Investigating the Effects of Non-thermal Air Plasma on Five Grains and Their Economically Important Pathogens

Melanie Ford

A thesis submitted for the degree of

Doctor of Philosophy

School of Agriculture, Food and Wine

The University of Adelaide

Adelaide, Australia



December 2021

Table of Contents

Table of Contents ..... **ii**
Abstract ..... **xiv**
Declaration ..... **xvi**
Acknowledgement of Country ..... **xvii**
Acknowledgements ..... **xviii**
1 Introduction and review of the literature **1**
1.1 General Introduction 1
1.2 Plasma 3
1.2.1 General background on plasma uses in food and agriculture 3
1.2.1.1 Non-thermal plasma 4
1.2.1.2 Role of the plasma generating apparatus 4
1.2.1.3 Ambient air plasma 6
1.2.2 Plasma treatment of seeds 6
1.2.2.1 The effect of plasma on seed surfaces 7
1.2.2.2 Plasma-treatment for pathogen inactivation 9
1.3 Plant seed morphology 11
1.3.1 Angiosperm seed germination 12
1.3.2 Grain crops of interest 13
1.3.2.1 Maize, *Zea mays* subsp. mays; GC 0645 14
1.3.2.1.1 Maize past and present 14
1.3.2.1.2 Maize grain morphology 15
1.3.2.2 Wheat, *Triticum aestivum*; GC 0654 17
1.3.2.2.1 Wheat grain past and present 17
1.3.2.2.2 Wheat grain morphology 18
1.3.2.3 Barley, *Hordeum vulgare*, GC 0640 19
1.3.2.3.1 Barley grain past and present 19
1.3.2.3.2 Barley grain morphology 20
1.3.2.4 Field pea, *Pisum sativum*; VD 0561 21
1.3.2.4.1 Field pea past and present 21
1.3.2.4.2 Field pea morphology 22
1.3.2.5 Psyllium, *Plantago ovata*; GC 3087 23
1.3.2.5.1 Psyllium past and present 23
1.3.2.5.2 Psyllium morphology 24

1.3.2.6 Summary 24
1.4 Fungal plant pathogens 25
1.4.1 *Aspergillus flavus*; MB#209842 27
1.4.2 *Bipolaris sorokiniana*; MB#293701 28
1.4.3 *Didymella pinodes*; MB#274545 29
1.4.4 *Fusarium graminearum*; MB#200256 30
1.4.5 *Penicillium chrysogenum*; MB#165757 31
1.5 Conclusions 32
1.6 Research aims and questions 33
1.6.1 Assess the impact of plasma exposure on grain surfaces 34
1.6.2 Evaluate the efficacy of plasma exposure for the inactivation of fungal pathogens on the grain surface 34
1.6.3 Determine the impact of plasma exposure on the physico-chemical properties of seeds. 35
1.6.4 Compare the effects of plasma exposure on seed viability, growth, and development 35
1.6.5 Apply knowledge gained throughout this thesis towards a real-world problem: deactivating fungal pathogens on an industrial contaminated grain sample 35
1.7 Significance of research 36
1.8 Structure of the thesis 36
2 A brief background on the events which lead to the conception of this research 38
2.1 Introduction 38
2.2 Previous work as the basis of this research project 38
2.2.1 Background 38
2.2.2 Plasma-treatment pilot trial 39
2.2.3 Plasma Tumbler (PT) pilot trials 40
2.3 Summary 41
3 General methodology 42
3.1 Plasma treatment 42
3.1.1 Plasma tumbler apparatus and modifications 42
3.1.1.1 Reasoning 42
3.1.1.2 Plasma tumbler apparatus 43
3.1.1.3 Modifications to the Michl et al., 2015 design 43
3.1.1.4 RF generator and matching system 44
3.1.2 Plasma tumbler operation 44
3.1.2.1 Treatment of single time points 45
3.1.2.2 Plasma tumbler treatment of time trial series 46
3.1.2.3 Tumbler and vacuum control treatment (T+V) 46

3.1.2.4 Untreated control 46
3.2 Grain procurement 47
3.2.1 Maize 47
3.2.2 Wheat 47
3.2.3 Barley 47
3.2.4 Field pea 47
3.2.5 Psyllium 47
3.2.6 Industry feed sample 48
3.3 Fungal culture 48
3.3.1 Media preparation 48
3.3.1.1 Full-strength Potato Dextrose Agar (PDA) 48
3.3.1.2 Half-strength Potato Dextrose Agar (½ PDA) 48
3.3.1.3 Water Agar 48
3.3.2 Fungal extraction buffer preparation 49
3.3.3 Microbe extractions 49
3.3.4 Haemocytometer quantification 49
3.3.5 Dilutions 50
3.3.6 Plating technique 50
3.3.7 Colony-forming unit counts 51
3.4 Statistical and data analysis 51
4 Assessing the impact of plasma treatment on grain surfaces via microscopy 52
4.1 Introduction 52
4.2 Materials and Methods 54
4.2.1 Grain treatment 54
4.2.2 Scanning electron microscopy 54
4.2.2.1 Sample preparation 54
4.2.2.2 Imaging 54
4.2.3 Profilometer 54
4.2.4 Statistical analysis 55
4.3 Results and Discussion 55
4.3.1 SEM 55
4.3.1.1 Maize 56
4.3.1.2 Wheat 59
4.3.1.3 Barley 62
4.3.1.4 Field Pea 66
4.3.1.5 Psyllium 67
4.3.1.6 Summary 71
4.3.2 Profilometry 72

4.4 Conclusion 77
5 Evaluating the efficacy of plasma treatment for the inactivation of fungal pathogens on the grain surface 79
5.1 Introduction 79
5.2 The culture of extant grain microbes 81
5.2.1 Introduction 81
5.2.2 Materials and Methods 82
5.2.2.1 Media preparation 82
5.2.2.1.1 Half-strength PDA (½ PDA) plates 82
5.2.2.1.2 Water agar (WA) plates 82
5.2.2.2 Grain treatment 82
5.2.2.3 Extraction buffer preparation 82
5.2.2.4 Microbe extractions 82
5.2.2.4.1 Pilot trial with maize 82
5.2.2.4.2 Experiment with four grain types 83
5.2.2.5 Colony counts 83
5.2.2.6 Fungal identification 83
5.2.2.7 Statistical analysis 83
5.2.3 Results and Discussion 84
5.2.3.1 Selection of culture media and refinement of methods 84
5.2.3.2 Quantification of extant culturable fungi 85
5.2.3.3 Fungal identification 88
5.2.4 Summary 88
5.3 Development of an assay to determine the relationships between fungal colony location and plasma exposure time 89
5.3.1 Introduction 89
5.3.1 Materials and Methods 90
5.3.1.1 Grain treatment 90
5.3.1.2 Well-plate preparation 90
5.3.1.3 Quantification of hyphal colonies 91
5.3.1.4 Data analysis 91
5.3.2 Results and Discussion 92
5.3.2.1 Maize 92
5.3.2.1 Wheat 93
5.3.3 Summary 96
5.4 The impact of the duration of plasma exposure on grain inoculated with fungal pathogens 97
5.4.1 Introduction 97
5.4.2 Materials and Methods 98
5.4.2.1 Plate preparation 98

5.4.2.2 Grain sterilisation prior to inoculation 98
5.4.2.3 Fungal extraction buffer preparation 98
5.4.2.4 Inoculum preparation and grain inoculation 98
5.4.2.4.1 Maize inoculated with *Aspergillus flavus*; ATCC 204304 98
5.4.2.4.1.1 Culture preparation 98
5.4.2.4.1.2 Grain inoculation 99
5.4.2.4.2 Field pea inoculated with *Penicillium chrysogenum* 100
5.4.2.4.2.1 Pathogen isolation 100
5.4.2.4.2.2 Culture preparation 101
5.4.2.4.2.3 Grain inoculation 101
5.4.2.4.3 Wheat inoculated with *Fusarium graminearum*; SARDI reference number 6894 101
5.4.2.4.3.1 Culture preparation 101
5.4.2.4.3.2 Grain inoculation 102
5.4.2.5 Experimental treatment 103
5.4.2.5.1 Untreated 103
5.4.2.5.2 T+V 103
5.4.2.5.3 Plasma treatment time series 103
5.4.2.6 Microbe extractions 103
5.4.2.7 Haemocytometer quantification 104
5.4.2.8 Dilutions 104
5.4.2.9 Plating technique 104
5.4.2.10 Cell viability Assay 104
5.4.2.11 Colony-forming unit quantification 104
5.4.2.12 Experimental replication and statistical analysis 105
5.4.3 Results and Discussion 105
5.4.3.1 Variations in inoculum 105
5.4.3.2 Spore/hyphal fragment viability assay 106
5.4.3.3 Colony-forming unit quantification 107
5.4.3.3.1 *Penicillium chrysogenum* on field pea 108
5.4.3.3.2 *Aspergillus flavus* on maize 111
5.4.3.3.3 *Fusarium graminearum* on wheat 113
5.4.4 Summary 113
5.5 Evaluation of plasma treatment for the deactivation of five inoculated pathogens on five grain types 114
5.5.1 Introduction 114
5.5.2 Materials and Methods 116
5.5.2.1 Grain sterilisation prior to inoculation 116
5.5.2.1.1 Maize, wheat, barley, and field pea 116

5.5.2.1.2 Psyllium 116
5.5.2.2 Inoculum preparation and grain inoculation 116
5.5.2.2.1 Maize inoculated with *Aspergillus flavus* 116
5.5.2.2.1.1 Culture preparation 116
5.5.2.2.1.2 Grain inoculation 116
5.5.2.2.2 Barley inoculated with *Bipolaris sorokiniana* 116
5.5.2.2.2.1 Culture preparation 116
5.5.2.2.2.2 Grain inoculation 117
5.5.2.2.3 Field pea inoculated with *Didymella pinodes* 118
5.5.2.2.3.1 Culture preparation 118
5.5.2.2.3.2 Grain inoculation 118
5.5.2.2.4 Wheat inoculated with *Fusarium graminearum* 119
5.5.2.2.4.1 Culture preparation 119
5.5.2.2.4.2 Grain inoculation 119
5.5.2.2.5 Psyllium inoculated with *Penicillium chrysogenum* 120
5.5.2.2.5.1 Culture preparation 120
5.5.2.2.5.2 Grain inoculation 120
5.5.2.3 Experimental treatment 120
5.5.2.4 Microbe extractions 120
5.5.2.5 Haemocytometer quantification 120
5.5.2.6 Dilutions 121
5.5.2.7 Plating technique 121
5.5.2.8 Colony-forming unit quantification 121
5.5.2.9 Scanning electron microscopy 121
5.5.2.9.1 Fixative preparation 121
5.5.2.9.2 Sample preparation 121
5.5.2.9.2.1 *Didymella pinodes* and *Penicillium chrysogenum* 121
5.5.2.9.2.2 *Aspergillus flavus, Bipolaris sorokiniana, Fusarium graminearum* and *Penicillium chrysogenum* 122
5.5.2.9.3 Imaging 122
5.5.2.10 Experimental replication and statistical analysis 123
5.5.3 Results and Discussion 123
5.5.3.1 *Aspergillus flavus* on maize host 123
5.5.3.2 *Bipolaris sorokiniana* on barley host 126
5.5.3.3 *Didymella pinodes* on field pea host 129
5.5.3.4 *Fusarium graminearum* inoculated wheat 132
5.5.3.5 *Penicillium chrysogenum* inoculated psyllium 135
5.5.3.6 Comparison of all fungal pathogen colony-forming unit concentrations 138

5.5.4 Summary 140
5.6 Conclusions 141
6 Determining the impact of plasma-treatment on the physico-chemical properties of grain 143
6.1 Introduction 143
6.2 Contact angle measurements 145
6.2.1 Introduction 145
6.2.2 Materials and Methods 146
6.2.2.1 Pilot trial grain treatment and experimentation 146
6.2.2.2 Plasma exposure trial grain selection and treatment 147
6.2.2.3 Tensiometer measurements 147
6.2.2.4 Data analysis 148
6.2.3 Results and Discussion 148
6.2.3.1 Water droplet on maize grain pilot trial 148
6.2.3.2 Contact angle measurements on three types of grains 150
6.2.4 Summary 153
6.3 Analysis of grain surface chemistry with ToF-SIMS 154
6.3.1 Introduction 154
6.3.2 Materials and Methods 155
6.3.2.1 Grain preparation 155
6.3.2.2 Time-of-flight secondary ion mass spectrometry 156
6.3.2.3 Data analysis 156
6.3.2.3.1 Principal component analysis 156
6.3.2.3.2 Two-way ANOVA 157
6.3.3 Results and Discussion 157
6.3.3.1 Principal component analysis 157
6.3.3.1.1 Comparisons of all fragments 158
6.3.3.1.2 Comparisons of organic fragments 161
6.3.3.2 Two-way ANOVA analysis of fragment abundance in each treatment and grain type 162
6.3.4 Summary 167
6.4 The effects of plasma exposure on grain moisture content and water sorption 167
6.4.1 Introduction 167
6.4.2 Materials and Methods 170
6.4.2.1 Treatment of grains 170
6.4.2.2 Seed moisture content 170
6.4.2.3 Dynamic vapour sorption trials 171
6.4.2.4 Modelling 172
6.4.2.5 Statistical analysis 173

6.4.3 Results and Discussion 173
6.4.3.1 Initial seed moisture content 174
6.4.3.2 Vapour sorption comparisons 175
6.4.3.3 Modelling grain hydration kinetics 180
6.4.3.3.1 Fitting the models 181
6.4.3.3.1 Using the Peleg model to interpret grain hydration 184
6.4.3.3.2 Using the 2-phase model to interpret grain hydration 185
6.4.4 Summary 192
6.5 Dye sorption assay to visualise the effect of plasma exposure on grain hydration 193
6.5.1 Introduction 193
6.5.2 Materials and Methods 194
6.5.2.1 Grain treatment 194
6.5.2.2 Trypan Blue incubation 194
6.5.2.3 Imaging 194
6.5.3 Results and Discussion 195
6.5.3.1 Maize 195
6.5.3.2 Wheat 197
6.5.3.3 Barley 198
6.5.3.4 Field pea 200
6.5.3.5 Psyllium 201
6.5.4 Summary 203
6.6 Mucilage hydration – a sticky situation 204
6.6.1 Introduction 204
6.6.2 Materials and Methods 204
6.6.2.1 Grain preparation 204
6.6.2.2 Sorption assay 205
6.6.2.3 Statistical analysis 205
6.6.3 Results and Discussion 205
6.6.4 Summary 208
6.7 The impact of plasma exposure on the prevalence of K+ on sample surfaces and in leachate 209
6.7.1 Introduction 209
6.7.2 Materials and Methods 210
6.7.2.1 Grain treatment 210
6.7.2.2 Dilution trial pilot 210
6.7.2.3 Experimental grain preparation 211
6.7.2.4 Flame photometry analysis 211
6.7.2.5 Statistical analysis 211

6.7.3 Results and Discussion 212
6.7.4 Summary 215
6.8 Conclusions 215
7 Comparing the effects of plasma treatment on seed viability, growth, and development 218
7.1 Introduction 218
7.2 Seed germination 220
7.2.1 Introduction 220
7.2.2 Materials and Methods 221
7.2.2.1 Grain treatment 221
7.2.2.2 Grain plating 221
7.2.2.3 Growth and development scores 222
7.2.2.4 Microbial contamination scores 223
7.2.2.5 Statistical analysis 224
7.2.3 Results and Discussion 224
7.2.3.1 Percent germination 225
7.2.3.1.1 Maize 225
7.2.3.1.2 Wheat 227
7.2.3.1.3 Barley 229
7.2.3.1.4 Field pea 229
7.2.3.1.5 Psyllium 229
7.2.3.1.6 Comparisons between grain types 230
7.2.3.2 Germination growth and development 230
7.2.4 Summary 231
7.3 Seedling growth trials 232
7.3.1 Introduction 232
7.3.2 Materials and Methods 233
7.3.2.1 Grain treatment 233
7.3.2.2 Experimental design 233
7.3.2.3 Grain sowing and growth trials 234
7.3.2.3.1 Maize 234
7.3.2.3.1.1 Short-term growth and development with an exposure time series 234
7.3.2.3.1.2 Long-term growth and development 234
7.3.2.3.2 Wheat 235
7.3.2.3.2.1 Short-term growth and development with a plasma exposure time series. 235
7.3.2.3.2.2 Repetition of short-term growth and development with three treatments... 235
7.3.2.3.3 Field pea 235
7.3.2.3.4 Psyllium 236

7.3.2.4 Statistical analysis 236
7.3.3 Results and Discussion 236
7.3.3.1 Early plant growth and development trials 237
7.3.3.1.1 Maize 237
7.3.3.1.2 Wheat exposure time series 237
7.3.3.1.3 Wheat three treatment comparisons 238
7.3.3.1.4 Field pea 241
7.3.3.1.5 Psyllium 242
7.3.3.2 Long-term growth of maize plants 242
7.3.4 Summary 244
7.4 Ethylene trial 245
7.4.1 Introduction 245
7.4.2 Materials and Methods 247
7.4.2.1 Grain preparation 247
7.4.2.1.1 Wheat 247
7.4.2.1.2 Maize 248
7.4.2.2 Hormone treatment preparation 248
7.4.2.2.1 Ethephon 248
7.4.2.2.2 AVG 248
7.4.2.3 Experimental procedures 249
7.4.2.4 Statistical analysis 249
7.4.3 Results and Discussion 250
7.4.3.1 Wheat 250
7.4.3.1.1 Water treatment 250
7.4.3.1.2 Ethephon treatment 250
7.4.3.1.3 AVG treatment 251
7.4.3.2 Maize 251
7.4.3.2.1 Water treatment 251
7.4.3.2.1 Ethephon treatment 255
7.4.3.2.2 AVG treatment 255
7.4.4 Summary 255
7.5 DNA oxidation 256
7.5.1 Introduction 256
7.5.2 Materials and Methods 258
7.5.2.1 Grain preparation 258
7.5.2.2 Grain growth 258
7.5.2.3 Embryo extraction 258
7.5.2.4 DNA extraction 259
7.5.2.5 Quantification of DNA concentration 260

7.5.2.6 ELISA assay for 8-Hydroxy-2'-deoxyguanosine 260
7.5.2.6.1.1 Pilot trial to establish dilutions 260
7.5.2.6.1.2 Experimental trial 260
7.5.2.7 Statistical analysis 260
7.5.3 Results and Discussion 261
7.5.4 Summary 262
7.6 Conclusions 263
8 Challenging the plasma tumbler system with contaminated industry grain samples 265
8.1 Introduction 265
8.2 Materials and Methods 267
8.2.1 Grain preparation 267
8.2.2 Plate preparation 268
8.2.3 Grain plating pilot trial 268
8.2.3.1 Grain treatment 268
8.2.3.2 Grain plating and visualisation 268
8.2.4 Experimental treatment 268
8.2.5 Microbe extractions and plating 269
8.2.5.1 Extractions 269
8.2.5.2 Dilutions 269
8.2.6 Plating 270
8.2.7 Colony-forming unit quantification 270
8.2.8 Pathogen descriptions and isolation 270
8.2.9 Pathogen identification 270
8.2.9.1 Visual identification 270
8.2.9.2 DNA extraction, sequencing, and analysis 271
8.2.9.3 qPCR 271
8.2.9.4 Data interpretation 271
8.2.10 Scanning electron microscopy 272
8.2.10.1 Sample preparation 272
8.2.10.2 Scanning 272
8.2.11 Mycotoxin analysis 272
8.2.11.1 Sample preparation 272
8.2.11.2 Sample analysis 272
8.2.12 Statistical analysis 273
8.3 Results and Discussion 273
8.3.1 Pilot trial grain plates 273
8.3.2 Colony-forming unit quantification 274
8.3.2.1 Filamentous fungal load on the contaminated grain 275

8.3.2.2 Comparisons of colony-forming units across treatments 276
8.3.3 Identification of pathogens present on the grain 279
8.3.4 Scanning electron microscopy 285
8.3.5 Mycotoxin sampling 288
8.4 Conclusions 291
9 Summary, limitations, and future directions 295
9.1 General summary 295
9.1.1 The impact of plasma exposure on grain surfaces 296
9.1.2 The efficacy of plasma exposure for the inactivation of grain fungal pathogens 296
9.1.3 The impact of plasma exposure on the physico-chemical properties of seeds 298
9.1.4 The effects of plasma exposure on seed viability, growth, and development 299
9.1.5 Challenging the system with a real-world problem: deactivating fungal pathogens on an industrial contaminated grain sample 300
9.2 Limitations of the research 301
9.2.1 Chapter 4 301
9.2.2 Chapter 5 302
9.2.3 Chapter 6 303
9.2.4 Chapter 7 303
9.2.5 Chapter 8 304
9.3 Future directions 304
9.4 Final remarks 306
10 References 307
Appendices 337
S1 Supplementary information for Chapter 4.2.3 337
S2 Supplementary information for Chapter 5.4.2.4.2.1 338
S3 Supplementary information for Chapter 5.4.2.8 339
S4 Supplementary information for Chapter 5.4.3.3.1 341
S5 Supplementary information for Chapter 5.5.2.6 342
S6 Supplementary information for Chapter 6.2.3 343
S7 Supplementary information for Chapter 6.3.4 346
S8 Supplemental information for Chapter 8.2.9.2 347
S9 Supplementary information for Chapter 8.2.8.3 350
S10 Supplementary information for Chapter 8.2.11.2 350
List of Figures 351
List of Tables 372
List of Equations 374

Abstract

Fungal contamination of post-harvest grain is a global problem, frequently resulting in economic loss and posing risks for human health and food security. Current methods for removing fungal contaminants from grain are often ineffective or may leave behind residues with downstream implications for consumers. This thesis explores the use of a novel air plasma tumbler apparatus to spin post-harvest grain through a field of plasma and inactivate fungal pathogens on the grain surface. Microbiological techniques were developed to inoculate grain with mycotoxigenic fungal pathogens and surface-sensitive analytical instrumentation were used to understand the physico-chemical changes to grains before and after exposure to plasma. Additionally, short-term seedling growth was investigated to understand the effects of plasma treatment on seed viability and seedling development.

Maize, wheat, barley, field pea and psyllium were selected for their economic importance and differing surface chemistries. Each type of grain was inoculated with an associated pathogen (e.g., *Aspergillus*, *Bipolaris, Didymella, Fusarium*, or *Penicillium* species) and exposed to a time series of plasma treatments. Cultures from grain samples were assessed for the number of viable pathogens following treatment. Furthermore, contaminated industry samples were procured and subjected to plasma exposure to determine if the technology could reduce high loads of mixed microbes.

Results showed varying efficacy of plasma exposure depending on grain type and associated pathogen. This may be attributed to seed surface chemistry, seed

morphology and the biochemical makeup of the pathogens. 90 minutes of plasma treatment was the most effective exposure time across all inoculated pathogens and grain types, resulting in up to 7-log reductions of microbial colony forming units. Industry sample microbial loads were reduced by five-fold, with 120-minutes of plasma exposure inactivating all filamentous fungi. SEM micrographs provided visual references, illustrating the plasma-induced weathering of both fungal pathogen structures and grain surfaces.

The effects of surface weathering had downstream implications for grain hydration and grain viability. Plasma treatment increased grain water sorption by roughly 25% and reduced water contact angles by over 50 degrees. It was also shown that plasma exposure altered the rate and direction of water ingress. The changes in grain-water relations may come at a cost to seed germination, growth, and development. Maize and wheat were negatively impacted by the long exposure to plasma necessary for microbial inactivation. However, in the context of food security, this may not be of interest.

This research applied aspects of microbiology, plasma physics and seed biology to gain insights into the deactivation of grain post-harvest fungal pathogens using air plasma. The outcomes of this systematic study advance the current knowledge of plasma agriculture and promote air plasma as a future technology, benefiting food security and food production, with possible future applications toward biosecurity.

Declaration

I certify that this work contains no material which has been accepted for the award of any other degree or diploma in my name, in any university or other tertiary institution and, to the best of my knowledge and belief, contains no material previously published or written by another person, except where due reference has been made in the text. In addition, I certify that no part of this work will, in the future, be used in a submission in my name, for any other degree or diploma in any university or other tertiary institution without the prior approval of the University of Adelaide and where applicable, any partner institution responsible for the joint-award of this degree.

I give permission for the digital version of my thesis to be made available on the web, via the University's digital research repository, the Library Search and also through web search engines, unless permission has been granted by the University to restrict access for a period of time.

Melanie Ford

December 2021

Acknowledgement of Country

I would like to begin by acknowledging and extending my deepest gratitude to the Kaurna People, the owners of the lands on which I have lived and worked whilst undertaking this research. I humbly recognise their deep connections to country, their culture, spirit, and knowledge. The scientific endeavours described in this thesis would not have been possible without Kaurna wisdom and guidance. I would like to dedicate and share this work with Kaurna people as a gesture of appreciation and respect. Thank you.

Acknowledgements

This thesis was developed in a time of deep uncertainty, loss and global change. Millions across the planet have lost their lives to a disease caused by a 29,903 base pair microbe - the SARS-Cov-19 virus. Millions more have lost their loved ones and livelihoods. It seems remarkable that throughout this tumultuous era my only loss was my previous research project. Under different circumstances this would have been momentous, yet the mere forfeiture of two years' work seems so flippant in our current times. This is especially so when looking back at the astonishing amount of research I have accomplished over the past year. If anything, this thesis is a testament to the power of collaboration and the generosity of those I work with.

The old proverb, 'it takes a village' certainly rings true for this body of work. It took the support of a whole university campus to finish a project in under 18 months. From the night shift security guards checking in and telling ghost stories to make sure I was safe and still awake at 2 am in the laboratory, the undergraduate teaching staff who happily let me use their instruments and equipment, the Head of School who personally drove to seven supermarkets to buy toilet paper and dry goods for international students in need during lockdown, the lab technicians who dutifully trained me and trusted me despite bloodshot eyes and sleep deprivation, through to the stolid support of my unflappable supervisory team, it took the encouragement and support of hundreds of people to get these words to print. While I cannot name each person who made an impact on my research, I would like to extend my sincere appreciation and thanks for all you have done.

There are a few individuals whose contributions not only shaped this work but, who supported my growth as a scientist and as a human. A brief sentence cannot begin to express my gratitude, but I hope they will take heart in these few words.

Bryan

Your quiet confidence in my research was, at times, my only motivation to push through.

Tara

You taught me to embrace my curiosity and to never forget my passion for knowledge.

Max

You showed me how to be a scientist. Your ability to brainstorm, pull concepts out of thin air and instantaneously calculate dilutions will forever amaze me.

I have attempted to collate a list of the ‘village’ which contributed to this thesis. Not all individuals are named but please know that I am grateful for all contributions, no matter how great or small.

Aaron Phillips
Alan McKay
Alex Cavallaro
Alison Gill
Anita Nedosyko
Ashleigh Panagaris
Beth Loveys
Bethany Murphy
Bryan Coad
Caitlin MacPherson
Carolyn Schultz
Chao Ma
Charlie Maxson
Chelsea Hocker
Chris Ford
Chris 'Rabby' Nicolson
Chris Stone
Danièle Giblot-Ducray
Dave Jeffery
Eliza Schioldann
Emma Aspin
Entesar Abood
Eva Tomczyk
Greg Naglis
Gwen Mayo
Hans Griesser
Harshal Patel
Helen Brown

Helen Collins
Herdina
Hugh Wallwork
Jade Saunders
James Cowley
Jane Sibbons
Janet Drake
Jared Thomas
Jenny Guerin
Jonathan Tyler
Julian Schwerdt
Karen Chance
Ken Neubauer
Kylie Neumann
Kym Edwards
Lisa O'Donovan
Makayla Lamb
Margret Evans
Mark Butt
Marne Durnin
Martin Cole
Matt Coulter
Matt Salomon
Matthew Gilliham
Matthew Tucker
Maxime François
Michael Taylor
Milica Grcic
Natalie Betts
Natalie Kibble
Oussama Yahiaoui
Patty Mulligan
Phil Brewer
Qi Wu
Rachel Burton
Renee Phillips
Roslyn Baird
Sandy Khor
Sarah Kidd
Stav Manafis
Stefanie Wege
Stephanie Watts-Williams
Steve Tyreman
Suzanne Balacey
Tara Garrard
Tate Hancox
Thomas Fallon
Thomas Michl
Tina Bianco-Miotto
Tom Mulligan
Tony Hall
Troy Campbell
Vinay Pagay
Vincent Bulone
Wayne Leifert
Wendy Sullivan
Ying Lily Meng
Yu Julian Que

Finally, I would like to thank the institutions which supported this work:

Adelaide Microscopy, Frome Road
ARC Plant Energy Biology
CSIRO Health and Biosecurity, Kintore Avenue
Future Industries Institute, University of South Australia
Intertek
Microscopy Australia
Molecular Diagnostics Centre
SARDI Cereal Pathology
South Australian Seed Conservation Centre
Sumitomo Chemical Australia Pty Ltd
University of Adelaide
Viterra
Waite Research Institute

1 Introduction and review of the literature

1.1 General Introduction

Food insecurity, or the inconsistent accessibility of nutritious food, is one of the most pressing concerns of our age, affecting one in three people, or roughly 2.37 billion (UN, 2021). As weather extremes, temperature changes, and the availability of water add stress to agricultural systems across the globe, climate variability is one of the major driving factors of food insecurity (Kang et al., 2009). This has been further exacerbated by the COVID-19 pandemic, which has decreased access to food, affected crop production, and driven economic changes around staple cereal and pulse crops. Current projections by the Food and Agriculture Organisation (FAO) of the United Nations (UN) forecast that pandemic-related inflation will further reduce access to staple grains for millions of people between now and 2030 (FAO, 2021a). The severity of this crisis cannot yet be fully estimated.

Global food security is reliant upon the safe and efficient production of staple grain crops (FAO, 2020; Dwivedi et al., 2017). Globally, humans consume a high amount of staple grains and grain products; roughly 166 kilograms per person, per year (Table 1-1), highlighting the dire need to reduce annual grain losses (FAO, 2021b). Every year, crop pathogens result in yield losses of roughly 22.5% for maize and 21.5% for wheat, not to mention the associated economic costs (Fisher et al., 2012; Savary et al., 2019). Fungal pathogens are of particular importance as many are capable of destroying crops and producing mycotoxins, which are secondary metabolites with dire

effects on human health, even at minute concentrations (Agriopoulou et al., 2020; Fausto et al., 2019). Mycotoxin contamination alone leads to the loss of million tonnes of harvested grain each year (Mesterházy et al., 2020). Any reduction in these losses will be beneficial in improving food security.

Table 1-1. Global figures for grain consumption and losses in 2018 (FAO, 2021b).

Grain & grain products	**kcal consumed per capita per day**	**kg consumed per capita per year**	**Losses (1000 tonnes)**
Rice	528	78.43	34070
Maize	156	18.76	62562
Wheat	544	67.04	26597
Barley	8	1.07	5058
Pea	7	0.77	687
Total	1243	166.07	128974

Some of the risks associated with crop fungal pathogens can be mitigated through improvements to hygiene, transport and storage practices, though these strategies tend to be less accessible in low-and middle-income countries (LMICs) (Pitt et al., 2012). Other risks, such as the increasing prevalence of fungicide resistance in crop pathogens, presently have no solution (Fisher et al., 2012; Hu and Chen, 2021). If we are therefore to achieve the UN Sustainable Development Goal (SDG) number two of zero hunger by 2030, innovative technologies must be rapidly developed to combat fungal pathogens, especially in staple crops (UN, 2015).

Despite the enormity of the situation, there are glimmers of hope. The scientific community has accepted the call to action for the improvement of food security and is currently proposing the use of plasma technologies, among other methods, to prevent loss throughout the food supply chain (Ohta, 2016; Puac et al., 2018). Non-thermal air plasmas are at the forefront of agricultural and biosecurity research due to their antimicrobial capabilities with low energy requirements, the lack of chemical input and scalability (Holubová et al., 2020; Kaur et al., 2020). Recent investigations have

explored the use of plasma for primary and secondary food production processes, including post-harvest grain crops, as reviewed by Bourke et al., 2018 and Misra et al., 2016. This rapidly expanding field of research is exciting with the potential to greatly impact food sustainability over the next decade given adequate funding, regulation and policy support, and targeted outcomes (Niemira, 2019). However, the current body of research surrounding plasma treatment of post-harvest grains is scattered and lacking in common goals and interests. Nine reviews over the past five years have sought to capture the evolving nature of this field (Bourke et al., 2018; Chizoba Ekezie et al., 2017; Holubová et al., 2020; Kaur et al., 2020; Misra et al., 2016; Niemira, 2019; Ohta, 2016; Puac et al., 2018; Siddique et al., 2018). What is clear from these literature reviews is the incredibly complex interaction of plasma with living seeds and microbes. Each seed type and microbe may respond to plasma treatment in a different manner. A detailed look at both seeds and target microbes is necessary prior to exploring their dynamic behaviour following plasma treatment. This chapter seeks to provide a review of the literature within the field of plasma agriculture, as well as a general background on plant seeds, a brief description of five grains of interest and five seed-borne pathogens of these crops. The synthesis of this information will be used to highlight gaps within the current body of research and lead to the conception of new research questions.

1.2 Plasma

1.2.1 General background on plasma uses in food and agriculture

As the fourth state of matter, plasma is a partially or fully ionised gas containing ions, electrons and neutrals (Von Keudell and Schulz-Von Der Gathen, 2017). While it exists around us in nature, the history of human research into plasma began in 1777 with the Lichtenberg figures (Merrill and Von Hippel, 1939) and was greatly advanced in 1857 when Siemens described a dielectric barrier discharge plasma (Misra et al., 2016). The

naming has yet to reach its centenary, with the term ‘plasma’ attributed to Irving Langmuir in 1927 (Smith, 1971). Since its discovery, the field of plasma physics has expanded from industrial applications to astrophysics, medicine, food production and beyond (Harry, 2010). The temperature of the electrons within a plasma determines the status as a high or low temperature plasma (Von Keudell and Schulz-Von Der Gathen, 2017). This review will focus on low temperature, specifically non-thermal (cold) plasmas for the treatment of living tissues.

1.2.1.1 Non-thermal plasma

Non-thermal plasmas exist in a non-equilibrium state where electron energies are much higher, and thus hotter, than the ions, radicals and neutral plasma species (Puligundla and Mok, 2019). This state is sufficient for excitation, dissociation and ionisation reactions to occur while allowing for a plasma treated surface to remain near room temperature (Harry, 2010). In this unique environment, a biological surface can remain within an ideal temperature range while energetic electrons initiate reactions (Whitehead, 2016). Applying this concept toward agricultural and food processing systems, ionized gases created in the plasma discharge are capable of altering features and deactivating microbes on food commodity surfaces without raising temperatures to levels detrimental to commodity quality (Puligundla and Mok, 2019). The concepts of non-thermal plasma treatment were first explored on rice in 1961 (Hogan and Roseman, 1961a, 1961b) and have steadily gained attention since.

1.2.1.2 Role of the plasma generating apparatus

The chemical composition of a plasma is dependent upon multiple factors including the type of plasma apparatus, gas composition, substrate composition, pressure, power, and duration of treatment (Butscher et al., 2020). Plasma can be generated using multiple types of apparatus including radio-frequency, dielectric barrier discharges, pulsed AC power sources, microwave and gliding arc systems

(Whitehead, 2016). Šerá et al., 2012 compared the four latter types of generators for treating the surfaces of buckwheat and found striking differences between each apparatus and downstream seed development. Others, including Bormashenko et al., 2015, 2012, Dauwe et al., 2021, Ling et al., 2015, 2014 and Singh et al., 2019 have reported on the effects of radiofrequency (RF) plasma. While it is recognised that the type of apparatus is of high importance, this research focuses on radiofrequency plasma and will generally discuss capacitively coupled RF reactors from this point forward. Detailed reviews including tables with various device types can be found in Ehlbeck et al., 2011, Kaur et al., 2020 and Muhammad et al., 2018.

Capacitively coupled low pressure radiofrequency plasma reactors are used in multiple fields ranging from semiconductor manufacturing to the treatment of agricultural products (Chen, 2008). These plasmas typically operate at the industry standard of 13.56 MHz generated between two parallel electrodes within a vacuum chamber (Wilczek et al., 2020) (Figure 1-1). A multitude of modifications to RF reactor designs have been used to accommodate samples of various sizes and the ability to move the sample during treatment (Michl et al., 2015).

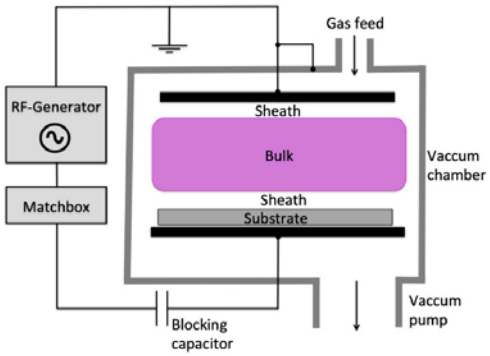


Figure 1-1. Diagram of a typical capacitively coupled radiofrequency plasma apparatus. Republished with permission of American Institute of Physics, from Electron dynamics in low pressure capacitively coupled radio frequency discharges, Wilczek, S., Schulze, J., Brinkmann, R.P., Donkó, Z., Trieschmann, J., Mussenbrock, T., 2020. J. Appl. Phys. 127; permission conveyed through Copyright Clearance Center, Inc.

1.2.1.3 Ambient air plasma

As previously mentioned, the gas composition also plays a role in plasma chemistry. In food and agricultural applications the gas is often ambient air, O_2, H_2, N_2, He, Ar or a combination of these gases (Dobrynin et al., 2009; Raballand et al., 2008; Šerá et al., 2010; Stolárik et al., 2015). From this point onward, there will be a focus on ambient air plasma. Air plasma contains a plethora of energetic species derived from the mixture of gases comprising air. For this reason, the exact chemical composition of the plasma cannot be determined. Instead, general assumptions can be made based on the main gases and their abundance in air, in the following order: nitrogen, oxygen, carbon dioxide, argon and trace amounts of other gases. In the plasma, the primary reactions are due to inelastic collisions of electrons with molecules and atoms, which cause different products such as ions, radicals, metastable species, and UV radiation. The ionisation and dissociation in these primary reactions can form highly reactive species, including O_3, O_2, $OH^{\bullet}$, H_2O, NO_2, N_2O, NO, CO_2, and HNO_3 (Holubová et al., 2020; Muhammad et al., 2018; Pavlovich et al., 2014). These newly formed species lead to secondary reactions which can create further reactive species and neutral fragments (Whitehead, 2016). As ions move throughout the field of plasma, they collide with the sample substrate, physically breaking apart surface molecules on the grains. The reactive species within the air plasma attack the freshly broken fragments causing many different chemical reactions (Dobrynin et al., 2009; Fridman, 2008). This process of physical ion bombardment and chemical reactivity is called chemical sputtering or etching and is responsible for the major weathering modifications to samples exposed to air plasma (Opretzka et al., 2007; Raballand et al., 2008).

1.2.2 Plasma treatment of seeds

Plasma in agriculture and food production processes has been explored for two main purposes: improvement to the surfaces of the treated commodities and the inactivation

of surface pathogens (Kaur et al., 2020; Whitehead, 2016). In both cases, the effects of chemical etching are thought to be the main mechanisms of action (Dobrynin et al., 2009). A short discussion of each purpose is listed below to understand how plasma treatment appears to impact the quality and microbiome.

1.2.2.1 The effect of plasma on seed surfaces

The surfaces of many agriculturally relevant seeds tend to be coated in an outer protective layer essential for regulating the manner in which a seed absorbs water (Werker et al., 1979). The ion bombardment and subsequent oxidation of seed surfaces during plasma treatment are thought to disrupt this outer layer which may have positive and negative effects. Hogan and Roseman, 1961a were the first to demonstrate this concept, describing changes to rice hydration capacity following plasma treatment. They observed that plasma altered the surfaces of grain, allowing for rice to absorb more water in a rapid manner. Plasma technology has developed by leaps and bounds over the sixty years since Hogan and Roseman's initial experiments. The concept of plasma-induced changes to grain hydration was greatly expanded upon by Bormashenko et al., 2012, who demonstrated that up to two minutes of RF plasma treatment altered the seed surface interaction with water and improved germination rates in wheat, green bean and lentil seeds. Subsequent research by Dufour et al., 2021 and Ling et al., 2014 validated this phenomenon with increased germination rates and the increased surface energies following plasma-treatment. On the other hand, up to 15 minutes of treatment in a gliding electric discharge system altered not only the maize seed surface topography but also the grain colour (Kamseu-Mogo et al., 2021). Furthermore, Dauwe et al., 2021 observed the formation of cracks on the surface of flax treated for 20 minutes using a RF apparatus, but little visible damage after five minutes of treatment. Although it is difficult to directly compare studies using different equipment, treatment regimens and types of seeds (Table 1-2), broad

Table 1-2. Selected plasma-treated seed germination research including plant species tested, apparatus, and treatment times. CDPJ = corona discharge plasma jet; DBD = dielectric barrier discharge; DCSBD = diffuse coplanar surface barrier discharge; GA = gliding arc; M = downstream microwave; RF = radiofrequency.

Treated species	**Common name**	**Plasma apparatus**	**Treatment time**	**Publication**
Arabidopsis thaliana	Arabidopsis	DBD, plasma jet	15 min	Bafoil et al., 2018
Arabidopsis thaliana	Arabidopsis	DBD	15 min	Bafoil et al., 2019
Triticum aestivum, Phaseolus vulgaris, lens culinaris	wheat, green bean, lentil	RF	15 s to 2 min	Bormashenko et al., 2012
Mimosa caesalpiniafolia	mimosa	DBD	3, 9, 15 min	da Silva et al., 2017
Linum usitatissimum	flax	RF	5, 10, 15, 20 min	Dauwe et al., 2021
Gossypium sp.	cotton	DBD	3, 27, 81 min	de Groot et al., 2018
Lens culinaris	lentil	DBD	up to 20 min	Dufour et al., 2021
Triticum aestivum	wheat	RF	15 s	Jiang et al., 2014
Zea mays	maize	GA	5 min, 15 min	Kamseu-Mogo et al., 2021
**Arabidopsis thaliana*	Arabidopsis	DBD	2,5,10,15 and 20 s	Kobayashi et al., 2020
Glycine max	soybean	RF	15 s	Ling et al., 2014
Brassica napus	rape seed	RF	15 s	Ling et al., 2015
Asparagus acutifolius	asparagus	RF	1, 15, 30 min	Lo Porto et al., 2019
Triticum aestivum	wheat	DBD	30 s, 1 min, 3 min	Los et al., 2019
Hordeum vulgare	barley	DCSBD	10 s, 20 s, 30s, 1 min, 3 min, 5 min	Pet'ková et al., 2021
Brassica napus	rape seed	CDPJ	up to 3 min	Puligundla et al., 2017
Avena sativa; Triticum aestivum	oat, wheat	M	3, 5, 10, 20, 40 min	Šerá et al., 2010
Cannabis sativa	hemp	GA, M	3, 5, 10 min	Sera et al., 2017
Capsicum annuum; Lens culinaris	capsicum, lentil	RF	1 min	Shapira et al., 2018
Ocimum basilicum	sweet basil	RF	10 min	Singh et al., 2019
Cucumis sativus, Capsicum annuum	cucumber, capsicum	DCSBD	4 s, 20 s	Štěpánová et al., 2018
Pisum sativum	pea	DCSBD	1 to 10 min	Stolárik et al., 2015
Pisum sativum	pea	DCSBD	1, 3, 5 min	Švubová et al., 2020
Sophora flavescens, Cassia torosa	sophora, senna	RF	1, 2, 3, 4 min	Yamauchi et al., 2012

generalisations can be made from the combined works. Chiefly, that the weathering processes of plasma alters the seed surface. In turn, this changes the way water interacts with the seed. Under optimal conditions plasma exposure may improve germination rates. However, there are many challenges to overcome if plasma is to be developed for broad agricultural use—plasma must treat living seeds with three-dimensional features such as grooves, wrinkles, and hairs, as well as a variety of surface chemistries. Much work is needed to determine ‘optimal’ plasma treatment conditions if this technology is to be expanded to meet the needs of the growing food crisis.

The investigation of plasma-activated water for enhanced seed germination (Lo Porto et al., 2018; Sivachandiran and Khacef, 2017; Zhou et al., 2019) is another area of interest but will not be discussed within this body of work, which focuses on the direct impact of plasma to seeds.

1.2.2.2 Plasma-treatment for pathogen inactivation

The impact of pathogens on food security cannot be understated, with the immediate need for mitigating technologies to prevent a worsening crisis (Fones et al., 2020; Savary et al., 2019). Plasma is seen as an emerging technology for consideration due to the ability to inactivate surface pathogens through chemical etching, while the non-equilibrium properties limit the impact on grain quality (Butscher et al., 2016; Dobrynin et al., 2009). These principles have been employed through the use of plasma sterilisation in the medical field (Laroussi, 2005; Scholtz et al., 2015) and are likely adaptable to suit the needs of agricultural and food production processes (Kaur et al., 2020; Misra et al., 2016). As sterilisation implies the complete elimination of all microbes (Mohapatra, 2017), the terms inactivation and disinfestation are preferred for agricultural and food applications since it is likely some microbes will remain viable

following treatment. Opretzka et al., 2007 demonstrated that on flat surfaces, plasma treatment can weather the surface structures of bacterial endospores to the point of inactivation. This concept has inspired research into the inactivation of plant pathogenic microbial cultures, as reviewed by Adhikari et al., 2020 and Scholtz et al., 2019, as well as a flurry of research evaluating the efficacy of plasma for the inactivation of microbes on grain surfaces (Butscher et al., 2016; Kordas et al., 2015; Los et al., 2020; Panngom et al., 2014; Selcuk et al., 2008). These studies have looked at both inoculations and extant microbes on the grain surface. Selcuk et al., 2008 performed a comprehensive study on the plasma treatment of multiple grain types inoculated with *Penicillium* spp. and *Aspergillus* spp. They recorded up to four-fold reductions of these pathogens while noting that the effect of plasma varied between grain types. It is speculated that specific features on the grain surface may contribute to the differences in efficacy (Butscher et al., 2016). It seems that plasma irradiation must be able to reach all surfaces and features of the grain if microbes are to be eliminated via weathering, yet few studies involve a plasma apparatus that rotates grains so all faces have equal exposure to plasma. Pet'ková et al., 2021, Švubová et al., 2020 and Tomeková et al., 2020 placed their plasma apparatus on an orbital shaker to rotate grains but it is unclear how effective this movement was at exposing all surfaces to plasma.

Los et al., 2020 investigated the effects of plasma on the extant wheat microbiome and noted log reductions of multiple types of fungal and bacterial pathogens. These results are encouraging in that plasma can simultaneously inactivate multiple types of pathogens. Overall, it appears that plasma treatment is capable of reducing the fungal and bacterial load on seeds, however the results may be dependent upon grain type and treatment protocols, as reviewed by Kaur et al., 2020. No known studies have yet explored the efficacy of plasma treatment on multiple fungal structures, e.g., hyphae,

conidia, etc. Additionally, steps should be taken to understand the plasma treatment conditions optimal for the complete inactivation of multiple pathogenic species. Understanding thresholds and limits is necessary to provide a framework for the future development of this technology if it is to be adapted on an industrial scale.

It is clear from the previous sections that establishing a foundational knowledge of seeds, their economic relevance and significant morphological features is necessary before exploring the applications of plasma. Additionally, a cursory discussion of plant pathogens is needed to understand their complex interactions with seeds. The remaining sections of this review will touch upon each of these fields.

1.3 Plant seed morphology

The appearance of seeds is arguably one of the most significant evolutionary benchmarks in earth history. Seed evolution in vascular plants during the Carboniferous, roughly 330 million years ago (Mya), has allowed plants to successfully reproduce on dry land and inhabit vast swathes of the earth (Magallón et al., 2013; Steeves, 1983). Gymnosperms, the naked seeds, were dominant until major extinctions during the Mesozoic paved the way for angiosperms, cased or enclosed seeds, to rapidly diversify (De La Torre et al., 2020; Doyle, 2012). The advantages of forming enclosed seeds led to countless modifications and variations along the theme with monocots and eudicots diverging in the Cretaceous (Sanderson et al., 2004). The ancestors to modern cereals and legumes spread across the globe following the Cretaceous-Paleogene boundary (Koenen et al., 2021; Strömberg, 2011) ultimately leading to the 405 families, 14,559 genera and an estimated 352,000 extant species (WFO, 2021). The astounding success of seeds as a form of reproduction is clearly apparent in the sheer diversity of living plant species covering all continents including Antarctica (Edwards and Lewis Smith, 1988).

As one would expect, seed morphology varies greatly among plants. This vast evolutionary timeline has allowed for countless shapes, sizes, structures and chemistries to aid in dispersal, protection and water sorption (WFO, 2021). Despite the incredible assortment of adaptations, all angiosperm seeds contain an embryo, nutrient reserves and an outer protective layer, with very few exceptions (Crang et al., 2018). The integrity of these structures is essential for the survival of the seed, and the protective envelope is designed to withstand the harsh natural environment and ensure a seed will not germinate until conditions are sufficient for embryo development (Kelly et al., 1992). The embryo is composed of a root (radicle), leaf tissues (cotyledon(s), plumule and/or coleoptile) and stem (hypocotyl). The storage tissues mobilise nutrients to fuel the metabolic activities of the rapidly developing embryo (Lopes and Larkins, 1993). While these fundamental structural traits are shared, each plant species has modified the tissues to suit specific needs. In the case of domesticated grain crops, the seed tissues have been selected to suit human needs.

1.3.1 Angiosperm seed germination

Germination is a complex event in which a dry and metabolically quiescent seed commences with the uptake of water to rehydrate and reactivate. This process occurs over three phases beginning with imbibition (Bewley, 1997) (Figure 1-2). The initial phase of water uptake is often tightly controlled through specific structures such as the micropyle, hilum and chalaza, where water is wicked toward the embryo via capillary action. It can also occur diffusely across the seed surface but often hydrophobic protective barriers limit diffusion in the early stages of imbibition (Miano and Augusto, 2018; Werker, 1997). Once the initial physical absorption of water occurs, the grain passes into phase II where water uptake plateaus as seed metabolic activity skyrockets. Cell elongation occurs in the embryonic tissues and culminates at phase III when the radicle protrudes from the seed. This event signals the completion of

germination and the beginning of seedling growth and development with the mobilisation of nutrients from storage tissues and rapid cell division (Bewley et al., 2013; Mei and Song, 2008). The phases of germination occur over different time points for each plant species and cultivar. In domesticated grain crops, such as wheat and barley, all three phases of germination may be complete in less than 24 hours given optimal conditions (Fincher and Stone, 1993).

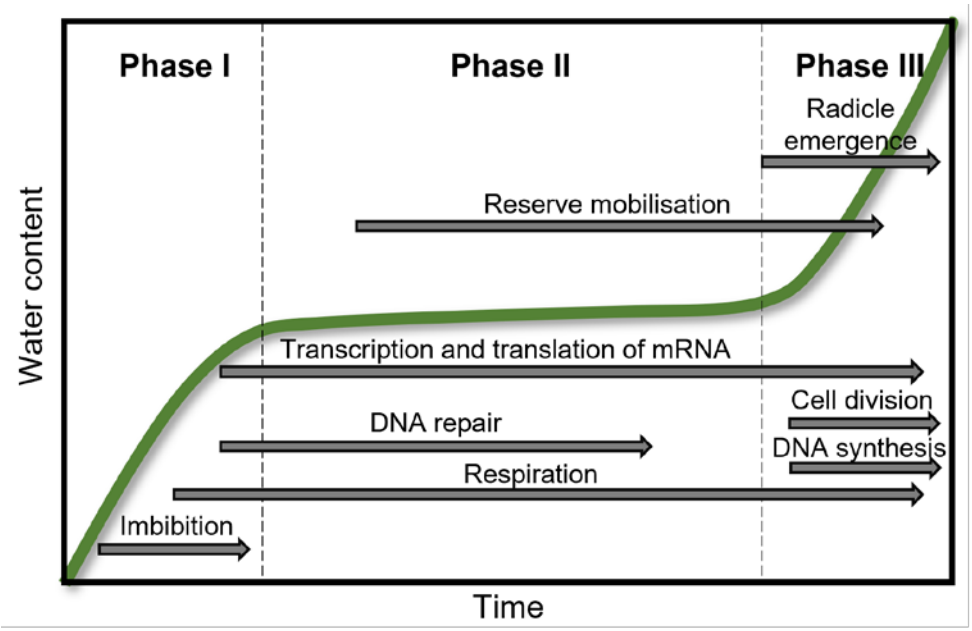


Figure 1-2. The triphasic model of seed germination modelled after Bewley et al., 2013 and Bewley and Black, 1978.

1.3.2 Grain crops of interest

The complex relationships between humans and seeds spans multiple millennia and has led to the breeding of specific traits designed to improve nutritional properties, grain size, disease resistance, ease of harvest and processing and ensure consistent germination rates (Cowling et al., 2019). A handful of these domesticated grains are staples within the diets of all humans on earth, including rice, wheat, maize, and soybean. Yet, over-reliance on these crops has led to much of the food security crisis facing the world today (Pingali, 2015). This highlights the importance of finding short-term solutions to postharvest grain pathogens to provide food security in the near future, while long-term strategies may be introduced to provide sustainability (Wei and

Frankel Davis, 2021). From this point onward, there will be a focus on five grain crops: maize, wheat, barley, field pea and psyllium. Each has been selected for both dietary and economic relevance, as well as classification and specific surface structures, the details of which will be described in the proceeding sections. Understanding the morphological features of each grain type will be important in later chapters when investigating the effects of plasma treatment on seed surface structures and water transport phenomena. The 2018 revised FAO and World Health Organisation (WHO) Codex Alimentarius, *Classification of Foods and Animal Feeds,* Commodity Groups are listed next to each grain type for the reader's ease of reference (FAO, 2019). These classifications are also used by the Australian Government and titled 'Crop Groups' (APVMA, 2021).

1.3.2.1 Maize, *Zea mays* subsp. mays; GC 0645

1.3.2.1.1 Maize past and present

Zea mays is a cereal crop domesticated from the wild grass, commonly known as teosinte, *Zea mays* subsp. *parviglumis,* roughly 7500 to 10,000 years ago in the Mexico-Central America region (Bonavia, 2013; Fukunaga et al., 2005; Matsuoka, 2005) (see Figure 1-3, A). Maize is currently grown on a global scale for human and animal consumption, as well as ethanol production (Ranum et al., 2014), with roughly 1.15 billion tonnes harvested in 2018 (FAO, 2021b). According to the FAO Food Balance Sheets (FAOSTAT), the 2018 global maize production was worth $243.6 billion USD, one of the top three food crops in economic value (FAO, 2021b). However, the mean annual losses due to pathogens and pests of 22.5%, as calculated by Savary et al., 2019, amount to roughly $54.9 billion USD. The effects of postharvest pathogens on maize production and safety should not be underestimated.

1.3.2.1.2 Maize grain morphology

The structure and chemical composition of maize kernels is thought to play a role in grain susceptibility to fungal infection with postharvest pathogens, such as *Aspergillus flavus* (Mutiga et al., 2019). For this reason, it is necessary to discuss the basic structure of maize grains (Figure 1-3). The outermost surface is coated in a layer

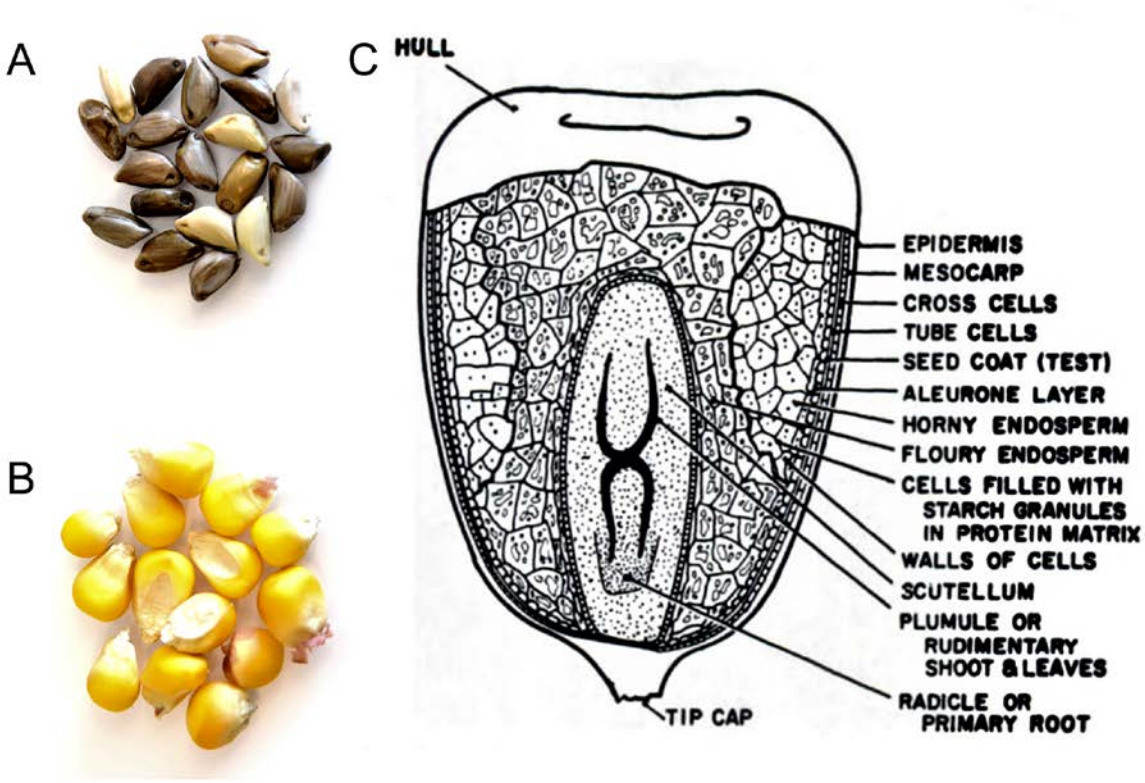


Figure 1-3. (A) Grains of maize wild relative, teosinte. (B) Modern maize cultivar B73. (C) Diagram of a modern maize kernel (republished with permission of Taylor and Francis Group, from Drying and storage of grains and oilseeds, Brooker, D.B., Bakker-Arkema, F.W., Hall, W., 1992. Van Nostrand Reinhold; permission conveyed through Copyright Clearance Center, Inc.).

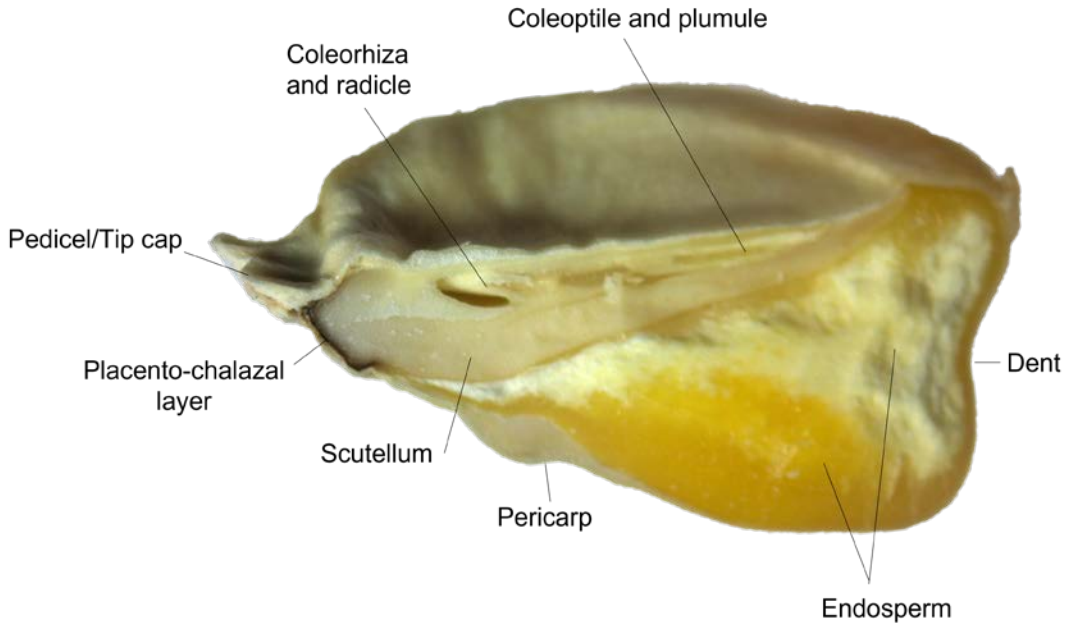


Figure 1-4. Longitudinal section of a *Zea mays* subsp. mays 'B73' grain with labels of important tissues and structures.

of wax, of which the composition differs between cultivars and types of maize (Russin et al., 1997). Under the waxy layer is the hull, consisting of the fused pericarp and seed coat (Song et al., 1992). Together, these dead maternal structures form the outer protective envelope of the grain. Underneath the pericarp is the aleurone layer which borders the endosperm. As in all cereals, the endosperm is the maize kernel storage tissue and makes up roughly 82% of the grain (Mejia, 2003). The embryo, or germ, is comprised of the radicle, with the outer protective coleorhiza sheath, and the plumule which is the rudimentary shoot and leaf (Figure 1-4). Adjacent to the embryonic root and leaf structures is the modified cotyledon called the scutellum (Brooker et al., 1992). Other structures of note include the tip cap, also known as the pedicle, the placenta-chalazal layer and the micropyle pore. These remnant maternal structures, like the pericarp, undergo programmed cell death at seed maturation and serve important functions in water uptake during seed imbibition (Domínguez and Cejudo, 2014).

1.3.2.2 Wheat, *Triticum aestivum*; GC 0654

1.3.2.2.1 Wheat grain past and present

Wild emmer wheat, *Triticum dicoccoides*, was first harvested in the Fertile Crescent, at least 19,000 years BP, with anthropogenic selection processes occurring over the next 10,000 years to form bread wheat, *T. aestivum*, between 8500 and 9000 years ago (Peng et al., 2011). Today, bread wheat is one of the three staple cereal crops with 766 million tonnes harvested globally in 2019 (FAO, 2021b). The global average annual yield losses of wheat due to pathogens is 21.5%, or 164.7 million tonnes (Savary et al., 2019). In Australia alone, pathogen losses total $913 million AUD each year, despite access to modern growing practices, harvest and storage hygiene (Murray and Brennan, 2009a). Compounding an already significant problem, climate change-related elevations in temperature and CO_2 are predicted to increase fungal pathogen pressures on wheat (Torres et al., 2019).

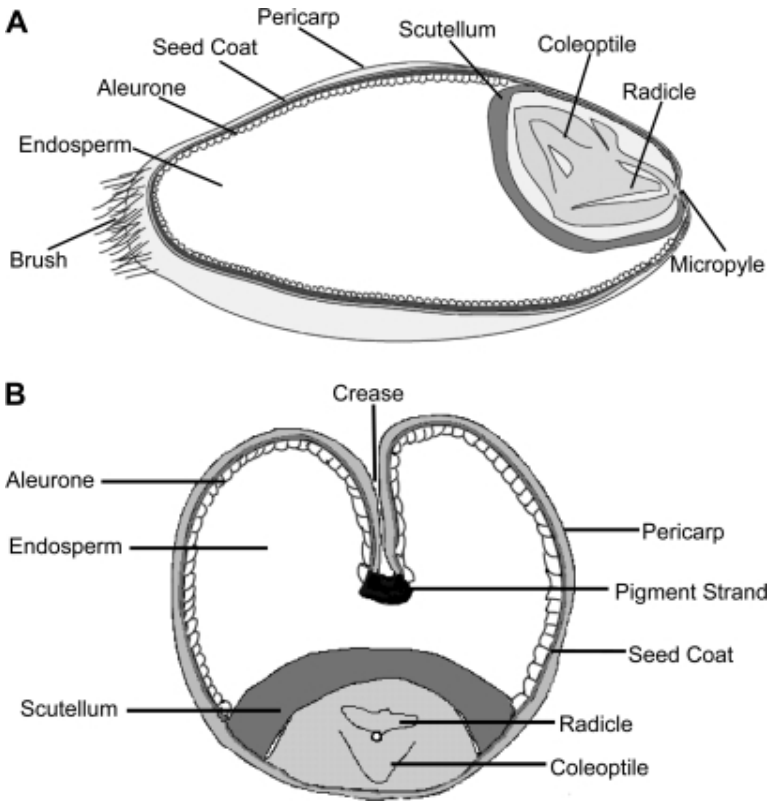


Figure 1-5. Wheat grain diagram. Republished with permission of Oxford University Press, from Water movement into dormant and non-dormant wheat (*Triticum aestivum* L.) grains, Rathjen, J.R., Strounina, E. V., Mares, D.J., 2009. J. Exp. Bot. 60; permission conveyed through Copyright Clearance Center, Inc.

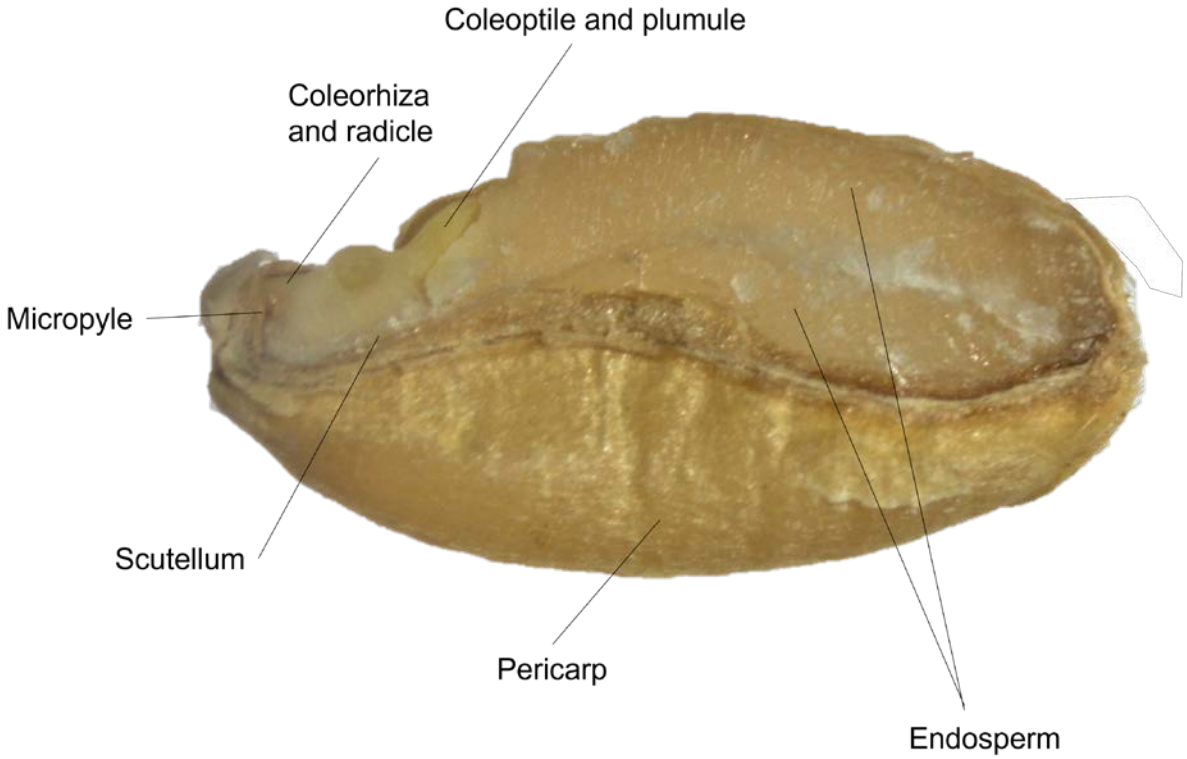


Figure 1-6. Longitudinal section along the crease of a *Triticum aestivum* 'Scepter' [sic], grain with labels of important tissues and structures.

1.3.2.2.2 Wheat grain morphology

To achieve reductions in post-harvest pathogens, understanding grain morphology is first necessary. Wheat grains contain distinct morphological features, including an embryo on one end of the dorsal surface and a tuft of hairs called the brush on the end opposite the embryo. Additionally, a ventral furrow, often called a crease, runs along the centre of the ventral surface (Wrigley, 2017) (Figure 1-5, B). The surface of the grain is covered in a thin, porous pericarp with a waxy outer microstructure (Rathjen, 2006). The outer pericarp cells, or exocarp, are elongated and arranged in a horizontal position. Underlying this layer is the testa, or seed coat, which is much less permeable (Rathjen et al., 2009) (Figure 1-5). Like maize, the grain nutrient storage is composed of the endosperm, and the embryo contains similar tissues, albeit in a different arrangement (Figure 1-6). The micropyle, a large pore which once served as the entry

point for the pollen tube, is easily distinguished on wheat near the radicle (Rathjen et al., 2009).

1.3.2.3 Barley, *Hordeum vulgare*, GC 0640

1.3.2.3.1 Barley grain past and present

The wild relative to barley, *Hordeum spontaneum*, occurred in two distinct populations, one in the Near East and another on the Tibetan Plateau, resulting in the independent domestication occurring twice in separate locations and times, to form the six-rowed modern *Hordeum vulgare* (Dai et al., 2012). The complex molecular processes behind the dual domestication processes are reviewed by Wang et al., 2019. The production of barley worldwide is predominantly for malting (Zhou, 2009). As such, it is more related to beverage production than food production, but is still an economically relevant crop with roughly 159 million tonnes produced worldwide in 2019 (FAO, 2021b). In Australia, it is a $1.29 billion AUD industry with $252 million AUD in annual losses attributed to pathogens (Murray and Brennan, 2009b).

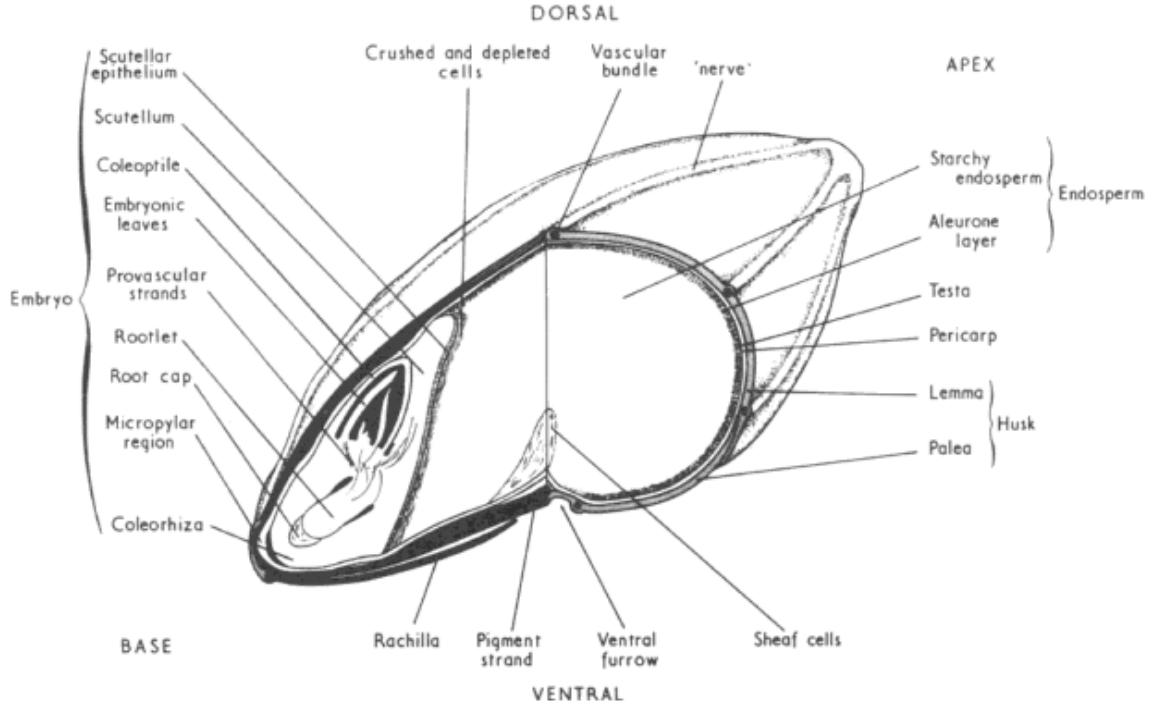


Figure 1-7. Diagram of a barley grain. Republished with permission of Wiley, from Barley, Briggs, D.E., 1978. 1st ed. Chapman and Hall, Ltd; permission conveyed through Copyright Clearance Center, Inc.

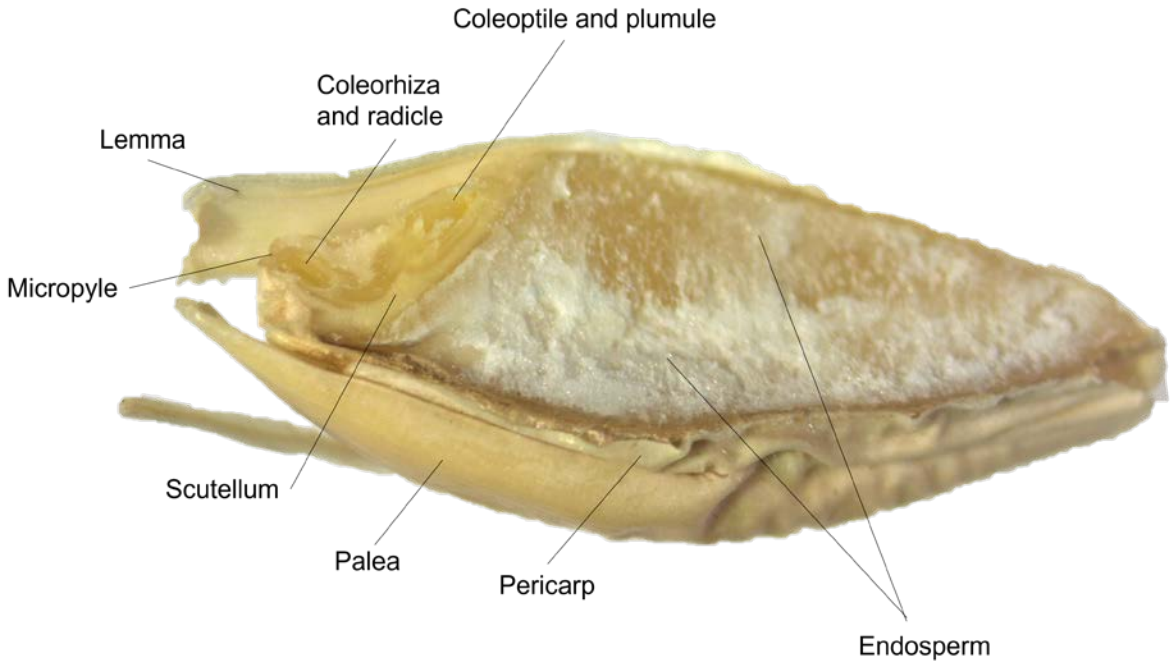


Figure 1-8. Longitudinal section of a *Hordeum vulgare* 'Compass,' grain with labels of important tissues and structures.

1.3.2.3.2 Barley grain morphology

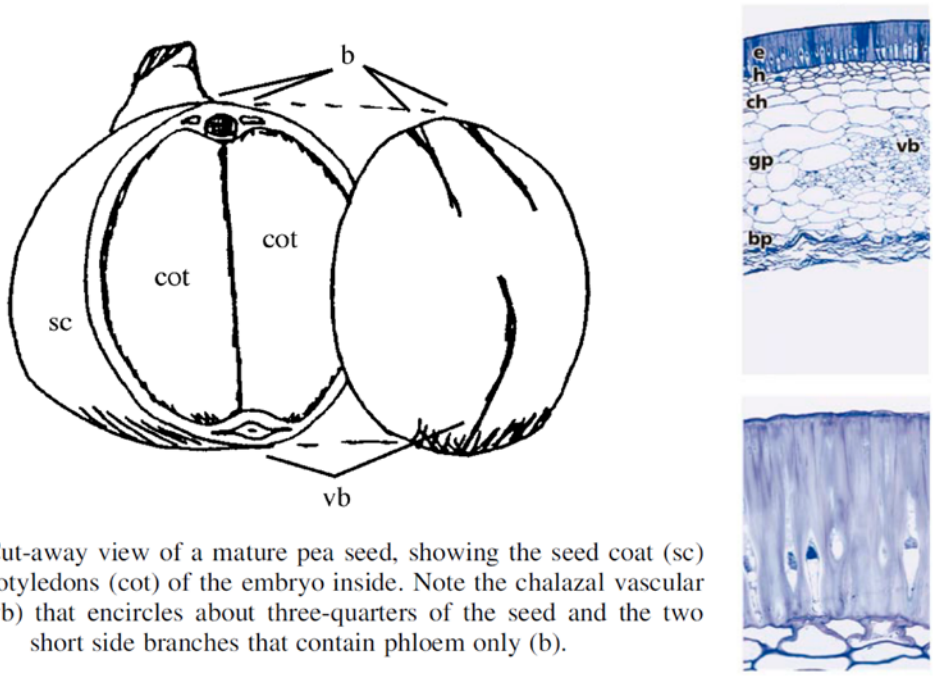
Barley grain structure is reminiscent to wheat but often retains a hull attached to the pericarp surface. While there are commercial hull-less varieties of barley, this review will focus on the general structures of hulled barley. The grain, or caryopsis, is enveloped in two flowering glumes; the dorsal glume (lemma), and ventral glume (palea) (Fincher and Stone, 1993) (Figure 1-7). The glumes are attached to the body of the grain pericarp except at the embryo and brush (Duffus and Cochrane, 1993) (Figure 1-8). The lemma and palea surfaces are often covered in trichomes, the number and structures of which vary with cultivar, but often consist of prickle-like and domed trichomes (Boateng et al., 2007). In addition to trichomes, barley surfaces are lined with ridges of silica-rich phytoliths, thought to be a defensive mechanism against insect predation (Imboden et al., 2018). Underneath the protective envelope of the hull,

the barley grain morphology resembles that of wheat with a similar positioning of tissues.

1.3.2.4 Field pea, *Pisum sativum*; VD 0561

1.3.2.4.1 Field pea past and present

Alongside wheat and barley, field pea is considered to be one of the six 'founder crops' of Near Eastern agriculture (Abbo et al., 2003). The domestication of *Pisum sativum* is thought to have occurred roughly 10,000 years BP in the Fertile Crescent, with various landraces and cultivars travelling across the Middle East, Africa and Europe along trade routes (Mikić et al., 2014). The leguminous grain does not have as high of a global production as the staple cereal crops, however 14.2 million tonnes were produced in 2019 (FAO, 2021b). The annual Australian production of field pea is valued at $78.1 million AUD with pathogen associated losses of 29.6% of the average annual yield, equating to roughly $23 million AUD (Murray and Brennan, 2012).



Cut-away view of a mature pea seed, showing the seed coat (sc) and the cotyledons (cot) of the embryo inside. Note the chalazal vascular bundle (vb) that encircles about three-quarters of the seed and the two short side branches that contain phloem only (b).

Figure 1-9. Diagrams of field pea grain. *Left*, drawing with labelled structures. *Right*, cross-section through the seed coat illustrating the epidermal layer with macrosclereid cells. Republished with permission of Oxford University Press, from Structure of the developing pea seed coat and the post-phloem transport pathway of nutrients, Van Dongen, J.T., Ammerlaan, A.M.H., Wouterlood, M., Van Aelst, A.C., Borstlap, A.C., 2003. Ann. Bot. 91; permission conveyed through Copyright Clearance Center, Inc.

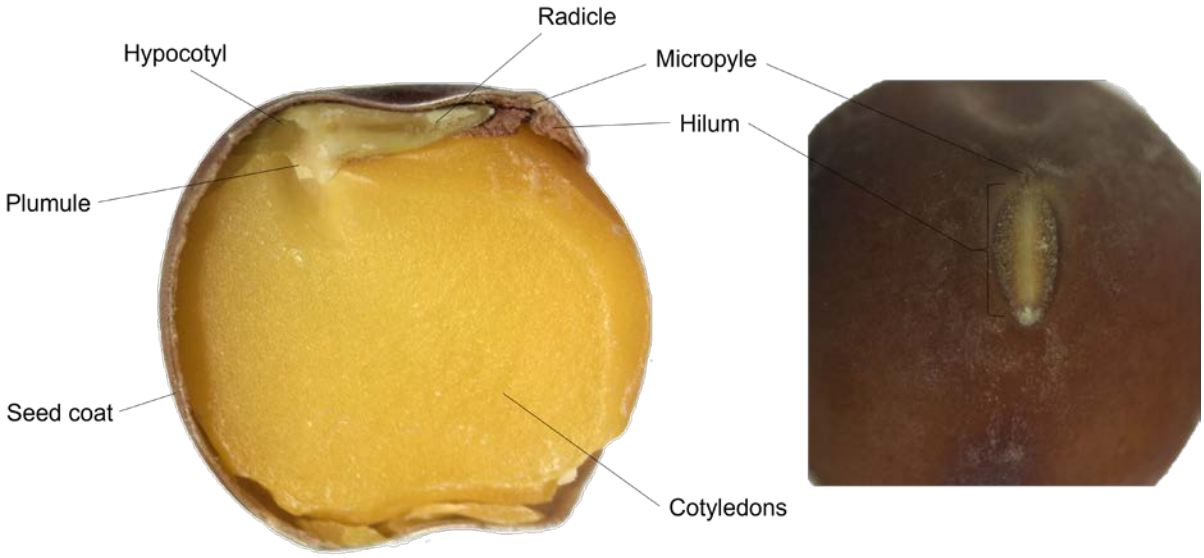


Figure 1-10. Longitudinal section of a *Pisum sativum* 'Butler' grain with labels of important tissues and structures. Note: the plumule fractured during grain sectioning and is difficult to distinguish from the base of the hypocotyl.

1.3.2.4.2 Field pea morphology

The outermost layer of the grain consists of the seed coat/testa. This relatively thick structure provides a protective, semi-permeable barrier between the inner seed tissues and the environment (Niemann et al., 2013) (Figure 1-9). The seed coat consists of a waxy cuticle layer covering elongated macrosclereid cells. Macrosclereids are arranged in a vertical position with the rounded, terminal ends facing the environment. Together with the underlying osteosclereid cells, the seed coats of cultivated *Pisum sativum* grains are between 80 and 90 µm (Zablatzká et al., 2021). Spanning the thickness of the seed coat is the micropyle (Werker, 1997). The adjacent hilum tissue formerly connected the seed to the mother plant (Werker et al., 1979). The embryo consists of a radicle, hypocotyl and plumule (Figure 1-10). In pea, the nutrient storage tissues are the modified cotyledons (Simpson, 2019).

1.3.2.5 Psyllium, *Plantago ovata*; GC 3087

1.3.2.5.1 Psyllium past and present

Plantago ovata is an herbaceous medicinal plant native to the Mediterranean and western Asia. It is one of two plants in the *Plantago* genus cultivated for the mucilaginous properties of the seeds; the other being *Plantago psyllium* (Kour et al., 2016). It is recognised that the term psyllium technically refers to the dried husk milled off the grains of both species. However, as psyllium is the common term for *Plantago ovata* used by agriculturists and the general public across Australia and North America, the grains of *P. ovata* will be referred to as psyllium throughout the body of this work.

The seed husk is coated with a polysaccharide mucilage which has been used as a traditional medicine for gut ailments. It is now a common ingredient in laxatives and ice creams, and is rapidly gaining popularity as an additive to gluten-free foods (Dhar et al., 2005; Marlett et al., 2000; Romão et al., 2021). Psyllium has traditionally been cultivated in India and was brought to Australia in the 1980s due to human rights concerns surrounding harvesting practices (McGhie, 1986).

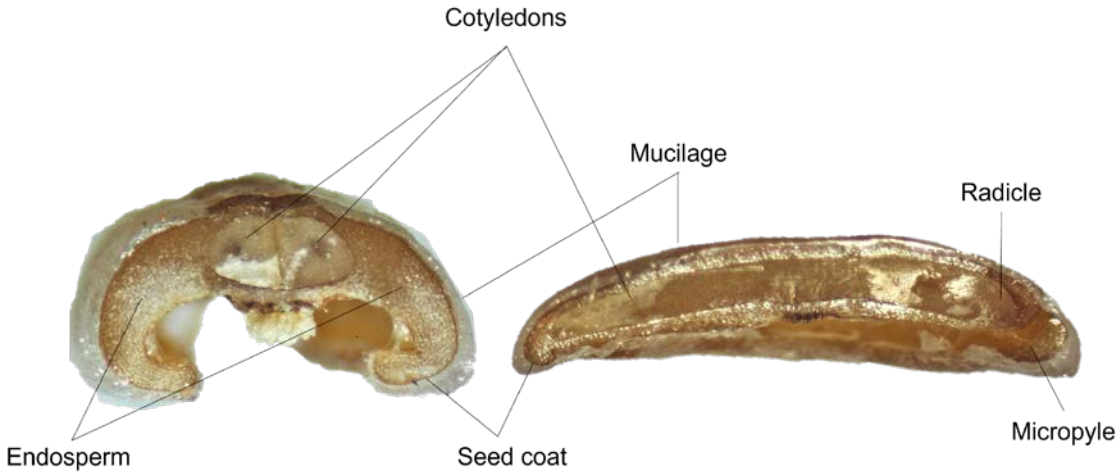


Figure 1-11. Transverse and longitudinal sections of *Plantago ovata* grains with labels of important tissues and structures.

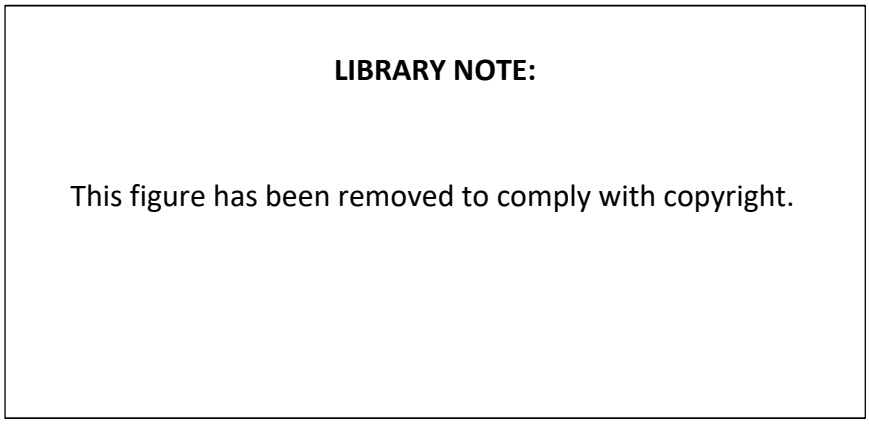


Figure 1-12. Diagram of *Plantago ovata* seed. (A) ventral view of the grain. (B) transverse section of the grain through the hilum. (C) Embryo with r = radicle, c = cotyledon. Republished from Seed morphological studies in the Indian isubgol of commerce, Malick, K.C., Safui, B., 1985. Bull. Bot. Surv. India 27; Nelumbo open access.

1.3.2.5.2 Psyllium morphology

The psyllium grain structure is boat-shaped with a convex dorsal surface and a ventral cavity (Figure 1-11). The outer surface is coated in laminated sheets of desiccated polysaccharide mucilage which rapidly expand upon contact with water (Phan et al., 2020). The seed coat lies underneath the mucilage and is visible in Figure 1-11 as a thin dark brown line between the endosperm and mucilage (Verma et al., 2017). The hilum sits roughly in the centre of the ventral cavity with the micropyle at one end due to the hemi anatropous ovule type (Malick and Safui, 1985) (Figure 1-12). The embryo is positioned longitudinally in the centre of the grain and consists of the radicle, hypocotyl and two cotyledons (Malick and Safui, 1985).

1.3.2.6 Summary

The five grain types described above are economically relevant and represent three families: *Poaceae*, *Fabacaea* and *Plantaginaceae* (WFO, 2021). Each of the grains has a complex morphology. Table 1-3 illustrates the basic differences in structure between grain types.

Table 1-3. Comparisons of features and structures of each of the five grain types (Briggs, 1978; Brooker et al., 1992; Duffus and Cochrane, 1993; Fincher and Stone, 1993; Malick and Safui, 1985; Mejia, 2003; Niemann et al., 2013; Phan et al., 2020; Rathjen et al., 2009; Song et al., 1992; Werker et al., 1979; Wrigley, 2017; Zablatzká et al., 2021).

Grain	Monocot	Dicot	Seed Coat	Endosperm	Radicle	Hypocotyl	Cotyledon(s)	Plumule	Coleoptile
Maize	✓	X	✓ Fused with pericarp	✓	✓	✓	1 Modified as scutellum	✓	✓
Wheat	✓	X	✓ Fused with pericarp	✓	✓	✓	1 Modified as scutellum	✓	✓
Barley	✓	X	✓ Fused with pericarp + husk	✓	✓	✓	1 Modified as scutellum	✓	✓
Field Pea	X	✓	✓	X Absorbed by cotyledons	✓	✓	2 Modified as storage tissue	✓	X
Psyllium	X	✓	✓ + layer of mucilage	✓	✓	✓	2	X	X

1.4 Fungal plant pathogens

Plant fungal pathogens have adversely affected humans' desire to maximise plant nutrition and productivity since the dawn of plant domestication and agriculture. The ancient Greeks were the first to document plant diseases and methods for control with Homer noting the use of sulphur 3000 years BP (Agrios, 2005). The earliest known scientific reports on agricultural fungal pathogens were made by Theophrastus, a student of Aristotle and noted '*father of botany*', in his descriptions of rust diseases 2300 years BP (Doehlemann et al., 2017). In essence, with agriculture comes the perpetual war against fungi (Stukenbrock and McDonald, 2008).

Fungal plant pathogens are not only relegated to the field where they destroy and/or reduce the quality of agricultural crops. Many pathogens and their toxic secondary metabolites, called mycotoxins, persist on harvested commodities and are easily spread during transport, storage, and processing (James and Zikankuba, 2018). An infection which begins on a head of wheat in the field can rapidly spread throughout harvested grain as spores land on other grains. Faced with sub-optimal storage conditions, these spores can germinate, leading to further infections and the possibility of mycotoxin production (Kumar et al., 2017). Once grains reach storage facilities, they

are often considered to represent an anthropogenic ecosystem (Magan et al., 2003). As such, the complex interactions between host grain and the microbiome must be managed via controlled environment conditions (Nopsa et al., 2015).

The main culprits of postharvest grain contamination fall into three mycotoxigenic genera: *Aspergillus*, *Fusarium* and *Penicillium* (Sharma and Bhandari, 2014). During colonisation, these fungi are capable of secreting mycotoxins, posing serious risks to human and animal health (Medina et al., 2017). Due to the toxicity of these compounds and the frequency in which they are found in harvested commodities, governments, and institutions like the FAO and WHO, have set limits on detectable levels in food and animal feed (FAO, 2019). The implications of both mycotoxin consumption, coupled with contaminated food waste, have led to the WHO IARC Report No. 158 (Pitt et al., 2012) and are considered in goals 2, 3 and 12 of the UN 17 Sustainable Development Goals for 2030 (UN, 2015). Discovering novel methods for controlling postharvest fungal pathogens which lead to grain contamination is a priority (Mesterházy et al., 2020).

The following sections will focus on five, often seed-borne, plant pathogens: *Aspergillus flavus, Bipolaris sorokiniana, Didymella pinodes, Fusarium graminearum* and *Penicillium chrysogenum*. These species have been chosen as model organisms due to their pathogenicity and global prevalence. A list of mycotoxins produced by these species is available in Table 1-4. Fungal repository, Mycobank.org (Crous et al., 2004; Robert et al., 2013), reference numbers are included in the section headings for the reader's convenience.

Table 1-4. List of mycotoxins produced by fungal species of interest for the purposes of this thesis.

Fungus	Associated mycotoxins	References
Aspergillus flavus	Aflatoxins B1, B2, G1, G2	Guan et al., 2021; Kumar et al., 2017; McKean et al., 2006
Bipolaris sorokiniana	Rehelminthosporol, dihydroprehelminthosporol, victoxinine, and prehelminthosporolactone	Marder et al., 2006
Fusarium graminearum	Deoxynivalenol, nivalenol, zearalenone	Mahato et al., 2019; Sobrova et al., 2010; Sweeney and Dobson, 1998
Penicillium chrysogenum	Citrinin; penicillin G	Flajs and Peraica, 2009; Reiss, 1977

1.4.1 *Aspergillus flavus*; MB#209842

Aspergillus flavus is a complex of saprophytic soil fungi with global distribution and are commonly found on both pre-harvest and post-harvest grains (Hedayati et al., 2007). *A. flavus* infects a broad range of plant hosts and is the causal agent of Aspergillosis in humans and animals (Fausto et al., 2019; Kidd et al., 2016). When growing under optimal conditions, the yellow-green coloured *A. flavus* culture is capable of producing highly carcinogenic aflatoxins with significant downstream effects on food and animal feed safety (Medina et al., 2017). A summary table of food products affected by aflatoxins can be found in Mahato et al., 2019.

A. flavus is thought to primarily use clonal reproduction, especially when colonising maize crops (Varga et al., 2011). The small globular asexual spores, called conidia, are characterised by their double cell wall impregnated with a layer of melanin (Garcia-Rubio et al., 2020) (Figure 1-13). The size and shape of the conidia, along with their electrostatic charge (Wargenau et al., 2011), allows for air-borne dispersal (Rogawansamy et al., 2015). For a detailed review see Amaike and Keller, 2011.



Figure 1-13. Coloured scanning electron micrograph of *Aspergillus flavus* conidia showing typical globose and echinulate morphology. Magnification = 20,000x; see Chapter 5.5.2 for experimental details.

1.4.2 *Bipolaris sorokiniana*; MB#293701

Bipolaris sorokiniana is a dynamic organism which causes black point, spot blotch and common root rot diseases. It infects a large range of host plants including cereal crops such as rice, wheat, barley and maize (Al-Sadi, 2021) across six continents (Gupta et al., 2018). Diseases are often seed-borne although they can be found on crop residues and in soil (Pandey et al., 2005). In the common root rot and crown rot diseases, *B. sorokiniana* is often associated with other fungi including *Fusarium, Pythium* and *Rhizoctonia* species (Al-Sadi, 2021).

B. sorokiniana colonies vary in colour from grey to black. Reproduction is primarily asexual through the formation of large, brown conidia with three to eight septa (Gupta et al., 2018) (Figure 1-14). Conidia are produced along short conidiophores and are often dispersed via air (Duveiller et al., 2005). The virulence of isolates is highly varied and dependent upon environmental conditions (Sultana et al., 2018).



Figure 1-14. *Bipolaris sorokiniana* conidia illustrated with a coloured scanning electron micrograph. Mature conidia can be up to 120µm. Note the indentation in the bottom left corner indicating the former connection to a conidiophore. Magnification = 10,000x.

1.4.3 *Didymella pinodes*; MB#274545

The nomenclature for this organism is varied (Chen et al., 2015) and is synonymous with *Peyronellaea pinodes* (Aveskamp et al., 2010)*, Mycosphaerella pinodes*, *Sphaeria pinodes* and *Ascochyta pinodes* on the NCBI Taxonomy database (Schoch et al., 2020). Herein, the widely recognised name *Didymella pinodes* will be used; it is considered to be of legitimate status on the Mycobank database as of December 2021 (Robert et al., 2013).

D. pinodes is one of four known causal agents of Ascochyta blight of field pea and is also capable of infecting *Lupinus albus* and *Medicago* spp. among others (Barilli et al., 2016). Within the Ascochyta blight complex, *D. pinodes* is considered to be the most destructive of the four fungal pathogens (Davidson et al., 2012) and causes major economic loss of field pea crops on a global scale (Sistani et al., 2017). Mancini and Romanazzi, 2014 have listed this organism as one of the main seed-transmissible fungal pathogens of *Pisum sativum*.

When grown on culture media, colonies of *D. pinodes* are grey to brown to black with concentric rings of pseudothecia and pycnidia (Davidson, 2012). Conidia generally

have one or two septa (Punithalingham and Gibson, 1976). Dispersal of conidia can occur via water or mechanical abrasion to release the conidia from the pycnidia (Barilli et al., 2016; Tran et al., 2016). A detailed review can be found in Khan et al., 2013 and the PhD thesis of Davidson, 2012.

1.4.4 *Fusarium graminearum*; MB#200256

Fusarium graminearum ranks fourth in the list of the 'Top 10' fungal plant pathogens (Dean et al., 2012). It is one of nine known causal agents of Fusarium Head Blight, infecting the floral tissues of cereal crops, reducing yield, quality and producing the mycotoxins deoxynivalenol (DON) and zearalenone (ZEA), among others (Torres et al., 2019). In addition to Fusarium Head Blight, fusariosis rots of many different agricultural crops are caused by this fungus (Adeniji and Babalola, 2018). *F. graminearum* is considered one of the main postharvest grain pathogens worldwide with infections spreading during points of the supply chain without strict environmental control (Nopsa et al., 2015). Current models are predicting an increase in economic losses from this pathogen both in-field and in-storage due to climate change-related rising temperatures and precipitation (Torres et al., 2019).

F. graminearum is generally used as the name for a complex of soil fungi which produce double-walled chlamydospores (Figure 1-15). It can persist in soil for years under harsh conditions before germinating and infecting plant tissues (Nyvall, 1970; Sitton and Cook, 1981). The thin, curved multi-septate macroconidia are easily recognisable and often used to distinguish *Fusarium* species from other filamentous soil fungi (Moss, 2002). Mycelial cultures are characterised by their pink to orange to white colouring and rapid growth on media containing nutrients (Galli et al., 2005). Detailed reviews can be found in Leplat et al., 2013, Torres et al., 2019, van der Lee et al., 2015, and Yang et al., 2013.



Figure 1-15. *Fusarium graminearum* chlamydospore shown in a coloured scanning electron micrograph. Magnification = 5000x. Note the bulbous structure of the chlamydospore compared to the hyphae.

1.4.5 *Penicillium chrysogenum*; MB#165757

Penicillium chrysogenum is a common environmental pathogen best known for its role in the production of penicillin (Gaynes, 2017). The *P. chrysogenum* complex contains five known species with worldwide distribution (Houbraken et al., 2014) and is a major allergen commonly found in homes and in agricultural dust (Rogawansamy et al., 2015; Singh and Chauhan, 2013). It can also be problematic in agricultural and food processing settings where it has been found to produce the mycotoxin citrinin in wheat products and bread (Reiss, 1977).

Colonies of *P. chrysogenum* are generally blue to grey to white and can grow across a wide range of temperatures (Cho et al., 2007). The small globose conidia have a double wall and the outside is dotted in echinulate rodlets (McCoy et al., 1971) (Figure 1-16). Dispersal is primarily airborne which contributes to the ability of this fungal complex to act as a food and grain contaminant (Burgain and Dantigny, 2016).

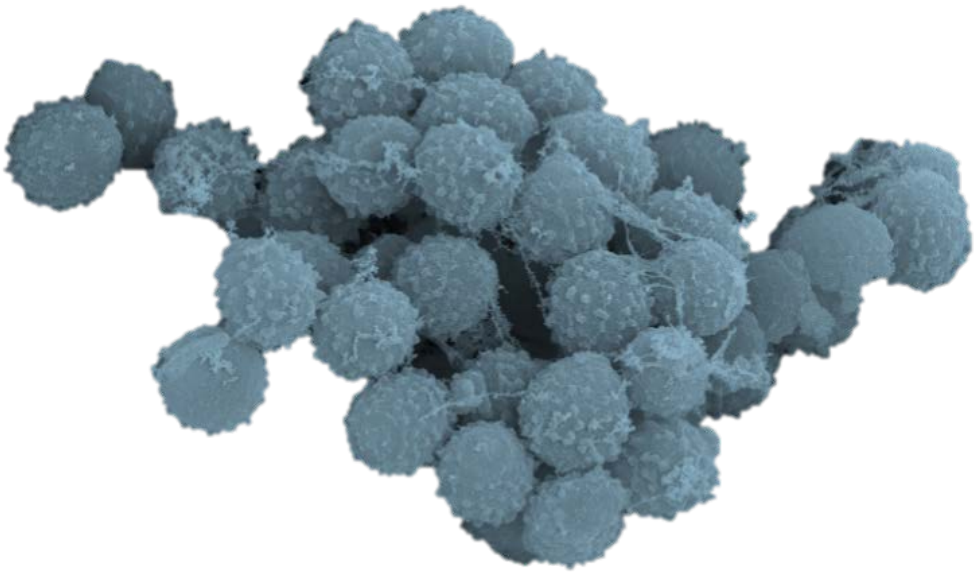


Figure 1-16. *Penicillium chrysogenum* clustered conidia seen in a coloured scanning electron micrograph. Magnification = 10,000x.

1.5 Conclusions

As sessile lifeforms, plants have an incredible toolbox for coping with a vast range of biotic and abiotic stresses. Nonetheless, the synthetic stresses created during plasma treatment are not encountered by plants, or their fungal pathogens, in nature. Seeds may have evolved biological pathways to deal with specific plasma-induced reactions such as oxidation, yet the intense plasma bombardment of a seed encasing a delicate embryo may trigger different signalling cascades depending upon treatment, species, and environmental factors. A holistic approach is needed to begin to unravel the intricacies of plasma-induced chemical and physical changes to different species of plant seeds. To conceptualise the plasma enigma, in-depth investigations into the way in which plasma alters agricultural grain surface structures, the grain response, and the reaction of microbes residing on the grain are necessary. For example, a plasma apparatus can be designed to rotate seeds, ensuring equal exposure to plasma. Once all grain faces are subjected to the same treatment, the surfaces should be visually

assessed to determine how plasma weathering impacts seed morphology. These observations may drive hypotheses and predictions about plasma interactions with microbes on the grain surfaces, as well as the grain response to exposure.

The current knowledge regarding plasma inactivation of microbes on grains is insufficient. A comprehensive study is needed to explore how both extant and inoculated microbial populations respond to plasma treatment across multiple model grain and pathogen systems. Ideally, this will include the plasma treatment of mycelial networks, conidia, and other asexual reproductive structures, such as chlamydospores, that are frequently present on infected grains. Understanding how plasma interacts with different pathogen structures is essential for understanding how this technology may be of use in an industrial application.

This multi-disciplinary work requires a broad understanding of not only the plasma-microbial interactions, but the seed surface structures and downstream grain viability. The plasma-induced changes to this micro ecosystem are likely connected. Therefore, research should be done to understand the mechanisms of varying plasma exposure durations on grain hydration as well as growth and development of the embryo. A comprehensive and systematic study is the best approach to understanding plasma treatment of grains and for determining possible points for development to scale in the near future.

1.6 Research aims and questions

The review of literature highlights the knowledge gaps and insufficiencies within the field of plasma agriculture. This research thesis seeks to provide a broad-spectrum survey of the microbiological, physico-chemical and seed growth and development aspects of plasma agriculture using five different grain types of economic relevance. Research aims are defined below.

1.6.1 Assess the impact of plasma exposure on grain surfaces

The current knowledge surrounding the impact of plasma on grain surface structures is inconsistent and varies with instrumentation, operating procedures, and grain type. This will be achieved by:

- Using microscopy techniques to survey the surface features of grains after treatment in a novel plasma system which allows for even exposure across all surfaces;
- Observing both macroscopic and microscopic alterations to determine areas of interest for subsequent study throughout this body of work;
- Building a better understanding of where plasma treatments can impact grains and which tissues from different species may be affected.

1.6.2 Evaluate the efficacy of plasma exposure for the inactivation of fungal pathogens on the grain surface

The use of a novel plasma tumbling system for reducing microbial populations on grain surfaces is currently unknown. The objectives for this aim are as follows:

- Establish methods for reducing extant grain microbes using the tumbler apparatus;
- Pinpoint the location of extant microbes to determine if physical features on the grain promote microbial aggregation;
- Challenge the plasma tumbler system with synthetically high fungal inoculum loads to understand how the duration of exposure effects the viability of fungi;
- Use various inoculation methods to test the efficacy of the plasma tumbler for the inactivation of multiple fungal structures;
- Develop knowledge about how plasma exposure differently impacts selected grain/pathogen systems.

1.6.3 Determine the impact of plasma exposure on the physico-chemical properties of seeds.

It is well established that plasma exposure changes the grain-water dynamic. Yet, a broad survey on the mechanisms behind the interactions has not been performed and a detailed study will improve this knowledge. This aim seeks to:

- Explore the changes to surface chemistry, and thus surface energy, which may impact grain water uptake;
- Understand the modifications to the direction of water entry into the grain;
- Understand how plasma exposure impacts the water sorption capacity of mucilaginous structures;
- Determine if changes to water ingress allow for solute egress.

1.6.4 Compare the effects of plasma exposure on seed viability, growth, and development

The modifications made to grains under long duration of plasma treatment may impact the viability, growth, and development of the underlying seed embryo, and previous studies have not thoroughly investigated these aspects. This aim hopes to:

- Address the impact of increasing plasma exposure times on seed germination;
- Understand how changes may alter the short-term and long-term growth and development of seedlings.

1.6.5 Apply knowledge gained throughout this thesis towards a real-world problem: deactivating fungal pathogens on an industrial contaminated grain sample

The foundational aspects of plasma research have been established but it is not yet known if the plasma system has the capacity to reduce the complex real-world issues associated with fungal pathogen contaminated grain. The specific objectives are to:

- Determine the baseline fungal load of an industry-rejected grain lot;

- Understand the culturable species that coexist on the grain surface;
- Determine the capacity for the plasma tumbler system to reduce the number of viable pathogens to negligible levels.

1.7 Significance of research

The project has a wide range of potential outcomes and applications for agriculture, biosecurity, and food safety. Overall, this thesis aims to achieve a better understanding of the use of plasma technologies for the inactivation of post-harvest pathogens and fit within the larger contexts of innovation for future food security and biosecurity. It will demonstrate the capabilities of a straightforward procedure to inactivate post-harvest grain pathogens, with implications for human and animal health. It will also apply different technologies to gain an understanding of how plasma-treatment may alter the physical properties, and to provide insight into grain hydration. It is hoped that the conclusions of this research can be used by Australian institutions including the Commonwealth Scientific Innovation and Research Organisation (CSIRO), South Australian Research and Development Institute (SARDI) and the University of Adelaide (UA), to address the relevant SDGs, namely Goal 2: Zero Hunger by 2030 (UN, 2015).

1.8 Structure of the thesis

This research sits in the crux between microbiology, the physico-chemical properties of plasma and seed physiology. Therefore, chapters are separated loosely by discipline, acknowledging that all fields play a role within these somewhat arbitrary groupings. Within each chapter, sections are comprised of a single or series of related experiments which build upon each other. Often, the conclusions from one section determined the direction of the experiments within the following section. Below is a list of each chapter for the reader's reference.

Chapter 1: Introduces the topic, literature, and the aims of the thesis.

Chapter 2: Describes the background work conducted by the author which led to the development of this research project.

Chapter 3: Describes the basic methods used throughout all experimentation.

Chapter 4: Describes a visual survey of the impacts of plasma on various grain types which led to the design of all experiments in subsequent chapters.

Chapter 5: Discusses the impact of plasma treatment on seed surface fungal pathogens.

Chapter 6: Provides insight into the physico-chemical changes to the grain acquired during plasma treatment.

Chapter 7: Describes how the physico-chemical changes may impact downstream seed germination, growth, and development.

Chapter 8: Combines the insight gained from previous chapters to challenge the plasma system with a contaminated real-world sample.

Chapter 9: Provides general conclusions and suggests future directions for research.

2 A brief background on the events which lead to the conception of this research

2.1 Introduction

Throughout the COVID-19 pandemic, researchers across the globe were forced to re-evaluate and prioritise their projects. This included the assessment of project viability under new health and safety regulations, frequent snap lockdowns, limited access to equipment and broad sweeping changes in funding. This was a major learning point for many early career researchers as they were forced to make critical decisions and exercise innovation during a time of great uncertainty. The contents of this thesis are no exception. Two years of research was set aside to explore a new scientific path forward through the pandemic. What began as a problem-solving side project, blossomed into a fascinating and ever-expanding study. A short mention of the previous study is necessary as it set the scene for the current work.

2.2 Previous work as the basis of this research project

2.2.1 Background

The foundations for this project were laid down while working on a previous project involving root exudates. It was necessary to grow sterile plants to ensure all root exudates were produced by the plant itself and not microbes residing on or in the roots. This is much easier said than done as the traditional methods of seed sterilisation are often fraught with complications. Bleach and ethanol alter the seed moisture content, which may cause downstream problems when working with mucilaginous seeds such

as *Plantago*, *Arabidopsis* and *Solanum* species. Ultraviolet light treatment fails to reach nooks and crannies in the grains. Chlorine gas fumigation stresses the seedling, often triggering the production of anthocyanins in 1-day-old maize. These drawbacks led to a pilot trial using non-thermal plasma treatment.

2.2.2 Plasma-treatment pilot trial

Maize grain was split into five aliquots of 10 grains each. One aliquot was placed in a custom-built, capacitively coupled, radio-frequency plasma system with a similar design to the system described by Griesser, 1989. Grain samples in a 45 mm Petri dish were placed on the grounded electrode, treated with ambient air plasma for five minutes, turned over and treated for another five minutes. This treatment was repeated on a separate aliquot of seeds using a water plasma. Conventional treatments of a 20-minute soak in 50% bleach, and four hours of chlorine gas fumigation were performed on two aliquots, respectively. The final aliquot of seeds was left as an untreated control.

Five seeds of each treatment were placed in Petri dishes with growth media (0.8% agar, 1% sucrose in full strength Hoagland's Solution) and incubated for seven days. The number of infected grains were counted to determine the efficacy of each treatment, summarised in Table 2-1.

Table 2-1. Percentage of maize grain displaying visible fungal contamination post-treatment with the stand plasma generator, chlorine gas fumigation, bleach, and Untreated control.

Treatment	**% Grain infected**
Untreated	100
Bleach	60
Cl_2 gas	10
Air plasma	30
Water plasma	100

As shown in the above table, chlorine gas fumigation and air plasma treatments were the most effective in reducing the number of infected grains. It was hypothesized that plasma treatment efficacy could be improved using a new plasma reactor design which allowed for even plasma treatments on all faces of grains within the plasma glow. For this project, Emeritus Professor Hans Griesser (University of South Australia) graciously loaned his rotating plasma reactor developed by Michl et al., 2015, called the plasma tumbler (PT) reactor. All future experiments were carried out using this reactor with modifications listed in Chapter 3.

2.2.3 Plasma Tumbler (PT) pilot trials

An initial pilot trial was conducted to evaluate the efficacy of the PT reactor. The previous pilot involved treating each side of the grain for 10 minutes with plasma for a total exposure time of 20 minutes. It was assumed a much longer time point of plasma treatment would be necessary in the PT due to the continuous movement of grains through the field of plasma. Time points of 60 and 90 minutes were chosen to ensure all faces of the grain would be sufficiently exposed to the plasma field and sheath.

Ten grams of maize grain were poured into a sterile, bevelled powder flask and attached to the PT. The spin speed was set to roughly 20 revolutions per minute (rpm) and a vacuum was pulled to 56 mTorr for ten minutes to degas the grain. Ambient air was introduced into the system and once the pressure inside the flask had stabilised, plasma was struck and run for 60 minutes. This process was repeated for a 90-minute exposure time. Grains were plated and incubated following the protocols described above and the number of visible fungal colonies were recorded after seven days to determine treatment efficacy (see Table 2-2).

Table 2-2. Percentage of maize grains displaying visible signs of fungal contamination post-treatment in the plasma tumbler for 60- and 90-minute treatments and the Untreated control.

Treatment	**% Grain infected**
Untreated	60
60 min plasma	5
90 min plasma	2.5

The 90-minute exposure time was relatively successful with no visible fungal growth on 97.5% of grains. This led to subsequent optimisation experiments varying pressure, power, spin speed, the volume of grain in the flask, and the species of grain. The data from these trials was collated and adapted to create a set of fundamental protocols for PT treatment of various grains, summarised in Table 2-3, which provided the groundwork from which all subsequent research in this thesis was built.

Table 2-3. Established operating parameters for the plasma tumbler system used throughout this work.

Power	50 W
Running pressure	250 mTorr
Spin speed	15 rpm (1.2 on dial)
Maximum sample volume	100 g depending upon grain size

2.3 Summary

This series of preliminary trials conducted during a different project, unfinished due to unforeseeable circumstances, created the standard operating procedures for use of the plasma tumbler apparatus. It was deemed worthwhile to briefly describe these experiments as they provide an explanation for the selection of time points and operating criteria which would otherwise be lost to the reader. Details of modifications to the PT system and operating protocols are listed in the following chapter.

3 General methodology

This chapter briefly describes methods used throughout the body of this thesis.

3.1 Plasma treatment

Plasma treatment involved the use of a 13.56 MHz radio-frequency ambient air plasma. The following general assumptions of air quality were made based on the location and timing of this research:

- Air pollution is relatively low in Adelaide, South Australia (Keywood et al., 2016);
- Work-from-home orders during the COVID-19 pandemic reduced the number of people working in the lab to a minimum and were in effect for the duration of this research;
- Bushfire smoke was not present during the experimental treatment phase of this project.

3.1.1 Plasma tumbler apparatus and modifications

3.1.1.1 Reasoning

If plasma treatment of grains is to be successful, chemical etching must be able to access all surfaces of the grains, no matter how the grains are initially loaded into the reactor. Plasmas in static reactors tend to be directional and therefore may only impact the side of the grain facing the plasma. Some studies have experimented with the use of a plasma reactor on an orbital shaker to roll seeds and ensure more than one surface of the grain is exposed to plasma (Pet'ková et al., 2021; Švubová et al., 2020;

Tomeková et al., 2020). While this innovative approach was successful in terms of the authors' desired outcomes, the shape and size of some grain types is problematic for orbital shaking. Instead, it was proposed that using a plasma system with a revolving seed treatment chamber would contribute to the development of an efficient seed treatment system compatible with a large range of seed sizes and morphologies.

3.1.1.2 Plasma tumbler apparatus

Michl et al., 2015 designed a radio frequency plasma apparatus based on a repurposed BUCHI Rotavapor® rotary evaporator. The straightforward design, which is relatively simple to replicate, was ideal for the purposes of this research. The research group was contacted, and the plasma apparatus was kindly loaned by Emeritus Professor Hans Griesser (University of South Australia), for the duration of the project. From this point forward, it will be described as the plasma tumbler (PT) system.

3.1.1.3 Modifications to the Michl et al., 2015 design

Small modifications were made to the PT system to ensure treated grains could remain sterile (Figure 3-1):

- A 10 cm piece of polytetrafluoroethylene (PTFE) plumber's tape, sprayed with 70% EtOH, was used to seal the connection between the flask and the rotary shaft. The seal was replaced each time the flask was removed from the system.
- An autoclaved Pyrex® fibre borosilicate glass wool plug was placed in the rotary shaft to trap as many microbial spores as possible from being pulled through the vacuum line.
- A 0.2 µm membrane filter (Sartorius) was cut to size and secured over both the inlet air valve and exhaust valve openings with Micropore™ surgical tape (3M) to allow air penetration but limit microbial movement into the system.

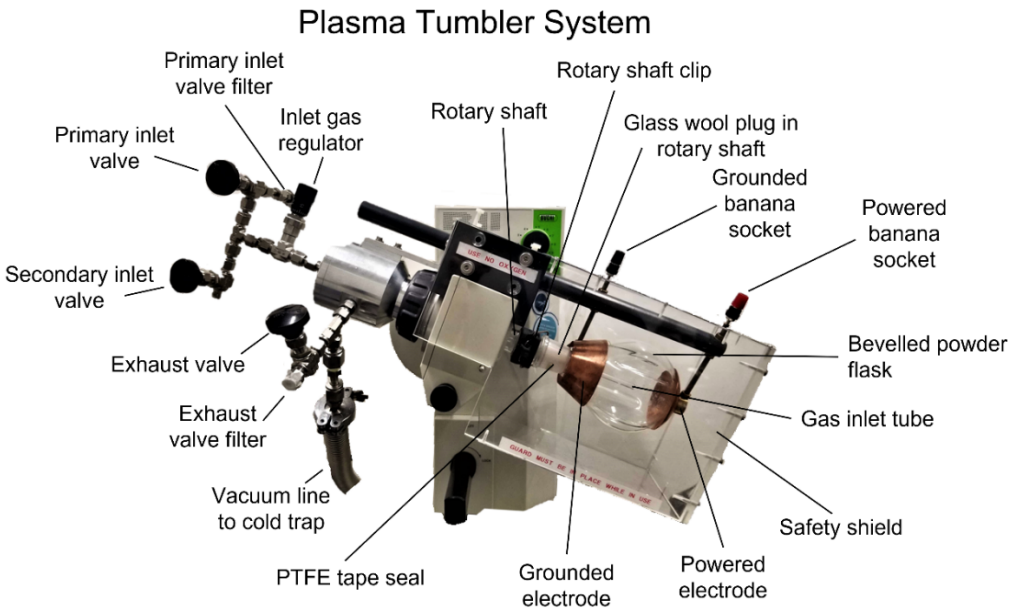


Figure 3-1. Diagram of the plasma tumbler apparatus designed by Michl et al. 2015 with labels of key features and modifications.

3.1.1.4 RF generator and matching system

A Coaxial Power Systems radio frequency generator RFG 050-50W at 13.56 MHz with a Coaxial Power Systems MMN 150 high efficiency manual matching network were used to generate plasma throughout this research.

3.1.2 Plasma tumbler operation

The PT system was connected to a vacuum with a 250 mL liquid nitrogen cold trap. The vacuum pump was primed while grain (up to 100 g depending on grain type) was loaded into an autoclaved bevelled 500 mL powder flask (BUCHI). The flask was connected to the PT system via PTFE tape sprayed with 70% EtOH. The rotary evaporator was set to 15 revolutions per minute (rpm), which corresponded to 1.2 on the spin dial. The flask was pressurised and once the pressure reached 250 mTorr, the plasma was ignited and adjusted to 50W, the maximum power setting on this instrument (Figure 3-2). The 50W of power and 250 mTorr pressure was maintained throughout the plasma run.

Upon completion of the run, the plasma was extinguished, and the flask restored to atmospheric pressure. The flask and rotary shaft were sprayed with 70% EtOH to reduce the chance of sample contamination with environmental microbes. Upon flask disconnection, an autoclaved and sterile piece of aluminium foil was quickly placed over the mouth of the flask. The flask was moved into a laminar flow where the treatment grain was poured into a sterile 50 mL tube.

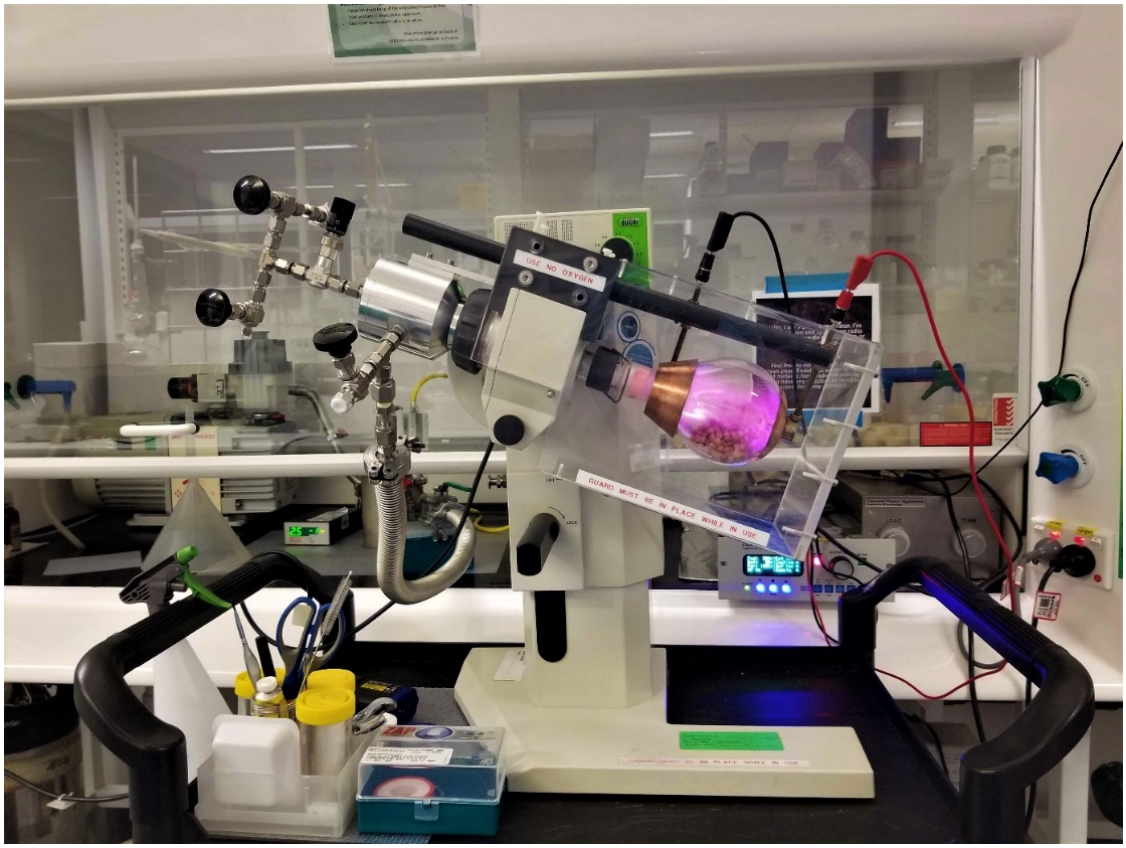


Figure 3-2.Plasma tumbler in operation. Field pea grains are seen in the rotating flask.

3.1.2.1 Treatment of single time points

A set duration of plasma exposure, usually 90 minutes (P90), was determined for the run. Once the plasma was struck, a timer was set for the appropriate amount of time. A run was completed when the plasma was extinguished at the end of the time duration. The flask was sprayed with 70% EtOH, disconnected from the PT system, capped with sterile foil and transferred to a laminar flow. Under sterile conditions in the

laminar flow, grain was poured into sterile 50 mL tubes and kept at laboratory temperature until use.

3.1.2.2 Plasma tumbler treatment of time trial series

The selection of time points was dependent upon the experiment. All treatment aliquots were combined in the flask. The plasma was ignited and run for the duration of the first time point at which the plasma was extinguished, and the flask restored to atmospheric pressure. The system was sprayed with 70% EtOH, flask disconnected and transferred to laminar flow with a sterile foil cap. Under laminar flow, an aliquot of grain was poured into a sterile 50 mL and labelled as the first treatment. The sterile foil cap was replaced, and the flask was returned to the PT system. A fresh 10 cm piece of PTFE tape was wrapped around the rotary shaft and sprayed with 70% EtOH. The flask was again sprayed with 70% EtOH prior to reconnection. The rotation and 250 mTorr pressure were restored and a plasma was struck again. This process was repeated until the treatment time series was complete. By removing small aliquots at each time point, it was ensured that all the grain up until that time point had been exposed to the same conditions, as a measure of limiting variability.

3.1.2.3 Tumbler and vacuum control treatment (T+V)

A set of control grains was prepared to compare the effects of the vacuum and mechanical tumbling to Untreated controls and plasma treatments. Treatment within the system was 90 minutes and corresponded to the longest time point for most experiments. The system was prepared following protocols in Chapter 3.1.1.3.1 for a single plasma treatment time, with a spin speed of 1.2 and 250 mTorr pressure, omitting plasma ignition.

3.1.2.4 Untreated control

An aliquot of grain from the same sample that was taken for T+V and all plasma time points was poured into a 50 mL sterile tube and labelled as the Untreated control.

3.2 Grain procurement

Five different grain types were selected based on their global agricultural and economic relevance, as well as classification and seed surface chemical properties.

3.2.1 Maize

The original seed stock of *Zea mays* ‘B73’ was kindly donated by Dr Brent Kaiser. This stock was grown to seed outdoors in 30-litre pots of Premium Potting Mix (Bio Gro, Mt. Gambier, South Australia) with a top layer of sugarcane mulch at the University of Adelaide, Waite Campus over spring and summer in 2019-2020. Grain was hand-harvested and oven-dried for three weeks at 45 °C. Viability was determined via germination tests on 100 grains each season. Grain was stored in the dark at 15 °C until use.

3.2.2 Wheat

Triticum aestivum ‘Scepter’ [sic] of food grade quality was donated by the Cereal Pathology Group (SARDI) from yield trials conducted in the South Australian Murray-Mallee region in 2019. Grain was stored at 5 °C post-harvest until use.

3.2.3 Barley

Hordeum vulgare ‘Compass’ of food grade quality was donated by the Cereal Pathology Group (SARDI) from yield trials conducted in the South Australian Murray-Mallee region in 2019. Grain was stored at 5 °C post-harvest until use.

3.2.4 Field pea

Pisum sativum ‘Butler’ of food grade quality was donated by the Soil Biology Group (SARDI). Grain was stored at 5 °C post-harvest until use.

3.2.5 Psyllium

Organic *Plantago ovata* grain of food grade quality was purchased from Accolent Dried Herbs, Queensland, Australia. Grain was stored at 15 °C until use.

3.2.6 Industry feed sample

A local South Australian grain network, Viterra, was contacted and asked to supply samples which tested positive for mycotoxins. Two months after harvest, Viterra returned a mixed feed sample of wheat, barley, and field pea with a positive test for the *Fusarium* produced mycotoxin, deoxynivalenol, rendering it unfit for human and animal consumption. A 20 kg sample was kindly donated prior to destruction of the lot and stored at 15 °C until use.

3.3 Fungal culture

3.3.1 Media preparation

3.3.1.1 Full-strength Potato Dextrose Agar (PDA)

Full-strength PDA, 39 g/L, (Oxoid) was prepared. Once the temperature cooled to 70 °C, 12 mL of media was poured into 90 x 14 mm gamma sterile Petri dishes (Technoplas). Plates were stored in a sterile container at lab temperature for up to two weeks prior to use.

3.3.1.2 Half-strength Potato Dextrose Agar (½ PDA)

Half-strength potato dextrose agar, 19.5 g/L, (½ PDA) (Oxoid) was prepared with an additional 7.5 g/L microbiology grade agar (Difco). Once the temperature cooled to 70 °C, 12 mL of media was poured into 90 x 14 mm gamma sterile Petri dishes (Technoplas). Plates were stored in a sterile container at lab temperature for up to two weeks prior to use.

3.3.1.3 Water Agar

A 1% water agar (Difco) was prepared and poured into 90 x 14 mm gamma sterile Petri dishes (Technoplas). Plates were stored in a sterile container at lab temperature for up to two weeks prior to use.

3.3.2 Fungal extraction buffer preparation

A non-toxic buffer was created to extract viable fungal spores and hyphal fragments from the grain surface for subsequent culture. 50 mL Tris-EDTA (TE) buffer, pH 8.0, RNAse-free (Invitrogen) was decanted into a sterile 50 mL tube (Technoplas). 2.5 µL Tween 20 (Fisher BioReagents) was added to the tube and vortexed for five seconds to create a 0.005% solution.

3.3.3 Microbe extractions

Inside a laminar flow hood, grain treatments of each species were divided into five 1 g replicates and poured into sterile 10 mL tubes. Each of the five tubes served as a biological replicate. 2 mL of extraction buffer (see preceding section) was added to each tube. Tubes were inverted twice and transferred to an orbital shaker (Ratek) for 20 minutes. Tubes were removed from the shaker and immediately used for haemocytometer quantification (see following section) and dilutions.

3.3.4 Haemocytometer quantification

10 µL of extraction liquid from section 3.3.3 was placed on a haemocytometer and quantified by counting the number of conidia present within the grids using a phase contrast compound microscope (Nikon, Eclipse Ci-L). The mean counts of four sections within the grids were used to establish initial colony-forming unit (CFU/mL) concentrations for each replicate (Figure 3-3). This allowed for the creation of a series of dilutions meant to capture between 30 and 300 CFU per plate. It was also used to assess the visual appearance of spores and hyphal fragments in each treatment.



Figure 3-3. *Bipolaris sorokiniana* extracts on a haemocytometer. Both conidia and hyphal fragments are visible on the grid.

3.3.5 Dilutions

Depending upon the experimental procedures, dilution factors were calculated based on haemocytometer estimates with an effort to keep colony-forming units per plate between 30 and 300 (Parker et al., 2016; Wilson et al., 2017). A pre-determined volume of extracted liquid was pipetted into a sterile 10 mL tube with an appropriate amount of autoclaved Milli-Q water. Serial dilutions may occur depending upon experimental design as outlined in the following chapters.

3.3.6 Plating technique

Tubes were inverted twice and 100 µL of liquid was removed with a sterile filter-tip pipette and placed in the centre of a pre-poured ½ PDA plate. The extraction liquid was spread across the plate with a sterile L-shaped glass cell spreader. This process was repeated three times, using aseptic technique, to produce triplicate technical replicates from each biological replicate tube. Plates were sealed with clingfilm (Glad, cut to 2.5 cm width with a bandsaw) and placed lid-side down on clean trays for incubation at 25 °C, 14h/10h light cycle for 96 hours, unless otherwise specified.

3.3.7 Colony-forming unit counts

Multiple dilutions were performed for each biological replicate in an attempt to create plates with between 30 and 300 colonies, ensuring statistical significance (Wilson et al., 2017). The dilution series which yielded colonies within this window were selected for counts. Plates were placed lid-side down on a lightbox with a magnification lamp. Using a counter pen (Thomas), all visible fungal colonies were counted and colony forming units were calculated using the following equation:

Eq. 3-1

$$\frac{CFU}{mL} = \frac{number\ of\ colonies\ counted\ on\ a\ plate * dilution\ factor}{volume\ of\ culture\ plated}$$

As the volume extract plated was always 100 µL, it can be written as:

$$\frac{CFU}{mL} = \frac{number\ of\ colonies\ counted\ on\ a\ plate * dilution\ factor}{0.1\ mL}$$

3.4 Statistical and data analysis

Most data throughout the body of this work were recorded and sorted in Microsoft Excel 365 (Microsoft Corporation, Seattle, WA, USA). Statistical analysis and graphs were created with GraphPad Prism 9.0.0 (GraphPad Software Inc, San Diego, CA, USA) unless otherwise specified, using a modified version of the pre-set Plasma colour theme. Data were expressed as mean ± standard error of the mean. Significance was accepted at $p<0.05$.

4 Assessing the impact of plasma treatment on grain surfaces via microscopy

4.1 Introduction

Imaging techniques can be powerful tools for surveying changes to surfaces. In scanning electron microscopy (SEM), electron beams interact with a surface to produce a signal, of which the position and intensity can be interpreted as images (Ul-Hamid, 2018). These images can provide qualitative information about the structure and topography of a surface. Advances in instrumentation for confocal profilometry, which uses the principles of laser confocal microscopy to scan a surface, are now capable of rendering three-dimensional images to determine profiles, quantify roughness and changes in surface area. When used in tandem, these analytical techniques offer detailed surface screenings from which to compare treatments (Scherrer et al., 2020).

Previous studies used scanning electron microscopy to explore the physical changes occurring on a grain surface prior to plasma treatment (Bafoil et al., 2018; Bormashenko et al., 2012, 2015; Dauwe et al., 2021; Kamseu-Mogo et al., 2021; Los et al., 2019; Šerá et al., 2010; Shapira et al., 2018; Štěpánová et al., 2018; Stolárik et al., 2015; Švubová et al., 2020; Zhou et al., 2019). These papers often describe the etching effects of plasma treatment which appeared to weather the grain surface. Occasionally, grain surface structures have been misidentified, which is understandable considering the complexities of morphologies and tissues, even

between cultivars of a species. This highlighted the need for a comprehensive survey to compare differences between plasma exposures and grain types to gain a better understanding of both micro and macro modifications induced during plasma treatment.

The overarching goal of this research is to understand how a non-thermal ambient air plasma alters the properties of the seed surface as well as the microbes that reside upon it. The first step taken toward the achievement of this goal was to assess the surface topography of control and treated grains. It was thought that the patterns of etching and modifications to the seed structure may yield clues to understanding why germinating grains may react in a certain manner. Samples of each treatment were screened using SEM and confocal profilometry to gain a visual understanding of how plasma impacts different biological surfaces. The observations from this chapter were then used to form hypotheses and design the experiments described throughout this thesis.

Five species of agriculturally important grain crops were selected for treatment based on phylogenetic classifications and variations in surface structures. Maize, wheat, and a hulled barley represented the cereal grains. Field pea was used as a model legume with a true seed coat. Finally, psyllium was chosen as a dicot with a polysaccharide mucilage surface structure. Three treatments were devised for each of the grain types. A 90-minute plasma treatment (P90) was chosen based on preliminary experiments as described in Chapter 2. As the PT system requires a partial vacuum for operation (33.33 Pa or 250 mTorr), it was unknown if the vacuum and tumbling of the grain would mechanically impact the grain surface, or if surface modifications are predominantly plasma related. Therefore, a tumbler and vacuum (T+V) treatment was established by subjecting grains to the same vacuum and spin speed, 15 rpm, as the plasma-treated samples. Finally, a subset of grain was set aside as an Untreated control. Treatments

were performed on each of the five grain types and screened via SEM. The surface topography of maize treatments was analysed with a confocal profilometer. The measurements taken from the profilometer were transformed to determine if surface area was altered due to mechanical damage induced by the tumbling action of the plasma system or the plasma etching process. Together, these techniques provided a baseline from which to launch all further experimentation.

4.2 Materials and Methods

4.2.1 Grain treatment

Three 10 g aliquots of each grain type (maize, wheat, barley, field pea and psyllium) were designated for treatment as either T+V, P90 or Untreated. Treatments were performed following protocols described in Chapter 3.1.2.

4.2.2 Scanning electron microscopy

4.2.2.1 Sample preparation

Untreated, T+V treatment and P90 treated grains of maize, wheat, barley, field pea and psyllium were adhered to 12.6 mm pin stubs (ProSciTech) with carbon tabs. Edges of the grain were painted with graphite conductive adhesive (ProSciTech) to ensure a flush connection between the rounded grain surface and the stub. Samples were sputter-coated with platinum by Adelaide Microscopy, Frome Road, prior to imaging.

4.2.2.2 Imaging

All stubs were analysed at Adelaide Microscopy, Frome Road, with a FEI Quanta 450 FEG Environmental SEM at acceleration voltages of 5.0 kV, except for maize at 10.0 kV.

4.2.3 Profilometer

Pericarp surfaces over the endosperm of Untreated, T+V and P90 treated maize grains were scanned with an Olympus LEXT OLS5000 confocal profilometer with a 405 nm

laser at Adelaide Microscopy, Frome Road. 130 μm^2 area scans were performed on six replicates of each treatment to determine maximum heights of peaks and troughs. This automatically generated area data sets with the LEXT software to describe the surface roughness of each sample. As the grain surface is uneven at the best of times, it was necessary to assess the three-dimensional standard deviation, also known as root mean square value (RMS or Sq). The percentage of additional surface area created by roughness (Sdr) was also compared between treatments via unpaired t-tests in GraphPad Prism 9.0.0 (see Appendix S1 for Sdr, Sq and Rq equation details). Additionally, four technical replicate profile scans were taken from each of the six grains per treatment. Standard two-dimensional root mean square values (RMS or Rq) were analysed alongside Sq values.

4.2.4 Statistical analysis

Statistical analysis was performed in GraphPad Prism 9.0.0 (GraphPad Software Inc, San Diego, CA, USA) with unpaired t-tests comparing significance of the developed interfacial area ratio (Sdr) between treatments. A two-way analysis of variance (ANOVA) with Tukey's multiple comparison analysis was performed to compare area height (Sq) and profile height (Rq) across all three treatments. Data were expressed as mean ± standard error of the mean. Significance was accepted at $p<0.05$.

4.3 Results and Discussion

4.3.1 SEM

A broad survey of the five grain types was performed via SEM to visually assess the impacts of each treatment on the surface structures of grains. Weathering, structural variations, mechanical damage and the presence of pathogens were observed to gain a better understanding of how plasma might be interacting with seed surfaces. The observations for each grain type are individually described in the following sections.

4.3.1.1 Maize

The Untreated micrographs (Figure 4-1, A, D) of the grain surface over the endosperm display the outlines of wax-covered elongated surface pericarp cells in parallel alignment. The relatively smooth appearance indicates a healthy covering of surface wax which plays a role in defence against fungal pathogens (Russin et al., 1997). The physical damage caused by tumbling the grains against each other is apparent in the T+V treatment samples (Figure 4-1, B, E). Large fragments of the surface waxes and/or pericarp have been broken off and lie strewn about the surface. The waxy ridges over the elongated pericarp cells have been reduced to faint outlines which indicates that the large shards of debris originally formed the ridges. Shards and fragments are also visible on the plasma treated grain, but the etching process has cleared both the surface of the seed and the debris field. The etching created a weathered appearance similar to the 20-minute plasma-treated flaxseed samples described by Dauwe et al., 2021. Clearly, the tumbling action and the plasma etching inflict damage to the seed surface.

The tissue of the pedicel, often called the tip cap, connected the grain to the maternal plant during grain development and is structurally different to the tissues covering the endosperm (Brooker et al., 1992; Domínguez and Cejudo, 2014). In Figure 4-2, the tubular or sausage-shaped cells of the pedicel are visible. The weathering caused by the 90-minute treatment is much more distinct in this region due to different tissues interacting with the plasma. What is exceptional to note is the presence of fungal spores on the surface of both the Untreated and P90 grains. The spore on the Untreated sample looks to be intact while the plasma-treated spore appears to be weathered. Overall, the etching processes of plasma treatment effect all tissue types and structures observed across the micrographs of P90 maize.

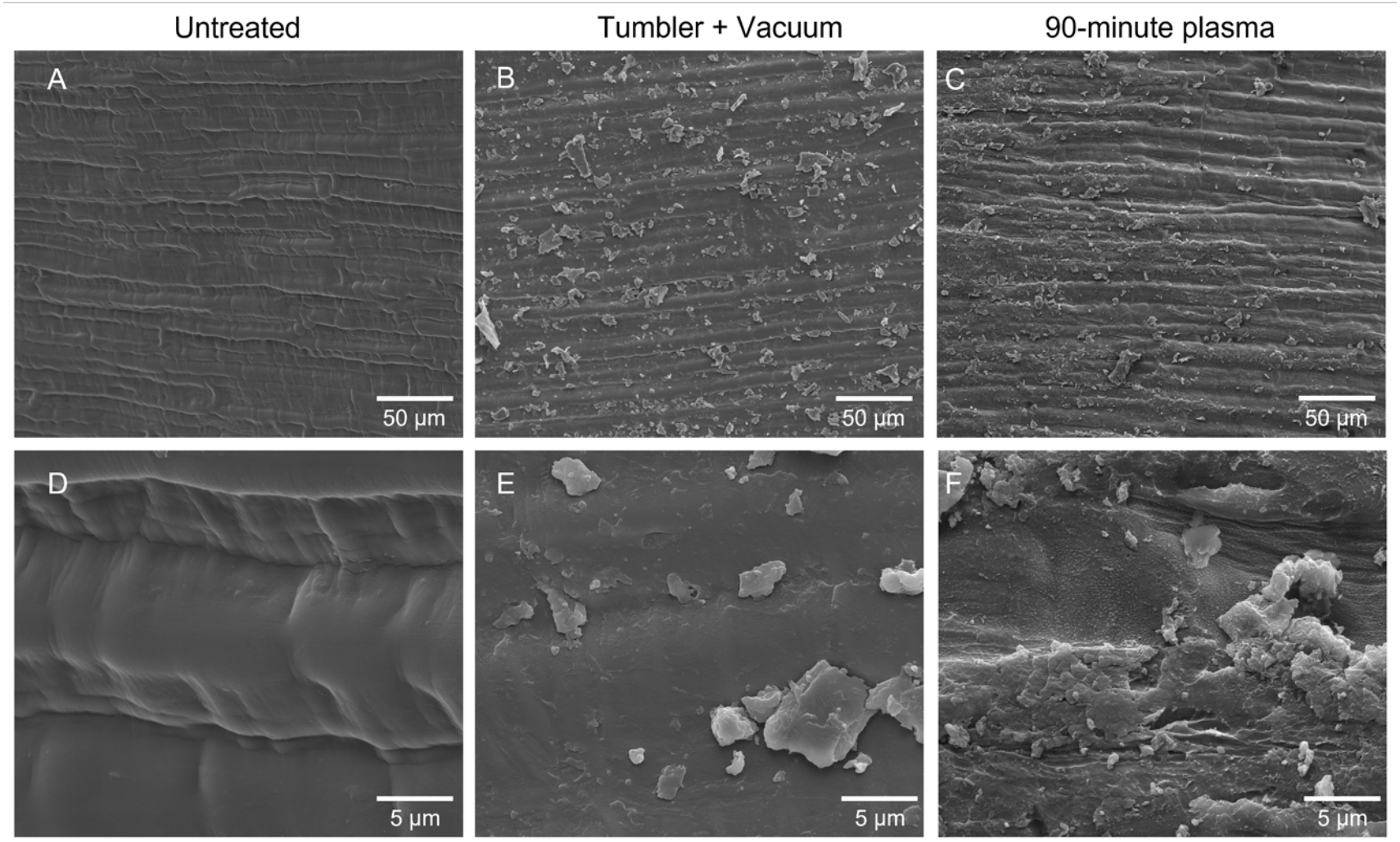


Figure 4-1. SEM micrographs of maize treatments show the exocarp surrounding the endosperm. Letters (A, D) are Untreated samples; (B, E) are T+V treatment; (C, F) are P90 treated grain.

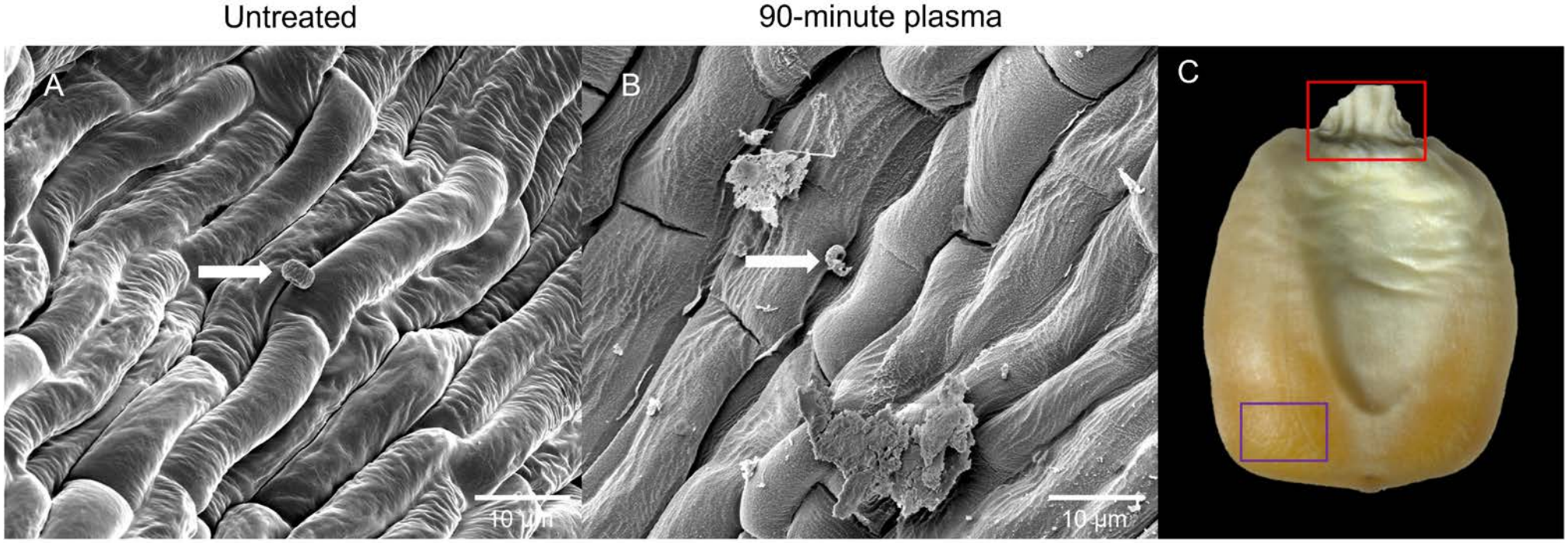


Figure 4-2. SEM micrographs of the surface of maize tip caps. (A) Untreated sample with a visible spore in the centre. (B) P90 treatment with visible weathering. Arrows indicate spores naturally present on the grain. Scale bar = 10 µm. (C) Maize grain with markings for areas of interest. Red square = tip cap area scanned; purple square = pericarp region scanned in Figure 4-1.

4.3.1.2 Wheat

SEM micrographs present views of the wheat grain exocarp (Figure 4-3). Much like maize, the Untreated samples have a smooth appearance with detectable outlines of the underlying cells. Large fragments can be seen on the surface of T+V treated wheat, albeit to a lesser extent than the T+V maize. This may be due to a different wax thickness and structure coating the seed surface. A distinctive granulated weathering pattern emerges on the P90 samples viewed at 10,000x magnification (Figure 4-3, F).

This pattern is reminiscent of the weathering effects of argon plasma documented by Butscher et al., 2016. It is interesting to visually compare wheat grains subjected to 90-minute air plasma treatment with a 10-minute high-powered argon plasma generated in a dielectric barrier system (Figure 4-4). Alongside the Ar plasma-treated images, it appears that long exposure times in the PT may produce a similar etching effect on the grain surface.

The effect of the plasma treatment is much more apparent when viewing grain macrostructures at 100x magnification (Figure 4-5). Untreated samples in A and B show the embryo and brush, respectively. Considerable damage to the embryo is visible in the P90 treatment (Figure 4-5, C). The exocarp has been torn away from the surface and the beak of the embryo appears to be crushed in multiple places. This may be a combination of both the mechanical damage inflicted by the tumbling action, and the weathering effects of plasma exposure. Even more evident is the modification of morphological structures in Figure 4-5, D. The entire brush has been removed during plasma treatment. The tumbling and chemical etching of the PT system figuratively shaves the brush off the wheat grain. It is speculated that the removal of this structure may alter the habitat of microbes present on the surface as they no longer have a protective shelter within the brush.

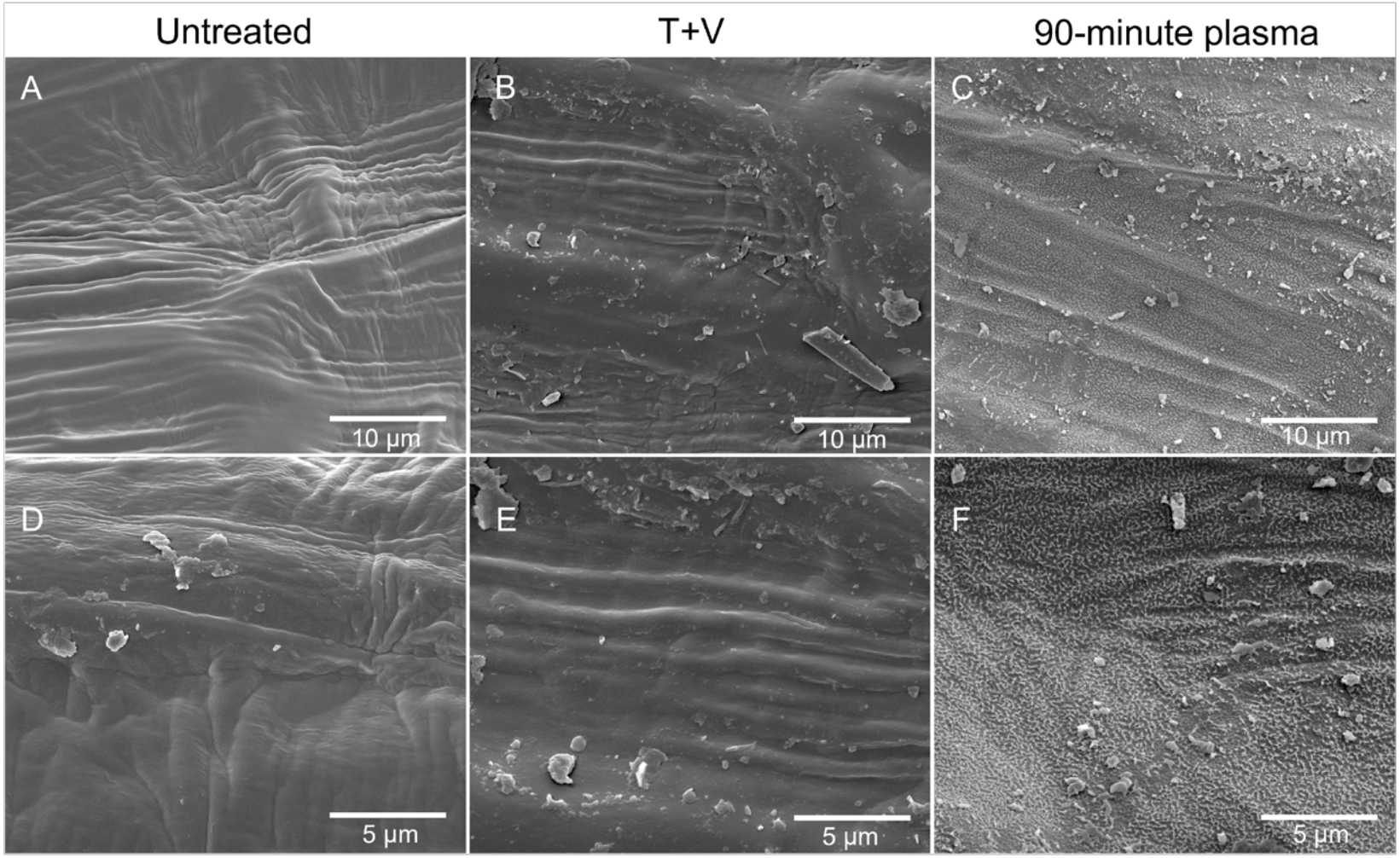


Figure 4-3. Dorsal exocarp SEM micrographs of wheat treatments. Letters (A, D) are Untreated samples; (B, E) are T+V treatment; (C, F) are P90 treated grain. (C, F) granulation of the grain surface is apparent on P90 treatments.

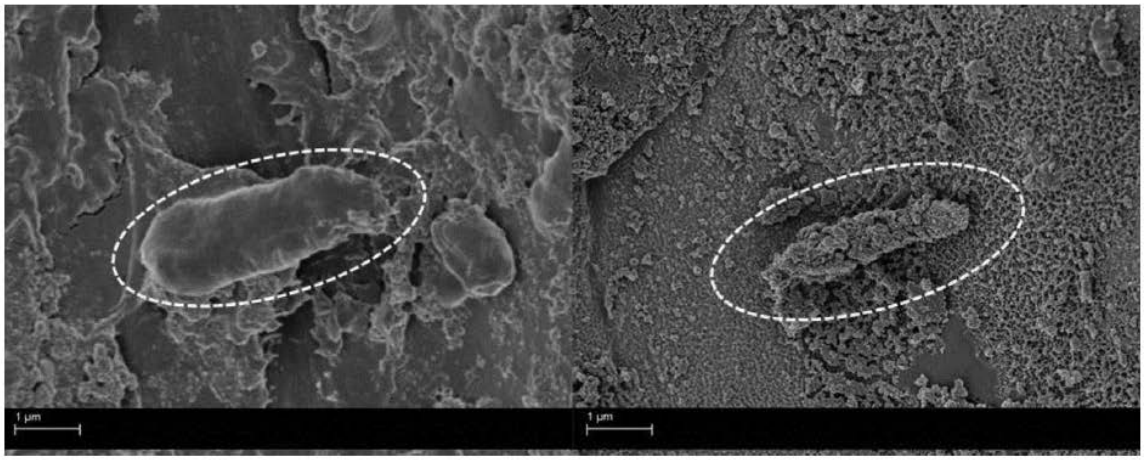


Figure 4-4. SEM image comparing wheat grain surfaces of control (left) and 10-minute argon plasma treatment in a DBD apparatus (right). Circles represent structures suspected to be bacteria endospores. Republished with permission of Elsevier Ltd., from Plasma inactivation of bacterial endospores on wheat grains and polymeric model substrates in a dielectric barrier discharge, Butscher, D., Zimmermann, D., Schuppler, M., Rudolf von Rohr, P., 2016. Food Control 60; permission conveyed through Copyright Clearance Center, Inc.

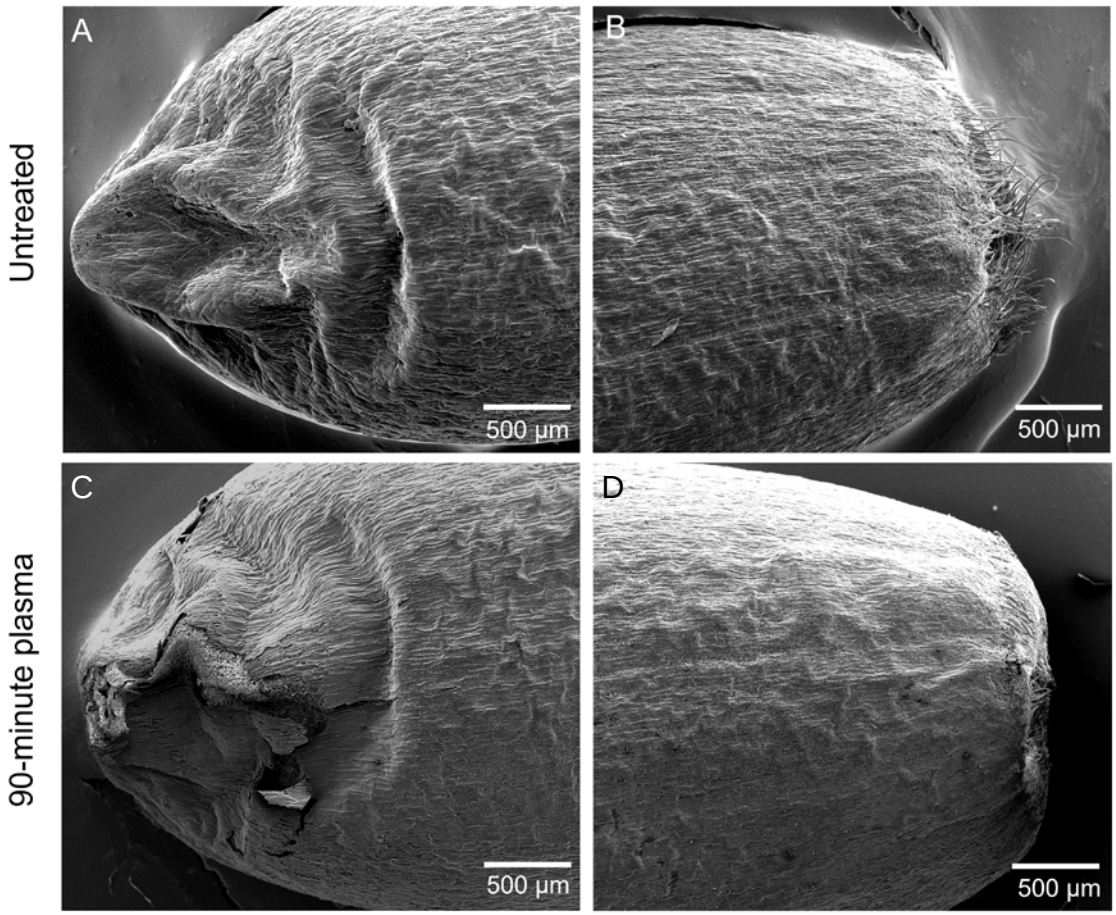


Figure 4-5. Wheat grains visualised under SEM. (A-B) are Untreated seeds. (C-D) are P90 treated grains. (A, C) focus on the embryo while (B, D) highlight the brush.

The domestication of wheat over multiple millennia has led to the loss of the protective hull and a gradual repositioning of the embryo on the outer edge of the grain with a thin covering (Dubcovsky and Dvorak, 2007). These phenotypic changes are the result of breeding for rapid and consistent germination and quick processing (Wrigley, 2017). The delicacy of wheat grains when compared to their emmer ancestors may leave them more vulnerable to the impacts of plasma treatment. Chapter 7 will explore the effects of plasma on grain growth and development to determine if the alterations visible under SEM have downstream consequences to seed viability and seedling health.

4.3.1.3 Barley

Unlike wheat, many barley cultivars have retained their protective hull surrounding the grain. The hull is made from the floral bract, called the lemma, and depending upon cultivar, may be coated in trichomes (Fincher and Stone, 1993). Untreated and T+V micrographs taken of the cultivar, Compass, reveal what are suspected to be two types of trichomes on the lemma surface, both prickle-like and dome-shaped (Imboden et al., 2018), giving the grain a very hairy appearance at 7500x magnification (Figure 4-6, D, E). They also display a series of parallel ridges which may correlate with the characteristic barley phytolith arrangement in the intercellular borders (Figure 4-6, A-C), as demonstrated in the reproduced image from Boateng et al., 2007 (Figure 4-7). P90 samples have a very different appearance to both controls. Hairs are completely absent, and the newly bald surfaces reveal details of the grain surface that were otherwise hidden (Figure 4-6, C, F). What are likely to be dome trichomes dot the surface giving the grain an almost plucked-chicken look. Additionally, the arrangement of intercellular phytolith ridges are much more distinct in the samples.

Comparisons between Untreated and P90 lemma at lower magnification highlight the general grain morphological features (Figure 4-8). The rachilla was present in

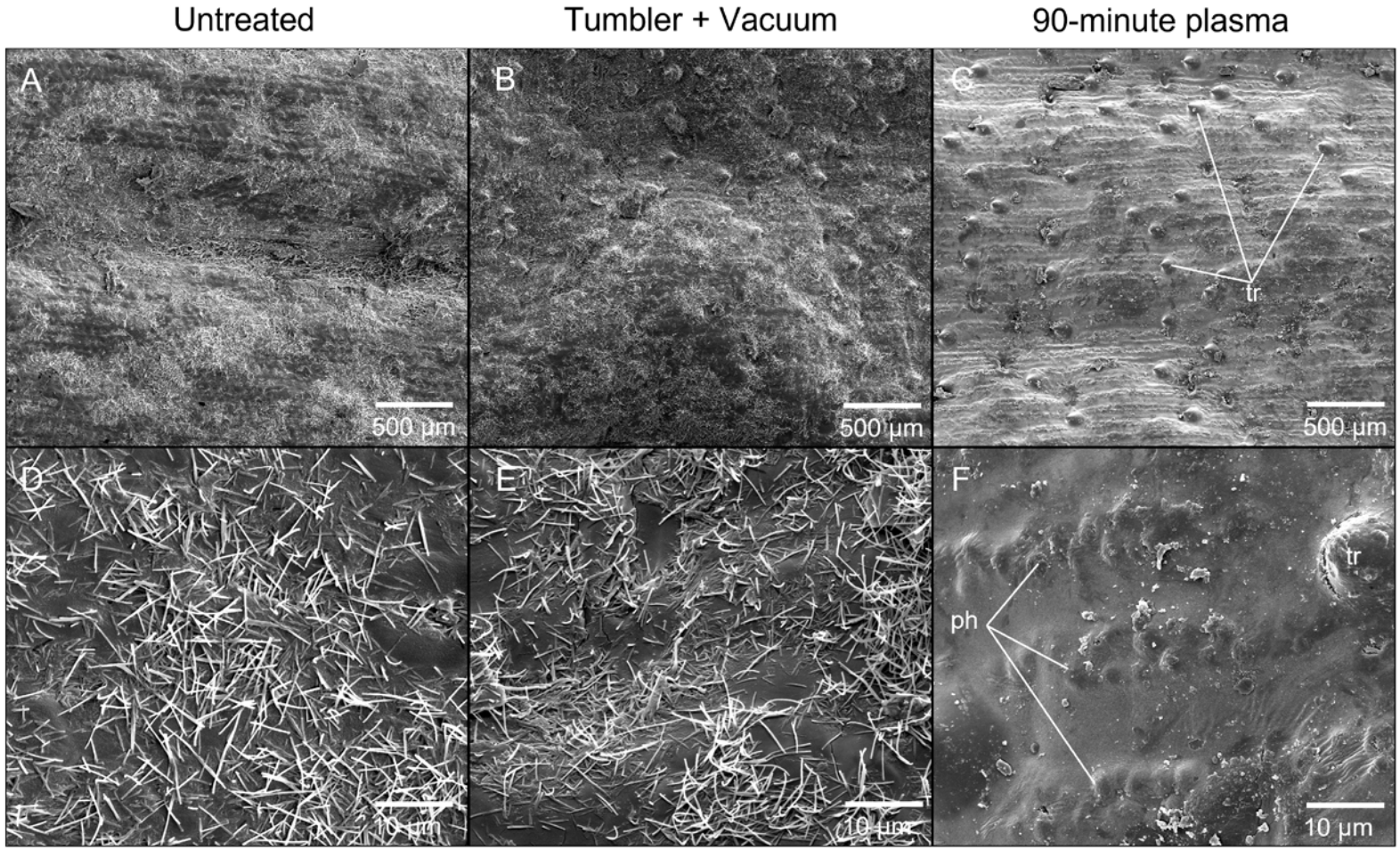


Figure 4-6. SEM micrographs of the hull of barley cultivar ‘Compass’. (A, D) are Untreated; (B, E) are T+V treatment; (C, F) are P90 treatment. Lemma hairs are visible in Untreated and T+V samples but not on P90 samples. ph = phytoliths below the surface on the intercellular borders; tr = dome trichomes; scale bars (A-C) = 50 µm; (D-F) = 10 µm.

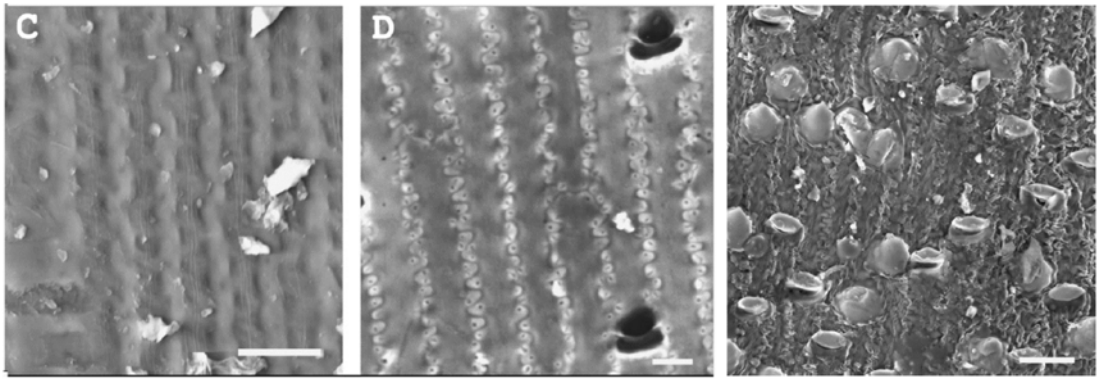


Figure 4-7. SEM micrographs of the surface of a barley lemma. *Left,* displays the outer surface with intercellular ridges. *Centre*, lines of phytoliths are exposed under the surface ridges. *Right*, dome trichomes dot the barley hull surface. Republished with permission of Elsevier Ltd., from Microstructure development of chars derived from high-temperature pyrolysis of barley (*Hordeum vulgare* L.) hulls, Boateng, A.A., Cooke, P.H., Hicks, K.B., 2007. Fuel 86; permission conveyed through Copyright Clearance Center, Inc.

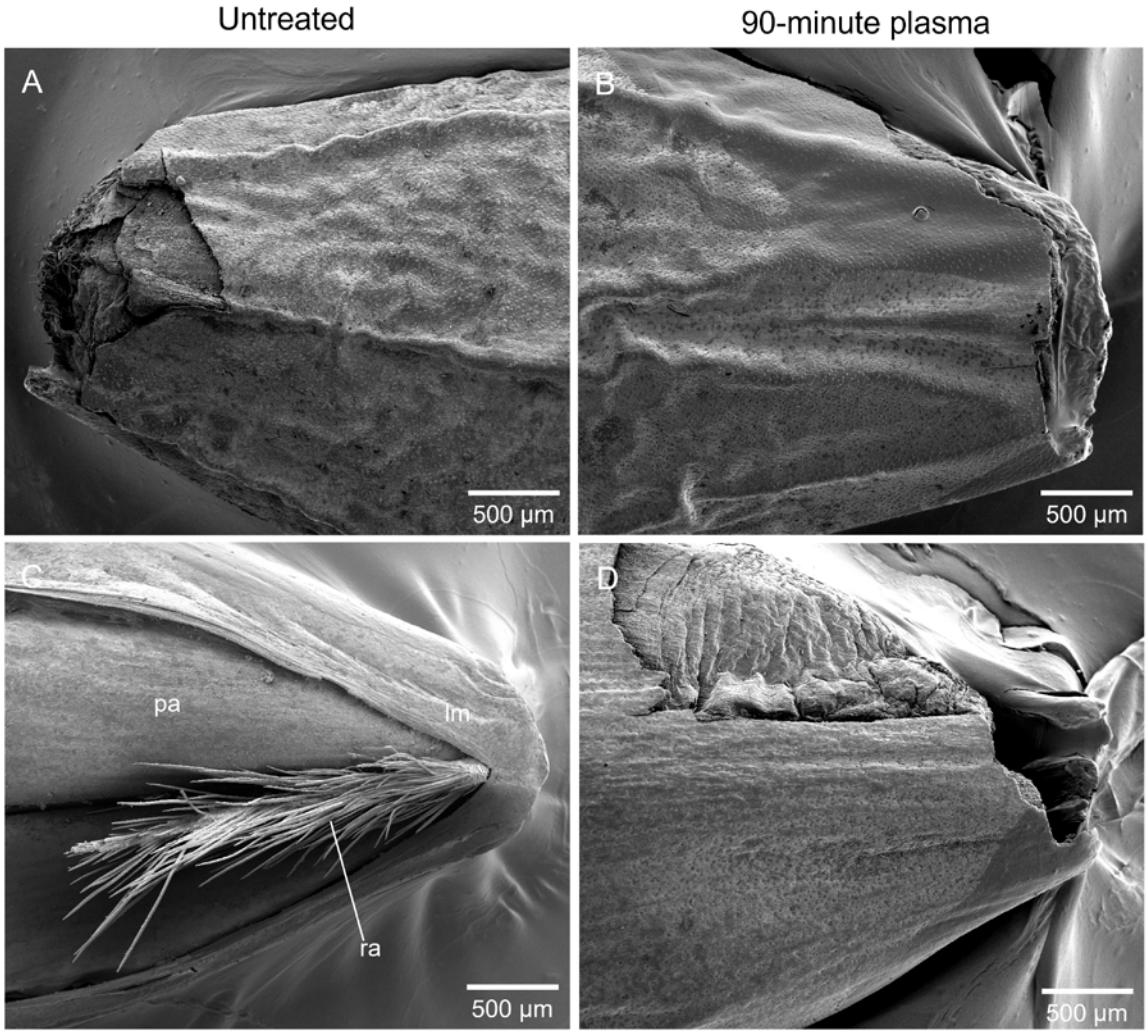


Figure 4-8. SEM micrographs of hulled barley. (A, C) are Untreated. (B, D) are 90-minute plasma-treated grains. (A) Damage to the lemma on an Untreated sample reveals the grain brush. (B) Modifications to lemma due to plasma treatment. Dome trichomes are much more apparent. (C) Ventral view of an Untreated grain with labelled structures. lm = lemma; pa = palea; ra = rachilla. (D) Damage on a plasma-treated grain reveals the underlying pericarp, seed coat and aleurone.

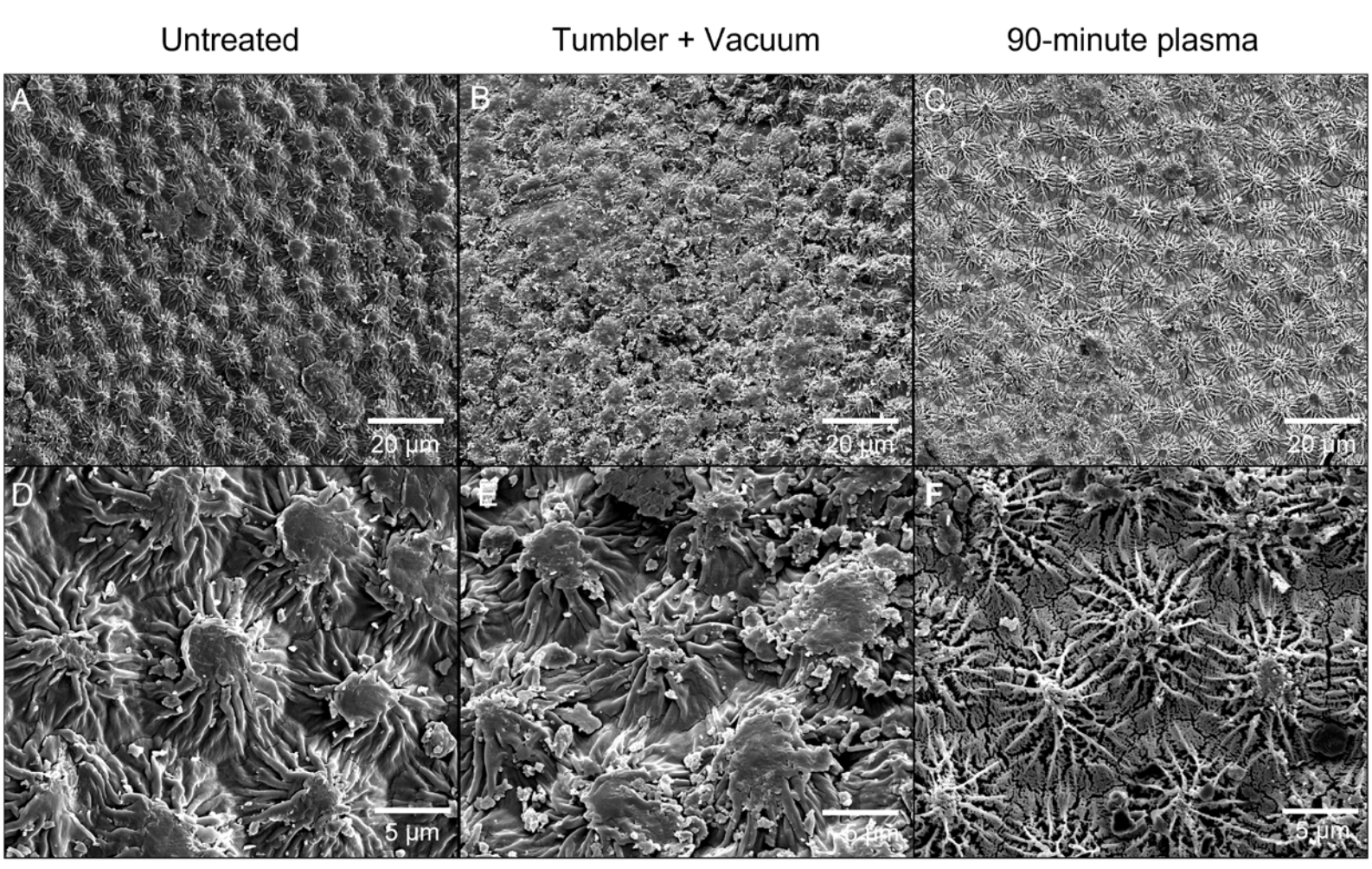


Figure 4-9. SEM micrographs of the seed coat surface of field pea. (A, D) are Untreated; (B, E) are T+V treatments; (C, F) are P90 treated grains. (A, B, D, E) The outline of star-shaped palisade cells are visible under the cuticle. (F) 90-minute plasma-treatment appears to strip away the seed coat cuticle, possibly exposing the primary cell wall structures below.

multiple Untreated samples and absent in all plasma-treated samples. The combined action of grain tumbling, and plasma etching may have physically removed this structure. Damage to both the lemma and grain pericarp are visible across both treatments. It appears that the barley hull may protect the seed from plasma-induced weathering. This also highlights the complexity of the barley surface structures, causing one to speculate on how the folds, nooks and crannies of the hull and grain surface may offer well-protected habitats for microbes.

4.3.1.4 Field Pea

SEM micrographs reveal the outline of the asterisk-shaped apical end of palisade cells of the pea seed coat (Figure 4-9). These macrosclereid cells run perpendicular to the grain surface with a thin protective cuticle that covers the cell surface (Werker, 1997; Zablatzká et al., 2021). The cuticle has a low wax content, covering only 1.34 µg cm^{-2} of the seed coat surface (Niemann et al., 2013; Van Dongen et al., 2003). A wrinkled dome of this lightly waxy cuticle covers the top of the palisade cells and highlights the characteristic surface structures of peas.

T+V treatments display a deformed surface with areas that appear to be flattened or crushed during the tumbling process (Figure 4-9, B and E). Despite the obvious damage, the cuticle does not appear to be fractured. The general seed surface structural integrity remains intact following T+V treatment. Yet, the impact of plasma-treatment on field pea is visually stunning (Figure 4-9 C and F). The wrinkled domes of cuticle covering the ends of the palisade cells have been stripped away. It appears that the primary cell wall structures of the underlying cell are now fully exposed on the grain surface. The complete removal of this layer may have significant consequences for seed permeability. It is speculated that water will enter the seed more rapidly through the fractures created across the plasma-treated surfaces, while Untreated and

T+V still retain their general structural integrity. These concepts will be further explored in Chapter 6.

4.3.1.5 Psyllium

Micrographs of Untreated grains display the characteristic wrinkled patterns (see Figure 4-10, A-B) and capsule imprint patterns (Figure 4-10, C) in the desiccated mucilage. The same structures are visible on T+V treated grains with a small debris field (Figure 4-10, D-F). Severe weathering is visible in all plasma-treated samples (Figure 4-10, G-I). Regardless of imprint shape, all surfaces have a granulated appearance. Some of the deep furrows in the capsule region only remain as hints and traces, which suggests that a very thin layer of the polysaccharide surface may be etched away in the plasma treatment process.

The surfaces of psyllium grains are coated in a 10 to 18 μm layer of laminated polysaccharide mucilage. The mucilage layer is formed between two mucilage secretion cells (MSCs) on the uppermost layer of the seed coat. The MSCs release polysaccharides into the intercellular space which compress into a thick layer. As the seed development begins to reach maturation, the MSC is sandwiched and crushed between the growing endosperm and the seed capsule. As this occurs, the mucilage is pressed into the capsule, leaving an imprint of the capsule surface structure behind on the top of the mucilage layer which subsequently desiccates (Phan et al., 2020). This creates a wonderful array of patterns on the psyllium seed surface (Figure 4-10, A-C). Regions near the capsule contain the imprints of long, parallel rows of cells. Areas of the grain under the operculum display imprints of hexagonal cells. This is further illustrated in Figure 4-11, A and B.

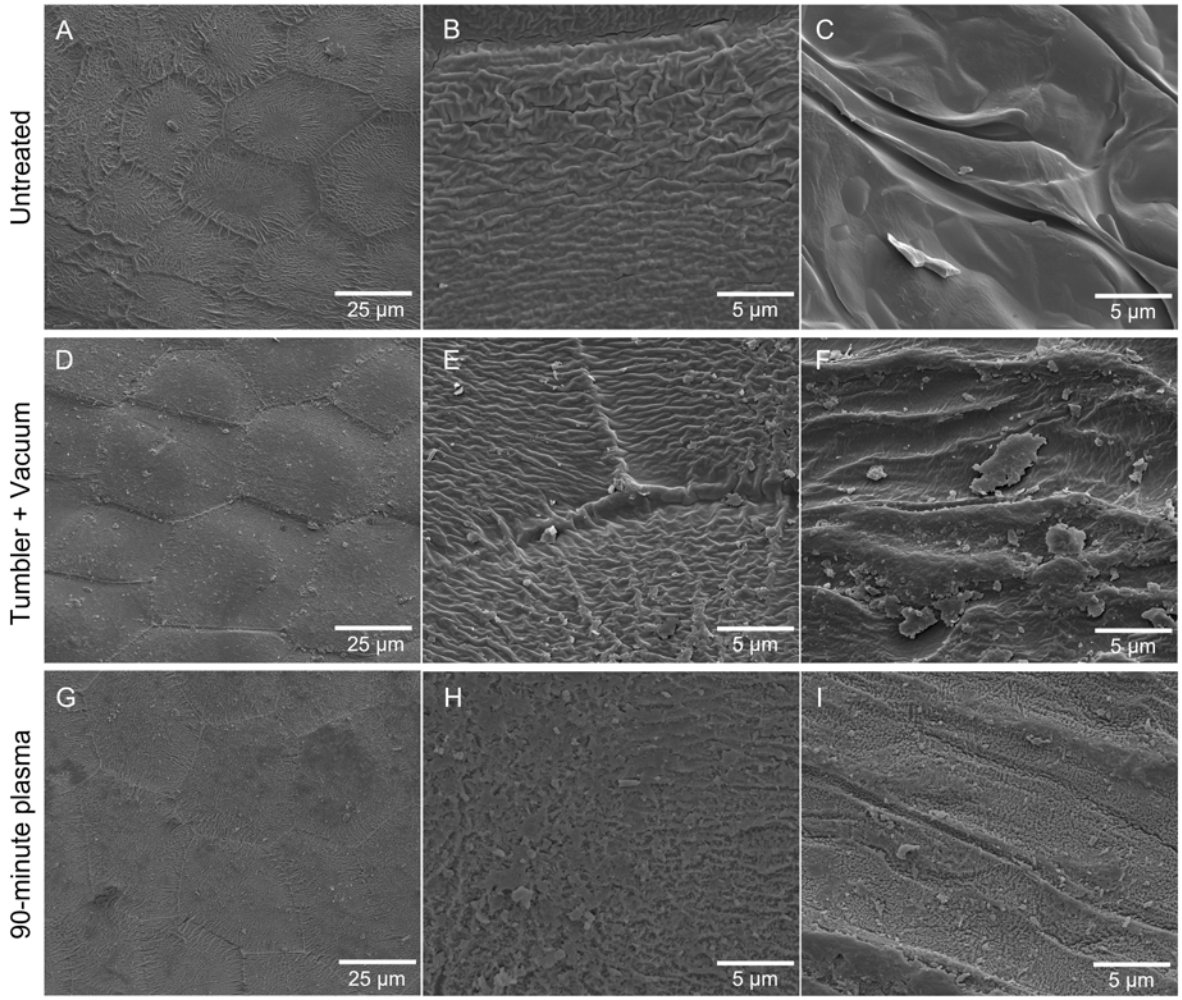


Figure 4-10. SEM micrographs of psyllium grains. Untreated (A-C), T+V (D-F) and 90-minute plasma-treated (G-I) display the characteristic wrinkles of desiccated mucilage on the grain surface. (A-B, D-E, G-H) are micrographs taken of the grain where the operculum was attached. (C, F, I) show the surface that was nearest to the capsule.

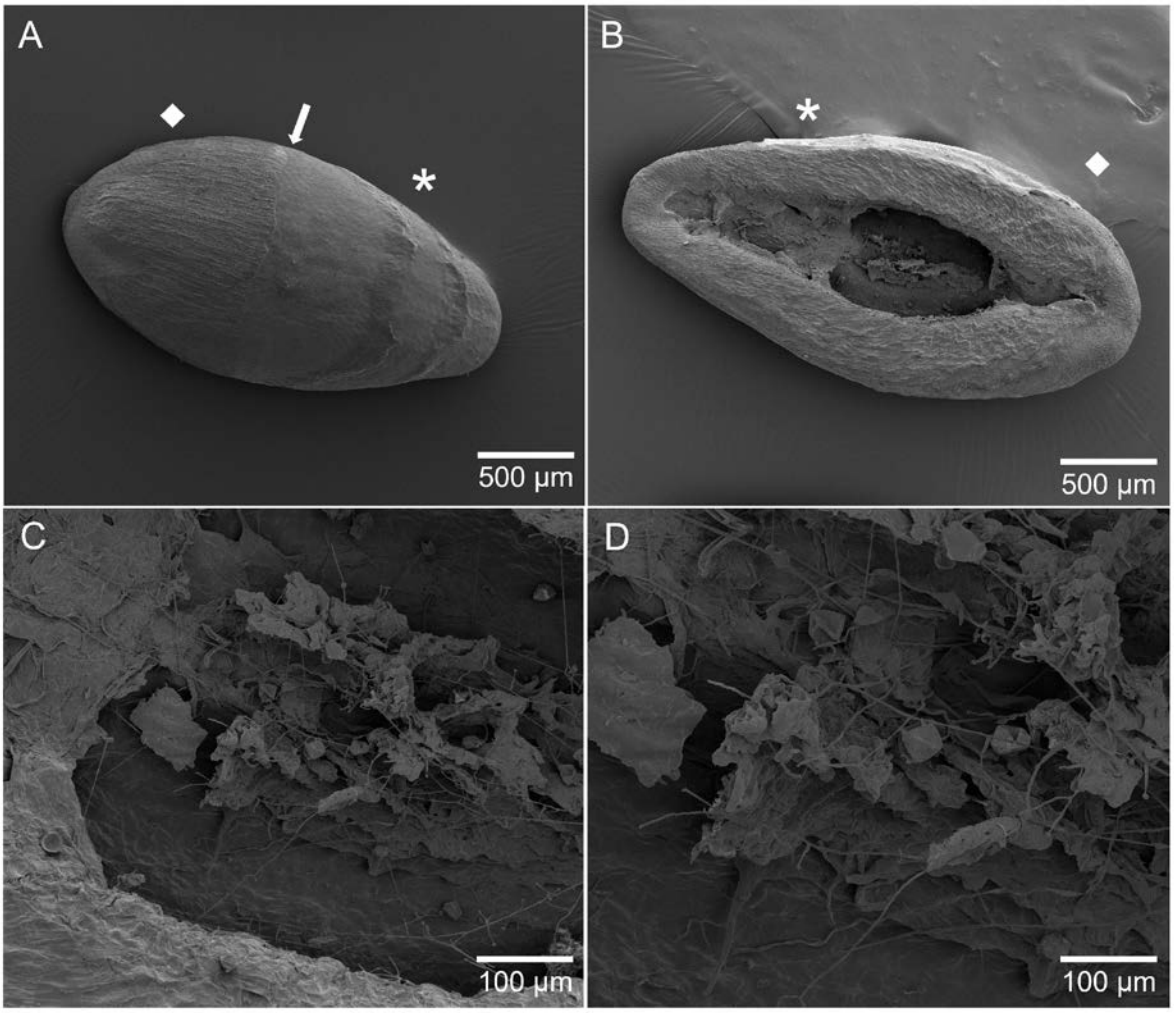


Figure 4-11. SEM micrographs of Untreated psyllium grains. (A) illustrates the dorsal surface of the grain. (B) pictures the ventral side of the grain. (C-D) Branching structures are suspected fungal hyphae growing throughout the ventral cavity of the grain. Diamonds indicate the region that was attached to the capsule. Asterisks indicate the region that was attached to the operculum. An arrow marks the equator where there are visible differences in surface patterns.

The surface modifications seen in psyllium are similar to those reported by Bafoil et al., 2018 in *Arabidopsis thaliana* where they describe the granulation of the 'volcano' structures on the seed surface (Figure 4-12). These 'volcano' structures are desiccated seed epidermal MSCs where the outer layers are the combination of both seed polysaccharide mucilage and the primary cell wall (Francoz et al., 2015). Plasma treatment appears to weather away the seed mucilage and reveal the primary cell wall. The surface cell structure and chemical composition differs greatly between psyllium

and *Arabidopsis* weathered seed surfaces, yet the pattern of etching and granulation is similar.

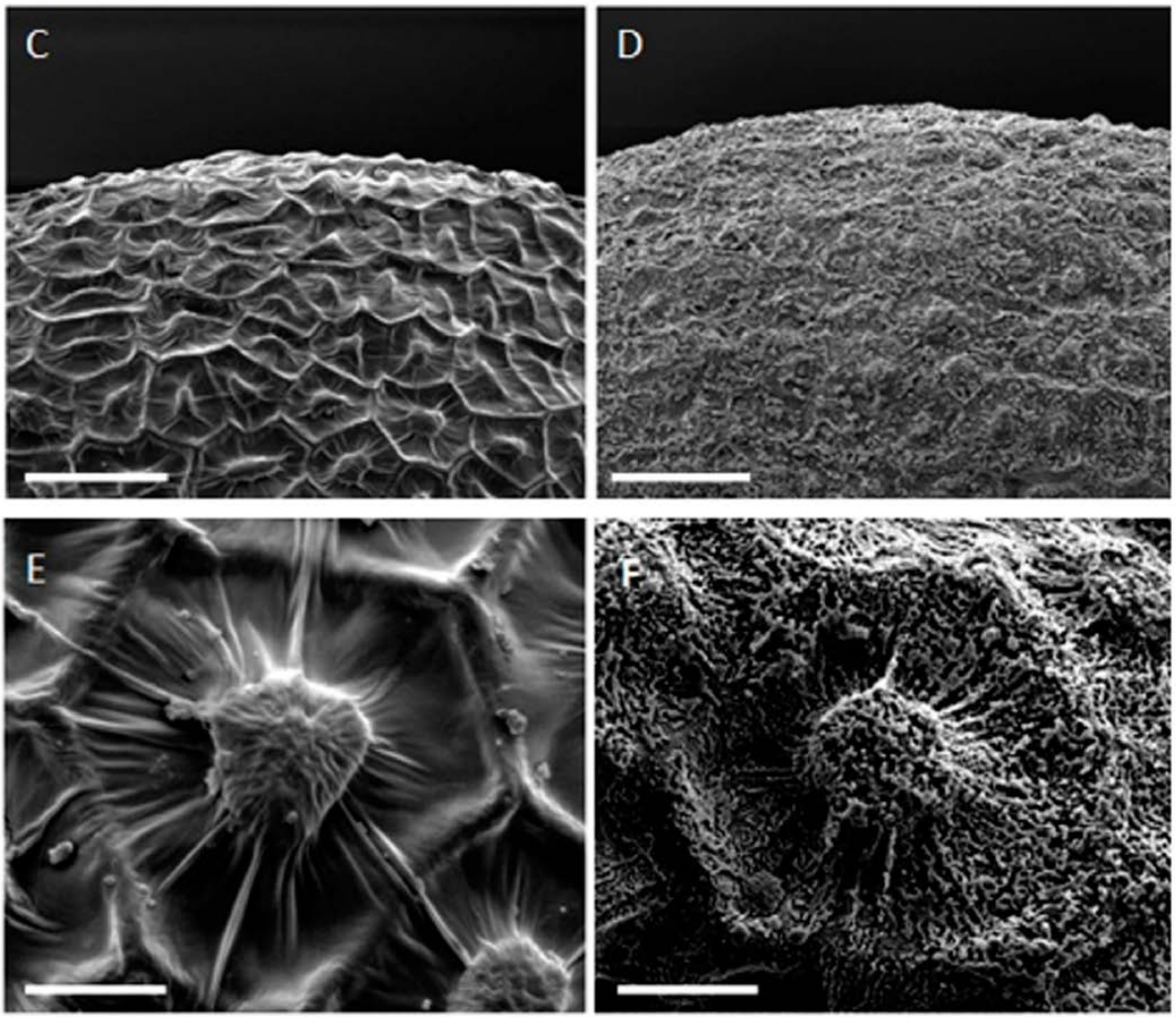


Figure 4-12. SEM micrographs of *Arabidopsis thaliana* seed surfaces. (C, E) represent control seeds while (D, F) were exposed to 15 minutes of air plasma in a floating electrode-dielectrode barrier discharge apparatus. The weathering of the surface of the mucilage secretion cells is reminiscent to the etching of the psyllium mucilage in Figure 4-10. Republished from Effects of low temperature plasmas and plasma activated waters on *Arabidopsis thaliana* germination and growth, Bafoil, M., Jemmat, A., Martinez, Y., Merbahi, N., Eichwald, O., Dunand, C., Yousfi, M., 2018. PLoS One 13; open access CC BY 4.0.

Unexpectedly, an Untreated grain and a T+V grain were observed with what is thought to be fungal growth throughout the ventral cavity of the grain (Figure 4-11, C-D). The filamentous structures are not part of the grain and closely resemble fungal hyphae and conidiophores. This somewhat protected region may act as a safe harbour for microbes which can feed on both the mucilage and the nutrient-rich embryo. The presence of fungal structures on these specific areas of grains raises two questions:

do specific grain morphological features encourage microbial colonisation; and can plasma treatments effectively deactivate secluded colonies? Experiments described in Chapter 5 will address these questions.

4.3.1.6 Summary

The SEM micrographs provide insight into how T+V and P90 treatments are interacting with the seed surface. Across all grain types, T+V treatment is correlated with mechanical damage. A debris field is visible, containing what are speculated to be chunks of the seed surface knocked loose as the grains collide in the spinning flask. An incredibly weathered version of the debris field appears on the P90 treatments, with minute channels etched into the grain surface. While the weathered surfaces resemble those published in other studies, there are notable differences. Some studies comment on a visible ‘cracking’ of the grain surface (Dauwe et al., 2021; Stolárik et al., 2015). This was not seen on any grain types, nor treatments in this research. Here, the field pea macrosclereid cells display a striking weathering pattern. Yet, these changes are not visible in the published works of Stolárik et al., 2015 and Švubová et al., 2020. As far as the author is aware, this is the first report of plasma treatment altering key morphological features, including the wheat brush, barley rachilla and prickle-like trichomes on barley.

Many of the plasma agriculture studies discussed throughout this section have been performed using dielectric barrier discharge and coplanar surface barrier discharge techniques which involve high power densities between 300 and 400W for shorter durations of exposure, usually 10 minutes or less. The plasma tumbler system was operating at 50W for a 90-minute exposure which may produce a very different type of seed surface reaction, as well as mechanical damage from the constant tumbling through the field of plasma and afterglow. Overall, this scanning electron microscopy

survey of grain surfaces demonstrates the ability of the plasma tumbler system to physically modify grain surfaces and features.

4.3.2 Profilometry

It was speculated that images and measurements from confocal profilometry might better describe and quantify the weathering processes of plasma treatment observed in the previous section. Maize was selected as an ideal candidate for screening due to the relatively flat grain surfaces when compared to the somewhat spherical field pea, canoe-shaped psyllium, and twinkie-shaped wheat grains (Figure 4-13). It is difficult to compensate for the strong curvature of the other grain surfaces, even when using filters, and may introduce unintentional artefacts. Following an unsuccessful attempt at collecting roughness measurements on psyllium, it was decided to nominate maize as the model grain type for analysis. Images from section 4.3.1 were referred to for the selection of a region of interest. The maize pericarp over the endosperm was ideal for scanning due to the more undulating topography of the grain without large curves.

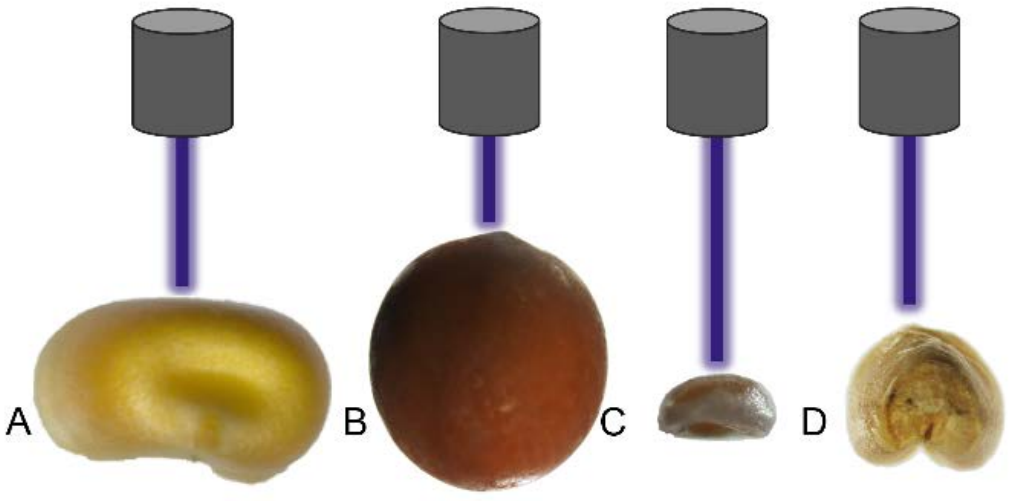


Figure 4-13. Diagram of grain surfaces with confocal 405 nm laser illustrates the difficulties when scanning curved surfaces. (A) maize; (B) field pea; (C) psyllium; (D) wheat.

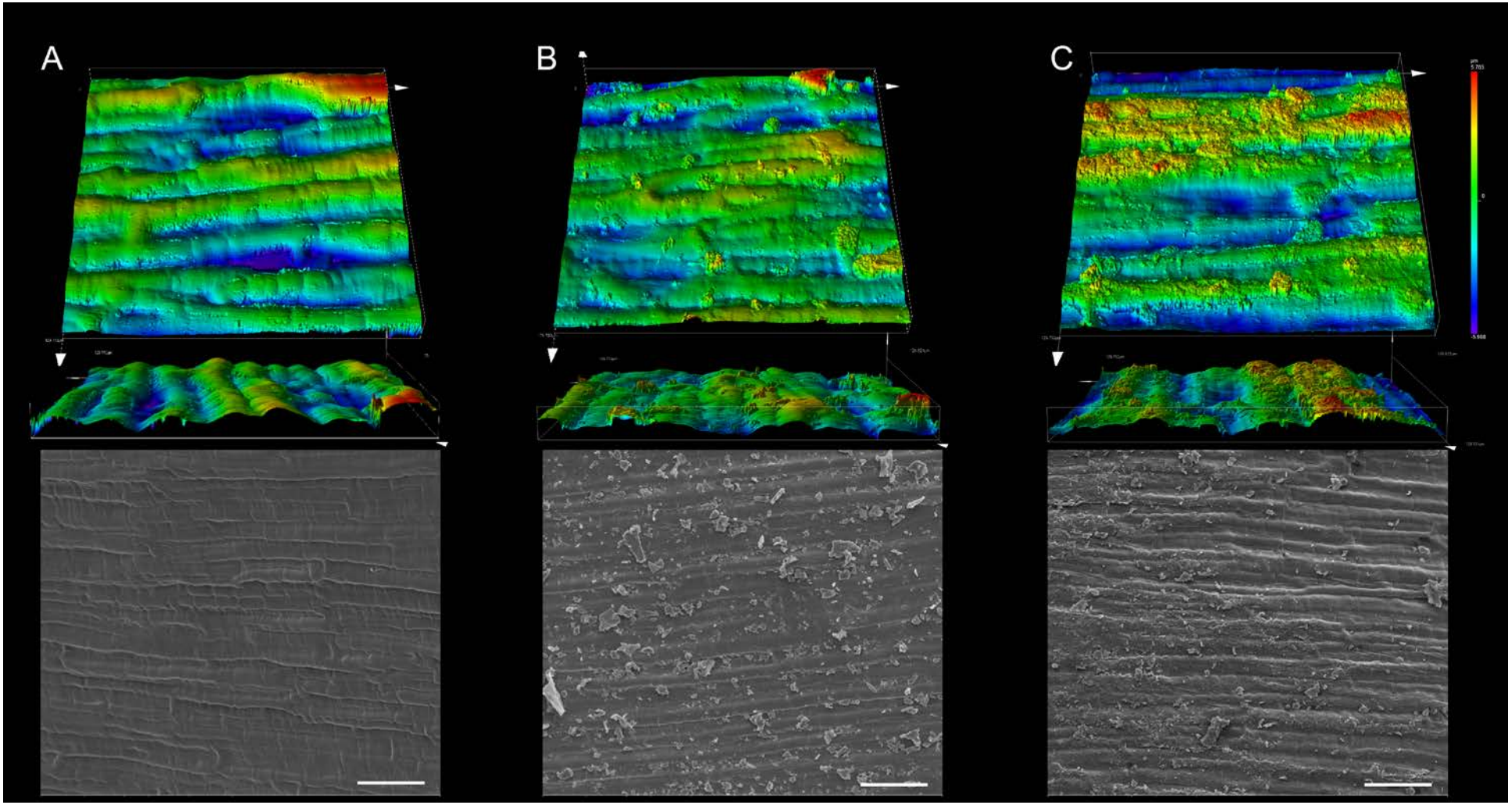


Figure 4-14. Confocal profilometer seed surface topographic maps of maize. (A) Untreated; (B) Tumbler + Vacuum; (C) 90-minute plasma treatment. Profilometer images are 129 µm wide. Scale bar on SEM micrographs is 50 µm.

Areal Z-stack scans of 129 μm^2 regions were performed to create topographic maps of each grain surface and assess the percent change in roughness. The maps were compared back to SEM micrographs to highlight the similarities between each method (Figure 4-14). The Untreated grain had a smooth and undulating surface. The tumbling action of the spinning flask again induced mechanical damage upon the grain surface. Large fragments of what appear to be the seed coat/pericarp are visible on both the T+V and P90 treatments. Like in SEM, plasma treatments appear to weather the surfaces in addition to the mechanical damage from tumbling. This was observed in the abraded appearance of P90 grain surfaces as seen in the areal Z-stack scan in Figure 4-14, C.

The visible alterations to the grain surface are supported by the change in interfacial area ratio (Sdr) which describes the percent change in surface area caused by roughness across treatments (Figure 4-15). As the chemical etching process caused by plasma weathers away the grain surface, the seed texture began to change. This is reflected in the significant difference between Untreated and P90 grain surfaces. The suspected shards of seed coat on the surface of T+V grain added enough roughness to make the means of this treatment intermediary between Untreated and 90-minute plasma.

The root mean square (RMS) value, also known referred to as Rq value, is often used to describe the standard deviation in height across a profile sample. The Sq value is similarly associated as the standard deviation in height across an area sample. These measurements are used to round out any peak/trough outliers across a sample, or in the case of this data, large fragments of debris on the seed surface. Four replicate profile measurements were taken across each seed and Rq values calculated. The Rq means of technical replicates for grain were compared via 2-way ANOVA and Tukey's multiple comparisons test to the Sq results (Figure 4-16).

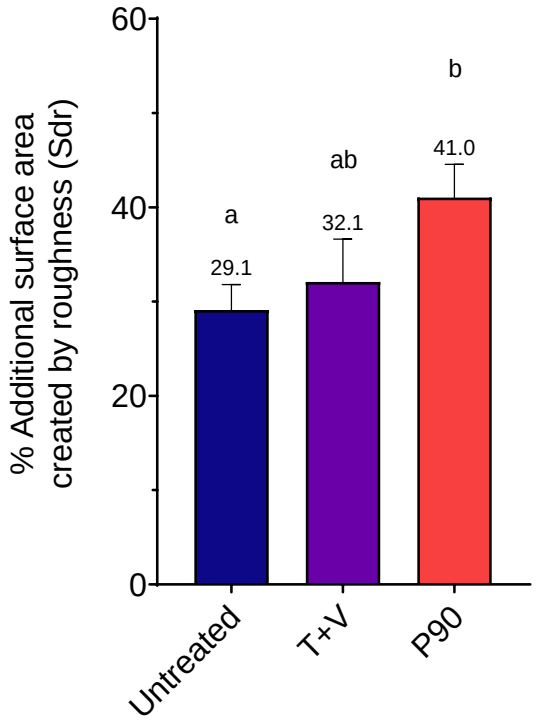


Figure 4-15. Unpaired t-test results for developed interfacial area ratio (Sdr) highlighting the percent change in surface area attributed to roughness in maize grain. Data is presented as SEM with significance accepted at p<0.05. Abbreviations: T+V (Tumbler + vacuum); P90 (90-minute plasma).

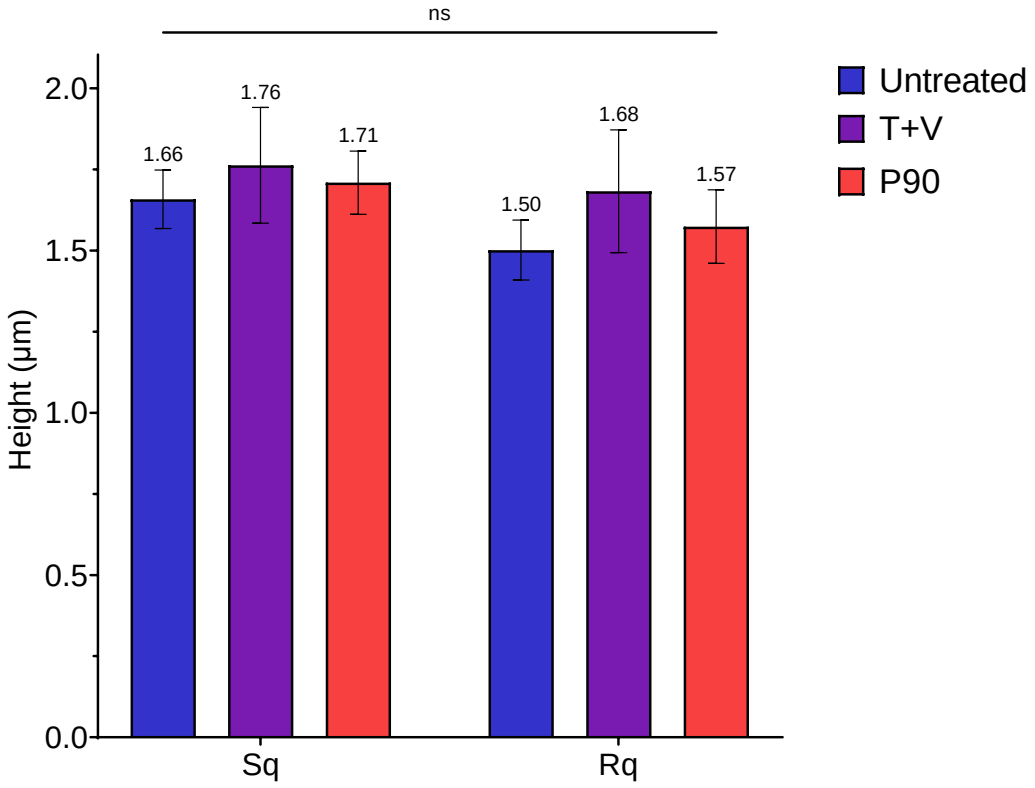


Figure 4-16. Two-way ANOVA analysis of both area height (Sq) and profile height (Rq). Data is presented as mean ± SEM with significance accepted at p<0.05. Abbreviations: T+V (Tumbler + vacuum); P90 (90-minute plasma); ns (non-significant).

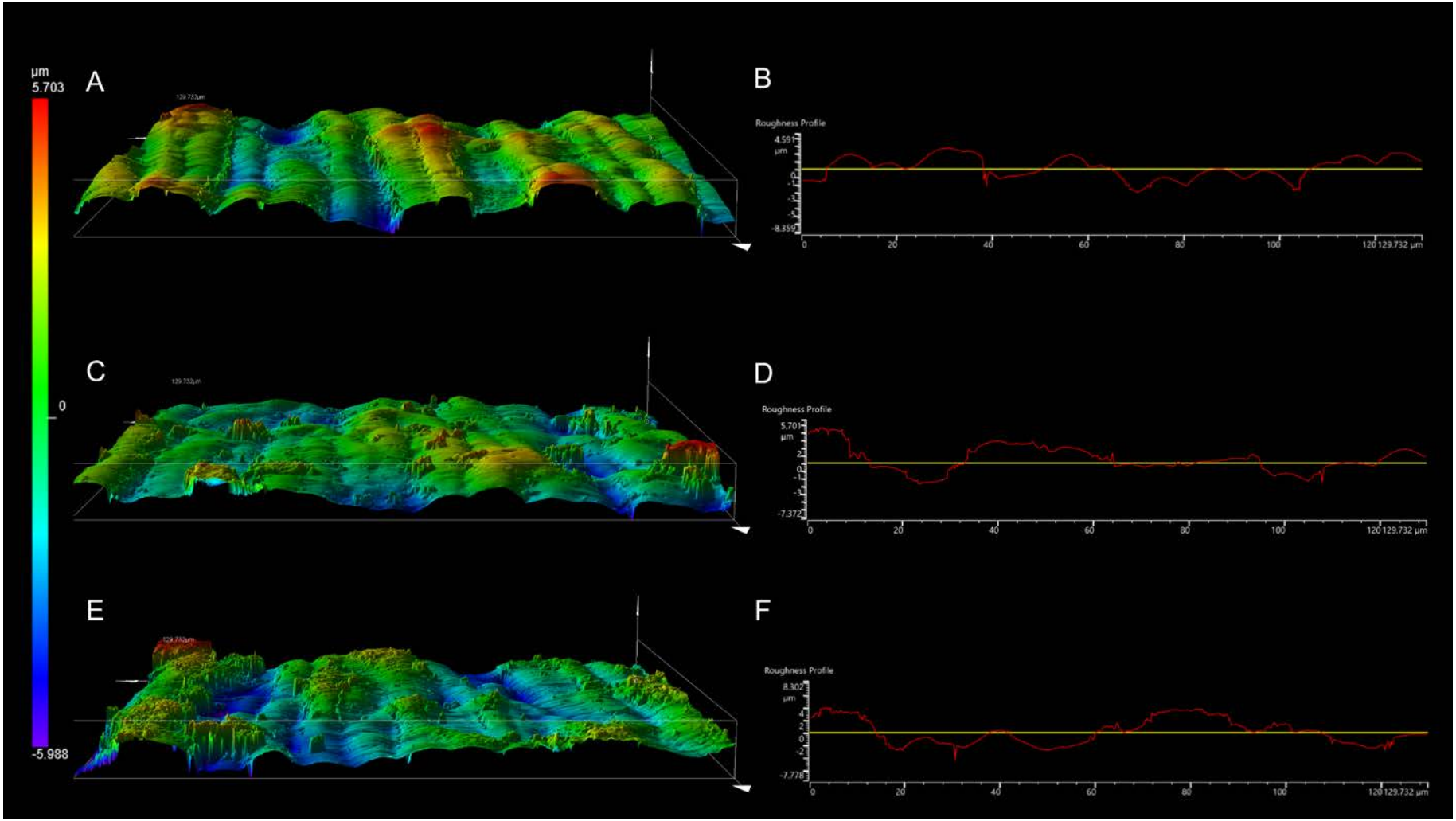


Figure 4-17. Visualisation of the data sets statistically described in Figure 4-16. Area scans (129 µm x 129 µm) compared to profile scans (129 µm) of each treatment. (A-B) = Untreated; (C-D) = T+V; (E-F) = P90.

Visual representations of the data statistically described in Figure 4-16, are useful for understanding the complexity of this analytical technique (Figure 4-17). When illustrated in this manner, it was unsurprising that there was no significance between samples. The fine roughness produced by plasma etching was strong enough to alter surface area but is masked in this analysis by the large variations in height from seed to seed. The application of a combination of filters within the LEXT software to reduce waviness, curves and noisiness could further elucidate smaller effects of the chemical etching process on the seed surface. Nevertheless, the goal of validating the effect of etching on the seed surface was accomplished. Additionally, the reliability of measurements is accurate to roughly 0.2 µm. As the etching process occurs at fractions of a nanometre, it was deemed to be outside of the scope of this project to further investigate the profile changes to the seed surface.

4.4 Conclusion

This chapter describes the use of imaging techniques to survey the surface structures of each grain type and the modifications induced by treatment. The striking images led to multiple lines of questioning for further investigation and formed the foundation from which all subsequent research in this thesis was conducted. It was clear that each grain type has distinct surface features which react differently when exposed to plasma. In maize, the elongated surface pericarp cells are visibly abraded, as if the grain surface had been sand-blasted. This was shown to increase surface area which may have implications on the way water droplets contact the grain surface (see Chapter 6.2). Plasma-treated wheat was notably missing the brush and displayed signs of possible embryo damage. This could have downstream impacts on seed viability, growth, and development (see Chapter 7.2 and 7.3). The barley husk was denuded of prickle-like trichomes, exposing the surface of the lemma. While these changes are fascinating, it is speculated that the husk may be protecting the grain from

the harshest of the chemical etching processes. On field pea, plasma stripped away the entire surface covering, leaving exposed remnants of the macrosclereid cells behind. This brought about conjectures that plasma-treated peas may respond differently to the Untreated cohort when exposed to water (see Chapter 6.4). Furthermore, the weathering of the psyllium polysaccharide coated surface may also impact grain-water relations, possibly affecting the mucilage swelling capacity (see Chapter 6.6).

In addition to the physical changes induced by plasma treatment, an unexpected microbiological component was observed. What are suspected to be fungal conidia were visible on the pedicel of both Untreated and P90 maize grains. The supposed plasma-treated conidium has been weathered and deformed, which led to speculation that plasma treatment may impact the viability of the extant seed fungal population. This concept formed the basis for Chapter 5. Moreover, what are likely fungal hyphae and conidiophores were seen in the psyllium grain cavity, indicating an infection, rather than the potential for infection due to the presence of quiescent spores. This inspired questioning about the efficacy of plasma against multiple types of fungal vegetative structures and necessitated further experiments with inoculated hyphal growth (see Chapter 5.5).

In summary, the results of this chapter prompted the experimentation described over the next three chapters. Due to the stepwise expanding nature of this work, the following three chapters will be structured in a different format. Individual experiments will be described in full so that the conclusions can form the basis of the following section, with an aim to communicate the evolving nature of this research.

5 Evaluating the efficacy of plasma treatment for the inactivation of fungal pathogens on the grain surface

5.1 Introduction

The increasing pressure of global food insecurity is driving the search for alternative methods for the removal of pathogens from post-harvest grain. Attention has turned toward technological approaches, such as the ionized gases created in plasma discharge, which are capable of deactivating or disinfesting pathogens on seed surfaces (Chizoba Ekezie et al., 2017; Misra et al., 2016). This is often attributed to the etching action of plasmas, particularly air and argon. As ion bombardment breaks apart surface compounds (Whitehead, 2016), superoxide and other reactive species interact with the newly-formed structural defects (Raballand et al., 2008). The repetition of this process creates a weathering effect across the surface exposed to plasma, as seen in the SEM micrographs in Chapter 4. Thus, the integrity of seemingly robust structures, like cell walls, can be quickly degraded. This principle is thought to be the mechanism of action behind microbial deactivation as chemical etching erodes the macrofibrils within the fungal or bacterial cell wall, ultimately leading to the destruction of the organism (Rossi et al., 2009).

Many studies have tested the efficacy of various plasma apparatus for the inactivation of microbes on grains, seeds and in culture, as reviewed by Adhikari et al., 2020; Kaur et al., 2020; and Siddique et al., 2018. Some have used seeds inoculated with

microbes to test plasma deactivation (Butscher et al., 2016; Dasan et al., 2016; Kopacki et al., 2017; Selcuk et al., 2008). Yet, few have compared the extant grain microbes or multiple grain types and pathogens. Los et al., 2020 isolated extant fungal pathogens from wheat grains, choosing six for inoculation to provide one of the most complete studies to date, using a dielectric barrier discharge system. However, wheat was the only model grain involved in the study which yielded colony-forming unit reductions of up to log 4 in *Aspergillus flavus*. Kordas et al., 2015 also identified extant fungal pathogens present on wheat grains and their response to short plasma exposures. Both foundational works highlighted the need for comprehensive studies exploring the efficacy of plasma inactivation on complex grain microbiomes. As neither grains nor pathogens fit into a one-size-fits-all category for plasma treatment, this research sought to fill the gap by exploring multiple host grains and pathogens to understand how features of each respond differently to treatment. This broad approach is essential if the technology will be considered for industrial use with near complete fungal deactivation in the future.

Grains are three-dimensional structures with layered surfaces, grooves, hulls, and other features. If plasma treatment is to be successful, chemical etching must occur across the entire surface of a grain. Butscher et al., 2016 compared endospore inoculated wheat grain to a polypropylene model and noted that morphological features on the wheat grain surface may shield endospores from plasma exposure. They also demonstrated that endospore reduction was directly related to plasma-generated chemical species and chemical etching. Here, we speculate that the plasma tumbler can overcome some of the difficulties posed by grain morphology. By perpetually spinning the grain, all surfaces continuously tumble in and out of the field of plasma. This may increase the ability of plasma-generated chemical species to react with more surface structures potentially shielding microbes.

A series of preliminary trials was conducted to establish whether the plasma tumbler could deactivate the extant population of fungi present on grain samples. Additionally, initial experiments were used to establish methods for subsequent fungal spore extraction and culture experiments. The outcome of these trials led to the development of an assay investigating the location of pathogens on maize and wheat. This data was applied to results in Chapter 4 with the conclusion that grain morphology plays a role in fungal spore load and position. It was then necessary to ascertain the exposure time when plasma treatment might be most effective, accounting for surface structures of the grain and potential hidey holes for microbes. Critical time windows were examined on maize and field pea inoculated with *Aspergillus flavus* and *Penicillium chrysogenum*, respectively. Finally, the newly established critical time window was challenged with five grain types and their associated fungal pathogens. The traditional quantitative methods of colony-forming unit counts were supported with qualitative SEM imagery.

The following sections are arranged into groups of related experiments. Aspects of the experimental process are described in each section, as each set of results helped to determine the subsequent research questions.

5.2 The culture of extant grain microbes

5.2.1 Introduction

This foundational experiment was designed to establish methods for extracting fungal species from grain and determine the baseline grain fungal spore loads. Generally, the extant population on a given grain type is highly variable and results in different initial pathogen loads depending on plant species, field location, weather patterns during the growing season, grain moisture content, grain handling hygiene and other factors. The aim was to develop a straightforward method for extracting fungal spores and hyphal

fragments from all grain types, characterising the fungal species present, and quantifying the fungal load. As the extant microbial population was unknown, pilot trial using maize grain, a broad range extraction buffer and two culture mediums were tested to ensure the greatest number of pathogens could be grown together on a plate. The data set gathered from the pilot trial was used to optimise methods and perform extractions of the extant microbes on wheat, barley, field pea and psyllium. From these data sets, the population of culturable microbes associated with each South Australian-grown grain type could be quantified.

5.2.2 Materials and Methods

5.2.2.1 Media preparation

5.2.2.1.1 Half-strength PDA (½ PDA) plates

Plates of media were prepared following protocols described in Chapter 3.3.1.2.

5.2.2.1.2 Water agar (WA) plates

Plates were poured using guidelines established in Chapter 3.3.1.3.

5.2.2.2 Grain treatment

Grain of maize, wheat, barley, and field pea was split into 10 g treatment aliquots of Untreated, T+V and P90. Treatments were performed as described in Chapter 3.1.2.

5.2.2.3 Extraction buffer preparation

Extraction buffer was created immediately prior to microbe extractions following protocols listed in Chapter 3.3.2.

5.2.2.4 Microbe extractions

5.2.2.4.1 Pilot trial with maize

Inside a laminar flow hood, grain treatments were divided into three 1 g replicates and poured into sterile 10 mL tubes. Each of the three tubes containing 1 g of seed served as a biological replicate. 4 mL of buffer was added to each tube and gently agitated for

20 minutes on an orbital mixer (Ratek). Tubes were inverted twice and 100 µL of liquid was removed with a sterile filter-tip pipette and placed in the centre of a pre-poured plate. Maize treatments were repeated using ½ PDA plates and WA plates. All subsequent experiments used ½ PDA. The extraction liquid was spread across the plate with a sterile L-shaped glass cell spreader. This process was repeated three times to produce triplicate technical replicates from each biological replicate tube. Plates were sealed with clingfilm (Glad, cut to 2.5 cm width with a bandsaw) and placed lid-side down on clean trays for incubation at 25 °C, 14h/10h light cycle for 96 hours.

5.2.2.4.2 Experiment with four grain types

Protocols described in section 5.2.2.4.1 (above) were repeated for four grain types (maize, wheat, barley, and field pea) except for three procedural amendments. The number of biological replicates was raised to five. The extraction buffer volume was reduced to 2 mL and only a ½ PDA plate medium was used.

5.2.2.5 Colony counts

Plates were placed on a light box and individual colonies were counted following procedures described in Chapter 3.3.7.

5.2.2.6 Fungal identification

Following colony counts, Untreated plates of maize, wheat, and field pea were incubated for another six days. At day 10, cello tape flag preparations (as described by Kidd et al., 2016) were made of each visually different fungal colony and viewed under a phase contrast compound microscope (Nikon, Eclipse Ci-L) for identification to genus level using Watanabe, 2010 as a reference.

5.2.2.7 Statistical analysis

All data was sorted in Microsoft Excel 365 (Microsoft Corporation, Seattle, WA, USA) before analysis. The significance between treatments and grain types were determined via two-way ANOVA and Tukey's multiple comparison analysis in GraphPad Prism

9.0.0 (GraphPad Software Inc, San Diego, CA, USA). All colony counts of zero were transformed to one for ease of statistical analysis on a logarithmic scale. Data were expressed as mean ± standard error of the mean. Significance was accepted at $p<0.05$.

5.2.3 Results and Discussion

5.2.3.1 Selection of culture media and refinement of methods

The culturing techniques established in the pilot trial were successful in extracting several visually distinct fungal colonies from maize grains. The mean of Untreated colony-forming units for ½ PDA medium was 278 CFU/mL; 311 CFU/mL was the mean for WA (Table 5-1). To help narrow down which culture medium should be used for subsequent experiments, a two-way ANOVA and multiple unpaired t-tests were performed to assess any differences in the number of colony-forming units that could be extracted on either medium. When comparing Untreated CFU/mL for both media, the p-value was 0.6611, indicating no significant difference. Interestingly, no viable colonies could be cultured from the T+V and P90 treatments using either medium. It is likely that the volume of extraction buffer used was too high, resulting in a very large spore dilution that could not be captured on culture plates. The buffer dilution of 1:5 (1 g of grain in 4 mL buffer) was reduced to 1:3 (1 g of grain in 2 mL buffer) for future trials throughout this chapter and Chapter 8.

Table 5-1. Summary of the pilot trial showing colony-forming units extracted from maize, *Zea mays* 'B73,' Untreated, T+V (Tumbler + vacuum), and P90 (90-minute plasma) grain and plated on two types of culture media.

Media	Treatment	Mean CFU/mL	Std
½ PDA	Untreated	278	42
	T+V	0	0
	P90	0	0
WA	Untreated	311	123
	T+V	0	0
	P90	0	0

Performing a visual inspection of the qualities of the fungal colonies was helpful to select the appropriate culture medium. Untreated colonies grown on ½ PDA were larger, displayed pigmentation and what appeared to be an accelerated growth rate, most likely due to increased nutrients in the media, when compared to Untreated colonies on WA. For this reason, ½ PDA was selected as the standard media for all subsequent colony forming unit experiments because it provided the optimal pathogen incubation time and supported the growth of fungal colonies with distinguishable phenotypical characteristics.

Overall, the initial extraction method and quantification of colony forming units was successful for the Untreated controls. The modifications listed above were then performed on wheat, barley, field pea and a second subset of maize grains to characterise the population of extant fungi and their numbers.

5.2.3.2 Quantification of extant culturable fungi

This series of experiments aimed to understand how P90 and T+V treatments impacted the extant fungi present on the grain surface. The aim was accomplished through the extraction, culture, and quantification of the seed surface fungi of four economically relevant grain types. The resulting data (Figure 5-1) indicates that each grain type is affected by plasma and T+V treatments in a different manner. In maize,

P90 treatment significantly reduced the concentration of colony-forming units when compared to Untreated controls. The effects of T+V treatment were not significantly different to either the control or plasma, suggesting that exposure to the mechanical tumbling and vacuum is an intermediary between the other treatments. On the other hand, wheat grains had dramatic decreases in CFU/mL between all three treatments. The T+V treatment had a much greater effect on the extant fungi in this grain type. Barley had significant reductions between the control and both treatments. However, there was no difference between T+V and P90. All three treatments were insignificant in field pea. In general, plasma treatment significantly decreased the concentration of colony-forming units when compared to the Untreated control. The relationship between T+V and plasma was less apparent. It was not possible to determine whether the action of T+V treatment or plasma treatment caused the reduction of CFUs, due to the lack of consistent trends between grain types. While the plasma-treatment does appear to have an effect, further experimentation is necessary to untangle the differences between treatments and grain types.

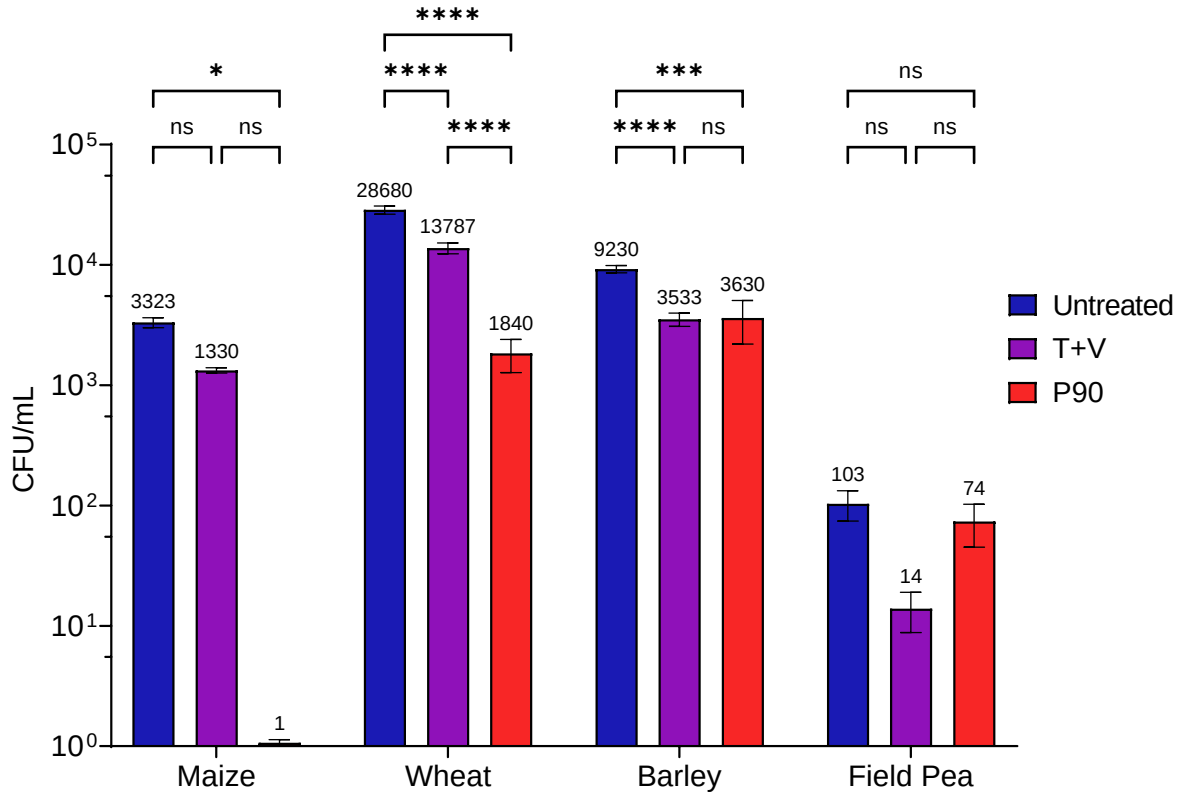


Figure 5-1. Two-way ANOVA and Tukey's multiple comparisons of colony-forming unit counts per grain type and treatment on a log scale. Data is presented as mean ± SEM. Abbreviations: T+V (Tumbler + vacuum); P90 (90-minute plasma); ns (non-significant); *p<0.05; ***p<0.001; ****p<0.0001.

Additionally, the data suggests that the naturally present fungal load of Untreated seeds varies between grain types. Surprisingly, wheat grains had the highest number of colony-forming units with 27,745% more than field pea, 763% more than maize and 211% more than barley. The food quality wheat grains appeared to be consistent in colour, shape, and size, ruling out a visible heavy infection. Instead, it was speculated that morphological features on the grain surface may promote fungal colonisation. As seen in Chapter 4, wheat has a wrinkled embryo, a ventral crease, and a brush, all of which may allow for the accumulation of fungal spores in these shelter-like features. It may be more difficult for spores to adhere to the rounded surfaces of field pea. Likewise, the maize pericarp over the endosperm is rather smooth. Only the pedicle and dent structures may provide refuge for spores. Should this concept be accurate,

grain surface features possibly play a role in the efficacy of plasma-treatment on inactivating fungal pathogens.

These initial trials set the foundation for the subsequent experiments within this chapter and Chapter 8. A series of research questions were developed to address whether morphological features can harbour pathogens on the grain surface and how plasma exposure time influences fungal colonies. These will be systematically investigated in the following sections.

5.2.3.3 Fungal identification

The identification to genus of fungal colonies cultured from the extraction process sought to evaluate the efficacy of the extraction method. Untreated plates from three grain types were further incubated following the colony-count process. Cello tape flag preparations, made on day 10 after inoculation, revealed at least five genera of fungal pathogens extracted from grain surfaces including *Aspergillus*, *Fusarium*, *Penicillium, Pyrenophora* and *Rhizopus*. All contained species that are known to be grain pathogens which may have downstream implications for human and animal health if consumed. The mycotoxigenicity of *Aspergillus, Fusarium* and *Penicillium* species as post-harvest grain contaminants is well-documented (Alshannaq and Yu, 2017; Cotuna et al., 2021; Guan et al., 2021; Muñoz et al., 2011; Pitt et al., 2012; Ponts, 2015; Torres et al., 2019) and may be of concern when considering concentration of CFU/mL found on Untreated wheat grains in the previous section. Overall, these results indicate that the techniques devised in section 5.2.2.4.1 and optimised in 5.2.2.4.2 are compatible with a diverse group of post-harvest pathogens.

5.2.4 Summary

This initial study involved the development of methods to extract and culture the extant fungi on grain surfaces. A diverse assortment of culturable grain pathogens were isolated and identified to gain an understanding of the compatibility of the methods with

multiple fungal genera and provide an insight into the pathogens occurring on South Australian grown grain. This series of experiments also explored the efficacy of 90-minute plasma treatment in reducing colony-forming units across multiple grain types, and how this may be related to the tumbling and vacuum process. In maize, wheat and barley, plasma treatment resulted in significant reductions in the colony-forming units of extant seed surface pathogens. However, the effect of the vacuum on the potential pathogen removal was not clear. It is also unclear why the concentrations of colony-forming units varied so greatly between grain types. Imagery in Chapter 4 suggested that grain morphological features may play a role in the effects of plasma on the seed surface. The same principles possibly contributed to the inactivation of spores on the seed surface as structures on the grain potentially shield microbes from plasma etching. Further studies are required to determine if seed surface features play a role in microbial shielding through the identification of fungal colony locations on the grain surface. Additionally, experiments are needed to untangle the relationship between T+V and plasma treatment. The following section seeks to address these concepts.

5.3 Development of an assay to determine the relationships between fungal colony location and plasma exposure time

5.3.1 Introduction

The SEM micrographs in Chapter 4 allowed one to visualise both the surface geography and the alteration of superficial features on grains which was caused by plasma treatment. This led to a series of questions about the removal of grain structures, such as buzz-cutting the wheat brush, and how this might impact spore position and viability. A simple well-plate assay was developed to uncover the location of fungal spores on the grain surface and determine if increasing plasma exposure time influenced hyphal growth sites. The aim was to untangle the relationships

between grain type, treatment conditions and colony locations that were confounded in the previous experiment. Using optical bottom well-plates, grains were encased in water agar to provide an adequate medium for hyphal growth without increasing vigour. Each well was divided into three-dimensional quadrants and visually assessed for locations of hyphal growth under a stereoscope. Scoring data were collected and analysed to understand the interactions between grain species, microbe positioning and plasma exposure.

5.3.1 Materials and Methods

5.3.1.1 Grain treatment

Maize, wheat, and field pea were selected as model species in this trial. Grains were divided into eight treatment aliquots of Untreated, T+V, P15, P30, P45, P60, P75 and P90 plasma treatments. The plasma treatment time series was performed using protocols established in Chapter 3.1.2.2. T+V and Untreated samples followed procedures in Chapter 3.1.2.3 and Chapter 3.1.2.4, respectively.

5.3.1.2 Well-plate preparation

Water agar was prepared following protocols in Chapter 3.3.1.3 and 500 µL or 1000 µL was pipetted into 12-well and 24-well sterile well plates (Nunc™, non-treated), respectively. Due to the size differences in grain, 2 x 12-well plates were prepared for each treatment in maize and field pea, and 1 x 24-well plate for wheat treatments. Once water agar media had cooled, a single grain was added to each corresponding well, embryo side up, using forceps sterilised between each seed. Additional water agar was cooled to 50 °C and added to each well until all surfaces of the grain were covered. The amount varied slightly depending upon individual differences in grain size and shape. Again, plates were cooled under a laminar flow hood prior to sealing with cling film (Glad). Plates were randomised in trays and left to incubate at 25 °C,

12hr/12hr light cycle for 48 hours. This process was repeated for maize, wheat, and field pea.

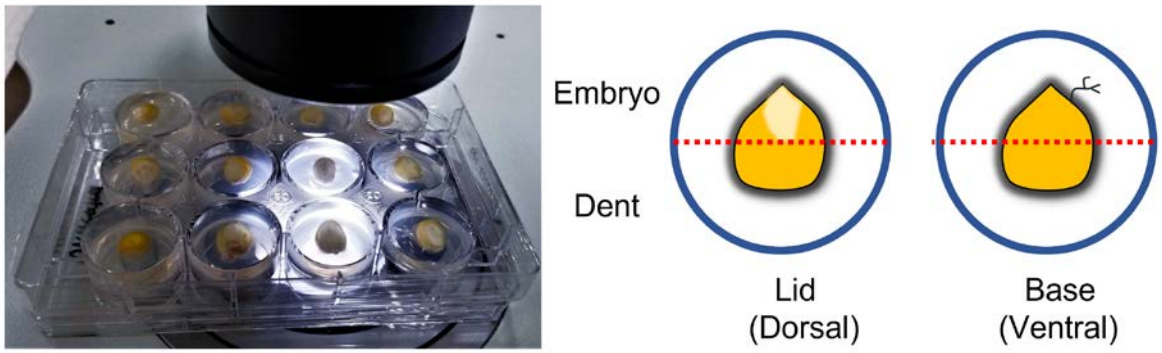


Figure 5-2. Well-plate assay quadrant diagram. Dorsal and ventral faces were viewed from the lid and base of the plate. Embryo and dent/brush quadrant were imagined as a line drawn roughly half-way across the grain.

5.3.1.3 Quantification of hyphal colonies

After 48 hours, all well-plates were inspected under a stereoscope (Olympus SZX10). Each well was divided into four quadrants based on dorsal, ventral, embryo, and dent/brush locations (Figure 5-2). Visible sites of hyphal growth were recorded with respect to the position within the well quadrant or grain morphological feature. Four counts were taken for each well with 96 counts in total for each treatment. This process was repeated at 72 and 96 hours to ensure the quantification of fungal colonies displaying hyphal growth.

5.3.1.4 Data analysis

All data analysis was completed in GraphPad Prism 9.0.0. One-way ANOVA with Tukey's multiple comparison tests were performed for each treatment to determine the significance of locations for each grain type. Two-way ANOVA and Tukey's multiple comparison tests investigated the interaction between plasma time points and location. Data were expressed as mean ± standard error of the mean. Significance was accepted at $p<0.05$.

5.3.2 Results and Discussion

This series of experiments was developed to test the relationship between plasma treatment time and fungal colony location on two cereal grains. Data were not collected for field pea due to grain swelling disrupting the media and rendering quantification impossible, a potential pitfall of this novel method.

5.3.2.1 Maize

In maize, the plasma exposure time had a strong effect on the visible number of hyphal colonies after 96 hours of incubation (Figure 5-3). A trend of significant reductions in pathogen counts at all locations were found between Untreated and T+V, T+V and P15, and also between P15 and P30. After 30 minutes of plasma treatment, the difference between treatments is minimal. Hyphae were still present until the 90-minute time point when complete fungal inactivation occurs. T+V treatment significantly impacted the number of visible hyphae however plasma treatment produces a stronger effect.

It is interesting to note that the Untreated maize grains had significantly more hyphal colony counts at the dent than at the embryo. The reverse is true for T+V and P15 treatment, which had significantly more colonies visible at the embryo. This may be linked to morphological features of the maize grains. On Untreated grains, the concave nature of the dent may allow more spores to collect in this region as compared to the embryo. The combination of vacuum and chemical etching processes of plasma treatment likely reduced the numbers and viability of the spores at the dent. It is speculated that the higher colony counts at the embryo of T+V and the shortest plasma exposure may be related to the rough edges where the grain separated from the cob, as well as the elongated and wavy pedicel cells (Figure 5-4). It is thought these structures may provide a small amount of shelter to fungal spores from plasma weathering. After 30 minutes of treatment, the weathering effects of plasma may alter

the surface structure to a point where it can no longer act as a refuge. SEM micrographs of the P90 grain pedicel region were much smoother than their Untreated counterparts.

5.3.2.1 Wheat

The location and number of visible hyphal colonies on wheat grains was very different to maize (Figure 5-3). No consistent trends were found between treatments, suggesting that plasma exposure is much less effective at deactivating fungi on the surface of wheat. These results were contrary to the log 2 reduction of colony-forming units seen in section 5.2.3.2. Numerous factors may have contributed to these confounding results, including varying numbers of extant spores on the grain surface. Future inoculation trials with known amounts of pathogens may be useful in untangling this problem and are addressed in section 5.4.

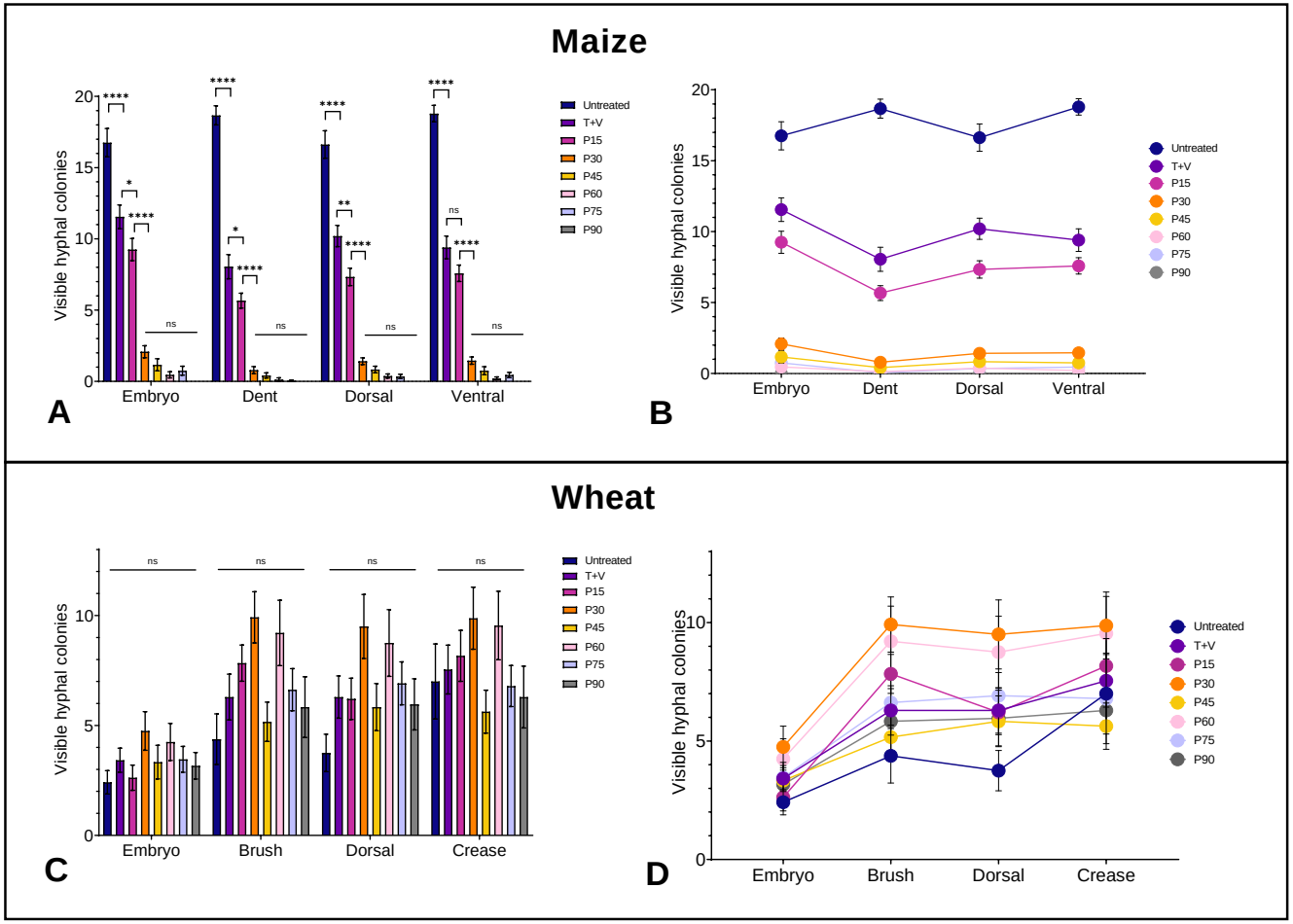


Figure 5-3. Comparisons of the number of visible hyphae and location after a 96-hour incubation for each grain type and treatment via two-way ANOVA with Tukey's multiple comparisons test. Data is presented as mean ± SEM; n = 24. (A, C) display the means of visible colonies at each location. (B, D) provide a different visualisation of the same data. Abbreviations: T+V (Tumbler + vacuum); P15 (15-minute plasma); P30 (30-minute plasma); P45 (45-minute plasma); P60 (60-minute plasma); P75 (75-minute plasma); P90 (90-minute plasma); ns (non-significant); *p<0.05; **p<0.01; ****p<0.0001.

The location of fungal colonies on wheat grain appears to be linked to treatment, with the lowest number of colonies near the embryo. Untreated, T+V, P15, P30 and P60 grains had significantly more colonies at the crease, than at the embryo. Additionally, P15, P30 and P60 had more colonies at the brush than at the embryo. There were no significant differences in location in P45, P75 and P90 treatments. This suggests that fungal colonies naturally aggregate toward the protective structure of the crease, which acts as a hidey-hole, protecting spores from the environment. SEM micrographs of Untreated wheat grains in Figure 5-5 illustrate the brush, crease, and embryo surface topography. Changes induced during shorter plasma exposures may alter the balance of fungal spore location. By 75 and 90 minutes of exposure, the overall effects of location are minimal. Overall, there is a relationship between wheat surface features and the number of visible hyphal colonies.

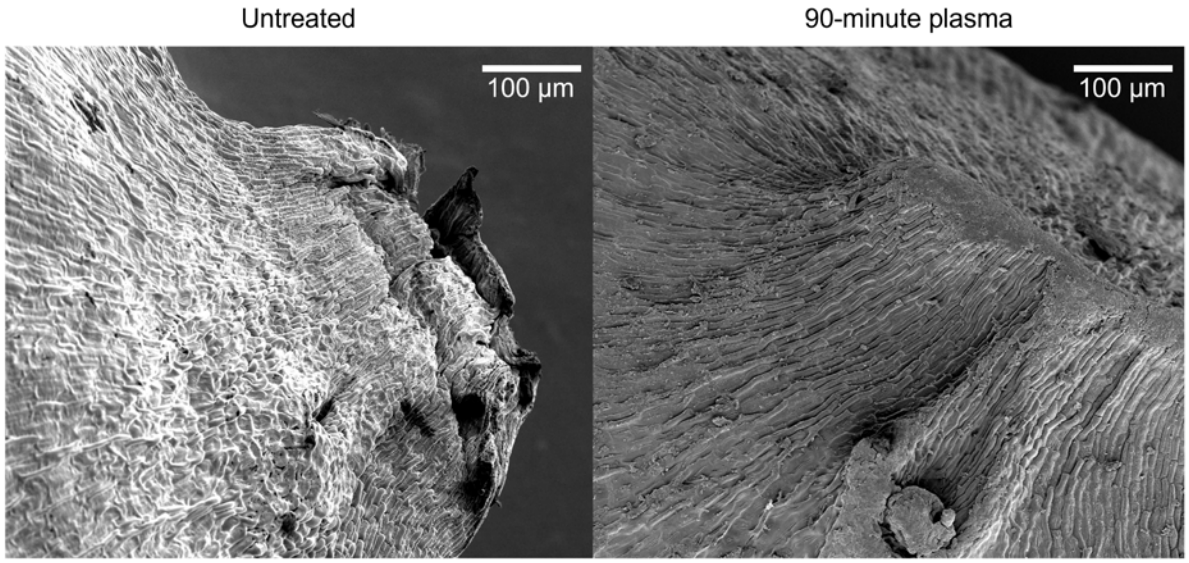


Figure 5-4. SEM micrographs of the maize pedicel, also known as the tip cap. It is speculated that the rough features of this part of the grain may provide shelter for fungal spores. By 90 minutes of treatment, the pedicle appears to be weathered and smooth.

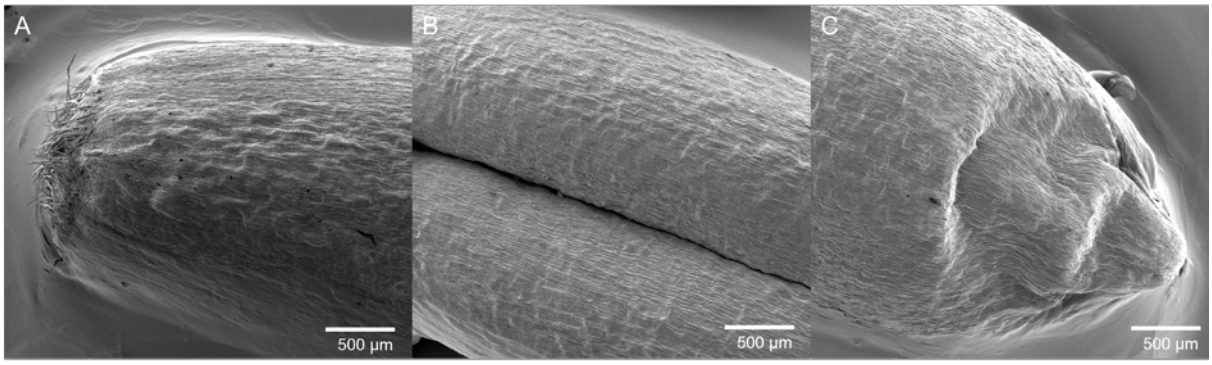


Figure 5-5. SEM micrographs of wheat grain surface features. (A) a dorsal view of the brush. (B) a ventral view of the crease. (C) a dorsal view of the embryo.

5.3.3 Summary

This experiment required the development of a simple assay to determine the natural distribution patterns of microbes across the surface of grains, and how this changes with increasing plasma exposure times. The findings indicate that microbial load and location may vary due to species and grain morphological features. In maize, there were more microbes associated with the embryo than other regions. In wheat, fungal colonies concentrated near the crease. However, prolonged plasma exposure altered this dynamic, reducing the effect of location. Moreover, the effects of all plasma exposure times on wheat fungal spore deactivation were negligible. In contrast, maize displayed a clear reduction curve; hyphal colonies decreased as plasma exposure time increased. By 90 minutes of plasma treatment, no visible hyphal colonies could be detected across the four quadrants in all 24 maize grains. The lack of data collection on field pea due to media disruption from grain swelling demonstrated a drawback of this novel method. The contrasting grain models require further experimentation to determine the efficacy of plasma treatment. The inoculation with known concentrations of pathogens, followed by treatment with a time series of plasma exposures may begin to untangle the enigmatic relationship between microbial concentrations, plasma exposure time and grain type.

5.4 The impact of the duration of plasma exposure on grain inoculated with fungal pathogens

5.4.1 Introduction

The initial results in section 5.2 suggested that 90 minutes of plasma exposure decreased the number of viable colonies of extant fungi on the grain surface. However, the use of extant microbes may not be generalisable to other systems worldwide where considerable variation in the types and number of fungal colonies initially present may make it difficult to predict the benefits of plasma. Additionally, results in 5.3 indicated that microbes on maize and wheat had different responses to plasma exposure times. This led to questioning whether a critical time window of plasma exposure could be established for each grain type. A systematic study was designed applying a time course of plasma exposures to grains inoculated with controlled numbers of a single pathogen.

Three grain types were selected because of their contrasting surface features: field pea, maize, and wheat. Grains were autoclave-sterilised and matched to a fungal pathogen. As *Aspergillus, Penicillium* and *Fusarium* genera are considered the most important pathogens of post-harvest grain due to their prevalence worldwide and mycotoxigenicity (Agriopoulou et al., 2020; Sharma and Bhandari, 2014; Solanki et al., 2019), one species from each of these genera was chosen. Synthetically high levels of inoculum were added to grains prior to treatment with one of eight different plasma exposure times. It is unlikely that microbial loads of 10^6 and 10^7 will be encountered in grain for human and animal consumption (as indicated in Figure 5-1 above). However, the high levels of inoculum were selected to test the full capabilities of the plasma system and aimed to tease apart relationships between exposure, grain type and pathogen species.

5.4.2 Materials and Methods

5.4.2.1 Plate preparation

Half-strength PDA plates (360 per independent experiment) were prepared following protocols described in Chapter 3.3.1.2.

5.4.2.2 Grain sterilisation prior to inoculation

250 g of grain was poured into a 500 mL glass beaker and thrice wrapped in aluminium foil. The layer of foil touching the flask was perforated to allow volatile components to leave the flask and condense on the outer layers of foil. Wrapped beakers were autoclaved for 17 minutes at 121 °C on a dry cycle then removed and left to rest overnight on the bench. The following day, the beakers were returned to the autoclave for a second cycle and left to rest overnight. Finally, the process was repeated for a third cycle to ensure any residual microbes would not survive the thrice autoclaving process. Once the grain cooled to laboratory temperature, it was transferred to a laminar flow where grain was decanted into sterile 120 mL specimen jars (Technoplas).

5.4.2.3 Fungal extraction buffer preparation

Extraction buffer was created immediately prior to microbe extractions following protocols listed in Chapter 3.3.2.

5.4.2.4 Inoculum preparation and grain inoculation

5.4.2.4.1 Maize inoculated with *Aspergillus flavus*; ATCC 204304

5.4.2.4.1.1 Culture preparation

A slope culture of *Aspergillus flavus* was kindly donated by Dr Sarah Kidd. Single spore cultures were grown on ½ PDA plates at 25 °C, 14h/10h light cycle for 10 days prior to inoculation.

5.4.2.4.1.2 Grain inoculation

Under post-harvest conditions, *A. flavus* spores can be transferred during the mechanical mixing of infected grains with the rest of the grain lot (Magan et al., 2003). A dry inoculation method was created to simulate these conditions. Plates with 10-day-old colonies, roughly 80 mm in diameter, were inspected under a stereoscope (Olympus SZX10) to ensure conidia development (Figure 5-6). Three plates were selected and transferred to a laminar flow. Lids were removed and placed upside down. 30 g of maize grain was poured into the lid. The base was replaced, and the plate was sealed with cling film. The plate was vigorously agitated for one minute to mix grain and conidia and left to rest for three minutes. This was repeated twice. Second and third plates were prepared with grain following the same protocols for a total of three plates with a combined 90 g of inoculated grain.

Using a sterile paper funnel, spore-covered grain was poured from the plates into a 120 mL sterile specimen jar (Technoplas). Jars were rolled back and forth to ensure thorough mixing of the grains from all three plates. 15 g of inoculated grain was transferred to a sterile 50 mL tube as the Untreated control. The remaining 75 g of grain was left in the 120 mL jar until plasma treatment.

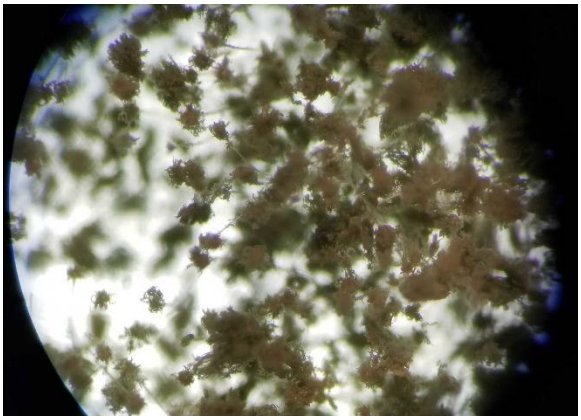


Figure 5-6. *Aspergillus flavus* culture with visible conidiophores and conidia ready for inoculation.

5.4.2.4.2 Field pea inoculated with *Penicillium chrysogenum*

5.4.2.4.2.1 Pathogen isolation

It was decided that one pathogen used in experimentation should be isolated from commercially grown, food quality samples. Fungi, speculated to be a species of *Penicillium*, were observed colonising psyllium grains in scanning electron microscope micrographs (see Chapter 4.3.1.1). To isolate this pathogen, three 1 g aliquots of psyllium grains were sprinkled across three ½ PDA plates and incubated for four days at 25 °C, 14h/10h light cycle. Plates were inspected under a phase contrast compound microscope (Nikon, Eclipse Ci-L) to visually identify *Penicillium*-like conidiophores and conidia following descriptions in Kidd et al., 2016. Any colonies appearing to resemble *Penicillium* were marked with a pen on the bottom of the plate. Using aseptic technique, 5 x 5 mm squares of marked colonies were transferred to fresh ½ PDA plates and incubated for five days at 25 °C, 14h/10h light cycle. Again, plates were inspected and any colonies resembling *Penicillium* were sub-cultured via the removal of 5 x 5 mm squares from the colony fringe and subsequent transfer to fresh ½ PDA plates.

A single plate with a vigorous colony was selected and submitted to the Molecular Diagnostics Centre (MDC) at the South Australia Research and Development Institute (SARDI). DNA was extracted from culture using a proprietary MDC method.

Universal primers were used to sequence fungal DNA in the Internal Transcribed Spacer (ITS) (Curran et al., 1994). Polymerase chain reaction (PCR) amplicons were sent to the Australian Genome Research Facility (AGRF) for sequencing. ITS sequences were interpreted by Dr Sarah Kidd, Head of the National Mycology Reference Laboratory, SA Health, Adelaide, Australia, to be *Penicillium chrysogenum* (the sequence is available in Appendix S2). *P. chrysogenum* is an extremely common airborne fungi with worldwide distribution and is relevant to both agriculture and food production due to mycotoxigenicity and spoilage (Rogawansamy et al., 2015).

5.4.2.4.2.2 Culture preparation

Single spore cultures of *P. chrysogenum* were grown on ½ PDA plates at 25 °C, 14h/10h light cycle for 10 days prior to inoculation (Figure 5-7).

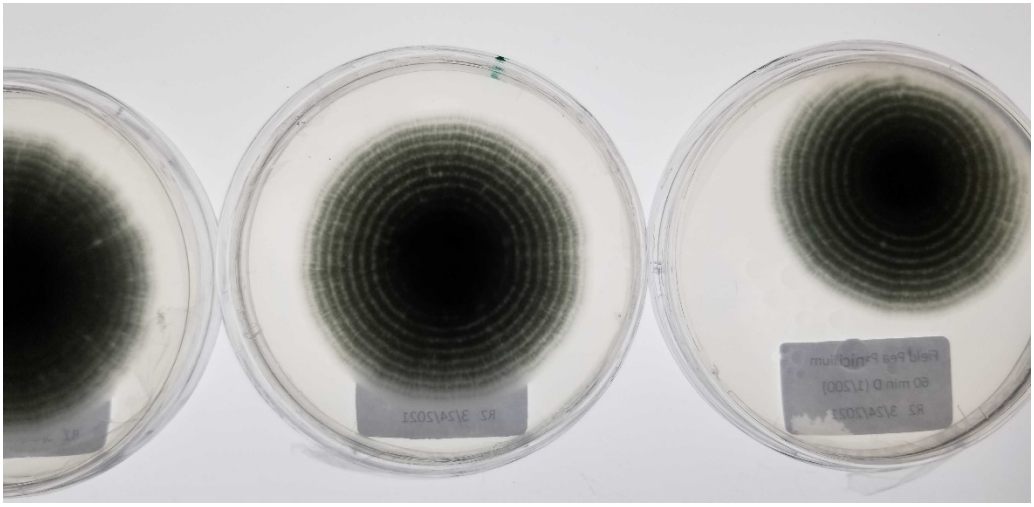


Figure 5-7. Single spore cultures of *Penicillium chrysogenum*.

5.4.2.4.2.3 Grain inoculation

P. chrysogenum contamination of post-harvest grains often occurs through the mechanical mixing of infected grains with uncontaminated grains, much like *A. flavus* (Nopsa et al., 2015). The dry shaking methods established in section 5.4.2.4.1.2 for *A. flavus* were followed using plates with 80 mm diameter, 10-day-old *P. chrysogenum* colonies from single-spore culture. Following inoculation, a 15 g aliquot of grain was transferred to a sterile 50 mL tube as the Untreated control. Another 15 g aliquot was set aside in a 50 mL tube for T+V treatment. The remaining 60 g of grain were left in the 120 mL specimen jar until plasma treatment.

5.4.2.4.3 Wheat inoculated with *Fusarium graminearum*; SARDI reference number 6894

5.4.2.4.3.1 Culture preparation

A freeze-dried *Fusarium graminearum* culture was donated by SARDI and grown on ½ PDA. Subcultures were prepared by removing 5 x 5 mm squares from the outer

edge of the original culture placing them in the centre of fresh ½ PDA plate. Ten subcultures were grown for 14 days at 25 °C, 14h/10h light cycle prior to inoculation.

5.4.2.4.3.2 Grain inoculation

Fusarium infections in the field and post-harvest generally occur via hyphal colonisation of grain (Torres et al., 2019). To accurately simulate colonisation conditions, a hyphal growth inoculation technique was developed. Six plates with 50 mm diameter, 7-day-old *Fusarium graminearum* colonies were selected based on salmon pink colour and fluffy hyphal growth. Under a laminar flow, plates were opened, and 35 g of sterile wheat was poured onto each plate. The plates were agitated to ensure an even spread of grain, sealed with cling film (Glad), and incubated for 10 days to allow colonisation of the grain (Figure 5-8).

After ten days, three plates were selected with the most filamentous hyphal growth across the grain. Under a laminar flow, the grain was gently disturbed with a scalpel blade then poured into a sterile 120 mL specimen jar. Any grain adhered to the media was left behind. The jar with the combined sample was rolled back and forth to mix the grain. Inoculated grain was treated and divided into Untreated control, T+V and plasma treatment aliquots as described in section 5.4.2.4.2.3.

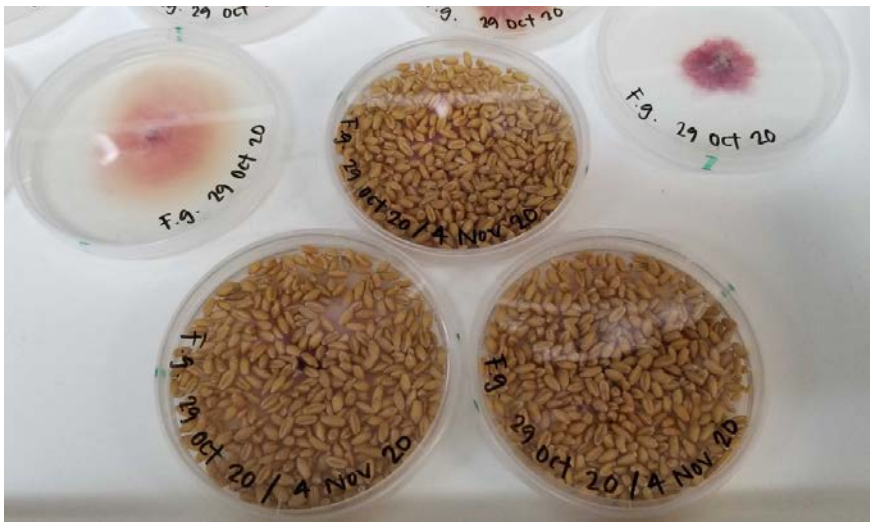


Figure 5-8. Sterile wheat added to *Fusarium graminearum* cultures for hyphal colonisation.

5.4.2.5 Experimental treatment

5.4.2.5.1 Untreated

Untreated grains were stored in sterile 50 mL tubes on the laboratory bench until extractions occurred, approximately four hours later.

5.4.2.5.2 T+V

A sterile 500 mL powder flask was prepared and the 15 mL aliquot of T+V grain was poured into the centre of the flask. A 90-minute treatment was conducted following protocols depicted in Chapter 3.1.2.3. The T+V method was only used in the *Penicillium* experiments. Treatments were stored in sterile 50 mL tubes until extractions occurred following all grain treatments, approximately two hours after T+V treatment.

5.4.2.5.3 Plasma treatment time series

A time series was developed for each grain type/pathogen combination. Combinations were limited to eight treatments due to the logistics of preparing 360 plates per experiment, in one day. All time trial treatments were prepared following protocols established in Chapter 3.1.2.2. *Aspergillus*-inoculated maize treatments included Untreated, P15, P30, P45, P60, P75, P90, and P105 treatments. *Penicillium*-inoculated field pea treatments were Untreated, T+V, P15, P30, P45, P60, P75 and P90. *Fusarium*-inoculated wheat experiments could not be completed for reasons described in the Results and Discussion section (5.4.3). Treatments were stored in sterile 50 mL tubes until extractions occurred, typically less than one hour after the completion of treatment.

5.4.2.6 Microbe extractions

Fungi were extracted from the surfaces of grains following protocols described in Chapter 3.3.3.

5.4.2.7 Haemocytometer quantification

Haemocytometer counts were performed following methods in Chapter 3.3.4.

5.4.2.8 Dilutions

Dilution factors were calculated based off haemocytometer estimates and varied with each experiment due to differences in inoculum load. A pre-determined volume of extracted liquid was pipetted into a sterile 10 mL tube with an appropriate amount of autoclaved Milli-Q water. A table of all dilutions is available in Appendix S3.

5.4.2.9 Plating technique

The plating of extracted fungi followed methods established in Chapter 3 3.6.

5.4.2.10 Cell viability Assay

A cell viability assay was conducted on an aliquot of remaining liquid from each extraction tube. Dilutions of stains were prepared 10 minutes prior to use and kept in the dark. 50 µL of extraction liquid was placed in the centre of a glass microscope slide. 10 µL of Syto™ 9 Green fluorescent nucleic acid stain (Invitrogen; diluted 1:1000 in Milli-Q water from stock) was pipetted into the liquid. A single drop of NucRed Dead™ (TO-PRO-3 iodide; Invitrogen) was added to droplet. Finally, 10 µL of SCRI Renaissance 2200 (SR2200; Renaissance Chemicals; diluted 1:2000 in Milli-Q water) was added to the slide and mixed thoroughly with a pipette. The mixture was incubated for 20 minutes prior to the addition of a coverslip and visualisation on a Zeiss Axio Imager M2. Viability assays were performed on one experiment per pathogen.

5.4.2.11 Colony-forming unit quantification

Colony-forming unit counts were conducted following methods described in Chapter 3.3.7.

5.4.2.12 Experimental replication and statistical analysis

Experiments on each species of pathogen and the associated host were conducted in triplicate. Individual experiments and combined triplicate data were analysed in GraphPad Prism 9.0.0. All CFU counts of zero were transformed to one for ease of statistical analysis on a logarithmic scale. Two-way ANOVA with Tukey's multiple comparisons were performed to compare all three experiments within a series. Additional one-way ANOVA with multiple comparisons analyses were carried out for the third and final experiment (Experiment 3) of the series for each pathogen/grain system. It was also necessary to compare treatments via t-tests with Welch's correction for differing standard deviations. Data were expressed as mean ± standard error of the mean. Significance was accepted at $p<0.05$.

5.4.3 Results and Discussion

Inoculation experiments were performed to gain a better sense of the capabilities of the plasma tumbler apparatus and how increasing exposure times may influence fungal spore viability. This involved the procurement and culture of three important post-harvest fungal pathogens of grain, followed by plasma treatment, fungal extractions, and culture. Due to the complexity of this series of experiments, not all inoculations were successful. The following section contains a brief description of the challenges faced during these experiments followed by results and discussion of the experimental series for each pathogen and grain host.

5.4.3.1 Variations in inoculum

The complex ecological networks in the field and throughout the supply chain mean that infection can occur through a variety of methods at multiple steps during processing. Methods of inoculation were created to simulate common ways in which spores and hyphae are transferred throughout lots of grain. The amount of moisture in the system was also limited due to the use of a vacuum during plasma treatment. With

this in mind, the initial inoculum load of each biological replicate and experimental series varied due to the lack of uniformity in the inoculation process. Initial inoculum loads were measured via haemocytometer and calculations of CFU/mL for three replicate trials are shown in Table 5-2. Results indicate that the enumerated colonies differed between experiments. This is most likely due to the nature of the inoculation processes. As the initial and final inoculum were within the same order of magnitude, the variations were not considered detrimental to subsequent statistical analysis.

Table 5-2. Variations within initial haemocytometer counts and final colony-forming units from plates. The means of haemocytometer counts of the initial inoculum load are compared to the means of the haemocytometer counts from Untreated extraction solutions.

Pathogen	Experiment Number	Initial CFU/mL	Final CFU/mL
Penicillium chrysogenum	1	2.79×10^7	1.21×10^7
	2	1.87×10^7	2.36×10^7
	3	1.78×10^7	5.61×10^7

Further discrepancies between the haemocytometer counts and final CFU/mL concentrations may be associated with the methods of spore extraction from the grain. Spores tightly adhered to the grain surface may not have been released into the buffer solution. Consequently, this may have led to lower spore counts once the solution was cultured. Moreover, each biological replicate consisted of a composite of 1 g of grain (roughly five maize grains, seven field peas and 26 wheat grains). The heterogeneity of the grain, their small numbers, and level of inoculum present on the surface of individual grains may have contributed to further variations in haemocytometer counts.

5.4.3.2 Spore/hyphal fragment viability assay

Spore/hyphal fragment viability was investigated to determine if another source of variation is present. The cell-impermeant stain, NucRed Dead™ fluoresces in far-red

when bound to DNA. As it can only enter cells with compromised cell membranes, it is often used in tandem with the cell permeant Syto™ 9 nucleic acid stain to distinguish between live and dead nuclei. SR2200 is a general fungal cell wall stain which binds to β-1,3 and β-1,4 linkages and has a similar spectra to DAPI (Harris et al., 2002; Renaissance Chemicals, 2021). In combination, the three fluorophores can highlight fungal cell walls, live and dead nuclei. This may be particularly helpful when trying to distinguish between viable hyphal fragments and multi-septate spores.

For the purposes of this research, the florescent cell viability assay was ineffective. Untreated samples contained many viable and unviable spores and hyphal fragments. However, no live cell nucleic acid (Syto™ 9) signals could be detected in the plasma-treated samples of the six plasma exposure times. It was unclear if this was an artefact or signalled high levels of inactivation. Furthermore, the SR2200 stain did not bind well with spore cell walls. Hyphal fragments were highly visible which indicated that differences in cell wall composition between hyphae and spores may have been a factor. Noothalapati et al., 2016, discussed the predominance of α-glucan in spore cell walls which may explain the lack of fluorescence as SR2200 binds to β linkages. For the above reasons, the assays were conducted on one experiment per fungal species but were not continued throughout the study. Instead, the number of colony-forming units were used as a measure of viability.

5.4.3.3 Colony-forming unit quantification

Colony-forming unit quantification from plates were the most valuable data sets collected in these experimental series. Multiple dilutions per sample allowed for up to nine technical replicates per biological replicate. This created a robust data set which could be analysed independently or compared to the other two experiments in the triplicate set. Technical issues with the nature of this experiment will be further discussed in Chapter 9.2.

5.4.3.3.1 *Penicillium chrysogenum* on field pea

The combined two-way ANOVA of data from all three independent *Penicillium* inoculated field pea experiments revealed clear trends across the treatments (Figure 5-9). While each experiment had a different inoculum load, all graphs followed a similar trend to the maize well-plate experiment data set described in 5.3.3.1. Dramatic log reductions in colony forming units were evident between all Untreated and plasma-treated time points. The P90 treatment in Experiment 1 yielded a 10^4 reduction. Improvements in the precision of dilutions led to a 10^6 reduction in Experiment 2 and a 10^7 reduction in Experiment 3. Both Experiment 2 and 3 consistently yielded less than ten CFU/mL for P90 treatments.

One-way ANOVA with Tukey's multiple comparisons test were performed on the data set from Experiment 3 (Figure 5-9, B). It was necessary to perform additional Welch's t-tests between each treatment as the high values in the Untreated controls skewed the results for lengthy treatments. The Welch's t-tests in combination with the large numbers from synthetic inoculation loads (Appendix S4), made it possible to deduce the impact of T+V treatments in comparison to each plasma time point and the Untreated control. Tumbling in a vacuum for 90 minutes had a significant effect on the number of colony-forming units present on plates. T+V plates had a mean of 1.05 x 10^7 less colony-forming units than the Untreated controls. This may be associated with the removal of spores loosely attached to the grain surface caused by the vacuum or from mechanical damage. While this treatment displayed a significant log reduction from the control, the larger effect was caused by plasma treatment.

A more detailed look at Experiment 3 (Figure 5-9, B) highlights the impact of treatment time. The relatively short 15-minute treatment produced a mean reduction of 1.17 x 10^7 colony-forming units when compared to Untreated and 1.29 x 10^6 when compared to T+V. The 30-minute window appears to be a key interval in the reduction of CFUs

as there was no significant difference between each of the means after the 30-minute treatment time point.

Despite the lack of statistical differences between P30, P45, P60, P75 and P90 treatments, there was a biological difference. The comparison between 10^2 CFUs to less than 10^1 is important in terms of spore deactivation. The presence of hundreds of viable spores may lead to mould growth, grain devaluation, grain contamination with mycotoxins and other downstream effects. This research is seeking to establish timepoints of complete spore deactivation. The 90-minute time point came very close with only five colonies counted across all experiments and dilutions. Due to the dilution factors associated with calculating CFUs/mL, this presented a mean of 7.47 CFUs/mL associated with that treatment.

It was hypothesized that extending plasma treatment to a 105-minutes may be enough to capture the critical exposure time when all conidia are inactivated. However, it was not logistically possible to add a ninth treatment to the experimental design. Statistically valid experiments conducted by a solo researcher were completed in a 16-hour working day. Adding another treatment would push the boundaries of work health and safety. Therefore, in subsequent experiments it was decided to replace the T+V treatment with the extended 105-minute plasma treatment. The three *Penicillium* experiments established that plasma treatments caused significantly greater spore deactivation than the T+V treatments. Accordingly, the omission of the T+V treatment was not detrimental to the aim of inactivating all spores.

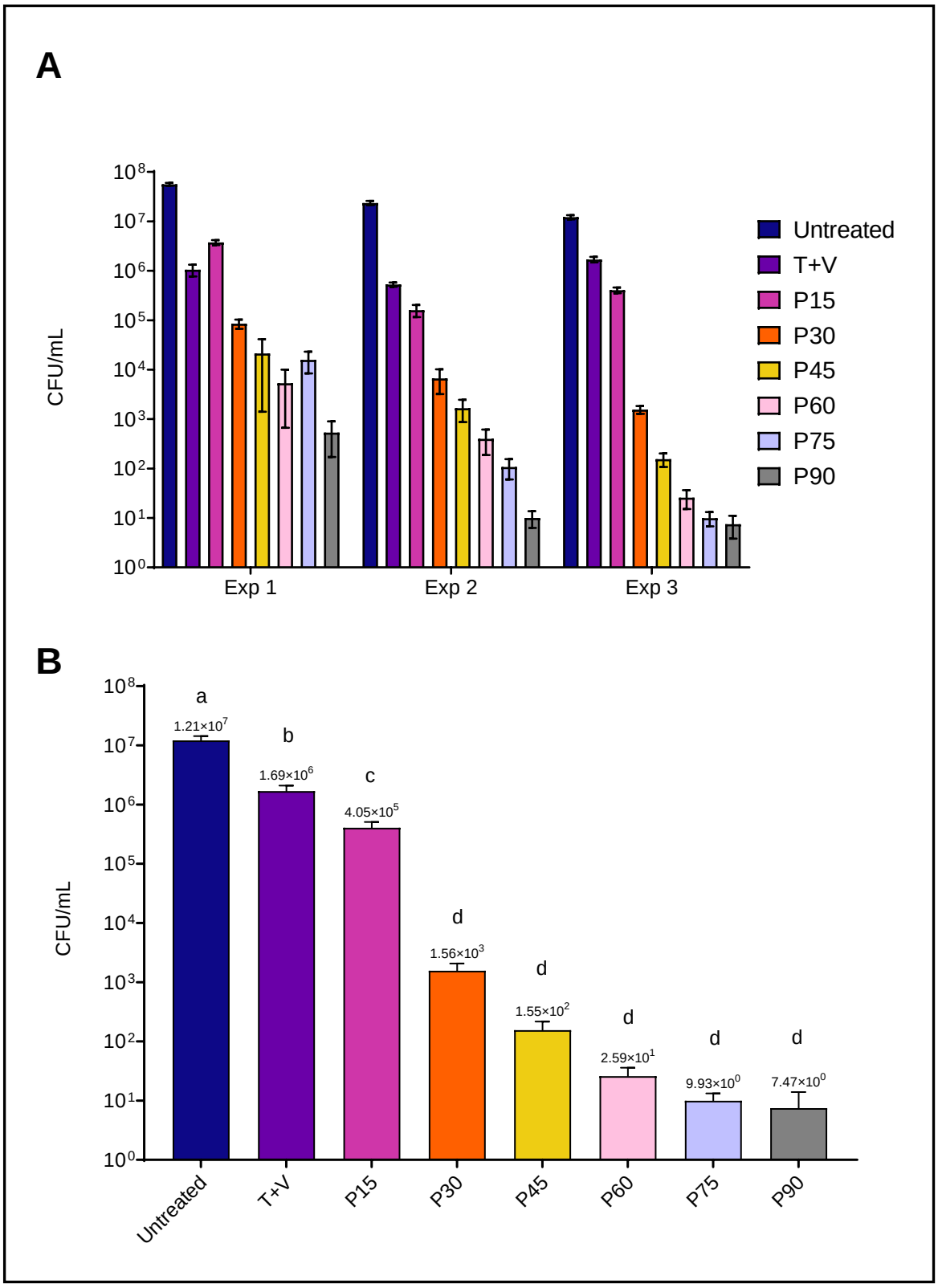


Figure 5-9. Field pea inoculated with *Penicillium chrysogenum* and subjected to varying durations of plasma exposure. Data is presented as mean ± SEM with significance accepted at $p<0.05$. (A) Results of each of the three independent experiments. (B) Detail of the results from Experiment 3 using one-way ANOVA comparing the means from each treatment. Letters indicate differences between means analysed in a stepwise comparison with Welch's t-test. Abbreviations: T+V (Tumbler+Vacuum); P15 (15-minute plasma); P30 (30-minute plasma); P45 (45-minute plasma); P60 (60-minute plasma); P75 (75-minute plasma); P90 (90-minute plasma).

5.4.3.3.2 *Aspergillus flavus* on maize

Much like the field pea experiments, the *Aspergillus flavus* colony forming units decreased in an exponential fashion over time (Figure 5-10). Yet, the critical time point appears to be different in each pathogen/grain system. The logarithmic reduction was more gradual in the *A. flavus*/maize system where it took up to 75 minutes to lower pathogen loads to less than 10^4 colony-forming units. While a decreasing trend was clear, there was no statistical difference between P75 and P105 treatments. By the 105-minute time point, no colonies could be counted, which may indicate that all spores were deactivated.

It is speculated that the slower reduction in *A. flavus* fungal spore viability, as compared to *P. chrysogenum*, may be related to the biological differences between these unrelated groups of fungi. The conidia of both species are small (2.4 to 5 µm) and globular with an outer layer of rodlets and thick double cell wall with a layer of melanin (Garcia-Rubio et al., 2020; McCoy et al., 1971). Despite these general similarities, the composition of the fungal cell walls is different (Lima et al., 2019). Plasma reactions with the cell wall surface chemistry will likely differ between the species, leading to variations in the effect of plasma exposure.

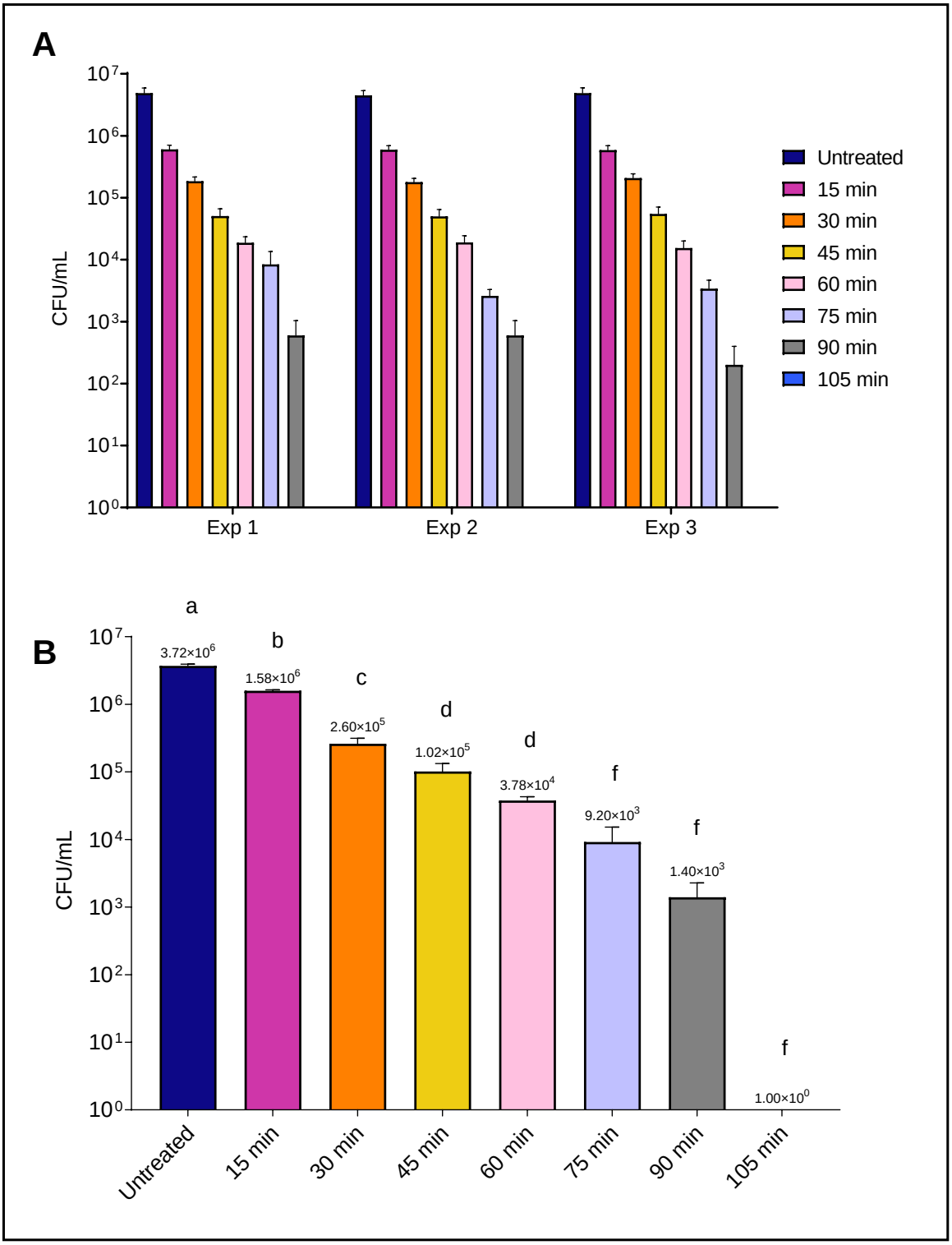


Figure 5-10. Maize inoculated with *Aspergillus flavus* and subjected to varying durations of plasma exposure. Data is presented as mean ± SEM with significance accepted at $p<0.05$. Note: T+V treatment was omitted from this experimental series and substituted with a 105-minute plasma exposure time. (A) Results of each of the three independent experiments. (B) Detail of the results from Experiment 3 using one-way ANOVA comparing the means from each treatment. Letters indicate differences between means analysed in a stepwise comparison with Welch's t test. Abbreviations: T+V (Tumbler+Vacuum); P15 (15-minute plasma); P30 (30-minute plasma); P45 (45-minute plasma); P60 (60-minute plasma); P75 (75-minute plasma); P90 (90-minute plasma).

5.4.3.3.3 *Fusarium graminearum* on wheat

The trials using wheat inoculated with *Fusarium graminearum* could not be carried out to completion as the inoculation method was not conducive to plasma treatment. It was found that growing the mycelium over wheat grains resting on an agar base increased the moisture content of each grain. When the moist inoculated grain was transferred to a flask and prepared for plasma treatment, it required a longer vacuum pump-down (a minimum of 30 minutes) to decrease the moisture content and establish a steady initial pressure. Not only did this confound comparisons with the other grain/pathogen systems by adding another unintentional vacuum treatment dimension into the experiment, but the higher partial pressure in the flask also made it tricky to strike the plasma after each time point. These complications were unsuitable for a rigorous, controlled experiment and therefore the *Fusarium*/wheat plasma time trial series were abandoned. Instead, a different method shown in the next section (5.5) was developed for growing mycelium over the top of wheat grain to understand how hyphal fragments behave after plasma treatment.

5.4.4 Summary

The robust series of experiments described in this chapter systematically established the relationship between plasma exposure time and the deactivation of fungal pathogens on the surface of grains. The statistical differences between each time point were robustly evaluated using several experimental and technical replicates that required more than 1080 plates per grain/pathogen series. It was discovered that each species of grain and its paired pathogen responded differently to plasma treatments. Generally, plasma exposures of 90 minutes or longer were effective for *Penicillium chrysogenum* and *Aspergillus flavus* spore inactivation. The tumbling and vacuum conditions within the PT system significantly reduced the number of colony-forming units. Yet, it was plainly evident that the chemical etching processes of plasma

treatment are responsible for the reduction of the fungal pathogen load to essentially zero.

The experimental design posed in this section challenged the PT system with synthetically high microbial loads. Promisingly, it was demonstrated that the plasma tumbler can deactivate small globose, echinulate conidia; *Aspergillus flavus* ranging from 3.5 to 4.5 µm; *Penicillium* spp. roughly 3.0-6.0 µm (Hedayati et al., 2007; Reponen et al., 2001). However, it was clear that modifications to the inoculation design are required to understand how plasma interacts with mycelial networks. Furthermore, the results of the well-plate assays in section 5.3.3, revealed differences between maize and wheat regarding the inactivation of extant microbes following P90 treatment. A much broader survey of grain types and pathogen species is necessary to understand how plasma interacts with different pathogens and their host grains.

5.5 Evaluation of plasma treatment for the deactivation of five inoculated pathogens on five grain types

5.5.1 Introduction

In the previous experiment, it was established that plasma exposure times of 90 minutes or more are optimal for the near complete deactivation of *P. chrysogenum* and *A. flavus* on the surfaces of field pea and maize. This led to speculation that 90-minutes is a critical time window and may be capable of deactivating a range of pathogens on the surfaces of multiple grain types. To examine this concept, all five model grain types were assembled: maize, field pea, wheat, barley, and psyllium. Associated fungal pathogens were selected based on their prevalence in the local South Australian region, mycotoxigenicity, and varying methods for inoculation. *Aspergillus flavus* and *Fusarium graminearum* are prevalent in stored grain and capable of producing highly problematic mycotoxins (Pitt et al., 2012). *Penicillium chrysogenum* is a common

mycotoxigenic environmental pathogen and was isolated from psyllium grain. *Bipolaris sorokiniana* is a pathogen of barley and wheat, often transmitted via seed (Al-Sadi, 2021). Finally, the frequently seed-borne *Didymella pinodes* is one of the causal agents of Ascochyta blight of field pea (Davidson, 2012). Together, these fungi represent a range of agriculturally important seed-borne and post-harvest pathogens which contribute to billions of dollars of loss every year (see Chapter 1 for detailed descriptions).

Inoculation methods were created to simulate field or post-harvest conditions in which fungal transmission is likely to occur. The dry inoculation methods outlined in section 5.4.2.4 were utilised for the often air-borne, small, globule conidia of *A. flavus* and the *P. chrysogenum.* A liquid inoculum was trialled for the single-septate *D. pinodes*, despite hesitancy in the previous experiments to create a liquid culture. *B. sorokiniana* sporulation occurred directly on the grain following mycelial colonisation. *F. graminearum* was again used as a model to assess the viability of hyphal fragments. New methods were adopted to ensure seed moisture content did not rise too high during the inoculation steps, preventing the prolonged vacuum exposures and plasma striking issues faced in section 5.4.3.3.3. As the previous experiments established the relationship between T+V and both the control and plasma treatment groups, it was no longer considered necessary to include that treatment within these trials. Inoculated grains were divided into an Untreated control group or 90-minute plasma treatment group.

In Chapter 4, scanning electron microscopy techniques were used to explore differences to the grain surface following 90-minute plasma treatment. However, it was unknown how fungi present on the grain surface would be impacted by plasma treatment. To address this gap in knowledge, inoculated grains were prepared and examined under SEM to understand how plasma interacts with various structures of

the five fungal pathogens. The striking images can be directly compared to colony-forming unit counts to create a broader understanding of how the PT system may be deactivating pathogens.

5.5.2 Materials and Methods

5.5.2.1 Grain sterilisation prior to inoculation

5.5.2.1.1 Maize, wheat, barley, and field pea

Procedures for grain sterilisation described in section 5.4.2.2 were followed for maize, wheat, barley, and field pea.

5.5.2.1.2 Psyllium

Due to the small size of psyllium grains (~ 3 mm) a sterile 50 mL polypropylene tube was used in lieu of a beaker. The tube was prepared by burning four 2 mm ventilation holes into the upper shaft of the tube with a soldering iron. 10 g of grain was added to the tube and the lid was sealed. The tube was then wrapped thrice in aluminium foil and followed autoclaving procedures listed in section 5.4.2.2.

5.5.2.2 Inoculum preparation and grain inoculation

5.5.2.2.1 Maize inoculated with *Aspergillus flavus*

5.5.2.2.1.1 Culture preparation

A. flavus culture preparation followed steps outlined in section 5.4.2.4.1.

5.5.2.2.1.2 Grain inoculation

Grain inoculation was performed following protocols established in section 5.4.2.4.1.

5.5.2.2.2 Barley inoculated with *Bipolaris sorokiniana*

5.5.2.2.2.1 Culture preparation

B. sorokiniana culture was donated by the SARDI Plant Health and Biosecurity Group in the form of inoculated barley grains. Three 1 g aliquots of grain were placed in sterile 10 mL tubes with 2 mL of extraction buffer. Grains were washed with buffer for five

minutes by gently rolling the tubes back and forth across the laminar flow bench. Grain and buffer poured onto full-strength PDA plates, sealed, and incubated for 10 days at 25 °C, 14h/10h light cycle. Ten 5 x 5 mm subculture squares were taken from the fringes of colonies and placed in the centre of plates with only 10 mL of full-strength PDA to ensure the thinnest spread of media across the plate, thereby reducing the amount of moisture available to barley grains. Subcultures were incubated for 10 days at 25 °C, 14h/10h light cycle prior to inoculation.

5.5.2.2.2.2 Grain inoculation

The technique developed for *Fusarium graminearum* inoculation in section 5.4.2.4.3 was used for *B. sorokiniana* to simulate a field and post-harvest-like infection via hyphal growth. Six plates with 50 mm diameter, 7-day-old *B. sorokiniana* colonies were selected. Under a laminar flow, plates were opened and 35 g of sterile barley was poured onto each plate. The plates were agitated to ensure an even spread of grain, sealed with cling film (Glad), and incubated for 14 days to allow colonisation of the grain (Figure 5-11).

After 14 days, three plates were selected with the most filamentous hyphal growth across the grain. Under a laminar flow, the grain was gently disturbed with a scalpel blade then poured into a sterile 120 mL specimen jar. Any grain adhered to the media was left behind. The jar with the combined sample was rolled back and forth to mix the grain. Inoculated grain was divided into even aliquots for Untreated and P90 treatment.

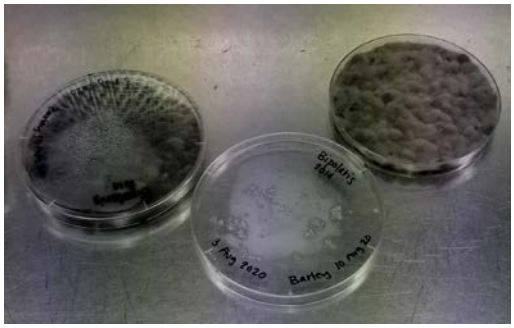


Figure 5-11. *Bipolaris sorokiniana* culture growing over the top of barley grains.

5.5.2.2.3 Field pea inoculated with *Didymella pinodes*

5.5.2.2.3.1 Culture preparation

Subcultures of 5 x 5 mm squares were taken from a single spore plate of *D. pinodes* donated by the SARDI Plant Health and Biosecurity Group and incubated under white light on full-strength PDA for 21 days at 25 °C, 14h/10h light cycle (Figure 5-12).

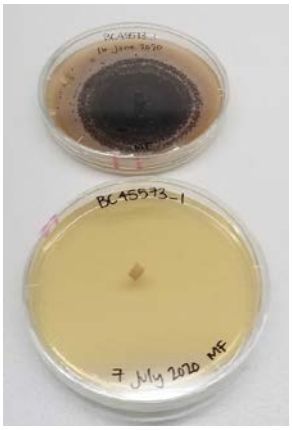


Figure 5-12. (Above) Original culture of *Didymella pinodes* donated by SARDI. (Below) Subculture taken from the original sample.

5.5.2.2.3.2 Grain inoculation

A liquid inoculum was created for *D. pinodes* to simulate the transfer of conidia via rain conditions near harvest, followed by a period of drying. Protocols were modified from Barilli et al., 2016 to suit this experiment. Three *D. pinodes* culture plates were opened in a laminar flow and 5 mL of extraction buffer (see Chapter 3.3.2 for preparation details) was added to each plate. The blunt side of a sterile scalpel blade was used to gently scrape spores from the surface of the gel and mix into the buffer. The liquid was removed with a pipette and transferred to a second plate. The process was repeated until the liquid contained spores scraped from all three plates. The inoculum was then poured into a sterile 50 mL tube containing 15 g of prepared field pea grain. The tube was rolled repeatedly across the laminar flow bench then placed on an orbital shaker for 20 minutes to ensure all grain was sufficiently coated with the inoculum.

At the conclusion of shaking, grain was poured onto sterile filter papers and left to dry in a laminar flow for two hours. Once dry, grain was portioned into two equal aliquots for Untreated and P90 treatments.

5.5.2.2.4 Wheat inoculated with *Fusarium graminearum*

5.5.2.2.4.1 Culture preparation

The preparation of cultures was conducted by repeated protocols developed in section 5.4.2.4.3.1.

5.5.2.2.4.2 Grain inoculation

The previous plasma-treated hyphal growth experiment failed due to the moisture content of the grain after inoculation. The protocols were adapted for use in 50 mL Mini Bioreactor tubes (Corning). Roughly 10 g portions of wheat grain were added to the bioreactor tubes. Using a pipette, 1 mL of sterile Milli-Q water was added to the grain to ensure a moisture content suitable for *Fusarium* growth. Tubes were rolled to disperse water throughout the grain. 1 x 1 cm squares of *F. graminearum*-covered agar were cut from the outer edges of 14-day old colonies grown on ½ PDA plates. These were placed mycelium side up along the side wall of the bioreactor tubes. Grain was gently rotated on top of the squares and incubated for 14 days.

Following incubation, bioreactor tubes were opened, and the semi-desiccated agar squares were removed. Grain from three tubes was poured into a sterile 120 mL specimen jar (Technoplas) and rolled back and forth to separate and mix grain. A 15 g aliquot of inoculated wheat grain was removed and placed in a sterile 50 mL tube as the Untreated control. The remaining grain was immediately transferred to the plasma reactor for P90 treatment.

5.5.2.2.5 Psyllium inoculated with *Penicillium chrysogenum*

5.5.2.2.5.1 Culture preparation

The cultures were prepared following protocols established in section 5.4.2.4.2.2.

5.5.2.2.5.2 Grain inoculation

Psyllium grain was selected for inoculation with *P. chrysogenum* due to the culture being isolated from this lot of grain. Grain inoculation followed protocols established in section 5.4.2.4.1.2 for *A. flavus* and used in section 5.4.2.4.2.3 for *P. chrysogenum* on field pea. Due to the small size of psyllium grain, roughly 2 g of sterile grain was poured onto each plate for a dry shaking method of inoculation. All inoculated grain was transferred to a sterile 50 mL tube. Roughly 3 g was then transferred to a fresh sterile tube as the Untreated control. The remaining 3 g was left in the first tube until plasma treatment.

5.5.2.3 Experimental treatment

Untreated grains were placed in a sterile 50 mL tube and kept on the laboratory bench for up to three hours prior to extraction. During this time, a 90-minute plasma treatment was performed following protocols in Chapter 3.1.2.1.

5.5.2.4 Microbe extractions

Extractions were performed as described in Chapter 3.3.3, except psyllium. Due to the small size of the grain, only 500 mg of grain was poured into five sterile tubes for biological replicates. Like all other systems, 2 mL of extraction buffer was added to each tube.

5.5.2.5 Haemocytometer quantification

Haemocytometer counts were completed using protocols described in Chapter 3.3.4.

5.5.2.6 Dilutions

Dilution factors were calculated based on haemocytometer estimates and varied with each experiment due to differences in inoculum load. A pre-determined volume of extracted liquid was pipetted into a sterile 10 mL tube with an appropriate amount of autoclaved Milli-Q water. A table of all dilutions is available in Appendix S5.

5.5.2.7 Plating technique

Plating of extracted fungi followed methods established in Chapter 3.3.6.

5.5.2.8 Colony-forming unit quantification

Colony-forming unit counts were calculated as described in Chapter 3.3.7.

5.5.2.9 Scanning electron microscopy

5.5.2.9.1 Fixative preparation

A custom fixative was designed to ensure the integrity of the pathogens on the surface of the grain, inspired by Hardham, 1985 and Qin et al., 2021. A 50 mM PIPES buffer (Piperazine-1,4-bis (2-ethanesulfonic acid); Sigma-Aldrich) was created and pH adjusted to 7.0 with NaOH. 2mM $CaCl_2$ and 10 mM sucrose were added to increase the osmotic potential of the solution. A combination of 4% paraformaldehyde (6% w/v aqueous solution, methanol free; Thermo Scientific) and 2% glutaraldehyde (25% w/v aqueous solution; Thermo Scientific) were added to ensure both quick and slower cross-linking. The buffer was stirred for two minutes then stored at 4 °C in the dark until use.

5.5.2.9.2 Sample preparation

5.5.2.9.2.1 *Didymella pinodes* and *Penicillium chrysogenum*

Following treatment, five inoculated Untreated and P90 field pea grains and ten psyllium grains of each treatment were set aside for microscopy. Within 24 hours of inoculation, inoculated grains were adhered to a 12.6 mm pin stubs (ProSciTech) with

carbon tabs. Edges of the grain were painted with graphite conductive adhesive (ProSciTech) to ensure a flush connection between the rounded grain surface and the stub. Samples were sputter-coated with platinum by Adelaide Microscopy, Frome Road, prior to imaging.

5.5.2.9.2.2 *Aspergillus flavus, Bipolaris sorokiniana, Fusarium graminearum* and *Penicillium chrysogenum*

Following treatment, five inoculated Untreated and P90 grains of each type were set aside for microscopy. Within 24 hours of inoculation, grains were placed in sterile 35 x 10 mm non-treated culture dishes (Nunc™). Fixative was added to each dish until the grains were fully covered. Dishes were wrapped in Parafilm® M (Amcor) and placed in a dark box at 4°C until COVID-19 restrictions were eased to allow for imaging (approximately five months). Once ready for processing, the fixative was removed from the dishes and a series of EtOH dehydrations were performed with three changes per concentration lasting ten minutes each. Concentrations were as follows: 70%, 80%, 90%, 100%. Once dehydrations were complete, grains were immediately placed in a Leica EM CPD300 Critical Point Dryer at Adelaide Microscopy, Waite Campus. Once dry, grains were adhered to 12.6 mm pin stubs (ProSciTech) with carbon tabs. Edges of the grain were painted with graphite conductive adhesive (ProSciTech) to ensure a flush connection between the rounded grain surface and the stub. Samples were sputter-coated with 5 nm platinum by Adelaide Microscopy, Frome Road, prior to imaging.

5.5.2.9.3 Imaging

All stubs were analysed at Adelaide Microscopy, Frome Road, with a FEI Quanta 450 FEG Environmental SEM at acceleration voltages of 5.0 kV for *B. sorokiniana* and *F. graminearum*; 10 kV for *A. flavus*, *D. pinodes* and *P. chrysogenum*.

5.5.2.10 Experimental replication and statistical analysis

A series of independent triplicate experiments were conducted for each grain type. All data analysis was conducted in GraphPad Prism 9.0.0. with CFU counts of zero transformed to one for statistical analyses on a logarithmic scale. Two-way ANOVA with Tukey's multiple comparison tests were performed to compare serial experiments within a species. Unpaired t-tests with Welch's correction were used to determine p-values between treatments within each experiment. Finally, the means of serial experiments across all species were compared with a two-way ANOVA, Tukey's multiple comparison tests and unpaired t-tests. Data were expressed as mean ± standard error of the mean. Significance was accepted at $p<0.05$.

5.5.3 Results and Discussion

This series of experiments was designed to explore the efficacy of the plasma tumbler on the deactivation of conidia and hyphal fragments of five economically relevant fungal grain pathogens paired with a specific host. The colony-forming unit counts derived from fungal pathogen extractions and culture were complemented with scanning electron micrographs to illustrate the effect of plasma treatment on fungal surface structures. The following sections are separated by fungal pathogen to ensure the seamless integration of CFU data sets and SEM imagery.

5.5.3.1 *Aspergillus flavus* on maize host

The combination of maize and *A. flavus* was repeated to ensure the methods established in section 5.4 continued to yield consistent data. Figure 5-13 demonstrates that in all three independent experiments, there were zero colonies present after 90 minutes of plasma treatment, yielding p-values of less than 10^{-6}. In other words, the plasma tumbler deactivated 99.999999% of *A. flavus* conidia on the surface of maize. The only variation between experiments can be found in Untreated CFU between

Experiment 2 and Experiment 3 with a mean difference of 802,000. Throughout the course of experimentation, methods were honed to produce consistent results.

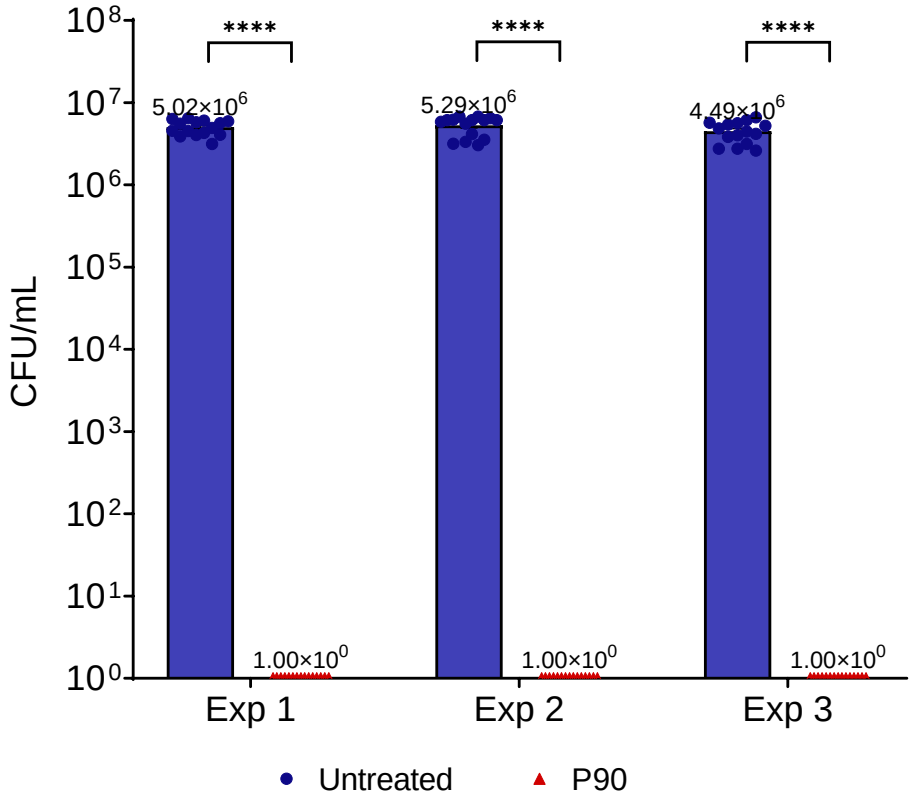


Figure 5-13. Data sets from three independent experiments with *Aspergillus flavus* on maize host following P90 (90-minute plasma) or Untreated control conditions. Individual values are plotted and bars present mean ± SEM; ****p<0.0001; n = 15.

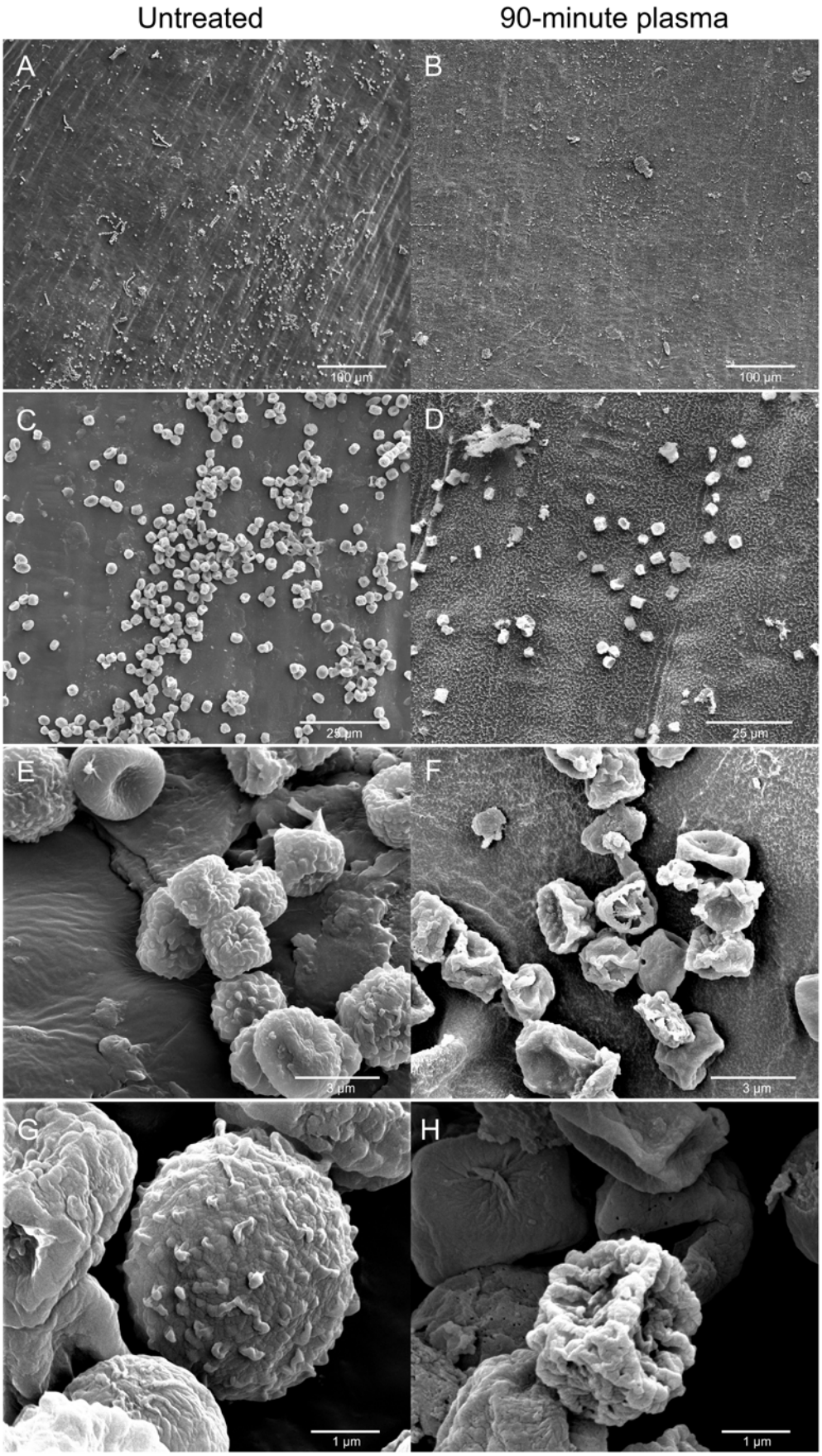


Figure 5-14. SEM micrographs of control and plasma treatments of *Aspergillus flavus* on maize grain. Images were captured of conidia on the maize pericarp surface over the endosperm; n = 3.

SEM micrographs of Untreated grains reveal the characteristic *A. flavus* globular conidia with rodlets covering the surface (Figure 5-14, A, C, E and G). Following plasma treatment, the shape of the conidia has been altered to resemble deflated balloons (Figure 5-14, F and H). Additionally, the fungal cell wall appears to be damaged in multiple areas. This indicates that the chemical etching processes of plasma treatment are eroding the conidia cell wall, which may be one of the deactivation mechanisms of action. The SEM images are similar to those captured by Dasan et al., 2016 on *A. flavus* inoculated hazelnuts treated with argon plasma. The differences between the present study and Dasan et al., 2016 are in the weathering of conidia surfaces. This study shows clear degradation of the fungal cell wall which supports the log 6 reductions in colony-forming units. This is likely due to variations in equipment, gas, and exposure times.

5.5.3.2 *Bipolaris sorokiniana* on barley host

During barley inoculations, the protocols established in 5.4.2.4.3.2 for *F. graminearum* were loosely followed to allow for the mycelial colonisation of the grain which, in turn, induced sporulation. It was assumed that the barley husk may act as a semi-permeable barrier and reduce grain moisture in this system in comparison to wheat. Additionally, modifications were made to the level of medium in the plates, with only 10 mL added, which was often not enough to cover the bottom of the entire plate. The success of this inoculation model is demonstrated in Figure 5-15 with colony-forming units of Untreated controls greater than 10^4/mL.

Colony-forming unit counts for *B. sorokiniana* were significantly reduced by plasma treatment throughout the experimental series (Figure 5-15). Plasma treatment was highly effective with p-values of 9×10^{-6}, $2.9 \times 10^{-5,}$ and less than 1×10^{-6}, respectively. The efficacy of plasma treatments on this species indicates that plasma is capable of deactivating robust, pigmented fungal conidia with a range of different morphologies,

including multiple septa. There were significant differences between Untreated groups across experiments, however, all plasma treatment groups gave essentially complete removal of pathogens, to the detection limit of the assay despite the higher fungal loads in Experiments 2 and 3. The nature of colony-forming unit calculations (see Chapter 3. 3.7 for equation) involves the multiplication of plate counts with a dilution factor. This means that a single colony present on a plate can give a CFU/mL value much higher than what was visualised. A dotted line has been added to the graph to demonstrate the variation between counting one colony on a plate, versus zero. Further discussion around the nature of colony-forming unit counts of under 30 can be found in Chapter 9.2.2. Regardless, the lack of difference between plasma treatment across the series demonstrates the efficacy of the system.

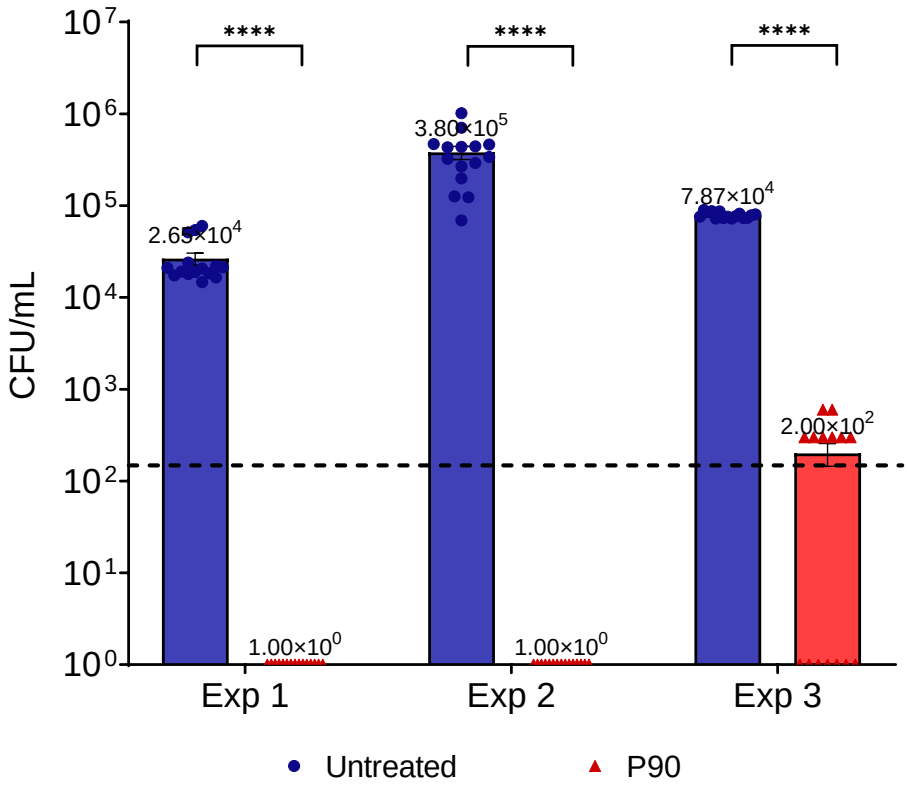


Figure 5-15. Experimental series of *Bipolaris sorokiniana* on barley host grain following P90 (90-minute plasma) or Untreated control conditions. Individual values are plotted with bar representing mean ± SEM; ****p<0.0001; n = 15. Dotted line indicates value for a single colony.

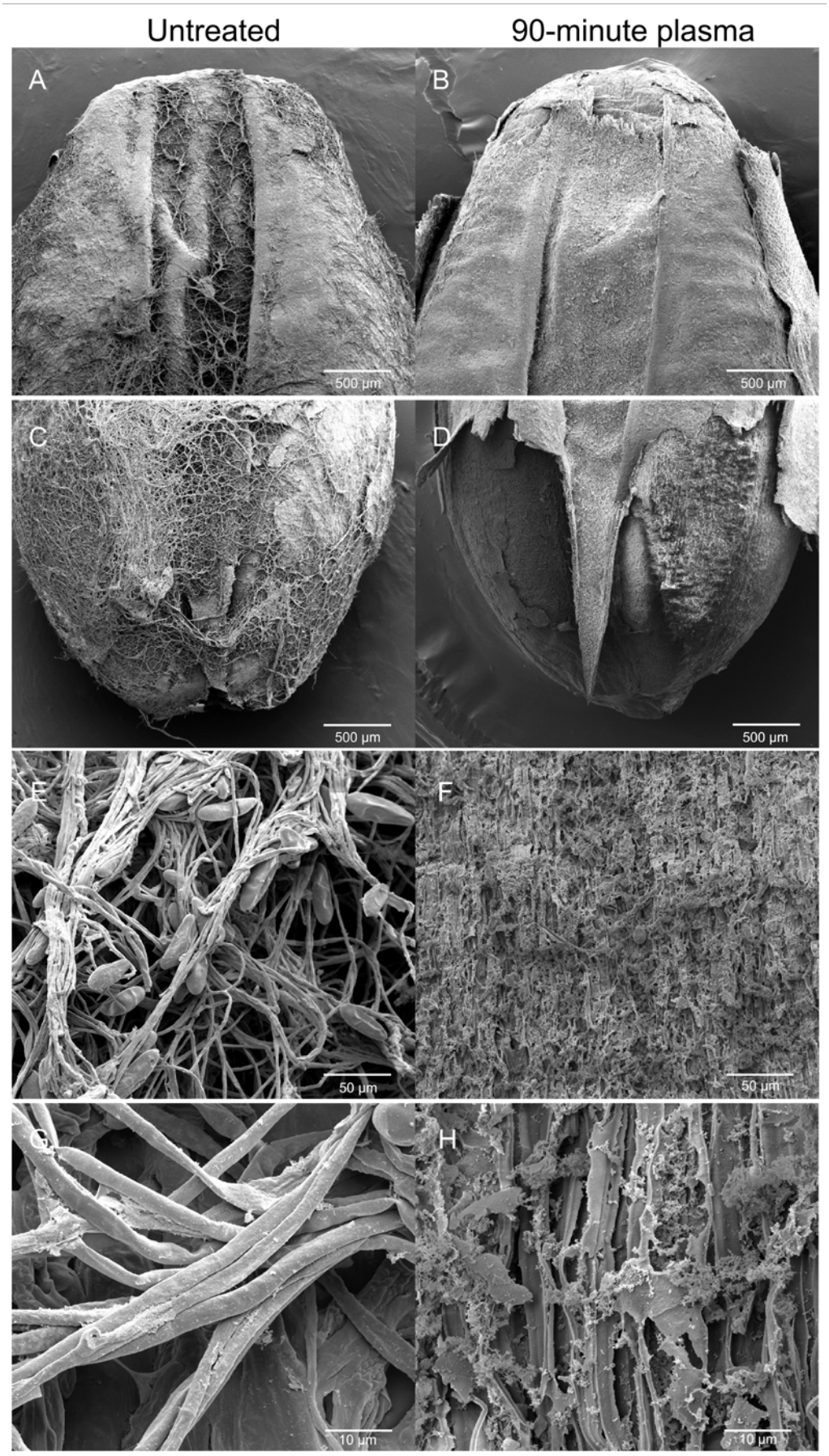


Figure 5-16. Barley grains inoculated with *Bipolaris sorokiniana*. Mycelial networks are clearly visible on Untreated grains and absent on plasma treatments. (A-B) Palea surface near the awn. (C-D) Palea surface near the embryo; n = 4.

The efficacy of plasma treatment is nowhere more apparent than in Figure 5-16. SEM micrographs of Untreated grains display a detailed mycelial network covering the barley surface. The elliptical, multi-septate conidia are visible in Figure 5-16, C. These structures were rendered unrecognisable following 90 minutes of plasma exposure. The entire mycelial network has been shredded during the chemical etching process and no conidia could be detected on any of the four plasma-treated replicates (Figure 5-16, B, D, F, H). The weathering effects of plasma most likely contribute to the near complete deactivation seen in the colony-forming unit counts. The impact of plasma exposure on the hyphae and conidia of *B. sorokiniana* is plainly evident.

5.5.3.3 *Didymella pinodes* on field pea host

In section 5.4, hesitancy to introduce a liquid inoculum was discussed. However, to simulate rain dispersal of spores, a method of applying a liquid-based inoculum, followed by immediate drying was introduced for *D. pinodes*. These conditions frequently occur under South Australian growing conditions (Davidson et al., 2012) and were not thought to influence conidium viability. Furthermore, it was speculated that the relatively slow water uptake rate of field pea would reduce the chance of elevated grain moisture content and associated problems with increased pressures and striking plasmas.

The use of a liquid inoculation method followed by air drying did not adversely impact the vacuum pressurization step prior to plasma strike. Instead, this method proved to be successful in securing high levels of inoculum to the grain surface (Figure 5-17). Untreated *D. pinodes* CFUs ranged between 10^5 and 10^6. The reduction in inoculum concentration with each subsequent experiment of 2.84×10^6 and 5.11×10^5, respectively, may be attributed to reduced sporulation after repeated subculturing of a mother single spore colony. Continually creating single-spore cultures was outside of the timeframe of this experiment and generally did not impact the outcomes of the trial

as the lowest concentration of 1.35 x 10^5 was still considered to be a synthetically high inoculum load. Unpaired t-tests between treatments in each experiment revealed discrepancies in statistical analysis. Repeated counts of zero or one are difficult to analyse and may result in skewed p-values. Nonetheless, there were strong levels of significance for each experiment with p-values of 1 x 10^{-6}, 2.8 x $10^{-3,}$ and 9.3 x 10^{-4}, respectively. Clearly, 90-minutes of plasma exposure impacts the viability of *D. pinodes* conidia.

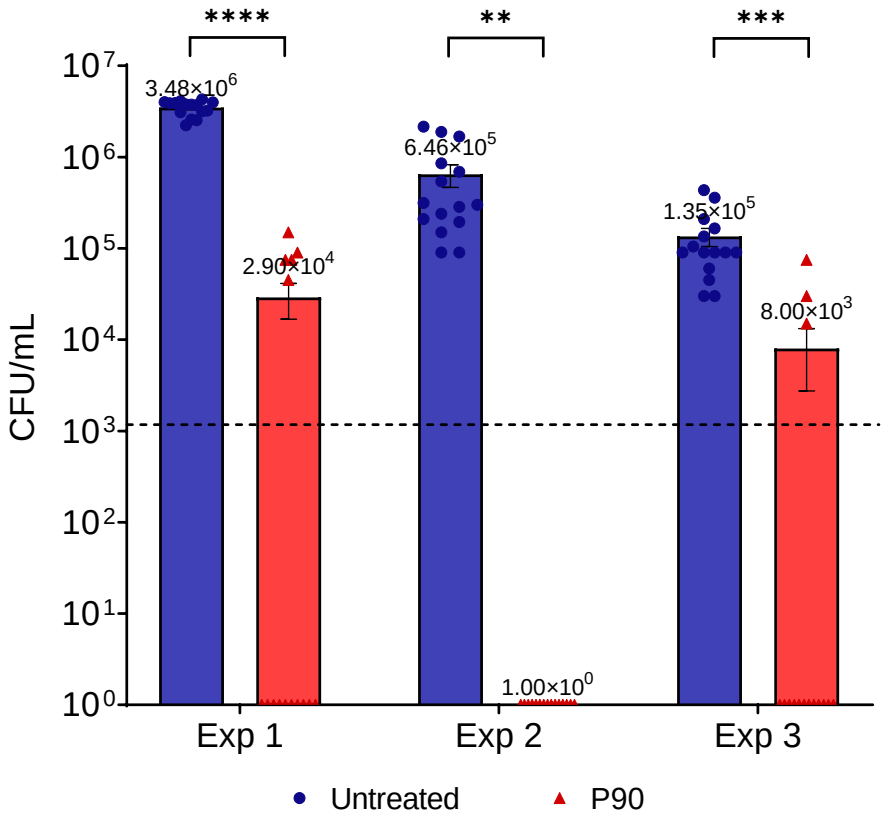


Figure 5-17. Experimental series of *Didymella pinodes* on field pea host treated with P90 (90-minute plasma) or Untreated control conditions. Individual values are plotted with bar representing mean ± SEM; ****p<0.0001; n = 15. Dotted line indicates value for a single colony.

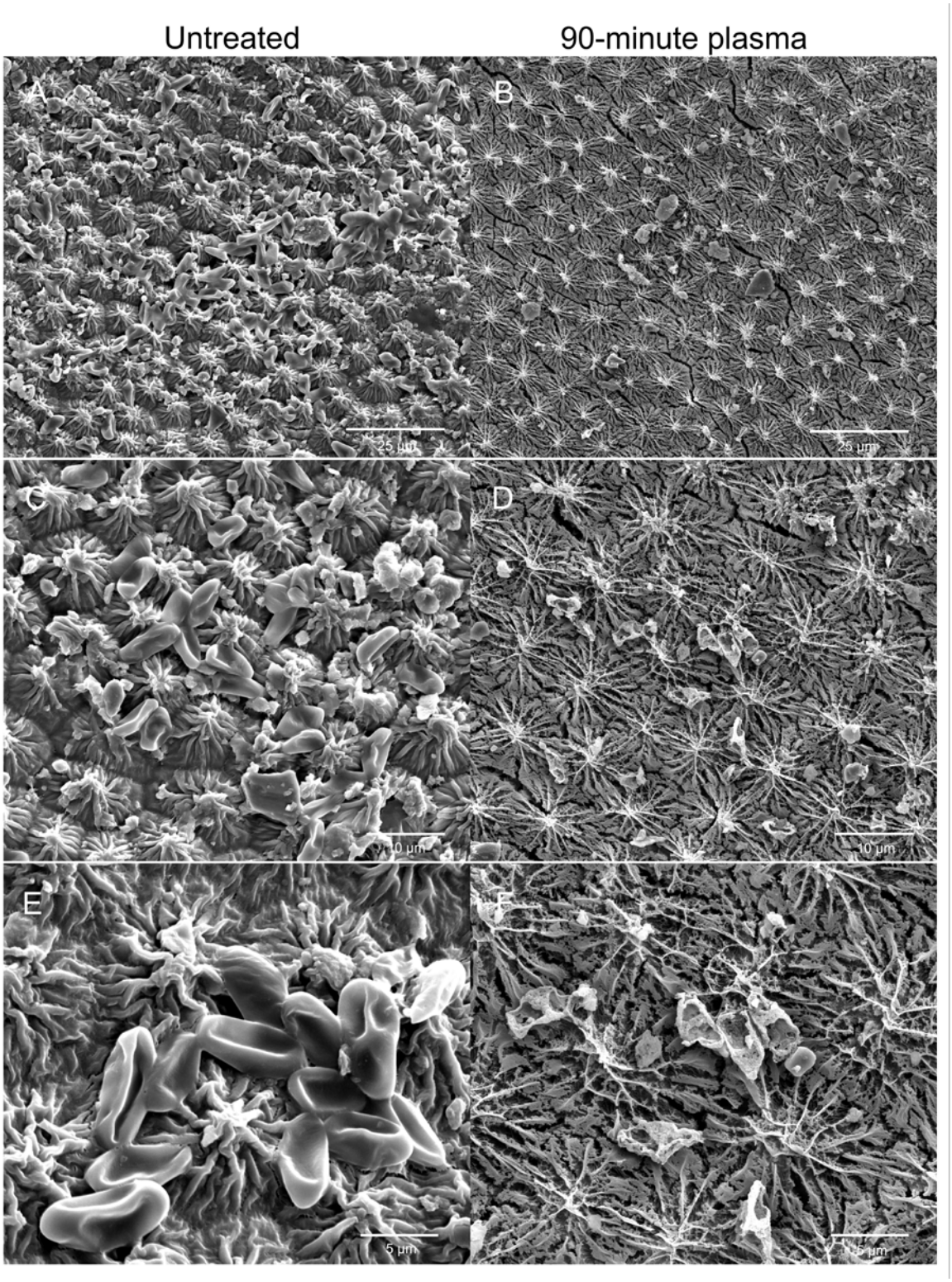


Figure 5-18.SEM micrographs of Untreated and 90-minute plasma-treated *Didymella pinodes* inoculated on field pea. Note: this was the first in the series of SEM screenings and spores were not prepared in fixative, dehydrated, or critically point dried prior to visualisation. n = 3.

The *D. pinodes* inoculated grains were the first in the experimental series to be screened under SEM, which requires a vacuum for operation. Field pea grains were not prepared in fixative, dehydrated or critically-point-dried prior to imaging. This

resulted in the deformation of conidia which had a deflated appearance on all Untreated controls (Figure 5-18, A, C, E). Except for dry psyllium, all subsequent inoculated grains for imaging were processed using methods developed and described in section 5.5.2.9.2.2 to preserve fungal surface structures. To prevent mucilage expansion on contact with the fixative solution, dry psyllium inoculated with *P. chrysogenum* was processed in the same manner as *D. pinodes*.

Despite the morphological artefacts induced by the negative pressure required for scanning at 10,000x magnification on the Quanta 450 instrument, the differences between treatments are evident (Figure 5-18, B, D, F). The fungal cell wall of *D. pinodes* has been completely eroded away during plasma treatment, exposing the intra-conidia structures, including the visible single septum. The complete destruction of the cell wall is likely the reason behind conidia deactivation. It is surprising any viable conidia persisted in Experiment 3 considering the extent of fungal cell wall damage.

5.5.3.4 *Fusarium graminearum* inoculated wheat

Following the failed attempts to treat *F. graminearum* inoculated grain with plasma in section 5.4, a different method was created using less moisture. Hyphae were successfully grown on grain using bioreactors and did not adversely impact the vacuum quality as in previous experiments. As expected, very few CFU in the Untreated controls grew from conidia. Upon inspection under a phase contrast compound microscope (Nikon, Eclipse Ci-L), a vast majority of the colonies grew from viable hyphal fragments. In Figure 5-19, the absence of plasma-treated colony-forming units in Experiments 1 and 3, and the average value below the limit of detection in Experiment 2, lends credit to the concept that plasma is capable of deactivating hyphae as well as conidia. It should be noted that only four colony-forming units in total were counted on plasma treated grain in Experiment 2 which led to the presence of two

values of 50 (refer to dotted line in Figure 5-19). Overall, the series of experiments on wheat were successful with unpaired t-tests yielding p-values of less than 1 x 10^{-6}.

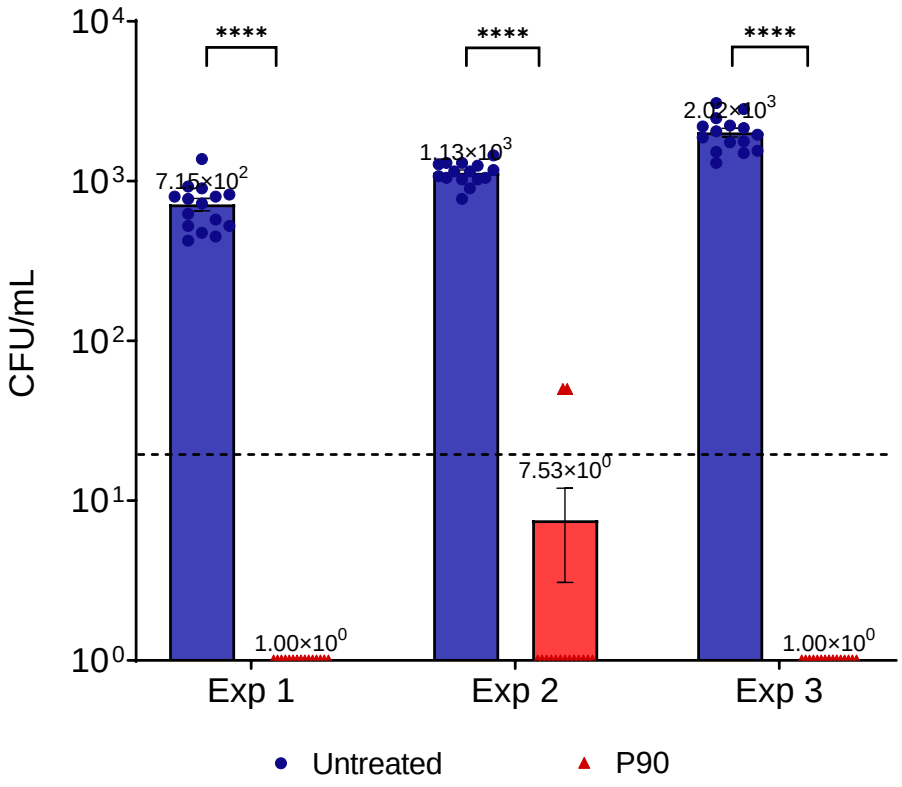


Figure 5-19. The results of three independent experiments on *Fusarium graminearum* inoculated wheat grains treated with P90 (90-minute plasma) or Untreated control conditions. Individual values are plotted with bar representing mean ± SEM; ****p<0.0001; n = 15. Dotted line indicates value for a single colony.

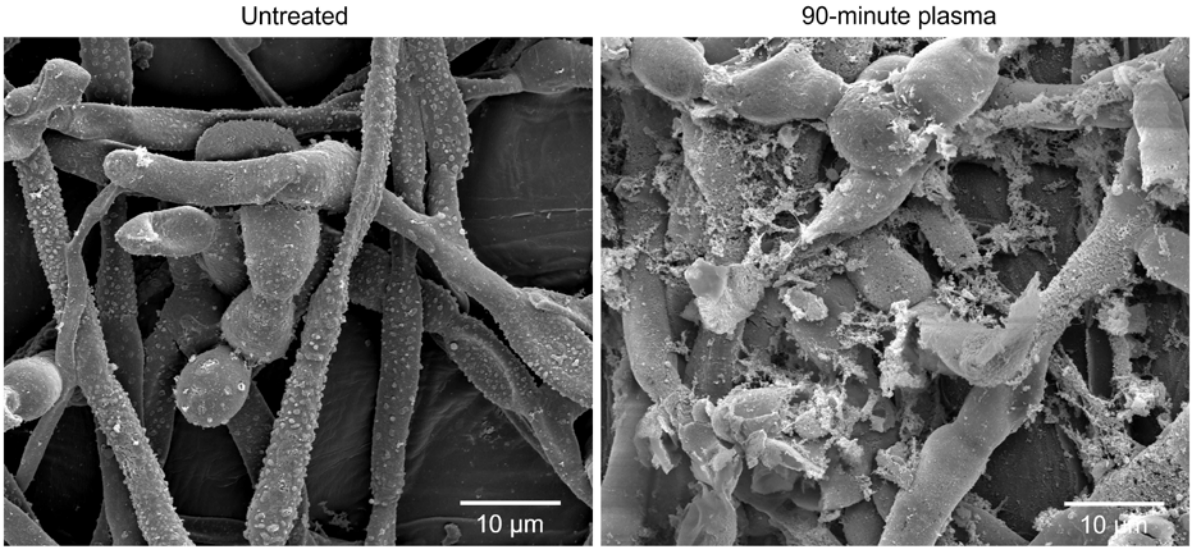


Figure 5-20. SEM imagery of what appear to be chlamydospores forming on the surface of *Fusarium graminearum*-inoculated wheat grains. The severely damaged remnant fungal structures are visible after plasma treatment.

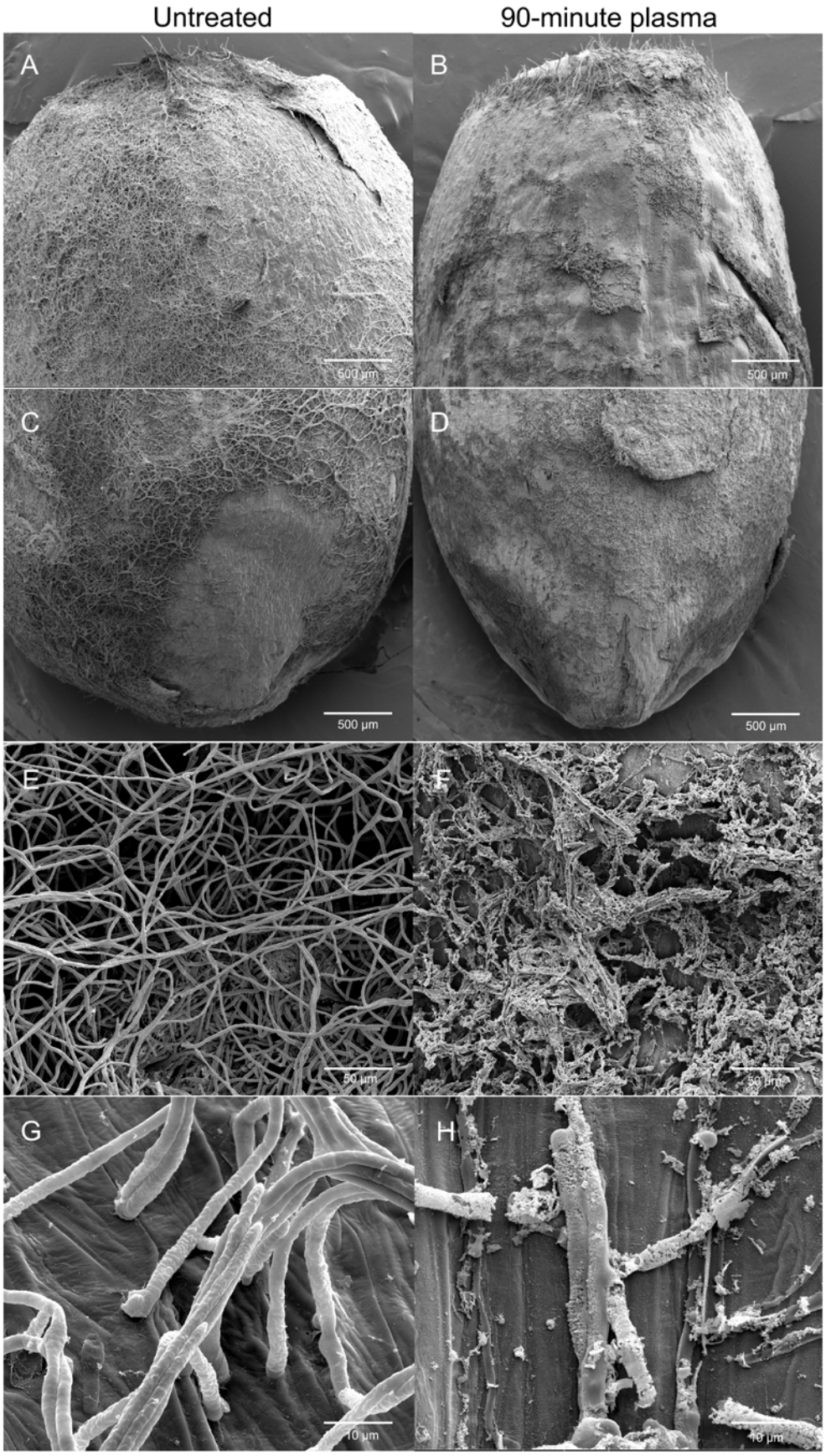


Figure 5-21. *Fusarium graminearum* inoculated wheat grains. (A and C) Visible mycelial network on Untreated grains. (E) Untreated hyphal network at 1000x magnification. (G) Hyphae penetrating the Untreated grain surface. (F) Remnants of mycelial network following 90 minutes of plasma exposure. (H) Remnants of what appear to be areas of hyphal penetration. n = 4.

SEM micrographs of Untreated and P90 grains reveal the efficacy of the plasma tumbler in deactivating *F. graminearum* hyphae. Much like *B. sorokiniana*, mycelial networks are visible on the Untreated grains (Figure 5-21, A, C, E). Figure 5-21, G reveals hyphal penetration of the wheat grain pericarp, present on all four Untreated grains, indicating the fungal infection went beyond the grain surface. When combined with CFU data sets, this astounding image suggests that the exposure in the plasma tumbler can deactivate a severe intracellular infection. Figure 5-21 B, D, F and H highlight the weathering effects of plasma which, like previous imagery, seem to leave behind remnant fungal structures. Furthermore, it appears that the inoculation method led to the production of chlamydospores or chlamydospore-like structures (Figure 5-20). This was unexpected as these structures often take weeks to form (Leslie and Summerell, 2006). Chlamydospores are enlarged vegetative cells with double-layered cell walls which serve as survival structures and can persist for years in the environment, often in crop residues and soil (Nyvall, 1970; Sitton and Cook, 1981). If the structures visible within the SEM imagery are true chlamydospores, it is remarkable that plasma can shred these robust survival structures.

5.5.3.5 *Penicillium chrysogenum* inoculated psyllium

The original *P. chrysogenum* culture for all inoculation experiments was isolated from psyllium grain. As such, it was fitting to incorporate this pathogen back into the system. There was a small learning curve to overcome, as seen in the results of Experiment 1 in Figure 5-22, as extraction liquid could not be in contact with the grain for over one minute due to the swelling of mucilage and consequent goo formation. This was not conducive to spreading along a plate and led to a more rapid method of spore extraction in Experiments 2 and 3. The mucilage complication had little impact on the resulting data as there was a strong trend of colony-forming unit reduction with plasma treatment, accounting for over 40% of the variation in the two-way ANOVA. Unpaired

t-test p-values of less than 1 x 10^{-6} were observed across all experiments. It should be noted that a single colony resulted in a count of roughly 10^5 due to initial high inoculum load and required serial dilutions for plating. As the 90-minutes of plasma treatment plates in Experiments 2 and 3 yielded zero CFU/mL, the high detection levels due to dilution were not considered to be analytical artefacts within this system. It appears that 90-minutes of treatment in the PT system may be sufficient to deactivate most *P. chrysogenum* conidia on the surface of psyllium.

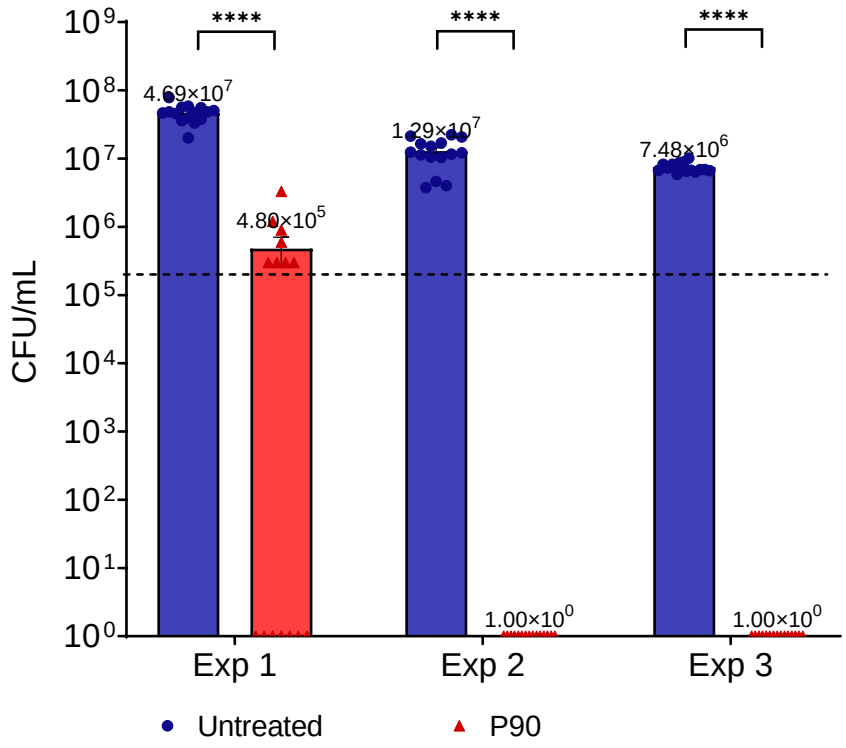


Figure 5-22. The results of three independent experiments with *Penicillium chrysogenum* inoculated psyllium grains and treated with P90 (90-minute plasma) or Untreated control conditions. Individual values are plotted with bar representing mean ± SEM; ****p<0.0001; n = 15. Dotted line indicates value for a single colony.

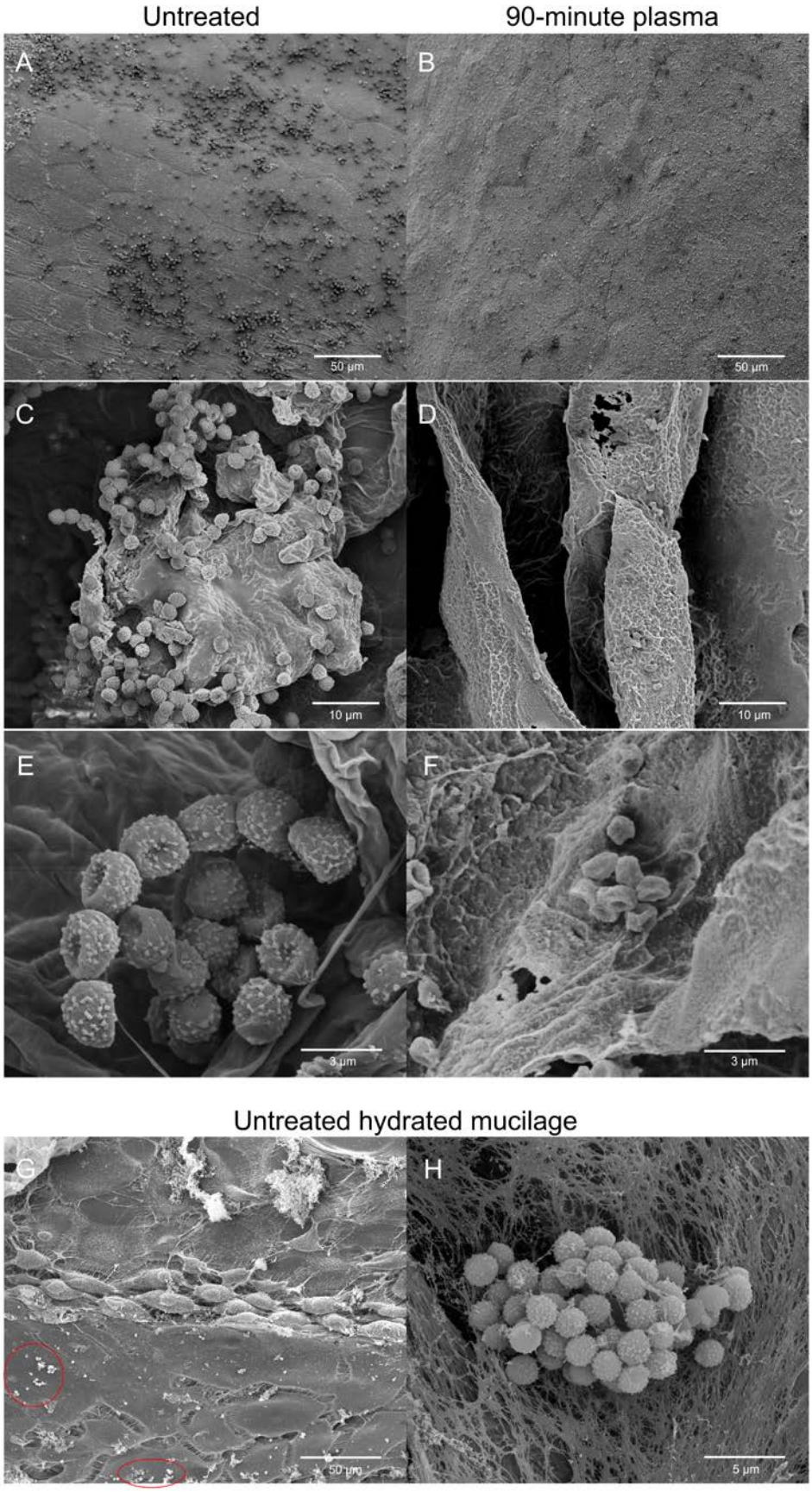


Figure 5-23. SEM micrographs of *Penicillium chrysogenum* inoculated dry psyllium grain. (A, G) View of Untreated grain dorsal surface. (C, H) Ventral view of psyllium grain with conidia. (G, H) Inoculated grains treated in fixative to hydrate mucilage and preserve conidia structures. (G) Red circles indicate conidia on partially hydrated mucilage (B, D, F) 90-minute plasma-treated grain surfaces with remnant conidia. n = 6.

The high inoculum load present in the CFU/mL counts were also apparent in SEM micrographs, with thousands of conidia visible across the surfaces of each Untreated grain (Figure 5-23). The ventral cavity of Untreated grains appeared to hold more visible conidia than the dorsal grain surface. It is also the region of visible hyphal growth in Chapter 4.3.1.1. When considered alongside the results of section 5.3, it is likely that the protective features of the ventral cavity allow for colonisation to occur more often in this region. It was speculated that following partial mucilage hydration, conidia would still be present in the cavity. This concept was confirmed in Figure 5-23, H where conidia were suspended in nets of expanding polysaccharide mucilage following partial hydration during fixation. Conidia were also visible on the dorsal surface of partially hydrated mucilage (Figure 5-23, G).

Few remnant conidia were visible on plasma-treated grains (Figure 5-23, B, D, F). It is speculated that the combination of plasma etching with the mechanical actions of tumbling and vacuum treatment removes many of the conidia from the grain surface of psyllium. The remaining fungal structures were highly weathered, lending credibility to the CFU/mL data sets obtained in Experiments 2 and 3.

5.5.3.6 Comparison of all fungal pathogen colony-forming unit concentrations

The means of technical replicates for each biological replicate in a series were analysed and compared across grain types and presented in Figure 5-24. As expected, there were significant variations between CFU in each grain type. Error bars for plasma treatments that span the zero CFU/mL value at the base of the x axis are indicative of the detection limits of the assay. These error bars indicate that some replicates had counts of zero or only very few colonies. This can be attributed to many factors including variations in inoculation method, dilution, concentration of conidia, size of conidia, or charge on the surface of the grain/conidia. While the statistical comparison

is not exceptionally helpful, the associated graph provides a visual summary of the entire experimental section.

The mean concentration of Untreated CFU/mL for each pathogen species reflected a conidia size natural sorting effect, with the smallest spores having the highest concentrations. This is reflective of the relative number of conidia produced by each of the organisms. The lowest Untreated CFU values were found in *Fusarium graminearum* which was designed to be a hyphal fragment study. While chlamydospores were potentially present, no micro or macroconidia were detected during haemocytometer counts. It is therefore unsurprising that lower colony-forming units were present when culturing viable hyphal fragments. As this data set falls within the range of expected outcomes based on known fungal pathogen behaviour and morphology, it can be assumed that no major errors in method have occurred. This final data set summarises the incredible efficacy of the PT system to reduce a variety of pathogenic fungi on five different grain types.

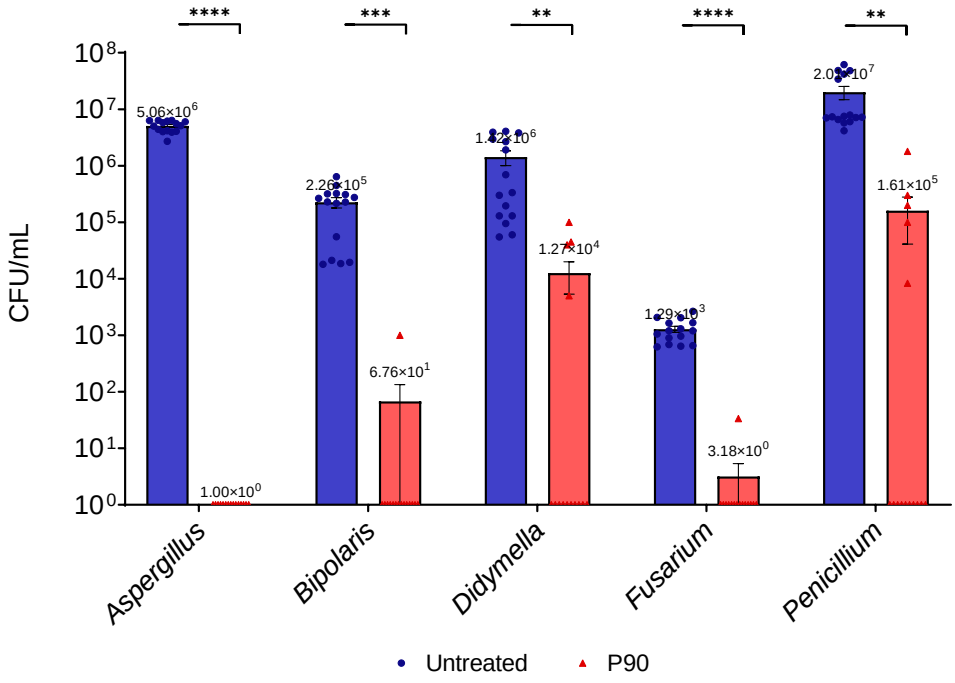


Figure 5-24. Summary of inoculation trials with combined data from each organism/host series. The means of biological replicates from all three independent experiments are plotted for each treatment. Data is presented as mean ± SEM; ** p<0.01; ***p<0.001; ****p<0.0001. Abbreviation: P90 (90-minute plasma).

5.5.4 Summary

This series of studies investigated the efficacy of 90-minute plasma tumbler treatments across multiple grain types and fungal pathogens. It was hypothesized that long plasma durations may be more effective in deactivating fungi that have colonised layered surfaces, grooves, hulls, and other features on grains. The results indicate the reduction of viable colony-forming units to near negligible levels for five economically relevant grains and pathogens. Variations in conidia and hyphal morphology did not appear to impact the efficacy of 90-minute plasma treatment. Although the consequences of differences in host grain surface structures and chemistry are unknown, they did not hinder the fungal deactivation process in this model.

The relative success of these broad-spectrum preliminary trials has been in the context of synthetically created host/pathogen relationships. The concentration of spores and the way they adhere to the grain surface will be different in a natural environment. Hyphal penetration of grains is common under suboptimal field conditions. The ability of the PT system to effectively reduce to nil the viability of a severe *Fusarium graminearum* infection, with grain penetration, is promising. If plasma treatment is to be considered as a technique for reducing post-harvest grain loss, it must be capable of minimizing both conidia and hyphal viability. As seen in sections 5.2 and 5.3, the extant microbes on the grain surface may or may not behave in a different manner when exposed to plasma treatment. Now that sufficient treatment timepoints have been established and the flexibility of plasma treatment across multiple species of host and pathogen has been demonstrated, the system should be tested on contaminated field samples with multiple fungal pathogens.

5.6 Conclusions

The reduction of post-harvest losses due to fungal contamination is necessary to ensure food supply demands are met for the future. This chapter sought to explore the potential of a plasma tumbler reactor to reduce extant and inoculated fungal pathogens on grain surfaces. Initially, five grain types were selected and treated with plasma to determine if the system could reduce the naturally present fungal load. It was discovered that the base fungal load varied by grain type. As grains with smoother surfaces had fewer extant culturable fungi, it was predicted that pathogen load may be related to morphological features on the grain surface. A novel assay was developed to assess the location of fungal colonies and how this differed over increasing plasma exposure times. While the exposure time varied with grain type, there was a correlation between morphological features on the grain surface and the number of hyphal colonies. The convoluted time exposure results led to a series of inoculation trials to better understand how plasma works under a synthetically high fungal load. Once the key exposure time of 90 minutes or more was identified, the system was challenged with five economically important pathogens on the five grain types to determine if the PT could inactivate synthetically high levels of fungal inoculum. Not only was plasma treatment capable of reducing fungal colonies by up to seven-fold, but SEM imagery also showed how each pathogen was affected. *B. sorokiniana* and *F. graminearum* hyphal infections, with visible grain penetration, were effectively shredded by the chemical etching processes of plasma. The surface features of conidia were extremely weathered and often featured compromised cell walls.

When considered as a whole, the results of this chapter demonstrate the efficacy of the PT system in almost complete deactivation of five seed-borne fungal pathogens. Furthermore, it was established that grain morphological features are capable of shielding microbes from environmental pressures. Long plasma exposure times of 90

minutes or more are essential to overcome the challenges imposed by grain structures. With this new understanding, it is evident that the plasma tumbler should be challenged with a contaminated industry sample to test the real-world application of the PT technology. However, it is first necessary to understand how the chemical etching process is impacting the grains themselves, not just the microbes on the surface. The stunning SEM micrographs in this chapter and Chapter 4 revealed both macro and micro level modifications brought about by 90 minutes of plasma treatment. Deep etching patterns in the grain surface may change the way the grain interacts with water. This side effect could have implications on whether plasma treatment may be appropriate for different grains. The following two chapters (Chapters 6 and 7) will explore the physico-chemical effects of plasma on the grain surface, how this impacts water uptake and any downstream consequences to grain germination, growth, and development. Only once these principles are established for multiple model grain systems, can complex microbially contaminated samples be introduced in Chapter 8.

6 Determining the impact of plasma-treatment on the physico-chemical properties of grain

6.1 Introduction

Within this project, the surfaces of grains are exposed to the effects of chemical and physical etching induced during plasma treatment. As demonstrated by the SEM micrographs in Chapter 4, substantial weathering occurs at both macro (e.g., the removal of the brush on wheat grains) and micro levels (e.g., weathering of the waxy seed coat cuticle on field pea). It is speculated that the plasma-induced oxidation may alter the hydrophobicity of grain surfaces, leading to potential downstream effects on seed-water relations. This has been demonstrated in other grain studies using air, helium, nitrogen and oxygen plasmas generated in a variety of plasma apparatus, yet not fully understood in the context of dynamic grain-water relations (Bormashenko et al., 2012; Dufour et al., 2021; Ling et al., 2015, 2014; Los et al., 2019). Grains have evolved complex hydration processes to regulate water uptake and the subsequent activation of specific tissues (Miano and Augusto, 2018). In the case of the five grains of interest, water typically enters through a pore on the grain surface called the micropyle. This structure once served as the location for pollen entry before fertilisation and now acts as a hydration point where water can be wicked toward the embryo via capillary action (Linkies et al., 2010; Rathjen et al., 2009). The rapid movement of water through the micropyle allows the embryo to hydrate and progress through the three

phases of germination more quickly than other tissues, such as the endosperm (Werker, 1997). Concurrently, water slowly diffuses across different regions of the grain surface to hydrate structures, such as the endosperm, and mobilises nutrients needed by the activating embryo (Niemann et al., 2013). Alterations to the grain surface can change the rate and direction in which water enters the grain. Subsequently leading to positive and negative downstream consequences on the timing of tissue hydration. Thus, changes in grain-water dynamics may affect germination if water enters at different locations and rates throughout the grain.

The weathering processes of plasma treatment necessitated experimentation to understand physico-chemical surface modifications and how these may play a role in grain-water relations. The increase in surface area on plasma-treated maize grain in Chapter 4, led to speculation that grain surface energy may also be increasing. Contact angle measurements were taken to explore this relationship. During this experimental process, it was observed that water ingress was modified, leading to water vapour sorption and aqueous dye uptake assays to determine changes in the rate and direction of water ingress. Additionally, plasma-treated grains were surface analysed via time-of-flight secondary ion mass spectrometry (ToF-SIMS) to gain insight into possible changes to the grain surface chemistry. Alterations to hydrocarbon fragments following plasma-treatment lowered surface hydrophobicity and confirmed the grain surface energy increases, which were established with contact angle measurement. Finally, ToF-SIMS data displaying spikes in K^+ on all plasma-treated grains, combined with observed staining of grain germination substrates following plasma treatment, led to a hypothesis that the weathering effects of plasma may expose intracellular contents. A flame photometry assay was conducted on grain extracts to understand this phenomenon. Together, this series of experiments sought to clarify the plasma-

induced physico-chemical alterations to grain surfaces and untangle the complicated story of grain hydration.

6.2 Contact angle measurements

6.2.1 Introduction

In Chapter 4, scanning electron micrographs illustrated the etching effect of plasma-treatment on seed surfaces. Additionally, the profilometry scanning of maize grains confirmed a 12% increase in grain surface area following plasma treatment. As each grain type has a different surface structure and chemistry, it was unknown if the potentially oxidising effects of air plasma etching alter the hydrophobic properties of the seed surface.

Contact angle measurements are a technique used to understand the free energy of a surface as it relates to wetting by a liquid. In the case of water, this is called its hydrophobicity or hydrophilicity. It should be noted that these descriptors are relative terms and should be interpreted within the context of a given experiment. Contact angle analysis is performed with an instrument called a tensiometer. It involves the placement of a small liquid droplet on a test substrate and measures the resulting angles within the three-phase boundary - in this case the solid grain surface, the liquid water droplet, and the surrounding air (Figure 6-1). On a low energy surface, the water droplet will often remain beaded with a relatively high contact angle due to strong cohesive forces. On the other hand, adhesive forces between the water droplet and the solid surface are strong on a high energy surface, creating a lower contact angle. The interaction between cohesive and adhesive forces determines the wettability of the surface. For the purposes of this thesis, high contact angles will be defined at greater than 90° and low contact angles will be less than 90°, following guidelines described by Elmogahzy, 2020.

A series of experiments was designed to understand how plasma may be impacting the surface free energy of seeds. A pilot experiment involved the placement of water droplets on Untreated, 90-minute plasma-treated and 60-second chloroform-treated maize grains to determine if there was a difference in grain surface free energy. The encouraging results of this experiment led to the development of a plasma exposure time-series experiment with the aim of determining how prolonged exposure in the plasma tumbler alters grain surface energy. Grains were placed on a tensiometer and contact angles between ultra-pure water droplets and grain surfaces were measured to determine if the hydrophobic properties of the seed surface were altered during the plasma etching process.



Figure 6-1. The contact angle of water droplets on the surface of wheat grains. (A) A more hydrophobic grain surface produces a high contact angle as the polar water molecules are attracted to each other through cohesive forces rather than the non-polar hydrocarbon chains on the grain surface. Arrows indicate the direction of attraction. (B) A more hydrophilic grain surface produces lower contact angles as adhesion forces attract the water molecules to a more polar grain surface.

6.2.2 Materials and Methods

6.2.2.1 Pilot trial grain treatment and experimentation

Maize cultivar ‘B73’ grains were divided into three 10 g treatment aliquots. One aliquot was treated on the plasma tumbler for 90 minutes (P90) following protocols in Chapter 3.1.2. Another aliquot was placed in a glass flask with 90 mL of chloroform (99.9% HPLC-grade, Sigma-Aldrich) for a 1:10 dilution (w/v). Following protocols in Russin et

al., 1997, the flask was agitated for 60 seconds before the grain was removed and allowed to evaporate to dryness in a fume cupboard. The remaining aliquot of grain was set aside as an Untreated control.

Ten grains of each treatment were placed embryo-side down on a paper towel. Using a P10 Ovation® pipette, 2 µL of Milli-Q water was dispensed onto the surface of the maize grain. Multiple observations were recorded over a period of two hours to determine how future experiments should be designed.

Furthermore, 50 µL drops of the wax and chloroform extract were placed on polished silicon wafers and allowed to evaporate to dryness to determine if maize surface waxes had been extracted.

6.2.2.2 Plasma exposure trial grain selection and treatment

Plasma treatments were conducted at 15-minute intervals for up to 90 minutes on maize, wheat and field pea following protocols in Chapter 3.1.2. Untreated and 90-minute Tumbler + Vacuum (T+V) controls were also prepared. Barley and psyllium were omitted from this experiment due to difficulties with grain surface features. The uneven outer husk on barley grains made it very difficult to place a level water droplet on the grain. The small size of psyllium grains, less than 3 mm, required the application of water droplet volumes of less than 1 µL which is outside of the range of accuracy of the instrument.

6.2.2.3 Tensiometer measurements

Maize and wheat grains were set on their ventral sides on glass slides to take measurements of the dorsal surfaces. Field pea grains were placed hilum-down on blue tack to avoid rolling around the slide. Slides were fitted onto an Attension® Theta Lite Auto 1 optical tensiometer. Milli-Q water droplets were dispensed at 2 µL for maize and field pea; 1 µL for wheat. The contact angles were measured twenty times per second over the course of five seconds for a total of 100 measurements per grain. This

procedure was repeated for ten replicates of each treatment and grain type. Contact angle means and dispersed surface energy were calculated within the Attension® software.

6.2.2.4 Data analysis

Two-way ANOVA with Tukey's multiple comparisons analyses were conducted in GraphPad Prism 9.0.0 (GraphPad Software Inc, San Diego, CA, USA) comparing treatments and grain types. Data were expressed as mean ± standard error of the mean. Significance was accepted at $p<0.05$.

6.2.3 Results and Discussion

6.2.3.1 Water droplet on maize grain pilot trial

The surface of maize grains is generally composed of hydrocarbon-rich waxes. A pilot experiment was conducted to compare Untreated and P90 treated grains with those that had been briefly immersed in chloroform to remove the wax (Russin et al., 1997). In this manner, the effects of plasma etching could be compared to both Untreated and wax-extracted grains. Observations of water droplet behaviour were recorded for each treatment. It was immediately apparent that water on plasma-treated grain behaved differently from Untreated and chloroform-treated grains (Figure 6-2). Relatively spherical bead-like droplets remained jauntily perched on the surfaces of the Untreated maize for the two-hour observation time. More rounded and convex droplets adsorbed to the surface on the chloroform-treated grains, over the two-hour time. Conversely, the interaction between water and plasma-treated grains did not produce a stable droplet. Instead, water is readily absorbed into the grain within one to two seconds after application. It was difficult to tell whether almost complete wetting of the surface had taken place or if the bulk of the droplet was incorporated into the grain.

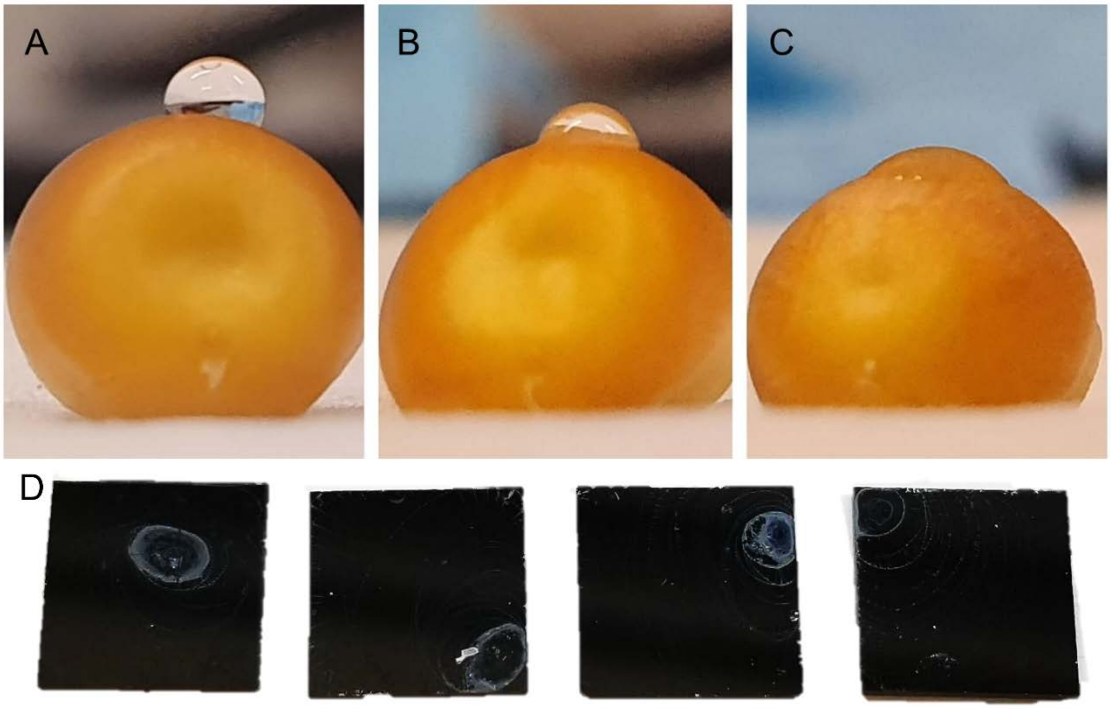


Figure 6-2. Maize grains with water droplets applied to the surface to observe wettability. Images taken in a burst-mode within two seconds of water application. (A) Untreated grains; (B) 60-second chloroform-treated grains to reduce the presence of seed surface waxes; (C) P90 grains. The relative hydrophobicity/hydrophilicity of the seed surface was demonstrated by the interaction of the water droplet with the maize kernel. (D) 50 µL drops of maize grain chloroform extracts placed onto silicon wafers illustrated the compounds extracted from the grain.

When chloroform extracts were dropped onto silicon wafers, concentric circles of a wax-like residue were formed, indicating that surface compounds were indeed extracted from the grain. This observation, when coupled with the visible interaction of water droplets with the grain surface, suggests that chloroform treatment altered the hydrophobic nature of the grain surface. Yet, this treatment was difficult to compare to P90 samples as water droplets retained their shape on chloroform-treated grains for two hours while droplets were immediately absorbed into plasma-treated seeds. It was speculated that the plasma oxidation of surface molecules increased surface energy while concurrent etching processes disrupted the waxy surface structures. This allowed water to spread across the grain surface and possibly penetrate the grain. The solvation power of chloroform is effective but is often insufficient for completely

dissolving plant cuticular waxes (Bewick et al., 1993). Plasma treatment likely raised the surface energy of the grain to a higher extent than chloroform treatment. For this reason, it was deemed necessary to proceed with a tensiometer assay to quantify the contact angle across a 15-minute interval plasma exposure series, with chloroform assays being replaced by a more relevant T+V control.

6.2.3.2 Contact angle measurements on three types of grains

Plasma-treated grains were analysed on an optical tensiometer to understand how exposure may influence water contact angle. Based on research by Bormashenko et al., 2012; Dufour et al., 2021; Ling et al., 2014; Los et al., 2019 and others, it was hypothesized that the oxidative effects of prolonged plasma exposures may increase the seed surface energy, greatly reducing contact angles. The resulting data present a slightly more complicated story. Relatively high contact angles were measured during interactions between water droplets and the surfaces of Untreated and T+V control grains. All control contact angle means were greater than 100°, regardless of grain type and presented as beaded drops on the grain surfaces (Figure 6-3). All plasma-treated sample contact angles were more challenging to measure as the water droplets quickly absorbed into the grain surface. Across all grain types, P45, P60, P75 and P90 treatments could not be reliably measured due to the rapid absorption rate coupled with the curvature of the grain surface. While the absorption rate may be compensated for by increasing the number of images per second within the software, it was not designed to factor in a high degree of water sorption into the grain. The measurement software could not distinguish between a water droplet and the grain surface when contact angles dropped below 45°. This resulted in data collection from only two plasma time exposures, P15 and P30, that could be repeatedly measured.

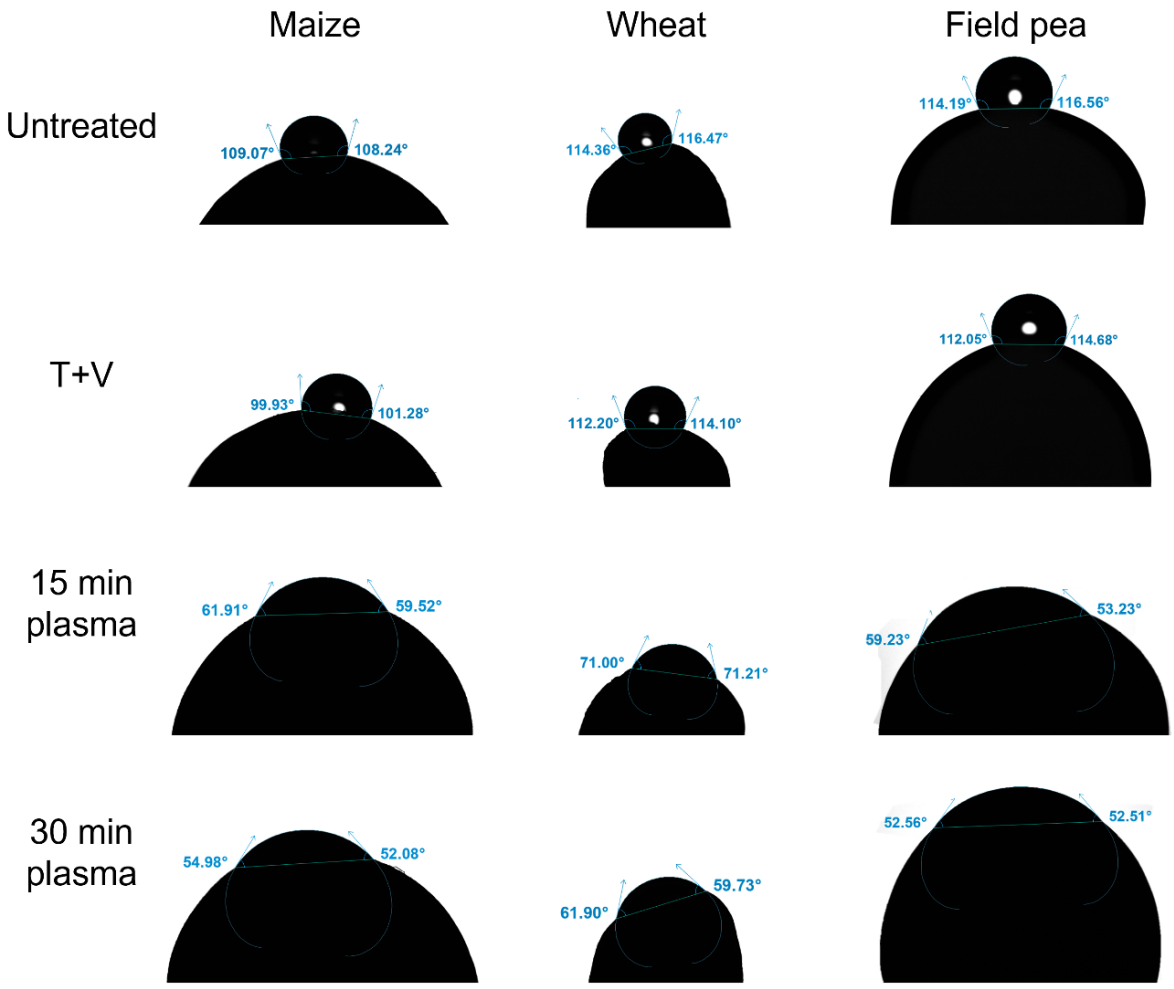


Figure 6-3. Contact angle images comparing maize, wheat, and field pea treatments. Water droplets form tight beads on control samples. Plasma-treated samples have sprawling droplets with much lower contact angles.

The initial hypothesis that plasma treatment may reduce water contact angles was validated in this experiment as angle measurements were effectively halved in P30 samples (Figure 6-4). By plotting the means of each grain type and treatment, the overall trend of contact angle reduction was clearly visible. There was a small but insignificant (p-value = 0.3605) increase in contact angle on field pea at 30-minutes of plasma exposure. This may be attributed to fallacies in software measurements because the contact angle for the field pea P45 treatment was not measurable due to grain curvature interfering with contact angle measurements lower than 45°. Tukey's multiple comparisons across grain types and treatments revealed no statistically

significant differences between the means of Untreated and T+V control samples. Conversely, p-values of less than 0.0001 were calculated between controls and plasma treatments, regardless of species (Appendix S6).

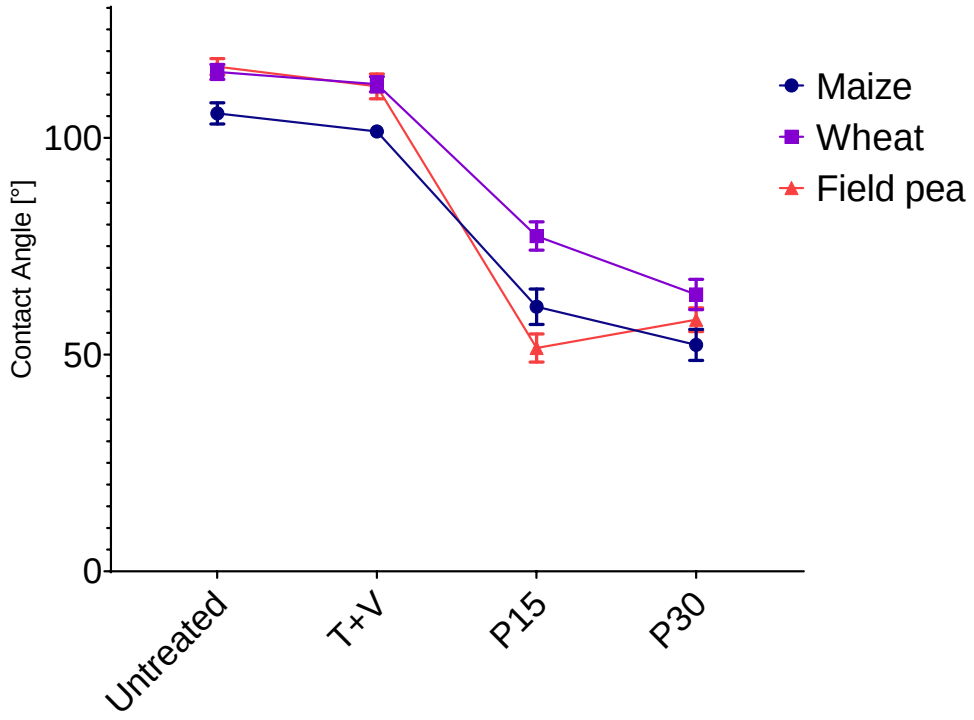


Figure 6-4. Comparison of the water droplet contact angle means of each grain type and treatment. Data is presented as mean ± SEM; n = 10. The difference between Untreated and T+V controls is insignificant (p values = 0.6167 to 0.8905). There is a highly significant difference between the controls and plasma treatments (p-values of less than 0.0001) in all grain types. Abbreviations: T+V (Tumbler + vacuum); P15 (15-minute plasma); P30 (30-minute plasma).

Plasma treatment evidently modified the grain, increasing seed surface energy and altering grain-water relations. It should be noted that increased surface roughness promotes wettability and lower contact angles (Good, 1992; Wenzel, 1949). SEM images and profilometry calculations presented in Chapter 4 demonstrated increased irregular roughness of plasma-treated grain surfaces and likely played a role in lowering contact angles. Furthermore, it is possible that the process of chemical etching breaks up large hydrocarbons on the grain surface and oxidises the remaining

fragments. This would greatly increase surface energy and adhesion between water molecules and the newly polar grain surface, allowing for better surface wetting. However, surface wetting does not explain the apparent absorption of almost the entire volume of the water drop into the seed in less than the five second recording period. Does a portion of the water droplet spread across the surface while the rest is absorbed into the grain?

Previous studies, including Bormashenko et al., 2012 and Los et al., 2019, found that water uptake increased following plasma treatment. Bormashenko et al., 2015 investigated the effects of plasma treatment on two layers of the seed coat of green beans, *Phaseolus vulgaris*, and observed that each tissue behaved differently following plasma treatment. The contact angle of water was greatly reduced on the exotestal. Conversely, the mesotesta contact angle remained the same before and after treatment, suggesting that water may not penetrate this layer. Instead, they propose that water uptake is occurring more rapidly through the micropyle. However, the water penetration observed in this assay occurred over the endosperm tissues of the seed. Understanding the spreading parameter of the water droplet on the grain surface may be useful but involves the measurement of contact angle with other liquids, such as ethylene glycol and diiodomethane, to calculate the polar component of the surface energy (Kalin and Polajnar, 2013). This is not an ideal experiment due to the difficulties imposed by the curvature of the grain surface. As the grain appears to rapidly absorb the water drop, measuring seed sorption would be a better indicator of whether the grain is absorbing water at a rapid rate after plasma-treatment. Section 6.4 will describe these experiments in detail.

6.2.4 Summary

This experiment employed contact angle techniques to gain an understanding of plasma-induced changes to seed surface energy. It was found that plasma exposure

greatly reduced contact angles, regardless of seed type, which correlates with an increase in surface energy. Surprisingly, contact angles could not be measured on grains exposed to plasma for over 30 minutes. Water droplets were instantly absorbed into the grain, indicating that prolonged exposure to plasma may disrupt the outer hydrophobic layers on the seed surface. This may strongly influence the relationship between water and the grain surface, which is often tightly controlled through specific channels and pores. A detailed investigation into the changes in surface chemistry will be explored in the following section to better understand the effects of plasma on the surface of grains. Additionally, section 6.4 explores seed water uptake following a series of plasma exposures to untangle the relationship between plasma treatment and water transport phenomena.

6.3 Analysis of grain surface chemistry with ToF-SIMS

6.3.1 Introduction

Time-of-flight secondary ion mass spectrometry (ToF-SIMS) is a highly sensitive analytical technique for understanding the surface chemical composition of a material. It involves pulsing primary ions at a surface with an aim to fragment the surface molecules into secondary ions and neutral fractions. The newly created ions and fragments are extracted into a mass spectrometer with mass-to-charge ratios (m/z) determined in the time-of-flight detector (Jasieniak et al., 2015). In this manner, the uppermost nanometre of the surface is semi-quantitatively analysed. ToF-SIMS analysis has been demonstrated on air plasma-treated bean, lentil and wheat grains by Bormashenko et al., 2012, revealing increases in O, CN, CNO and $C_2H_3O_2$ fragments. Their results suggested that reactive nitrogen species (RNS) and reactive oxygen species (ROS) created in the field of plasma react with grain surfaces. It also highlighted the need for further analysis on a large suite of fragments to understand

the reactions in greater detail across different grain types and the prolonged plasma exposures required for microbial deactivation within the plasma tumbler system.

The physico-chemical effects of air plasma on grain are poorly understood. This is partly due to the complicated and non-uniform chemistry of air plasma and the variations in surface chemistry of the grains treated. Each grain type and cultivar will have different surface structures and chemical makeup. While the general principles of air plasma reactions will apply to all grains treated in the PT system, subtle differences may occur due to morphological and chemical differences, visually demonstrated in the SEM micrographs in Chapter 4. As grains are living organisms, exploring the variations in plasma reactions with each grain surface chemistry is necessary to predict subsequent grain responses.

An experiment was designed to study the surface chemistries of Untreated, P30 and P90 maize, wheat, field pea and psyllium grains. It was hypothesized that plasma exposure would cause changes to the outer coverings of grains, particularly the hydrocarbons which provide a waxy protective barrier to the environment. By looking at positive and ion fragments, this study sought to expand knowledge surrounding plasma interactions with grain surfaces and understand the possible oxidation levels.

6.3.2 Materials and Methods

6.3.2.1 Grain preparation

Three aliquots of maize, wheat, field pea and psyllium grain were separated for treatment. P30 and P90 treatments were conducted as per Chapter 3.1.2. The third grain aliquot was set aside as the Untreated control. Plasma treatments were performed back-to-back with maize, wheat and field pea treated one day and psyllium treated the following morning. Grains from each treatment were then placed in a sterile 12-well plate (Nunc™, non-treated) and transported to the Future Industries Institute

node of Microscopy Australia at the University of South Australia, Mawson Lakes campus. All samples were submitted for analysis within 24 hours of treatment.

6.3.2.2 Time-of-flight secondary ion mass spectrometry

Samples were submitted to the Future Industries Institute node of Microscopy Australia at the University of South Australia, Mawson Lakes campus for analysis. ToF-SIMS analysis was conducted on a Physical Electronics Inc. PHI TRIFT V nanoTOF instrument equipped with a pulsed liquid metal $^{79+}$Au primary ion gun (LMIG), operating at 30 kV. Dual charge neutralisation was provided by an electron flood gun and 10 eV Ar^+ ions. Two grains were selected for each treatment with six analysis locations per grain. The spectra of positive inorganic ion peaks and positive fragments containing carbon, hydrogen, oxygen, and nitrogen (C_xH_y, $C_xH_yO_z$ and $C_xH_yNO_z$) were chosen for analysis.

ToF-SIMS imagery collected during analysis are visual displays of ToF-SIMS fragment mass spectral data rastered in two dimensions. Images of the highest intensity, K ions, were collated and are presented and discussed in section 6.7 of the chapter.

6.3.2.3 Data analysis

Integrated peak values of selected ions were normalised to the total selected secondary ion intensities, to correct for differences in total ion yield between particles. The resulting data were then compared qualitatively by preparing plots of average normalised counts.

6.3.2.3.1 Principal component analysis

Principal component analyses (PCA) were performed on the averaged normalised counts of each grain type using MATLAB with NESAC/BIO Toolbox plugin (https://www.nb.uw.edu/mvsa/multivariate-surface-analysis-homepage) and scaled to the square root mean centre. Initially, PCAs compared all four types of fragments (C_xH_y, $C_xH_yO_z$, $C_xH_yNO_z$ and positive inorganic ions). The data was analysed a second

time for each grain type omitting the positive inorganic ions. Ellipses represented the 95% confidence interval (CI).

6.3.2.3.2 Two-way ANOVA

A two-way ANOVA was performed in GraphPad Prism 9.0.0 to compare normalised fragment counts and treatment within grain type. Data were expressed as mean ± standard error of the mean. Significance was accepted at $p<0.05$. Statistically significant C_xH_y fragments, as well as $C_xH_yO_z$, $C_xH_yNO_z$ and positive inorganic ions were plotted in a heat map to display the relationships between treatment and grain type.

6.3.3 Results and Discussion

ToF-SIMS surface analysis was conducted to explore the changes in seed surface chemistry following plasma treatment. It was suspected that grain fragments might vary between Untreated controls and plasma-treated grains due to the chemical etching processes. Etching may have exposed underlying layers of the epidermal cell walls with different chemical components. It is also possible that ROS and RNS created within the plasma field may have reacted with broken fragments on the seed surface, altering the chemical fingerprint. As each grain type has different surface chemistry, comparisons were made to determine if patterns were detectable across grain types following plasma treatment. The data gathered in this section was used to inform subsequent experiments regarding seed surface chemical and physical properties.

6.3.3.1 Principal component analysis

PCA is one of the recommended analytical techniques for untangling trends within the large data sets collected with ToF-SIMS analysis (Jasieniak et al., 2015). Here, PCA plots compared correlations between selected ToF-SIMS positive fragments from each grain type and displayed trends caused by different treatments. The loadings indicate fragments which had the greatest influence on the PCA plots. The initial PCA analysis

comparing all fragments are discussed first, followed by a secondary PCA series omitting the positive inorganic ions to gain a sense of potential patterns and trends.

6.3.3.1.1 Comparisons of all fragments

PCA plots of each grain type (Figure 6-5) showed the differences in grain surface chemistry following plasma treatment. Across all grain types, the Untreated control sample set separated from the plasma-treated sample sets with principal component one (x-axis). This result indicated a strong influence caused by plasma treatments on the surface chemistry of the samples when compared to the controls. The analysis of both the P30 and the P90 treatments showed little variation in the data sets for maize, wheat, and field pea. With field pea, there was close clustering on both PC1 and PC2 axes for the P30 samples, with a shift to greater PC2 and PC1 values for the P90 treatments. More distinct data clustering becomes apparent for psyllium which showed similar trends to field pea (increased PC2 and PC1 values), but relatively tighter clustering of the data for the P90 samples. Interestingly, there is little overlap within the 95% confidence interval ellipses in psyllium: the only grain with a polysaccharide surface chemistry. A useful starting point to interpret these trends may come from the biological differences between the grains, as discussed in Chapter 1.3.2.

To understand the chemical reasons for clustering within the PCA plots, it was necessary to examine the loadings (Figure 6-6). In all four grain types, inorganic cations influenced the plasma treatment groups toward the positive side of the x-axis. This correlates with high normalised values of inorganic ion fragments. Higher values of Mg, K and Ca ions may be associated with plasma weathering the seed surface structures and exposing the intercellular contents. K^+ is one of the most abundant macronutrients found in all plant cells. It may have been released if plasma etching damaged the peripheral cell walls. In addition to K^+, it is thought that compromising the integrity of cell walls may also lead to the release of cross-linked minerals, such as

Ca^{2+} and Mg^{2+} (Gilliham et al., 2011; White et al., 2018). More surprising is the presence of Al ions on the surface of field pea. It is possible these ions are associated with pre-harvest fungicide application, such as Fosetyl-aluminium, which is commonly used in this crop (Aslam et al., 2019). Regardless of their origins, the inorganic ions on the seed surface appear to be a main factor driving the PCA plots in this preliminary analysis. To better understand how the organic fragments influence grain surface chemistry, a separate series of analyses were conducted, excluding the inorganic ions.

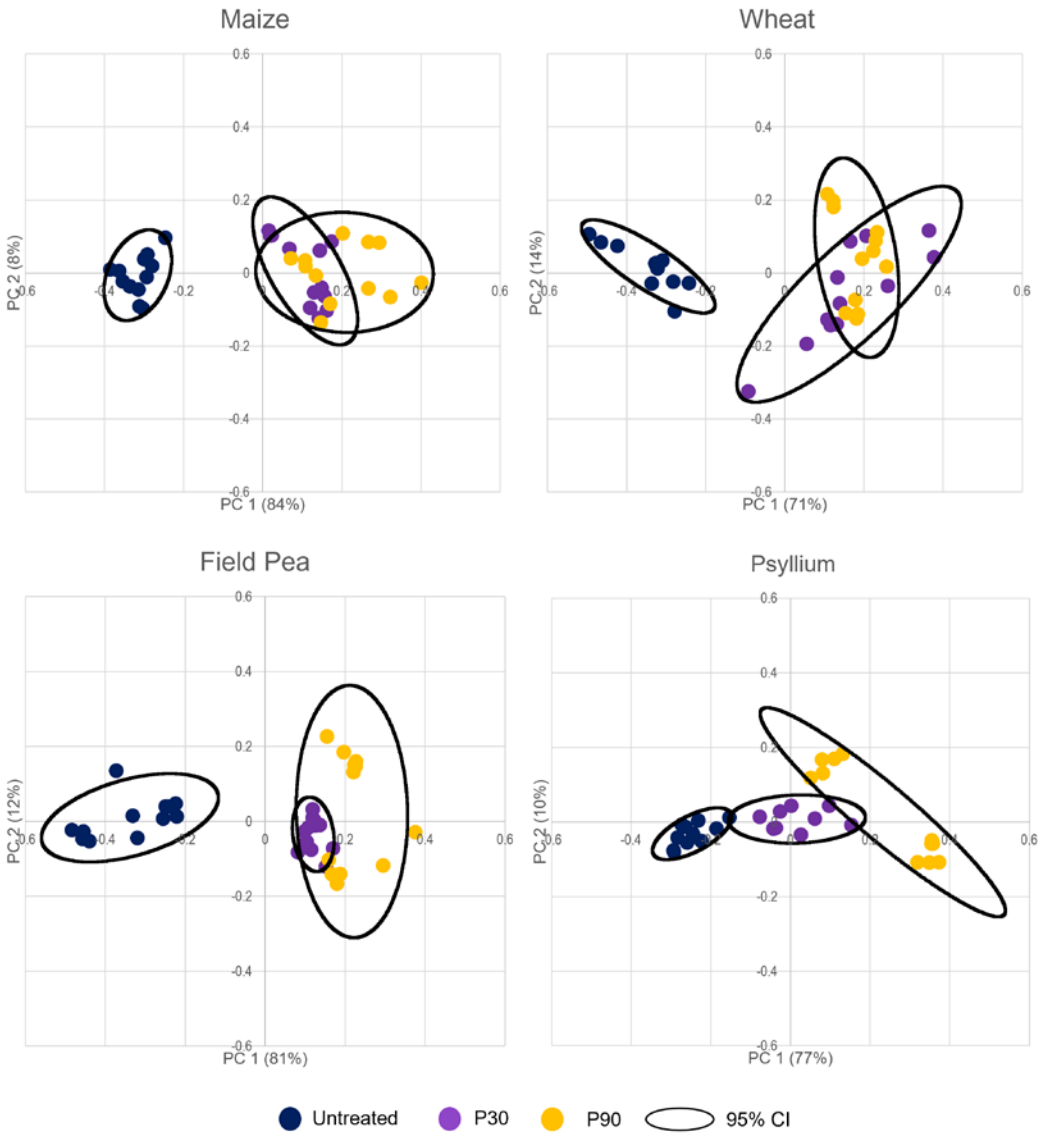


Figure 6-5. PCA plots comparing all fragments analysed during ToF-SIMS. Across all grain types, the Untreated control group is mostly separated from the plasma treatments along with principal component 1 (x-axis). Ellipses represent the 95% confidence interval (95% CI). Abbreviations: P30 (30-minute plasma); P90 (90-minute plasma).

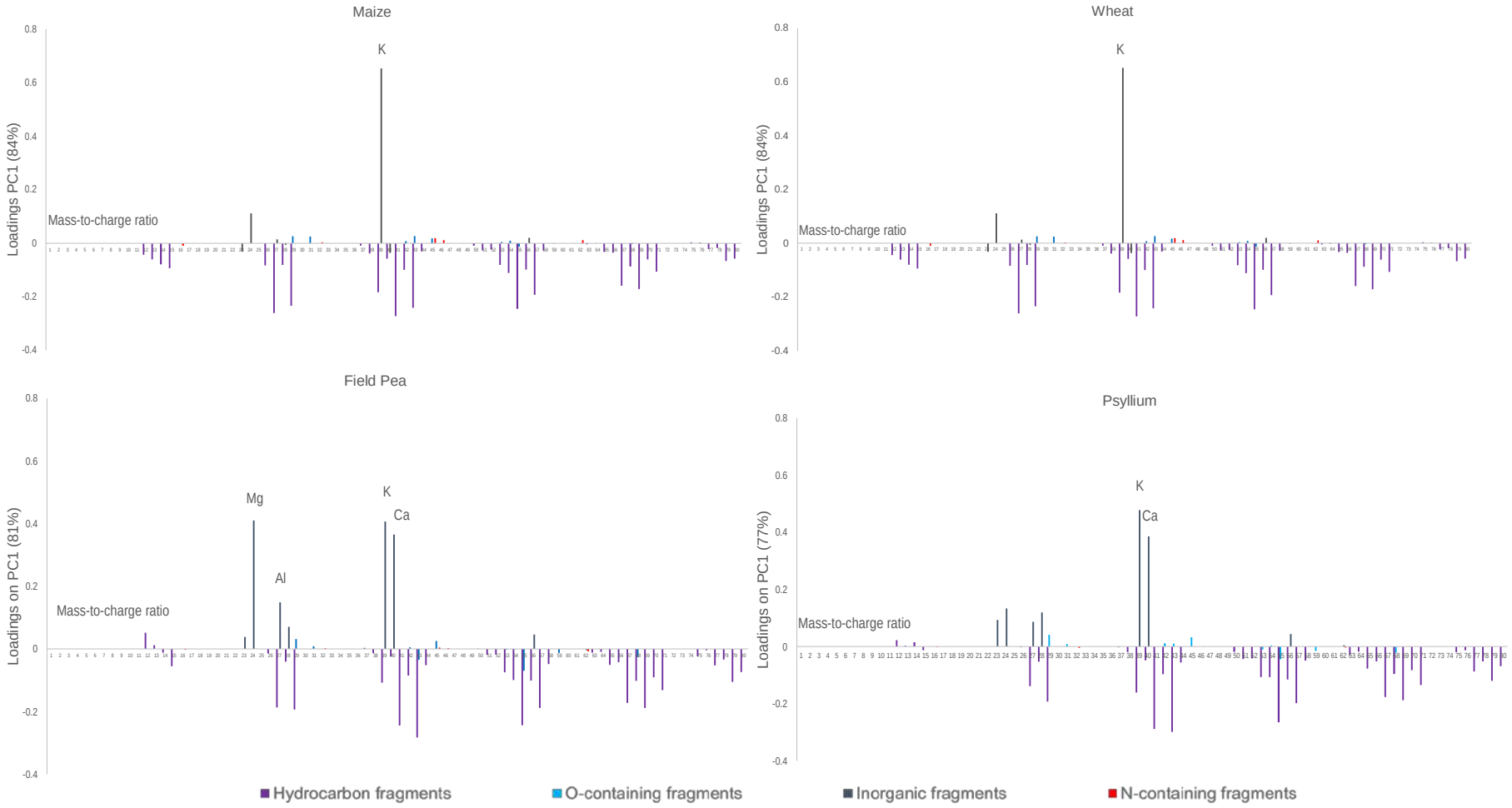


Figure 6-6. Combined PCA loadings of all treatments within a grain type to allow comparisons of fragments analysed during ToF-SIMS. The inorganic cations were a driving factor in the separation of treatments in this first analysis.

6.3.3.1.2 Comparisons of organic fragments

The PCA plots excluding the inorganic cations (Figure 6-7) were different to the plots in Figure 6-5. Yet, they displayed a similar trend in separating Untreated controls from P30 and P90 treatments. The percentage of principal component 1 driving the plots has increased without the inorganic cations (Figure 6-8). C_xH_y fragments appeared to contribute the most to negative loadings on PC1. The oxygen-containing fragments influenced negative PC1 loadings to a lesser extent. Instead, many $C_xH_yO_z$ fragments contributed to positive PC1 loadings, which was evident for field pea and psyllium. In general, the influence of N-containing fragments was small, but perhaps slightly biased due to very small changes to positive loadings on PC1. This varies from the results of ToF-SIMS analysis presented in Bormashenko et al., 2012. They found evidence for plasma exposure increasing the relative abundance of O, CN, CNO and $C_2H_3O_2$ fragments. However, it is difficult to make direct comparisons between their work and the present study. Bormashenko et al. 2012 used different plasma parameters, notably short durations of plasma exposure (up to two minutes) and lower powers (20 W), as well as the selected analysis of negative ions. As far as the author is aware, this is to-date the most comprehensive ToF-SIMS analysis of the surface chemistry of plasma-treated grains.

Overall, the PCA analyses showed there were differences in the surface chemistry of grains following plasma exposure. A higher prevalence of inorganic cation counts following plasma treatment appears to be the most common difference, yet alterations to hydrocarbon fragments also drive changes in the surface chemistry. Due to the nature of ToF-SIMS analysing fragments, the chemical modifications are unknown however, a deeper understanding can be made using a statistical analysis to further explore the differences between fragments and treatments.

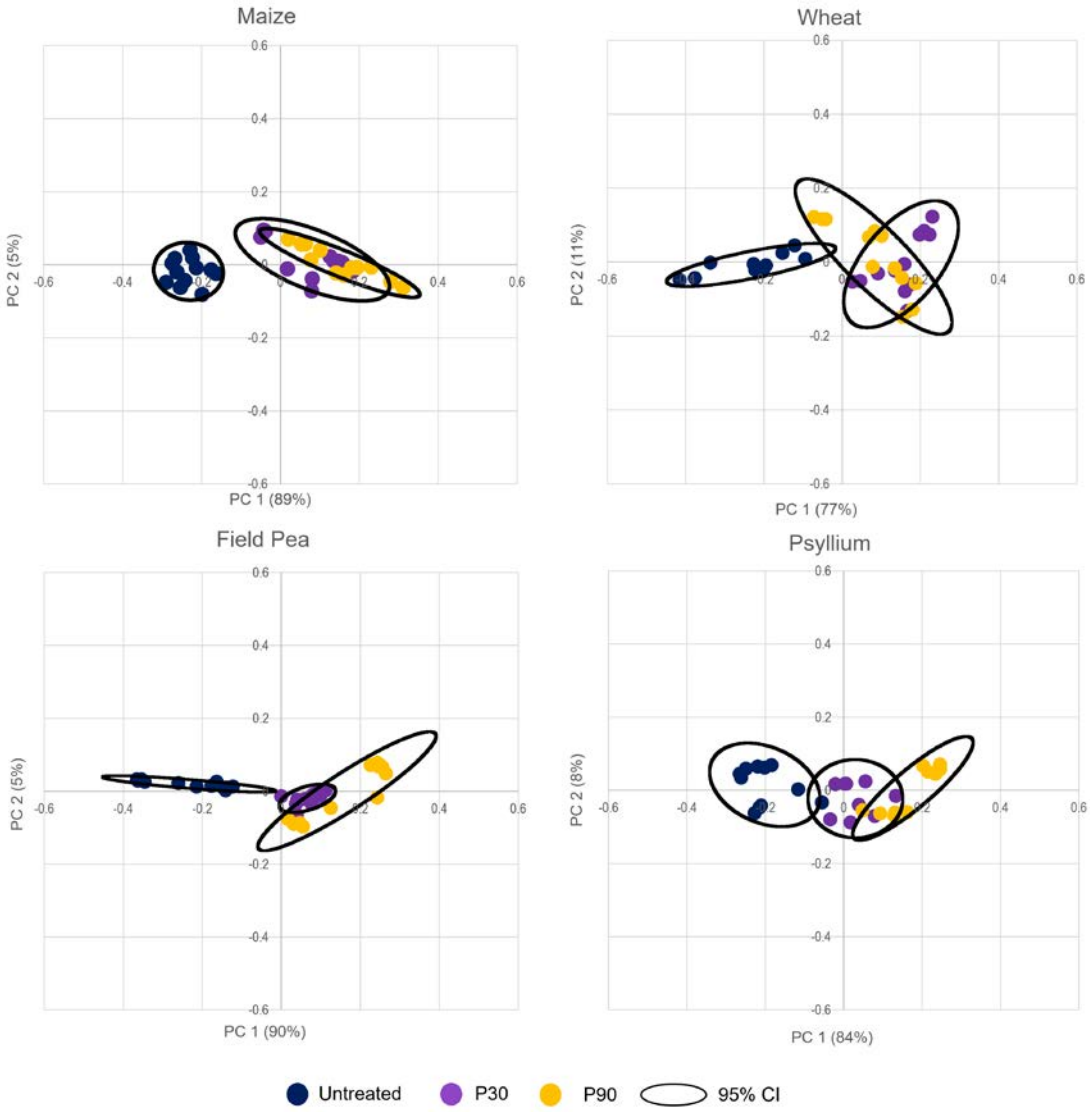


Figure 6-7. PCA plots comparing organic fragments analysed during ToF-SIMS. When inorganic ions are removed, the Untreated control group is separated from the plasma treatments along with principal component 1 (x-axis). Ellipses represent the 95% confidence interval (95% CI). Abbreviations: P30 (30-minute plasma); P90 (90-minute plasma).

6.3.3.2 Two-way ANOVA analysis of fragment abundance in each treatment and grain type

ToF-SIMS is a semi-quantitative analysis and can help display general trends when used as a method to survey unknown surface chemistries. A two-way AVOVA was conducted to compare the normalised means of counts for fragments of each treatment and grain type. Fragments with statistical significances between treatments were

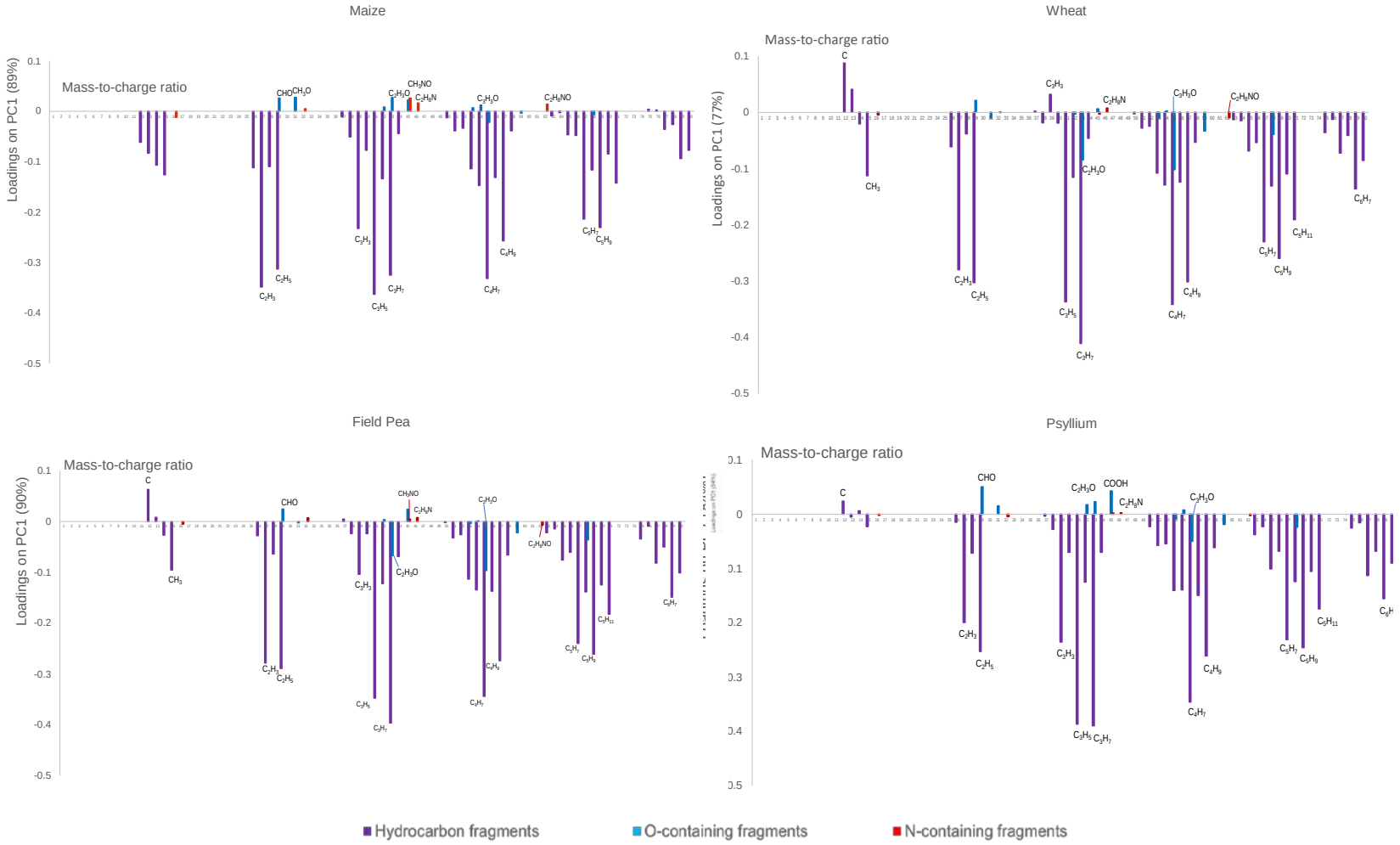


Figure 6-8. Combined PCA loadings of all treatments within a grain type to allow comparisons of fragments analysed during ToF-SIMS. When the inorganic cations are removed from the analysis, the hydrocarbon fragments become the dominant components shaping the plots.

	Maize			Wheat			Field Pea			Psyllium		
Fragment	**U vs P30**	**U vs P90**	**P30 vs P90**	**U vs P30**	**U vs P90**	**P30 vs P90**	**U vs P30**	**U vs P90**	**P30 vs P90**	**U vs P30**	**U vs P90**	**P30 vs P90**
C				0.0406	0.9202	0.1007						
CH_2	0.2096	0.0401	0.7266									
CH_3	0.0665	0.0112	0.7769									
C_2H_3	<0.0001	<0.0001	0.0789	<0.0001	<0.0001	0.8327	<0.0001	<0.0001	0.2653	<0.0001	<0.0001	0.9478
C_2H_5	<0.0001	<0.0001	0.3598	<0.0001	<0.0001	0.7253	<0.0001	<0.0001	0.445	<0.0001	<0.0001	0.1194
C_3H_3	<0.0001	<0.0001	0.4726				0.0072	0.0046	0.9886	<0.0001	<0.0001	0.4461
C_3H_5	<0.0001	<0.0001	0.0619	<0.0001	<0.0001	0.7105	<0.0001	<0.0001	0.1502	<0.0001	<0.0001	0.0006
C_3H_6	0.1007	0.0315	0.8771				<0.0001	<0.0001	0.3709			
C_3H_7	<0.0001	<0.0001	0.7004	<0.0001	<0.0001	0.5284				<0.0001	<0.0001	0.0004
C_4H_6	0.0848	0.0306	0.907									
C_4H_7	<0.0001	<0.0001	0.3954	<0.0001	<0.0001	0.7628	<0.0001	<0.0001	0.7887	<0.0001	<0.0001	0.0305
C_4H_9	<0.0001	<0.0001	0.6361	<0.0001	<0.0001	0.8274	<0.0001	<0.0001	0.9236	<0.0001	<0.0001	0.1979
C_5H_7	<0.0001	<0.0001	0.8031	0.0043	0.0077	0.9806	0.0018	0.0008	0.9692	0.0097	0.0004	0.5876
C_5H_9	<0.0001	<0.0001	0.808	0.0002	0.0006	0.9703	0.0002	0.0001	0.9811	0.0037	<0.0001	0.5379
K^+	<0.0001	<0.0001	0.0069	<0.0001	<0.0001	<0.0001	<0.0001	<0.0001	0.9209	0.1786	0.0013	0.0917
Mg^{2+}							0.0528	0.001	0.2372			
Ca^{2+}							0.0348	0.006	0.7287			
CHO							0.0036	0.3373	0.1044			
C_2H_3O							0.4597	0.0001	0.0032			
C_3H_3O				0.0006	0.002	0.8871	<0.0001	<0.0001	0.64			
CH_3NO	<0.0001	0.0261	0.0093				0.0162	0.7999	0.0045			
C2H8NO	0.0035	0.2453	0.0927									

Table 6-1. Fragments with significant differences between treatments are listed with accompanying p-values to compare trends between grain types. Highlighted cells show statistically different trends for fragments between treatments shared in all grains. Blank cells indicate that no statistically significant values were found for this fragment within a grain type. Significance was accepted at $p<0.05$. Abbreviations: U (Untreated); P30 (30-minute plasma); P90 (90-minute plasma).

extracted and placed in Table 6-1 to compare p-values and look for similarities and differences between grain types. Due to variations in surface structure between grain types, as shown in SEM imagery in Chapter 4, we can expect differences. However, the similarities observed may provide insight to the reactions occurring within the field of plasma.

There are eight fragments shared across all four grain types with significant patterns between treatments; one of which is potassium, while the other seven were hydrocarbon fragments. This trend of hydrocarbon modifications is expected given the prevalence of waxes and complex sugars across the grain surface. Noteworthy is the level of significance within treatment comparisons. Many of the p-values comparing Untreated to P30 and P90 were less than 0.0001, which indicated that the fragment counts have changed with plasma treatment. When comparing P30 and P90 treatments, much larger p-values were obtained, suggesting that chemical changes to the grain surface were less influenced by exposure time. In other words, most of the significant chemical changes are likely occurring within the first 30 minutes of plasma exposure.

The heatmap in Figure 6-9, compares the mean normalised counts for each fragment within groupings and illustrates increases and decreases between treatments and grain types. The counts of oxygen-containing fragments, CHO and COOH, increased with plasma exposure, hinting at the possible oxidation of the seed surface, yet no significant trends were visible. Additionally, no visible patterns could be detected between treatments for nitrogen-containing fragments. The most apparent patterns were found within the hydrocarbon fragments (C_xH_y). Untreated grains had significantly higher counts, which decreased with increasing plasma treatment. Such changes suggest the possible weathering of hydrocarbon-based waxes on the grain surface, which was visually observed by scanning electron microscopy in Chapter 4. While it is

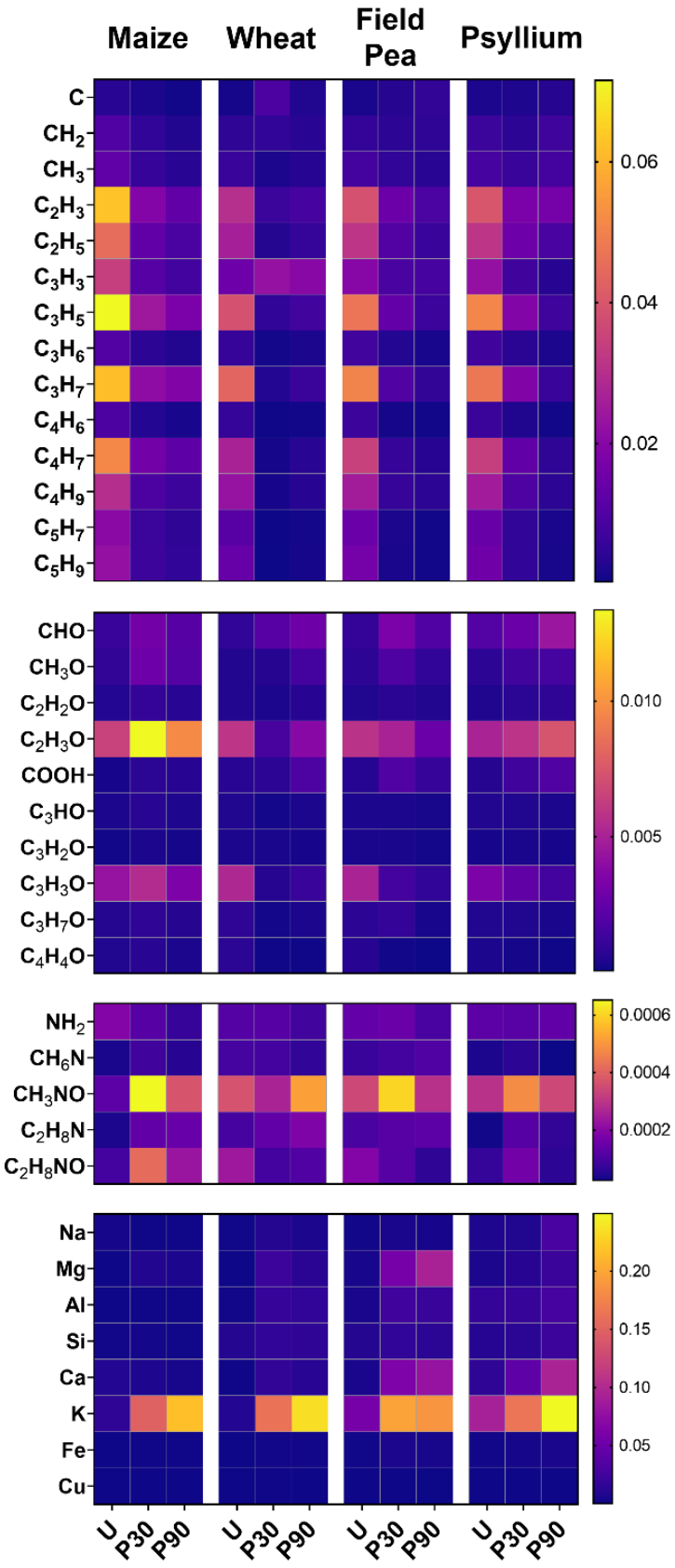


Figure 6-9. Heatmap displaying the means of mass peak area per fragment and treatment. Due to the large number of hydrocarbon (C_xH_y) fragments analysed, only fragments with significant differences between treatments were selected for representation in this heatmap. The full heatmap of hydrocarbon fragments is available in Appendix S7. Note that comparisons should be made only within groupings due to differences in scale. Abbreviations: U (Untreated); P30 (30-minute plasma); P90 (90-minute plasma).

tempting to hypothesize, the details of the chemical reactions occurring between the plasma and grain surface are undoubtedly complex and beyond the scope of this project. Instead, this technology was used as a screening tool to explore possible similarities and differences in surface chemistry fragments following plasma treatment.

6.3.4 Summary

The ToF-SIMS study was conducted to survey the surface chemistry of multiple grain types and to look for variations between treatments. It is evident that plasma-treatment changed the seed surface chemistry. In the PCA plots of all grain types, Untreated controls are segregated from their plasma treated P30 and P90 counterparts. Hydrocarbon fragments and inorganic cations drive the variations. Maize, wheat, and field pea have an uppermost surface layer of wax which serves as a protective covering for the grain. The decrease in hydrocarbon fragments confirms the results from section 6.2 which speculated that the immediate absorption of water droplets into the grain may be due to changes in the outer hydrophobic layer on the seed surface. The enormous increases in inorganic cations may be an artefact of the ready ability of these fragments to ionise. However, it may also indicate that plasma etching is releasing the cations previously bound within cell wall matrices and intracellular structures. Further studies investigating plasma-treated grain interactions with water are necessary to untangle the complexities of the physico-chemical changes.

6.4 The effects of plasma exposure on grain moisture content and water sorption

6.4.1 Introduction

The interaction between water droplets and treatment seed surfaces, shown in section 6.2. above, indicated that the plasma-treatment process increased seed wettability. If water droplets become readily absorbed into the seed surface following exposure to

plasma, the rate of water uptake may also be affected. Water absorption, or imbibition, is the process of seed water uptake and is generally considered the first of three phases of germination. It typically occurs through physico-chemical processes prior to the biological activation of the seed. If the grain does not reach the water potential threshold, it can remain suspended between phases I and II (Figure 6-10) (Bewley et al., 2013). Diffusion will happen in some areas, but each of the five grains in this study contains specific structures, chiefly the micropyle, which aid in grain hydration through capillary action (Miano and Augusto, 2018). Germination phases II and III involve cellular processes which alter the rate of water uptake in the grain (see Chapter 1, Figure 1-2). For this reason, understanding physical water interactions within phase I will provide a better understanding of how plasma treatment may impact initial grain water sorption. To test this concept, it was first necessary to establish the baseline seed moisture content of Untreated, T+V and P90 grains. It was hypothesized that the moisture content would be reduced in both T+V and P90 samples due to the 90-minute vacuum process. A standard oven-drying moisture content assay was performed to measure the mean initial moisture content.

A series of water sorption trials immediately followed this experiment. Traditionally, water sorption is measured by soaking grains, recording their weights at various time intervals, and comparing to the initial grain weights to estimate the bulk water sorption. This time-consuming process can be difficult to interpret as each grain type, and treatment will absorb water at a different rate, posing issues with capturing only phase I of germination. If grains are held at high humidity, but just under the water potential threshold for cell expansion, they will remain indefinitely in phase II (Bewley et al., 2013). Taking advantage of this physiological phenomenon, grains were placed under the water potential threshold in a highly sensitive vapour sorption meter for 72 hours or 120 hours at 90% relative humidity (RH) and 25 °C to allow for water absorption

weights without the risk of cell expansion. This allowed for the capture of data reflecting the physical processes of grain sorption. The data sets were compared to the initial moisture content to determine how the rate of water uptake is altered with plasma-treatment. Finally, the use of the vapour sorption meter allowed for the capture of over 430 measurements per replicate which could then be fitted to grain hydration models to determine the differences in hydration rate and method – diffusion or capillary action. Together, these data sets can be used to understand how plasma exposure influenced grain water relations.

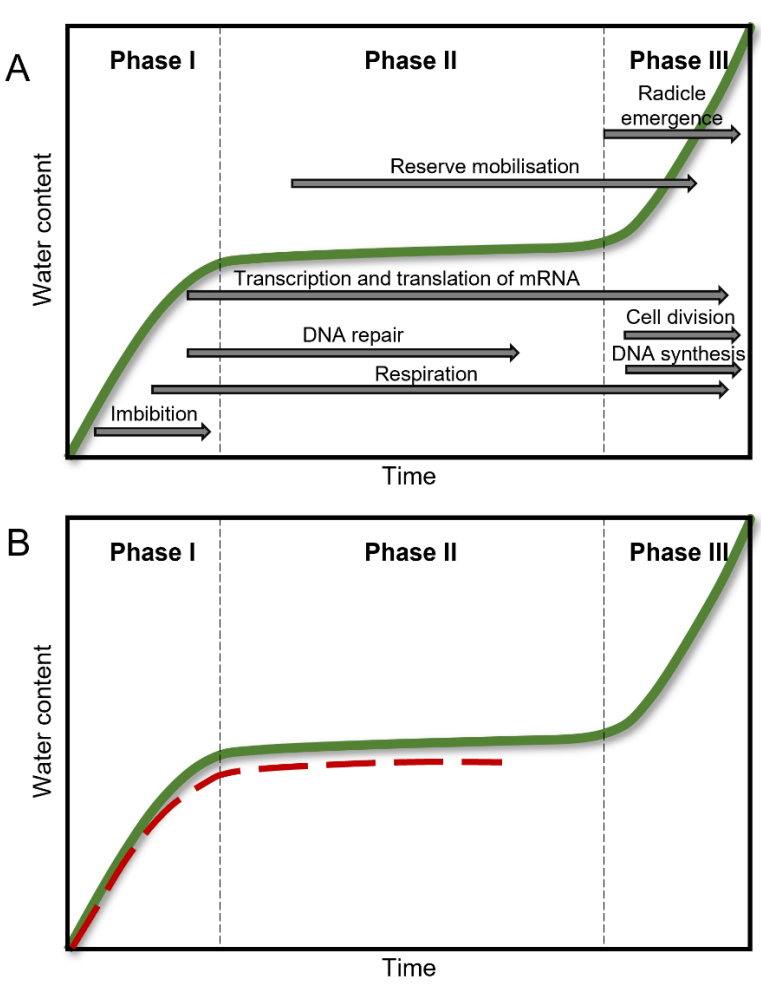


Figure 6-10. Grain water sorption curves based on Bewley et al. 2013. (A) Illustration of the processes occurring across different water content and time points, reproduced from Chapter 1.3.1 for the reader's convenience. (B) This graph displays the standard water sorption curve in green. The red dashed line illustrates where seeds were held below the water potential threshold. Seeds will not proceed through phases II and III until the water potential increases.

6.4.2 Materials and Methods

6.4.2.1 Treatment of grains

60 g of grain was divided into six 10 g treatment aliquots. One aliquot was prepared as a T+V control (Chapter 3.1.2). Four others were placed in the plasma tumbler and treated following protocols in Chapter 3.1.2 for 90 minutes with 10 g removed at 15, 30 and 60-minute intervals to produce P15, P30, P60 and P90 treatments. The remaining aliquot was left as an Untreated control.

Once all treatments were completed, each 10 g aliquot was divided in half. One portion was used for seed moisture content measurements, while the other was left for vapour sorption trials. One grain type was treated each morning for five consecutive mornings. The reasoning behind this complicated treatment process was to ensure the grains were under identical treatment conditions prior to each of the two experiments so datasets could be compared without treatment bias. All grains were kept in 50 mL sterile tubes with Parafilm® M (Amcor) sealing the lids.

6.4.2.2 Seed moisture content

Following plasma exposure, the grain from each treatment was poured into a bladed coffee grinder and pulsed for 20 seconds. Four replicates of 1 g of coarsely ground grain were immediately weighed, recorded, and sealed in 2 mL tubes with Parafilm around the edges. One litre of desiccant beads was poured into a 4 x 40 x40 cm plastic container. A small baking tray was placed on top of the beads with 12 pre-weighed 43 mm aluminium weigh boats (labForce®). Grain from each treatment was swiftly transferred into a weigh boat. Once the boats were filled, the lid of the plastic box was replaced to avoid moisture exposure during transportation to the oven. The baking tray of weigh boats was rapidly transferred to the oven and dried at 120 °C for four hours. Once drying was complete, the tray was transferred back to the desiccant box and left

to cool for 45 minutes as per Grabe, 1989. Final weights were recorded, and percent moisture content was calculated with the equation below.

Equation 6-1.

$$\frac{initial\ weight\ (g)}{dry\ weight\ (g)}\ x\ 100 = \%\ moisture\ content$$

6.4.2.3 Dynamic vapour sorption trials

A vapour sorption analyser was used for sorption measurements as the weights are fully automated and kept under a set temperature and humidity. A pilot trial to establish relative humidity was conducted using maize grain. Aliquots of approximately 1 g of grain were placed in pre-calibrated 33 mm dishes on a ProUmid SPSx-1µ Advance vapour sorption analyser. The instrument was set to 25 °C and 98% RH for 120 hours with weights taken every 10 minutes. Another set of 1 g aliquots of maize grain were run at 25 °C and 90% RH for 120 hours. The results of each experiment were compared, and 90% RH was selected for all experimental trials.

The remaining 5 g aliquot of each grain treatment (Untreated, T+V, P15, P30, P60, P90) from the previous experiment were weighed and split into four roughly 1 g replicates, except for the P15 treatment. The vapour sorption analyser holds 23 samples; therefore, it was decided that the P15 treatment would have only three 1 g replicates. Each of the 23 samples were immediately placed in pre-calibrated 33 mm dishes (Figure 6-11). The instrument was set at 90% relative humidity (RH) and 25 °C with weights taken every ten minutes and images taken every hour. Wheat, barley, and psyllium data collection ran for 72 hours as grains generally reach germination stage three within 24 hours at high water potential. Maize and field pea data collection lasted for 120 hours as it typically takes between 72 and 96 hours for these grains to reach germination phase III at a high water potential. Data was collected within the

accompanying SPS Software and exported to GraphPad Prism 9.0.0 for statistical analysis.

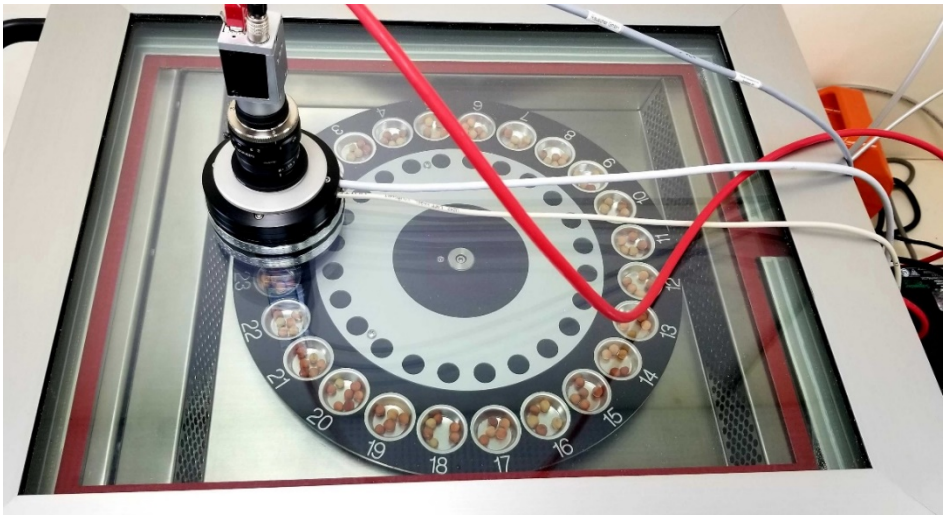


Figure 6-11. Field pea grains in the carousel of a ProUmid SPSx-1µ Advance vapour sorption analyser.

6.4.2.4 Modelling

The hydration kinetics of maize, wheat, barley, and psyllium grains follow a downward concave shape (DCS) which can be described by grain hydration models developed for the food processing industry. Two mathematical models, Peleg (Peleg, 1988) and the 2-step hydration model (Miano et al., 2017) were selected to describe the rate of water uptake and how this is balanced between capillary action and diffusion. Field pea, which displays a sigmoidal hydration behaviour data, was variable between replicates. This may be associated with the large variations between grains in size, and therefore surface area. The errors in replicate measurements created large uncertainties in the fitting algorithm, resulting in poor data fits and were omitted from modelling. Model equations were transposed for analysis in GraphPad Prism 9.0.0 software (Figure 6-12). Each grain type was fitted to the model and the goodness of fit was determined by R^2 values.

Equation 6-2. Peleg equation: $$M_t = M_0 + \frac{t}{k_1 + (k_2 t)}$$ Fitting interpretation of Peleg model in x y coordinates, assuming M0 = 0: $$y = \frac{x}{k_1 + (k_2 x)}$$ Equation 6-3. 2-phase equation: $$\frac{(M_t - M_\infty)}{(M_0 - M_\infty)} = p(1 - e^{-k_{M1}t}) + (1-p)(1 - e^{-k_{M2}t})$$ $$M_t = M_0 + (M\infty - M0)\,(p(1 - e^{-k_{M1}t}) + (1-p)(1 - e^{-k_{M2}t}))$$ Fitting interpretation of 2-phase model in x y coordinates, assuming M0 = 0: $$y = y_\infty p(1 - e^{-k_{M1}x}) + y_\infty(1-p)(1 - e^{-k_{M2}x})$$	$\frac{1}{k1}$ = rate of hydration (h-1) $\frac{1}{k2}$ = % change in dry mass kM1 = rate of capillary flow (h-1) kM2 = rate of diffusional flow (h-1) M_∞ = equilibrium moisture content (%) M_0 = initial moisture content (%) M_t = moisture content as a function of time (%) p = % fast water absorption $$p = \frac{\Delta M1 t}{(M_t - M_0)}$$ t = time (h

Figure 6-12. Modelling equations and the interpretation for use in GraphPad Prism 9.0.0.

6.4.2.5 Statistical analysis

GraphPad Prism 9.0.0. software was used to analyse data throughout this section. A grouped analysis with two-way ANOVA and Tukey's multiple comparison tests were used to compare initial seed moisture content and initial to final seed moisture content. One-way ANOVA with Tukey's multiple comparisons tests were performed on the final seed moisture content to determine the water sorption in mg. Data were expressed as mean ± standard error of the mean. Significance was accepted at $p<0.05$.

6.4.3 Results and Discussion

Observations of water droplets absorbing into the seed surface during contact angle measurements led to the speculation that plasma treatment may be altering the rate of water sorption into the grain. As this section is focused on the plasma-induced changes to the seed surface that may be impacting the rate of water sorption, it is ideal to consider the initial water surface sorption and first stage of uptake. The first step

was to establish a baseline measurement by calculating the initial moisture content for each grain type and treatment. Next, grains were placed in a sorption meter and held at 25 °C and 90% RH to allow vapour sorption into the grain but suspend further germination phases, illustrated in Figure 6-10. It should be noted that a pilot trial was conducted on maize held at 25 °C and 98% RH, which triggered fungal growth (Figure 6-13). As fungal water sorption could confound the measurements, RH was dropped to 90% for all experimental data gathering.



Figure 6-13. A pilot trial with maize grain held at 25 °C and 98% relative humidity for 120 hours. At 98% relative humidity, the water potential was high enough to trigger fungal growth as seen (suspected to be *Rhizopus arrhizus*) colonising maize in dishes 14 and 15.

6.4.3.1 Initial seed moisture content

The initial seed moisture content of each grain type and treatment was calculated and compared via two-way ANOVA with Tukey's multiple comparisons tests (Figure 6-14). The moisture content varied greatly between grain type and treatment. Maize moisture content appeared to be influenced by the 90-minute vacuum in both T+V and plasma treatments rather than the plasma alone. Conversely, wheat and barley moisture contents were influenced more by plasma treatment than the vacuum. Psyllium moisture content was reduced by both vacuum and plasma treatments. There were no differences between the field pea treatments possibly due to the variations in grain size and total sample surface area.

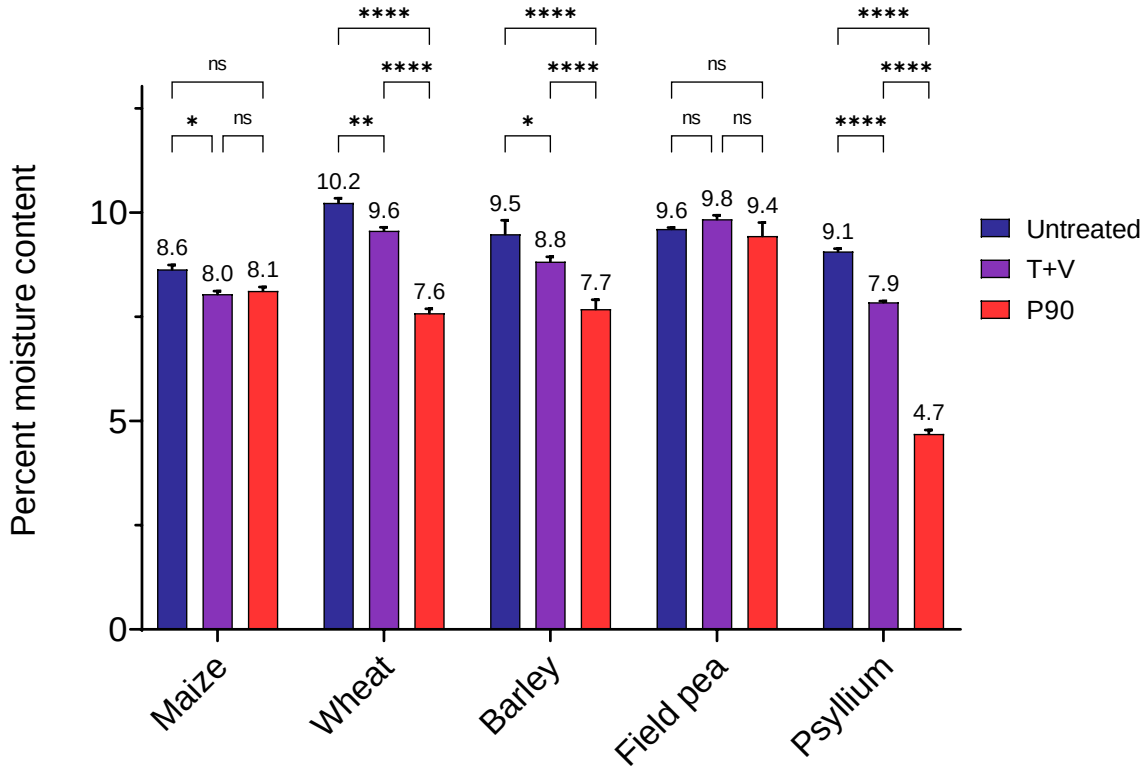


Figure 6-14. Comparison of initial seed moisture content for all grain types and treatments. Data is presented as mean ± SEM. Abbreviations: T+V (Tumbler + vacuum); P90 (90-minute plasma); ns (non-significant); *p<0.05; **p>0.01; ****p>0.0001.

6.4.3.2 Vapour sorption comparisons

This experiment sought to use the detailed data sets collected from the vapour sorption meter to understand patterns within each grain type. Sorption curves were plotted to determine the difference in water uptake between treatments (Figure 6-15). The steep initial slopes, followed by a plateau, suggested that grain has progressed through the physical phase of imbibition and is suspended at the water potential threshold created by 90% RH. Wheat, barley, and psyllium produced textbook style curves over their 72-hour measurement window. These smaller grains have been bred for consistent germination within 24 hours of imbibition. Unsurprisingly, the rate of water sorption increased rapidly over the first 20 hours then begins to slow. Maize and field pea required longer measurement windows due to the large grain size and slower germination rate, typically occurring between three or four days after imbibition. Maize

curves followed a similar pattern to wheat, barley, and psyllium over the longer time course, with distinct separation of treatments occurring around 40 hours, as compared to the 10-hour timepoint seen in the other three grains. On the other hand, the rate of water sorption in field pea continued to increase up to 120 hours. 90-minute plasma exposure resulted in a curve most consistent with the other species, while Untreated and T+V curves did not quite reach the plateau after 120 hours.

The amount of water absorbed per treatment was calculated by subtracting the initial weight from the final weight. These data sets were analysed by one-way ANOVA with Tukey's multiple comparison tests to determine the statistical differences between treatment means (Figure 6-16). Overall, a general pattern was observed across all grain types. Plasma treated grains absorbed more water than the Untreated and T+V control samples. The difference was most significant at the 90-minute exposure time point. Water sorption increased by 38%, 35%, 33%, 16% and 32% for maize, wheat, barley, field pea and psyllium, respectively. These data suggest that plasma treatment had a strong effect on the water sorption capacity of grain.

While plasma treated grains absorbed more water than both the Untreated and T+V controls, it was unclear if this may be attributed to compensation. It was unclear if the lower initial seed moisture content allowed the grains to take up water lost in the vacuum during plasma treatment. To investigate the effects of initial moisture content on water sorption, comparisons were made between the final percent moisture content from the vapour sorption meter data sets and the initial moisture content (Figure 6-17). In all cases, plasma-treated grains absorbed more water than was originally lost due to vacuum-treatment. The initial moisture content in every grain type was lowest for plasma-treated grains; the final moisture content was the highest. This data set showed that the water sorption capacity of grains increased following plasma treatment, despite initial moisture loss due to the vacuum.

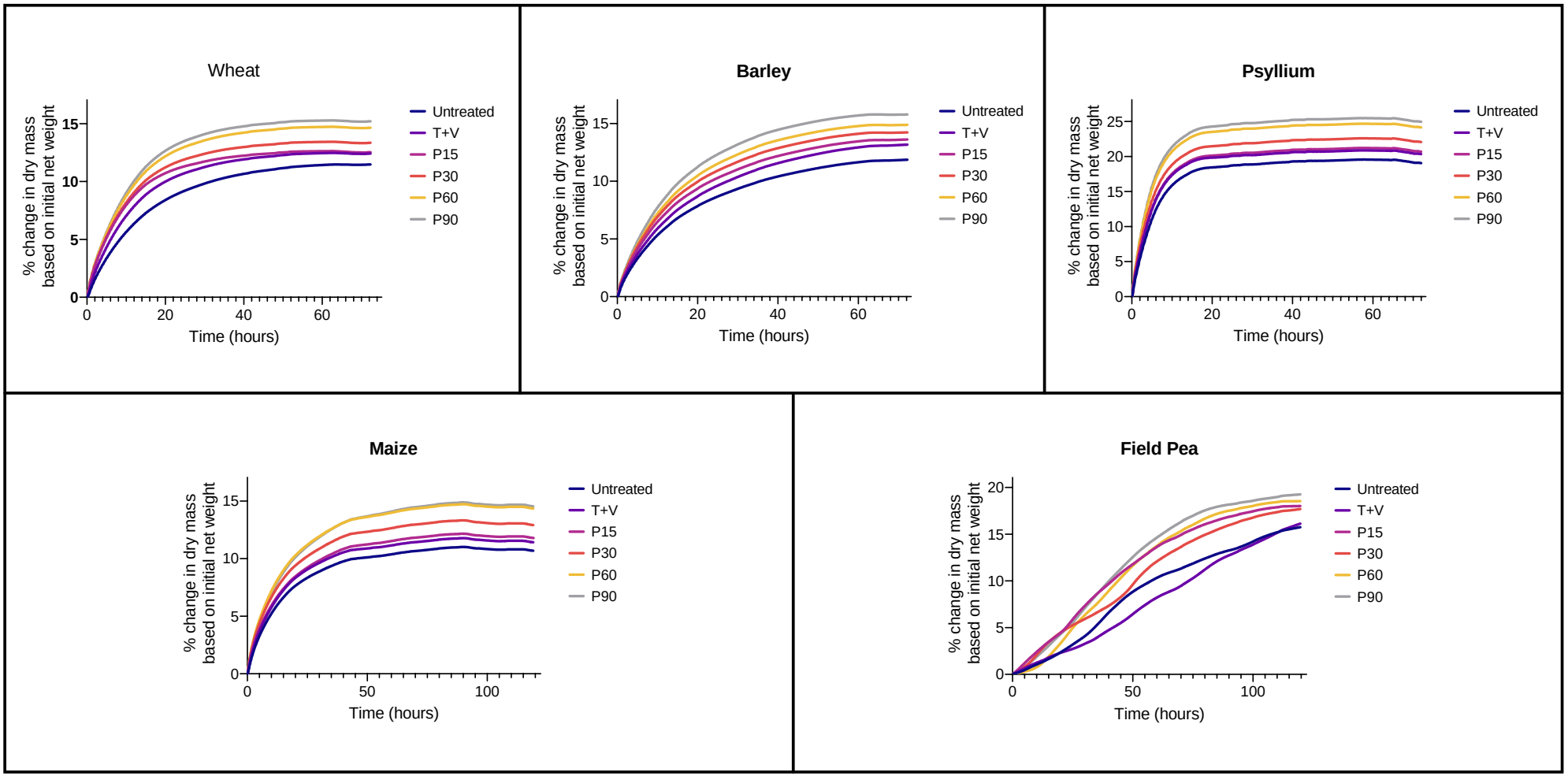


Figure 6-15. Water sorption curves comparing each treatment within a grain type. Maize and field pea were measured over the course of 120 hours. Wheat, barley, and psyllium were measured over 72 hours. All grains, except field pea, appeared to follow the standard sorption curve with a steep initial slope that flattened over time.

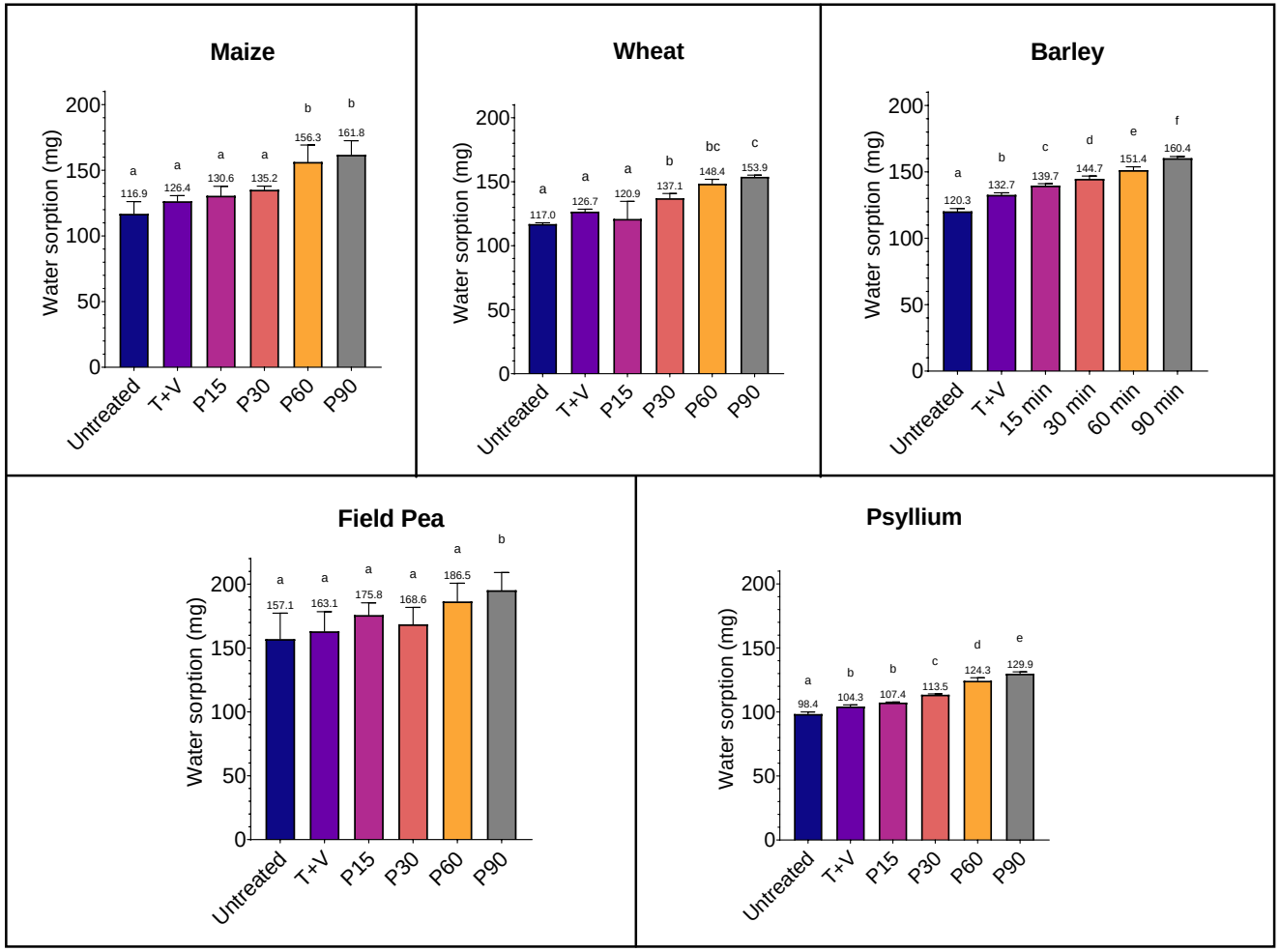


Figure 6-16. Comparisons between water sorption means of each treatment. In all grain types, the P90 (90-minute plasma) treatment absorbed significantly more water than the Untreated controls. Data is presented as mean ± SEM with significance accepted at $p<0.05$. Letters indicate statistical differences between means. Abbreviations: T+V (Tumbler + vacuum); P15 (15-minute plasma); P30 (30-minute plasma); P60 (60-minute plasma); P90 (90-minute plasma).

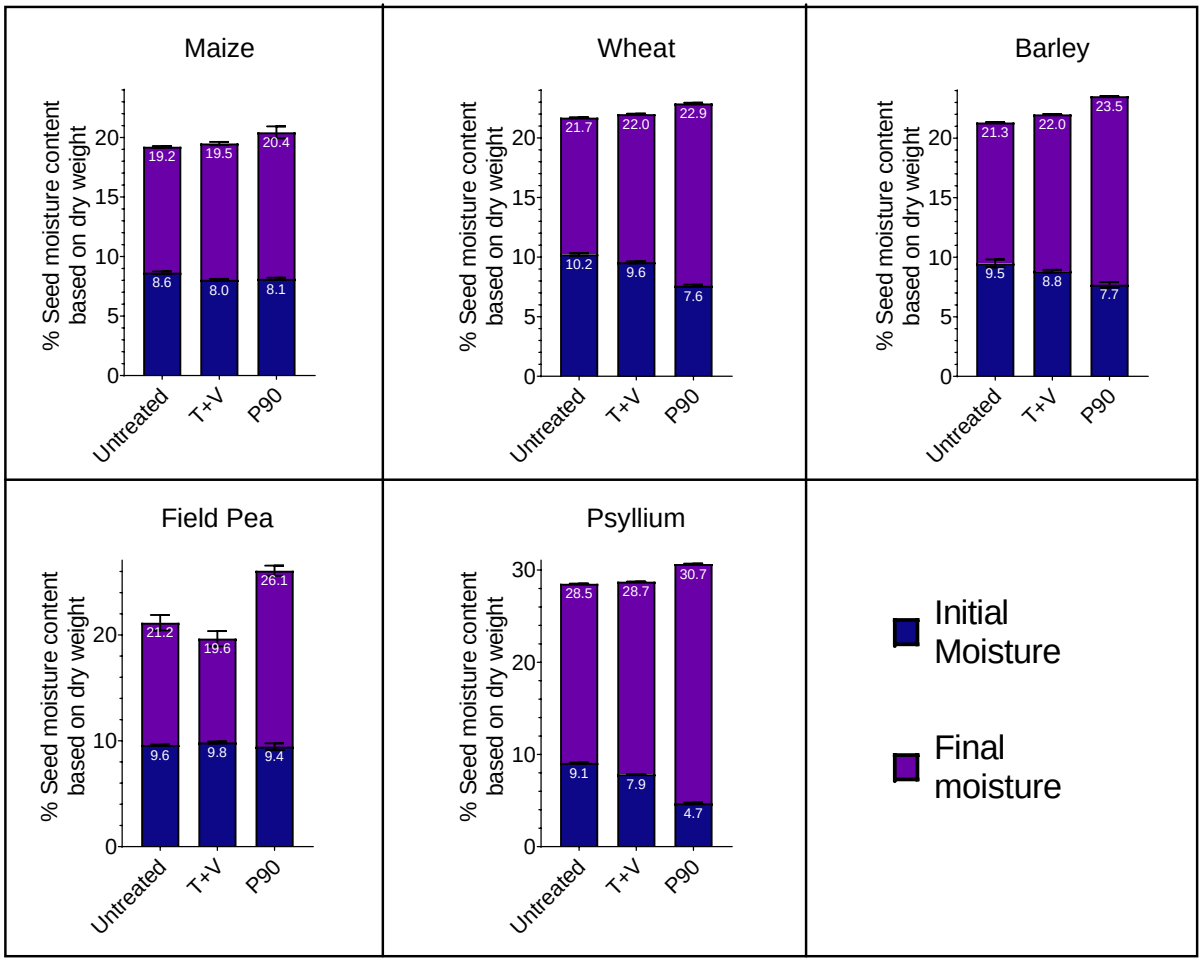


Figure 6-17. Comparison between final sorption meter moisture content and initial moisture content. Data is presented as mean ± SEM. These data sets were used to determine if plasma-treated samples were absorbing more water to compensate for the initial moisture loss due to vacuum treatment. Abbreviations: T+V (Tumbler + vacuum); P90 (90-minute plasma).

The increase in grain water sorption capacity following plasma treatment was pronounced. It was speculated that plasma changed the seed surface properties, allowing water to enter the grain differently. Etching of hydrophobic surface compounds and a slight increase in surface area due to changes in roughness (see Chapter 4), may have allowed more water to diffuse through seed surfaces. It is also unknown if seed interactions between water in a liquid state and vapour state caused differences in sorption capacity. In soil, seeds typically encounter water vapour within soil pores where imbibition can occur by gas diffusion. However, it has been established that vapour imbibition alone is generally insufficient to raise the seed water potential past phase II, thus preventing the onset of germination (Bewley et al., 2013). This concept was taken advantage of during these experiments but may also induce unknown artefacts due to the paucity of research surrounding water vapour sorption in seeds. Experiments to understand plasma-induced changes to water uptake patterns across grain tissues are explored in section 6.5.

6.4.3.3 Modelling grain hydration kinetics

Upon contact with water, grains begin to hydrate through both diffusion and capillary action. The processes of capillary flow occur as water follows specific pathways and pores, such as the micropyle, as well as empty spaces between cells and tissues. It is a rapid process and takes place in all five grains in this study (Miano and Augusto, 2018). Diffusion is a much slower process as water transport is influenced by concentration gradients through semi-permeable barriers such as the seed coat. Due to the statistically significant increases in water sorption capacity of plasma treated grains, it was speculated that the hydration kinetics may be altered. The best way to test this concept was with hydration kinetic models. The Peleg model (Peleg, 1988) describes the rate ($\frac{amount\ of water}{time}$) of bulk water sorption. It is an empirical model which generally fits sorption data with physical significance for both constants (k_1 and k_2).

The 2-phase model (Miano et al., 2017) considers the different rates of water uptake by the exponential association of water in two phases. The fast term is interpreted as being influenced by capillary forces and the slow term is interpreted as being influenced by diffusion. Thus, the 2-phase model is derived from physical laws and the constants are directly related to the rate of hydration in each phase. When used in tandem, the Peleg and 2-phase models can illustrate how plasma treatment alters the rate and process of grain hydration. It should be noted that both equations are suitable for grains with a downward concave shape pattern of hydration. Field pea had a sigmoidal shape hydration pattern and was omitted from this study. Future research may consider using a sigmoidal Kaptso model to study this grain (Kaptso et al., 2008).

6.4.3.3.1 Fitting the models

Prior to analysis, all grain types and treatments were fitted to the models (Figure 6-18). The goodness of fit was determined by R^2 values which varied between grain type and treatment (Table 6-2). Wheat and barley nicely fitted the Peleg model across all treatments, maize, and psyllium less so. This generalisation has also been documented in maize by Miano et al., 2017, and led to the proposal of the 2-phase model by these authors. Wheat, barley, and psyllium treatments fit the 2-phase model remarkably well ($R^2 > 0.99$). Despite the development of the model for maize, this grain type did not fit as well as the other grains, with R^2 values reducing with increasing plasma treatments. Nonetheless, the variations in correlation coefficients were not detrimental to model fitting and all grain types were considered acceptable for both models.

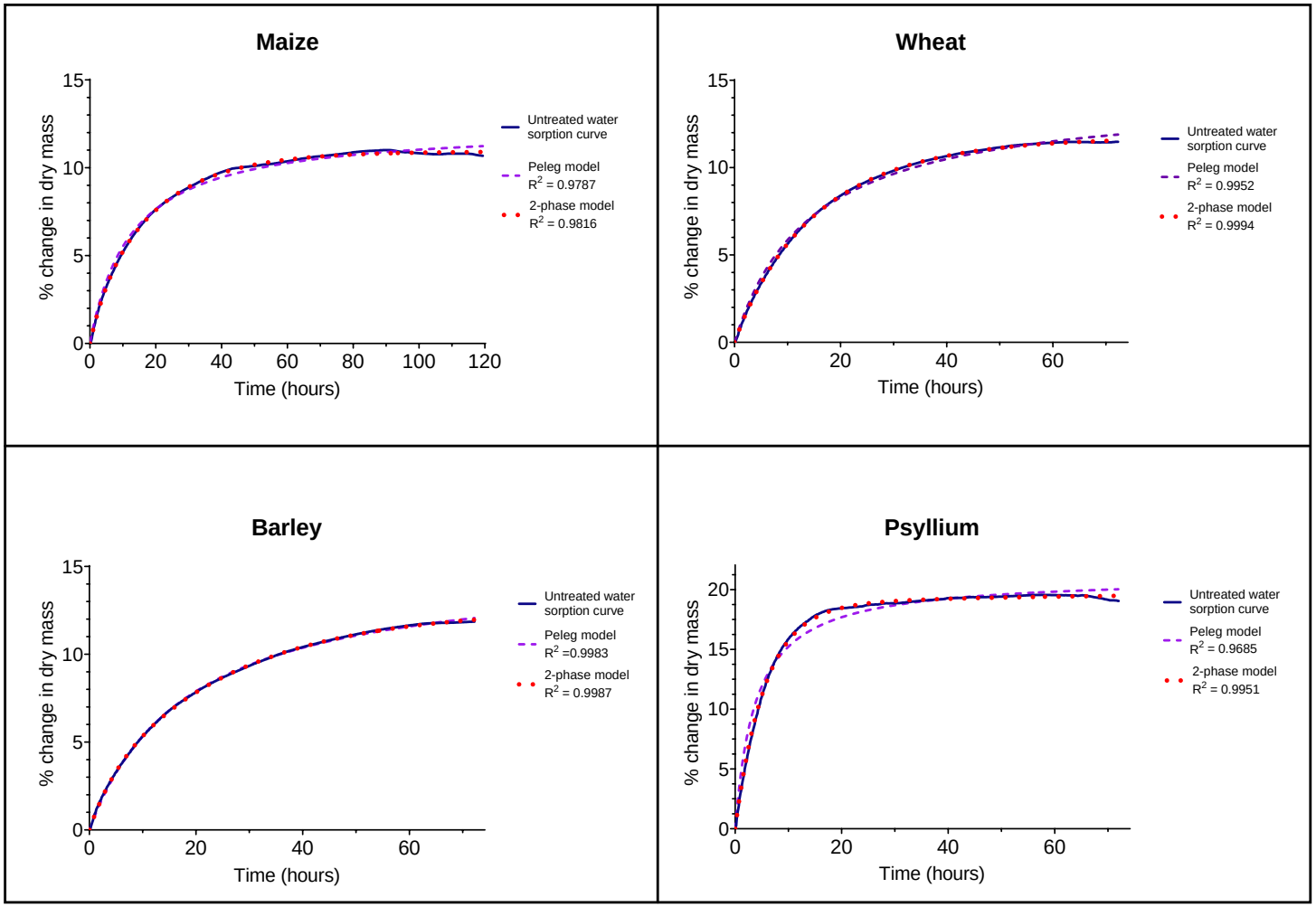


Figure 6-18. Fitting the Peleg and 2-phase models to Untreated replicates of each grain type (maize, wheat, barley, and psyllium) in GraphPad Prism 9.0.0.

Peleg Model																				
Grain		**Untreated**			**T + V**			**P15**			**P30**			**P60**			**P90**		
Maize	R^2	0.9787			0.9800			0.9384			0.9821			0.9547			0.9278		
	k_1	1.008	±	0.011	0.885	±	0.009	0.839	±	0.015	0.767	±	0.007	0.725	±	0.011	0.768	±	0.015
	k_2	0.0806	±	0.0002	0.0759	±	0.0002	0.0715	±	0.0003	0.0673	±	0.0001	0.0604	±	0.0002	0.0592	±	0.0003
Wheat	R^2	0.9952			0.9842			0.9907			0.9908			0.9887			0.9884		
	k_1	1.007	±	0.006	0.644	±	0.007	0.549	±	0.007	0.541	±	0.005	0.522	±	0.005	0.509	±	0.005
	k_2	0.0701	±	0.0002	0.0686	±	0.0002	0.0688	±	0.0002	0.0646	±	0.0002	0.0584	±	0.0002	0.0561	±	0.0002
Barley	R^2	0.9983			0.9980			0.9991			0.9983			0.9983			0.9979		
	k_1	1.212	±	0.004	1.096	±	0.004	0.947	±	0.003	0.867	±	0.003	0.827	±	0.003	0.759	±	0.003
	k_2	0.0661	±	0.0001	0.0594	±	0.0001	0.0589	±	0.0001	0.0566	±	0.0001	0.0539	±	0.0001	0.0510	±	0.0001
Psyllium	R^2	0.9685			0.9709			0.9726			0.9748			0.9745			0.9737		
	k_1	0.183	±	0.003	0.155	±	0.002	0.155	±	0.003	0.139	±	0.002	0.124	±	0.002	0.121	±	0.002
	k_2	0.0474	±	0.0001	0.0447	±	0.0001	0.0439	±	0.0001	0.0414	±	0.0001	0.0379	±	0.0001	0.0367	±	0.0001

2-phase Model																				
Grain		**Untreated**			**T + V**			**P15**			**P30**			**P60**			**P90**		
Maize	R^2	0.9861			0.9881			0.9465			0.9894			0.9615			0.9341		
	k_{M1}	0.19	±	0.03	0.23	±	0.03	0.36	±	0.09	0.33	±	0.04	0.33	±	0.07	0.37	±	0.11
	k_{M2}	0.049	±	0.002	0.052	±	0.001	0.052	±	0.002	0.052	±	0.001	0.051	±	0.002	0.049	±	0.002
Wheat	R^2	0.9994			0.9920			0.9993			0.9992			0.9978			0.9989		
	k_{M1}	0.17	±	0.02	0.17	±	0.03	0.21	±	0.02	0.41	±	0.06	0.87	±	0.20	1.34	±	0.26
	k_{M2}	0.057	±	0.001	0.071	±	0.008	0.079	±	0.002	0.084	±	0.001	0.084	±	0.001	0.0854	±	0.0004
Barley	R^2	0.9987			0.9985			0.9996			0.9990			0.9994			0.9993		
	k_{M1}	0.22	±	0.01	0.25	±	0.02	0.25	±	0.01	0.25	±	0.01	0.27	±	0.01	0.27	±	0.02
	k_{M2}	0.039	±	0.001	0.040	±	0.001	0.0433	±	0.0004	0.046	±	0.001	0.0489	±	0.0005	0.051	±	0.001
Psyllium	R^2	0.9951			0.9983			0.9986			0.9987			0.9991			0.9988		
	k_{M1}	0.180	±	0.002	0.195	±	0.001	0.195	±	0.002	0.208	±	0.002	0.213	±	0.001	0.211	±	0.002
	k_{M2}	0.024	±	0.009	0.029	±	0.005	0.033	±	0.006	0.044	±	0.004	0.047	±	0.004	0.046	±	0.004

Table 6-2. Fitting the Peleg and 2-phase model to the sorption data sets. The R^2 values and means of best-fit values ± 95% CI are listed for each grain type and treatment.

6.4.3.3.1 Using the Peleg model to interpret grain hydration

In the Peleg model, the inverse of parameter k_1 is equivalent to the rate of water sorption (h^{-1}), while the technically dimensionless parameter k_2 reflects the percent change in dry mass caused by water absorption. When the means of each treatment are plotted (Figure 6-19) it allows the comparison of hydration rate and bulk water sorption with increasing plasma exposure for each treatment. Across all grain types, T+V and plasma treatments increased the rate of water uptake and the total amount of water uptake. It is unsurprising that T+V increased the total ingress by about 6% as this is likely replacing the moisture content lost during the 90-minute vacuum exposure. The changes in rate of water uptake for all T+V treatments demonstrated that the vacuum altered the seed water potential, allowing for more rapid movement of water into the grain.

In maize, the hydration rate (inverse k_1) increased with plasma exposure until 90-minutes when the rate matched that of 30-minutes, roughly 31% higher than the Untreated grains. Interestingly, the bulk water sorption (inverse k_2) increased between 60 and 90-minutes of plasma, even though the rate of water ingress was slightly lower by 90-minutes.

Wheat grains displayed a dramatic increase in hydration rate with P90 absorbing water vapour 97% faster than Untreated grains. Surprisingly, the T+V treatment had a 56% rate increase when compared to Untreated but only a 2% increase in bulk sorption. This suggests that water rapidly re-enters the grain following vacuum treatment, but the total water uptake is relatively unaffected.

Both barley and psyllium displayed similar trends in hydration rate (inverse k_1) with increased rates of 59% and 51%, respectively, between Untreated and P90. The bulk sorption increased by 29% in both grain types. The baseline of water sorption for psyllium was much higher than the other three grains with a 21% increase in mass for

Untreated control grains and 27% for P90 grains. This is most likely explained by the hydrogel properties of the polysaccharide mucilage on the grain surface. Overall, the Peleg model showed there was a positive correlation between plasma treatment and both the rate and amount of water uptake.

6.4.3.3.2 Using the 2-phase model to interpret grain hydration

The 2-phase model describes the difference in water sorption rate over time. The initial steep slope (germination phase I) is interpreted as water sorption via capillary transport (k_{M1}). As the rate of absorption reduces over time (transition from germination phase I to phase II), this is thought to correspond with a greater influence of slower mode water transport. The slower processes of hydration are interpreted to be diffusion (k_{M2}). Like the Peleg model, the means of the two constants for each treatment were plotted to visualise how these constants are influenced by plasma treatment. In other words, the graphs illustrate the changes in capillary flow and diffusional flow (Figure 6-20).

In a broad sense, plasma treatment increased the rate of capillary transport (k_{M1}). Yet, the impact of plasma treatment varied widely between grain types. The diffusional water ingress increased in wheat, barley and psyllium but remained constant in maize. This highlighted the differences in surface chemistry and seed morphology, as these factors determined the impact of plasma exposure on water ingress.

In maize grains, all plasma exposures greatly affected capillary water transport. Plasma exposure increased the capillary hydration rate (k_{M1}) by 76% to 97% when compared to Untreated grains. The dominance of this value was remarkable because, across all treatments the diffusion rate (k_{M2}) remained unchanged. When considered in tandem with the Peleg model for maize, the improvement of water sorption in plasma-treated grain was likely due to the increase in capillary flow.

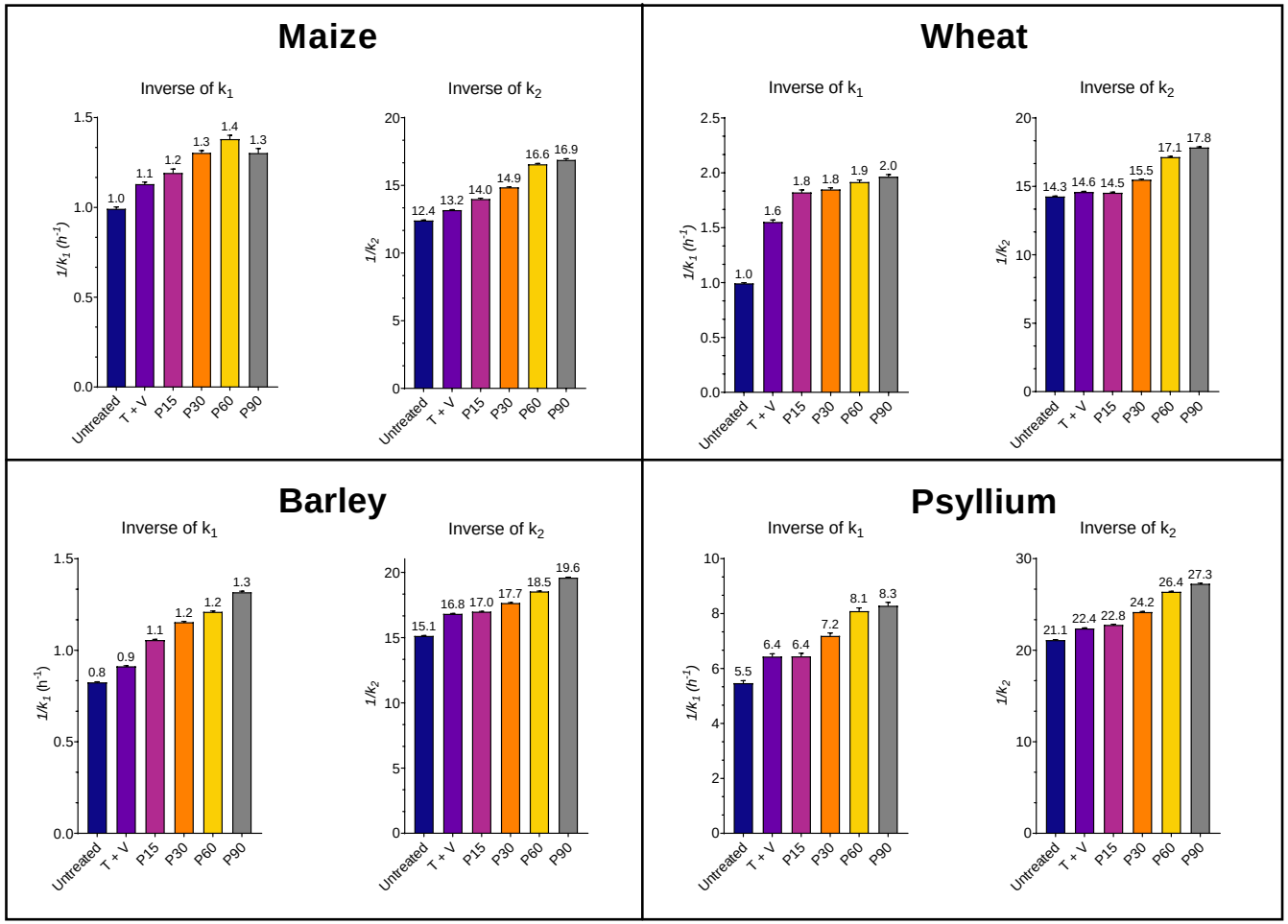


Figure 6-19. Sorption data fitted to the Peleg model (Peleg, 1988) of grain hydration. The inverse of the means of best-fit values ± 95% CI are plotted for each treatment. The inverse of k_1 (h^{-1}) corresponds to the rate of water ingress into the grain. The inverse of k_2 is equivalent to the % change in dry mass as seen in Figure 6-15. Abbreviations: T+V (Tumbler + vacuum); P15 (15-minute plasma); P30 (30-minute plasma); P60 (60-minute plasma); P90 (90-minute plasma).

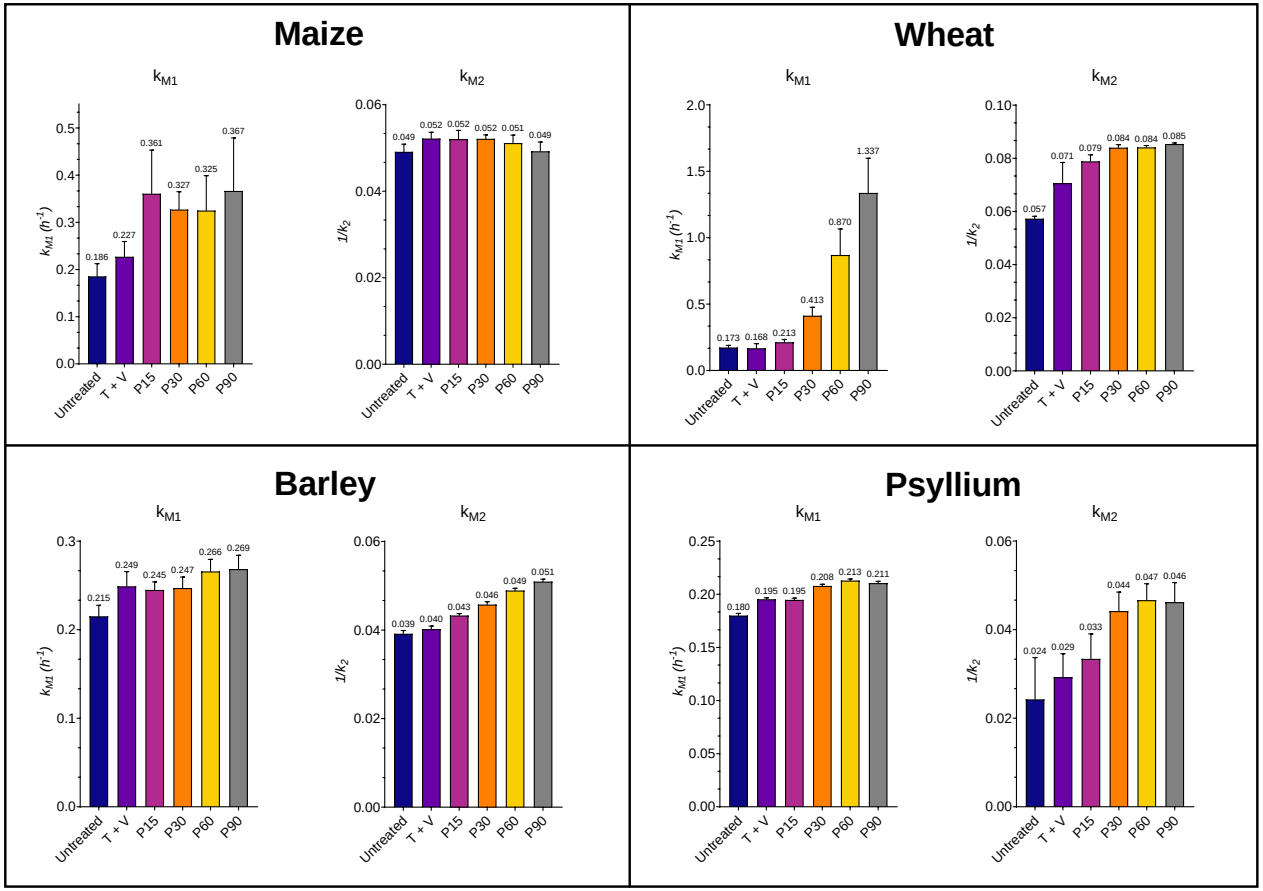


Figure 6-20. Sorption data fitted to the 2-phase model (Miano et al., 2017). The means of best-fit values ± 95% CI are plotted for each treatment. k_{M1} represents the constant for rate of fast water ingress, interpreted as water entry via capillary action. k_{M2} represents the constant for rate of slow water ingress, interpreted as water entry via diffusion. Note the differences in scale bars between grain types, with particular attention to wheat k_{M1}. Abbreviations: T+V (Tumbler + vacuum); P15 (15-minute plasma); P30 (30-minute plasma); P60 (60-minute plasma); P90 (90-minute plasma).

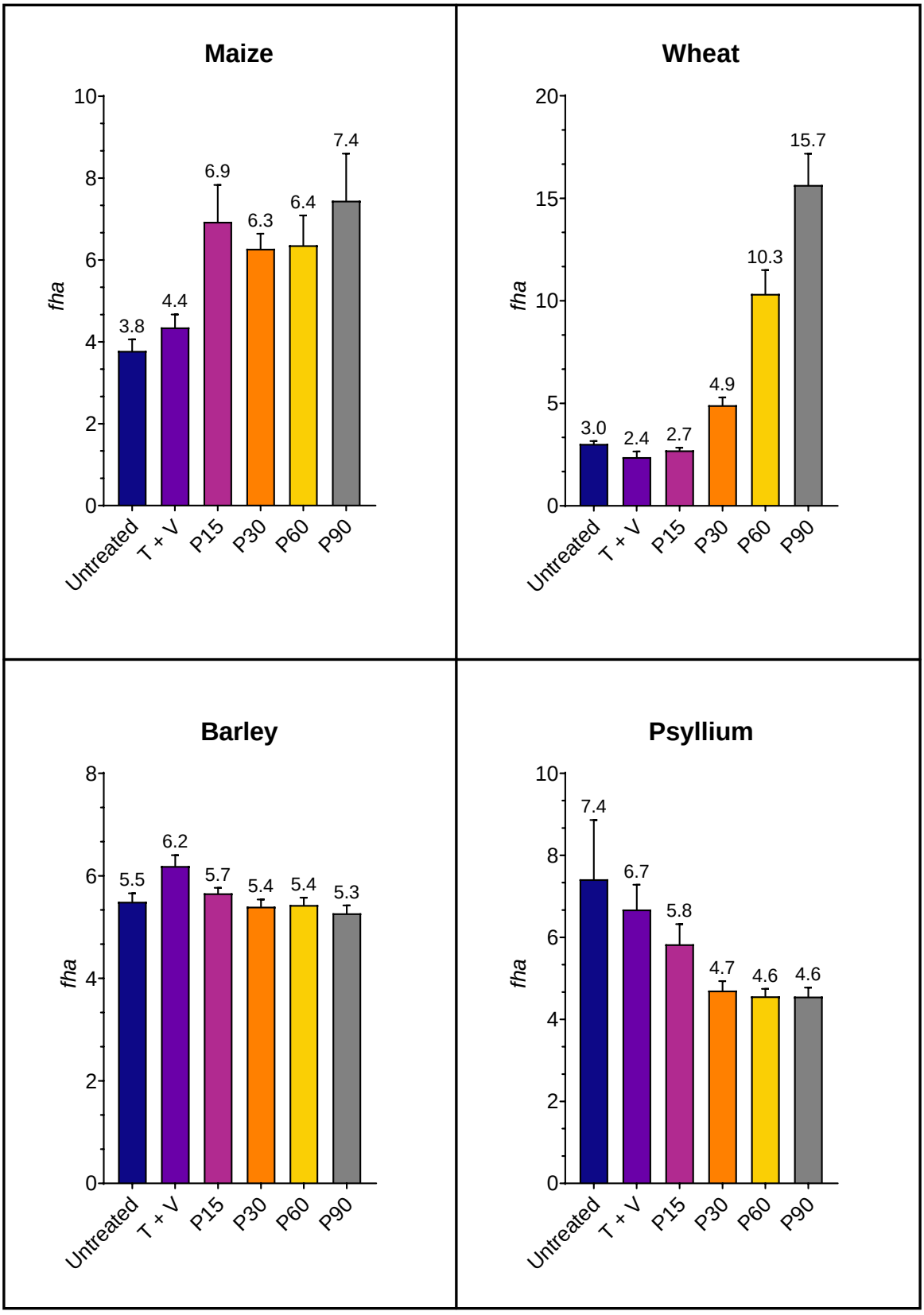


Figure 6-21. Ratio of k_{M1} constant means to k_{M2} constant means ± 95% CI. Capillary action values are always larger than diffusion values which means the ratio is much greater than one. Abbreviations: T+V (Tumbler + vacuum); P15 (15-minute plasma); P30 (30-minute plasma); P60 (60-minute plasma); P90 (90-minute plasma).

In wheat grains, the plasma-induced changes to capillary flow were astounding, with increases of 672% when comparing P90 to Untreated grains. As the model fitting R^2 value for Untreated was 0.9994, and 0.9899 for P90, the changes in k_{M1} are genuine and unlikely to be artefacts of the model. Additionally, diffusional hydration increased by 50% with P90 treatment. This signified that major changes in water flow were occurring following plasma treatment which may have downstream impacts on seed growth and development and will be further investigated in Chapter 7.

Barley grains displayed moderate changes in capillary and diffusional flow, 25% and 30%, respectively, with increasing plasma exposure. This may be interpreted as a general increase in water sorption due to plasma treatment without shifting the processes of water uptake toward one form or another.

In psyllium a very different effect was seen. Increases in hydration due to capillary action were small. Instead, it appeared that diffusion is the dominant process of water uptake. Again, this likely occurred due to the presence of the mucilage layer on the seed surface.

The pronounced differences in hydration action between grain types led to the comparison of the ratio of capillary hydration to diffusive hydration (Figure 6-21). k_{M1} values were always greater than k_{M2} values, which led to ratios greater than one. Increasing values correspond with a greater influence of capillary water ingress. Conversely, decreasing ratio values indicate a shift toward the influence of diffusion. In this manner, the four grain types exhibited incredibly different behaviour following plasma treatment.

In maize, all plasma treatments increased the rate of capillary uptake compared with Untreated and T+V controls. There was little difference between P15, P30, P60 and P90 exposures. On the other hand, wheat exhibited a massive influence toward greater capillary flow with prolonged plasma exposure. For P90 treatments, the ratio of the

capillary constant to the diffusional constant increased to 15 times. This observation is striking when compared to a five-times increase for Untreated samples. Barley maintained a relatively steady ratio of around five times capillary/diffusional flow across all treatments. Psyllium presented an interesting trend compared to the other grain types. The ratio above one showed that capillary water transport dominated for all plasma treatments. Yet, increased plasma exposure strengthened the influence of diffusional water transport. This led to an overall decrease in ratio which was noticeable in T+V and P15 treatments. By 30 minutes, plasma treatments had an equal influence for both constants resulting in steady values. Overall, it was clear that plasma exposure uniquely affected grain hydration for each grain type.

To further contextualise grain hydration, it was useful to compare the results of this section with other studies conducted on the same grain species. Rathjen et al., 2009 performed magnetic resonance micro-imaging on imbibing wheat grains. They found that hydration began in the embryo and scutellum, likely through the micropyle, and increased over the course of 18 hours (Figure 6-22). The endosperm began to visibly hydrate via the crease between 9 and 12 hours after exposure to water. This data correlated with the results from the 2-phase model which predicted that capillary action is the dominant form of water uptake in imbibing wheat. At the beginning of imbibition, water likely travelled through the micropyle and wicked toward the embryo along the embryo-scutellum interface. It isn't until many hours later that diffusion begins through the crease. As water diffuses through the outer protective layers of the seed, it is again influenced by capillary flow as water wicks between the outer pericarp and testa layers before passing into the aleurone.

Barley shares a similar hydration model with wheat where water rapidly travels into the grain via the micropyle, hydrating the scutellum and embryo. The bran and aleurone are the next tissues to hydrate, followed by the endosperm (Fincher and Stone, 1993).

Yet, according to the 2-phase model, wheat and barley grains treated with plasma have incredibly different responses during imbibition. P90 treatments of wheat greatly increased capillary action by 672%, while barley only increased by 25%. This further reflected in the ratio between capillary ingress and diffusional ingress, as wheat had a dramatic increase in capillary action between Untreated and P90. The ratio in barley had a slight reduction between Untreated and P90, which illustrated that increasing plasma exposure shifted the influence slightly from capillary water uptake to diffusion. It is speculated that the differences lie in the presence of a husk protecting the outer layer of the barley grain. Wheat grains have a relatively thin and soft layer of pericarp on the outer surface (Rathjen, 2006) which is likely being etched away, creating new pathways for water to enter the grain. The barley husk shields the seed surface from the main impact of chemical etching and therefore has less of an effect on water ingress.

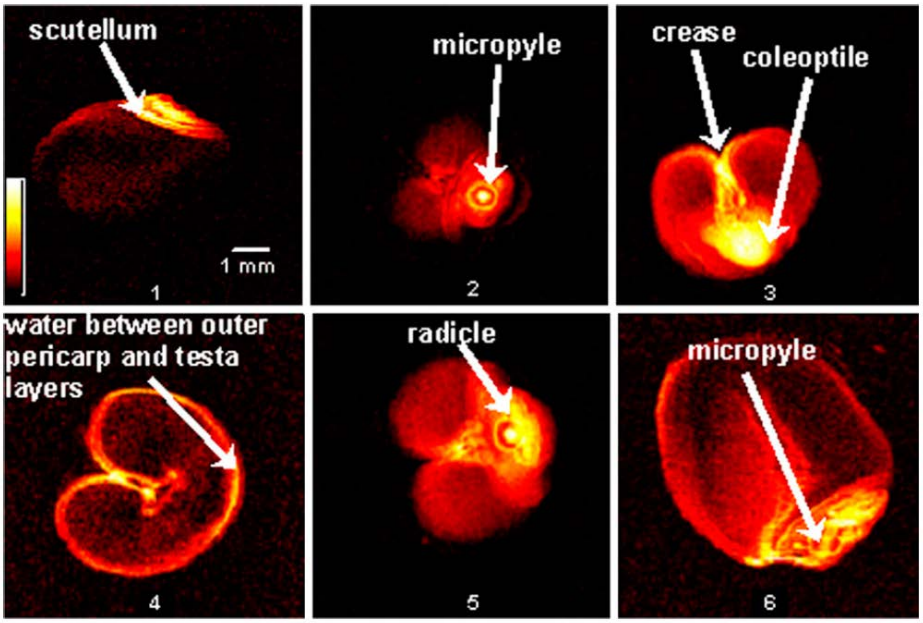


Figure 6-22. Magnetic resonance micro-imaging of wheat imbibing for 11-14 hours. The red to yellow gradient represents the presence of water. This study showed that the embryo and scutellum were the first tissues to hydrate, likely through capillary action via the micropyle. The endosperm hydrated more slowly through the crease where water began to travel between the outer pericarp and testa. Republished with permission of Oxford University Press, from Water movement into dormant and non-dormant wheat (*Triticum aestivum* L.) grains, Rathjen, J.R., Strounina, E. V., Mares, D.J., 2009. J. Exp. Bot. 60; permission conveyed through Copyright Clearance Center, Inc.

In maize, the initial water uptake occurs through the pedicle or tip cap. This tissue consists of both a micropyle and tubular cell remnants which conduct water rapidly toward the embryo (Miano et al., 2017). Treatment of maize with plasma increased the rate of capillary hydration, possibly allowing water to enter the pedicle more rapidly. Diffusional hydration was also raised, probably due to plasma weathering of the protective surface waxes surrounding the grain, as demonstrated in section 6.3. Finally, psyllium likely hydrates through both capillary action through the micropyle and remnant placental tissue in the dorsal cavity. Diffusion is also thought to occur as water passes from the surrounding high-water potential mucilage to a lower water potential dehydrated grain.

6.4.4 Summary

Understanding the changes in seed moisture content and seed water sorption are helpful when assessing the impact of plasma treatment on the surface of grains. Previous studies have explored this subject across all three phases of germination using traditional methods of grain soaking and weighing (Bormashenko et al., 2012, 2015; Dauwe et al., 2021; de Groot et al., 2018; Dufour et al., 2021; Lo Porto et al., 2019; Los et al., 2019; Stolárik et al., 2015). The experiments in this section differ in the use of a highly sensitive vapour sorption meter to capture weights every ten minutes and hold grains between phases I and II of germination. Large data sets were captured using this instrument, which were analysed to understand subtle differences in the amount of water absorbed, rate of sorption and the kinetic processes through which sorption likely occurred. The initial moisture content varied with treatment and grain type but was generally reduced in both T+V and plasma treatments. Despite the initial reductions, all plasma treatments and T+V were able to cause more water uptake over time. The increase in moisture sorption in T+V grains was small and likely represented the restoration of initially lost moisture. However, all plasma-treatments

saw increased hydration rates and water sorption capacity, with differences in sorption kinetics. This suggests that the etching processes of plasma treatment can alter the grain surface to a degree in which water can penetrate the surface. The next section explores the use of a water-soluble dye to detect the areas where surface damage allows for greater water penetration.

6.5 Dye sorption assay to visualise the effect of plasma exposure on grain hydration

6.5.1 Introduction

During imbibition, the direction of water ingress within a grain is a highly concerted process designed to promote tissue activation and hormone signalling at specific time points (Bewley, 1997). Changes to the manner which grains uptake water will impact the processes of germination. Some species might be able to take advantage of rapid and more efficient water sorption, such as when placed in soils lacking available moisture. On the other hand, extensive alteration could lead to breaches in tissue integrity and may cause nutrient leaching. Hence, the effect of plasma should be studied for different treatment durations and across different grain species. In section 6.2, it was shown that water appeared to readily absorb into surfaces over the endosperm in plasma-treated maize, wheat, and field pea. It was also demonstrated in section 6.4 that the rate of water uptake increased with plasma treatment. Considering these observations, it was unknown if the chemical etching process of plasma treatment may alter permeability and the direction of water uptake within the grain. A straightforward dye assay was performed to look for hydration points and potential areas of damage.

Trypan Blue is a soluble azo dye with a molecular weight of 960.81 Da. It is frequently used as a cell viability stain as it generally only penetrates cells with compromised

membranes (Chan et al., 2020). Additionally, it has been used in the brewing industry to illustrate grain permeability before and after abrasion damage in barley (Briggs and MacDonald, 1983). The large size of the molecule means it is generally excluded during grain water uptake with the exceptions of large porous structures and tissue damage. Untreated, P30 and P90 treated grains were incubated with Trypan Blue and visually inspected after 1 hour and 24 hours to assess the permeability and hydration patterns of each treatment.

6.5.2 Materials and Methods

6.5.2.1 Grain treatment

Untreated, P30 and P90 treatments of each grain type were prepared following protocols established in Chapter 3.1.2.

6.5.2.2 Trypan Blue incubation

Plates were prepared by placing a 90 mm glass microfibre filter, GF/C (Whatman), on the upside-down lid of a 90 mm cell culture plate. Glass microfibre filters were chosen instead of filter papers as the Trypan Blue can bind to cellulose. For maize, wheat, barley, and field pea, 20 grains of each treatment were scattered across the glass fibre; ten ventral-side down; ten dorsal-side down. Due to the small size of psyllium grains, approximately 100 grains were scattered across the glass microfibre filter surface. 6 mL of a 0.1% aqueous Trypan Blue solution was added to each plate. The plate bases were placed over the lids to reduce evaporation. Grains were incubated at 25 °C for 24 hours with visualisation and imaging on a Zeiss Stemi 2000-C stereo microscope with a Zeiss AxioCam ERc 5s, at 1 hour and 24 hours.

6.5.2.3 Imaging

Following one hour of incubation, five representative grains of each treatment were selected for imaging on a Zeiss Stemi 2000-C stereo microscope. This process was

repeated following a 24-hour incubation. Additionally, four grains of each treatment were selected for hand-sectioning with a razor blade followed by imaging.

6.5.3 Results and Discussion

Plant seeds have evolved multiple structures to regulate water uptake across tissue types. Changes in seed surface water permeability may impact viability and germination. On the one hand, there have been multiple reports where plasma treatments have been shown to improve seed germination. This is likely caused by more efficient grain hydration due to the removal of the outer hydrophobic layer of the grain (Bormashenko et al., 2012; Dufour et al., 2021; Los et al., 2019). On the other hand, the lengthy plasma treatments necessary for the inactivation of pathogens may damage grain tissues directly or indirectly through changes to water ingress. To understand the impact of the plasma etching process on grain hydration, an assay was conducted with a soluble, high molecular weight dye, Trypan Blue. Areas of increased dye uptake are associated water influx and/or the presence of porous structures. This led to discussions on how grain water uptake and mucilage hydration may be changing due to the weathering of protective surface structures.

6.5.3.1 Maize

Plasma treatment altered the Trypan Blue staining of maize grains (Figure 6-23). Untreated grains showed very little staining with only a tiny amount of blue at the pedicel. The embryo appeared to be hydrating in the longitudinal section taken at 24 hours of incubation which suggests that water uptake is occurring within the grain, but the high molecular weight dye is being excluded. Conversely, 30-minute and 90-minute treatments had intense staining of the surface pericarp cells. The pattern of staining followed the usual pattern of hydration for maize, however it appeared to be taking place at an accelerated pace. This result is consistent with changes to the hydration rate and capillary flow demonstrated in section 6.4. The micropyle, located in the

pedicel or tip cap, wicks moisture toward the embryo via capillary action. Once the scutellum and embryo have progressed into germination phase I, hydration continues into the endosperm from both the embryo and dent ends of the grain (Miano and Augusto, 2018). This pattern was clearly visible using Trypan Blue on the 30-minute treatment. After one hour of incubation, the stain travelled up the pericarp, over the embryo, and toward the dent. Only the regions over the pericarp on the dorsal surface were not stained. In P90 treatments, the entire grain surface pericarp had taken up the stain. The aqueous dye travelled rapidly, hydrating the pericarp in one hour when it can take up to a day on control grains.

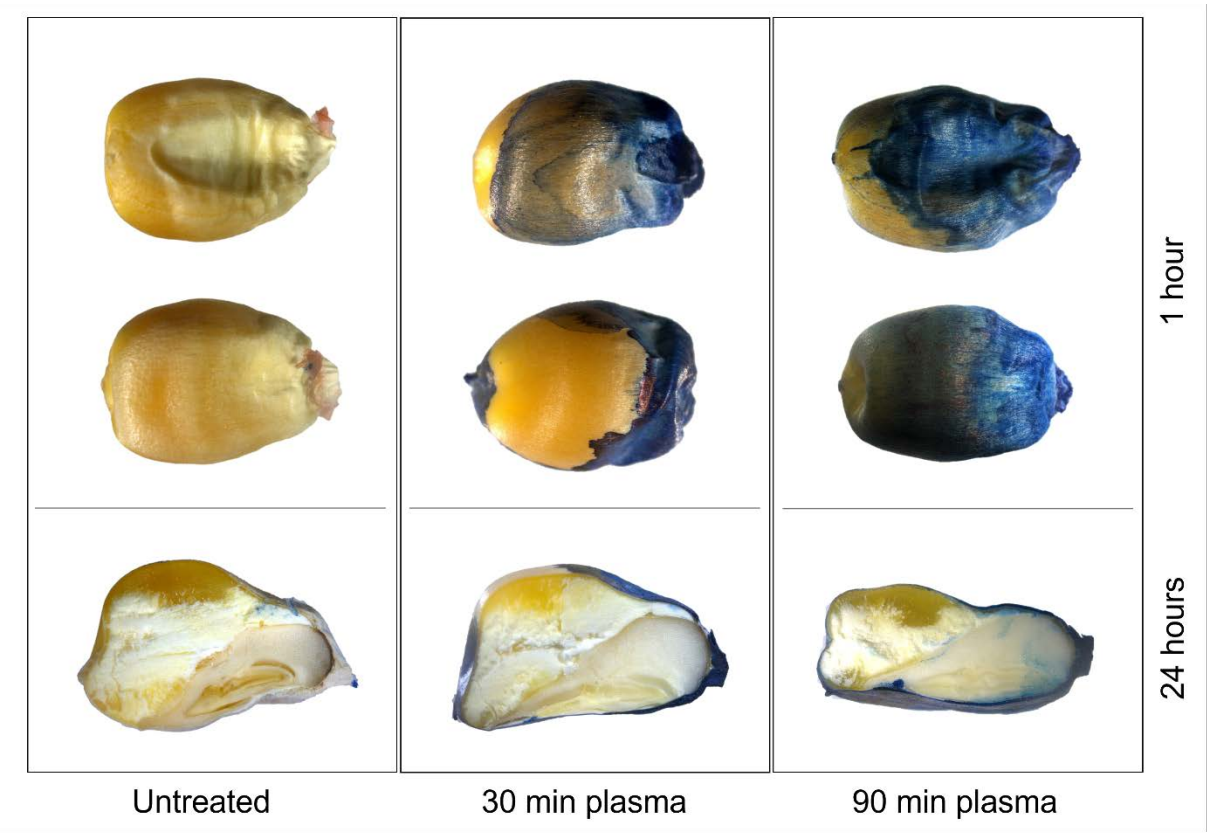


Figure 6-23. Trypan blue staining of treated maize grains after one hour in dorsal and ventral views, and after 24 hours in longitudinal sections. Plasma treatment alters the rate of grain staining. The patterns of staining follow typical maize grain hydration patterns but occur within one hour, as opposed to one to three days.

The lack of staining on Untreated grains indicated that the grain surface was healthy and intact. It is supposed that the tumbling and etching processes in the plasma treated

samples abraded the surface to the point where a hydrated, 960 Da molecule could freely enter the pericarp. The stain did not appear to penetrate further than the pericarp. Instead, the small traces of dye visible on the P90 longitudinal section are artefacts created during grain sectioning as the blade transferred dye from the saturated pericarp into the grain.

6.5.3.2 Wheat

Trypan blue staining showed markedly different effects on wheat grains compared to maize. Untreated grains displayed staining near the brush at the one-hour time point, which is expected as this region is likely slightly damaged during the threshing process (Figure 6-24). By 24 hours, there was staining below the micropyle which, again, was likely caused during threshing when the grain separated from the glumes. Hydration was visible in the embryo, indicating that water uptake was occurring with the exclusion of Trypan Blue stain. P30 and P90 treated grains treated displayed very different behaviours with Trypan Blue uptake occurring across the entire grain surface at a remarkable pace. Within 15 seconds of the addition of 0.1% aqueous Trypan Blue, the whole grain was stained blue for the P90 treatment. It is suspected this observation is linked to the 672% increase in capillary action seen in section 6.4.3.3.3. P30 grain was stained blue in roughly five minutes after the addition of Trypan Blue. This suggests that plasma treatment significantly weathers the wheat bran surface, leading to dramatically altered rates of dye penetration.

Longitudinal sections revealed complete staining of the pericarp for both plasma treatments and light staining of regions in the endosperm. The micropyle and small areas of the embryo radicle were darkly stained. It is unknown if the radicle staining was due to abrasion during radicle protrusion or if minor damage occurred to this tissue during the combination of tumbling, ion bombardment and oxidation for 30 and 90 minutes. If it is the latter, radicle damage may have serious downstream consequences

on germination for these lengthy plasma treatments. It was worth noting that all five sectioned replicate P30 and P90 grains had reached germination phase III while all Untreated grains appeared to be in phase II. This observation, along with potential radicle damage, led to speculation that the increased rate of water uptake for these samples may impact germination rates and will be investigated in Chapter 7.

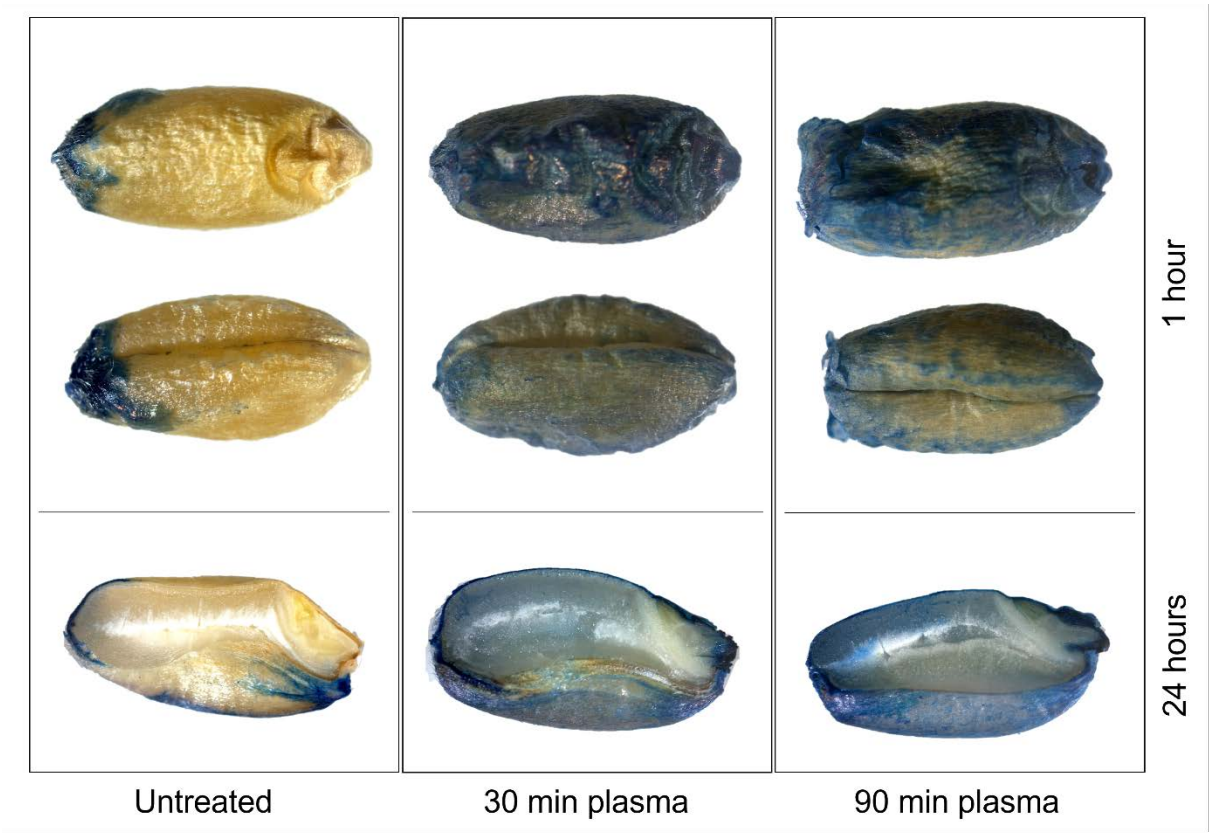


Figure 6-24. Trypan Blue staining of treated wheat grains after one hour in dorsal and ventral views, and after 24 hours in longitudinal sections. There was considerable difference in staining patterns between Untreated and plasma-treated grains. By hour 24, Untreated grains were in phase II of germination while both plasma treatments had reached phase III.

6.5.3.3 Barley

Hulled-barley grains have a similar morphology to wheat grains, however the lemma and palea remain attached, providing an outer protective layer. Despite the presence of the hull, barley displayed a similar staining pattern to wheat grains with a much slower rate of stain uptake (Figure 6-25). Untreated grains were stained at the

micropyle, the damaged regions where the awn was attached prior to threshing, and the regions where the lemma connects to the pericarp. On all plasma-treated grains, the entire palea on the ventral surface was darkly stained as well as a large portion of the lemma. Areas of the pericarp adjacent to the husk showed light staining with swelling in areas of the endosperm. This indicated more water uptake in the endosperm of plasma-treated grains when compared to Untreated grains, and correlates to the increases in water sorption seen in section 6.4.3. It appears that the barley husk and possibly areas of pericarp were abraded during plasma treatment, allowing more water and the high molecular weight dye to penetrate the tissues. Unlike the wheat grains, all 20 grains of each treatment had reached germination phase III by 24 hours.

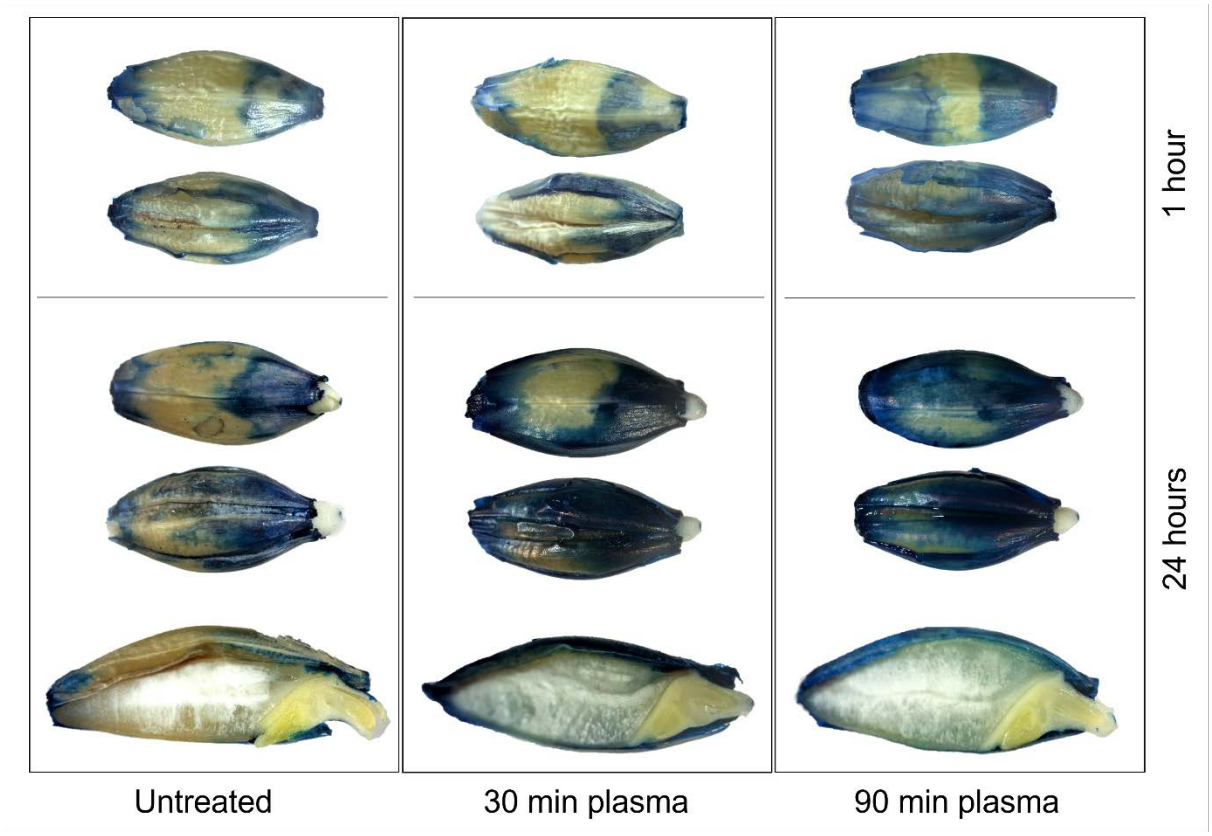


Figure 6-25. Trypan Blue staining of treated barley grains after one hour in dorsal and ventral views, and after 24 hours in longitudinal sections. Dye-accessible areas were stained blue. Untreated grains are show damage where the awn was attached, around the micropyle and attachment to the maternal structures and around the areas where the lemma connects with the pericarp.

6.5.3.4 Field pea

Field pea embryos generally hydrate through the micropyle as their seed coats are largely hydrophobic and impermeable to water (Bewley et al., 2013; Niemann et al., 2013). In this experiment, the seed coat cuticle on Untreated grains was able to uptake dye (Figure 6-26). This was unexpected and only occurred in the regions surrounding the micropyle that were immersed in dye. The dye also penetrated a portion of the palisade layer near the micropyle. Plasma-treated grains saw a similar pattern of staining near the micropyle with additional staining of the tracheid bar underneath the hilum in all P90 grains. This may indicate plasma-induced changes to the hilar fissure, allowing the stain to penetrate the tissue below.

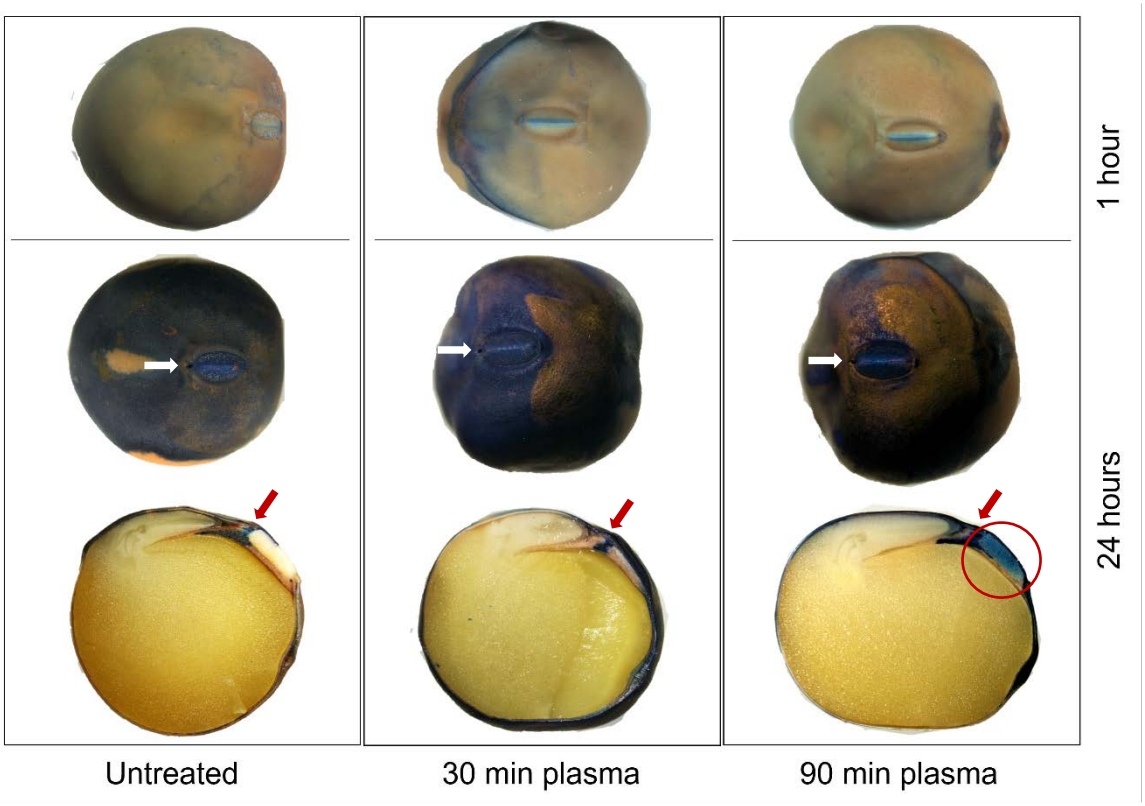


Figure 6-26. Trypan Blue staining of treated field pea grains after one hour in dorsal and ventral views, and after 24 hours in longitudinal sections. Plasma-treated grains showed pronounced swelling, indicating rapid water uptake. All grains displayed stain uptake at the micropyle (arrows) with additional staining of the tracheid bar (circle) in 90-minute plasma treatments.

Over the course of 24 hours, the embryo and cotyledons slightly swelled and appeared moist. All plasma-treated grains displayed much more swelling than the controls, with pronounced grain distortion visible in P90 treatments. At one hour, the seed coats appeared to be flexible. By 24 hours, the entire grain surface was stained with Trypan Blue in both the P30 and P90 treatments. Curiously, areas with the darkest staining began to turn a copper colour near the 24-hour time point. It is speculated that this may be due to oxidative processes occurring during imbibition, such as the production of ROS for signalling. Oxidation is known to decolour Trypan Blue and this concept is employed in the textile industry to decolour wastewater containing this dye (Ghime and Ghosh, 2020). In any case, plasma treatment is altering the rate of water uptake within the grain.

6.5.3.5 Psyllium

The surfaces of psyllium grains are coated in at least two layers of polysaccharide mucilage which expands upon hydration. The outer-most layer is composed of a more hydrophilic and pectinaceous mucilage, while the layer closest to the grain contains more heteroxylans (Phan et al., 2020). The application of the aqueous Trypan Blue solution hydrated the mucilage and revealed differences between treatments (Figure 6-27). Untreated grains followed traditional mucilage hydration patterns (Yu et al., 2017) with the outer pectinaceous layer of mucilage expanding within 20 minutes and full expansion of the inner heteroxylan layer by 60 minutes. The pectinaceous layer of mucilage was reduced in the P30 treatment and completely absent in P90 treatments. Instead, a thick hydrophobic layer with deep staining was visible on P90 grains. Additionally, the area of hydrated mucilage was greatly reduced.

Following a 24-hour incubation, all P90 grains had reached phase III of germination with hydrated endosperm. This is unsurprising as the water sorption capacity (in

section 6.4.3.2) increased by 32% for this treatment. Most of the P30 grains had reached phase III but endosperm was not as saturated as the P90 samples. Roughly half of the Untreated grains had germinated with endosperm hydration yet to be completed. Overall, the images suggest that the outermost layer of mucilage was being modified by the etching processes of plasma treatment, greatly reducing the capacity for expansion. The hydration of the endosperm appeared to be occurring faster following prolonged plasma exposure, which may be attributed to the increased diffusion rate. It is unknown if plasma treatment therefore decreases mucilage sorption and increases seed sorption. A mucilage sorption assay was conducted in section 6.6 to tease apart these observations.

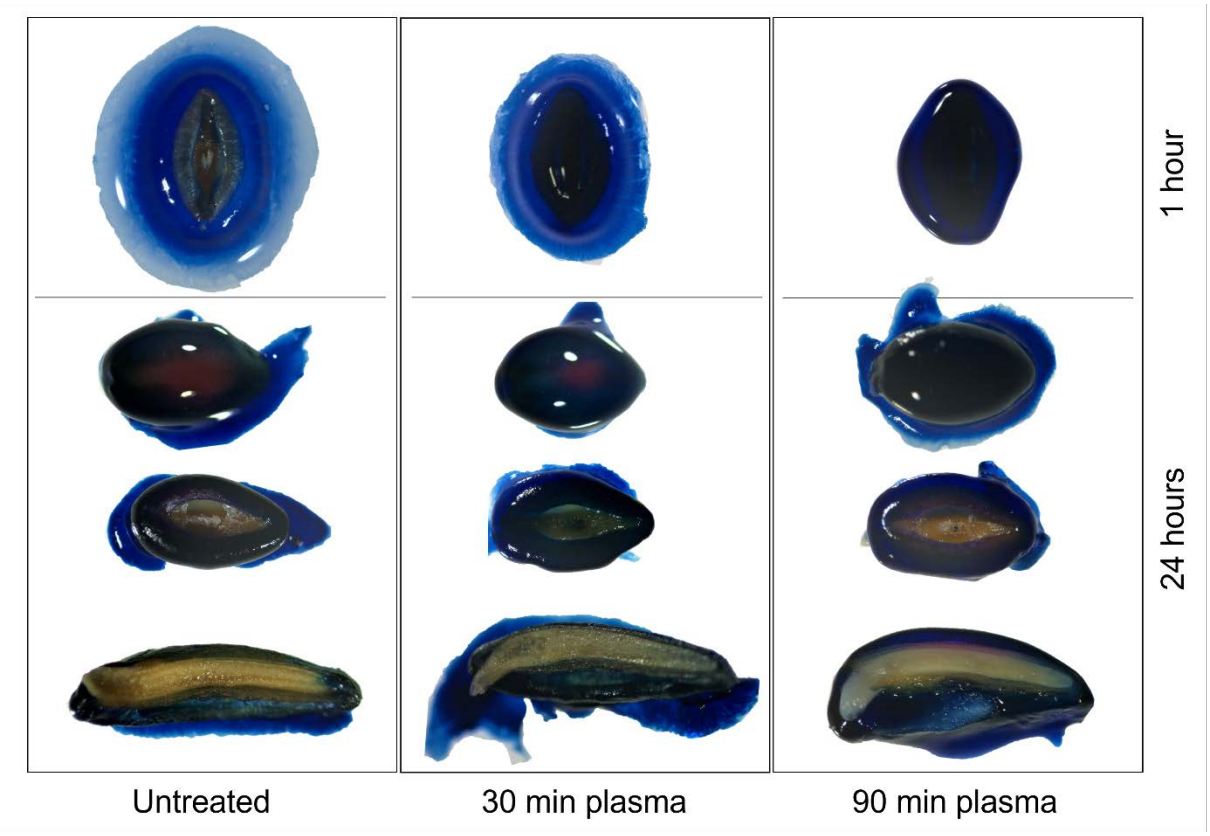


Figure 6-27. Trypan Blue staining of treated psyllium grains after one hour in dorsal and ventral views, and after 24 hours in longitudinal sections. At one-hour, Untreated grains showed the fully expanded mucilage layer while mucilage area on the plasma-treated grains was reduced.

6.5.4 Summary

In sections 6.3 and 6.4, it was established that the properties of the grain surface changed following plasma treatment, altering water transport. The seed hydrophobicity was reduced, water appeared to readily penetrate the grain, and grains absorbed more water than controls. To visualise grain hydration, a straightforward staining assay was performed with 0.1% aqueous solution of the large molecular weight azo dye, Trypan Blue. Overall, control grains hydrated in patterns like those described in the literature. Plasma treatment greatly affected water transport phenomena with full surface staining by the 24-hour time point for P90 grains. In addition to vast areas of stain coverage, Trypan Blue was often able to penetrate structures below the seed surface. The tracheid bar underneath the hilum was stained in all P90 field peas. This signified substantial weathering of the grain surface during plasma exposure. It also demonstrated the changes in direction of water and stain uptake within the grain. Instead of water tracking along defined pathways, it appeared to rapidly penetrate the weathered pericarp in the monocots and the seed coat in the legume.

Perhaps the most surprising plasma-induced alteration was seen in psyllium, where the amount of hydrated surface mucilage was dramatically reduced. Not only did the hydrophilic upper layer of pectin appear to be absent but the mucilage swelling capacity appeared to shrink. The reduction of mucilage hydration may be partly due to the reduction of surface sugars due to plasma etching. It is therefore necessary to understand the role of plasma in both seed sorption and mucilage sorption. The following section describes an experiment carried out to understand the effect of plasma exposure on the psyllium mucilage sorption capacity.

6.6 Mucilage hydration – a sticky situation

6.6.1 Introduction

Psyllium grains are coated in a 10 to 18 µm layer of laminated polysaccharide mucilage which fully hydrates into a sticky goo within 60 minutes of water exposure. The outermost polysaccharides tend to be more hydrophilic and composed of pectin, while layers closer to the seed display hydrophobic properties and are composed of heteroxylans (Phan et al., 2020). During the Trypan Blue staining assay conducted in section 6.5.3.5, mucilage hydration patterns appeared to be greatly reduced with plasma exposure. The outer hydrophilic layers of mucilage were not observed in 90-minute plasma-treated grains. Furthermore, the endosperm appeared to be fully hydrated in only the 90-minute plasma grains. These observations led to speculation that the hydration properties of the outermost layer of mucilage was being physically or chemically changed by plasma, reducing the water sorption capacity of the mucilage layer itself, but not the grain.

As described by Cowley et al., 2020, a straightforward mucilage sorption assay was conducted to determine if plasma treatment was altering the mucilage water sorption capacity. This involved incubating pre-weighed grains with ultrapure water for 45 minutes. Final weights were taken and compared back to the initial weights to determine the amount of water absorbed by the mucilage layer. It was thought this data set may provide a clue as to how plasma interacts with the surface of a mucilaginous seed.

6.6.2 Materials and Methods

6.6.2.1 Grain preparation

Excess psyllium grain prepared for the Trypan Blue assay (see section 6.5.2.1) was utilised in this trial to compare data sets from both assays.

6.6.2.2 Sorption assay

Following protocols described by Cowley et al., 2020, four replicates of 20 grains per treatment were placed in 2 mL Eppendorf tubes and weighed. The weights of the tubes containing grain were recorded. 1 g of Milli-Q water was added to each tube and placed in an incubation block for 45 minutes at 25 °C. Following incubation, excess water was removed from each tube using a P200 Ovation® pipette, followed by a P10 Ovation® pipette, leaving behind only the grains and water bound within the hydrated mucilage. The excess water was deposited into pre-weighed Eppendorf tubes and water weights were recorded. Weights of each tube containing grain were again recorded and water sorption capacity was calculated using the following equation:

Equation 6-4.

$$\frac{(initial\ water\ weight\ (g) - weight\ of\ excess\ water\ (g))}{initial\ weight\ of\ grain\ (g)} = water\ sorption\ capacity\ of\ mucilage\ (g)$$

6.6.2.3 Statistical analysis

A one-way ANOVA with Tukey's multiple comparison test was conducted in GraphPad Prism 9.0.0 to determine the significance of mucilage water sorption. Data were expressed as mean ± standard error of the mean. Significance was accepted at $p<0.05$.

6.6.3 Results and Discussion

Observations made while conducting the Trypan Blue assay in section 6.5.3, suggested that plasma-treatment may be altering the water sorption capacity of the laminated layers of polysaccharide mucilage on the psyllium grain surface. A mucilage sorption assay was undertaken to understand how plasma may be impacting the psyllium grain surface. It is thought that psyllium mucilage takes up to 60 minutes to fully hydrate all layers. Grain hydration tends to occur shortly after mucilage hydration,

once it is no longer competing with the mucilage hydrogel for water (Cowley et al., 2020). This assay captures mucilage water uptake at the 45-minute timepoint to avoid excess water sorption by the seed.

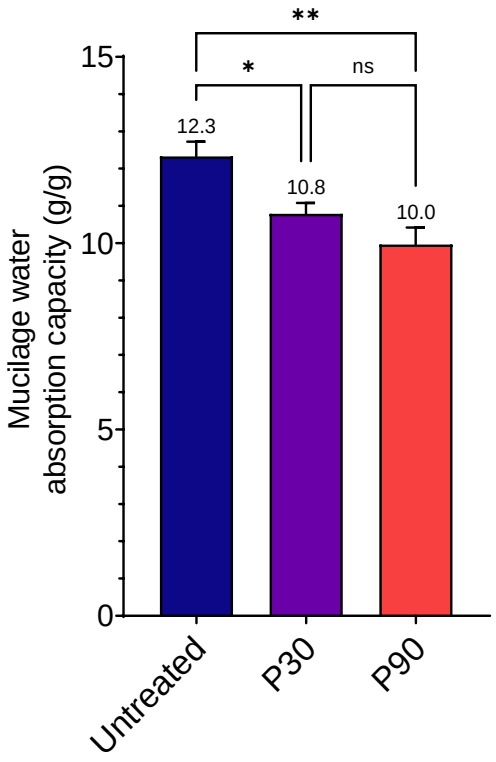


Figure 6-28. Psyllium grain surface mucilage water sorption capacity. Plasma exposure reduces the water holding capacity of the mucilage. Data is presented as mean ± SEM. Abbreviations: P30 (30-minute plasma); P90 (90-minute plasma); ns (non-significant); *p<0.05; **p<0.01.

Consistent with observations in section 6.5.3, the mucilage water sorption capacity diminished with increasing plasma exposure (Figure 6-28). P30 treatment reduced the mucilage sorption capacity by 12.2%, while P90 treatment lowered sorption by 19%. Mucilage is composed of polysaccharides that form a hydrogel-like polymer responsible for its water sorption properties (Yu et al., 2017). The abundance of hydrophilic functional groups contributes to hydrogen bonding with water. Given the oxidative properties of air plasma, it is reasonable to propose that plasma significantly interferes with the ability of water to hydrate the polysaccharide chains. This is possibly due to the loss of hydrogen-bond forming functional groups that could associate with

water molecules. It is also likely that plasma bombardment may be physically cleaving the polysaccharide chains. The weathering of the grain surface visible during scanning electron microscopy (Figure 6-29) supports the idea that etching may be altering the large polysaccharide chains on the seed surface. The raised wrinkles of desiccated mucilage on the surface of untreated grains are absent following plasma treatment. Instead, plasma leaves behind an abraded and indented surface.

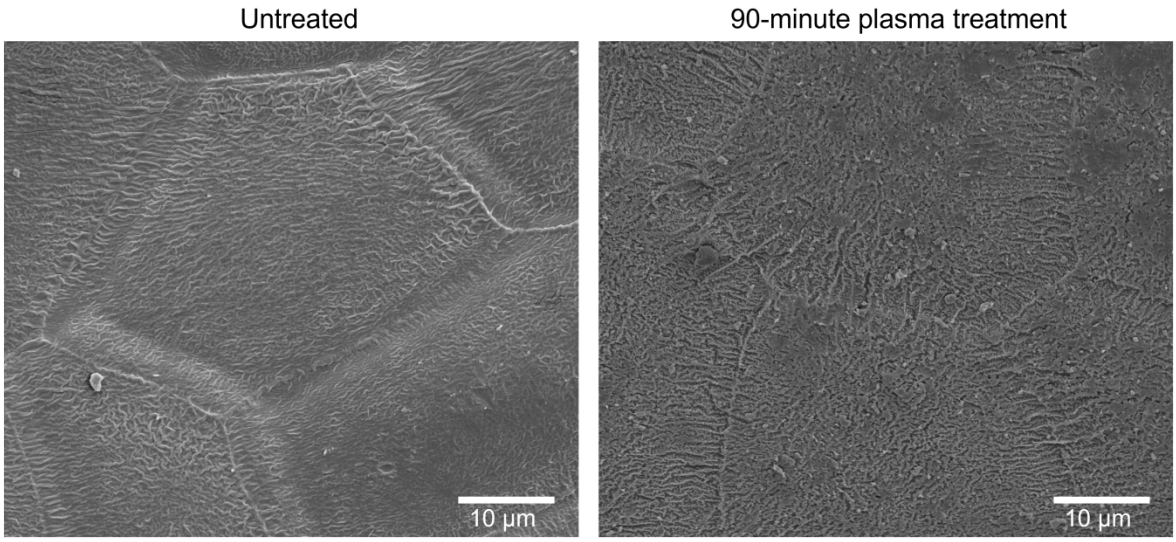


Figure 6-29. Scanning electron micrographs of Untreated and 90-minute plasma treated psyllium grains. Plasma appears to affect the polysaccharide microstructures of mucilage on the surface.

It should be noted that plasma exposure appeared to increase the water vapour sorption capacity of psyllium grains (see section 6.4). P90 treatment raised the water vapour sorption of the grains by 32%. This data appeared to contrast observations of the reduction in mucilage water sorption. It is speculated that the differences may be attributed to the state of the water being absorbed. Liquid water rapidly interacts with mucilage coating the seed surface to create a sticky hydrogel within seconds to minutes of water contact. In this state, the mucilage is absorbing water before it can reach the grain surface. On the other hand, water vapour can diffuse across the grain

surface and slowly hydrate both the mucilage and the grain tissues. Grain surface mucilage was slightly sticky following 72 hours in the vapour sorption meter at 90% RH but far from fully hydrated, as described in section 6.4. This suggests that the sorption measurements taken in the vapour phase may better represent seed sorption, rather than mucilage sorption. Future research to understand the interaction of seed surfaces with multiple states of water is necessary to fully understand grain hydration, yet it is not within the scope of this project. Plasma treatment displayed initial and rather puzzling opposite effects on psyllium mucilage absorption. Despite the contrast, the data gathered in this experiment and the Trypan Blue Assay in section 6.5, suggested that plasma treatment reduced mucilage sorption capacity. From this assay, it is not possible to determine whether the amount of mucilage has changed or the chemical properties of the mucilage which allow for water sorption. Future research is necessary to untangle this complicated relationship.

6.6.4 Summary

Psyllium grains were selected as a model system within this body of research due to the seed surface chemistry. The psyllium mucilage water holding capacity was greatly reduced by plasma treatment; 12% in P30 grains and 19% in P90 grains, when compared to Untreated samples. It is proposed that the etching process of plasma treatment is both etching and oxidising the surface polysaccharides. Water will no longer interact in the same manner with the newly broken and oxidised sugar chains. The repetition of these physical and chemical reactions over the course of 90 minutes of treatment has the overall effect of lowering the mucilage hydration capacity.

6.7 The impact of plasma exposure on the prevalence of K+ on sample surfaces and in leachate.

6.7.1 Introduction

The processes in grain hydration are complex and follow carefully evolved pathways to ensure optimum success in germination. If water rapidly enters a grain during imbibition, it can cause cellular damage and the leakage of cell contents. This may be due to the gel state of desiccated cell membranes in dry seeds. In this state, the rigid membranes are more susceptible to damage and the consequent leakage of cell contents. Conversely, the slow entry of water into the grain hydrates the membranes and allows them to transition back into a crystalline liquid state which can more fluidly adapt to turgidity (Bewley et al., 2013). As it has been shown throughout this chapter, the rate of grain hydration increases with plasma treatment. It is possible that the rapid influx of water into plasma-treated grains may cause cellular damage. It is also likely that the etching of grain surfaces (as seen in Chapter 4) compromised the outermost layer of the seed surface, exposing intracellular contents.

Following plasma treatment, water readily diffused into the grain, which suggests that intracellular solutes from damaged cells can diffuse out of the grain into a solution with a low solute potential. Plasma-treated grains frequently displayed a yellowish leachate when plated on agar, filter paper and glass fibre paper (Figure 6-30). It was speculated from the results of the ToF-SIMS analysis in section 6.3 that this leachate may be a combination of oxidised hydrocarbon fragments and the contents of damaged cells on the surface of the grain. As potassium is one of the most abundant macronutrients found in grains, it is possible that the high K^+ peaks displayed with ToF-SIMS analysis may also correlate with contents of the grain leachate. The energetic bombardment of the plasma may be exposing K^+ that is usually stored in cell walls and intracellular structures and oxidising it to KOH.

Another possibility is that the abundance of potassium in the ToF-SIMS spectra may be attributed to the ease of ionizability of potassium and is an artefact. It was therefore necessary to conduct a leachate assay to detect and quantify potassium in solution following grain hydration. Untreated, T+V, P30, P60 and P90-treated grains of maize and wheat were soaked in sterile Milli-Q water overnight. The leachate was removed, diluted, and analysed for potassium on a flame photometer. The analysed data was compared to ToF-SIMS data in section 5.2 to determine if correlations exist between K^+ measurements in each analysis.



Figure 6-30. 90-minute plasma-treated wheat grains on half-strength PDA. A yellowish leachate surrounds each grain.

6.7.2 Materials and Methods

6.7.2.1 Grain treatment

Untreated, T+V, P30, P60, and P90 treatments for both maize and wheat were prepared following protocols laid out in Chapter 3.1.2.

6.7.2.2 Dilution trial pilot

A pilot trial using Untreated and P90 grains was conducted to ensure meaningful dilutions were prepared for each sample. Two replicates of 2 g of grain were placed in sterile 10 mL tubes with 8mL of autoclaved Milli-Q water. Tubes were incubated overnight in a dark box. The following morning, all tubes were inverted five times to mix the grains and leachate. Aliquots were removed from each tube and placed in

fresh, sterile 10 mL tubes for the preparation of dilutions. Sterile Milli-Q water was added to each tube to create 1:10, 1:50 and 1:100 dilutions for each grain type and treatment. These dilutions were analysed for potassium on a flame photometer to determine ideal dilutions for the main experiment.

6.7.2.3 Experimental grain preparation

Based on the data collected in the pilot trial, a series sterile 10 mL tubes were labelled for each grain type with four replicates of each treatment. 2 g of grain of each treatment was placed into the corresponding tube with 2 mL of sterile Milli-Q water. Tubes were inverted five times and placed in a tube rack inside a dark box overnight. The following morning, tubes were removed from the box and inverted five times to mix the sample. 1 mL aliquots of extracted leachate were removed from each tube and placed in sterile tubes with 9 mL of sterile Milli-Q water. These tubes were used directly on the flame photometer.

6.7.2.4 Flame photometry analysis

Analysis was conducted on a Sherwood Scientific 410 Flame Photometer using 0 g/L, 2 g/L, 4 g/L, 6 g/L, 8 g/L and 10 g/L potassium standards. Tubes of liquid were again inverted five times prior to readings to ensure thorough mixing. Measurements were recorded once a stable number was achieved for each sample. Two technical replicate measurements were taken for each tube. The instrument was blanked with sterile Milli-Q water between each reading.

6.7.2.5 Statistical analysis

A standard curve was generated in GraphPad Prism 9.0.0 with all measurements fitted along the curve to generate normalised values for each reading. Dilution factors were calculated for each normalised value and a two-way ANOVA with Tukey’s multiple comparisons test was performed on the means of technical replicates to compare

treatments and grain types. Data were expressed as mean ± standard error of the mean. Significance was accepted at $p<0.05$.

6.7.3 Results and Discussion

The surface chemical analysis of Untreated, P30 and P90 grains revealed the presence of hydrocarbon fragments, oxidised fragments, and high K^+ levels across all grain types. It was also observed that following hydration, plasma-treated grains leaked pigmented substances onto the surrounding substrates. While imbibitional leakage is normal during grain hydration, there were visually distinct differences between Untreated and plasma-treated seeds. It was thought there may be a correlation between the changes in surface chemistry, rapid grain hydration and the pigmented leachate. A flame photometry assay was performed on the grain leachate of treated maize and wheat to look for correlations between data sets gathered throughout this chapter.

Maize grain displayed a trend of increasing K^+ concentration with increasing plasma exposure by 12%, 27% and 38%, respectively (Figure 6-31). Both the P60 and P90 treatments were significantly different from the Untreated control, with respective p-values of 0.0449 and 0.0037. In wheat grain extracts, all plasma and T+V treatments had significantly higher K^+ concentrations than the Untreated control, ranging between 29% and 45%. Clearly, the weathering effects of long exposures to plasma in this system increase the likelihood that K^+ will leach into the environment upon grain hydration. This does not however, explain why T+V treatments had increased potassium leachate concentrations. It is possible that the removal of moisture during vacuum treatment was increasing the fragility of cell membranes which can cause downstream cellular damage upon hydration. Dauwe et al., 2021 conducted experiments on imbibitional leakage in plasma-treated flax seeds and found no difference between untreated and 250 mTorr vacuum treated controls; an identical

vacuum pressure was used throughout this research. This may be due to shorter vacuum treatments of 20 minutes and different grains. They did find that plasma treatment increased initial solute leakage. It can also be speculated there may be some mechanical damage induced by seed tumbling, as seen in SEM micrographs in Chapter 4. Damage to the pericarp, may allow more intracellular K^+ to leach out upon grain hydration, especially in the embryo region.

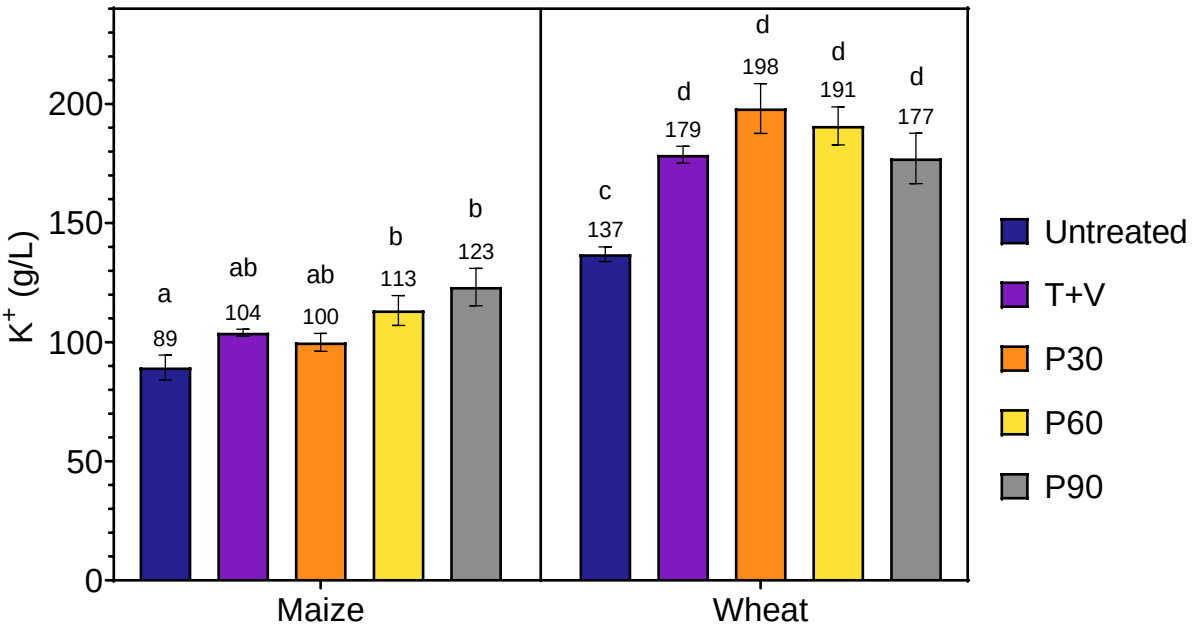


Figure 6-31. Potassium concentrations in the leachate of hydrated maize and wheat grains. Grains were soaked overnight in Milli-Q water and the extracts were analysed via flame photometry to calculate K^+ concentrations. Data is presented as mean ± SEM with significance accepted at $p<0.05$. Letters indicate significant differences between means. Abbreviations: T+V (Tumbler + vacuum); P30 (30-minute plasma); P60 (60-minute plasma); P90 (90-minute plasma).

This experiment showed the variations between grain types with the Untreated control concentration of K^+ in wheat leachate measuring 53% higher than the Untreated control in maize. This trend continued throughout the treatments with the highest concentration in wheat (P30) being 61% more than the highest concentration in maize (P90). Once hydrated, wheat can release more K^+ into the surrounding environment than maize. Nonetheless, there were significant differences between controls and plasma treatments in both grain types.

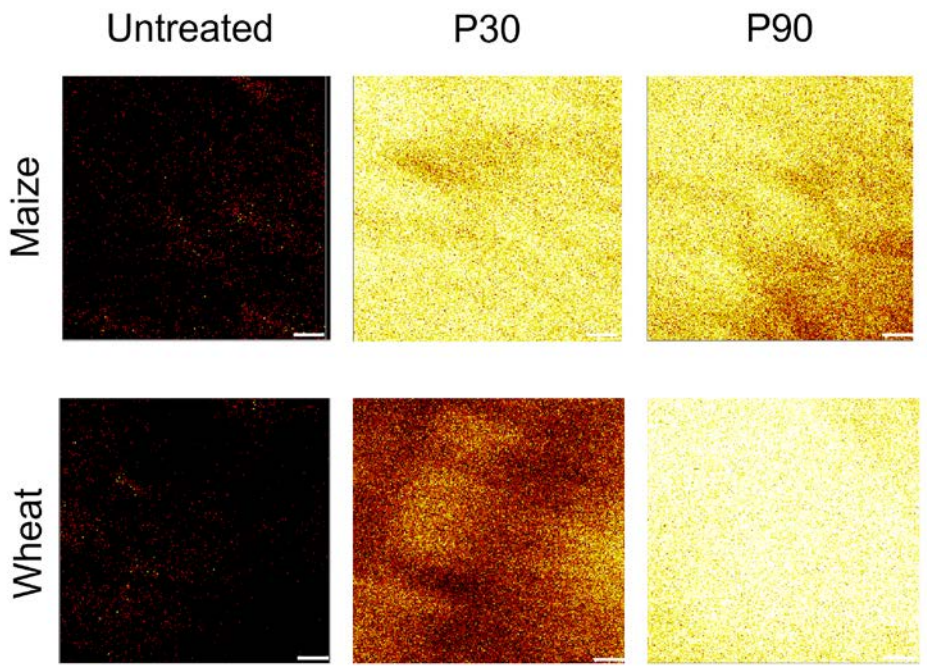


Figure 6-32. ToF-SIMS imagery of the maize grain surface as a visual display of fragment intensity. The presence of K^+ increased with plasma treatment. Scans were taken over the endosperm on the dorsal surface of each grain. Scale bars = 10 µm. Abbreviations: P30 (30-minute plasma); P90 (90-minute plasma).

The results of the flame photometry assay loosely correlate with the imagery produced during ToF-SIMS analysis (Figure 6-32). ToF-SIMS images are a visual display of fragment intensity, with 256 x 256-pixel images depicting 90 μm^2 surface areas. Overall, the imagery displayed an increased presence of K^+ following plasma treatment. For maize, the K^+ signature is highest in 30-minute plasma treated grains, as opposed to 90-minutes in the leachate assay. Conversely, wheat displayed an increasing K^+ signature with increasing plasma exposure in the ToF-SIMS analysis, while the leachate assay resulted in the highest concentration of K^+ at 30 minutes and decreasing over time. It should be noted that ToF-SIMS describes the presence of K^+ on the grain surface, while the leachate assay illustrates the mobility of K^+ from grain tissues into solution. In this context, it is unknown if the discrepancies between experiments are due to the nature of the assays or the small numbers of ToF-SIMS

replicates (two biological replicates sampled at six locations). Despite the inconsistencies, plasma treatment of grains changes the presence of potassium on the grain surface and in solution.

6.7.4 Summary

This experiment was conducted to determine if a correlation exists between plasma treatment and potassium content of imbibitional leachate. While there was a significant trend for increased potassium leaching following plasma treatment, this was likely due to multiple factors. It appears that the etching process of plasma treatment is exposing K^+, which can be detected in both the leachate and ToF-SIMS analysis. It is also possible that the tumbling process causes mechanical damage which may have caused the leaching of nutrients. Additionally, the vacuum process, followed by rapid rehydration may have damaged cell walls and allowed intracellular content leakage. Overall, the release of potassium from the grain following plasma treatment may have downstream consequences, including the reduction of nutritional properties which may impact food production. It may also induce complications during germination as vital nutrients may leak out of the seeds, both depriving the embryo of nutrition and signalling soil-borne seed pathogens. Further research should aim at using more analytical techniques to understand the chemical composition of imbibitional leakage from plasma treated grains. Specifically, a thorough analysis by HPLC may aid in the understanding the origin of leached compounds following plasma exposure.

6.8 Conclusions

This chapter sought to investigate how plasma exposure altered seed surface chemistry and if said changes influenced the interaction between the grain and water. SEM imagery from Chapter 4 led to speculation that large, hydrophobic molecules on the grain surface may be fragmented during plasma treatment, raising the surface

energy of the grain. To test this concept, contact angle measurements were conducted with water droplets. While this assay confirmed a much higher surface energy on plasma-treated grains, it also provided observations that water may be rapidly penetrating the grain, within a manner of seconds. This led to dual pathways of investigation: an exploration of chemical changes to grain surfaces with the use of ToF-SIMS analysis and detailed studies into grain hydration. ToF-SIMS analysis demonstrated that plasma treatment altered the chemical signature of the grain surface, with differences in surface fragment composition depending upon grain type and treatment. Grain hydration analyses, with a high precision sorption meter, provided excellent insights into water transport and the effects of plasma treatment. Modelling data with Peleg and 2-phase absorption models, illustrated the variation between grain types and plasma treatments. The changes to rapid water ingress, interpreted as capillary action, led to an assay using a high molecular weight dye to track flow into the grain. It became clear that plasma treatment modified the grain surface (pericarp and/or testa) cells, potentially reducing viability. It also appeared to reduce the surface mucilage of psyllium. A further investigation into changes in mucilage water sorption was performed and confirmed that mucilage sorption capacity is reduced following plasma treatment. A final experiment on seed leachate suggested that chemical modifications and cellular damage on the plasma-treated grain surface influenced the concentration of potassium leakage. Changes to water ingress go hand-in-hand with changes to solute egress.

When taken together, the results of this chapter push the boundaries of knowledge surrounding plasma interactions with seed surfaces. The prolonged exposure times deemed necessary to deactivate mycotoxigenic post-harvest fungi not only alter the fungal cell walls, but treatment changes the surface structures and water dynamics of the grain host. While plasma is often touted as a panacea, this research suggests that

there are pros and cons with each exposure time. Improved grain hydration rates are both a benefit and pitfall, depending on the path of postharvest production. The dry manner of fungal deactivation is clearly a positive for psyllium processing which relies upon desiccated seed mucilage. However, the changes to mucilage chemistry and content may have consequences for product quality. The negative implications of plasma treated grains releasing intracellular contents, including macronutrients, into the surrounding environment is also of concern. This highlights the need for further investigations into how plasma treatment is impacting the biological processes of each grain type. Do changes in water sorption alter germination rates? How does this impact seedling growth and development? These essential questions must be answered for each grain type before plasma-treatment can be recommended as a technology for solving food security issues. Overall, the decision to apply plasma technology toward a grain should be carefully weighed with understanding of the implications toward the physical, chemical, biological, and microbiological properties of each grain type.

7 Comparing the effects of plasma treatment on seed viability, growth, and development

7.1 Introduction

Over their vast evolutionary timeline, plant seeds have evolved countless strategies to combat both biotic and abiotic stresses in their natural environments. Quiescent, dry grains can remain viable in the soil for months to millennia (Shen-Miller et al., 1995). Seeds can survive bushfires, pass through the digestive tracts of animals and be dispersed across continents by wind before germinating and beginning their life as a sessile plant (Nelson, 2018). While they are often equipped to deal with harsh conditions and levels of oxidation, the synthetic stresses created within the field of plasma are unlike anything that occurs in nature. The combination of ion bombardment and chemical oxidation within a vacuum may influence the viability and growth of the treated seeds. Previous studies have explored the impacts of time plasma exposure time, ranging between 15 seconds and 40 minutes on a variety of apparatus (da Silva et al., 2017; Dauwe et al., 2021; Jiang et al., 2014; Lo Porto et al., 2019; Los et al., 2019; Šerá et al., 2010, 2017). The results vary between instrumentation and species treated yet, there is a general trend of germination improvement following brief plasma exposure, often under six minutes. Longer exposures tend to have a negative impact due to changes in seed biochemistry, including changes to levels of endogenous hormones, increased enzymatic activity, and altered metabolism (Bafoil et al., 2019; Šerá et al., 2010; Stolárik et al., 2015). The mechanisms behind these changes are

poorly understood and likely involve complex pathways and signalling cascades. Nonetheless, these studies suggest that prolonged plasma exposures, like those established in Chapter 5 as optimal for the deactivation of microbes on seed surfaces, may have a negative effect on seed viability.

Research conducted in Chapter 6 showed that physico-chemical changes induced during extended plasma treatment altered the manner in which seeds absorb water. Each grain type responded differently to contact with water, either increasing capillary flow or diffusion. The changes to water ingress also impacted solution egress and imbibitional leakage. It is unknown if these changes may alter seed health and the metabolic activation of each tissue within the grain.

While this study focuses on grain destined for food and feed production where germination will not occur, it is still important to understand the downstream consequences of treatment. There are many occasions where researchers may need to grow plants in a sterile environment and therefore consider the use of long time point plasma treatment to deactivate microbes on the grain surface. In consideration, it was deemed necessary to perform a series of experiments to understand how long plasma exposure times, up to 90-minutes, may affect seed viability, growth, and development. Trials were conducted to understand how plasma exposure time impacts the germination of each grain type. These were followed by seedling growth assays to track developmental trends within treatments. Variations in the results from these trials led to the conjecture that hormone signalling may play a role in the differences in development between treatments. As ethylene is an important hormone in both germination and oxidative stress response (Wang et al., 2020), a simple ethylene trial was conducted to see if trends could be detected across treatments. Finally, it has been suggested by Dobrynin et al., 2009 and Šerá et al., 2010 that DNA oxidation may occur with long plasma exposures. This concept was explored in a final assay to

elucidate oxidative damage to the DNA of germinating embryos. Ultimately, these experiments were conducted to gain insight into the way plasma exposure may impact the living grains.

7.2 Seed germination

7.2.1 Introduction

Grains are desiccated and quiescent plant embryos with very low metabolic activity. This resting state allows them to remain viable for long periods of time under harsh conditions. Upon contact with water under ideal conditions, imbibition occurs leading the seeds into metabolic overdrive. Cells hydrate, biochemical signalling occurs, DNA and mitochondria are repaired and the embryo begins to elongate through cell expansion (Bewley et al., 2013). Eventually the radicle will rupture the testa, signifying the occurrence of germination. Next begins the complex processes of seedling growth and development. Success is dependent on countless environmental factors, as well as internal signalling. Disruptions to the balance can lead to developmental delays and even seedling death (Rajjou et al., 2012). It is unknown how the stages of germination and early seedling growth will be impacted by the conditions involved in relatively long plasma treatments. The chemical etching process that is capable of deactivating microbes on the seed surface and may also be capable of harming the grain.

A series of experiments was conducted to gain insight into the relationships between plasma exposure time, seed viability and seedling development. Seeds of each grain type were exposed to incremental time points of plasma then placed on sterile plates for germination. Plates were monitored over multiple days to document the different stages of germination. The resulting data were used to understand how plasma treatment impacts the development of each grain type.

7.2.2 Materials and Methods

7.2.2.1 Grain treatment

Grains of each species were divided into six treatment aliquots: Untreated control, Tumbler + Vacuum (T+V) control, 15-minute (P15), 30-minute (P30), 60-minute (P60) and 90-minute (P90) plasma treatments. T+V control grains were treated in the plasma tumbler under a 250 mTorr vacuum for 90 minutes following protocols in Chapter 3.1.2.3. The plasma time series of grains was prepared following protocols in Chapter 3.1.2.2. Grains were treated 24 hours prior to the commencement of germination experiments with separate plasma runs for each independent experiment.

7.2.2.2 Grain plating

Sterile 100 mm x 25 mm culture dishes (Merck; Z358762) were prepared by placing a pre-autoclaved 90 mm C/E glass fibre filter (Whatman) into the upside-down lid. Grains of each treatment were randomly placed on the glass fibre and 6 mL of autoclaved deionised water was added to each plate. Dish bases were placed on top of the lids and secured with 25 mm Micropore™ surgical tape (3M) to allow gas exchange. Plates contained differing numbers of seeds for each grain type due to variations in size (Table 7-1). Due to the mucilaginous nature of psyllium grains, seeds were arranged in a row and the plate tilted upright in a rack. This allowed the radicles to grow downward in response to gravity for more accurate scoring on small seeds (Figure 7-1). For all other grain types, upside-down plates were randomised and placed in trays. All trays and racks of plates were incubated in a controlled environment (CE) cabinet at 25/18 °C, over a 14/10 hr light cycle at 60% relative humidity (RH).

Table 7-1. List of germination experimental design factors for each grain type.

Grain type	# seeds per plate	# plates per treatment	# of seeds per treatment	# independent experiments	Total # seeds per treatment	Total # seeds
Maize	6	6	36	3	108	648
Wheat	10	5	50	2	100	600
Barley	10	5	50	2	100	600
Field pea	6	6	36	3	108	648
Psyllium	12	5	60	2	120	720

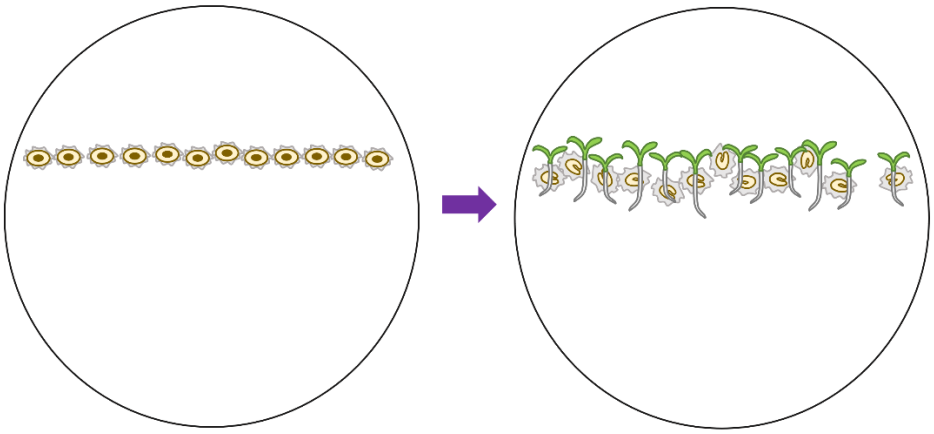


Figure 7-1. Diagram of psyllium germination layout for optimal observations of BBCH stages 00-09 (see Table 7-2 for growth stage descriptions) of germination.

Germination was considered to have occurred once a visible radicle had protruded from a seed. At 96 hours after sowing, counts of the germinated seeds were recorded and the germination percentage was calculated. The mean percentage of germination was calculated based on the germination percentages from all plates across the independent experiments.

7.2.2.3 Growth and development scores

In addition to percent germination, the early stages of seedling growth and development of Untreated, P30 and P90 grains were recorded. Seeds from three

plates of each treatment of maize and wheat, four plates from field pea and 5 plates of psyllium were selected for scoring. The differing number of plates per grain type were due to policy changes in shared controlled environment cabinet space due to COVID-19. Seeds on each plate were individually scored at set time points following the two-digit general BBCH scale (Lancashire et al., 1991) for maize, wheat, barley and field pea. The extended BBCH scale (Hess et al., 1997) was used for psyllium. Scores were recorded for the germination stages 00 to 09 (Table 7-2). Stage 01 marked the addition of water to each plate. A true soil emergence stage could not be recorded at 09 as growth occurred in culture plates. Therefore, the soil emergence stage was accepted to have occurred when cereal seed coleoptiles or pea shoots reached roughly 3 cm in length. The 3 cm measurement was designed to simulate the average sowing depth.

Table 7-2. Description of BBCH scale from dry seed to emergence. Adapted from Lancashire et al., 1991.

BBCH Score	Description
00	dry seed
01	imbibition begins
03	imbibition complete
05	radicle emergence
06	radicle elongation and root hair development
07	coleoptile, cotyledon or shoot emergence
09	emergence from soil

7.2.2.4 Microbial contamination scores

It was assumed that microbial growth may hinder germination, therefore each plate was scored for visible fungal contamination. A plate was given a score of 1 for the presence of fungi or zero for the absence of visible fungal contamination. The mean scores for each plate were calculated and combined to establish the percent grain microbial contamination.

7.2.2.5 Statistical analysis

One-way analysis of variance (ANOVA) was carried out to determine the significance of the percent germination measured between each grain type. Pairwise comparison of significance between the groups was determined using Tukey's test. ANOVA values were calculated using GraphPad Prism 9.0.0 (GraphPad Software Inc, San Diego, CA, USA). Two-way ANOVAs were also performed with multiple comparison analysis. Data were expressed as mean ± standard error of the mean. Significance was accepted at $p<0.05$.

7.2.3 Results and Discussion

Seed germination trials were conducted to understand how different exposure times of plasma-treatment may impact seed viability and vigour. Seed were germinated on plates with glass fibre filters to capture all BBCH stages of germination across fixed time points for each grain type. Glass fibre filters were selected over filter paper due to the uniformity of weave and the lack of air bubble formation between the polystyrene plate and filter. This allowed for all grains to sit evenly on the filter and have consistent exposure to water for imbibition. Due to variations in grain size and available space within CE cabinets, differing numbers of seeds and plates were used for each grain type. The available CE cabinet had a capacity of up to 36 plates split across three trays. The large grain size of maize and field pea allowed for up to six grains per plate, therefore the experiment was conducted three times to ensure a minimum of 100 grains per treatment. The smaller grain size of wheat and barley allowed for up to 10 grains per plate which reduced the number of replicates in the experiment to two to achieve 100 grains per treatment. Finally, a novel technique was developed for plating psyllium to compensate for the mucilaginous grain, small size, and rapid germination rate, within 18 hours. The uniform placement within an inverted plate allowed for more accurate assessment of each growth stage. The BBCH stages for barley were not

recorded due to a COVID-19 snap lockdown restricting daily access to CE cabinets. Limited access meant only 96-hour percent germination could be recorded for each experiment. Repetition of the experiments post-lockdown was not possible due to CE cabinet booking constraints.

7.2.3.1 Percent germination

The percent germination varied widely across grain types and treatments (Figure 7-2). Trends are not immediately apparent within this data set. The differences between plasma exposure time and grain type may be influenced by grain morphology and surface chemistry. For this reason, each grain type is discussed below in detail.

7.2.3.1.1 Maize

Maize grains had the lowest percent germination within the control treatments, Untreated and T+V. Previous work on this grain lot yielded percent germination above 90% after seed disinfestation involving a 20-minute seed dip in a solution of 50% bleach, 25% ethanol and 25% water. The grain was grown for research purposes at the University of Adelaide, Waite Campus and stored at 15 °C and used for germination trials within six months of harvest. For these reasons, it is suspected that the reduced percent germination may be attributed to microbial contamination. By hour 96, maize Untreated and T+V grains were visibly inundated with fungal contamination, possibly a *Rhizopus* species. A similar problem was encountered in Chapter 6.4.3 with the same lot of grain (see Figure 6-13). A fungal infection rapidly grew on control and treatments with plasma exposures less than 60 minutes. To further elucidate this phenomenon, the number of contaminated grains per treatment were recorded and analysed (Figure 7-3).

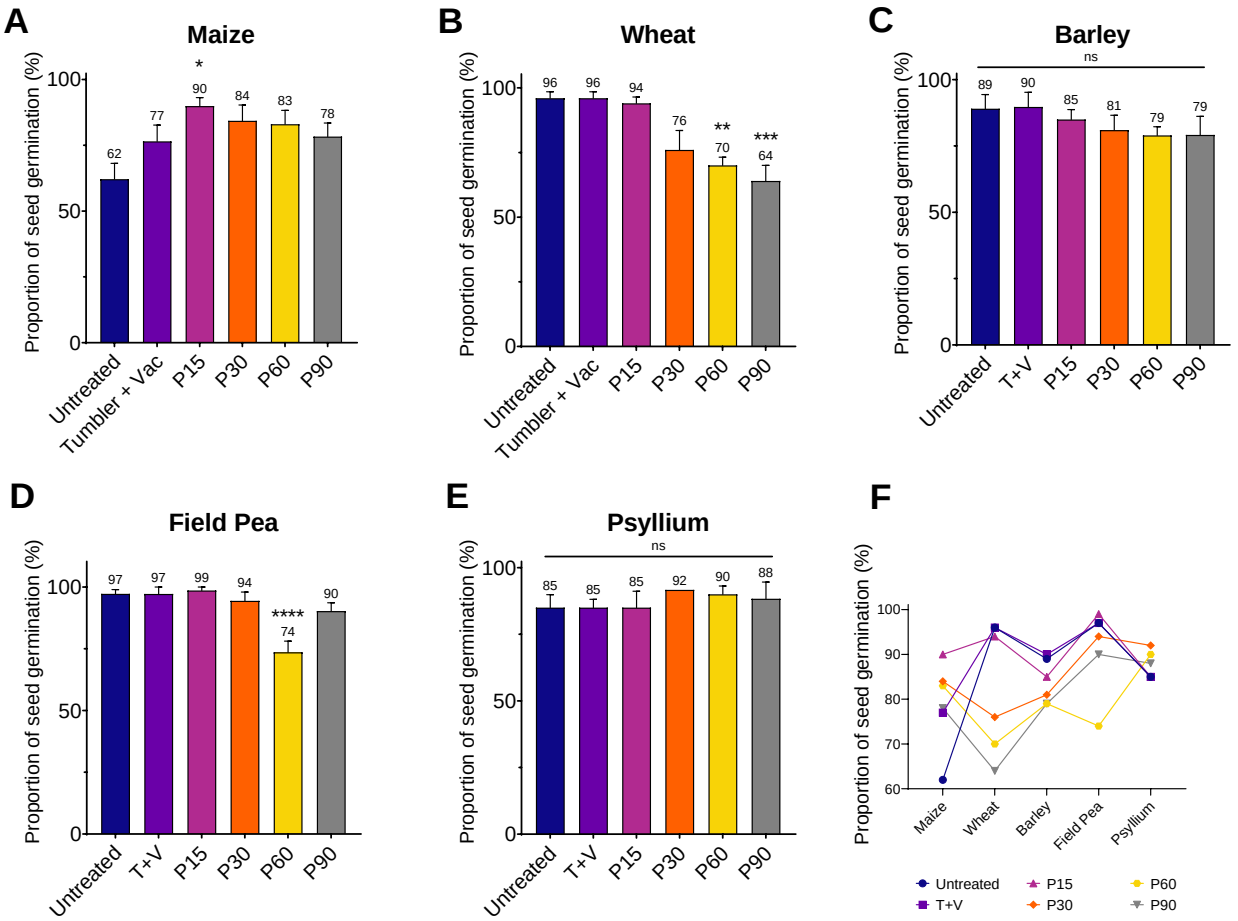


Figure 7-2. Mean percent germination for all treatments and grain types. (A-E) represent the means of combined experiment data (n = 100+). (F) compares the means of treatments for each grain type and highlights the variation in germination with prolonged plasma exposure. Data is presented as mean ± SEM. Abbreviations: T+V (Tumbler + vacuum); P15 (15-minute plasma); P30 (30-minute plasma); P60 (60-minute plasma); P90 (90-minute plasma); ns (non-significant). P-values are in comparison to the Untreated control; *p<0.05; **p<0.01; ***p<0.001; ****p<0.0001.

As expected, the visual observation of fungal contaminants was greatly reduced by plasma treatment. It may be that fungal infections hindered germination in control grains. A short plasma treatment of 15-minutes did not remove all fungi but was sufficient to restore percent germination back to expected levels. Increasing plasma exposure reduced both the percent germination and fungal contamination. This data set suggests that the exposure time for microbial deactivation does not necessarily match the time point for enhancing germination. In maize, shorter periods of plasma treatment may be more conducive to enhancing germination. Longer exposures should be considered if the goal of treatment is microbial deactivation.

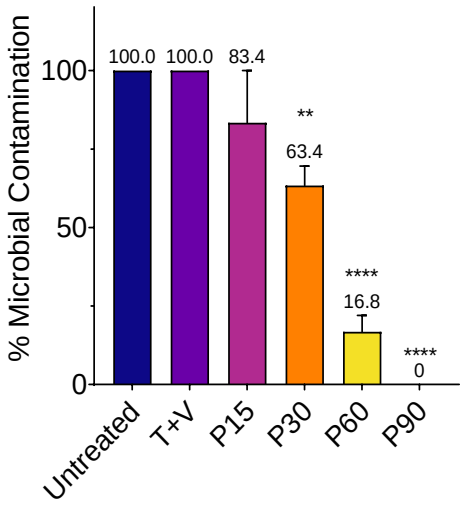


Figure 7-3. Maize percent of grain with visible fungal contamination in relation to different treatments. It is suspected that high levels of fungal infection may have inhibited germination on the control Untreated and T+V grains. Data is presented as mean ± SEM. Significance to both control treatments is displayed as **p<0.01; ****p<0.0001. The lack of error bars on both the Untreated and T+V controls indicate that every grain displayed visible fungal contamination. Abbreviations: T+V (Tumbler + vacuum); P15 (15-minute plasma); P30 (30-minute plasma); P60 (60-minute plasma); P90 (90-minute plasma).

7.2.3.1.2 Wheat

Unlike maize, industry grown food-grade wheat grains did not display visible fungal contamination, nor reduced germination in control grains (Figure 7-2). Instead, the percent germination on control grains followed the industry standard, of above 90%, for this cultivar, Scepter [sic], (GRDC, 2016). However, an inverse correlation was seen where the percent germination gradually decreased with increasing plasma exposure.

This suggests that prolonged plasma-treatment has a negative effect on seed viability. It is speculated this may be attributed to grain morphology. Thousands of years of domestication have led to the development of a hull-less, or naked, grain. While this adaptation allows for rapid germination under normal conditions, the less protected embryo is vulnerable to injury. In Chapter 4, Figure 4-5, SEM imagery of plasma-treated grains showed significant changes to grain surface features, including the embryo and the brush. Mechanical damage inflicted during the tumbling process, combined with the physical etching and chemical weathering of the seed surface during lengthy plasma treatment may have compromised embryo viability. Damage to the pericarp surrounding the embryo was captured on SEM micrographs of numerous plasma-treated grains (Figure 7-4). It is possible that the structure and position of tissues, including a protective hull, may have influenced the efficacy of extended plasma-treatment on germination. Damage to the pericarp may not only influence embryo health but also the direction of water uptake within the grain, as seen in Chapter 6, Figure 6-24. The combined data and imaging suggest that plasma treatments greater that 15-minutes are counterproductive for wheat grain germination.

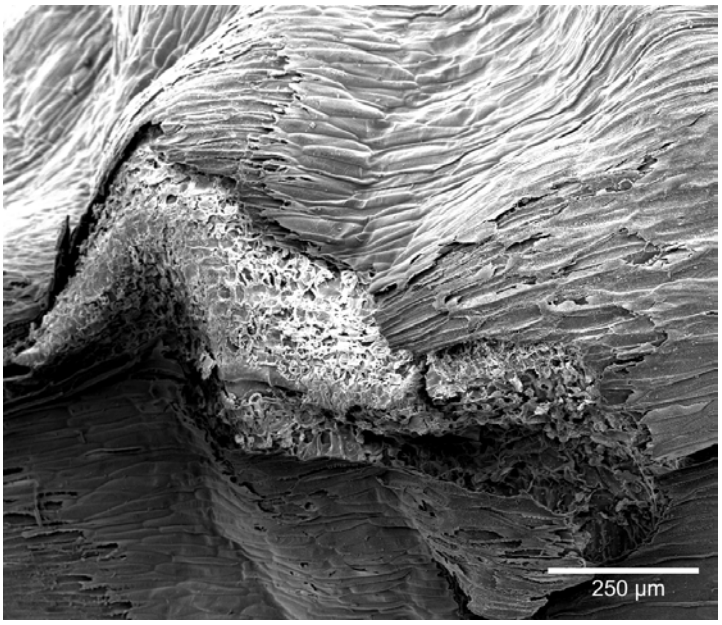


Figure 7-4. SEM micrograph showing damage to the pericarp covering the embryo on a 90-minute plasma-treated grain. More detailed images and comparisons with other treatments can be seen in Chapter 4, Figures 4-3 and 4-5.

7.2.3.1.3 Barley

Hulled barley grains possess a similar structure to wheat with an added protective layer of the husk. Like wheat, barley germination followed a trend of reduced germination percentage with increasing plasma exposure (Figure 7-2). While the reductions were not statistically significant, growers and malters/brewers may baulk at the idea of a 10% decrease in germination. It is possible that the protective barley hull contributed to the higher percent germination following long plasma exposure when compared to wheat. The husk may have shielded the embryo from the mechanical and physico-chemical changes caused by plasma treatment. It seems that grain morphological features may play a role in the capacity of plasma-treatment to impact grain growth and development.

7.2.3.1.4 Field pea

Field pea grains showed a rather convoluted relationship with plasma treatment. All treatments were not statistically significant, except the P60 treatment (Figure 7-2). Across all experiments, the percentage of germination after 60-minutes of plasma exposure was lower but partially recovered at 90-minutes. This baffling effect is suspected to be related to growth and development of the grain and will be discussed further in section 7-3.

7.2.3.1.5 Psyllium

Psyllium grain percent germination was relatively unaffected by plasma treatment (Figure 7-2). These robust grains have a layer of laminated polysaccharide mucilage covering the seed coat. It is thought that this outer layer may have acted as a protective shield against the weathering processes of plasma treatment. This may explain why psyllium was the only grain type which did not display decreased percent germination from prolonged plasma exposure.

7.2.3.1.6 Comparisons between grain types

The percent germination data are rather complex with differences between each grain type (Figure 7-2, F). It is thought that the different morphologies and surface structures play a role in the efficacy of plasma treatment. It appears that shorter exposures may be beneficial, depending upon species. Whereas long exposure times can inflict damage to specific grain structures which can lead to reduced germination and viability. This dose-dependent reaction is different for each grain type and is further explored with initial germination growth and development scores.

7.2.3.2 Germination growth and development

In addition to recording the percent germination, seeds of three treatments were scored to track changes in the germination growth and development stages using the BBCH scale. This scale describes trends in a more qualitative manner than compared to simple counts of radicle emergence from the seed (Figure 7-5). In maize, plasma-treated grains displayed slower radicle protrusion and did not develop as quickly as the Untreated grains across the recording window. Plasma-treated wheat showed faster initial radicle emergence, but this was followed by subsequent delays in radicle elongation and coleoptile emergence. The lag in coleoptile growth could have both short-term and long-term consequences for wheat growth and development. When compared to the similar delays in maize, it appears that the cell elongation processes involved in germination sensu stricto are uninhibited by plasma treatment. However, the metabolic processes and biochemical signalling involved in activation of the embryo may be hampered by plasma exposure.

In contrast, post-germination developmental delays were not observed in the eudicots. Like wheat, psyllium displayed accelerated emergence but by 96 hours the Untreated seedlings had matched their plasma-treated counterparts. Finally, in field pea, there were no differences in growth and development between treatments throughout the

growth window. An additional 168-hour time point was recorded to look for variations at a longer time point, yet no differences between treatments were observed. This data set confirms that plasma exposure has a very different impact on each grain type. Overall, the cereals had delayed growth and development while the eudicots were less effected. This may be due to numerous factors including but not limited to grain morphology, water uptake, embryo damage and microbial contamination. Longer term growth experiments are needed to untangle the dynamic effects between grain type and plasma exposure on seedling development.

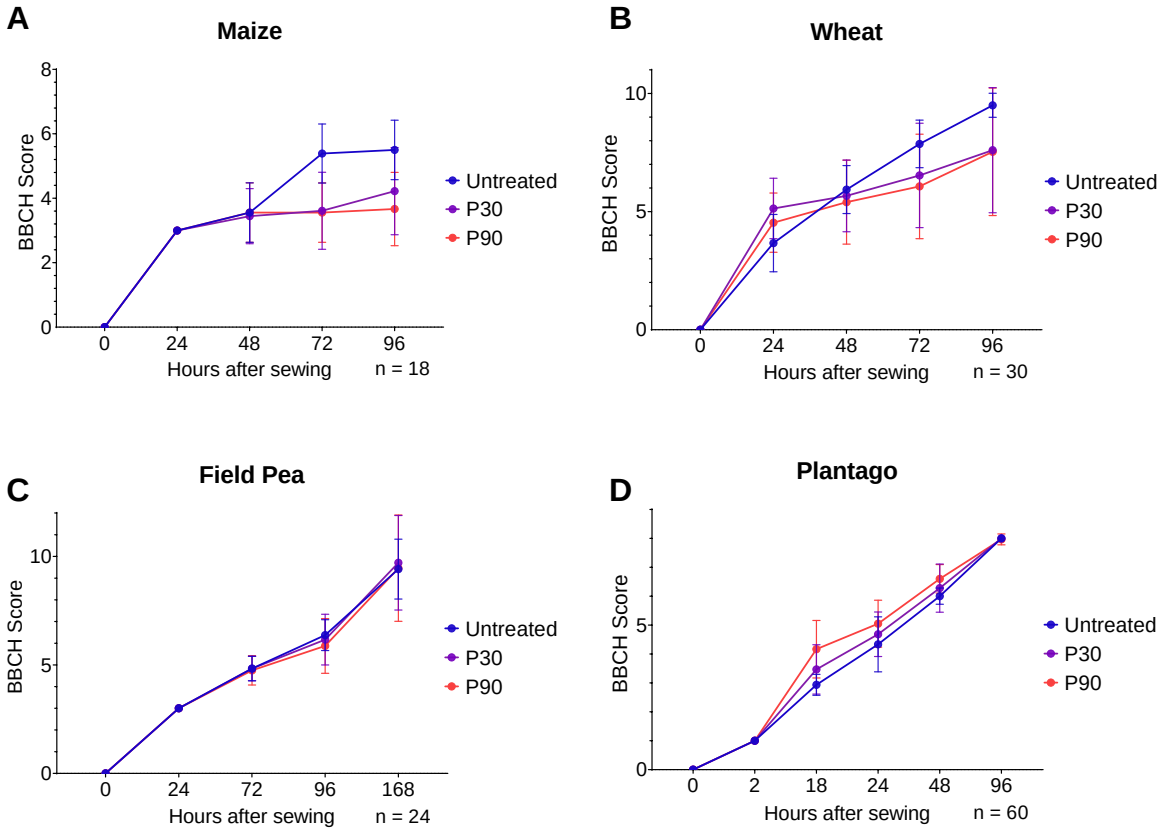


Figure 7-5. Growth and development scores for seedlings across the germination time frame. Data is presented as mean ± SEM. Note that barley data was not collected due to COVID-19 restrictions to controlled environment cabinet access. Abbreviations: P30 (30-minute plasma); P90 (90-minute plasma).

7.2.4 Summary

This study sought to provide insight on the interactions between seed germination, seedling growth and plasma exposure times. Germination assays were conducted in

a synthetic plate environment to aid in the observation of minute changes at each time point. The resulting data suggested that the behaviour of a seed following plasma treatment is dependent upon both time exposure and species. Factors such as grain morphology and surface chemistry likely play a significant role in the prediction of how plasma may interact with a seed. Severe etching involved in long exposure times may cause developmental delays or worse, reduce viability. Shorter exposure times may increase percent germination but may also be less efficient at removing microbial contamination. Depending upon the subsequent use of seeds following treatment, it may be worthwhile to have knowledge of both the positive and negative aspects of prolonged plasma exposure. The downstream impacts of plasma treatment on plant growth and development beyond the narrow germination window will be further explored in the next section.

7.3 Seedling growth trials

7.3.1 Introduction

Like most living organisms, the early stages of growth and development are critical for the establishment of a healthy and vigorous plant. Rapid radicle protrusion and the emergence of photosynthetic structures are essential for the success of the seedling. The delays in maize and wheat radicle elongation and coleoptile emergence seen in section 7.2.3.2 led to speculation that long plasma exposure may have detrimental effects on seedling vigour. To better understand the effects of plasma treatment, another series of seedling growth assays were conducted. Seeds of each treatment were sown into Jiffy-7® soil pellets and measured daily following seedling emergence.

7.3.2 Materials and Methods

7.3.2.1 Grain treatment

Grain plasma treatment and T+V treatment followed protocols established in Chapter 3.1.2. Short-term growth trials of maize, wheat and psyllium involved a time series of treatments, as specified in the following sections.

7.3.2.2 Experimental design

A randomised complete block design (RCBD) was established for each grain type using R Studio with Agricolae and BiometryTraining packages (Figure 7-6). Due to the nature of the packages, individual completely randomised design (CRD) plots were created for each ‘block’ or tray. These were based on trays holding 5 x 6 Jiffy-7® soil pellets. Depending upon the availability of space in CE cabinets, two or three trays were used per grain type for a total of 60 plants over two trays for maize, wheat, and field pea; 90 plants over three trays for psyllium. Wheat Trial B held 150 Jiffy-7® soil pellets across five trays. The ‘seed’ number (see code in Figure 7-6) was chosen at random to produce different plots for each tray.

```
#RCBD
trt <- c ("Untreated","T+V","P15", "P30", "P60", "P90")
rep <- 5
outdesign <- design.crd(trt = trt, r = rep, seed = 42)
des.out <- des.info(design.obj = outdesign, nrows = 5, ncols = 6)


#Latin square
trt <- c("U", "T+V", "P90","U", "T+V", "P90")
outdesign <- design.lsd(trt)
des.out <- des.info(design.obj = outdesign, nrows = 6, ncols = 6)
```

Figure 7-6. Code used with the BiometryTraining package in RStudio to create a randomised complete block design and Latin square design.

7.3.2.3 Grain sowing and growth trials

7.3.2.3.1 Maize

7.3.2.3.1.1 Short-term growth and development with an exposure time series

Ten replicates of each treatment were sown in Jiffy-7® pellets and placed in trays with a capacity of 30 pellets in a 5 x 6 arrangement. Treatments were randomised across two trays following the RCBD established in 3.2.2. Trays were placed in a controlled environment cabinet for eleven days at 28/20 °C, 14/10 hr light cycle at 60% RH. Once the shoot protruded through the soil, measurements were recorded daily from the point of emergence/top of Jiffy-7® pellet to the tip of the youngest leaf. Measurements concluded seven days after emergence.

7.3.2.3.1.2 Long-term growth and development

Untreated, T+V and 90-minute plasma treatments were selected for this trial. Two seeds were sown in 30 L pots with Premium Potting Mix (Bio Gro, Mt. Gambier, South Australia), and topped with sugarcane mulch. Pots were placed outdoors along benches at the University of Adelaide Waite Campus, Adelaide Australia in a 6 x 6 Latin Square design (see code in Figure 7-6). Plants were grown for 18 weeks from mid-October 2020 to the end of February 2021. At 21 days after sowing, any pots with two seedlings were reduced to a single plant per pot. The plant closest to the centre of the pot was retained to ensure the most even spacing between pots and not bias the experiment by selecting for phenotypic traits. Plants were monitored throughout the growing season. Harvest occurred once all plants had completely dried in the pots. Plant height was measured from soil level to the base of the tassel. Following grain harvest, all above ground vegetative tissue from each plant was placed in pre-weighed paper bags and oven dried at 50 °C for two weeks. After drying, weights were recorded for each plant.

7.3.2.3.2 Wheat

7.3.2.3.2.1 Short-term growth and development with a plasma exposure time series

Ten replicates of each treatment were sown in Jiffy-7® pellets and placed in trays with a capacity of 30 pellets in a 5 x 6 arrangement. Treatments were randomised across two trays following the RCBD established in section 7.3.2.2. Trays were placed in a controlled environment cabinet for nine days at 22/16 °C,14/10 hr light cycle at 60% RH. Once the shoot protruded through the soil, measurements were recorded daily from the point of emergence/top of Jiffy-7® pellet to the tip of the youngest leaf. Measurements concluded six days after emergence.

7.3.2.3.2.2 Repetition of short-term growth and development with three treatments

Fifty replicates of each treatment were sown in Jiffy-7® pellets and placed in trays with a capacity of 30 pellets in a 5 x 6 arrangement. Treatments were randomised across five trays following the RCBD established in section 7.3.2.2. Trays were placed in a controlled environment cabinet for fourteen days at 22/16 °C, 14/10 hr light cycle at 60% RH. Once the shoot protruded through the soil, measurements were recorded daily from the point of emergence/top of Jiffy-7® pot to the tip of the youngest leaf. Measurements concluded ten days after emergence.

7.3.2.3.3 Field pea

Twenty replicates of Untreated, T+V and 90-minute plasma treated seeds were sown in Jiffy-7® pellets and placed in trays with a capacity of 30 pellets in a 5 x 6 arrangement. Treatments were randomised across two trays following a RCBD design. Trays were placed in a controlled environment cabinet for eighteen days at 20/14 °C, 14/10 hr light cycle at 60% RH. Once the shoot protruded through the soil, measurements were recorded daily from the point emergence/top of Jiffy-7® pot to the tip of the youngest leaf. Measurements concluded ten days after emergence.

7.3.2.3.4 Psyllium

Fifteen replicates of each treatment were sown in Jiffy-7® pellets and placed in trays with a capacity of 30 pellets in a 5 x 6 arrangement. Treatments were randomised across three trays following the RCBD established in 7.3.2.2. Trays were placed in a controlled environment cabinet for twenty-six days at 28/20 °C, 14/10 hr light cycle at 60% RH. Once the shoot protruded through the soil, measurements were recorded every four days from the point of emergence/top of Jiffy-7® pot to the tip of the youngest leaf. Measurements concluded sixteen days after emergence.

7.3.2.4 Statistical analysis

Two-way ANOVA were performed with multiple comparison analysis to determine the significance of treatment on growth height at each time point. One-way analysis of variance (ANOVA) was carried out to determine the significance of treatment in dry weight and plant height at harvest. Pairwise comparison of significance between the groups was determined using Tukey's test. ANOVA values were calculated using GraphPad Prism 9.0.0. Data were expressed as mean ± standard error of the mean. Significance was accepted at $p<0.05$.

7.3.3 Results and Discussion

In section 7.2.3.2, developmental lags following radicle protrusion were observed in plasma-treated maize and wheat. This led to questions regarding the impact of plasma treatment on early seedling development in a synthetic plate environment. To further understand the influence of plasma exposure, a time series of plasma treatments was conducted on seeds of maize, wheat, field pea and psyllium. Barley was omitted from this study due to interruptions caused by COVID-19 lockdowns. Seedlings were grown in soil with plant growth tracked over various time points (Figure 7-7). Descriptions of growth and development across grain types and treatments are listed below.



Figure 7-7. Seedlings grown in Jiffy-7® pellets for growth and development measurements. (A) Maize at 7 days after emergence (DAE); (B) wheat at 6 DAE (C) field pea at 11 DAE; (D) psyllium at 16 DAE.

7.3.3.1 Early plant growth and development trials

7.3.3.1.1 Maize

Over the time course of seven days, maize seedlings displayed consistent growth within each treatment (Figure 7-8). By day 7 after emergence, Untreated, T+V and 30-minute plasma treated seedlings grew on average 40% taller than all other treatments. The differences between treatments were statistically insignificant due to variation within treatment replicates. It is speculated that changes would be biologically relevant because the differences in growth patterns during early development are vitally important to growers.

7.3.3.1.2 Wheat exposure time series

Like maize, wheat seedlings displayed a dovetailing effect with treatments appearing to separate into two, statistically insignificant groups (Figure 7-8). At six days after

emergence, the Untreated, P15 and P60 seedlings were on average 27% taller than the other treatments.

The results of maize and wheat heights (separating without statistical significance) necessitated the plotting of individual plant growth height (Figure 7-9). In maize, the rate of growth ($\frac{\text{height}}{\text{time}}$) is much slower for many plants as highlighted in the black rectangle. In wheat, many plants failed to grow following soil emergence, resulting in a plateauing growth rate. When taken into context with the germination growth and development for maize and wheat in section 7.2.3.2 (Figure 7-5, A and B), this appears to be a continuation of the same trend where some plants hit a plateau in growth and development. To further understand these patterns, a second wheat seedling growth trial was conducted (see below), as well as a long-term maize growth trial (7.3.3.2).

7.3.3.1.3 Wheat three treatment comparisons

A second wheat growth trial was conducted with 50 plants of three different treatments to look for trends within a larger data set. The above soil tissues were harvested at Day 10 after emergence (14 DAS), oven-dried and weighed to capture differences in dry mass between treatments. Across all time points, 90-minute plasma treated seedlings had a significantly slower growth rate than both Untreated and T+V seedlings, with p-values of less than 0.0001 across each day (Figure 7-10). There were no differences between the Untreated and T+V controls. In addition, the dry mass of P90 seedlings was significantly lower than the controls, by roughly 22%. Together, these data sets demonstrate the negative impact of 90-minute plasma treatment on seedling growth and development.

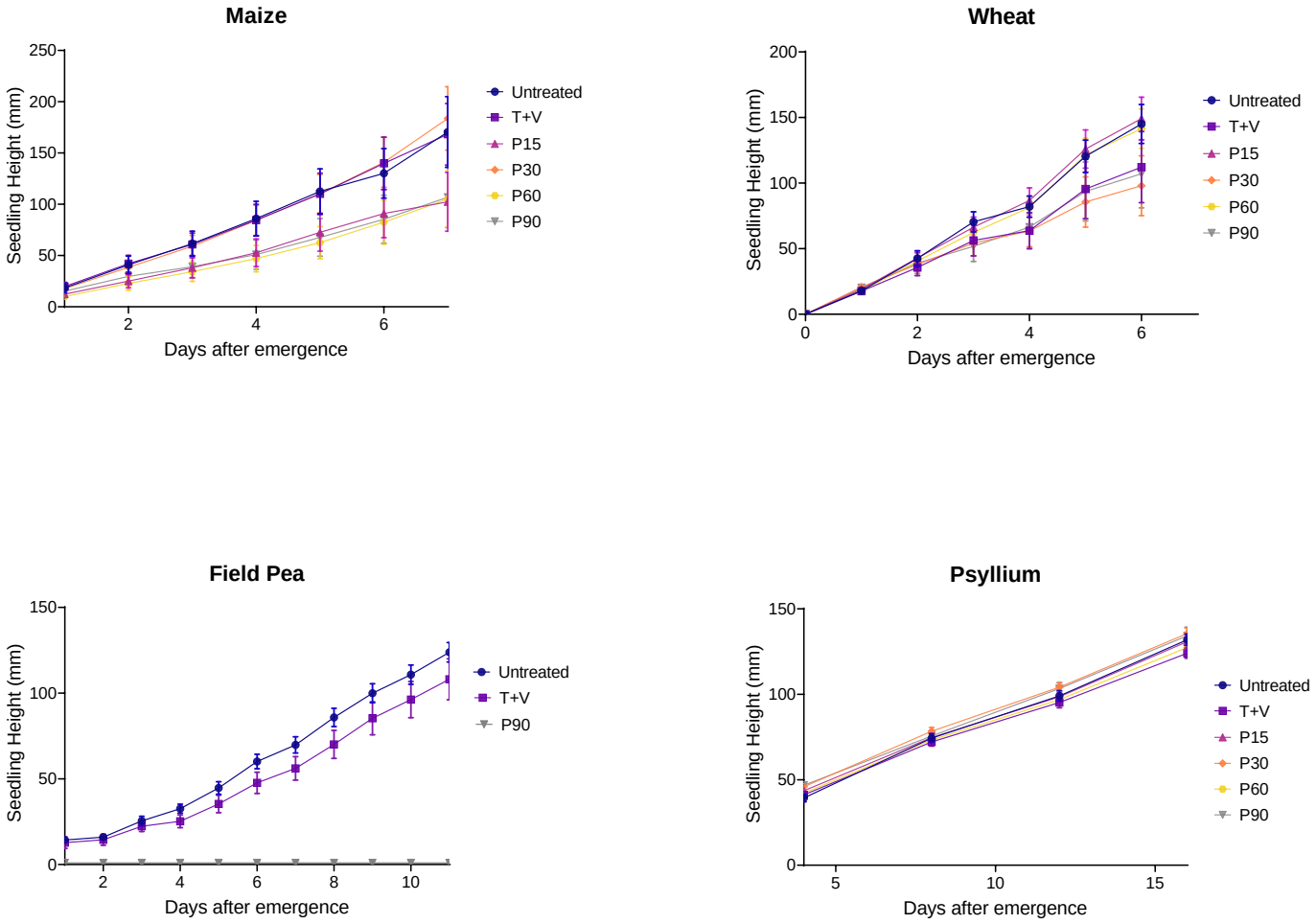


Figure 7-8. Seedling height following emergence from the soil. Data is presented as mean ± SEM. Abbreviations: T+V (Tumbler + vacuum); P15 (15-minute plasma); P30 (30-minute plasma); P60 (60-minute plasma); P90 (90-minute plasma).

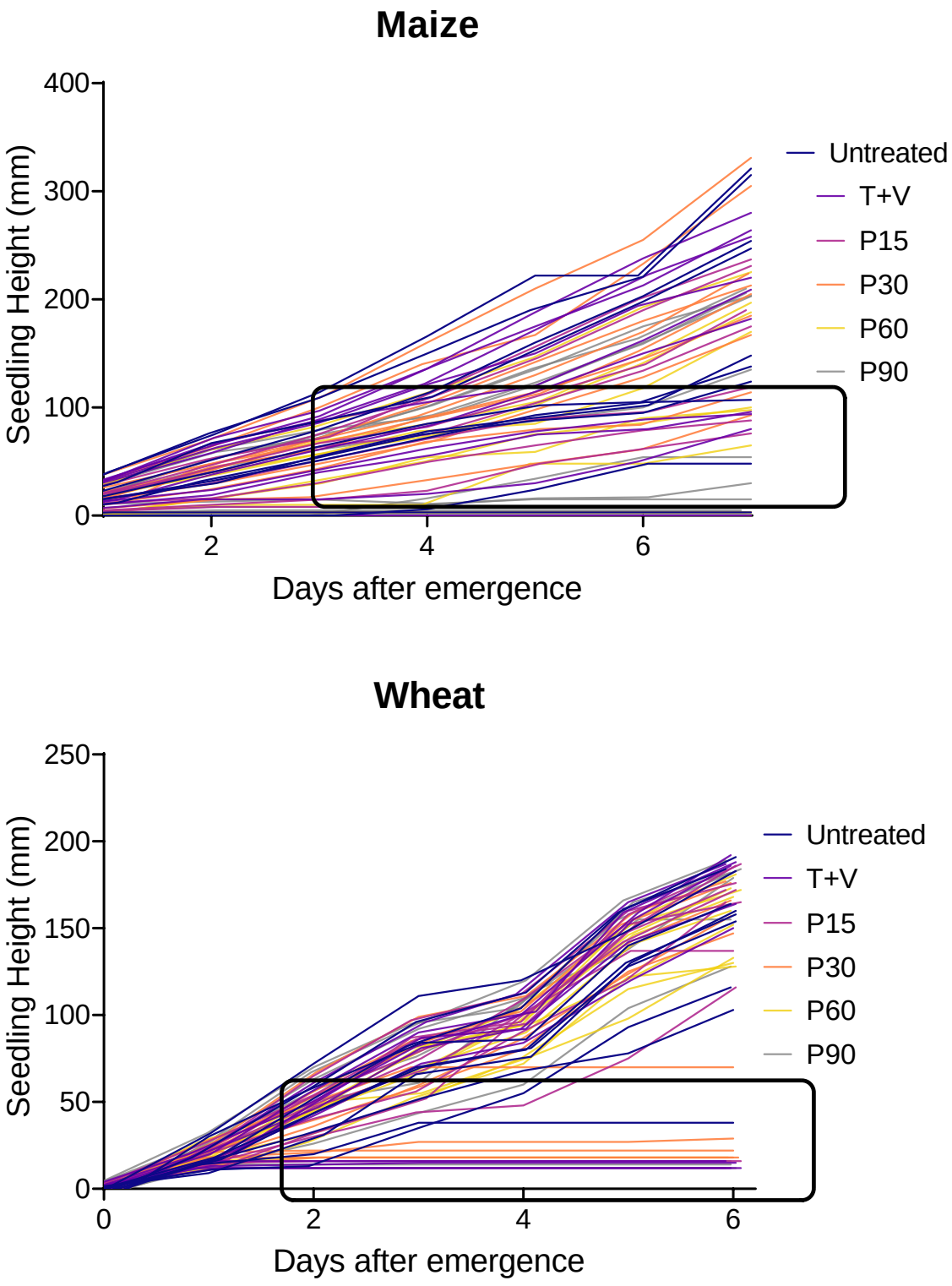


Figure 7-9. Growth of individual replicates over the course of six days following emergence. Black rectangles display the stagnation of growth in many replicates which contributed to large but insignificant differences in mean growth rate. Abbreviations: T+V (Tumbler + vacuum); P15 (15-minute plasma); P30 (30-minute plasma); P60 (60-minute plasma); P90 (90-minute plasma).

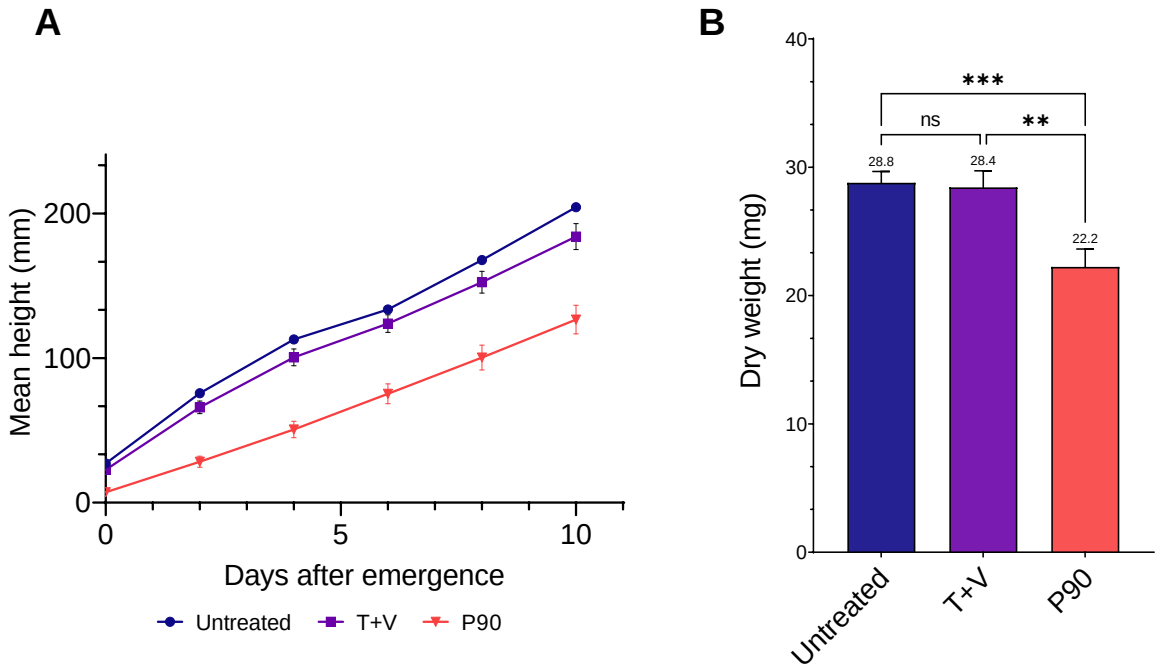


Figure 7-10. Wheat seedling growth trial. (A) Seedling height recorded for 10 days from emergence at 4 DAS. (B) Dry weights of above ground plant material harvested at 10 days after emergence, 14 DAS. Data is presented as mean ± SEM. Abbreviations: T+V (Tumbler + vacuum); P90 (90-minute plasma); ns (non-significant); **p<0.01; ***p<0.001.

7.3.3.1.4 Field pea

Due to COVID-19 restrictions and limited space available in controlled environment cabinets, field pea growth trials were conducted with only three treatments (n=20) (Figure 7-8). The growth rate was recorded for Untreated and T+V seedlings only. None of the 90-minute plasma treated seeds emerged from the soil. Of the seedlings that did emerge, there was no statistical difference between Untreated and T+V. The complete absence of plasma-treated seedlings was puzzling and led to the dissection of soil pellets to observe the condition of the plasma-treated seeds. Unexpectedly, almost all had visible fungal contamination which was not present in Untreated and T+V treatments. The previous growth experiment in section 7.2.3.2 occurred under sterile conditions which led to the speculation that the removal of the outer layers may leave the grain more susceptible to infection with soil fungi. It should be noted that pathogenic fungi are not typically found in Jiffy-7® pellets and may have been

unintentionally introduced during treatment. Due to further COVID-19 lockdown limitations, a secondary experiment could not be completed for this grain type.

7.3.3.1.5 Psyllium

Psyllium seedling data collection began at Day 4 following emergence when unfurled cotyledons were at a measurable stage. Over the course of 16 days, there were no differences in height between treatments (Figure 7-8). When taken into consideration with percent germination (section 7.2.3.1) and germination growth and development (7.2.3.2), it appears that psyllium was unaffected by all lengths of plasma exposure. It is speculated this may be due to the thick layer of laminated polysaccharides on the seed surface, above the seed coat. The effects of plasma treatments may etch off layers of mucilage with minimal impact on seed viability and development.

7.3.3.2 Long-term growth of maize plants

The growth of maize cv. B73 plants from seed to seed was explored to see if the effects of plasma-treatment could be seen throughout the plant lifecycle. Plants were grown outdoors over the 2020-2021 summer season as glasshouse space for plants of this size was not available for the 18-week lifecycle. Initially, two seeds were placed in each pot as a bet-hedging method to ensure the survival of at least one seedling across the germination and early development period. At 21 DAS, any pots with two seedlings were reduced to the one. It was understood that this process may introduce bias by not capturing data from seeds that may have had compromised germination and early development due to treatment. However, this data set was gathered to complement the early growth and development data by providing a long-term look at plant health. As all pots had at least one seedling persist until 21 DAS, the selection of a seedling based on position closest to the centre of the pot was not considered detrimental to the experiment.



Figure 7-11. Maize seed-to-seed pot growth experiment. Images were captured at 4, 8, 12 and 18 weeks after sowing. Overall, there were no visible differences between the treatments.

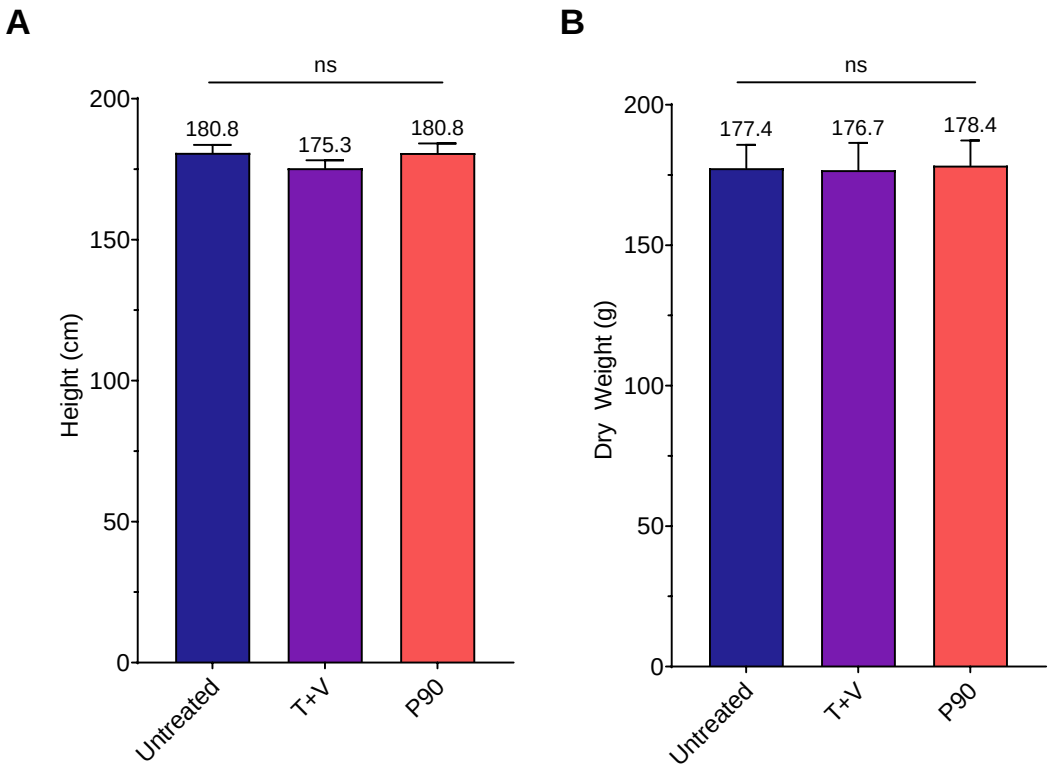


Figure 7-12. Maize harvest data at 18 weeks after sowing. (A) Mean height of plants from soil level to the base of the tassel. (B) Mean dry weights of all above ground vegetative material. Data is presented as mean ± SEM with significance accepted at $p<0.05$. Abbreviations: T+V (Tumbler + vacuum); P90 (90-minute plasma); ns (non-significant).

Overall, there was little difference between Untreated, T+V and P90 plants. All treatments produced healthy plants with no visible differences between treatments across the growing season (Figure 7-11). Data sets collected at harvest (Figure 7-12) revealed that by the end of the lifecycle, the three treatments were indistinguishable, with no difference among the 12 replicates of each treatment in plant height or dry weight. While plasma may have impacted early growth and development, long-term growth and development of maize was unaffected.

7.3.4 Summary

This study was conducted to gain an understanding of how different plasma exposures may impact seedling growth and development under non-sterile soil conditions. While some of the growth trials were limited, each grain type displayed a different response to prolonged plasma exposure. Early seedling growth and development in cereals was greatly reduced by 90-minutes of plasma exposure. However, maize seedlings which persisted past 21 days displayed no difference in long-term growth and biomass at harvest. It appears that plasma may reduce early growth rates but has lessened the effect on later growth and development. In the model legume system of field pea, plasma-treated seeds were unable to emerge from the soil, while their Untreated and T+V counterparts thrived. Under the growth conditions of this experiment, plasma-treated field pea grains were degraded to non-viable, possibly caused by an opportunistic fungal infection. Finally, the early growth rate of psyllium was largely unaffected by plasma treatment. Chapter 6 demonstrated the dramatic effects of plasma treatment on water transport. It is likely that differences in grain water sorption and the downstream metabolic processes are impacting the early seedling growth. It is also possible that plasma treatment may be influencing biological processes such as hormone signalling and the repair of oxidative damage mechanisms resulting in stunted growth. The remaining sections of this chapter will be dedicated toward

investigating possible biological explanations for the inhibition of seedling development covered within sections 7.2 and 7.3.

7.4 Ethylene trial

7.4.1 Introduction

Seed hormone signalling is an incredibly complex field of research and even the most rigorous of studies may be difficult to interpret as signalling pathways are convoluted and often confounded by countless variables. Yet, a cursory survey of the impacts of plasma-treatment on early seed germination and development would not be complete without briefly discussing the potential effects of plasma on seed hormones. It is clear from the previous sections that plasma exposure can influence seed germination, growth, and development. The intensity of the effects is dependent upon seed type, the length of plasma exposure time, and can range from improvements in percent germination to dramatic decreases. This may be attributed to plasma weathering of the grain surface, as seen in Chapter 4, which appears to impact grain-water relations, demonstrated in Chapter 6. While the changes in water transport most likely play a large role in the changes to seed viability, growth and development, oxidative stress induced by plasma-treatment has the potential to trigger hormone responses. Stolárik et al., 2015, investigated changes to pea seedling auxin and cytokinin concentrations following 0-, 2- and 10-minute plasma exposures. Auxin levels generally decreased, while cytokinins increased, offering speculation that short-term plasma treatments are capable of influencing hormone signalling in pea. This led to conjectures that early germination signalling hormones, such as ethylene and ROS, may also be impacted by plasma treatment.

ROS are essential for germination, yet there is a delicate balance as high levels can have deleterious effects through lipid peroxidation, protein and nucleic acid damage

(Bailly et al., 2008; Choudhury et al., 2013). As suggested by Ling et al., 2015, the peroxidation of lipids, due to the ROS involved in plasma treatment, may increase intracellular concentrations of malondialdehyde (MDA), a mutagenic compound formed from the oxidation of tri-unsaturated fatty acids. Inducing high levels of MDA via plasma treatment may be one of the factors contributing to the efficacy of plasma in the deactivation of microbes (Dobrynin et al., 2009). However, these same processes may also impact seed embryos. Wang et al., 2020, found that the addition of exogenous ethylene to the seeds of the legume alfalfa can reduce intracellular MDA and H_2O_2, lessening the negative impact of oxidative stress. This is intriguing as ethylene is an essential hormone deeply involved in early germination of many species. In cereals, ethylene synthesis begins in Phase II of germination and interacts with ROS to promote radicle elongation and germination (Corbineau et al., 2014; Locke et al., 2000). While the interplay between ethylene and ROS during germination is still relatively unknown, it is worth questioning whether the potential oxidative stress induced by plasma triggers a response involving ethylene signalling during germination and early seedling growth. Therefore, could the addition of exogenous ethylene counteract the negative effects of long exposure plasma treatment on wheat and maize seeds?

Extensive research should be undertaken to thoroughly investigate these questions. Nevertheless, this section presents an experiment designed to tentatively address the question and satisfy curiosity about the role of ethylene in the germination of plasma-treated cereals using materials readily available in the laboratory. Ethephon (ET), 2-chloroethylphosphonic acid, is often used as a source of ethylene as it can be diluted with water to generate an equal molar amount of ethylene. This reagent can be added to small, contained environments to increase exogenous ethylene concentrations (Tucker et al., 2017). 2-aminoethoxyvinyl glycine (AVG) is an ethylene biosynthesis

inhibitor which works by preventing the enzymatic conversion of S-adenosyl-L-methionine to ethylene through the inhibition of ACC synthase (Schaller and Binder, 2017). Both relatively inexpensive reagents are commonly found in plant science laboratories and can be useful in small-scale studies. Together these reagents were used to explore the hypothesis that ethylene may play a role in diminishing the negative effects of prolonged plasma exposure on cereal grains.

7.4.2 Materials and Methods

7.4.2.1 Grain preparation

Two plasma treatment time points were selected for this experiment. As the experimental goal was to determine if ethylene exposure could rescue plasma-treated seeds, it was necessary to select two treatments, mid-term and long-term, where there was an observable decline in germination, growth, and development.

7.4.2.1.1 Wheat

Treatment time points were selected based on data from section 7.2.3.1, where a significant decrease was observed in percent germination between 30-minute and 60-minute treatments. Therefore, a 45-minute plasma exposure (P45) was selected as the mid-term exposure time, while a 90-minute treatment (P90) served as a long exposure time point.

Wheat grains were split into three aliquots of 10 g each. One aliquot remained untreated as a negative control. Another aliquot was treated for 45-minutes in the plasma tumbler following protocols in Chapter 3.1.2.1. The final aliquot was treated for 90-minutes in the plasma tumbler. Following treatment, grains were transferred to a laminar flow for plating.

7.4.2.1.2 Maize

Like wheat, treatment time points were selected based on percent germination data in section 7.2.3.1. There was no difference between mid-range treatments of 30 and 60 minutes, therefore a 60-minute treatment (P60) was selected as the mid-term exposure time and 90-minutes (P90) acted as the long-term exposure.

Maize grains were split into three 10 g aliquots with one Untreated control, a P60 treatment and a P90 treatment. Following treatment, grains were transferred to a laminar flow hood for plating.

7.4.2.2 Hormone treatment preparation

Concentrations of hormones were determined following protocols described by Sun et al., 2020. Their research suggests that ethephon concentrations of 10 µm will not inhibit root growth, while AVG concentrations of 1 mM will inhibit growth without further toxic effect to the seedling. As the goal was to determine if ethylene can restore vigour to plasma-treated seeds, 10 µm concentration was selected as the optimal concentration for ethephon.

7.4.2.2.1 Ethephon

A 1 mM stable stock solution of Ethephon (Sigma-Aldrich) was prepared in 99.5% ultrapure molecular grade ethanol (Fisher Scientific). The solution was kept in the dark at 4 °C for two hours until use. Immediately prior to application, a 10 µM working solution was created by adding stock solution into autoclaved deionized water, pH 7. The solution was sealed, inverted ten times, and quickly dispensed onto plates.

7.4.2.2.2 AVG

The agrichemical ReTain® was kindly donated to the laboratory by Sumitomo Chemical Australia Pty Ltd. ReTain® contains 15% active AVG and a 1 mM aqueous working solution was made with autoclaved DI water, factoring in the initial

concentration. The working solution was stored in the dark at 4 °C for two hours prior to application.

7.4.2.3 Experimental procedures

Under a laminar flow, treated maize and wheat grains were placed in sterile culture dishes with autoclaved glass fibre filters following protocols established in section 7.2.2.2. Three replicates were created for each plasma exposure and hormone treatment for a total of 27 plates per grain type. Once plates were prepared, 6 mL of either autoclaved DI water, AVG working solution or ET working solution were added to each plate. All ET plates were prepared last to ensure gaseous ethylene did not contaminate other treatments. All plates were immediately sealed with Parafilm® M (Amcor) then double wrapped in cling film (Glad). Plates were then transferred to controlled environment cabinets. Water and AVG treatments were randomised throughout one cabinet and ET treatments were randomised in the second cabinet to prevent ethylene contamination. Wheat grains were incubated at 22/18 °C at 14/10hr light cycle for four days. Maize grains were incubated at 28/20 °C at 14/10hr light cycle for six days. BBCH scores were recorded daily for each grain with percent germination scores on the final day following protocols established in sections 7.2.2.3 and 7.2.2.4.

7.4.2.4 Statistical analysis

Two-way ANOVA were performed with multiple comparison analysis to determine the significance of treatment on percent germination and BBCH scores at each time point. ANOVA values were calculated using GraphPad Prism 9.0.0 (GraphPad Software Inc, San Diego, CA, USA). Data were expressed as mean ± standard error of the mean. Significance was accepted at $p<0.05$.

7.4.3 Results and Discussion

This trial was designed to investigate trends between plasma exposures and hormone treatments to see if ethylene application could counteract the negative effects of prolonged plasma exposure on wheat and maize grains. From the onset, it was understood that this experiment would not answer questions regarding the nature of hormone signalling within plasma-treated germinating seedlings. It was conducted to gain insights into whether ethylene could improve germination and seedling development. In both grain types, Untreated seeds displayed developmental delays with ET and AVG exposure when compared to water-treated controls (see Figures 7-13, 7-14 and 7-15). This suggests that the 10 µM concentration of ethylene was too high, despite the findings of Sun et al., 2020. In fact, the strong effects of ethylene overshadowed the effects of the plasma treatment which makes it difficult to draw meaningful conclusions from this dataset. Nevertheless, trends could be observed from the experiment and are discussed here.

7.4.3.1 Wheat

7.4.3.1.1 Water treatment

Untreated wheat grains exposed to water followed typical growth and development, reaching BBCH stage 09 by 4 DAS (Figure 7-13). Following similar trends previously seen in sections 7.2 and 7.3, roughly 40% of the plasma-treated grains failed to develop beyond stage 05 (Figure 7-14). The cell elongation processes of embryo swelling, and radicle protrusion occurred, but no further development was visible. It is clear that plasma treatment had a negative impact on germination for many of the wheat grains.

7.4.3.1.2 Ethephon treatment

As mentioned above in 7.4.3, the 10 µm dose of ethephon applied in this pilot trial was too high and had an inhibitory effect on early seedling growth, as opposed to the

proposal by Wang et al., 2020, that low doses may recover seedlings from stress (Figure 7-14). Germination was unaffected but radicle and coleoptile elongation were severely stunted. However, an interesting trend appeared in the P45 grain where ethephon treatment exhibited a 10% increase in germination over P45 water-treated grain. Additionally, P45 ethephon-treated grain had markedly better seedling development than Untreated ET and P90 ET grain. All P45 ET grains had radicle and coleoptile elongation. The 10 µm dose of ethylene had less of an inhibitory effect on mid-term plasma treated grains. It is speculated that halving the concentration of ethylene, to 5 µM, may be beneficial for medium length plasma treatments. This hypothesis could not be tested due to time constraints but may be of interest for future research.

7.4.3.1.3 AVG treatment

As expected, the inhibition of ethylene synthesis by 1 mM AVG did not impact germination in plasma Untreated grains however, growth and development were stunted. Complementary to the P45 ethephon treatment results, P45 with AVG had the lowest percent germination and BBCH scores. This indicated that ethylene likely plays a role in the recovery of seed germination following mid-term plasma exposure. However, the effects of P90 exposure cannot be overcome by hormone treatment.

7.4.3.2 Maize

7.4.3.2.1 Water treatment

The response of all maize grain treatments germinated in water was different to section 7.2.3.1.1, in that fungal infection did not inhibit percent germination (Figure 7-15). Instead, Untreated grains followed the predictable pattern of high percent germination which gradually decreased with plasma exposure. It appears that fungal contamination of the previous lot of grain may have played a heavy role in reduced germination described in section 7.2.3. Overall, maize grown in water followed the expected trends.

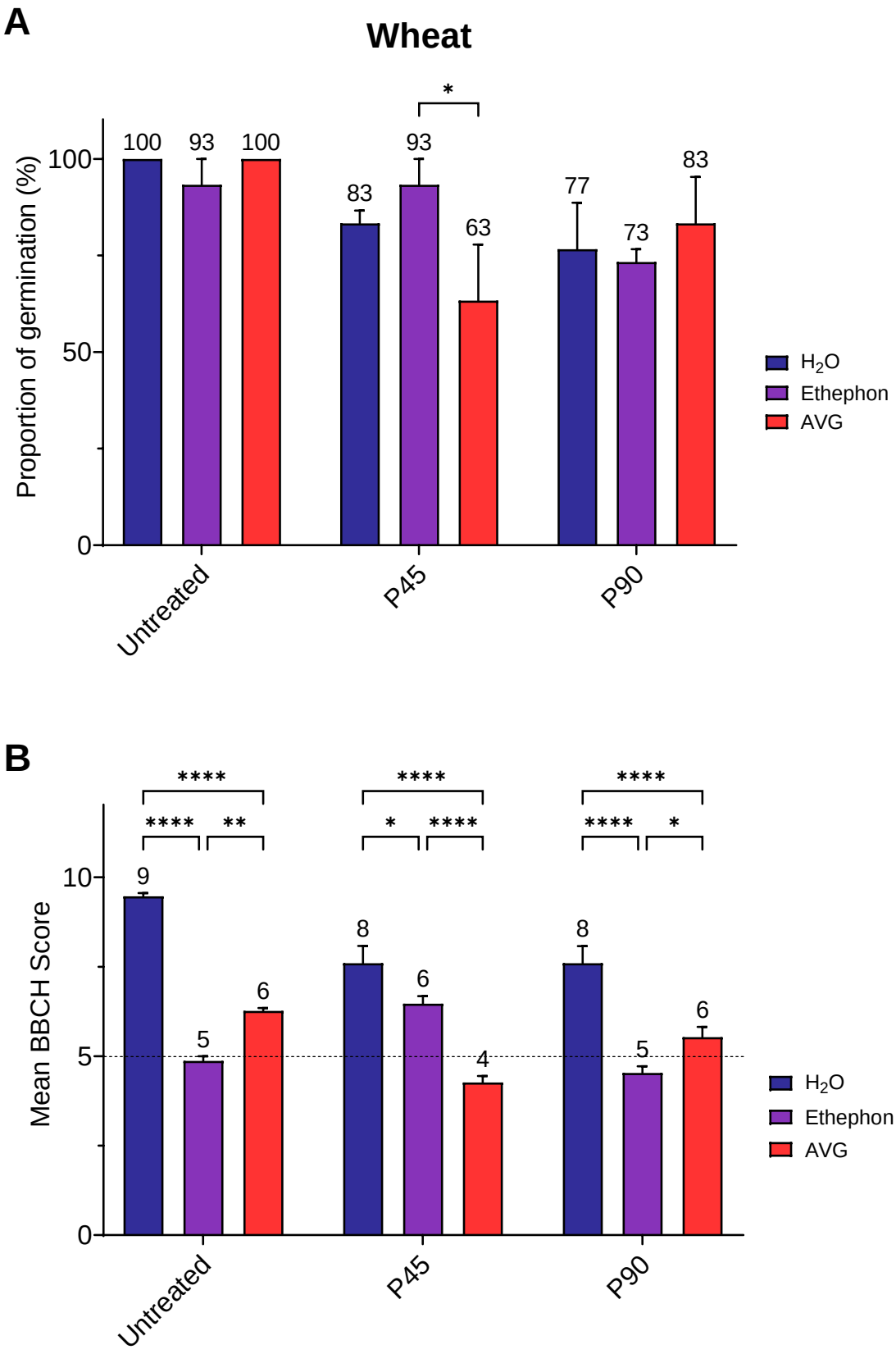


Figure 7-13. Ethylene trial results for wheat, *Triticum aestivum* 'Scepter' [sic]. (A) Comparisons of percent germination. (B) Comparisons of the mean BBCH score for each treatment at 4 DAS. The dotted line represents radicle protrusion/germination at stage 05. Data is presented as mean ± SEM. Abbreviations: AVG (2-aminoethoxyvinyl glycine treatment); P45 (45-minute plasma); P90 (90-minute plasma); ns (non-significant); *p<0.05; **p<0.01; ****p<0.0001. All pairwise comparisons were calculated based on two-way ANOVA with Tukey's multiple comparison tests.



Figure 7-14. Images of wheat grains from one plate of each treatment at 4 DAS. This visualisation highlights the influence of prolonged plasma exposure on seedling development as seen in the H_2O treatments (left). It also displays the impact of unintentionally high concentrations of ethylene (centre). It is of note that ethylene treatment improved development of P45 grains when compared to the Untreated ethylene grains.

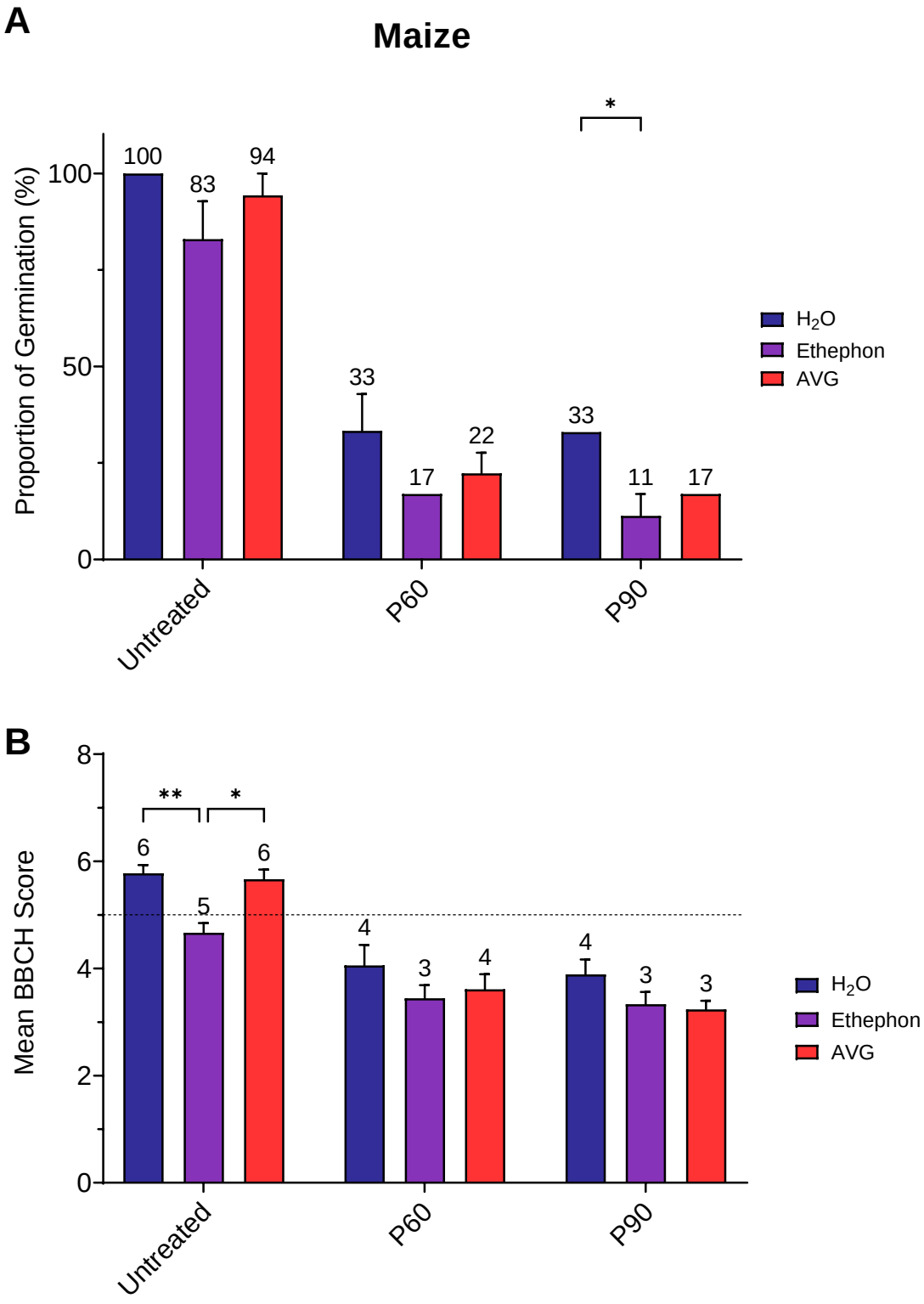


Figure 7-15. Percent germination and mean BBCH scores at 6 DAS in maize grains, *Zea mays* 'B73.' (A) Comparisons of percent germination. (B) Comparisons of the mean BBCH score for each treatment at 6 DAS. The dotted line represents radicle protrusion/germination at stage 05. Data is presented as mean ± SEM. Abbreviations: AVG (2-aminoethoxyvinyl glycine treatment); (P60 (60-minute plasma); P90 (90-minute plasma); ns (non-significant); *p<0.05; **p<0.01. All pairwise comparisons were calculated based on two-way ANOVA with Tukey's multiple comparison tests.

7.4.3.2.1 Ethephon treatment

The 10 µM concentration of ethephon had a significant impact on Untreated grains, reducing the BBCH scores (Figure 7-15). This effect was not as apparent in plasma-treated grains which had relatively similar BBCH scores between H_2O, ET and AVG treatments. There was a significant reduction in percent germination between Untreated ET and P90 ET grains. While ethylene production is linked to germination rate in maize (Kong et al., 2020), these results simply emphasize the powerful nature of ethylene and the delicate balance of goldilocks conditions that are required to ensure healthy growth and development.

7.4.3.2.2 AVG treatment

The presence of 1 mM AVG did not impact maize percent germination or growth and development across all plasma exposures. When taken into context with the ethephon results, this suggests that maize seedlings are likely very sensitive to ethylene in the early stages of development.

7.4.4 Summary

Due to the complexities of air plasma reactions with both seed surface chemistry and the underlying living embryo, it is difficult to isolate and identify the multitude of plasma-induced factors impacting germination and growth. Changes to seed water uptake likely play a role in this process. However, it is possible that the stresses created during plasma exposure, including oxidation, may alter the downstream hormone signalling of germinating seeds. Wang et al., 2020 noticed an improvement in the growth and development of alfalfa seedlings under oxidative stress conditions with the application of exogenous ethylene, a volatile hormone involved in germination. While wheat is physiologically different to alfalfa, it is known to be ethylene sensitive, especially in regard to transcriptional control of endosperm degradation (Sun et al., 2020). It was hypothesized that ethylene application might counteract the negative effects of plasma

treatment, including oxidative stress. Unfortunately, the ethephon concentration utilised in this study was too high and confounded the results by inhibiting root and coleoptile elongation. Yet, there does appear to be a relationship in wheat between ethylene signalling at the 45-minute plasma exposure. Here, the addition of exogenous ethylene improved BBCH scores when compared to Untreated ET and P90 ET treated wheat. There was also a decrease in BBCH scores in P45 grains with the inhibition of ethylene synthesis. While no conclusions can be drawn from these observations, they highlight the need for future research into changes in hormone signalling following plasma exposure. It should also be noted that across all hormone treatments and grain types, there was a significant decrease in seedling health with 90-minutes of plasma exposure. This resulted in developmental delays and the reduction of overall percent germination. It seems that prolonged plasma exposure alters seed germination, growth, and development beyond the point of rescue with exogenous ethylene. This led to speculation that chemical species created within the field of plasma may penetrate further into the grain, especially in areas where the mechanical tumbling has damaged the outer surface. If this occurs, the possibility of DNA oxidation through the chemical etching processes is increased and may lead to alterations in seed viability and seedling development. A final study was conducted to investigate the impact of long plasma treatment on seed embryo DNA oxidation.

7.5 DNA oxidation

7.5.1 Introduction

The environment created within the air plasma tumbler is dynamic and the effects of plasma will variably impact the surface chemistry of different grain samples. It is often assumed that a radiofrequency air plasma will contain both reactive oxygen and nitrogen species. Recently, both Dufour et al., 2021 and Holubová et al., 2020,

suggested that active species within the plasma may diffuse into the seed and form secondary reactive species which act upon the inner seed tissues. If this is occurring, the thickness and chemical makeup of seed surface and subsurface structures may determine the impact of plasma treatment on seed viability, growth, and development. Furthermore, Dobrynin et al., 2009 and Šerá et al., 2010 discussed the potential for plasma to oxidise seed DNA. Oxidative damage to nucleic acids has been reported during treatment with ozone, especially in grains with damage to the outer layers of pericarp and testa (Pandiselvam et al., 2020). As ozone is likely a chemical species produced within the plasma tumbler, it is reasonable to speculate that oxidative damage to grain tissues may occur. This could explain why some seeds of the same grain type are able to germinate and grow while others struggle to develop following germination. Grains that have mechanical damage may be more susceptible to plasma oxidation and active species penetration into exposed tissues.

Tomeková et al., 2020 investigated the effects of air plasma, pure O_2, pure N_2 and various mixed ratio plasmas on the DNA of pea seedling roots and found that air plasma did induce DNA damage. However, the amount of damaged DNA was not quantifiable by their comet assay, as only the percent of DNA fragments streaked across a gel versus in a band were compared. Other research has investigated secondary plasma products, such as malondialdehyde (MDA) formed from the oxidation of lipids, which can have mutagenic effects. Los et al., 2019 showed that MDA within wheat seedling roots increased following plasma exposure, leading to speculation that this could cause DNA damage. Instead of using MDA as a proxy for measuring DNA damage, a quantifiable DNA damage assay analysing seed embryos, rather than roots, is necessary to understand the effects of plasma on a living grain.

8-Hydroxy-2'-deoxyguanosine (8-OHdG) is a commonly used biomarker of oxidative DNA damage. It is formed when hydroxyl radicals attack guanine residues (Shigenaga

and Ames, 1991) and is readily detectable through a number of assays, including commercially available enzyme-linked immunosorbent assays (ELISA). To test for the presence of 8-OHdG in plasma-treated embryos, seeds were germinated on sterile plates. Following radicle protrusion, embryos were dissected from the grains and DNA extracted. An 8-OHdG ELISA assay was conducted using DNA extracts from multiple grain types and plasma exposures. The resulting data was compared to look for trends between oxidised DNA and plasma exposures.

7.5.2 Materials and Methods

7.5.2.1 Grain preparation

Maize, wheat, and field pea grains were divided into three 10 g treatment aliquots. Psyllium was separated into three 2 g treatment aliquots due to the small size. Untreated grains were set aside until germination. The remaining aliquots were treated on the plasma tumbler for 30 and 90-minutes following protocols established in Chapter 3.1.2.1.

7.5.2.2 Grain growth

Sterile plates with autoclaved glass fibre filters were prepared following methods in section 7.2.2.2. For each grain type and treatment, roughly one gram of grain was added to a plate, replicated twice. Plates were sealed with Micropore™ tape (3M) to allow gas exchange and incubated in the dark at 25 °C.

7.5.2.3 Embryo extraction

Once grains reached BBCH stage 05 with radicle protrusion, embryos were dissected from the grains using a No. 11 scalpel blade and forceps. Roughly 100 mg of embryos were immediately placed in a 1.5 mL Eppendorf tube with 100 µL TES, 99% (Fisher Scientific) to prevent further oxidation and snap frozen in liquid nitrogen. This was repeated to produce four biological replicates. All embryos were stored at -80 °C until DNA extractions were performed.

7.5.2.4 DNA extraction

DNA extractions followed protocols modified from (Healey et al., 2014). The detailed Healey extraction buffer was made up as described. 3 µL β-mercaptoethanol was added to the buffer solution and preheated to 65 °C. Once heated, 150 µL of buffer solution was added to a 1.5 mL tube containing embryos. The solution and embryos were immediately ground in the tube with a micro-pestle. The pestle was then washed in 720 µL of buffer solution. Samples were incubated for 60 minutes in a water bath at 65 °C, inverted every 15 minutes, twice. Following incubation, samples were centrifuged at 16,100 xg for 10 minutes and the supernatant was transferred to a new 2 mL Eppendorf tube. 125 µL of neat R40 buffer R40 buffer (40 ug/ml RNAse A in Tris-EDTA buffer) was added to each tube and incubated in a 37°C water bath for 15 minutes, with gentle mixing every 5 minutes.

A chloroform wash step was performed twice by adding 1x the volume of chloroform: isoamyl alcohol (ratio of 24:1). The tubes were placed on a rotor for five minutes then centrifuged at 10,000 xg for 10 minutes. The upper aqueous phase was pipetted into a new 2 mL Eppendorf tube.

5 M sodium chloride was added at half the volume of the aqueous phase extract and mixed by inversion. Three times the volume of cold 95% ethanol was added and mixed via inversion. Tubes were incubated at -20 °C for 60 minutes then centrifuged at 15,000 xg for 10 minutes. The supernatant was removed, and the remaining pellet was washed in 70% ethanol followed by centrifugation at 15,000 xg for 10 minutes. Again, the supernatant was decanted, and the pellet was suspended in 100 µL 0.01 M Tris-EDTA (TE) Buffer.

7.5.2.5 Quantification of DNA concentration

Immediately following extraction, the DNA concentration of samples was determined with the (Qubit™ dsDNA BR Assay Kit; Q32851) using a Qubit 4 Fluorometer. Samples were then frozen at -80 °C until the ELISA assay could be performed.

7.5.2.6 ELISA assay for 8-Hydroxy-2'-deoxyguanosine

This section was completed using a DNA Damage Competitive ELISA Kit (Invitrogen; EIADNAD).

7.5.2.6.1.1 Pilot trial to establish dilutions

A pilot trial was conducted using a P90 wheat sample to determine the appropriate dilution needed for DNA extractions to fall within the standard curve of the ELISA kit. In one well-strip, standards of 8000, 1000 and 62.5 pg/mL were added to create a concentration reference. A P90 wheat sample was added to three wells as neat, 1:10, and 1:100 dilutions. The assay was performed following the kit manual and the absorbance at 450 nm was measured. It was determined empirically that a 1:2 dilution would be sufficient for all experimental samples

7.5.2.6.1.2 Experimental trial

Three biological replicates were selected for each treatment. Samples were thawed and vortexed for 10 seconds to resuspend the DNA pellets. 25 µL of sample was added per well, followed by 100 µL Assay Buffer for a 1:2 sample in-well dilution. All other protocols were followed as directed in the kit. Two technical replicates of each biological replicate were measured. Plates were read at 450 nm on a SpectraMax 250 (Molecular Devices) with SOFTMax Pro software.

7.5.2.7 Statistical analysis

A standard curve was generated in GraphPad Prism 9.0.0. The read values were fit to the curve to determine concentration of deoxyguanosine per well. The means of technical replicates were divided by the initial Qubit concentration to determine amount

of oxidised DNA per ng of DNA. Two-way ANOVA were performed with Tukey's multiple comparison analysis to determine the significance between plasma exposure and grain type. ANOVA values were calculated using GraphPad Prism 9.0.0. Data were expressed as mean ± standard error of the mean. Significance was accepted at $p<0.05$.

7.5.3 Results and Discussion

In previous sections, it was observed that some germinating seeds, markedly plasma-treated wheat, were capable of radicle protrusion but did not progress through any subsequent developmental stages. It was speculated that the stunted growth and development in plasma-treated seedlings may be due to oxidative damage to embryo DNA. To test this hypothesis, DNA was extracted from the embryos of plasma-treated germinating seeds at BBCH stage 05. This was the stage at which development appeared to lag and coincided with the completion of DNA and mitochondrial DNA repair following imbibition. The concentration of oxidised DNA in the embryos of treated seeds was measured by proxy using 8-OHdG (Figure 7-16).

The resulting data proved the null hypothesis – there was no relationship between plasma-treatment and 8-OHdG concentration in extracted embryo DNA. No significant trends were detected between plasma treatments for all grain types. While P30 wheat had one biological replicate with a high reading of 341 pg 8-OHdG /ng DNA, it was not statistically significant. As the readings of both technical replicates were nearly identical, it is possible that at least one embryo within this somewhat anomalous biological replicate had been mechanically damaged prior to germination. Furthermore, this data suggests that plasma primary active species and secondary active species were not capable of penetrating into the embryo of healthy, intact food quality grains. The observed differences in growth and development were more likely attributed to

changes in water uptake (as seen in Chapter 6) which have downstream effects on metabolism, enzymatic processes, and hormone signalling.

It is interesting to note the highest concentration of 8-OHdG, a mean of 301 pg/ng of DNA, was found in Untreated psyllium embryos. As these grains are coated in a dehydrated layer of mucilage, it is possible that the complex processes of seed and mucilage desiccation, which are often associated with the accumulation of free radicals and lipid peroxidation, may be causing oxidative damage to the embryo DNA (Bailly et al., 2008). If so, psyllium is well-equipped to handle and repair DNA damage as it is observed to have consistent germination with radicle protrusion occurring at roughly 18 hours after sowing.

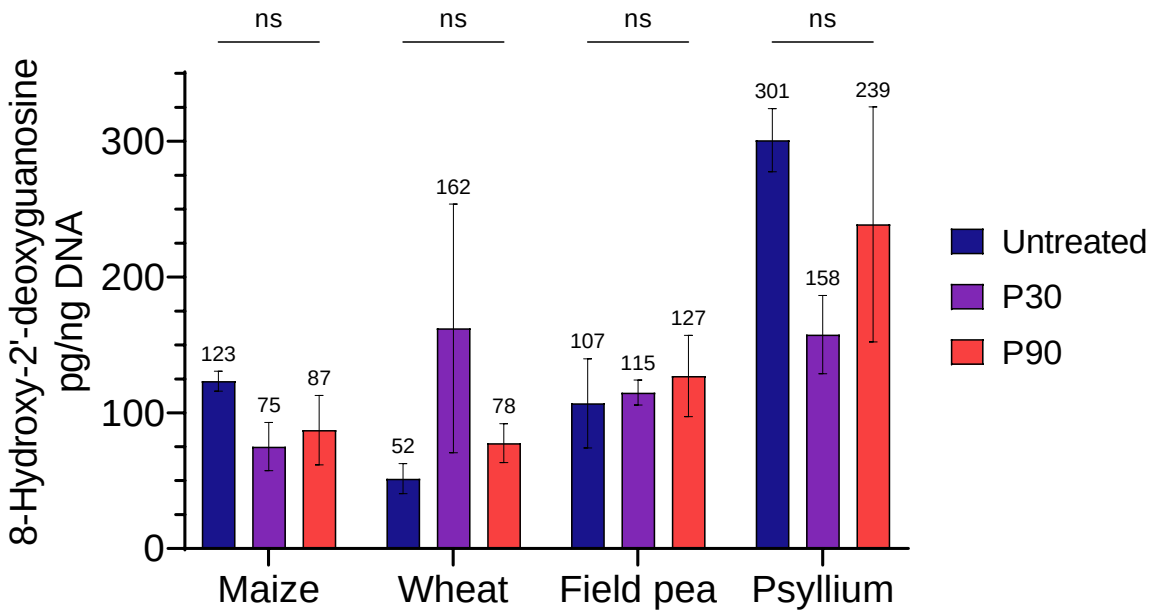


Figure 7-16. Concentrations of 8-OHdG per ng of DNA for each grain type and plasma treatment compared to the Untreated control. There were no significant differences between treatments within each grain type. Data is presented as mean ± SEM with significance accepted at $p<0.05$. Abbreviations: P30 (30-minute plasma); P90 (90-minute plasma); ns (non-significant).

7.5.4 Summary

The DNA damage assay conducted in this trial showed that plasma treatment did not oxidise seed embryo DNA in the four grain types analysed. This finding suggests that

active primary and secondary species generated in the PT system were unable to pass through the multiple protective structures and tissues covering the embryo to a significant degree. The lack of mutagenic effects is an encouraging indicator that plasma may be a beneficial technology for deactivating microbes on grain prior to food production. However, 8-OHdG is only one of about 20 oxidative adducts formed during radical attack on DNA. To truly understand the processes involved in plasma-induced stress, future studies should be undertaken to investigate different oxidative adducts, including MDA, and transcriptional changes within the hydrating embryo.

7.6 Conclusions

This chapter has explored the effects of plasma exposure on the biological processes involved in seed germination and early seedling development. Plasma exposure times of 90-minutes were considered optimal for the deactivation of fungal pathogens on the seeds surface (see Chapter 5). In addition to damaging fungal pathogens, it was speculated that prolonged plasma treatment may also impact seed health and viability. In general, cereal grains displayed inhibited germination and delayed growth and development stages with increasing plasma exposure times. On the other hand, psyllium seemed to be impervious to the effects of up to 90-minutes of plasma treatment. Investigations into the effects of ethylene, a volatile hormone intrinsically involved in germination of cereal grains, were inconclusive. While it is possible that plasma treatment impacts seed hormone signalling, within the context of this research, ethylene could not be identified as a factor for inhibiting seedling development in wheat and maize. Additionally, there was no difference in the amount of oxidative damage to DNA between treatments and grain types, suggesting that active primary and secondary plasma species are not penetrating the layers of tissue protecting the

embryo. Instead, it seems likely that changes to grain hydration properties (see Chapter 6) are the major biological consequence of lengthy plasma treatments.

While these experiments provide more insight into the way plasma interacts with grains as living organisms, it is important to highlight that the overarching aim of this research was to inactivate grain fungal pathogens. Depending upon the destined food and feed processing pathways of the grain, the inhibition of plant growth and development from extended plasma treatment may not be relevant. Rather, the results of this chapter can be used to better understand the mechanism of action behind plasma treatment for fungal deactivation. If the viability of quiescent seeds with complex morphologies and tissues can be influenced by plasma exposure, so too can the viability of fungal pathogens. This newly found knowledge brings us to the final experimental chapter of this thesis project – challenging the plasma tumbler system with naturally contaminated grains.

8 Challenging the plasma tumbler system with contaminated industry grain samples

8.1 Introduction

Harvested grains contain widely diverse populations of filamentous fungi, yeasts, and bacteria; the composition of which is dependent upon site location, weather patterns and harvesting processes. Throughout the supply chain, from field to storage, there are numerous opportunities for microbes to thrive given adequate temperature and humidity. This can lead to quality loss, product spoilage and the production of harmful fungal secondary metabolites, called mycotoxins (Magan et al., 2003). Each year, millions of tonnes of grain are destroyed due to microbial contamination and mycotoxin production, with implications toward economic losses and food security, as well as human and animal health (Sharma and Bhandari, 2014). International organisations, including the Food and Agriculture Organization (FAO) of the United Nations and the World Health Organization (WHO) have made calls for the development of new and scalable technologies to reduce microbial and mycotoxin contamination of grains prior to storage. The drive to reduce post-harvest pathogens is incorporated into steps toward achieving goals 2, 3 and 12 of the UN 17 Sustainable Development Goals for 2030 (Pitt et al., 2012; UN, 2015).

Postharvest fungal grain pathogens of significance are found within three genera: *Aspergillus*, *Fusarium* and *Penicillium* (Thompson and Raizada, 2018). While countless other microbes are present, these fungi are capable of antagonistic and

mycotoxigenic behaviours which allow them to outcompete other species in grain storage (Magan et al., 2003). In high-income countries, such as Australia, post-harvest fungal pathogens are generally managed through hygiene practices and strict climate control of storage facilities (Nopsa et al., 2015). Even so, fungal infections may have been established prior to storage, and the mixing of grain can distribute pathogens throughout the grain lot. Deactivating the grain microbiome within the early stages of the supply chain is necessary to reduce the risk of grain contamination. In Chapter 5, it was demonstrated that the straightforward and easily scalable plasma tumbler (PT) apparatus was capable of log 7 reductions of synthetically inoculated postharvest pathogens. Chapter 6 looked at changes to the physico-chemical properties of the seed surface following plasma treatment. This data may be used as a proxy for the potential impact of plasma on microorganisms residing on the seed surface. Finally, Chapter 7 demonstrated that plasma treatment can influence the viability of seeds which are exponentially larger than fungal spores. If prolonged plasma exposure influences the viability of a comparatively larger organism, it was speculated that the plasma tumbler technology may be able to inactivate the complex grain microbiome of real-world contaminated grain samples.

A final study was designed to challenge the PT apparatus against a wide range of naturally occurring exogenous microbes on contaminated wheat grain. Wheat has been a slightly difficult model system to interpret, without consistent trends in results across multiple experiments in Chapter 5 (5.2.3.2 and 5.3.3.2). These data sets were less convincing of the ability of the PT to reduce extant pathogens below log 3 colony-forming units on the seed surface of wheat. On the other hand, maize, field pea and psyllium have all displayed characteristic patterns of microbial reduction across the project. It is speculated that lengthy plasma durations may be required to compensate for both the wheat grain morphological features and the complexities of the mixed

microbiome on highly contaminated grain. To investigate this hypothesis, a request was made with a local agricultural network, Viterra, for a sample of grain which had tested positive for mycotoxins. It was assumed that the existence of mycotoxins would correlate with a relatively high microbial load. A sample of composite feed grain was reported to be positive for the mycotoxin deoxynivalenol (DON) which indicated the presence of *Fusarium* species. A 20 kg subsample of this grain was kindly donated by Viterra for research purposes and used throughout the final trials. As spore inactivation on wheat was rather convoluted under previous experimental conditions, a modified plasma time trial was performed with 30, 60 90 and 120-minute treatments. Subsamples were taken of cultured colonies for identification via both the traditional visual method and internal transcribed spacer (ITS) sequencing. When combined, the resulting data described the culturable microbiota of the sample, and the relative persistence of each species with respect to plasma time points. Scanning electron micrographs of grain samples from each treatment were compared to visually assess the locations of microbes and the morphological variations after plasma treatment. Finally, the microbial diversity of the grain sample led to speculation that further mycotoxin analysis would reveal the presence of multiple toxins produced by a range of pathogens.

This final research chapter describes a large and multi-faceted experiment. As such, a more conventional layout is appropriate. The following sections are arranged in a similar manner to Chapter 4.

8.2 Materials and Methods

8.2.1 Grain preparation

A one-kilogram aliquot of the composite feed sample (containing wheat, barley, canola, and field pea) was hand sorted to isolate the wheat grain. The roughly 200 grams of

material other than wheat was discarded. The remaining wheat grain was divided into 120 mL sterile specimen jars (Technoplas) until further use.

8.2.2 Plate preparation

Half-strength potato dextrose agar (PDA) plates were poured following protocols in Chapter 3.3.1.1.

8.2.3 Grain plating pilot trial

8.2.3.1 Grain treatment

A 120 mL specimen jar of sorted wheat grain was divided into six equal portions for treatment. One aliquot was exposed to 90 minutes of T+V treatment (see Chapter 3.1.2.3). Four aliquots were treated with plasma via protocols established in Chapter 3.1.2.2 for 15, 30, 60 and 90-minutes, respectively. The remaining portion of grain was left as the Untreated control.

8.2.3.2 Grain plating and visualisation

Roughly one gram of grain from each plasma treatment was scattered across a 90 mm half-strength PDA plate. Plates were sealed with cling film (Glad) and incubated at 25 °C with 12hr/12hr light dark cycles for seven days. Following incubation, plates were inspected under a stereoscope (Olympus SZX10) and with the naked eye. Tentative pathogen identification to the genus level was made. Based on observations of rough numbers and diversity of microbial species present, it was determined that future experimental plasma treatments from this grain allotment should be performed at 30, 60, 90 and 120 minutes of exposure.

8.2.4 Experimental treatment

Untreated, T+V, P30, P60, P90 and P120-minute plasma treatments were prepared following protocols established in section 8.2.4.1. The pilot experiment suggested that

plasma exposure longer than 90 minutes may be necessary to accommodate for a diverse microbial load.

8.2.5 Microbe extractions and plating

8.2.5.1 Extractions

As described in Chapter 3.3.3, five aliquots of 1 g of grain from each treatment were placed in individual sterile 10 mL tubes with 2 mL of extraction buffer (Chapter 3.3.2). Each tube was rolled back and forth against the lab bench prior to orbital shaking (Ratek) for 20 minutes to suspend conidia and hyphal fragments present on the grain surface. Additionally, five replicates of Untreated food-quality wheat grain, as described in Chapter 3.2.2 and Chapter 5.2.2.2, were extracted, in the manner listed above, to compare the fungal load of the Untreated contaminated sample with an Untreated food quality sample.

8.2.5.2 Dilutions

10 µL aliquots of extraction solutions were removed for haemocytometer counts to establish serial dilutions for each treatment. See Table 8-1 for a list of all dilutions prepared for this experiment. Notes were made of visually distinct spore types present on the haemocytometer.

Table 8-1. List of dilutions prepared for each plasma treatment.

Treatment	**Dilutions**
Untreated	1:100; 1:1000
T+V	1:100; 1:1000
30 min plasma	1:10; 1:100
60 min plasma	neat; 1:10
90 min plasma	neat; 1:10
120 min plasma	neat

8.2.6 Plating

Microbial extract solutions were plated as described in Chapter 3.3.6.

8.2.7 Colony-forming unit quantification

As established in Chapter 3.3.7, colonies with visible hyphae were counted at days 3, 4 and 5 after plating to ensure a representative quantification of all culturable fungi. Bacterial and yeast cultures were not included in counts. One dilution was selected to represent each treatment based on the general rule of 30 to 300 colonies per plate. As most long plasma exposure plates contained less than 30 colonies, the dilution with the highest number of colonies per plate was utilised in CFU/mL calculations.

8.2.8 Pathogen descriptions and isolation

During CFU counts, a separate data set was created with visual descriptions of each fungal colony. Representative subcultures were taken from plates with less interactions between species. These were isolated following a series of subcultures on half-strength PDA plates. The isolates were then prepared for visual and genomic identification (see below).

8.2.9 Pathogen identification

8.2.9.1 Visual identification

Plates were inspected on an Olympus SZX10 stereoscope to confirm the presence of fungal conidia. Cello tape flag preparations of conidia were created following steps outlined by Kidd et al., 2016, and visualised under a phase contrast compound microscope (Nikon, Eclipse Ci-L). Visual identification to genus level was attempted using Watanabe, 2010 as a reference.

Yeast and bacterial colonies were subsampled with a wire loop and placed on glass slides for visualisation on a phase contrast microscope. Cultures were marked as yeast

or bacteria based on cell size and morphology. Bacterial colony categorisation was attempted by Gram-staining, as detailed by (Froböse et al., 2020).

8.2.9.2 DNA extraction, sequencing, and analysis

ITS sequencing of pure cultures including DNA extraction, amplification and sequencing analysis was conducted through the Molecular Diagnostics Centre at the South Australia Research and Development Institute (SARDI). DNA was extracted from pure cultures; a small amount of mycelium from single conidium-derived cultures or single bacterial colonies were transferred to individual microtubes containing glass beads. Bacterial and fungal cells were disrupted using a Precellys cell disrupter (Bertin Technologies) and DNA was extracted using the commercial in confidence SARDI protocol.

Universal primers were used to sequence fungal DNA in the Internal Transcribed Spacer (Curran et al., 1994) and bacterial DNA in the 16s rDNA (Schabereiter-Gurtner et al., 2003; Weisburg et al., 1991). PCR amplicons were sent to the Australian Genome Research Facility (AGRF) for sequencing. Sequences were identified using the Basic Local Alignment Search Tool (BLAST) in Genbank (https://www.ncbi.nlm.nih.gov/genbank). A list of sequences is available in Appendix S8.

8.2.9.3 qPCR

Two 100g grain samples were sent to the Molecular Diagnostics Centre at SARDI for qPCR analysis through their Routine DNA-based Testing Service (RDTS) (Ophel-Keller et al., 2008). Established qPCR tests (Evans et al., 2010) were conducted on *Fusarium* spp. See Appendix S9 for details.

8.2.9.4 Data interpretation

ITS sequences were interpreted by Dr Sarah Kidd, Head of the National Mycology Reference Laboratory, South Australia Health, Adelaide, Australia.

8.2.10 Scanning electron microscopy

8.2.10.1 Sample preparation

Two grains of each treatment were adhered to 12.6 mm pin stubs (ProSciTech) with carbon tabs. Edges of the grain were painted with graphite conductive adhesive (ProSciTech) to ensure a flush connection between the rounded grain surface and the stub. Samples were sputter-coated with 5 µm of platinum by Adelaide Microscopy, Frome Road, prior to imaging.

8.2.10.2 Scanning

All stubs were analysed at Adelaide Microscopy, Frome Road with a FEI Quanta 450 FEG Environmental SEM at acceleration voltages of 2.0 kV.

8.2.11 Mycotoxin analysis

8.2.11.1 Sample preparation

300 g of sorted wheat grain was divided into 50 g aliquots for Untreated, T+V, P30, P90 and P120 treatments. T+V treatment followed protocols described in Chapter 3.1.2.3. All plasma exposures were run individually for the required timeframe using the standard techniques developed in Chapter 3.1.2.1. Post treatment, grain was split into three 10 g aliquots to serve as biological replicates of each treatment. The remaining grain was set aside. Each 10 g aliquot was ground to flour in a ball mill (Retsch, MM 400, 30 Hz). Jars and balls were washed with hot soapy water followed by a 100% EtOH soak between aliquots and treatments to prevent cross contamination between samples.

8.2.11.2 Sample analysis

Three 10 g flour replicates of Untreated, T+V, P30, P90 and P120 treatments were sent to a commercial laboratory (Intertek, Adelaide, Australia) for a full suite mycotoxin analysis via HPLC. See Appendix S10 for a list of all mycotoxins tested.

8.2.12 Statistical analysis

All data were sorted in Microsoft Excel 365 (Microsoft Corporation, Seattle, WA, USA) before analysis. Cultured pathogen data sets were analysed in Microsoft Excel. 365. The significance between treatments and grain types were determined via one-way ANOVA with Tukey's multiple comparison analysis and Welch's t test in GraphPad Prism 9.0.0 (GraphPad Software Inc, San Diego, CA, USA). All colony counts of zero were transformed to one for ease of statistical analysis on a logarithmic scale. Data were expressed as mean ± standard error of the mean. Significance was accepted at $p<0.05$.

8.3 Results and Discussion

8.3.1 Pilot trial grain plates

This series of experiments sought to challenge the PT device against highly contaminated industry grain samples. The grain procured for treatment had tested positive for the mycotoxin, DON, which was used as a proxy measurement for grain contamination. It was necessary to conduct a pilot trial prior to experimentation to determine if the assumed levels of grain contamination were accurate and to gain a better sense of the microbes that may be cultured. Grain from each treatment was scattered over half-strength PDA on 90 mm plates to encourage the growth of fungal pathogens. Following a seven-day incubation, grain plates were inspected for microbial growth (Figure 8-1). The abundance and vigour of fungal growth across the plates revealed the level of contamination and gave an indicator of the fungal species present within the samples. Visually distinct *Rhizopus*, *Aspergillus* and *Penicillium* genera were tentatively identified. There also appeared to be multiple yeasts and bacteria present.

During observations of the pilot trial plates, it was noted that P90 treatments contained many fungal colonies (Figure 8-1). This led to speculation that much longer plasma exposure times may be necessary to reduce the diverse loads of microbes on the

contaminated grain. Thus, for all subsequent experiments, the 15-minute plasma exposure time point was replaced with a 120-minute plasma exposure. This pilot experiment also informed the design of culturing methods and appropriate dilution factors to accurately capture manageable colony counting on culture plates.

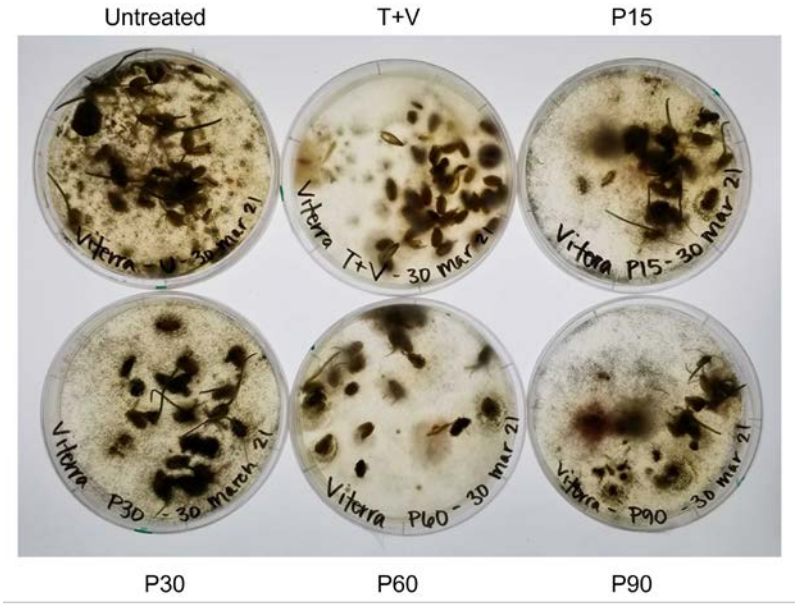


Figure 8-1. Pilot trial plates of wheat grain with four plasma treatments compared to the Untreated and T+V controls. Plates were incubated for seven days to determine the potential fungal pathogens and levels of contamination. Multiple species of fungi and bacteria are visible across all treatments. Abbreviations: T+V (tumbler + vacuum); P15 (15-minute plasma); P30 (30-minute plasma); P60 (60-minute plasma); P90 (90-minute plasma).

8.3.2 Colony-forming unit quantification

The calculation of colony-forming units is a traditional method for estimating the number of viable conidia and hyphal fragments and was used in this context to determine the filamentous fungal load on grains of each treatment. Only filamentous fungal colonies were counted in this experiment as they could be reliably distinguished on plates, whereas yeast and bacterial colonies were often mixed. This was not considered to be detrimental to understanding the efficacy of the PT as the most significant and mycotoxigenic postharvest fungi are filamentous members of the genera *Aspergillus*, *Fusarium* and *Penicillium* (Agriopoulou et al., 2020; Solanki et al., 2019).

It was originally assumed that the mycotoxin contaminated grains would have a higher microbial load than food production quality grain. The pilot trial used grain sprinkled on plates, which provided a qualitative visual reference yet, a quantitative measure was necessary to compare the differences between contaminated and food quality grain. Colony-forming units were calculated of the Untreated contaminated wheat samples and Untreated food production quality samples to characterise the fungal load. Next, the colony-forming units between all contaminated grain treatments were compared to understand how different time exposures in the PT alter the viability of conidia and hyphal fragments extracted from the grain. Together, these data sets provide insights into the efficacy of plasma treatment on real-world contaminated grain samples.

8.3.2.1 Filamentous fungal load on the contaminated grain

The mean fungal load on the contaminated grain contained 10^3 times more colony-forming units per millilitre than the food production-quality grain described in Chapter 3.2.2 and used throughout this thesis (Figure 8-2). This indicates a heavy filamentous fungal load and justifies their use within this set of experiments. The larger numbers present in a natural system, allow the PT system to be challenged in an applied manner on a problematic industry sample. Additionally, the heavy fungal load may allow for a better comparison between T+V treatments and plasma treatments which were slightly more difficult to interpret in the food quality samples in Chapter 5.2.3.2 and 5.3.3.2.

The data set in Figure 8-2 also suggests that a correlation exists between mycotoxin presence and filamentous fungal load on grain. The original mixed grain contaminated samples had tested positive for the mycotoxin DON, which is produced by *Fusarium graminearum, F. pseudograminearum and F. culmorum* (Ramirez et al., 2004; Sweeney and Dobson, 1998; Torres et al., 2019). The high concentrations of colony-forming units indeed confirmed the original presumptions that mycotoxin contaminated

grain would contain higher microbial loads than food quality grain. Further analysis of mycotoxins can be found in section 8.3.5.

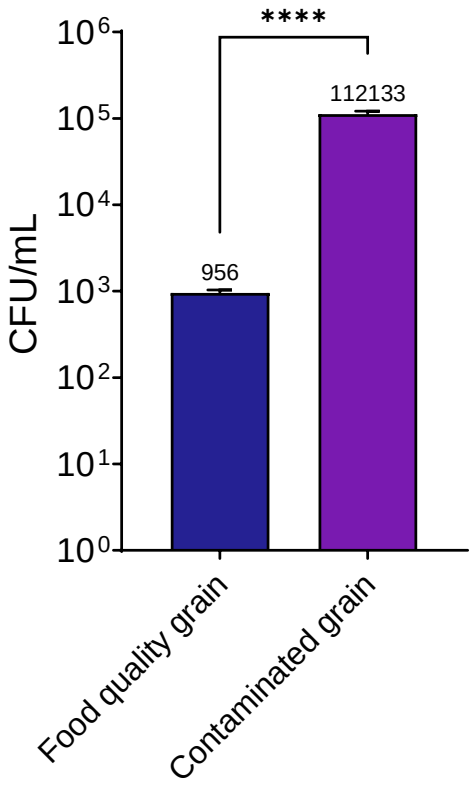


Figure 8-2. Comparison of the contaminated wheat with food quality wheat. There is a log 3 increase in colony-forming units in the contaminated grain, suggesting heavy levels of filamentous fungal pathogens across the contaminated samples. Data is presented as mean ± SEM; ****p<0.0001.

8.3.2.2 Comparisons of colony-forming units across treatments

Once the mean level of culturable fungi on Untreated samples was ascertained, the means of colony-forming units per treatment were compared to understand the relationship between plasma exposure and viable conidia and hyphal fragments. Following similar trends seen in plasma time exposure experiments in Chapter 5.4, the T+V treatment caused a slight but insignificant reduction of colony-forming units compared to Untreated samples (Figure 8-3, A). Plasma treatment was responsible for the log 5 decreases in CFU/mL, with negligible hyphal colonies by 120 minutes of treatment (Figure 8-4). This is rather exceptional considering the lack of clear inactivation results in previous experiments on wheat (see Chapters 5.2.3.2 and

5.3.3.2), the heterogeneous nature of the original samples and diverse range of pathogens present. The differences between means of plasma treatments are not statistically significant due to variations within the treatments and the low colony counts when compared to Untreated and T+V treatments (Figure 8-3, B). While the statistical significance is lacking, the data is meaningful from a biological perspective: it indicates near complete inactivation of all seed surface filamentous fungi by 120 minutes of plasma exposure. The inactivation levels of highly microbially diverse samples showcase the plasma tumbler's capacity and its potential future use as a simple and scalable technology for improving food safety.

It is interesting to note the non-linear trend seen within Figure 8-3, A. The graph is reminiscent to that of the visible hyphal colonies of extant fungi on food quality wheat in Figure 5-3, C in Chapter 5.3.3.1. Further analysis of these data sets was conducted to ensure the validity of the one-way ANOVA. A Welch's t test (p-value = 0.2860) revealed no significant difference between P60 and P90 treatments. Instead, the 9.49 CFU/mL mean of P60 treatments, and the 189 CFU/mL mean of P90 treatments indicates high variability within the samples. If the data is fitted into a graph displaying the values of each replicate plate (Figure 8-3, B), it illustrates the variations within a treatment on a logarithmic scale. It suggests that the extant microbial load across the grain samples is highly variable which may impact the efficacy of the plasma treatment at shorter plasma exposure times. Regardless of the variations within P30, P60, and P90 treatments, P120 is the most effective and consistent treatment with almost complete inactivation of filamentous fungi.

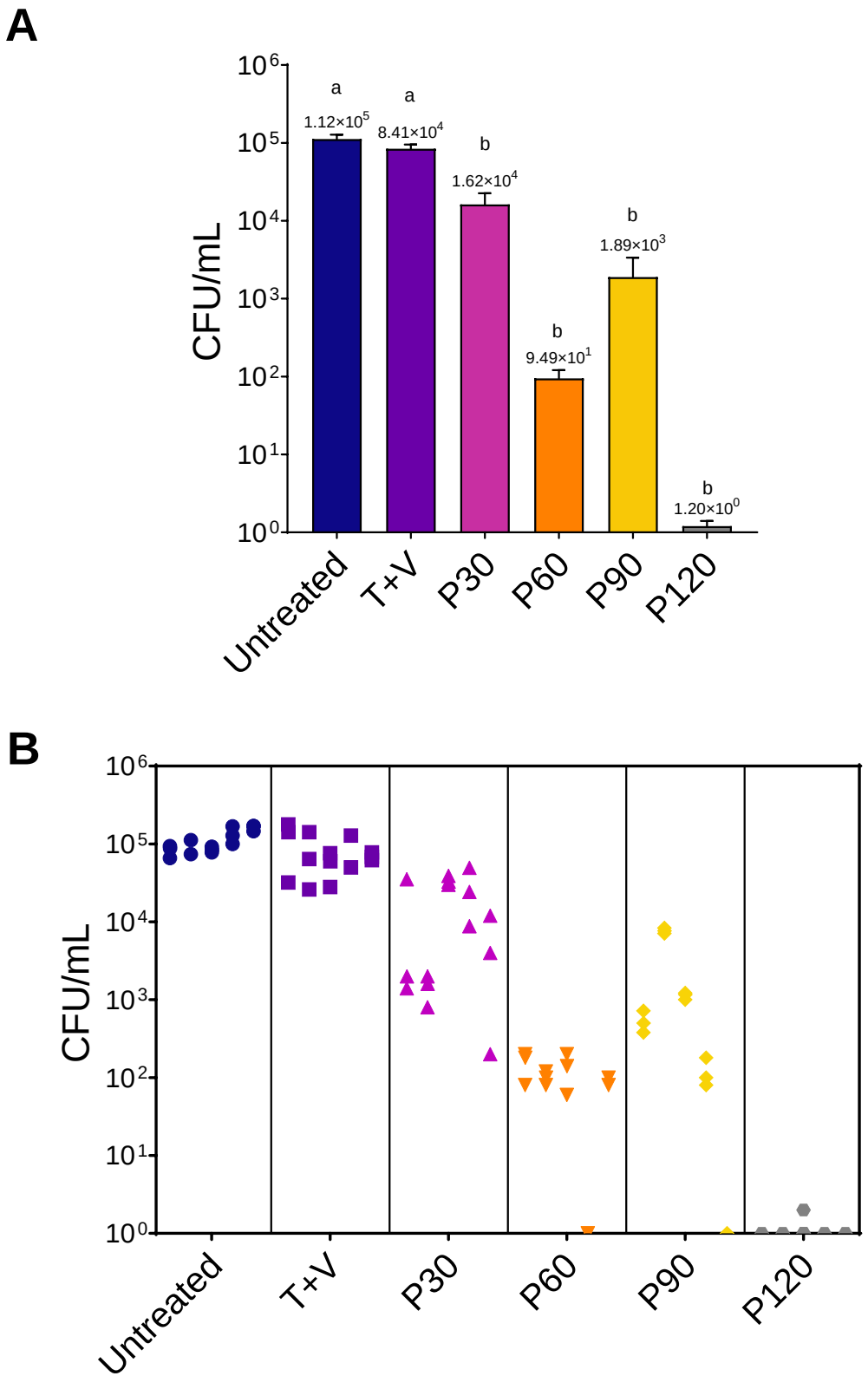


Figure 8-3. (A) Comparisons of colony-forming unit counts per grain type and treatment on a log scale. Data is presented as mean ± SEM with significance accepted at $p<0.05$; n = 15. Letters indicate differences between means Plasma treatment significantly reduces the number of culturable colony-forming units. (B) Individual CFU/mL values plotted for each replicate. This figure highlights the variability within treatments, which is likely due to the heterogeneity of the naturally occurring microbial load. Abbreviations: T+V (Tumbler + vacuum); P30 (30-minute plasma); P60 (60-minute plasma); P90 (90-minute plasma); P120 (120-minute plasma).

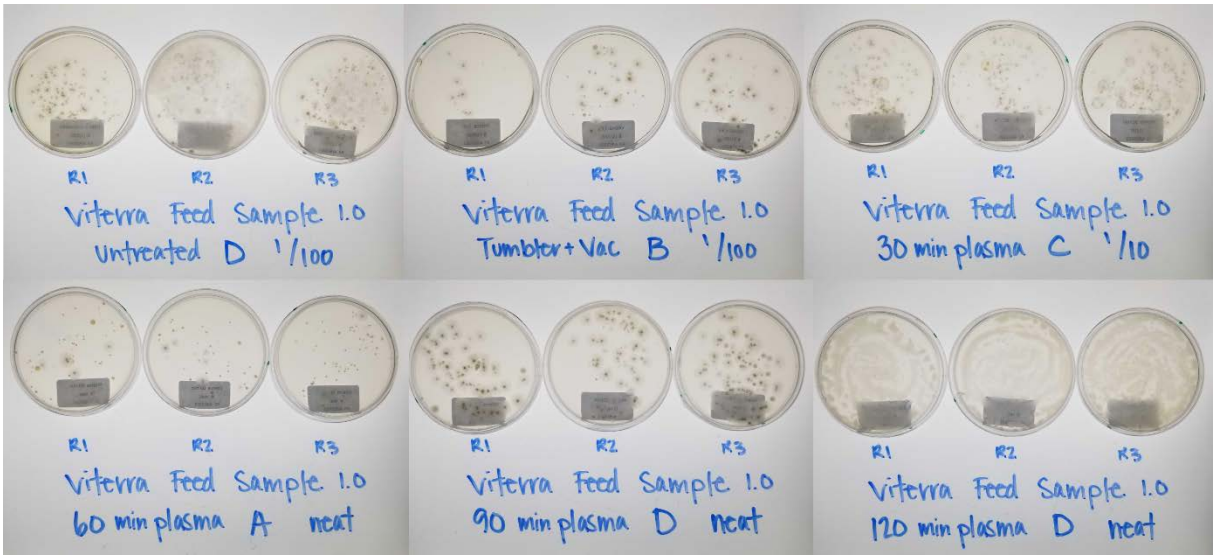


Figure 8-4. Images of one group of representative technical replicate plates from each treatment. Dilutions are indicated in the bottom right corner of each treatment. Filamentous fungi are notably absent on 120-minute plasma treatment plates. Colonies present on this treatment are composed of yeast and bacteria.

8.3.3 Identification of pathogens present on the grain

The plates from the colony-forming unit experiment (section 8.3.2) displayed a complex assortment of fungi which diminished with plasma exposure. Each of the 180 plates (of the two dilutions per treatment, only one was selected for CFU/mL calculations based on the general rule of 30-300 colonies per plate) was visually assessed and tentatively categorised by genus based on morphological features (Kidd et al., 2016). Traditional subculturing methods were used to isolate distinct microbes from plates of each treatment. Following incubation, cultures were visually assessed via microscopy (Figure 8-5) and were identified to species following ITS sequencing. Together, these data sets were collated to understand the most abundant fungal pathogens and how they were impacted by plasma treatment. It is recognised that NGS techniques are the preferred method for discovery surveys of grain samples. Given the difficulty of establishing an NGS pipeline for grain samples, qPCR analysis was instead used to identify *Fusarium* spp.

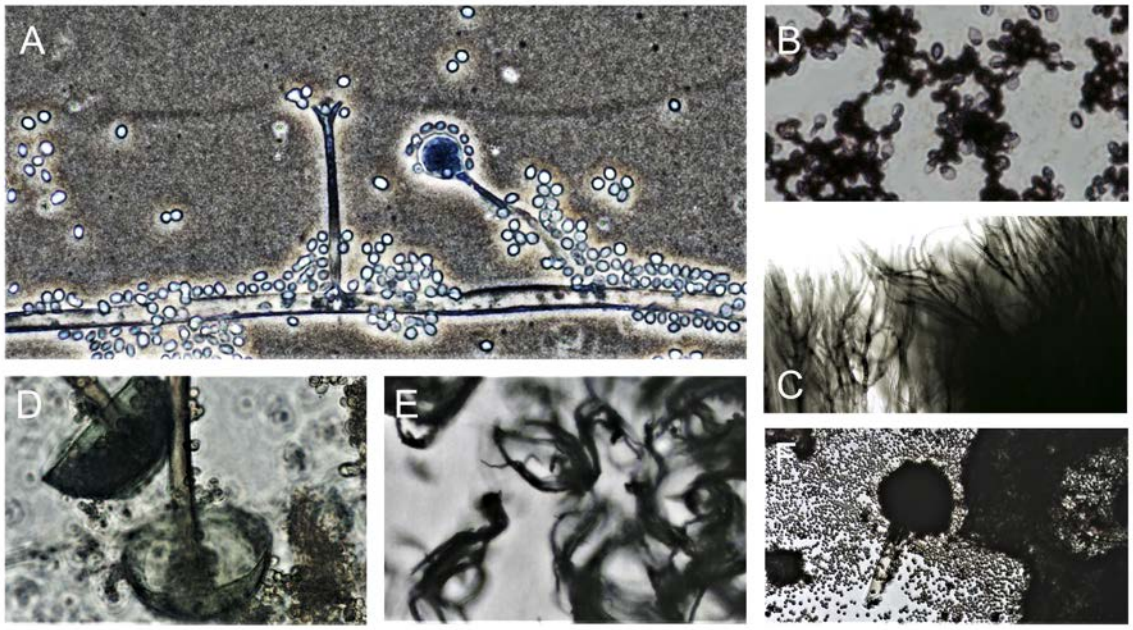


Figure 8-5. Flag preparations of isolated cultures. (A) *Lichtheimia corymbifera*; (B) mixed culture of yeast and bacteria; (C) *Aureobasidium pullulans*; (D) *Rhizopus arrhizus*; (E) *Penicillium corylophilum*; (F) *Aspergillus niger.* No scale bars were set.

The astounding diversity of the extant grain microbiota represented at least eight sequenced fungal genera and one bacterial genus. The data set displayed in Figure 8-6 shows the number of plates containing each of the cultured microbes that were identified via ITS and 16S. All species identified are common environmental microbes in South Australia and it is therefore unsurprising that they were found on the wheat samples. *Aspergillus flavus* was the most prevalent pathogen and appeared on 66% of the 180 plates. Half of all plates contained the thermophilic *Bacillus safensis*, while 45% supported growth of the encapsulated yeast, *Cryptococcus magnus*. Over 42% of plates contained mixed bacterial and yeast cultures. Despite all efforts to isolate bacterial colonies on sequentially created streak plates, three of the four visually distinct colonies sent for ITS were mixed and could not be identified. The presence of mixed microbial cultures highlights one of the drawbacks of using traditional plating methods to isolate and survey the grain microbiota. It can be very challenging to separate highly mixed cultures of unknown species with potentially complicated

symbioses. Nonetheless, this data set presents a glimpse at the diversity and relative abundance of culturable filamentous fungi, yeast and bacteria present on commercially grown grain samples.

It was unknown if plasma treatment would impact select species or the entire grain microbiota. Thus, the identification of species at each plasma exposure time was essential to understand how the length of plasma exposure may impact each microbe. Each of the 180 plates was given a +/- score for the presence of every microbe. The number of positive plates was summed for each species and a two-way ANOVA was performed to compare the variations in species across plasma exposure times (see Figure 8-7). There is an inverse relationship between species abundance and plasma exposure time in most cases, except for *Cryptococcus magnus*. The number of plates containing *C. magnus* colonies appeared to increase with time. By 120-minutes of plasma exposure, only *C. magnus*, *Bacillus safensis* and mixed bacterial and yeast cultures were present on plates. It is possible that the successful removal of other pathogen species may have reduced the competition for resources on plates, allowing *C. magnus* and *B. safensis* to thrive. *C. magus* may survive long durations of plasma treatment due to the robust capsule and modified fungal cell wall structure protecting this yeast from the impacts of plasma chemical etching (Garcia-Rubio et al., 2020). Along similar reasoning, *Bacillus safensis* survival was predicted from the fact that this hardy, spore-forming thermophilic soil microbe is a persistent contaminant of sterile NASA cleanrooms and space craft assembly areas, and warrants concern for interplanetary protection (Tirumalai et al., 2018). One technical replicate in the 120-minute exposure contained two *Aspergillus flavus* colonies. These were the only hyphae-forming fungal colonies found in this treatment. It appears that increasing the plasma exposure time decreases the total viable population of grain microbes, regardless of Kingdom.

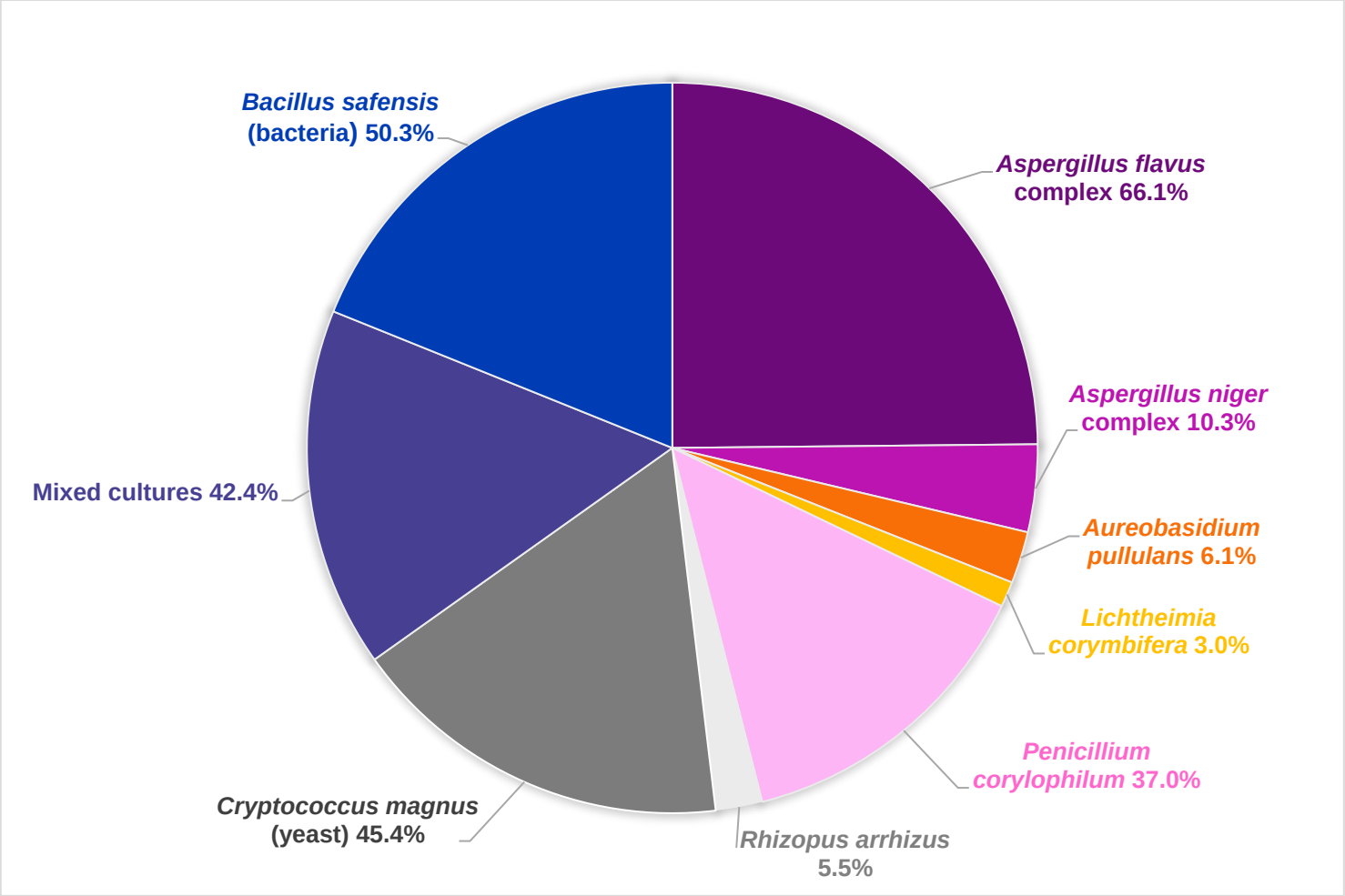


Figure 8-6. Percent of plates with visible colonies of each species identified through ITS sequencing. Please note that conidia of *Alternaria* and *Bipolaris* genera were visible under the microscope but did not appear in culture. *Fusarium* species were identified via qPCR but also did not appear in culture.

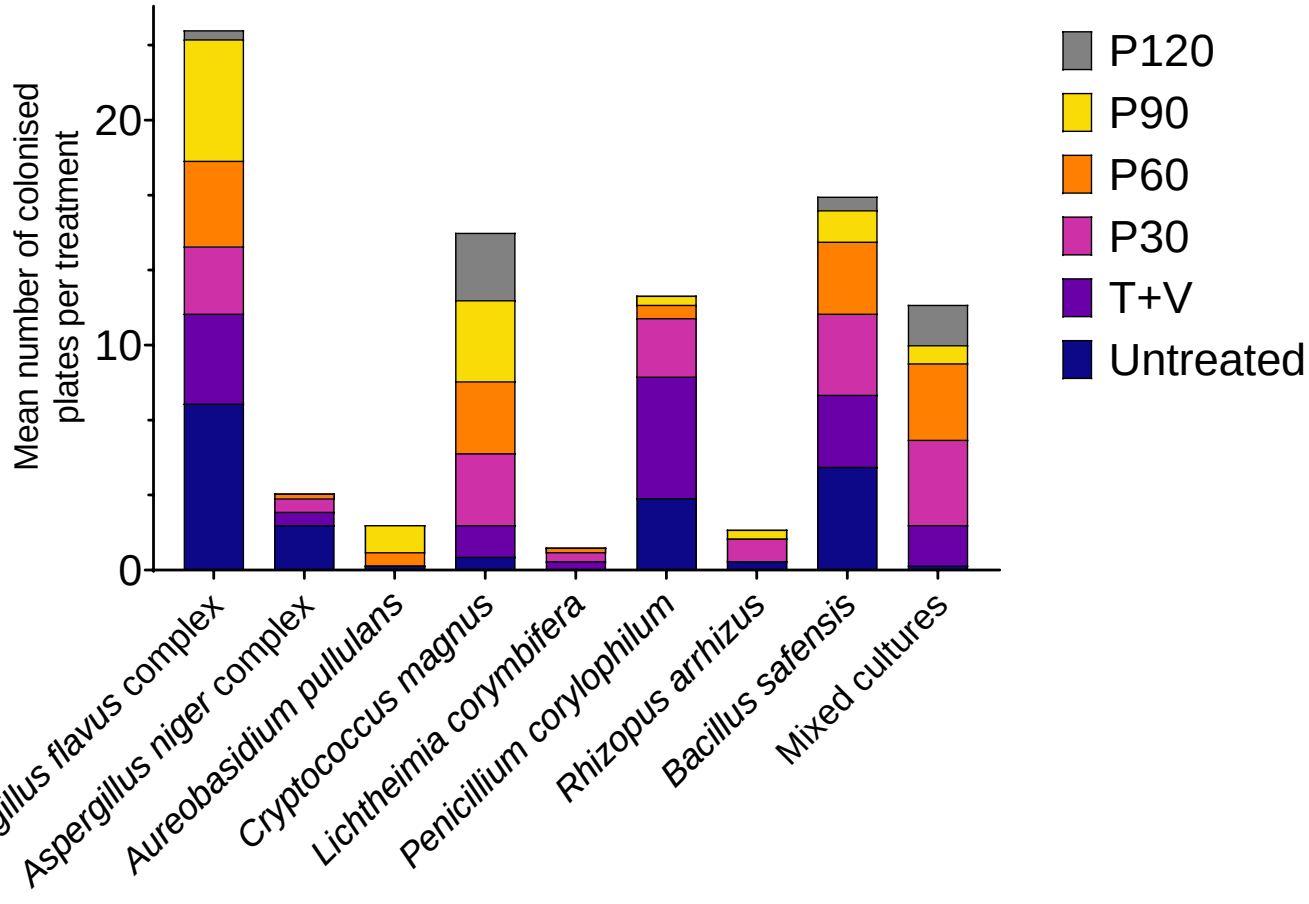


Figure 8-7. Graph illustrating the changes in species abundance across treatments. Two-way ANOVA data is presented as the mean. All plates were scored on a +/- scale for the presence/absence of each known species. The number of technical replicate plates (out of 6) with positive scores were summed and used as a total score for each biological replicate as indicated on the y-axis. Abbreviations: T+V (Tumbler + vacuum); P30 (30-minute plasma); P60 (60-minute plasma); P90 (90-minute plasma); P120 (120-minute plasma).

Perhaps the most notable information from this data set is the absence of common pathogens in the *Fusarium*, *Alternaria*, *Pyrenophora* and *Bipolaris* genera. *Alternaria* and *Bipolaris* species were prevalent during initial haemocytometer inspections of extracted spores but were not identifiable on plates. *Fusarium* colonies were observed growing on the pilot trial grain plates but could not be cultured. The presence of the mycotoxin, DON, further alludes to the existence of *Fusarium* species within this grain allotment, despite the absence in culture. qPCR was performed on two grain samples in collaboration with the Molecular Diagnostics Centre at the South Australian Research and Development Institute (SARDI). This led to the identification of *Fusarium pseudograminearum* and *Fusarium culmorum* (see Appendix S9). The presence of *F. pseudograminearum* and *F. culmorum* was further supported in the mycotoxin analysis (see section 8.3.5 below) by the presence of Zearalenone, a metabolite of these species (Ropejko and Twarużek, 2021; Torres et al., 2019).

The confirmation of *F. pseudograminearum* and *F. culmorum* on the grain sample highlighted the limitation of using traditional methods of spore extraction and plating. Although these methods are simple and affordable for the relative quantification of colony-forming units, there are drawbacks. In the *Fusarium* inoculation trials in Chapter 5.5.3.4, it was observed that macroconidia were rarely present on culture plates. Instead, colonies formed from viable hyphal fragments. It is possible that the extraction methods used within this thesis may be unsuitable for the culture of *Fusarium* species from macroconidia. The absence of *Bipolaris* and *Alternaria* conidia on culture plates may be another sign that this method was less than ideal for the culture of larger conidia. However, *Bipolaris* conidia could be cultured in Chapter 5.5.3.2, suggesting otherwise. The lack of representation on plates may be due to a paucity of spores present across the grain. It is difficult to tell considering the heterogeneity of the original sample. It is also likely that many of the species extracted from the grain and spread

onto plates were competing against each other for resources. The interspecies competition may have led to antagonism and a reduction of colony growth in certain species. Magan et al., 2003 found that mycotoxigenic *Penicillium*, *Aspergillus* and *Fusarium* species displayed dominance in mixed cultures. With this in mind, there are multiple factors contributing to the inconsistencies in species, including but not limited to the heterogeneity of inoculum across samples, interspecific competition and antagonism and the methods used in this project. More species were likely present on the grain but could not be identified.

While many species may not have been identified within the bounds of this experiment, it is still notable that plasma treatment inactivated a broad range of filamentous fungi, reducing the culturable microbial load by log 5. The only remaining culturable species after 120-minutes of plasma exposure were incredibly robust, encapsulated or spore-forming single-celled microbes. The reduction of 99.999% of seed surface fungi is astounding with deep implications for the improvement of grain quality, as well as the minimisation of food and/or feed loss. Yet, these benefits do come at a cost of two hours of plasma exposure, a rather long treatment time. This suggests the need for future research with a focus on treatment optimisation and upscaling of this technology.

8.3.4 Scanning electron microscopy

Scanning electron micrographs in Chapter 5.5.3 illustrated the effect of plasma etching on a single species of inoculated fungal pathogen in situ. It was unknown how plasma treatment may interact on a microscopic level with the highly complex grain microbiome of the contaminated industry samples. SEM was performed on samples of each treatment to assess the plasma-induced physical alterations to fungal pathogens on the grain surface (Figure 8-8).

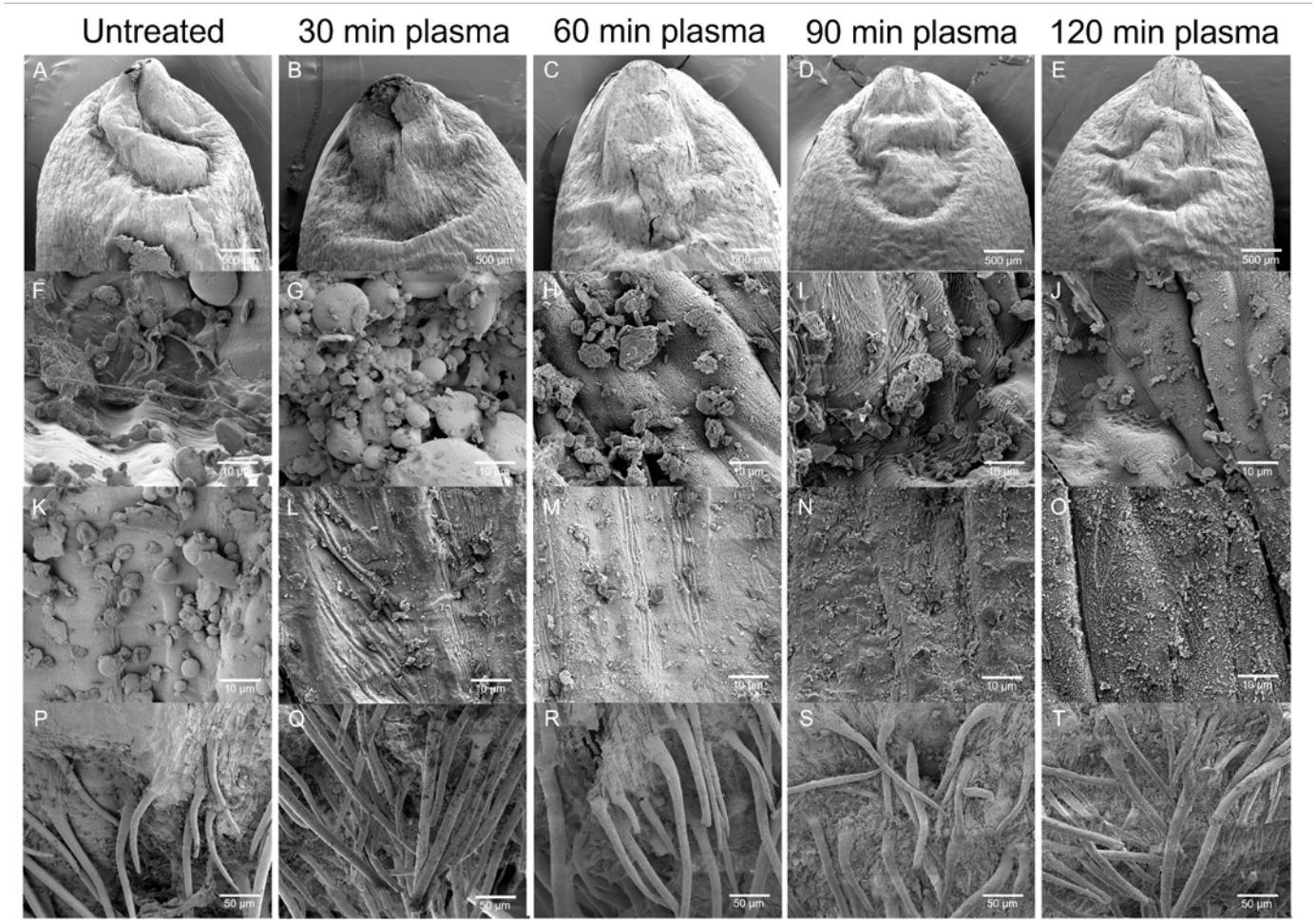


Figure 8-8. SEM micrographs of mycotoxin contaminated wheat grain samples. (A-E) display the embryo region of the grain. Note the debris within creases on the Untreated grain. (F-J) show the embryo region at 5000 x magnification with microbes clearly visible in the Untreated image and increasingly damaged with plasma exposure. (K-O) are micrographs of the dorsal region of the grain with clear weathering of both grain and microbe surfaces. (P-T) visualise the wheat grain brush which becomes severely damaged with extended plasma treatment.

Micrographs of Untreated samples display what appear to be multiple types of spores, hyphae, and other debris on all surfaces of the grain. These objects of interest are concentrated in the brush and between folds near the embryo. This validates the concept explored in Chapter 5.3, that microbes may aggregate in protected topographical areas on the grain. P30 exposures distorted the surfaces of microbes, debris, and grain. After 60 minutes of exposure, it is no longer possible to discern which structures were formerly microbes and which were detritus. By 90-minutes, weathering is apparent with significant damage to the brush and few objects larger than 10 µm visible on the surface. These observations align with similar damage in wheat following 90-minutes of plasma treatment in Chapter 4.3.1.2. 120 minutes of plasma exposure severely abraded all surface structures. Both the grain and objects located on it, became deeply etched and fragmented.

It is interesting to note the difficulty in procuring micrographs without distortions and other artefacts due to sample charging. All previous SEM micrographs on wheat (see Chapters 4.3.1.2 and 5.5.3.4) were performed with an acceleration voltage of 5 kV and scanning speed of 30 µs. On the contaminated grain samples, particular objects, which strongly resemble microbes, were highly charged, and required a reduction in acceleration voltage to 2 kV and scanning speed to 3µs for all grains in this experiment (Figure 8-9). Strong streaking and bright spots appeared on Untreated grain images but were reduced on samples exposed to longer than 30-minutes of plasma. It is unclear why this happened but may be attributed to the highly charged nature of many fungal spores (Wargenau et al., 2011). The charging could be altered during the plasma-induced chemical etching of spore surfaces.

Overall, SEM micrographs of the contaminated samples provided striking visual examples of heavy microbial loads on the grain surfaces. The fragmentation of surface objects increased with plasma exposure time and provided clues as to how the etching

process may be concurrently degrading many species of microbes on the grain surface. These visuals led to speculation that the deep etching may impact small molecules on the grain surface, including mycotoxins. Future studies should be undertaken to explore if prolonged plasma exposure can weather mycotoxins, as well as the microbes that produce them.

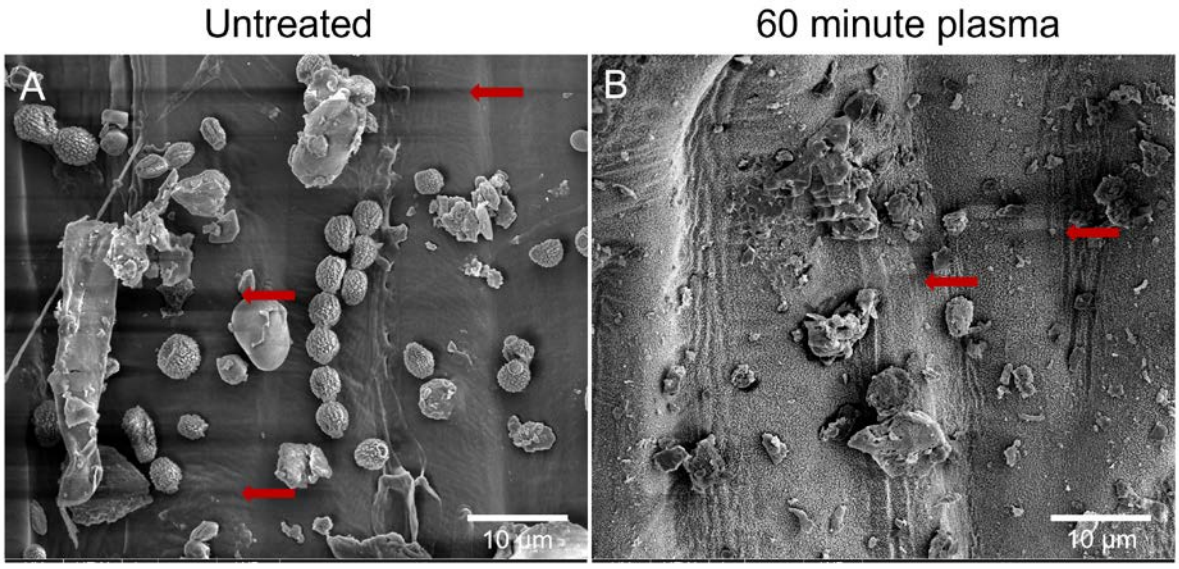


Figure 8-9. SEM micrographs with sample charging. Red arrows highlight the streaking which was more pronounced in Untreated samples and gradually reduced with plasma exposure.

8.3.5 Mycotoxin sampling

The premise of this experiment was to test the capacity of the plasma tumbler to inactivate a diverse population of microbiota on real-world samples, where the detection of mycotoxins led destruction of grain. Due to the severe risks to both human and animal health, the FAO and national agencies have established thresholds for allowable mycotoxins present in grain, requiring testing prior to processing and export (FAO, 2019). Subsamples of the grain donated for these experiments had been previously analysed for mycotoxins and were shown to contain 320 µg/Kg of (DON), a secondary metabolite of *Fusarium* spp. (Torres et al., 2019). It was assumed that the grain became infected in the field as *Fusarium* spp. colonisation generally does not

occur postharvest (Hope et al., 2005). The nature of grain fungal infections and mycotoxin production in the field is sporadic and may or may not be indicative of widespread colonisation. It was unknown if mycotoxins would be present throughout the entire grain allotment or only within a handful of samples. It was therefore deemed necessary to conduct a small sampling on grain to determine if mycotoxins were present across all samples, regardless of treatment. It was also hypothesized that Aflatoxins, a group of mycotoxins produced by *Aspergillus flavus* and *Aspergillus parasiticus* (Kumar et al., 2017) may be present within the samples given the prevalence of *A. flavus* on 66% of the plates in section 8.3.3. Samples were ground to flour and HPLC mycotoxin analysis was conducted by the commercial laboratory Intertek, Agricultural Services, Adelaide, Australia.

The results from mycotoxin analysis indicated that multiple, isolated fungal infections were present across the grain samples. Roughly 40% of the samples sent for testing returned positive mycotoxin results. Zearalenone was detected in T+V, 30-minute and 120-minute plasma treated samples, which suggested that the grain was infected by *Fusarium* spp. (Figure 8-10) (Ropejko and Twarużek, 2021). This corresponds to the detection of *F. pseudograminearum* and *F. culmorum* via qPCR in section 8.3.3. Unexpectedly, no detectable levels of DON were present in the 15 samples tested, despite an initial positive test. Aflatoxins, 2 µg/Kg, were found in two T+V replicates but not in the rest of the samples. The low detection levels of Aflatoxins are slightly surprising when considering *A. flavus* was present in over 66% of all culture plates. However, this may be attributed to multiple factors including whether *A. flavus* infections had occurred prior to grain procurement, or if spores were present but had not reached optimal conditions for sporulation and/or aflatoxin production. Both temperature and humidity significantly affect sporulation and mycotoxin aflR gene expression (Mahato et al., 2019; Umesha et al., 2016). It is probable that the high

frequency of *A. flavus* found on culture plates is attributed to quiescent spores on the grain surface.

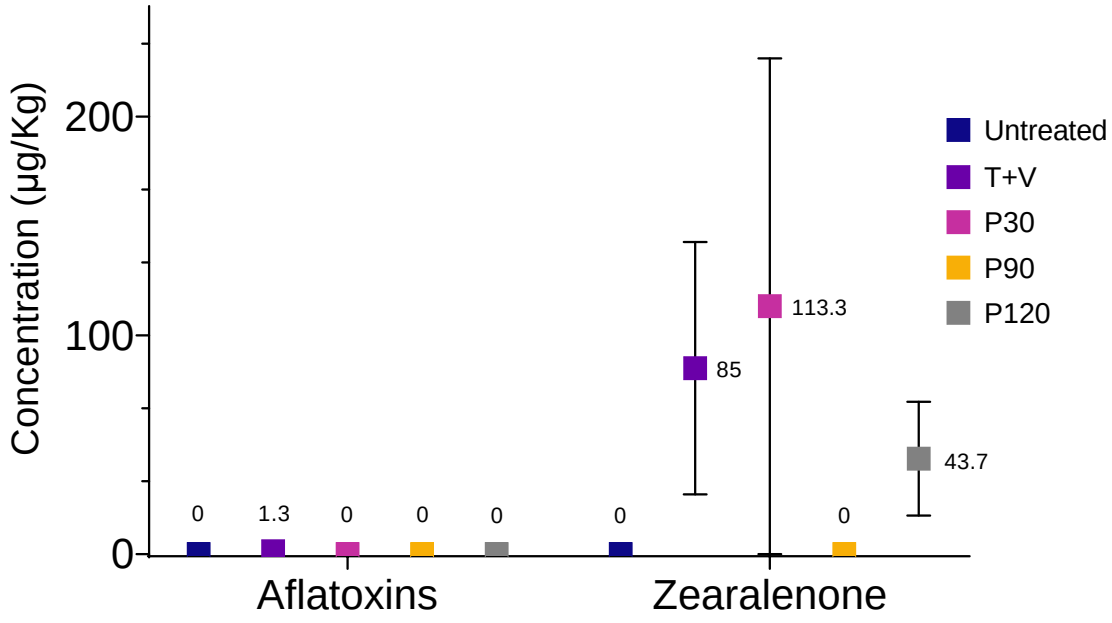


Figure 8-10. Comparisons of mean concentrations of Aflatoxins and Zearalenone found in each treatment. DON was detected in the original testing but not present in the sampling of each treatment. Two-way ANOVA data is presented as mean ± SEM. Abbreviations: T+V (Tumbler + vacuum); P30 (30-minute plasma); P90 (90-minute plasma); P120 (120-minute plasma).

The episodic nature of mycotoxigenic grain fungal infections occurring in the field and during transport likely plays a major role in the variations between samples. It is also highly probable that sampling error, caused by the small 10 g aliquots, occurred within this experiment. This design flaw was considered prior to testing but could not be overcome due to the very small laboratory scale of the plasma tumbler and ball mill. The necessary large volumes of grain could not be treated, ground into flour, and homogenised prior to sampling. Instead, this trial was treated as a discovery pilot to determine if cultured pathogens and their associated mycotoxins could be matched between samples. In this context, the mycotoxin testing experiment was successful. It also raised questions regarding the potential for plasma treatment to degrade mycotoxins through the chemical etching process. Within this survey, Zearalenone was

detected in 120-minute plasma treated samples. However, it is unknown if the initial concentration of Zearalenone was the same or higher prior to plasma treatment. It is not without reason to speculate the ion bombardment and oxidation within the plasma environment may be capable of denaturing these compounds. Future research involving the inoculation of grains with known levels of mycotoxins is necessary to establish whether plasma treatment has the capacity to improve grain quality through the reduction of toxic compounds

8.4 Conclusions

Harvested grain contains a mixed consortium of filamentous fungi, yeasts, and bacteria. The grain microbiota is often established in the field and can vary across a block and/or region. Once grains are mixed together post-harvest, the microbiota can be distributed throughout the stored lots (Magan et al., 2003). This increases the spread of the inoculum and may have cascading effects including deterioration of grain quality and increased mycotoxin production. It is therefore necessary to explore new technologies capable of deactivating microbes prior to grain storage. While there are many studies (reviewed by Kaur et al., 2020) investigating the use of plasma for the disinfestation of grains and seeds with inoculated pathogens, as far as the author is aware, this is the first research to use contaminated samples provided by industrial partners. These contaminated wheat samples were procured based on mycotoxin testing, which served as a proxy measurement for grain contamination. Concentrations of up to 10^3 more colony-forming units were found in the Untreated contaminated grain control samples, in comparison to the food quality wheat samples. This demonstrated the obstacles faced within the industry when confronted with low quality grain that may be harmful to human and animal health.

There were difficulties determining the species present on the grain due to the heterogeneity of the inoculum load throughout the samples, fungal species resource competition and drawbacks with the methods employed in this study. The traditional extraction and plating method for the quantification of viable spores is a simple yet powerful tool but may not be suitable for all pathogen species. *Fusarium* spp. were absent on culture plates but were identified via qPCR of grain samples and implicated by the presence of mycotoxin residues. Conversely, an analysis with NGS would be ideal to understand the full extent of microbes present, but outside of the scope of this project and would not reflect viability, just simply DNA present within the sample. There were likely many more pathogens present on the grain that were not culturable or identifiable through traditional plating methods. It should also be noted that *Aspergillus* spp. and *Penicillium* spp. become dominant in culture, which may attribute to the underrepresentation of other fungi (Magan et al., 2003). All these points should be taken into consideration when interpreting the efficacy of the plasma tumbler to inactivate fungal pathogens.

Overall, plasma treatment greatly reduced the culturable filamentous fungi extracted from the grain surface. The colony-forming unit concentration decreased with prolonged plasma exposure. Substantial inactivation, by a magnitude of 5, occurred throughout all replicates of the P120 treatment. Most of the identified fungal pathogen species, including *Aspergillus niger*, *Rhizopus arrhizus*, *Penicillium chrysogenum* and *Lichtheimia corymbifera* were significantly reduced by 90-minutes of treatment and completely absent by 120-minutes. The extremely hardy encapsulated yeast, *Cryptococcus magnus* and thermophilic endospore-forming *Bacillus safensis* appear to be the main persistent microorganisms present following 120-minutes of plasma exposure. *Cryptococcus* species are often distinguished from other fungi due to the presence of an exopolysaccharide capsule covering a double layer cell wall (Garcia-Rubio et al., 2020). Both the capsule and cell wall are tightly linked to virulence and

persistence in the environment. In *Cryptococcus neoformans*, the 3-5 µm diameter yeast cell can produce a capsule up to 30 µm thick depending upon environmental stress conditions (Wang et al., 2018). It is no wonder that this microorganism can withstand even 120-minutes of plasma treatment and it is speculated that much longer treatment times may be required for inactivation. As for *Bacillus safensis*, this endospore-forming extremophile was originally isolated from the Jet Propulsion Lab, California, USA, from which its name was derived -- spacecraft assembly facility (SAF) (Abril et al., 2019). A plasma study was shown to inactivate a 100 µL cell suspension dried onto a disc with 90-minutes of plasma treatment with a surface micro-discharge apparatus (Shimizu et al., 2014). Within the context of this system, *B. safensis* endospores are located across a three-dimensional grain surface as opposed to a relatively flat disc. It is possible that, like *C. magnus*, longer exposure times are necessary to inactivate this microbe on variable grain surfaces. However, as *B. safensis* is a common environmental/soil microbe without known pathogenicity, it may not be necessary to inactivate it for agricultural and food/feed production proposes.

These experiments sought to apply the knowledge gained throughout previous chapters toward a pervasive problem challenging the agriculture and food production industries with real impacts on food sustainability and human health. The exponential reduction of multiple pathogenic species indicates the plasma tumbler system is suitable for further investigation as a clean technology for the improvement of post-harvest grain quality. One finding of this chapter is that different treatment times are necessary to inactivate different pathogens. Clear goals of plasma treatment must be established prior to use for agricultural and food production processes. Which microbes are of the most concern? Is inactivation of 99.999% of microbes sufficient for the food production processes? What types of grains will be treated? The answers to these questions, among others, will dictate the application of plasma. As many

pathogens are greatly reduced by 90-minutes of treatment, it may be desirable to shorten the treatment time. Longer treatments may be necessary to ensure food safety regulations are met. Additionally, rigorous studies investigating the effects of plasma treatment on mycotoxins are needed.

In summary, the plasma tumbler appears to be a successful method for concurrently deactivating multiple species of wheat fungal pathogens. The complexity of the samples tested the limits of the PT system with a diversity of unknown pathogens and infection loads. In previous experiments using wheat as the model grain, there were no established patterns of microbial reductions. Instead, wheat-specific morphological features, within this research called 'hidey holes,' may confound spore inactivation. The data presented here suggests that 120 minutes of exposure in the plasma tumbler may be required to inactivate most pathogens and reach microbes residing in protective structures on the grain surface. The outcome of this experiment, in a translatable real-world sample, is promising and should be considered for further research as a future method for the inactivation of fungal pathogens on post-harvest grain.

9 Summary, limitations, and future directions

9.1 General summary

The growing food security crisis across the globe has been exacerbated by the COVID-19 pandemic and increasing climate variability (FAO, 2021a). With one third of the world population now food insecure, the Sustainable Development Goal for 2030 of zero hunger is becoming much more difficult to achieve (UN, 2021). Increasing the safe and sustainable production of staple crops are key targets toward mitigation of this crisis (UN, 2015). As fungal crop pathogens are leading causes of crop yield and food production losses, there is pressure to explore technologies which can rapidly and efficiently reduce fungal contamination of post-harvest grains (Fausto et al., 2019; Fisher et al., 2012; Fones et al., 2020; Savary et al., 2019; Strange and Scott, 2005). Non-thermal plasma technologies are emerging as potential solutions due to the lack of chemical input, reduction of grain moisture content, and low energy requirements (Bourke et al., 2018; Kaur et al., 2020). The ion bombardment and chemical weathering processes of non-thermal air plasmas are capable of inactivating microbes as well as altering the surface properties of seeds (Bormashenko et al., 2012; Dauwe et al., 2021; Kordas et al., 2015; Los et al., 2020; Selcuk et al., 2008). Yet, each grain is a three-dimensional living organism. As such, Butscher et al., 2016, speculated that morphological features on the grain surface will play a role in the efficacy of plasma treatment. A suitable plasma apparatus must concurrently expose all faces of a grain to the field of plasma if high levels of microbial inactivation are to occur. This thesis

sought to provide a comprehensive and systematic study using a novel rotating plasma tumbler apparatus to understand how plasma impacts post-harvest grains and fungal pathogens on the grain surface. The following subsections will consist of research aims (as discussed in Chapter 1.6) with conclusions of each aim described below.

9.1.1 The impact of plasma exposure on grain surfaces

Initially, it was unknown how the plasma tumbler apparatus impacted the surface structures of grains. A broad qualitative survey of untreated and treated grains, using scanning electron microscopy, was performed to explore seed surface topography, as well as alterations to surfaces following tumbler and vacuum treatment and plasma treatment (see Chapter 4). While the tumbler and vacuum treatment caused mechanical damage to grain surfaces, plasma treatment dramatically weathered the grain surfaces, including areas of mechanical damage. The patterns of weathering were dependent upon grain type and surface features, which confirmed the findings of Butscher et al., 2016 and Dauwe et al., 2021. It was also demonstrated that plasma impacts macro structures on the grain surface, in addition to the microscopic weathering, which has not been reported until now. Maize was further analysed with a confocal profilometer which resulted in a 12% increase in surface area following plasma treatment. Across all grain types, it was speculated that the newly weathered state may alter the interaction of water with grain surfaces. This led to the development of multiple assays involving grain-water relations in Chapter 6. Additionally, the SEM imagery highlighted the presence of extant fungi on grains. The damaged appearance of what are speculated to be conidia near the pedicle of plasma-treated maize grain led to the culture of extant fungi on the grain surface in Chapter 5.

9.1.2 The efficacy of plasma exposure for the inactivation of grain fungal pathogens

Preliminary trials described in the brief background section in Chapter 2, hinted toward the ability of the plasma tumbler to inactivate extant microbes on the grain surface. A

90-minute exposure timeframe was established as sufficient for reducing the microbial load on maize grains. In Chapter 5, this concept was explored in detail to understand how plasma interacts with the micro-ecosystems of each grain type. The extant microbes on the surfaces of Untreated, T+V and 90-minute plasma-treated grains were cultured to determine if plasma was able to reduce the number of colony-forming units. While plasma treatment reduced the number of fungal colonies across all grain types, it was unclear whether the 90-minute tumbler and vacuum treatment or the 90-minute plasma exposure were the mechanisms of action. Variations between grain types, especially wheat, led to speculation that morphological features on the grain surface may shield microbes from the effects of plasma treatment. A novel well-plate-based assay was developed to survey the location of extant microbial colonies growing on the grain surface, and how these change with varying plasma time exposures. Maize grains displayed large reductions in colony-forming units with increasing plasma exposure, regardless of location. In contrast, microbes on wheat grains tended to aggregate near the brush and crease regions. The time length of plasma exposure did not influence the location and viability of hyphal colonies. The results suggested that morphological features on the grain surface influence the efficacy of the plasma tumbler to inactivate microbes.

The significant differences between maize and wheat in the well-plate assays led to the development of inoculation trials. By adding specific pathogens to the grain surface, it became easier to compare how the time exposure of plasma affects the viability of fungal conidia. The efficacy of the tumbler system was highlighted in these trials as *Penicillium chrysogenum* inoculated on field pea grains displayed up to log 7 reductions between Untreated and 90-minute plasma treated grain. *Aspergillus flavus* inoculated on maize was completely deactivated by 105 minutes of treatment. The consistent reduction of *Penicillium* and *Aspergillus* spp. to negligible levels across all

independent experiments has not yet been demonstrated within the current body of literature. If small, yet robust, airborne spores could be inactivated at highly significant levels, it was speculated that plasma may impact the viability of other filamentous fungal structures. Therefore, a series of final inoculation assays were developed to challenge the plasma tumbler system with multiple fungal structures using five relevant seed-borne pathogens on five grain hosts. The significant reductions in colony-forming units were furthered via scanning electron microscopy, which for the first time, illustrated the effects of plasma chemical etching on multiple fungal structures, including hyphae and chlamydospores. Overall, Chapter 5 confirmed that the plasma tumbler system can reduce multiple types of fungal seed pathogens to relatively low levels.

9.1.3 The impact of plasma exposure on the physico-chemical properties of seeds

If plasma technology is to be developed for agricultural purposes, it is necessary to understand how the physico-chemical processes interact with different grain surfaces. In Chapter 6, it was speculated that plasma exposure may have altered the surface energies of each grain, due to the increases in surface area described in Chapter 4. This led to water droplet contact angle analysis using a tensiometer. The resulting data suggest that plasma exposure significantly increases surface energy, lowering contact angles by over 50 degrees. It was also observed that water droplets interacted in a different manner with plasma treated grains, which drove the development of water sorption assays. It also led to the analysis of four grain types using ToF-SIMS techniques to look for differences in surface chemistry following plasma exposure. Bormashenko et al., 2012 were the first to use this technique on plasma-treated seeds and looked at small, negative fragments. The data collected in this thesis greatly expanded the number and types of fragments analysed and used PCA to look for

relationships between fragments and plasma exposure. Across all four grain types, there were clear differences between control and plasma treatments.

The relationship between grains and water is of the utmost importance as seed germination is dependent upon hydration. To understand how plasma treatment may alter grain-water interactions, grains were placed in a highly sensitive vapour sorption meter to track changes in water uptake over time. Not only did plasma exposure significantly impact the rate and weight of water uptake, but it was shown for the first time, through modelling, that the mechanisms of water entry vary after plasma treatment. This was confirmed via a qualitative staining experiment which demonstrated the differences in grain uptake patterns of a high molecular weight stain. Psyllium grains are coated in a layer of polysaccharide mucilage, which displayed very different hydration patterns between treatments when exposed to the stain. A mucilage sorption assay was used to compare treatments. This assay showed a 19% decrease in mucilage sorption following 90 minutes of plasma exposure, highlighting the effects of plasma on seed physico-chemical properties. Finally, it was hypothesized that changes to grain water uptake may result in nutrient leaching. Grain leachate was analysed for Potassium concentrations which increased with both T+V and plasma treatment, suggesting that mechanical damage from tumbling, and weathering effects of plasma, likely increase the concentrations of solutes leaching into solution. This may have downstream consequences for food production and nutrition. In summary, plasma exposure alters seed surface chemistry, grain-water relations and the ability of Potassium, and potentially other solutes, to leach from the grain into the surrounding environment.

9.1.4 The effects of plasma exposure on seed viability, growth, and development

The discoveries in Chapter 6 regarding physico-chemical changes induced during plasma treatment, were speculated to have downstream consequences for seed

viability, growth, and development. Chapter 7 explored how plasma exposure influences seed health through a series of germination and growth trials. In contrast to other studies (Los et al., 2019; Šerá et al., 2010), each grain type was shown to have a different response to varying exposures of plasma treatment. Psyllium was relatively unaffected by even 90 minutes of plasma exposure, while wheat experienced reduced germination and seedling growth at the same exposure time. Maize seedling growth and development was hindered by 90 minutes of plasma exposure but recovered to show no significant differences between treatments in mature plants. This led to investigations into ethylene signalling and DNA oxidative damage to better explain why each grain type exhibited different responses to plasma treatment. However, the results of these studies were inconclusive, suggesting that other mechanisms may be reducing seed health following long plasma exposure times. Further research into the seed biological responses to plasma treatment is necessary.

9.1.5 Challenging the system with a real-world problem: deactivating fungal pathogens on an industrial contaminated grain sample

When considered as a whole, the physico-chemical effects of plasma treatment can alter both seed surfaces and microbe surfaces. A final series of experiments were conducted in Chapter 8 to use the new-found understanding of plasma-seed and plasma-microbe dynamics to inactivate the diverse extant seed microbiome on industrial contaminated grain samples. Previous studies have looked at plasma inactivation of the extant grain microbiome (Kordas et al., 2015; Los et al., 2020), however, this appears to be the first real-world application of plasma technology toward a problematic lot of grain. South Australian-grown industrial samples of mycotoxin contaminated grain were procured and shown to have a three-fold increase of fungal colonies when compared to food-quality grain. Subsamples were treated with varying exposures of plasma and cultured. By 120 minutes of exposure, filamentous fungal

cultures were inactivated with only the encapsulated yeast, *Cryptococcus magnus,* and endospore-forming bacteria, *Bacillus safensis,* remaining. This exciting data set demonstrated the efficacy of the plasma tumbler for treating and inactivating post-harvest fungal pathogens on diverse industry samples. It acts as a proof-of-concept toward future potential uses for plasma while highlighting future technologies to fight food loss.

9.2 Limitations of the research

The research described within this thesis was conducted between June 2020 and September 2021; and was therefore limited in capacity due to the COVID-19 pandemic. Access to instruments, controlled environment cabinets and laboratory space were subject to snap lockdowns, evolving regulations surrounding health and safety, and the subsequent backlogs associated with mass cancellations of instrument bookings. This required flexibility and adaptability within experimental planning and design. It also meant that many techniques could not be adequately optimised for the purposes of this research and some experiments, especially plant growth and development (Chapter 7), could not be replicated. The following subsections briefly describe specific limitations within each chapter.

9.2.1 Chapter 4

The Olympus LEXT OLS5000 confocal profilometer with a 405 nm laser is a powerful tool for assessing seed surface topography and analysing surface roughness and surface area. Within this research, only maize grains were analysed due to their relatively flat surface features. However, the LEXT software allows for the application of various filters to compensate for surface curves and waviness. These tools could have been applied to the curved surfaces of the other four grain types. Due to time and booking constraints, surface area data was only collected for maize. Had the software

been used to its full capacity, a better understanding of the weathering effects of plasma treatment across all grain types would have been possible.

9.2.2 Chapter 5

The microbiological experiments detailed in this chapter were limited due to the nature of calculating colony-forming units using conventional plate counts, statistical analysis compensating for scores of zero, as well as the lack of development of a consistent spore/hyphal fragment viability assay. Colony-forming units, or viable cell renumeration, are generally counted on plates with between 30 and 300 units (Wilson et al., 2017). Counts below 30 may have reduced statistical reliability (Parker et al., 2016). When combined with dilution factors, a single colony on a plate could yield a result of 3000 CFU/mL. To compensate for this, a median dose of plasma exposure could be calculated, in a similar fashion to an LD_{50}. However, due to the nature of plasma treatment, and variations between grain types and fungal pathogens, the creation of plasma exposure times which yielded median dose values were not possible within the scope of this research. Instead, a series of dilutions were performed for each biological replicate, at each plasma exposure time, to capture counts between 30 and 300. Even so, many treatments yielded counts of zero, which are statistically difficult to analyse. Therefore, all counts of zero were transformed to counts of one, which was thought to be acceptable as all analysis was compared on a log scale. It is recognised that both the nature of counting colony-forming unit counts of less than 30 and transformation of zeros to ones, may have added artefacts into the data sets which could not be detected by the author.

Additionally, fluorescent cell viability assays were inconclusive due to the nature of the fluorophores used, including NucRed Dead™, Syto™ 9 and SCRI Renaissance 2200. Had the fluorescent viability assays been optimised, artefacts induced by colony-forming unit counts may have been detectable.

9.2.3 Chapter 6

Understanding the plasma treatment-induced physico-chemical changes to the seed surface was challenging and limited by time and instrumentation. The available tensiometer was not capable of releasing a water droplet smaller than one mL, which was too large to fit on the surface of psyllium grains. Additionally, the software struggled to calculate contact angle on a curved seed surface. This led to the lack of data collection for all grain types treated with plasma exposures greater than 30 minutes. Had more time and different instrumentation been available, the collection of data across all plasma exposure times may have resulted in a better understanding of changes to grain surface energy and water sorption. Furthermore, grain water sorption experiments were conducted in a vapour sorption meter. While water exists in the vapour phase within the soil matrix, no known studies analyse the effects of vapour versus liquid water sorption by grains. It is therefore unknown if the results of this section are biased toward water sorption in a vapour phase.

The ToF-SIMS analysis hoped to provide a better understanding of the chemical changes to the seed surface following plasma treatment. The resulting data sets were enormous and could not be fully analysed within the timeframe of this research. Only the inorganic and small organic fragment datasets are presented within this thesis and may not be representative of the total surface chemistry changes caused by plasma treatment. Further analysis of larger fragments is ongoing with the aim of publishing in the future.

9.2.4 Chapter 7

Seedling growth and development assays were hindered by frequent changes to controlled environment cabinet accessibility due to COVID-19. In the interest of completing experiments on four of the five grain types, with respect to pandemic-related booking constraints, barley was omitted from growth and development assays.

Additionally, replication of all growth and development experiments was not possible. Having the ability to conduct these experiments in full would have enabled a more detailed understanding of the downstream effects of plasma treatment on seedling health. However, as seedling growth is generally irrelevant to the food production aspects of maize, wheat, field pea and psyllium, that lack of data collection within this chapter was not considered detrimental to the main goals of this research project.

9.2.5 Chapter 8

As in Chapter 5, the nature of colony-forming unit counts may have limited the data collected in this chapter. Additionally, it became clear through subculturing, ITS sequencing and PCR identification that not all grain microbes were able to be identified. *Fusarium pseudograminearum* and *Fusarium culmorum* were detected via qPCR, but not through subcultures or ITS. Had next-generation-sequencing (NGS) techniques been available during this research, it is possible that many more seed-borne microbes may have been identified within the contaminated grain samples.

9.3 Future directions

Despite these limitations, the research described within this thesis has generated new knowledge in the field of plasma agriculture. The results also pave the way for multiple new directions of future research, which will be critical if plasma is to be adapted for agricultural applications of scale. Chapters 5 and 8 demonstrated that the air plasma tumbler system is effective at reducing fungal pathogen loads on food quality grain. However, the level of microbial inactivation will be dependent upon the intended production processes which may or may not be tightly regulated by industry-standards and government policy. Early value chain protective and preventative grain treatment strategies to reduce microbial load, such as prior to storage, may require less plasma exposure time (Misra et al., 2016). Whereas food safety is often tightly regulated at multiple stages within global supply chains and may require extended exposure times.

Detailed research into specific applications is necessary prior to scaling instrumentation to industry levels. Regulation of plasma use for food production is currently in its infancy (Niemira, 2019). Optimisation of technology will need to closely follow the regulatory space to ensure instrumentation, treatment times and levels of inactivation fall within newly developing policies within and between countries. While the possible applications toward biosecurity and import/export policies are promising, international trade regulations must be developed between global trade partners prior to the consideration of plasma technology.

While plasma-induced alterations to grain-water dynamics may improve grain hydration for food processing, it may come at a cost of reduced nutritional value if key minerals are lost during the soaking process (Dauwe et al., 2021). Studies into the nutritional properties of grains, pre- and post-plasma treatment, are essential prior to understanding scalability. Moreover, if plasma treatments are to be used to improve the hydration kinetics of imbibing grains for production purposes (e.g., soaking chickpea for processing into hummus), detailed models must be developed. Treatment of cereals prior to storage may reduce the fungal load but may also render the grains more susceptible to changes in humidity and moisture content. For psyllium grain, the ability to remove fungal pathogens in a dry manner, without hydrating the mucilage, is a huge step forward in improving grain quality. However, the potential reduction in quantity of mucilage or changes in chemical composition of the mucilage must be considered before plasma technology is applied to this grain system.

Understanding the impacts of plasma treatment on seed viability and seedling health will also require further investigation. An integrated -omics approach is necessary to understand how both the embryo, and other signalling tissues within a seed, (e.g., scutellum and aleurone), are affected by varying exposures to plasma. Proteomics and

metabolomics studies may highlight the metabolic changes to seed tissues and the pathways which are most affected by treatment.

Ensuring that the growing food security needs of our current world population are met will require the prioritisation of studies into plasma agricultural technology. Engineering projects to upscale a non-thermal, rotating, air plasma system for use with subsistence level farming in LMICs should be considered as a high priority. These countries have the greatest immediate need and would benefit from the rapid adoption of this comparatively inexpensive technology. This will also require detailed work into the level of microbial inactivation and the possibility of plasma reducing mycotoxin loads, as discussed by Kaur et al., 2020. Overall, future developments in plasma agriculture are crucial before this technology can be considered as a tool for improving food security and sustainability.

9.4 Final remarks

The relatively new field of plasma agriculture sits at the interface between plasma physics, microbiology, and seed biology, requiring a broad knowledge and skill base within research teams. This project has highlighted the positive outcomes of open communication and transparency across scientific disciplines and research institutions. The accomplishments of this research are a testament to what is possible when curiosity, patience, and the dedication to the scientific process are embraced. The skills gained during these studies are immeasurable and will be of great benefit to my future endeavours. It is hoped that the work presented within this thesis not only benefits the individuals involved but adds to the current body of scientific knowledge around plasma treatment of grains for the improvement of food security. Meanwhile, the challenges associated with achieving the UN Sustainable Development Goals are not limited to the field of science alone, underscoring the importance of multi-disciplinary collaboration in tackling global issues.

10 References

Abbo, S., Shtienberg, D., Lichtenzveig, J., Lev-Yadun, S., Gopher, A., 2003. The chickpea, summer cropping, and a new model for pulse domestication in the ancient Near East. Q. Rev. Biol. 78, 435–448. https://doi.org/10.1086/378927

Abril, A.G., Rama, J.L.R., Feijoo-Siota, L., Calo-Mata, P., Salazar, S., Peix, A., Velázquez, E., Villa, T.G., 2019. *Bacillus safensis* subsp. osmophilus subsp. nov., isolated from condensed milk, and description of *Bacillus safensis* subsp. safensis subsp. nov. Int. J. Syst. Evol. Microbiol. 69, 189–195. https://doi.org/10.1099/ijsem.0.003126

Adeniji, A.A., Babalola, O.O., 2018. Tackling maize fusariosis: in search of *Fusarium graminearum* biosuppressors. Arch. Microbiol. 200, 1239–1255. https://doi.org/10.1007/s00203-018-1542-y

Adhikari, B., Pangomm, K., Veerana, M., Mitra, S., Park, G., 2020. Plant Disease Control by Non-Thermal Atmospheric-Pressure Plasma. Front. Plant Sci. 11, 1–15. https://doi.org/10.3389/fpls.2020.00077

Agriopoulou, S., Stamatelopoulou, E., Varzakas, T., 2020. Advances in Occurrence, Importance, and Mycotoxin Control Strategies: Prevention and Detoxification in Foods. Foods 9, 137. https://doi.org/10.3390/foods9020137

Agrios, G.N., 2005. History of Plant Pathology and Early Significant Plant Diseases, in: Plant Pathology. Academic Press, Burlington, MA, pp. 8–29.

Al-Sadi, A.M., 2021. *Bipolaris sorokiniana*-Induced Black Point, Common Root Rot, and Spot Blotch Diseases of Wheat: A Review. Front. Cell. Infect. Microbiol. 11, 1–9. https://doi.org/10.3389/fcimb.2021.584899

Alshannaq, A., Yu, J.H., 2017. Occurrence, toxicity, and analysis of major mycotoxins in food. Int. J. Environ. Res. Public Health 14, 632.

https://doi.org/10.3390/ijerph14060632

Amaike, S., Keller, N.P., 2011. *Aspergillus flavus*. Annu. Rev. Phytopathol. 49, 107–133. https://doi.org/10.1146/annurev-phyto-072910-095221

APVMA, 2021. Crop Groups [WWW Document]. URL https://apvma.gov.au/crop-groups (accessed 11.14.21).

Aslam, S., Ghazanfar, M.U., Munir, N., Hamid, M.I., 2019. Managing *Fusarium* wilt of pea by utilizing different application methods of fungicides. Pakistan J. Phytopathol. 31, 81–88. https://doi.org/10.33866/phytopathol.031.01.0482

Aveskamp, M.M., de Gruyter, J., Woudenberg, J.H.C., Verkley, G.J.M., Crous, P.W., 2010. Highlights of the Didymellaceae: A polyphasic approach to characterise *Phoma* and related pleosporalean genera. Stud. Mycol. 65, 1–60. https://doi.org/10.3114/sim.2010.65.01

Bafoil, M., Jemmat, A., Martinez, Y., Merbahi, N., Eichwald, O., Dunand, C., Yousfi, M., 2018. Effects of low temperature plasmas and plasma activated waters on *Arabidopsis thaliana* germination and growth. PLoS One 13, e0195512. https://doi.org/10.1371/journal.pone.0195512

Bafoil, M., Ru, A. Le, Merbahi, N., Eichwald, O., Dunand, C., Yousfi, M., 2019. New insights of low-temperature plasma effects on germination of three genotypes of *Arabidopsis thaliana* seeds under osmotic and saline stresses. Sci. Rep. 9, 8649. https://doi.org/10.1038/s41598-019-44927-4

Bailly, C., El-Maarouf-Bouteau, H., Corbineau, F., 2008. From intracellular signaling networks to cell death: the dual role of reactive oxygen species in seed physiology. Comptes Rendus - Biol. 331, 806–814. https://doi.org/10.1016/j.crvi.2008.07.022

Barilli, E., Cobos, M.J., Rubiales, D., 2016. Clarification on host range of *Didymella pinodes* the causal agent of pea ascochyta blight. Front. Plant Sci. 7, 592. https://doi.org/10.3389/fpls.2016.00592

Bewick, T.A., Shilling, D.G., Querns, R., 1993. Evaluation of Epicuticular Wax Removal from Whole Leaves with Chloroform. Weed Technol. 7, 706–716. https://doi.org/10.1017/S0890037X00037581

Bewley, J.D., 1997. Seed germination and dormancy. Plant Cell 9, 1055–1066. https://doi.org/10.1105/tpc.9.7.1055

Bewley, J.D., Black, M., 1978. Physiology and Biochemistry of Seeds in Relation to Germination. Springer Berlin Heidelberg, New York. https://doi.org/10.1007/978-3-642-66668-1

Bewley, J.D., Bradford, K.J., Hilhorst, H.W.M., Nonogaki, H., 2013. Structure and composition, in: Seeds: Physiology of Development, Germination and Dormancy. Springer Science+Business, New York, pp. 1–392. https://doi.org/10.1007/978-1-4614-4693-4

Boateng, A.A., Cooke, P.H., Hicks, K.B., 2007. Microstructure development of chars derived from high-temperature pyrolysis of barley (*Hordeum vulgare* L.) hulls. Fuel 86, 735–742. https://doi.org/10.1016/j.fuel.2006.08.024

Bonavia, D., 2013. The Domestication of Maize, in: Maize : Origin, Domestication, and Its Role in the Development of Culture. Cambridge University Press, Cambridge, pp. 61–117. https://doi.org/10.1017/cbo9781139149433.004

Bormashenko, E., Grynyov, R., Bormashenko, Y., Drori, E., 2012. Cold Radiofrequency Plasma Treatment Modifies Wettability and Germination Speed of Plant Seeds. Sci. Rep. 2, 1–8. https://doi.org/10.1038/srep00741

Bormashenko, E., Shapira, Y., Grynyov, R., Whyman, G., Bormashenko, Y., Drori, E., 2015. Interaction of cold radiofrequency plasma with seeds of beans (*Phaseolus vulgaris*). J. Exp. Bot. 66, 4013–4021. https://doi.org/10.1093/jxb/erv206

Bourke, P., Ziuzina, D., Boehm, D., Cullen, P.J., Keener, K., 2018. The Potential of Cold Plasma for Safe and Sustainable Food Production. Trends Biotechnol. 36, 615–626. https://doi.org/10.1016/j.tibtech.2017.11.001

Briggs, D.E., 1978. Barley, 1st ed. Chapman and Hall, Ltd., London. https://doi.org/10.1007/978-94-009-5715-2

Briggs, D.E., MacDonald, J., 1983. The permeability of the surface layers of cereal grains, and implications for tests of abrasion in barley. J. Inst. Brew. 89, 324–332. https://doi.org/10.1002/j.2050-0416.1983.tb04197

Brooker, D.B., Bakker-Arkema, F.W., Hall, W., 1992. Drying and storage of grains and oilseeds, Van Nostrand Reinhold, New York.

Burgain, A., Dantigny, P., 2016. Inoculation of airborne conidia of *Penicillium chrysogenum* on the surface of a solid medium. Food Microbiol. 54, 162–166.

https://doi.org/10.1016/j.fm.2015.10.002

Butscher, D., Waskow, A., von Rohr, P.R., 2020. Disinfection of granular food products using cold plasma, in: Bermudez-Aguirre, D. (Ed.), Advances in Cold Plasma Applications for Food Safety and Preservation. Academic Press, pp. 185–228. https://doi.org/10.1016/B978-0-12-814921-8.00006-2

Butscher, D., Zimmermann, D., Schuppler, M., Rudolf von Rohr, P., 2016. Plasma inactivation of bacterial endospores on wheat grains and polymeric model substrates in a dielectric barrier discharge. Food Control 60, 636–645. https://doi.org/10.1016/j.foodcont.2015.09.003

Chan, L.L.Y., Rice, W.L., Qiu, J., 2020. Observation and quantification of the morphological effect of trypan blue rupturing dead or dying cells. PLoS One 15, 1–17. https://doi.org/10.1371/journal.pone.0227950

Chen, F.F., 2008. Radiofrequency Plasma Sources for Semiconductor Processing, in: d'Agostino, R., Favia, P., Kawai, Y., Ikegami, H., Sato, N., Arefi-Khonsari, F. (Ed.), Adv. Plasma Technol. 99–115. https://doi.org/10.1002/9783527622184.ch6

Chen, Q., Jiang, J.R., Zhang, G.Z., Cai, L., Crous, P.W., 2015. Resolving the Phoma enigma. Stud. Mycol. 82, 137–217. https://doi.org/10.1016/j.simyco.2015.10.003.

Chizoba Ekezie, F.G., Sun, D.W., Cheng, J.H., 2017. A review on recent advances in cold plasma technology for the food industry: Current applications and future trends. Trends Food Sci. Technol. 69, 46–58. https://doi.org/10.1016/j.tifs.2017.08.007

Cho, H.Y., Bancerz, R., Ginalska, G., Leonowicz, A., Cho, N.S., Ohga, S., 2007. Culture conditions of psychrotrophic fungus, *Penicillium chrysogenum* and its lipase characteristics. J. Fac. Agric. Kyushu Univ. 52, 281–286. https://doi.org/10.5109/9315

Choudhury, S., Panda, P., Sahoo, L., Panda, S.K., 2013. Reactive oxygen species signaling in plants under abiotic stress. Plant Signal. Behav. 8. https://doi.org/10.4161/psb.23681

Corbineau, F., Xia, Q., Bailly, C., El-maarouf-bouteau, H., 2014. Ethylene, a key factor in the regulation of seed dormancy. Front. Plant Sci. 5, 1–13. https://doi.org/10.3389/fpls.2014.00539

Cotuna, O., Paraschivu, M., Sărăţeanu, V., Partal, E., Durău, C.C., 2021. Influence of *Fusarium graminearum* infection on the accumulation of mycotoxins in wheat grains. Preprints. https://doi.org/10.20944/preprints202106.0429.v1

Cowley, J.M., Herliana, L., Neumann, K.A., Ciani, S., Cerne, V., Burton, R.A., 2020. A small-scale fractionation pipeline for rapid analysis of seed mucilage characteristics. Plant Methods 16, 1–12. https://doi.org/10.1186/s13007-020-00569-6

Cowling, W.A., Li, L., Siddique, K.H.M., Banks, R.G., Kinghorn, B.P., 2019. Modeling crop breeding for global food security during climate change. Food Energy Secur. 8, 1–10. https://doi.org/10.1002/fes3.157

Crang, R., Lyons-Sobaski, S., Wise, R., 2018. Fruits, seeds, and seedlings, in: Plant Anatomy: A Concept Based Approach to the Structure of Seed Plants. Springer Nature, Cham, Switzerland, pp. 650–678. https://doi.org/10.1007/978-3-319-77315-5

Crous, P.W., Gams, W., Stalpers, J.A., Robert, V., Stegehuis, G., 2004. MycoBank: An online initiative to launch mycology into the 21st century. Stud. Mycol. 50, 19–22.

Curran, J., Driver, F., Ballard, J.W.O., Milner, R.J., 1994. Phylogeny of Metarhizium: analysis of ribosomal DNA sequence data. Mycol. Res. 98, 547–552. https://doi.org/10.1016/S0953-7562(09)80478-4

da Silva, A.R.M., Farias, M.L., da Silva, D.L.S., Vitoriano, J.O., de Sousa, R.C., Alves-Junior, C., 2017. Using atmospheric plasma to increase wettability, imbibition and germination of physically dormant seeds of *Mimosa Caesalpiniafolia*. Colloids Surfaces B Biointerfaces 157, 280–285. https://doi.org/10.1016/j.colsurfb.2017.05.063

Dai, F., Nevo, E., Wu, D., Comadran, J., Zhou, M., Qiu, L., Chen, Z., Beiles, A., Chen, G., Zhang, G., 2012. Tibet is one of the centers of domestication of cultivated barley. PNAS 109, 16969–16973. https://doi.org/10.1073/pnas.1215265109

Dasan, B.G., Mutlu, M., Boyaci, I.H., 2016. Decontamination of *Aspergillus flavus* and *Aspergillus parasiticus* spores on hazelnuts via atmospheric pressure fluidized bed plasma reactor. Int. J. Food Microbiol. 216, 50–59.

https://doi.org/10.1016/j.ijfoodmicro.2015.09.006

Dauwe, R., Roulard, R., Ramos, M., Thiombiano, B., Mesnard, F., Gontier, E., Jamali, A., 2021. Etching of the seed cuticle by cold plasma shortens imbibitional leakage in *Linum usitatissimum* L. Ind. Crops Prod. 167. https://doi.org/10.1016/j.indcrop.2021.113536

Davidson, J., 2012. Epidemiology and management of *Ascochyta* blight of field pea (*Pisum sativum*) in South Australia. University of Adelaide.

Davidson, J.A., Krysinska-Kaczmarek, M., Herdina, McKay, A., Scott, E.S., 2012. Comparison of cultural growth and in planta quantification of *Didymella pinodes*, *Phoma koolunga* and *Phoma medicaginis* var. pinodella, causal agents of ascochyta blight on field pea (*Pisum sativum*). Mycologia 104, 93–101. https://doi.org/10.3852/11-118

de Groot, G.J.J.B., Hundt, A., Murphy, A.B., Bange, M.P., Mai-Prochnow, A., 2018. Cold plasma treatment for cotton seed germination improvement. Sci. Rep. 8, 1–10. https://doi.org/10.1038/s41598-018-32692-9

De La Torre, A.R., Piot, A., Liu, B., Wilhite, B., Weiss, M., Porth, I., 2020. Functional and morphological evolution in gymnosperms: A portrait of implicated gene families. Evol. Appl. 13, 210–227. https://doi.org/10.1111/eva.12839

Dean, R., Van Kan, J.A.L., Pretorius, Z.A., Hammond-Kosack, K.E., Di Pietro, A., Spanu, P.D., Rudd, J.J., Dickman, M., Kahmann, R., Ellis, J., Foster, G.D., 2012. The Top 10 fungal pathogens in molecular plant pathology. Mol. Plant Pathol. 13, 414–430. https://doi.org/10.1111/j.1364-3703.2011.00783.x

Dhar, M.K., Kaul, S., Sareen, S., Koul, A.K., 2005. *Plantago ovata*: genetic diversity, cultivation, utilization and chemistry. Plant Genet. Resour. 3, 252–263. https://doi.org/doi:10.1079/PGR200582

Dobrynin, D., Fridman, G., Friedman, G., Fridman, A., 2009. Physical and biological mechanisms of direct plasma interaction with living tissue. New J. Phys. 11. https://doi.org/10.1088/1367-2630/11/11/115020

Doehlemann, G., Ökmen, B., Zhu, W., Sharon, A., 2017. Plant Pathogenic Fungi. Microbiol. Spectr. 5, 1–23. https://doi.org/10.1128/9781555819583.ch34

Domínguez, F., Cejudo, F.J., 2014. Programmed cell death (PCD): An essential process of cereal seed development and germination. Front. Plant Sci. 5, 1–11.

https://doi.org/10.3389/fpls.2014.00366

Doyle, J.A., 2012. Molecular and fossil evidence on the origin of angiosperms. Annu. Rev. Earth Planet. Sci. 40, 301–326. https://doi.org/10.1146/annurev-earth-042711-105313

Dubcovsky, J., Dvorak, J., 2007. Genome Plasticity a Key Factor in the Success of Polyploid Wheat Under Domestication. Science (80-.). 316, 1862–1866. https://doi.org/10.1126/science.1143986

Duffus, C.M., Cochrane, M.P., 1993. Formation of the barley grain morphology, physiology, and biochemistry, in: MacGregor, A.W., Bhatty, R.S. (Eds.), Barley: Chemistry and Technology. American Association of Cereal Chemists, St. Paul, pp. 33–72.

Dufour, T., Gutierrez, Q., Bailly, C., 2021. Sustainable improvement of seeds vigor using dry atmospheric plasma priming: Evidence through coating wettability, water uptake, and plasma reactive chemistry. J. Appl. Phys. 129. https://doi.org/10.1063/5.0037247

Duveiller, E., Kandel, Y.R., Sharma, R.C., Shrestha, S.M., 2005. Epidemiology of foliar blights (spot blotch and tan spot) of wheat in the plains bordering the Himalayas. Phytopathology 95, 248–256. https://doi.org/10.1094/PHYTO-95-0248

Dwivedi, S.L., Lammerts van Bueren, E.T., Ceccarelli, S., Grando, S., Upadhyaya, H.D., Ortiz, R., 2017. Diversifying Food Systems in the Pursuit of Sustainable Food Production and Healthy Diets. Trends Plant Sci. 22, 842–856. https://doi.org/10.1016/j.tplants.2017.06.011

Edwards, J.A., Lewis Smith, R.I., 1988. Photosynthesis and respiration of *Colobanthus quitensis* and *Deschampsia antarctica* from the maritime Antarctic. Br. Antarct. Surv. Bull. 81, 43–63.

Ehlbeck, J., Schnabel, U., Polak, M., Winter, J., Von Woedtke, T., Brandenburg, R., Von Dem Hagen, T., Weltmann, K.D., 2011. Low temperature atmospheric pressure plasma sources for microbial decontamination. J. Phys. D. Appl. Phys. 44. https://doi.org/10.1088/0022-3727/44/1/013002

Elmogahzy, Y.E., 2020. Finished fibrous assemblies, in: Mogahzy, Y.E. El (Ed.), Engineering Textiles. Woodhead Publishing, pp. 275–298.

https://doi.org/10.1016/b978-0-08-102488-1.00011-3

Evans, M.L., Hollaway, G.J., Dennis, J.I., Correll, R., Wallwork, H., 2010. Crop sequence as a tool for managing populations of *Fusarium pseudograminearum* and *F. culmorum* in south-eastern Australia. Australas. Plant Pathol. 39, 376–382. https://doi.org/10.1071/AP09092

FAO, 2021a. Agricultural and food markets: Trends and prospects, OECD-FAO Agricultural Outlook 2021-2030. Rome.

FAO, 2021b. FAOSTAT Food Balances [WWW Document]. Food Balanc. URL https://www.fao.org/faostat/en/?#data/FBS (accessed 10.20.21).

FAO, 2019. Codex Alimentarius: General standard for contaminants and toxins in food and feed. Food & Agriculture Organization of the United Nations.

FAO, 2017. Plant health and food security, International Plant Protection Convention. Rome.

Fausto, A., Rodrigues, M.L., Coelho, C., 2019. The still underestimated problem of fungal diseases worldwide. Front. Microbiol. 10, 1–5. https://doi.org/10.3389/fmicb.2019.00214

Fincher, G.B., Stone, T.A., 1993. Physiology and biochemistry of germination in barley, in: MacGregor, A.W., Bhatty, R.S. (Eds.), Barley: Chemistry and Technology. American Association of Cereal Chemists, St. Paul, Minnesota, USA, pp. 247–295.

Fisher, M.C., Henk, D.A., Briggs, C.J., Brownstein, J.S., Madoff, L.C., McCraw, S.L., Gurr, S.J., 2012. Emerging fungal threats to animal, plant and ecosystem health. Nature 484, 186–194. https://doi.org/10.1038/nature10947

Flajs, D., Peraica, M., 2009. Toxicological properties of citrinin. Arh. Hig. Rada Toksikol. 60, 457–464. https://doi.org/10.2478/10004-1254-60-2009-1992

Fones, H.N., Bebber, D.P., Chaloner, T.M., Kay, W.T., Steinberg, G., Gurr, S.J., 2020. Threats to global food security from emerging fungal and oomycete crop pathogens. Nat. Food 1, 332–342. https://doi.org/10.1038/s43016-020-0075-0

Francoz, E., Ranocha, P., Burlat, V., Dunand, C., 2015. *Arabidopsis* seed mucilage secretory cells: Regulation and dynamics. Trends Plant Sci. 20, 515–524. https://doi.org/10.1016/j.tplants.2015.04.008

Fridman, G., 2008. Direct Plasma Interaction with Living Tissue. Drexel University.

Froböse, N.J., Bjedov, S., Schuler, F., Kahl, B.C., Kampmeier, S., Schaumburg, F., 2020. Gram staining: A comparison of two automated systems and manual staining. J. Clin. Microbiol. 58, 1–6. https://doi.org/10.1128/JCM.01914-20

Fukunaga, K., Hill, J., Vigouroux, Y., Matsuoka, Y., Sanchez G., J., Liu, K., Buckler, E.S., Doebley, J., 2005. Genetic diversity and population structure of teosinte. Genetics 169, 2241–2254. https://doi.org/10.1534/genetics.104.031393

Galli, J.A., Fessel, S.A., Panizzi, R.C., 2005. Effect of *Fusarium graminearum* and infection index on germination and vigor of maize seeds. Fitopatol. Bras. 30, 470–474. https://doi.org/10.1590/s0100-41582005000500002

Garcia-Rubio, R., de Oliveira, H.C., Rivera, J., Trevijano-Contador, N., 2020. The Fungal Cell Wall: *Candida*, *Cryptococcus*, and *Aspergillus* Species. Front. Microbiol. 10, 1–13. https://doi.org/10.3389/fmicb.2019.02993

Gaynes, R., 2017. The discovery of *Penicillin*-new insights after more than 75 years of clinical use. Emerg. Infect. Dis. 23, 849–853. https://doi.org/http://dx.doi.org/10.3201/eid2305.161556

Ghime, D., Ghosh, P., 2020. Decolorization of diazo dye trypan blue by electrochemical oxidation: Kinetics with a model based on the Fermi's equation. J. Environ. Chem. Eng. 8, 102792. https://doi.org/10.1016/j.jece.2018.11.037

Gilliham, M., Athman, A., Tyerman, S.D., Conn, S.J., 2011. Cell-specific compartmentation of mineral nutrients is an essential mechanism for optimal plant productivity-another role for TPC1? Plant Signal. Behav. 6, 1656–1661. https://doi.org/10.4161/psb.6.11.17797

Good, R.J., 1992. Contact Angle, Wetting, and Adhesion: A Critical Review. J. Adhes. Sci. Technol. 6, 1269–1302. https://doi.org/10.1163/156856192X00629

Grabe, D.F., 1989. Measurement of Seed Moisture, in: Stanwood, P.C., McDonald, M.B. (Eds.), Seed Moisture. Crop Science Society of America, Madison, Wisconsin, pp. 69–92. https://doi.org/10.2135/cssaspecpub14.c5

Grains Research and Development Corporation (GRDC), 2016. GRDC GrowNotes: Wheat. Canberra, Australia.

Griesser, H.J., 1989. Small scale reactor for plasma processing of moving substrate

web. Vacuum 39, 485–488. https://doi.org/10.1016/0042-207X(89)90272-8

Guan, Y., Chen, J., Nepovimova, E., Long, M., Wu, W., Kuca, K., 2021. Aflatoxin Detoxification Using Microorganisms and Enzymes. Toxins (Basel). 13, 1–17. https://doi.org/10.3390/toxins13010046

Gupta, P.K., Chand, R., Vasistha, N.K., Pandey, S.P., Kumar, U., Mishra, V.K., Joshi, A.K., 2018. Spot blotch disease of wheat: the current status of research on genetics and breeding. Plant Pathol. 67, 508–531. https://doi.org/10.1111/ppa.12781

Hardham, A.R., 1985. Studies on the cell surface of zoospores and cysts of the fungus *Phytophthora cinnamomi*: The influence of fixation on patterns of lectin binding. J Histochem Cytochem 33, 110–118. https://doi.org/10.1177/33.2.3918095

Harris, K., Crabb, D., Young, I.M., Weaver, H., Gilligan, C.A., Otten, W., Ritz, K., 2002. In situ visualisation of fungi in soil thin sections: Problems with crystallisation of the fluorochrome FB 28 (Calcofluor M2R) and improved staining by SCRI Renaissance 2200. Mycol. Res. 106, 293–297. https://doi.org/10.1017/S0953756202005749

Harry, J.E., 2010. Introduction To Plasma Technology: Science, Engineering and Applications. Wiley VCH, Weinheim, Germany. https://doi.org/10.1002/9783527632169

Healey, A., Furtado, A., Cooper, T., Henry, R.J., 2014. Protocol: A simple method for extracting next-generation sequencing quality genomic DNA from recalcitrant plant species. Plant Methods 10, 1–8. https://doi.org/10.1186/1746-4811-10-21

Hedayati, M.T., Pasqualotto, A.C., Warn, P.A., Bowyer, P., Denning, D.W., 2007. *Aspergillus flavus*: Human pathogen, allergen and mycotoxin producer. Microbiology 153, 1677–1692. https://doi.org/10.1099/mic.0.2007/007641-0

Hess, M., Barralis, G., Bleiholder, H., Buhr, L., Eggers, T., Hack, H., Stauss, R., 1997. Use of the extended BBCH scale - General for the descriptions of the growth stages of mono- and dicotyledonous weed species. Weed Res. 37, 433–441. https://doi.org/10.1046/j.1365-3180.1997.d01-70.x

Hogan, J.T., Roseman, A.S., 1961a. Gas plasma irradiation of rice: I. Hydration. Cereal Chem. 38.

Hogan, J.T., Roseman, A.S., 1961b. Gas plasma irradiation of rice: II. Effect of heat on hydratio and cooking characteristics. Cereal Chem. 38, 423.

Holubová, L., Kyzek, S., Ďurovcová, I., Fabová, J., Horváthová, E., Ševčovičová, A., Gálová, E., 2020. Non-thermal plasma—a new green priming agent for plants? Int. J. Mol. Sci. 21, 1–16. https://doi.org/10.3390/ijms21249466

Hope, R., Aldred, D., Magan, N., 2005. Comparison of environmental profiles for growth and deoxynivalenol production by *Fusarium culmorum* and *F. graminearum* on wheat grain. Lett. Appl. Microbiol. 40, 295–300. https://doi.org/10.1111/j.1472-765X.2005.01674.x

Houbraken, J., de Vries, R.P., Samson, R.A., 2014. Modern taxonomy of biotechnologically important *Aspergillus* and *Penicillium* species, 1st ed, Advances in Applied Microbiology. Elsevier Inc. https://doi.org/10.1016/B978-0-12-800262-9.00004-4

Hu, M., Chen, S., 2021. Non-target site mechanisms of fungicide resistance in crop pathogens: A review. Microorganisms 9, 1–19. https://doi.org/10.3390/microorganisms9030502

Imboden, L., Afton, D., Trail, F., 2018. Surface interactions of *Fusarium graminearum* on barley. Mol. Plant Pathol. 19, 1332–1342. https://doi.org/10.1111/mpp.12616

James, A., Zikankuba, V.L., 2018. Mycotoxins contamination in maize alarms food safety in sub-Sahara Africa. Food Control 90, 372–381. https://doi.org/10.1016/j.foodcont.2018.03.018

Jasieniak, M., Coad, B.R., Griesser, H.J., 2015. ToF-SIMS multivariate analysis of surface-grafted small bioactive molecules. Biointerphases 10. https://doi.org/10.1116/1.4937464

Jiang, J., He, X., Li, L., Li, J., Shao, H., Xu, Q., Ye, R., Dong, Y., 2014. Effect of Cold Plasma Treatment on Seed Germination and Growth of Wheat. Plasma Sci. Technol. 16, 54–58. https://doi.org/10.1088/1009-0630/16/1/12

Kalin, M., Polajnar, M., 2013. The correlation between the surface energy, the contact angle and the spreading parameter, and their relevance for the wetting behaviour of DLC with lubricating oils. Tribol. Int. 66, 225–233. https://doi.org/10.1016/j.triboint.2013.05.007

Kamseu-Mogo, J.P., Kamgang-Youbi, G., Djepang, S.A., Tamo, B.S., Laminsi, S.,

2021. Treatment of Maize Seeds (*Zea mays*) by Nonthermal Plasma Generated by Gliding Electric Discharge for Application in Agriculture. IEEE Trans. Plasma Sci. 49, 2318–2328. https://doi.org/10.1109/TPS.2021.3094935

Kang, Y., Khan, S., Ma, X., 2009. Climate change impacts on crop yield, crop water productivity and food security - A review. Prog. Nat. Sci. 19, 1665–1674. https://doi.org/10.1016/j.pnsc.2009.08.001

Kaptso, K.G., Njintang, Y.N., Komnek, A.E., Hounhouigan, J., Scher, J., Mbofung, C.M.F., 2008. Physical properties and rehydration kinetics of two varieties of cowpea (*Vigna unguiculata*) and bambara groundnuts (*Voandzeia subterranea*) seeds. J. Food Eng. 86, 91–99. https://doi.org/10.1016/j.jfoodeng.2007.09.014

Kaur, M.A., Hüberli, D.B., Bayliss, K.L., 2020. Cold plasma: exploring a new option for management of postharvest fungal pathogens, mycotoxins and insect pests in Australian stored cereal grain. Crop Pasture Sci. 71, 715–724. https://doi.org/10.1071/CP20078

Kelly, K.M., Van Staden, J., Bell, W.E., 1992. Seed coat structure and dormancy. Plant Growth Regul. 11, 201–209. https://doi.org/10.1007/BF00024559

Keywood, M., Hibberd, M., Emmerson, K., 2016. Australia State of the Environment: Atmosphere. Canberra, Australia.

Khan, T.N., Timmerman-Vaughan, G.M., Rubiales, D., Warkentin, T.D., Siddique, K.H.M., Erskine, W., Barbetti, M.J., 2013. *Didymella pinodes* and its management in field pea: Challenges and opportunities. F. Crop. Res. 148, 61–77. https://doi.org/10.1016/j.fcr.2013.04.003

Kidd, S., Halliday, C., Alexiou, H., Ellis, D., 2016. Descriptions of medical fungi, 3rd ed. Published by the authors, Adelaide, Australia.

Kobayashi, M., Wang, Y., Kumagai, S., Uraoka, Y., Ito, T., 2020. Effects of cold atmospheric plasma irradiation on *Arabidopsis* seedlings. Jpn. J. Appl. Phys. 59. https://doi.org/10.7567/1347-4065/ab4e7b

Koenen, E.J.M., Ojeda, D.I., Bakker, F.T., Wieringa, J.J., Kidner, C., Hardy, O.J., Pennington, R.T., Herendeen, P.S., Bruneau, A., Hughes, C.E., 2021. The Origin of the Legumes is a Complex Paleopolyploid Phylogenomic Tangle Closely Associated with the Cretaceous-Paleogene (K-Pg) Mass Extinction Event. Syst. Biol. 70, 508–526. https://doi.org/10.1093/sysbio/syaa041

Kong, D., Fu, X., Jia, X., Wang, W., Li, Y., Li, J., Yang, X., Ju, C., 2020. Identification of Quantitative Trait Loci Controlling Ethylene Production in Germinating Seeds in Maize (*Zea mays* L.). Sci. Rep. 10, 1677. https://doi.org/10.1038/s41598-020-58607-1

Kopacki, M., Pawlat, J., Terebun, P., Kwiatkowski, M., Starek, A., Kiczoroski, P., 2017. Efficacy of non-thermal plasma fumigation to control fungi occurring on onion seeds, in: 2017 International Conference on Electromagnetic Devices and Processes in Environment Protection with Seminar Applications of Superconductors (ELMECO & AoS). pp. 1–4. https://doi.org/10.1109/ELMECO.2017.8267746

Kordas, L., Pusz, W., Czapka, T., Kacprzyk, R., 2015. The effect of low-temperature plasma on fungus colonization of winter wheat grain and seed quality. Polish J. Environ. Stud. 24, 433–438.

Kour, B., Kotwal, S., Dhar, M.K., Kaul, S., 2016. Genetic diversity analysis in Plantago ovata and some of its wild allies using RAPD markers. Russ. Agric. Sci. 42, 37–41. https://doi.org/10.3103/s1068367416010055

Kumar, P., Mahato, D.K., Kamle, M., Mohanta, T.K., 2017. Aflatoxins: A Global Concern for Food Safety, Human Health and Their Management. Front. Microbiol. 7, 1–10. https://doi.org/10.3389/fmicb.2016.02170

Lancashire, P.D., Bleiholder, H., Van den Boom, T., Langeluddeke, P., Stauss, R., Weber, E., Witzenberger, A., 1991. A uniform decimal code for growth stages of crops and weeds. Ann. Appl. Biol. 119, 561–601. https://doi.org/10.1111/j.1744-7348.1991.tb04895.x

Laroussi, M., 2005. Low temperature plasma-based sterilization: Overview and state-of-the-art. Plasma Process. Polym. 2, 391–400. https://doi.org/10.1002/ppap.200400078

Leplat, J., Friberg, H., Abid, M., Steinberg, C., 2013. Survival of Fusarium graminearum, the causal agent of *Fusarium* head blight. A review. Agron. Sustain. Dev. 33, 97–111. https://doi.org/10.1007/s13593-012-0098-5

Leslie, J.F., Summerell, B.A., 2006. Species Descriptions, in: The *Fusarium* Laboratory Manual. Blackwell Publishing, pp. 111–118.

Lima, S.L., Colombo, A.L., de Almeida Junior, J.N., 2019. Fungal Cell Wall: Emerging

Antifungals and Drug Resistance. Front. Microbiol. 10, 1–9. https://doi.org/10.3389/fmicb.2019.02573

Ling, L., Jiafeng, J., Jiangang, L., Minchong, S., Xin, H., Hanliang, S., Yuanhua, D., 2014. Effects of cold plasma treatment on seed germination and seedling growth of soybean. Sci. Rep. 4, 1–7. https://doi.org/10.1038/srep05859

Ling, L., Jiangang, L., Minchong, S., Chunlei, Z., Yuanhua, D., 2015. Cold plasma treatment enhances oilseed rape seed germination under drought stress. Sci. Rep. 5, 1–10. https://doi.org/10.1038/srep13033

Linkies, A., Graeber, K., Knight, C., Leubner-Metzger, G., 2010. The evolution of seeds. New Phytol. 186, 817–831. https://doi.org/10.1111/j.1469-8137.2010.03249.x

Lo Porto, C., Sergio, L., Boari, F., Logrieco, A.F., Cantore, V., 2019. Cold plasma pretreatment improves the germination of wild asparagus (*Asparagus acutifolius* L.) seeds. Sci. Hortic. (Amsterdam). 256. https://doi.org/10.1016/j.scienta.2019.108554

Lo Porto, C., Ziuzina, D., Los, A., Boehm, D., Palumbo, F., Favia, P., Tiwari, B., Bourke, P., Cullen, P.J., 2018. Plasma activated water and airborne ultrasound treatments for enhanced germination and growth of soybean. Innov. Food Sci. Emerg. Technol. 49, 13–19. https://doi.org/10.1016/j.ifset.2018.07.013

Locke, J.M., Bryce, J.H., Morris, P.C., 2000. Contrasting effects of ethylene perception and biosynthesis inhibitors on germination and seedling growth of barley (*Hordeum vulgare* L.). J. Exp. Bot. 51, 1843–1849. https://doi.org/10.1093/jexbot/51.352.1843

Lopes, M.A., Larkins, B.A., 1993. Endosperm origin, development, and function. Plant Cell 5, 1383–1399. https://doi.org/10.2307/3869790

Los, A., Ziuzina, D., Boehm, D., Bourke, P., 2020. Effects of cold plasma on wheat grain microbiome and antimicrobial efficacy against challenge pathogens and their resistance. Int. J. Food Microbiol. 335, 108889. https://doi.org/10.1016/j.ijfoodmicro.2020.108889

Los, A., Ziuzina, D., Boehm, D., Cullen, P.J., Bourke, P., 2019. Investigation of mechanisms involved in germination enhancement of wheat (*Triticum aestivum*) by cold plasma: Effects on seed surface chemistry and characteristics. Plasma

Process. Polym. 16, 1–12. https://doi.org/10.1002/ppap.201800148

Magallón, S., Hilu, K.W., Quandt, D., 2013. Land plant evolutionary timeline: Gene effects are secondary to fossil constraints in relaxed clock estimation of age and substitution rates. Am. J. Bot. 100, 556–573. https://doi.org/10.3732/ajb.1200416

Magan, N., Hope, R., Cairns, V., Aldred, D., 2003. Post-harvest fungal ecology : Impact of fungal growth and mycotoxin accumulation in stored grain. Eur. J. Plant Pathol. 109, 723–730.

Mahato, D.K., Lee, K.E., Kamle, M., Devi, S., Dewangan, K.N., Kumar, P., Kang, S.G., 2019. Aflatoxins in Food and Feed: An Overview on Prevalence, Detection and Control Strategies. Front. Microbiol. 10, 1–10. https://doi.org/10.3389/fmicb.2019.02266

Malick, K.C., Safui, B., 1985. Seed morphological studies in the Indian isubgol of commerce. Bull. Bot. Surv. India 27, 63–68. https://doi.org/10.20324/nelumbo/v27/1985/74742

Mancini, V., Romanazzi, G., 2014. Seed treatments to control seedborne fungal pathogens of vegetable crops. Pest Manag. Sci. 70, 860–868. https://doi.org/10.1002/ps.3693

Marder, L., Corbellini, V.A., Ferrão, M.F., Scroferneker, M.L., Schneider, R.D.C.D.S., 2006. Quantitative analysis of total mycotoxins in metabolic extracts of four strains of *Bipolaris sorokiniana* (*Helminthosporium sativum*). Process Biochem. 41, 177–180. https://doi.org/10.1016/j.procbio.2005.06.021

Marlett, J.A., Kajs, T.M., Fischer, M.H., 2000. An unfermented gel component of psyllium seed husk promotes laxation as a lubricant in humans. Am. J. Clin. Nutr. 72, 784–789. https://doi.org/10.1007/978-1-60327-919-2_5

Matsuoka, Y., 2005. Origin matters: Lessons from the search for the wild ancestor of maize. Breed. Sci. 55, 383–390. https://doi.org/10.1270/jsbbs.55.383

McCoy, E.C., Girard, A.E., Kornfeld, J.M., 1971. Fine structure of resting and germinating *Penicillium chrysogenum* conidiospores. Protoplasma 73, 443–456. https://doi.org/10.1007/BF01273945

McGhie, D.A., 1986. Agricultural progress on the Ord. J. Dep. Agric. West. Aust. 27, 1–4.

McKean, C., Tang, L., Tang, M., Billam, M., Wang, Z., Theodorakis, C.W., Kendall, R.J., Wang, J.S., 2006. Comparative acute and combinative toxicity of aflatoxin B1 and fumonisin B1 in animals and human cells. Food Chem. Toxicol. 44, 868–876. https://doi.org/10.1016/j.fct.2005.11.011

Medina, A., Gilbert, M.K., Mack, B.M., OBrian, G.R., Rodríguez, A., Bhatnagar, D., Payne, G., Magan, N., 2017. Interactions between water activity and temperature on the *Aspergillus flavus* transcriptome and aflatoxin B1 production. Int. J. Food Microbiol. 256, 36–44. https://doi.org/10.1016/j.ijfoodmicro.2017.05.020

Mei, Y. qin, Song, S. quan, 2008. Early Morphological and Physiological Events Occurring During Germination of Maize Seeds. Agric. Sci. China 7, 950–957. https://doi.org/10.1016/S1671-2927(08)60134-0

Mejia, D., 2003. Maize Post-harvest Operations. Rome, Italy.

Merrill, F.H., Von Hippel, A., 1939. The atomphysical interpretation of Lichtenberg figures and their application to the study of gas discharge phenomena. J. Appl. Phys. 10, 873–887. https://doi.org/10.1063/1.1707274

Mesterházy, A., Oláh, J., Popp, J., 2020. Losses in the grain supply chain: Causes and solutions. Sustainability 12, 1–18. https://doi.org/10.3390/su12062342

Miano, A.C., Augusto, P.E.D., 2018. The Hydration of Grains: A Critical Review from Description of Phenomena to Process Improvements. Compr. Rev. Food Sci. Food Saf. 17, 352–370. https://doi.org/10.1111/1541-4337.12328

Miano, A.C., Ibarz, A., Augusto, P.E.D., 2017. Ultrasound technology enhances the hydration of corn kernels without affecting their starch properties. J. Food Eng. 197, 34–43. https://doi.org/10.1016/j.jfoodeng.2016.10.024

Michl, T.D., Coad, B.R., Husler, A., Vasilev, K., Griesser, H.J., 2015. Laboratory Scale Systems for the Plasma Treatment and Coating of Particles. Plasma Process. Polym. 12, 305–313. https://doi.org/10.1002/ppap.201400141

Mikić, A., Medović, A., Jovanović, Ž., Stanisavljević, N., 2014. Integrating archaeobotany, paleogenetics and historical linguistics may cast more light onto crop domestication: The case of pea (*Pisum sativum*). Genet. Resour. Crop Evol. 61, 887–892. https://doi.org/10.1007/s10722-014-0102-9

Misra, N.N., Schlüter, O., Cullen, P.J., 2016. Plasma in Food and Agriculture, Cold

Plasma in Food and Agriculture: Fundamentals and Applications. Academic Press, Amsterdam. https://doi.org/10.1016/B978-0-12-801365-6.00001-9

Mohapatra, S., 2017. Sterilisation and disinfection, in: Prabhakar, H. (Ed.), Essentials of Neuroanethesia. New Delhi, India, pp. 929–944. https://doi.org/10.1016/B978-0-12-805299-0.00059-2

Moss, M.O., 2002. Mycotoxin review - 2. *Fusarium*. Mycologist 16, 158–161. https://doi.org/10.1017/S0269915X02004135

Muhammad, A.I., Liao, X., Cullen, P.J., Liu, D., Xiang, Q., Wang, J., Chen, S., Ye, X., Ding, T., 2018. Effects of Nonthermal Plasma Technology on Functional Food Components. Compr. Rev. Food Sci. Food Saf. 17, 1379–1394. https://doi.org/10.1111/1541-4337.12379

Muñoz, K., Vega, M., Rios, G., Geisen, R., Degen, G.H., 2011. Mycotoxin production by different ochratoxigenic *Aspergillus* and *Penicillium* species on coffee- and wheat-based media. Mycotoxin Res. 27, 239–247. https://doi.org/10.1007/s12550-011-0100-0

Murray, G., Brennan, J.P., 2012. The Current and Potential Costs from Diseases of Field Pea in Australia. Canberra, Australia.

Murray, G.M., Brennan, J.P., 2009a. The current and potential costs from diseases of wheat in Australia, The current and potential costs from diseases of wheat in Australia. Canberra, Australia.

Murray, G.M., Brennan, J.P., 2009b. The Current and Potential Costs from Diseases of Barley in Australia. Canberra, Australia.

Mutiga, S.K., Chepkwony, N., Hoekenga, O.A., Flint-Garcia, S.A., Nelson, R.J., 2019. The role of ear environment in postharvest susceptibility of maize to toxigenic *Aspergillus flavus*. Plant Breed. 138, 38–50. https://doi.org/10.1111/pbr.12672

Nelson, E.B., 2018. The seed microbiome: Origins, interactions, and impacts. Plant Soil 422, 7–34. https://doi.org/10.1007/s11104-017-3289-7

Niemann, S., Burghardt, M., Popp, C., Riederer, M., 2013. Aqueous pathways dominate permeation of solutes across *Pisum sativum* seed coats and mediate solute transport via diffusion and bulk flow of water. Plant, Cell Environ. 36, 1027–1036. https://doi.org/10.1111/pce.12035

Niemira, B.A., 2019. Regulatory status of cold plasma in food applications, Advances in Cold Plasma Applications for Food Safety and Preservation. Elsevier Inc. https://doi.org/10.1016/B978-0-12-814921-8.00013-X

Noothalapati, H., Sasaki, T., Kaino, T., Kawamukai, M., Ando, M., Hamaguchi, H.O., Yamamoto, T., 2016. Label-free Chemical Imaging of Fungal Spore Walls by Raman Microscopy and Multivariate Curve Resolution Analysis. Sci. Rep. 6, 1–10. https://doi.org/10.1038/srep27789

Nopsa, J.F.H., Daglish, G.J., Hagstrum, D.W., Leslie, J.F., Phillips, T.W., 2015. Ecological Networks in Stored Grain: Key Postharvest Nodes for Emerging Pests, Pathogens, and Mycotoxins. Bioscience 65, 985–1002. https://doi.org/10.1093/biosci/biv122

Nyvall, R.F., 1970. Chlamydospores of *Fusarium roseum* “Graminearum” as survival structures. Phytopathology 60, 1175–1177.

Ohta, T., 2016. Plasma in Agriculture, in: Cold Plasma in Food and Agriculture: Fundamentals and Applications. Elsevier Inc., pp. 205–221. https://doi.org/10.1016/B978-0-12-801365-6.00008-1

Olympus Corporation, 2018. Introduction to Surface Roughness Measurement: Roughness measurement guidebook. Olympus Corporation, Tokyo, Japan.

Ophel-Keller, K., McKay, A., Hartley, D., Herdina, Curran, J., 2008. Development of a routine DNA-based testing service for soilborne diseases in Australia. Australas. Plant Pathol. 37, 243–253. https://doi.org/10.1071/AP08029

Opretzka, J., Benedikt, J., Awakowicz, P., Wunderlich, J., Von Keudell, A., 2007. The role of chemical sputtering during plasma sterilization of *Bacillus atrophaeus*. J. Phys. D. Appl. Phys. 40, 2826–2830. https://doi.org/10.1088/0022-3727/40/9/024

Pandey, S.P., Kumar, S., Kumar, U., Chand, R., Joshi, A.K., 2005. Sources of inoculum and reappearance of spot blotch of wheat in rice-wheat cropping systems in eastern India. Eur. J. Plant Pathol. 111, 47–55. https://doi.org/10.1007/s10658-004-2404-9

Pandiselvam, R., Mayookha, V.P., Kothakota, A., Sharmila, L., Ramesh, S. V., Bharathi, C.P., Gomathy, K., Srikanth, V., 2020. Impact of Ozone Treatment on Seed Germination–A Systematic Review. Ozone Sci. Eng. 42, 331–346.

https://doi.org/10.1080/01919512.2019.1673697

Panngom, K., Lee, S.H., Park, D.H., Sim, G.B., Kim, Y.H., Uhm, H.S., Park, G., Choi, E.H., 2014. Non-thermal plasma treatment diminishes fungal viability and up-regulates resistance genes in a plant host. PLoS One 9. https://doi.org/10.1371/journal.pone.0099300

Parker, N., Schneegurt, M., Thi Tu, A.-H., Lister, P., Forster, B.M., Allen, S., Auman, A., Brelles-Marino, G., Alhadeff Feldman, M., Flowers, P., Pinchuk, G., Rowley, B., Sutherland, M., Franklund, C., Paterson, A., 2016. Microbiology. American Society for Microbiology Press & OpenStax, Washington D.C.

Pavlovich, M.J., Clark, D.S., Graves, D.B., 2014. Quantification of air plasma chemistry for surface disinfection. Plasma Sources Sci. Technol. 23. https://doi.org/10.1088/0963-0252/23/6/065036

Peleg, M., 1988. An empirical model for the description of moisture sorption curves. J. Food Sci. 53, 1216–1217.

Peng, J., Sun, D., Nevo, E., 2011. Wild emmer wheat, *Triticum dicoccoides*, occupies a pivotal position in wheat domestication process. Aust. J. Crop Sci. 5, 1127–1143.

Peťková, M., Švubová, R., Kyzek, S., Medvecká, V., Slováková, L., Ševčovičová, A., Gálová, E., 2021. The effects of cold atmospheric pressure plasma on germination parameters, enzyme activities and induction of DNA damage in barley. Int. J. Mol. Sci. 22, 1–16. https://doi.org/10.3390/ijms22062833

Phan, J.L., Cowley, J.M., Neumann, K.A., Herliana, L., O'Donovan, L.A., Burton, R.A., 2020. The novel features of *Plantago ovata* seed mucilage accumulation, storage and release. Sci. Rep. 10, 1–14. https://doi.org/10.1038/s41598-020-68685-w

Pingali, P., 2015. Agricultural policy and nutrition outcomes – getting beyond the preoccupation with staple grains. Food Secur. 7, 583–591. https://doi.org/10.1007/s12571-015-0461-x

Pitt, J.I., Wild, C.P., Baan, R.A., Gelderblom, W.C.A., Miller, J.D., Riley, R.T., Wu, F., 2012. IARC Scientific Publication No. 158: Improving public health through mycotoxin control. World Health Organization, Lyon, France.

Ponts, N., 2015. Mycotoxins are a component of *Fusarium graminearum* stress-

response system. Front. Microbiol. 6, 1–5. https://doi.org/10.3389/fmicb.2015.01234

Puac, N., Gherardi, M., Shiratani, M., 2018. Plasma agriculture: A rapidly emerging field. Plasma Process. Polym. 15, 1–5. https://doi.org/10.1002/ppap.201700174

Puligundla, P., Kim, J.W., Mok, C., 2017. Effect of corona discharge plasma jet treatment on decontamination and sprouting of rapeseed (*Brassica napus* L.) seeds. Food Control 71, 376–382. https://doi.org/10.1016/j.foodcont.2016.07.021

Puligundla, P., Mok, C., 2019. Microwave- and radio-frequency-powered cold plasma applications for food safety and preservation, Advances in Cold Plasma Applications for Food Safety and Preservation. Elsevier Inc. https://doi.org/10.1016/B978-0-12-814921-8.00011-6

Punithalingham, E., Gibson, I.A.S., 1976. *Phoma medicaginis*. Commonw. Med. Inst. Descr. Pathog. fungi Bact. 5.

Qin, Y., Jiang, W., Li, A., Gao, M., Liu, H., Gao, Y., Tian, X., Gong, G., 2021. The combination of paraformaldehyde and glutaraldehyde is a potential fixative for mitochondria. Biomolecules 11, 1–14. https://doi.org/10.3390/biom11050711

Raballand, V., Benedikt, J., Wunderlich, J., Von Keudell, A., 2008. Inactivation of *Bacillus atrophaeus* and of *Aspergillus niger* using beams of argon ions, of oxygen molecules and of oxygen atoms. J. Phys. D. Appl. Phys. 41. https://doi.org/10.1088/0022-3727/41/11/115207

Rajjou, L., Duval, M., Gallardo, K., Catusse, J., Bally, J., Job, C., Job, D., 2012. Seed germination and vigor. Annu. Rev. Plant Biol. 63, 507–533. https://doi.org/10.1146/annurev-arplant-042811-105550

Ramirez, M.L., Chulze, S., Magan, N., 2004. Impact of environmental factors and fungicides on growth and deoxinivalenol production by *Fusarium graminearum* isolates from Argentinian wheat. Crop Prot. 23, 117–125. https://doi.org/10.1016/j.cropro.2003.07.005

Ranum, P., Peña-Rosas, J.P., Garcia-Casal, M.N., 2014. Global maize production, utilization, and consumption. Ann. N. Y. Acad. Sci. 1312, 105–112. https://doi.org/10.1111/nyas.12396

Rathjen, J.R., 2006. Role of the Seed Coat in the Dormancy of Wheat (*Triticum*

aestivum) Grains. University of Adelaide.

Rathjen, J.R., Strounina, E. V., Mares, D.J., 2009. Water movement into dormant and non-dormant wheat (*Triticum aestivum* L.) grains. J. Exp. Bot. 60, 1619–1631. https://doi.org/10.1093/jxb/erp037

Reiss, J., 1977. Mycotoxins in foodstuffs x production of citrinin by *Penicillium chrysogenum* in bread. Cosmet. Toxicol. 15, 303–307.

Renaissance Chemicals, 2021. SCRI Renaissance Stain 2200 [WWW Document]. URL http://renchem.co.uk/index.php/specialty-chemicals-division/item/48-selected-fluorescent-dyes-and-brighteners-for-microscopists (accessed 8.3.21).

Reponen, T., Grinshpun, S.A., Conwell, K.L., Wiest, J., Anderson, M., 2001. Aerodynamic versus physical size of spores: Measurement and implication for respiratory deposition. Grana 40, 119–125. https://doi.org/10.1080/00173130152625851

Robert, V., Vu, D., Amor, A.B.H., van de Wiele, N., Brouwer, C., Jabas, B., Szoke, S., Dridi, A., Triki, M., Daoud, S. ben, Chouchen, O., Vaas, L., de Cock, A., Stalpers, J.A., Stalpers, D., Verkley, G.J.M., Groenewald, M., dos Santos, F.B., Stegehuis, G., Li, W., Wu, L., Zhang, R., Ma, J., Zhou, M., Gorjón, S.P., Eurwilaichitr, L., Ingsriswang, S., Hansen, K., Schoch, C., Robbertse, B., Irinyi, L., Meyer, W., Cardinali, G., Hawksworth, D.L., Taylor, J.W., Crous, P.W., 2013. MycoBank gearing up for new horizons. IMA Fungus 4, 371–379. https://doi.org/10.5598/imafungus.2013.04.02.16

Rogawansamy, S., Gaskin, S., Taylor, M., Pisaniello, D., 2015. An evaluation of antifungal agents for the treatment of fungal contamination in indoor air environments. Int. J. Environ. Res. Public Health 12, 6319–6332. https://doi.org/10.3390/ijerph120606319

Romão, B., Falcomer, A.L., Palos, G., Cavalcante, S., Botelho, R.B.A., Nakano, E.Y., Raposo, A., Shakeel, F., Alshehri, S., Mahdi, W.A., Zandonadi, R.P., 2021. Glycemic index of gluten-free bread and their main ingredients: A systematic review and meta-analysis. Foods 10, 1–22. https://doi.org/10.3390/foods10030506

Ropejko, K., Twarużek, M., 2021. Zearalenone and Its Metabolites-General Overview, Occurrence, and Toxicity. Toxins (Basel). 13, 1–12.

https://doi.org/10.3390/toxins13010035

Rossi, F., Kylián, O., Rauscher, H., Hasiwa, M., Gilliland, D., 2009. Low pressure plasma discharges for the sterilization and decontamination of surfaces. New J. Phys. 11. https://doi.org/10.1088/1367-2630/11/11/115017

Russin, J.S., Guo, B.Z., Tubajika, K.M., Brown, R.L., Cleveland, T.E., Widstrom, N.W., 1997. Comparison of kernel wax from corn genotypes resistant or susceptible to *Aspergillus flavus*. Phytopathology 87, 529–533. https://doi.org/10.1094/PHYTO.1997.87.5.529

Sanderson, M.J., Thorne, J.L., Wikström, N., Bremer, K., 2004. Molecular evidence on plant divergence times. Am. J. Bot. 91, 1656–1665. https://doi.org/10.3732/ajb.91.10.1656

Savary, S., Willocquet, L., Pethybridge, S.J., Esker, P., McRoberts, N., Nelson, A., 2019. The global burden of pathogens and pests on major food crops. Nat. Ecol. Evol. 3, 430–439. https://doi.org/10.1038/s41559-018-0793-y

Schabereiter-Gurtner, C., Lubitz, W., Rölleke, S., 2003. Application of broad-range 16S rRNA PCR amplification and DGGE fingerprinting for detection of tick-infecting bacteria. J. Microbiol. Methods 52, 251–260. https://doi.org/10.1016/S0167-7012(02)00186-0

Schaller, G.E., Binder, B.M., 2017. Inhibitors of Ethylene Biosynthesis and Signaling, in: Binder, B.M., Schaller, G.E. (Eds.), Methods in Molecular Biology: Ethylene Signaling Methods and Protocols. Springer Nature, New York, pp. 223–235. https://doi.org/10.1007/978-1-4939-6854-1

Scherrer, D., Bragger, U., Ferrari, M., Mocker, A., Joda, T., 2020. In-vitro polishing of CAD/CAM ceramic restorations: An evaluation with SEM and confocal profilometry. J. Mech. Behav. Biomed. Mater. 107. https://doi.org/10.1016/j.jmbbm.2020.103761

Schoch, C.L., Ciufo, S., Domrachev, M., Hotton, C.L., Kannan, S., Khovanskaya, R., Leipe, D., Mcveigh, R., O'Neill, K., Robbertse, B., Sharma, S., Soussov, V., Sullivan, J.P., Sun, L., Turner, S., Karsch-Mizrachi, I., 2020. NCBI Taxonomy: a comprehensive update on curation, resources and tools. [WWW Document]. Database (Oxford). URL https://www.ncbi.nlm.nih.gov/Taxonomy/Browser/wwwtax.cgi (accessed

11.16.21).

Scholtz, V., Pazlarova, J., Souskova, H., Khun, J., Julak, J., 2015. Nonthermal plasma - A tool for decontamination and disinfection. Biotechnol. Adv. 33, 1108–1119. https://doi.org/10.1016/j.biotechadv.2015.01.002

Scholtz, V., Šerá, B., Khun, J., Šerý, M., Julák, J., 2019. Effects of Nonthermal Plasma on Wheat Grains and Products. J. Food Qual. https://doi.org/10.1155/2019/7917825

Selcuk, M., Oksuz, L., Basaran, P., 2008. Decontamination of grains and legumes infected with *Aspergillus* spp. and *Penicillum* spp. by cold plasma treatment. Bioresour. Technol. 99, 5104–5109. https://doi.org/10.1016/j.biortech.2007.09.076

Šerá, B., Gajdová, I., Černák, M., Gavril, B., Hnatiuc, E., Kováčik, D., Kříha, V., Sláma, J., Šerý, M., Špatenka, P., 2012. How various plasma sources may affect seed germination and growth. Proc. Int. Conf. Optim. Electr. Electron. Equipment, OPTIM 1365–1370. https://doi.org/10.1109/OPTIM.2012.6231880

Šerá, B., Sery, M., Gavril, B., Gajdova, I., 2017. Seed Germination and Early Growth Responses to Seed Pre-treatment by Non-thermal Plasma in Hemp Cultivars (*Cannabis sativa* L.). Plasma Chem. Plasma Process. 37, 207–221. https://doi.org/10.1007/s11090-016-9763-9

Šerá, B., Špatenka, P., Šerý, M., Hrušková, I., Materials, A.S., 2010. Influence of Plasma Treatment on Wheat and Oat Germination and Early Growth. IEEE Trans. Plasma Sci. 38, 2963–2968. https://doi.org/10.1109/TPS.2010.2060728

Shapira, Y., Chaniel, G., Bormashenko, E., 2018. Surface charging by the cold plasma discharge of lentil and pepper seeds in comparison with polymers. Colloids Surfaces B Biointerfaces 172, 541–544. https://doi.org/10.1016/j.colsurfb.2018.09.004

Sharma, N., Bhandari, A.S., 2014. Management of Pathogens of Stored Cereal Grains, in: Lichtfouse, E. (Ed.), Sustainable Agriculture Reviews. Springer International Publishing, Cham, Switzerland, pp. 87–107. https://doi.org/10.1007/978-3-319-00915-5

Shen-Miller, J., Mudgett, M.B., Schopf, J.W., Clarke, S., Berger, R., 1995. Exceptional seed longevity and robust growth: ancient Sacred Lotus from China.

Am. J. Bot. 82, 1367–1380. https://doi.org/10.1002/j.1537-2197.1995.tb12673.x

Shigenaga, M.K., Ames, B.N., 1991. Assays for 8-hydroxy-2′-deoxyguanosine: A biomarker of in vivo oxidative DNA damage. Free Radic. Biol. Med. 10, 211–216. https://doi.org/10.1016/0891-5849(91)90078-H

Shimizu, S., Barczyk, S., Rettberg, P., Shimizu, T., Klaempfl, T., Zimmermann, J.L., Hoeschen, T., Linsmeier, C., Weber, P., Morfill, G.E., Thomas, H.M., 2014. Cold atmospheric plasma - A new technology for spacecraft component decontamination. Planet. Space Sci. 90, 60–71. https://doi.org/10.1016/j.pss.2013.10.008

Siddique, S.S., Hardy, G.E.S.J., Bayliss, K.L., 2018. Cold plasma : a potential new method to manage postharvest diseases caused by fungal plant pathogens. Plant Pathol. 67, 1011–1021. https://doi.org/10.1111/ppa.12825

Simpson, M.G., 2019. Plant Embryology. Plant Syst. 567–582. https://doi.org/10.1016/b978-0-12-812628-8.50011-0

Singh, P., Chauhan, M., 2013. Influence of environmental factors on the growth of building deteriorating fungi: *Aspergillus flavus* and *Penicillium chrysogenum*. Intrenational J. pharmceutical Sci. Res. 4, 425–429.

Singh, R., Prasad, P., Mohan, R., Verma, M.K., Kumar, B., 2019. Radiofrequency cold plasma treatment enhances seed germination and seedling growth in variety CIM-Saumya of sweet basil (*Ocimum basilicum* L.). J. Appl. Res. Med. Aromat. Plants 12, 78–81. https://doi.org/10.1016/j.jarmap.2018.11.005

Sistani, N.R., Kaul, H.P., Desalegn, G., Wienkoop, S., 2017. Rhizobium impacts on seed productivity, quality, and protection of pisum sativum upon disease stress caused by didymella pinodes: Phenotypic, proteomic, and metabolomic traits. Front. Plant Sci. 8. https://doi.org/10.3389/fpls.2017.01961

Sitton, J.W., Cook, R.J., 1981. Comparative morphology and survival of chlamydospores of *Fusarium roseum* “Culmorum” and “Graminearum.” Ecol. Epidemiol. 71, 85–90.

Sivachandiran, L., Khacef, A., 2017. Enhanced seed germination and plant growth by atmospheric pressure cold air plasma: combined effect of seed and water treatment. RSC Adv. 7, 1822–1832. https://doi.org/10.1039/c6ra24762h

Smith, H.M.M., 1971. History of Plasmas. Nature 233, 1971.

Sobrova, P., Adam, V., Vasatkova, A., Beklova, M., Zeman, L., Kizek, R., 2010. Deoxynivalenol and its toxicity. Interdiscip. Toxicol. 3, 94–99. https://doi.org/10.2478/v10102-010-0019-x

Solanki, M.K., Abdelfattah, A., Britzi, M., Zakin, V., Wisniewski, M., Droby, S., Sionov, E., 2019. Shifts in the composition of the microbiota of stored wheat grains in response to fumigation. Front. Microbiol. 10, 1–13. https://doi.org/10.3389/fmicb.2019.01098

Song, H.P., Litchfield, J.B., Morris, H.D., 1992. Three-dimensional microscopic MRI of maize kernels during drying. J. Agric. Eng. Res. 53, 51–69. https://doi.org/10.1016/0021-8634(92)80073-2

Steeves, T.A., 1983. The evolution and biological significance of seeds. Can. J. Bot. 61, 3550–3560. https://doi.org/10.1139/b83-404

Štěpánová, V., Slavíček, P., Kelar, J., Prášil, J., Smékal, M., Stupavská, M., Jurmanová, J., Černák, M., 2018. Atmospheric pressure plasma treatment of agricultural seeds of cucumber (*Cucumis sativus* L.) and pepper (*Capsicum annuum* L.) with effect on reduction of diseases and germination improvement. Plasma Process. Polym. 15, 1–9. https://doi.org/10.1002/ppap.201700076

Stolárik, T., Henselová, M., Martinka, M., Novák, O., Zahoranová, A., Černák, M., 2015. Effect of Low-Temperature Plasma on the Structure of Seeds, Growth and Metabolism of Endogenous Phytohormones in Pea (*Pisum sativum* L.). Plasma Chem. Plasma Process. 35, 659–676. https://doi.org/10.1007/s11090-015-9627-8

Strange, R.N., Scott, P.R., 2005. Plant disease: A threat to global food security. Annu. Rev. Phytopathol. 43, 83–116. https://doi.org/10.1146/annurev.phyto.43.113004.133839

Strömberg, C.A.E., 2011. Evolution of grasses and grassland ecosystems. Annu. Rev. Earth Planet. Sci. 39, 517–544. https://doi.org/10.1146/annurev-earth-040809-152402

Stukenbrock, E.H., McDonald, B.A., 2008. The origins of plant pathogens in agro-ecosystems. Annu. Rev. Phytopathol. 46, 75–100. https://doi.org/10.1146/annurev.phyto.010708.154114

Sultana, S., Adhikary, S.K., Islam, M.M., Rahman, S.M.M., 2018. Evaluation of

pathogenic variability based on leaf blotch disease development components of *Bipolaris sorokiniana* in *Triticum aestivum* and agroclimatic origin. Plant Pathol. J. 34, 93–103. https://doi.org/10.5423/PPJ.OA.08.2017.0175

Sun, M., Tuan, P.A., Izydorczyk, M.S., Ayele, B.T., 2020. Ethylene regulates post-germination seedling growth in wheat through spatial and temporal modulation of ABA / GA balance 71, 1985–2004. https://doi.org/10.1093/jxb/erz566

Švubová, R., Kyzek, S., Medvecká, V., Slováková, Ľ., Gálová, E., Zahoranová, A., 2020. Novel insight at the Effect of Cold Atmospheric Pressure Plasma on the Activity of Enzymes Essential for the Germination of Pea (*Pisum sativum* L. cv. Prophet) Seeds. Plasma Chem. Plasma Process. 40, 1221–1240. https://doi.org/10.1007/s11090-020-10089-9

Sweeney, M.J., Dobson, A.D.W., 1998. Mycotoxin production by *Aspergillus*, *Fusarium* and *Penicillium* species. Int. J. Food Microbiol. 43, 141–158. https://doi.org/10.1016/S0168-1605(98)00112-3

Thompson, M.E.H., Raizada, M.N., 2018. Fungal pathogens of Maize gaining free passage along the silk road. Pathogens 7. https://doi.org/10.3390/pathogens7040081

Tirumalai, M.R., Stepanov, V.G., Wünsche, A., Montazari, S., Gonzalez, R.O., Venkateswaran, K., Fox, G.E., 2018. *Bacillus safensis* FO-36b and *Bacillus pumilus* SAFR-032 : a whole genome comparison of two spacecraft assembly facility isolates. BMC Microbiol. 18, 1–16. https://doi.org/10.1186/s12866-018-1191-y

Tomeková, J., Kyzek, S., Medvecká, V., Gálová, E., Zahoranová, A., 2020. Influence of Cold Atmospheric Pressure Plasma on Pea Seeds: DNA Damage of Seedlings and Optical Diagnostics of Plasma. Plasma Chem. Plasma Process. 40, 1571–1584. https://doi.org/10.1007/s11090-020-10109-8

Torres, A.M., Palacios, S.A., Yerkovich, N., Palazzini, J.M., Battilani, P., Leslie, J.F., Logrieco, A.F., Chulze, S.N., 2019. *Fusarium* head blight and mycotoxins in wheat: Prevention and control strategies across the food chain. World Mycotoxin J. 12, 333–355. https://doi.org/10.3920/WMJ2019.2438

Tran, H.S., You, M.P., Khan, T.N., Barbetti, M.J., 2016. Pea black spot disease complex on field pea: dissecting the roles of the different pathogens in causing

epicotyl and root disease. Eur. J. Plant Pathol. 144, 595–605. https://doi.org/10.1007/s10658-015-0798-1

Tucker, M.L., Kim, J., Wen, C.-K., 2017. Treatment of Plants with Gaseous Ethylene and Gaseous Inhibitors of Ethylene Action, in: Binder, B.M., Schaller, G.E. (Eds.), Methods in Molecular Biology: Ethylene Signaling Methods and Protocols. Springer Nature, New York, pp. 27–39. https://doi.org/10.1007/978-1-4939-6854-1

Ul-Hamid, A., 2018. A beginners guide to scanning electron microscopy. Springer Nature Switzerland, Cham, Switzerland. https://doi.org/10.1007/978-3-319-98482-7

Umesha, S., Marichenne, H., Chandrasekhar, B., Shivakumara, P., Kumar, J.S., Raghava, S., Avinash, P., Shirin, M., Bharathi, T.R., Rajini, S.B., Nandhini, M., Rani, V., Shobha, M., Prakash, H.S., 2016. Aflatoxins and food pathogens : impact of biologically active aflatoxins and their control strategies. J. Sci. Food Agric. 97, 1698–1707. https://doi.org/10.1002/jsfa.8144

UN, 2021. Progress towards the Sustainable Development Goals: Report of the Secretary-General. New York.

UN, G.A., 2015. Transforming our world: the 2030 Agenda for Sustainable Development. New York, United Nations.

van der Lee, T., Zhang, H., van Diepeningen, A., Waalwijk, C., 2015. Biogeography of *Fusarium graminearum* species complex and chemotypes: a review. Food Addit. Contam. - Part A 32, 453–460. https://doi.org/10.1080/19440049.2014.984244

Van Dongen, J.T., Ammerlaan, A.M.H., Wouterlood, M., Van Aelst, A.C., Borstlap, A.C., 2003. Structure of the developing pea seed coat and the post-phloem transport pathway of nutrients. Ann. Bot. 91, 729–737. https://doi.org/10.1093/aob/mcg066

Varga, J., Frisvad, J.C., Samson, R.A., 2011. Two new aflatoxin producing species, and an overview of *Aspergillus* section Flavi. Stud. Mycol. 69, 57–80. https://doi.org/10.3114/sim.2011.69.05

Verma, A.K., Gautam, N., Bharti, K.A., 2017. Macro and micro-morphological characteristics of Plantago seeds and its implication for species identification.

Curr. Bot. 8, 159–163. https://doi.org/10.19071/cb.2017.v8.3243

Von Keudell, A., Schulz-Von Der Gathen, V., 2017. Foundations of low-temperature plasma physics - An introduction. Plasma Sources Sci. Technol. 26. https://doi.org/10.1088/1361-6595/aa8d4c

Wang, Y., Diao, P., Kong, L., Yu, R., Zhang, M., 2020. Ethylene Enhances Seed Germination and Seedling Growth Under Salinity by Reducing Oxidative Stress and Promoting Chlorophyll Content via ETR2 Pathway. Front. Plant Sci. 11, 1–14. https://doi.org/10.3389/fpls.2020.01066

Wang, Y.L., Ye, H., Liu, L., Wu, J.H., Ru, W.M., Sun, G.L., 2019. Molecular Insights on the Domestication of Barley (*Hordeum vulgare* L.). CRC. Crit. Rev. Plant Sci. 38, 280–294. https://doi.org/10.1080/07352689.2019.1658856

Wang, Z.A., Li, L.X., Doering, T.L., 2018. Unraveling synthesis of the cryptococcal cell wall and capsule. Glycobiology 28, 719–730. https://doi.org/10.1093/glycob/cwy030

Wargenau, A., Fleißner, A., Bolten, C.J., Rohde, M., Kampen, I., Kwade, A., 2011. On the origin of the electrostatic surface potential of *Aspergillus niger* spores in acidic environments. Res. Microbiol. 162. https://doi.org/10.1016/j.resmic.2011.07.006

Watanabe, T., 2010. Pictorial Atlas of Soil and Seed Fungi, 3rd ed. CRC Press. https://doi.org/10.1201/ebk1439804193

Wei, D., Frankel Davis, K., 2021. Culturally appropriate shifts in staple grain consumption can improve multiple sustainability outcomes. Environ. Res. Lett. 16. https://doi.org/https://doi.org/10.1088/1748-9326/ac32fc

Weisburg, W.G., Barns, S.M., Pelletier, D.A., Lane, D.J., 1991. 16S ribosomal DNA amplification for phylogenetic study. J. Bacteriol. 173, 697–703. https://doi.org/10.1128/jb.173.2.697-703.1991

Wenzel, R.N., 1949. Surface Roughness and Contact Angle. J. Phys. Chem. 53, 1466–1467. https://doi.org/10.1021/j150474a015

Werker, E., 1997. Seed Anatomy, Encyclopaedia of plant anatomy Bd. 10. Gebrüder Borntraeger, Berlin, Germany. https://doi.org/10.2307/1223825

Werker, E., Marbach, I., Mayer, A.M., 1979. Relation between the anatomy of the

testa, water permeability and the presence of phenolics in the genus Pisum. Ann. Bot. 43, 765–771. https://doi.org/10.1093/oxfordjournals.aob.a085691

WFO, 2021. World Flora Online [WWW Document]. URL http://www.worldfloraonline.org/

White, P.J., Broadley, M.R., El-Serehy, H.A., George, T.S., Neugebauer, K., 2018. Linear relationships between shoot magnesium and calcium concentrations among angiosperm species are associated with cell wall chemistry. Ann. Bot. 122, 221–226. https://doi.org/10.1093/aob/mcy062

Whitehead, J.C., 2016. The Chemistry of Cold Plasma, Cold Plasma in Food and Agriculture: Fundamentals and Applications. Elsevier Inc. https://doi.org/10.1016/B978-0-12-801365-6.00003-2

Wilczek, S., Schulze, J., Brinkmann, R.P., Donkó, Z., Trieschmann, J., Mussenbrock, T., 2020. Electron dynamics in low pressure capacitively coupled radio frequency discharges. J. Appl. Phys. 127. https://doi.org/10.1063/5.0003114

Wilson, C., Lukowicz, R., Merchant, S., Valquier-Flynn, H., Caballero, J., Sandoval, J., Okuom, M., Huber, C., Durham Brooks, T., Clement, B., Wentworth, C.D., Holmes, A.E., 2017. Quantitative and Qualitative Assessment Methods for Biofilm Growth: A Mini-review. Res Rev J Eng Technol. 6.

Wrigley, C., 2017. Cereal-Grain Morphology and Composition, Second Edi. ed, Cereal Grains: Assessing and Managing Quality: Second Edition. Elsevier Ltd. https://doi.org/10.1016/B978-0-08-100719-8.00004-8

Yamauchi, Y., Kuzuya, M., Sasai, Y., Kondo, S. ichi, 2012. Surface treatment of natural polymer by plasma technique-promotion of seed germination. J. Photopolym. Sci. Technol. 25, 535–538. https://doi.org/10.2494/photopolymer.25.535

Yang, F., Jacobsen, S., Jørgensen, H.J.L., Collinge, D.B., Svensson, B., Finnie, C., 2013. *Fusarium graminearum* and its interactions with cereal heads: Studies in the proteomics era. Front. Plant Sci. 4, 1–8. https://doi.org/10.3389/fpls.2013.00037

Yu, L., Yakubov, G.E., Zeng, W., Xing, X., Stenson, J., Bulone, V., Stokes, J.R., 2017. Multi-layer mucilage of *Plantago ovata* seeds: Rheological differences arise from variations in arabinoxylan side chains. Carbohydr. Polym. 165, 132–

141. https://doi.org/10.1016/j.carbpol.2017.02.038

Zablatzká, L., Balarynová, J., Klčová, B., Kopecký, P., Smýkal, P., 2021. Anatomy and histochemistry of seed coat development of wild (*Pisum sativum* subsp. *elatius* (m. bieb.) Asch. et Graebn. and domesticated pea (*Pisum sativum* subsp. *sativum* l.). Int. J. Mol. Sci. 22. https://doi.org/10.3390/ijms22094602

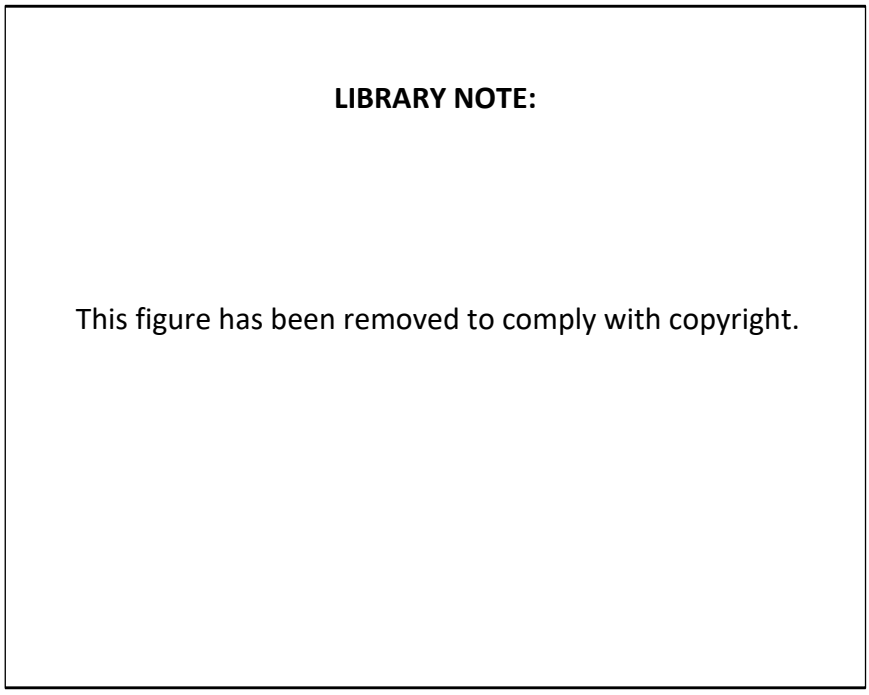
Zhou, M.X., 2009. Barley production and consumption, in: Zhang, G., Li, C. (Eds.), Genetics and Improvement of Barley Malt Quality. Springer Berlin Heidelberg, Berlin, Germany, pp. 1–17.

Zhou, Renwu, Li, J., Zhou, Rusen, Zhang, X., Yang, S., 2019. Atmospheric-pressure plasma treated water for seed germination and seedling growth of mung bean and its sterilization effect on mung bean sprouts. Innov. Food Sci. Emerg. Technol. 53, 36–44. https://doi.org/10.1016/j.ifset.2018.08.006

Appendices

S1 Supplementary information for Chapter 4.2.3

Equations and figures have been extracted from the Olympus Corporation Surface Roughness Guidebook, Olympus Corporation, 2018. These figures provide more detail regarding the equations used within Chapter 4.2.3.



S2 Supplementary information for Chapter 5.4.2.4.2.1

ITS sequence for *Penicillium chrysogenum*; 505 kb Q20 bases;7708 signal sequence intensity

TAGGGACAGAGTGGCGGGCCCCACTGCGGGTCNAACCTTCCCACCCGTGTATC
ATTTACCTTGTTGCTTCGGCGGGCCCGCCTTAACTGGCCGCCGGGGGGCTTAC
GCCCCCGGGCCCGCGCCCGCCGAAGACACCCTCGAACTCTGTCTGAAGATTGT
AGTCTGAGTGAAAATATAAATTATTTAAAACTTTCAACAACGGATCTCTTGGTTCC
GGCATCGATGAAGAACGCAGCGAAATGCGATACGTAATGTGAATTGCAAATTCA
GTGAATCATCGAGTCTTTGAACGCACATTGCGCCCCCTGGTATTCCGGGGGGC
ATGCCTGTCCGAGCGTCATTGCTGCCCTCAAGCACGGCTTGTGTGTTGGGCCC
CGTCCTCCGATCCCGGGGGACGGGCCCGAAAGGCAGCGGCGGCACCGCGTC
CGGTCCTCGAGCGTATGGGGCTTTGTCACCCGCTCTGTAGGCCCGGCCGGCG
CTTGCCGATCAACCCAAATTTTTATCCAGGTTGACCTCGGATCAGGTAGGGATA
CCCGCTGATTAAAAACCATATAN

S3 Supplementary information for Chapter 5.4.2.8

Table of dilutions performed for all biological replicates within each treatment described. Abbreviations: U (Untreated control); T+V (tumbler + vacuum); P15 (15-minute plasma); P30 (30-minute plasma); P45 (45-minute plasma); P60 (60-minute plasma); P75 (75-minute plasma); P90 (90-minute plasma).

Pathogen/ Host	**Experiment Number**	**Treatment**	**Dilutions**
***Penicillium chrysogenum*/Field Pea**	1	U	(1/2000), (1/10000)
		T+V	(1/2000), (1/10000)
		P15	(1/1000), (1/2000)
		P30	(1/1000), (1/2000)
		P45	(1/500), (1/1000)
		P60	(1/500), (1/1000)
		P75	(1/100), (1/500)
		P90	(1/100), (1/500)
	2	U	(1/5000), (1/10000)
		T+V	(1/1000), (1/2000)
		P15	(1/1000), (1/2000)
		P30	(1/500), (1/1000)
		P45	(1/250), (1/500)
		P60	(1/100), (1/200)
		P75	(1/10), (1/100)
		P90	neat, (1/10), (1/100)
	3	U	(1/5000), (1/10000), (1/20000)
		T+V	(1/100), (1/1000), (1/2000)
		P15	(1/100), (1/1000), (1/2000)
		P30	neat, (1/10), (1/100)
		P45	neat, (1/10)
		P60	neat, (1/10)
		P75	neat, (1/10)
		P90	neat, (1/10)
***Aspergillus flavus*/maize**	1	U	(1/1000), (1/2000)
		P15	(1/1000), (1/2000)
		P30	(1/1000), (1/2000)
		P45	(1/1000), (1/2000)
		P60	(1/1000), (1/2000)
		P75	(1/1000), (1/2000)
		P90	(1/1000), (1/2000)
		P105	(1/1000)
	2	U	(1/100), (1/1000), (1/2000)
		P15	(1/100), (1/1000), (1/2000)
		P30	(1/100), (1/1000), (1/2000)
		P45	(1/100), (1/1000), (1/2000)
		P60	(1/100), (1/1000), (1/2000)
		P75	(1/100), (1/1000), (1/2000)

		P90	(1/100), (1/1000), (1/2000)
		P105	(1/100)
	3	U	(1/100), (1/500), (1/1000), (1/2000)
		P15	(1/100), (1/500), (1/1000)
		P30	(1/100), (1/500), (1/1000)
		P45	(1/100), (1/500), (1/1000)
		P60	(1/100), (1/500), (1/1000)
		P75	(1/100), (1/500), (1/1000)
		P90	(1/100), (1/500), (1/1000)
		P105	(1/100)

S4 Supplementary information for Chapter 5.4.3.3.1

Field pea inoculated with *Penicillium chrysogenum* Experiment 3 Tukey's multiple comparisons test vs Welch's t-tests. Abbreviations: T+V (tumbler + vacuum); P15 (15-minute plasma); P30 (30-minute plasma); P45 (45-minute plasma); P60 (60-minute plasma); P75 (75-minute plasma); P90 (90-minute plasma).

Field pea/*Penicillium* spp.	**Tukey's multiple comparisons test**		**Welch's t test**	
Experiment 3	**Summary**	**Adjusted P Value**	**Summary**	**Adjusted P Value**
Untreated vs. T+V	****	<0.0001	**	0.0079
Untreated vs. P15	****	<0.0001		
Untreated vs. P30	****	<0.0001		
Untreated vs. P45	****	<0.0001		
Untreated vs. P60	****	<0.0001		
Untreated vs. P75	****	<0.0001		
Untreated vs. P90	****	<0.0001		
T+V vs. P15	ns	0.9376	*	0.03
T+V vs. P30	ns	0.7898		
T+V vs. P45	ns	0.7891		
T+V vs. P60	ns	0.789		
T+V vs. P75	ns	0.789		
T+V vs. P90	ns	0.789		
P15 vs. P30	ns	>0.9999	*	0.0126
P15 vs. P45	ns	>0.9999		
P15 vs. P60	ns	>0.9999		
15 min Plasma vs. P75	ns	>0.9999		
P15 vs. P90	ns	>0.9999		
P30 vs. P45	ns	>0.9999	ns	0.0518
P30 vs. P60	ns	>0.9999		
P30 vs. P75	ns	>0.9999		
P30 vs. P90	ns	>0.9999		
P45 vs. P60	ns	>0.9999	ns	0.1055
P45 vs. P75	ns	>0.9999		
P45 vs. P90	ns	>0.9999		
P60 vs. P75	ns	>0.9999	ns	0.1937
P60 vs. P90	ns	>0.9999		
P75 vs. P90	ns	>0.9999	ns	0.7586

S5 Supplementary information for Chapter 5.5.2.6

Table of dilutions performed for all biological replicates within each treatment described. Note that unlike the plasma exposure time series dilutions described in Appendix S2, the same dilutions were performed for both Untreated and P90 treatments.

Pathogen/Host	Experiment Number	Dilutions
***Aspergillus flavus*/maize**	1	(1/500), (1/1000), (1/2000)
	2	(1/500), (1/1000), (1/2000)
	3	(1/500), (1/1000), (1/2000)
***Bipolaris sorokiniana*/ barley**	1	(1/10), (1/100), (1/200)
	2	(1/100), (1/200), (1/500)
	3	(1/10), (1/100), (1/200)
***Didymella pinodes*/ field pea**	1	(1/500), (1/1000), (1/5000)
	2	(1/500), (1/1000), (1/5000)
	3	(1/500), (1/1000), (1/5000)
***Fusarium graminearum*/ wheat**	1	neat (1/10)
	2	neat (1/10)
	3	neat (1/10)
***Penicillium chrysogenum*/ psyllium**	1	(1/1000), (1/5000), (1/10000)
	2	(1/1000), (1/5000), (1/10000)
	3	(1/1000), (1/5000), (1/10000)

S6 Supplementary information for Chapter 6.2.3

Two-way ANOVA table with Tukey's multiple comparisons for contact angle measurements. Abbreviations: T+V (tumbler + vacuum); P15 (15-minute plasma); P30 (30-minute plasma).

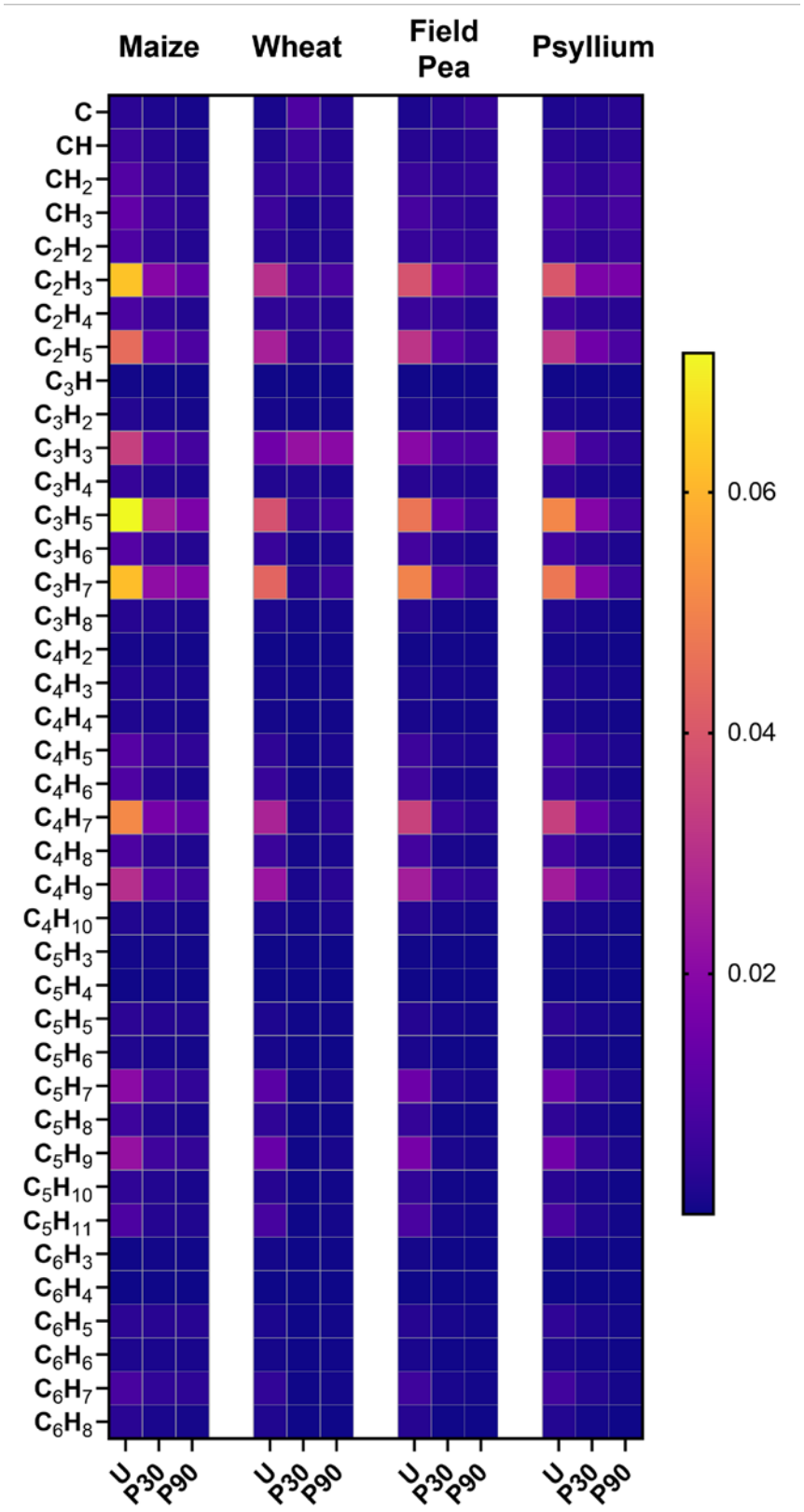
Two-way ANOVA	Ordinary				
Alpha	0.05				
Source of Variation	% of total variation	P value	P value summary	Significant?	
Interaction	3.102	<0.0001	****	Yes	
Row Factor	3.363	<0.0001	****	Yes	
Column Factor	84.88	<0.0001	****	Yes	
ANOVA table	SS (Type III)	DF	MS	F (DFn, DFd)	P value
Interaction	2427	6	404.5	F (6, 97) = 5.791	P<0.0001
Row Factor	2631	2	1316	F (2, 97) = 18.84	P<0.0001
Column Factor	66400	3	22133	F (3, 97) = 316.9	P<0.0001
Residual	6775	97	69.84		
Data summary					
Number of columns (Column Factor)	4				
Number of rows (Row Factor)	3				
Number of values	109				
Within each row, compare columns (simple effects within rows)					

Number of families	3				
Number of comparisons per family	6				
Alpha	0.05				
Tukey's multiple comparisons test	Predicted (LS) mean diff.	95.00% CI of diff.	Below threshold?	Summary	Adjusted P Value
Maize					
Untreated vs. T+V	4.164	-5.606 to 13.93	No	ns	0.6817
Untreated vs. P15	44.59	34.22 to 54.95	Yes	****	<0.0001
Untreated vs. P30	53.4	42.12 to 64.68	Yes	****	<0.0001
T+V vs. P15	40.42	30.06 to 50.79	Yes	****	<0.0001
T+V vs. P30	49.24	37.96 to 60.52	Yes	****	<0.0001
P15 vs. P30	8.815	-2.983 to 20.61	No	ns	0.2131
Wheat					
Untreated vs. T+V	2.821	-7.478 to 13.12	No	ns	0.8905
Untreated vs. P15	37.84	27.54 to 48.14	Yes	****	<0.0001
Untreated vs. P30	51.33	41.29 to 61.37	Yes	****	<0.0001
T+V vs. P15	35.02	24.72 to 45.32	Yes	****	<0.0001
T+V vs. P30	48.51	38.47 to 58.55	Yes	****	<0.0001
P15 vs. P30	13.49	3.450 to 23.53	Yes	**	0.0037
Field Pea					
Untreated vs. T+V	4.554	-5.216 to 14.32	No	ns	0.6167
Untreated vs. P15	64.88	55.11 to 74.65	Yes	****	<0.0001
Untreated vs. P30	58.37	48.01 to 68.74	Yes	****	<0.0001
T+V vs. P15	60.33	50.56 to 70.10	Yes	****	<0.0001
T+V vs. P30	53.82	43.46 to 64.18	Yes	****	<0.0001

P15 vs. P30	-6.507	-16.87 to 3.856	No	ns	0.3605

S7 Supplementary information for Chapter 6.3.4

Heatmap of all CxHy fragments. Abbreviations: U (Untreated); P30 (30-minute plasma); P90 (90-minute plasma).



S8 Supplemental information for Chapter 8.2.9.2

ITS sequences analysed for each fungus and 16s rDNA for the bacteria extracted from contaminated industry grains.

Aspergillus flavus; 495 kb Q20 bases;11091 signal sequence intensity

AATGGAAGAGTGGTCGGGTTCCCAAGCGAGCCCAACCTCCCACCCGTGTCCAC
TGTACCTTAGTTGCTTTCGGCGGGCCCGCCATTCATGGCCGCCGGGGGCTCTC
AGCCCCGGGCCCGCGCCCGCCGGAGACACCACGAACTCTGTCTGATCTAGTGA
AGTCTGAGTTGATTGTATCGCAATCAGTTAAAACTTTCAACAATGGATCTCTTGG
TTCCGGCATCGATGAAGAACGCAGCGAAATGCGATAACTAGTGTGAATTGCAGA
ATTCCGTGAATCATCGAGTCTTTGAACGCACATTGCGCCCCCTGGTATTCCGGG
GGGCATGCCTGTCCGAGCGTCATTGCTGCCCATCAAGCACGGCTTGTGTGTTG
GGTCGTCGTCCCCTCTCCGGGGGGGACGGGCCCCAAAGGCAGCGGCGGCAC
CGCGTCCGATCCTCGAGCGTATGGGGCTTTGTCACCCGCTCTGTAGGCCCGGC
CGGCGCTTGCCGAACGCAAATCAATCTTTTTCCAGGTTGACCTCGGATCAGGTA
GGGATACCCGCTGANNAAAAAACCAAATACAA

Aspergillus niger; 506 kb Q20 bases;9960 signal sequence intensity

AATGGAAGAGTGGCCGGGTCCNNCNTGCGGCCCAACCTCCCATCCGTGTCTAT
CATACCCTGTCTGCTTCGGCGGGCCCGCCGCTTGTCGGCCGCCGGGGGGGCG
CCTTTGCCCCCCGGGCCCGTGCCCGCCGGAGACCCCAACACGAACACTGTCTG
AAAGCGTGCAGTCTGAGTTGATTGAATGCAATCAGTTAAAACTTTCAACAATGGA
TCTCTTGGTTCCGGCATCGATGAAGAACGCAGCGAAATGCGATAACTAATGTGA
ATTGCAGAATTCAGTGAATCATCGAGTCTTTGAACGCACATTGCGCCCCCTGGT
ATTCCGGGGGGCATGCCTGTCCGAGCGTCATTGCTGCCCTCAAGCCCGGCTTG
TGTGTTGGGTCGCCGTCCCCCTCTCCGGGGGGACGGGCCCGAAAGGCAGCGG
CGGCACCGCGTCCGATCCTCGAGCGTATGGGGCTTTGTCACATGCTCTGTAGG
ATTGGCCGGCGCCTGCCGACGTTTTCCAACCATTTTTTCCAGGTTGACCTCGGA
TCAGGTAGGGATACCCGCTGATTAAAAACCATATATAA

Aureobasidium pullulans; 525 kb Q20 bases;6815 signal sequence intensity

AAGGANAGAGNACGGGTGCTCAGCGCCCGACCTCCAACCCTTTGTTGTTAAACT
ACCTTGTTGCTTTGGCGGGACCGCTCGGTTCCGAGCCGCTGGGGATTCGTCCC
AGGCGAGCGCCCGCCAGAGTTAAACCAAACTCTTGTTATTTAAACCGGTCGTCT
GAGTTAAAATTTTGAATAAATCAAAACTTTCAACAACGGATCTCTTGGTTCTCGCA
TCGATGAAGAACGCAGCGAAATGCGATAAGTAATGTGAATTGCAGAATTCAGTG
AATCATCGAATCTTTGAACGCACATTGCGCCCCTTGGTATTCCGAGGGGCATGC
CTGTTCGAGCGTCATTACACCACTCAAGCTATGCTTGGTATTGGGTGCCGTCCT
TAGTTGGGCGCGCCTTAAAGACCTCGGCGAGGCCTCACCGGCTTTAGGCGTAG
TAGAATTTATTCGAACGTCTGTCAAAGGAGAGGACTTCTGCCGACTGAAACCTTT
TATTTTTTCTAGGTTGACCTCGGATCAGGTAGGGATACCCGCTGATATAAAAACC
ATAATAA

Cryptococcus magnus; 502 kb Q20 bases;12376 signal sequence intensity

NTANGGCGGGNAGAAGANTNCNGAATCCAAAGGGCGAAAGCCAGTGGGTTNTC
CCTTTAATATCCCATCACACCTTGTTGCACTTGTCTGGATGCTTTGCATCCACTC
CCCAACTAAACATTCATCCGTAACAAATGTAGTCTTATTATAACATAATAAAACTT
CTCAACAACGGATCTCTTGGCTCTCGCATCGATGAAGAACGCAGCGAAATGCGA

TAAGTAATGTGAATCGCAGAATTCAGTGAATCATCGAATCTTTGAACGCACCTTG
CGCTCCTTGGTATTCCGAGGAGCATGCCTGTTTGAGTATCATGAAACCCTCAAA
CCCAAGTTTTGGATTTCGATCCATGCTTGAGTTTGGATTTGGATGTTTGCCGGTG
ATGAACCGACTCATCTTAAAAGTATTAGCTTGGATCTGTCTATATGACTGGTTTG
ACTTGGCATAATAAGTATTTTGCTGAGGACATCTTCGGATGGCCAGGACCTAGA
CTACTGTCTGCTAACTAAACCATCACTTTAAGTGCATCTTTGGATGTTACTCATTG
TGTAACTTTGACATCTGGCCTCAAATCAAGTAGGACTACCCGCTATTTAAAACCC
AATAAA

Lichtheimia corymbifera; 714 kb Q20 bases;1443 signal sequence intensity

AAGGGANAGAAAGTAATTAAGCCTTGGGGGGTTGGCCTAACTTAAGGTCTTCTC
TTAAGGTTCCTCACAGTTATGTGCAATGTTGGGTCACCTTGGTTGACTCTGCCTA
AAGCTTTTGACTTGAAAAAAGACTTGAGCAATGGGCTGGCCTTAGGGGCCCCTA
GTATGTTTATCATACTAACCCCAAAGGTTTTTTCTACTATGTCTATGAATTGATGT
ATGAAAAAAAAGTTATTTGTTAACTTGAAGGCTTCTGTAAAAAGAGTCTTTAAAAA
CAACTCTTGGCAATGGATCTCTTGGTTCTCGCATCGATGAAGAGCGTAGCAAAG
TGCGATAATTATTGCGACTTGCATTCATAGTGAATCATCGAGTTCTTGAACGCAT
CTTGCGCCTAGTAGTCAATCTACTAGGCACAGTTGTTTCAGTATCTGCATCCACC
AATCAACTTAACCTTTTGTGTTGAGTTGGAACTGGGCTTCTAGTTGATGGCATTT
AGTTGCTGTCATGGCCTTAAATCAATGTCCTAGGTGTTAGAACATCTAACACCGG
ATGGAAACTTTAGAGCGCTTTAAGAGCAGCTTGGATAGTGAGTTCAATAATTCCA
AGCATTAAGTCTTTTAATGAACTAGCTTTTCTATCTATGGGACACTACTTGGAGA
AATCCAAGTAACCTTTAAACTCACATTTAGATCTGAAATCAACTGAGACCACCCG
CTGAACTTAAAACCATATAA

Penicillium corylophilum; 483 kb Q20 bases;11091 signal sequence intensity

NNNGNGAGGAGTGGACGGGCCCTCACTGCGGTTCNAACCTACCACCCATGTAC
NNTGTACCCTGTTGCTTCGGCGGGCCCGCCTCACGGCCGCCGGGGGGCTTTC
TGCCCTCTGGCCCGCGCCCGCCGAAGACACCATTGAACACTGTCTGAAGATTG
CAGTCTGAGCAATTAGCTAAATAAGTTAAAACTTTCAACAACGGATCTCTTGGTT
CCGGCATCGATGAAGAACGCAGCGAAATGCGATACGTAATGTGAATTGCAGAAT
TCAGTGAATCATCGAGTCTTTGAACGCACATTGCGCCCCTTGGTATTCCGGGGG
GCATGCCTGTCCGAGCGTCATTGCTGCCCTCAAGCACGGCTTGTGTGTTGGGC
CCCGTCCTCCTTCCCGGGGGACGGGCCCGAAAGGCAGCGGCGGCACCGCGTC
CGGTCCTCGAGCGTATGGGGCTTTGTCACCCGCTCTTGTAGGCCCGGCCGGCG
CTTGCCGACAACCATCAATCTTTTTTCAGGTTGACCTCGGATCAGGTAGGGATA
CCCGCTGATATAAAGACCATATATAA

Rhizopus arrhizus; 536 kb Q20 bases;11096 signal sequence intensity

TTATGGNAAAAGTTACACAGCGCCTTATACTTCAAGGGTTCTCCTCTGGGGTAA
GTGATTGCTTCTACACTGTGAAAATTTGGCTGAGAGACTCAGACTGGTCATGGG
TAGACCTATCTGGGGTTCTGATCGATGCCACTCCTGGTTTCAGGAGTACCCTTC
ATAATAAACCTAGAAATTCAGTATTATAAAGTTTAATAAAAAACAACTTTCTAACAA
TGGATCTCTTGGTTCTCGCATCGATGAAGAACGTAGCAAAGTGCGATAACTAGT
GTGAATTGCATATTCAGTGAATCATCGAGTCTTTGAACGCAGCTTGCACTCTATG
GTTTTTCTATAGAGTACGCCTGCTTCAGTATCATCACAAACCCACACATAACATT
TGTTTATGTGGTGATGGGTCGCATCGCTGTTTTATTACAGTGAGCACCTAAAATG
TGTGTGATTTTCTGTCTGGCTTGCTAGGCAGGAATATTACGCTGGTCTCAAGATC
TTTTTTTTTGGTTCGCCCAGGAAGTAAAGTACAAGAGTATAATCCAGTAACTTTC
AAACTATGATCTGAAGTCAGGTGGGATTACCCGCTGATTTAAAACCCATAAGAAC
T

Bacillus safensis; 848 kb Q20 bases;8817 signal sequence intensity

TTCGGGGGGGGGCCCAAAGACTTGCAAGTTCGAGCGGACAGAAGGGAAGCTC
TGCTCCCGGATGTTAGCGGCGGACGGGTGAGTAACACGTGGGTAACCTGCCTG
TAAGAGTGGGATAACTCCGGGAAACCGGAGCTAATACCGGATAGTTCCTTGAAC
CGCATGGTTCAAGGATGAAAGACGGTTTCGGCTGTCACTTACAGATGGACCCG
CGGCGCATTAGCTAGTTGGTGGGGTAATGGCTCACCAAGGCGACGATGCGTAG
CCGACCTGAGAGGGTGATCGGCCACACTGGGACTGAGACACGGCCCAGACTC
CTACGGGAGGCAGCAGTAGGGAATCTTCCGCAATGGACGAAAGTCTGACGGAG
CAACGCCGCGTGAGTGATGAAGGTTTTCGGATCGTAAAGCTCTGTTGTTAGGGA
AGAACAAGTGCGAGAGTAACTGCTCGCACCTTGACGGTACCTAACCAGAAAGC
CACGGCTAACTACGTGCCAGCAGCCGCGGTAATACGTAGGTGGCAAGCGTTGT
CCGGAATTATTGGGCGTAAAGGGCTCGCAGGCGGTTTCTTAAGTCTGATGTGAA
AGCCCCCGGCTCAACCGGGGAGGGTCATTGGAAACTGGGAAACTTGAGTGCAG
AAGAGGAGAGTGGAATTCCACGTGTAGCGGTGAAATGCGTAGAGATGTGGAGG
AACACCAGTGGCGAAGGCGACTCTCTGGTCTGTAACTGACGCTGAGGAGCGAA
AGCGTGGGGAGCGAACAGGATTAGATACCCTGGTAGTCCACGCCGTAAACGAT
GAGTGCTAAGTGTTAGGGGGTTTCCGCCCCTTAGTGCTGCAGCTAACGCATTAA
GCACTCCGCCTGGGGAGTACGGTCGCAAGACTGAATAGGGGNTTTTTTTTTGNN
NGG

S9 Supplementary information for Chapter 8.2.8.3

F. pseudograminearum **pg DNA/g Sample***	***F. culmorum / F. graminearum*** **pg DNA/g Sample***	***Fusarium culmorum*** **kDNA copies/g Sample***	***Fusarium graminearum*** **kDNA copies/g Sample***
1418	1539	26	0
1092	405	8	0

S10 Supplementary information for Chapter 8.2.11.2

List of analysed mycotoxins and the thresholds provided by Intertek

Mycotoxin	**Threshold**
DEOXYNIVALENOL/VOMITOXIN	<400 PPB
AFLATOXIN TOTAL (B1, B2, G1, G2)	<1 PPB
OCHRATOXIN	<2 PPB
ZEARALENONE	<40 PPB
FUMONISIN TOTAL (B1, B2)	<100 PPB
HT-2 TOXIN	<100 PPB
T-2 TOXIN	<100 PPB
3-ACETYL DEOXYNIVALENOL	<40 PPB
15-ACETYL DEOXYNIVALENOL	<40 PPB

List of Figures

Figure 1-1. Diagram of a typical capacitively coupled radiofrequency plasma apparatus. Republished with permission of American Institute of Physics, from Electron dynamics in low pressure capacitively coupled radio frequency discharges, Wilczek, S., Schulze, J., Brinkmann, R.P., Donkó, Z., Trieschmann, J., Mussenbrock, T., 2020. J. Appl. Phys. 127; permission conveyed through Copyright Clearance Center, Inc. 5

Figure 1-2. The triphasic model of seed germination modelled after Bewley et al., 2013 and Bewley and Black, 1978. 13

Figure 1-3. (A) Grains of maize wild relative, teosinte. (B) Modern maize cultivar B73. (C) Diagram of a modern maize kernel (republished with permission of Taylor and Francis Group, from Drying and storage of grains and oilseeds, Brooker, D.B., Bakker-Arkema, F.W., Hall, W., 1992. Van Nostrand Reinhold; permission conveyed through Copyright Clearance Center, Inc.)..... 15

Figure 1-4. Longitudinal section of a *Zea mays* subsp. mays ‘B73’ grain with labels of important tissues and structures..... 16

Figure 1-5. Wheat grain diagram. Republished with permission of Oxford University Press, from Water movement into dormant and non-dormant wheat (Triticum aestivum L.) grains, Rathjen, J.R., Strounina, E. V., Mares, D.J., 2009. J. Exp. Bot. 60; permission conveyed through Copyright Clearance Center, Inc. 17

Figure 1-6. Longitudinal section along the crease of a *Triticum aestivum* ‘Scepter’ [sic], grain with labels of important tissues and structures. 18

Figure 1-7. Diagram of a barley grain. Republished with permission of Wiley, from Barley, Briggs, D.E., 1978. 1st ed. Chapman and Hall, Ltd; permission conveyed through Copyright Clearance Center, Inc. 19

Figure 1-8. Longitudinal section of a *Hordeum vulgare* ‘Compass,’ grain with labels of important tissues and structures. 20

Figure 1-9. Diagrams of field pea grain. Left, drawing with labelled structures. Right, cross-section through the seed coat illustrating the epidermal layer with macrosclereid cells. Republished with permission of Oxford University Press, from Structure of the developing pea seed coat and the post-phloem transport pathway of nutrients, Van Dongen, J.T., Ammerlaan, A.M.H., Wouterlood, M., Van Aelst, A.C., Borstlap, A.C., 2003. Ann. Bot. 91; permission conveyed through Copyright Clearance Center, Inc. 21

Figure 1-10. Longitudinal section of a *Pisum sativum* ‘Butler’ grain with labels of important tissues and structures. Note: the plumule fractured during grain sectioning and is difficult to distinguish from the base of the hypocotyl. 22

Figure 1-11. Transverse and longitudinal sections of *Plantago ovata* grains with labels of important tissues and structures. 23

Figure 1-12. Diagram of *Plantago ovata* seed. (A) ventral view of the grain. (B) transverse section of the grain through the hilum. (C) Embryo with r = radicle, c = cotyledon. Republished from Seed morphological studies in the Indian isubgol of commerce, Malick, K.C., Safui, B., 1985. Bull. Bot. Surv. India 27; Nelumbo open access. 24

Figure 1-13. Coloured scanning electron micrograph of *Aspergillus flavus* conidia showing typical globose and echinulate morphology. Magnification = 20,000x; see Chapter 5.5.2 for experimental details. 28

Figure 1-14. *Bipolaris sorokiniana* conidia illustrated with a coloured scanning electron micrograph. Mature conidia can be up to 120µm. Note the indentation in the

bottom left corner indicating the former connection to a conidiophore. Magnification = 10,000x. 29
Figure 1-15. *Fusarium graminearum* chlamydospore shown in a coloured scanning electron micrograph. Magnification = 5000x. Note the bulbous structure of the chlamydospore compared to the hyphae. 31
Figure 1-16. Penicillium chrysogenum clustered conidia seen in a coloured scanning electron micrograph. Magnification = 10,000x. 32
Figure 3-1. Diagram of the plasma tumbler apparatus designed by Michl et al. 2015 with labels of key features and modifications. 44
Figure 3-2.Plasma tumbler in operation. Field pea grains are seen in the rotating flask. 45
Figure 3-3. Bipolaris sorokiniana extracts on a haemocytometer. Both conidia and hyphal fragments are visible on the grid. 50
Figure 4-1. SEM micrographs of maize treatments show the exocarp surrounding the endosperm. Letters (A, D) are Untreated samples; (B, E) are T+V treatment; (C, F) are P90 treated grain. 57
Figure 4-2. SEM micrographs of the surface of maize tip caps. (A) Untreated sample with a visible spore in the centre. (B) P90 treatment with visible weathering. Arrows indicate spores naturally present on the grain. Scale bar = 10 µm. (C) Maize grain with markings for areas of interest. Red square = tip cap area scanned; purple square = pericarp region scanned in Figure 4-1. 58
Figure 4-3. Dorsal exocarp SEM micrographs of wheat treatments. Letters (A, D) are Untreated samples; (B, E) are T+V treatment; (C, F) are P90 treated grain. (C, F) granulation of the grain surface is apparent on P90 treatments. 60
Figure 4-4. SEM image comparing wheat grain surfaces of control (left) and 10-minute argon plasma treatment in a DBD apparatus (right). Circles represent structures suspected to be bacteria endospores. Republished with permission of Elsevier

Ltd., from Plasma inactivation of bacterial endospores on wheat grains and polymeric model substrates in a dielectric barrier discharge, Butscher, D., Zimmermann, D., Schuppler, M., Rudolf von Rohr, P., 2016. Food Control 60; permission conveyed through Copyright Clearance Center, Inc. 61

Figure 4-5. Wheat grains visualised under SEM. (A-B) are Untreated seeds. (C-D) are P90 treated grains. (A, C) focus on the embryo while (B, D) highlight the brush. 61

Figure 4-6. SEM micrographs of the hull of barley cultivar ‘Compass’. (A, D) are Untreated; (B, E) are T+V treatment; (C, F) are P90 treatment. Lemma hairs are visible in Untreated and T+V samples but not on P90 samples. ph = phytoliths below the surface on the intercellular borders; tr = dome trichomes; scale bars (A-C) = 50 µm; (D-F) = 10 µm. 63

Figure 4-7. SEM micrographs of the surface of a barley lemma. Left, displays the outer surface with intercellular ridges. Centre, lines of phytoliths are exposed under the surface ridges. Right, dome trichomes dot the barley hull surface. Republished with permission of Elsevier Ltd., from Microstructure development of chars derived from high-temperature pyrolysis of barley (Hordeum vulgare L.) hulls, Boateng, A.A., Cooke, P.H., Hicks, K.B., 2007. Fuel 86; permission conveyed through Copyright Clearance Center, Inc. 64

Figure 4-8. SEM micrographs of hulled barley. (A, C) are Untreated. (B, D) are 90-minute plasma-treated grains. (A) Damage to the lemma on an Untreated sample reveals the grain brush. (B) Modifications to lemma due to plasma treatment. Dome trichomes are much more apparent. (C) Ventral view of an Untreated grain with labelled structures. lm = lemma; pa = palea; ra = rachilla. (D) Damage on a plasma-treated grain reveals the underlying pericarp, seed coat and aleurone. 64

Figure 4-9. SEM micrographs of the seed coat surface of field pea. (A, D) are Untreated; (B, E) are T+V treatments; (C, F) are P90 treated grains. (A, B, D, E) The outline of star-shaped palisade cells are visible under the cuticle. (F) 90-minute plasma-treatment appears to strip away the seed coat cuticle, possibly exposing the primary cell wall structures below. 65
Figure 4-10. SEM micrographs of psyllium grains. Untreated (A-C), T+V (D-F) and 90-minute plasma-treated (G-I) display the characteristic wrinkles of desiccated mucilage on the grain surface. (A-B, D-E, G-H) are micrographs taken of the grain where the operculum was attached. (C, F, I) show the surface that was nearest to the capsule. 68
Figure 4-11. SEM micrographs of Untreated psyllium grains. (A) illustrates the dorsal surface of the grain. (B) pictures the ventral side of the grain. (C-D) Branching structures are suspected fungal hyphae growing throughout the ventral cavity of the grain. Diamonds indicate the region that was attached to the capsule. Asterisks indicate the region that was attached to the operculum. An arrow marks the equator where there are visible differences in surface patterns. 69
Figure 4-12. SEM micrographs of Arabidopsis thaliana seed surfaces. (C, E) represent control seeds while (D, F) were exposed to 15 minutes of air plasma in a floating electrode-dielectrode barrier discharge apparatus. The weathering of the surface of the mucilage secretion cells is reminiscent to the etching of the psyllium mucilage in Figure 4-10. Republished from Effects of low temperature plasmas and plasma activated waters on Arabidopsis thaliana germination and growth, Bafoil, M., Jemmat, A., Martinez, Y., Merbahi, N., Eichwald, O., Dunand, C., Yousfi, M., 2018. PLoS One 13; open access CC BY 4.0 70
Figure 4-13. Diagram of grain surfaces with confocal 405 nm laser illustrates the difficulties when scanning curved surfaces. (A) maize; (B) field pea; (C) psyllium; (D) wheat. 72

Figure 4-14. Confocal profilometer seed surface topographic maps of maize. (A) Untreated; (B) Tumbler + Vacuum; (C) 90-minute plasma treatment. Profilometer images are 129 µm wide. Scale bar on SEM micrographs is 50 µm. 73

Figure 4-15. Unpaired t-test results for developed interfacial area ratio (Sdr) highlighting the percent change in surface area attributed to roughness in maize grain. Data is presented as SEM with significance accepted at $p<0.05$. Abbreviations: T+V (Tumbler + vacuum); P90 (90-minute plasma). 75

Figure 4-16. Two-way ANOVA analysis of both area height (Sq) and profile height (Rq). Data is presented as mean ± SEM with significance accepted at $p<0.05$. Abbreviations: T+V (Tumbler + vacuum); P90 (90-minute plasma); ns (non-significant). 75

Figure 4-17. Visualisation of the data sets statistically described in Figure 4-16. Area scans (129 µm x 129 µm) compared to profile scans (129 µm) of each treatment. (A-B) = Untreated; (C-D) = T+V; (E-F) = P90. 76

Figure 5-1. Two-way ANOVA and Tukey's multiple comparisons of colony-forming unit counts per grain type and treatment on a log scale. Data is presented as mean ± SEM. Abbreviations: T+V (Tumbler + vacuum); P90 (90-minute plasma); ns (non-significant); *$p<0.05$; ***$p<0.001$; ****$p<0.0001$. 87

Figure 5-2. Well-plate assay quadrant diagram. Dorsal and ventral faces were viewed from the lid and base of the plate. Embryo and dent/brush quadrant were imagined as a line drawn roughly half-way across the grain. 91

Figure 5-3. Comparisons of the number of visible hyphae and location after a 96-hour incubation for each grain type and treatment via two-way ANOVA with Tukey's multiple comparisons test. Data is presented as mean ± SEM; n = 24. (A, C) display the means of visible colonies at each location. (B, D) provide a different visualisation of the same data. Abbreviations: T+V (Tumbler + vacuum); P15

(15-minute plasma); P30 (30-minute plasma); P45 (45-minute plasma); P60 (60-minute plasma); P75 (75-minute plasma); P90 (90-minute plasma); ns (non-significant); *p<0.05; **p<0.01; ****p<0.0001. 94

Figure 5-4. SEM micrographs of the maize pedicel, also known as the tip cap. It is speculated that the rough features of this part of the grain may provide shelter for fungal spores. By 90 minutes of treatment, the pedicle appears to be weathered and smooth. 95

Figure 5-5. SEM micrographs of wheat grain surface features. (A) a dorsal view of the brush. (B) a ventral view of the crease. (C) a dorsal view of the embryo. 96

Figure 5-6. *Aspergillus flavus* culture with visible conidiophores and conidia ready for inoculation. 99

Figure 5-7. Single spore cultures of *Penicillium chrysogenum*. 101

Figure 5-8. Sterile wheat added to *Fusarium graminearum* cultures for hyphal colonisation. 102

Figure 5-9. Field pea inoculated with *Penicillium chrysogenum* and subjected to varying durations of plasma exposure. Data is presented as mean ± SEM with significance accepted at p<0.05. (A) Results of each of the three independent experiments. (B) Detail of the results from Experiment 3 using one-way ANOVA comparing the means from each treatment. Letters indicate differences between means analysed in a stepwise comparison with Welch's t-test. Abbreviations: T+V (Tumbler+Vacuum); P15 (15-minute plasma); P30 (30-minute plasma); P45 (45-minute plasma); P60 (60-minute plasma); P75 (75-minute plasma); P90 (90-minute plasma). 110

Figure 5-10. Maize inoculated with *Aspergillus flavus* and subjected to varying durations of plasma exposure. Data is presented as mean ± SEM with significance accepted at p<0.05. Note: T+V treatment was omitted from this experimental series and substituted with a 105-minute plasma exposure time.

(A) Results of each of the three independent experiments. (B) Detail of the results from Experiment 3 using one-way ANOVA comparing the means from each treatment. Letters indicate differences between means analysed in a stepwise comparison with Welch's t test. Abbreviations: T+V (Tumbler+Vacuum); P15 (15-minute plasma); P30 (30-minute plasma); P45 (45-minute plasma); P60 (60-minute plasma); P75 (75-minute plasma); P90 (90-minute plasma). 112

Figure 5-11. *Bipolaris sorokiniana* culture growing over the top of barley grains. ... 117

Figure 5-12. (Above) Original culture of *Didymella pinodes* donated by SARDI. (Below) Subculture taken from the original sample. 118

Figure 5-13. Data sets from three independent experiments with *Aspergillus flavus* on maize host following P90 (90-minute plasma) or Untreated control conditions. Individual values are plotted and bars present mean ± SEM; ****p<0.0001; n = 15. 124

Figure 5-14. SEM micrographs of control and plasma treatments of *Aspergillus flavus* on maize grain. Images were captured of conidia on the maize pericarp surface over the endosperm; n = 3. 125

Figure 5-15. Experimental series of *Bipolaris sorokiniana* on barley host grain following P90 (90-minute plasma) or Untreated control conditions. Individual values are plotted with bar representing mean ± SEM; ****p<0.0001; n = 15. Dotted line indicates value for a single colony. 127

Figure 5-16. Barley grains inoculated with *Bipolaris sorokiniana*. Mycelial networks are clearly visible on Untreated grains and absent on plasma treatments. (A-B) Palea surface near the awn. (C-D) Palea surface near the embryo; n = 4. .. 128

Figure 5-17. Experimental series of *Didymella pinodes* on field pea host treated with P90 (90-minute plasma) or Untreated control conditions. Individual values are

plotted with bar representing mean ± SEM; ****p<0.0001; n = 15. Dotted line indicates value for a single colony. 130
Figure 5-18.SEM micrographs of Untreated and 90-minute plasma-treated *Didymella pinodes* inoculated on field pea. Note: this was the first in the series of SEM screenings and spores were not prepared in fixative, dehydrated, or critically point dried prior to visualisation. n = 3. 131
Figure 5-19. The results of three independent experiments on *Fusarium graminearum* inoculated wheat grains treated with P90 (90-minute plasma) or Untreated control conditions. Individual values are plotted with bar representing mean ± SEM; ****p<0.0001; n = 15. Dotted line indicates value for a single colony. 133
Figure 5-20. SEM imagery of what appear to be chlamydospores forming on the surface of *Fusarium graminearum*-inoculated wheat grains. The severely damaged remnant fungal structures are visible after plasma treatment. 133
Figure 5-21. *Fusarium graminearum* inoculated wheat grains. (A and C) Visible mycelial network on Untreated grains. (E) Untreated hyphal network at 1000x magnification. (G) Hyphae penetrating the Untreated grain surface. (F) Remnants of mycelial network following 90 minutes of plasma exposure. (H) Remnants of what appear to be areas of hyphal penetration. n = 4. 134
Figure 5-22. The results of three independent experiments with *Penicillium chrysogenum* inoculated psyllium grains and treated with P90 (90-minute plasma) or Untreated control conditions. Individual values are plotted with bar representing mean ± SEM; ****p<0.0001; n = 15. Dotted line indicates value for a single colony..... 136
Figure 5-23. SEM micrographs of *Penicillium chrysogenum* inoculated dry psyllium grain. (A, G) View of Untreated grain dorsal surface. (C, H) Ventral view of psyllium grain with conidia. (G, H) Inoculated grains treated in fixative to hydrate mucilage and preserve conidia structures. (G) Red circles indicate conidia on

partially hydrated mucilage (B, D, F) 90-minute plasma-treated grain surfaces with remnant conidia. n = 6. 137

Figure 5-24. Summary of inoculation trials with combined data from each organism/host series. The means of biological replicates from all three independent experiments are plotted for each treatment. Data is presented as mean ± SEM; ** p<0.01; ***p<0.001; ****p<0.0001. Abbreviation: P90 (90-minute plasma). 139

Figure 6-1. The contact angle of water droplets on the surface of wheat grains. (A) A more hydrophobic grain surface produces a high contact angle as the polar water molecules are attracted to each other through cohesive forces rather than the non-polar hydrocarbon chains on the grain surface. Arrows indicate the direction of attraction. (B) A more hydrophilic grain surface produces lower contact angles as adhesion forces attract the water molecules to a more polar grain surface. 146

Figure 6-2. Maize grains with water droplets applied to the surface to observe wettability. Images taken in a burst-mode within two seconds of water application. (A) Untreated grains; (B) 60-second chloroform-treated grains to reduce the presence of seed surface waxes; (C) P90 grains. The relative hydrophobicity/hydrophilicity of the seed surface was demonstrated by the interaction of the water droplet with the maize kernel. (D) 50 µL drops of maize grain chloroform extracts placed onto silicon wafers illustrated the compounds extracted from the grain. 149

Figure 6-3. Contact angle images comparing maize, wheat, and field pea treatments. Water droplets form tight beads on control samples. Plasma-treated samples have sprawling droplets with much lower contact angles. 151

Figure 6-4. Comparison of the water droplet contact angle means of each grain type and treatment. Data is presented as mean ± SEM; n = 10. The difference

between Untreated and T+V controls is insignificant (p values = 0.6167 to 0.8905). There is a highly significant difference between the controls and plasma treatments (p-values of less than 0.0001) in all grain types. Abbreviations: T+V (Tumbler + vacuum); P15 (15-minute plasma); P30 (30-minute plasma).....152

Figure 6-5. PCA plots comparing all fragments analysed during ToF-SIMS. Across all grain types, the Untreated control group is mostly separated from the plasma treatments along with principal component 1 (x-axis). Ellipses represent the 95% confidence interval (95% CI). Abbreviations: P30 (30-minute plasma); P90 (90-minute plasma). 159

Figure 6-6. Combined PCA loadings of all treatments within a grain type to allow comparisons of fragments analysed during ToF-SIMS. The inorganic cations were a driving factor in the separation of treatments in this first analysis.....160

Figure 6-7. PCA plots comparing organic fragments analysed during ToF-SIMS. When inorganic ions are removed, the Untreated control group is separated from the plasma treatments along with principal component 1 (x-axis). Ellipses represent the 95% confidence interval (95% CI). Abbreviations: P30 (30-minute plasma); P90 (90-minute plasma). 162

Figure 6-8. Combined PCA loadings of all treatments within a grain type to allow comparisons of fragments analysed during ToF-SIMS. When the inorganic cations are removed from the analysis, the hydrocarbon fragments become the dominant components shaping the plots. 163

Figure 6-9. Heatmap displaying the means of mass peak area per fragment and treatment. Due to the large number of hydrocarbon (C_xH_y) fragments analysed, only fragments with significant differences between treatments were selected for representation in this heatmap. The full heatmap of hydrocarbon fragments is available in Appendix S7. Note that comparisons should be made only within

groupings due to differences in scale. Abbreviations: U (Untreated); P30 (30-minute plasma); P90 (90-minute plasma). 166

Figure 6-10. Grain water sorption curves based on Bewley et al. 2013. (A) Illustration of the processes occurring across different water content and time points, reproduced from Chapter 1.3.1 for the reader's convenience. (B) This graph displays the standard water sorption curve in green. The red dashed line illustrates where seeds were held below the water potential threshold. Seeds will not proceed through phases II and III until the water potential increases. 169

Figure 6-11. Field pea grains in the carousel of a ProUmid SPSx-1µ Advance vapour sorption analyser. 172

Figure 6-12. Modelling equations and the interpretation for use in GraphPad Prism 9.0.0. 173

Figure 6-13. A pilot trial with maize grain held at 25 °C and 98% relative humidity for 120 hours. At 98% relative humidity, the water potential was high enough to trigger fungal growth as seen (suspected to be *Rhizopus arrhizus*) colonising maize in dishes 14 and 15. 174

Figure 6-14. Comparison of initial seed moisture content for all grain types and treatments. Data is presented as mean ± SEM. Abbreviations: T+V (Tumbler + vacuum); P90 (90-minute plasma); ns (non-significant); *p<0.05; **p>0.01; ****p>0.0001. 175

Figure 6-15. Water sorption curves comparing each treatment within a grain type. Maize and field pea were measured over the course of 120 hours. Wheat, barley, and psyllium were measured over 72 hours. All grains, except field pea, appeared to follow the standard sorption curve with a steep initial slope that flattened over time. 177

Figure 6-16. Comparisons between water sorption means of each treatment. In all grain types, the P90 (90-minute plasma) treatment absorbed significantly more water than the Untreated controls. Data is presented as mean ± SEM with significance accepted at $p<0.05$. Letters indicate statistical differences between means. Abbreviations: T+V (Tumbler + vacuum); P15 (15-minute plasma); P30 (30-minute plasma); P60 (60-minute plasma); P90 (90-minute plasma). 178

Figure 6-17. Comparison between final sorption meter moisture content and initial moisture content. Data is presented as mean ± SEM. These data sets were used to determine if plasma-treated samples were absorbing more water to compensate for the initial moisture loss due to vacuum treatment. Abbreviations: T+V (Tumbler + vacuum); P90 (90-minute plasma). 179

Figure 6-18. Fitting the Peleg and 2-phase models to Untreated replicates of each grain type (maize, wheat, barley, and psyllium) in GraphPad Prism 9.0.0. 182

Figure 6-19. Sorption data fitted to the Peleg model (Peleg, 1988) of grain hydration. The inverse of the means of best-fit values ± 95% CI are plotted for each treatment. The inverse of k_1 (h^{-1}) corresponds to the rate of water ingress into the grain. The inverse of k_2 is equivalent to the % change in dry mass as seen in Figure 6-15. Abbreviations: T+V (Tumbler + vacuum); P15 (15-minute plasma); P30 (30-minute plasma); P60 (60-minute plasma); P90 (90-minute plasma)..... 186

Figure 6-20. Sorption data fitted to the 2-phase model (Miano et al., 2017). The means of best-fit values ± 95% CI are plotted for each treatment. k_{M1} represents the constant for rate of fast water ingress, interpreted as water entry via capillary action. k_{M2} represents the constant for rate of slow water ingress, interpreted as water entry via diffusion. Note the differences in scale bars between grain types, with particular attention to wheat k_{M1}. Abbreviations: T+V (Tumbler + vacuum);

P15 (15-minute plasma); P30 (30-minute plasma); P60 (60-minute plasma); P90 (90-minute plasma). 187

Figure 6-21. Ratio of k_{M1} constant means to k_{M2} constant means ± 95% CI. Capillary action values are always larger than diffusion values which means the ratio is much greater than one. Abbreviations: T+V (Tumbler + vacuum); P15 (15-minute plasma); P30 (30-minute plasma); P60 (60-minute plasma); P90 (90-minute plasma). 188

Figure 6-22. Magnetic resonance micro-imaging of wheat imbibing for 11-14 hours. The red to yellow gradient represents the presence of water. This study showed that the embryo and scutellum were the first tissues to hydrate, likely through capillary action via the micropyle. The endosperm hydrated more slowly through the crease where water began to travel between the outer pericarp and testa. Republished with permission of Oxford University Press, from Water movement into dormant and non-dormant wheat (Triticum aestivum L.) grains, Rathjen, J.R., Strounina, E. V., Mares, D.J., 2009. J. Exp. Bot. 60; permission conveyed through Copyright Clearance Center, Inc. 191

Figure 6-23. Trypan blue staining of treated maize grains after one hour in dorsal and ventral views, and after 24 hours in longitudinal sections. Plasma treatment alters the rate of grain staining. The patterns of staining follow typical maize grain hydration patterns but occur within one hour, as opposed to one to three days. 196

Figure 6-24. Trypan Blue staining of treated wheat grains after one hour in dorsal and ventral views, and after 24 hours in longitudinal sections. There was considerable difference in staining patterns between Untreated and plasma-treated grains. By hour 24, Untreated grains were in phase II of germination while both plasma treatments had reached phase III. 198

Figure 6-25. Trypan Blue staining of treated barley grains after one hour in dorsal and ventral views, and after 24 hours in longitudinal sections. Dye-accessible areas were stained blue. Untreated grains are show damage where the awn was attached, around the micropyle and attachment to the maternal structures and around the areas where the lemma connects with the pericarp. 199

Figure 6-26. Trypan Blue staining of treated field pea grains after one hour in dorsal and ventral views, and after 24 hours in longitudinal sections. Plasma-treated grains showed pronounced swelling, indicating rapid water uptake. All grains displayed stain uptake at the micropyle (arrows) with additional staining of the tracheid bar (circle) in 90-minute plasma treatments. 200

Figure 6-27. Trypan Blue staining of treated psyllium grains after one hour in dorsal and ventral views, and after 24 hours in longitudinal sections. At one-hour, Untreated grains showed the fully expanded mucilage layer while mucilage area on the plasma-treated grains was reduced. 202

Figure 6-28. Psyllium grain surface mucilage water sorption capacity. Plasma exposure reduces the water holding capacity of the mucilage. Data is presented as mean ± SEM. Abbreviations: P30 (30- minute plasma); P90 (90-minute plasma); ns (non-significant); *p<0.05; **p<0.01. 206

Figure 6-29. Scanning electron micrographs of Untreated and 90-minute plasma treated psyllium grains. Plasma appears to affect the polysaccharide microstructures of mucilage on the surface. 207

Figure 6-30. 90-minute plasma-treated wheat grains on half-strength PDA. A yellowish leachate surrounds each grain. 210

Figure 6-31. Potassium concentrations in the leachate of hydrated maize and wheat grains. Grains were soaked overnight in Milli-Q water and the extracts were analysed via flame photometry to calculate K^+ concentrations. Data is presented as mean ± SEM with significance accepted at p<0.05. Letters indicate significant

differences between means. Abbreviations: T+V (Tumbler + vacuum); P30 (30-minute plasma); P60 (60-minute plasma); P90 (90-minute plasma)..... 213
Figure 6-32. ToF-SIMS imagery of the maize grain surface as a visual display of fragment intensity. The presence of K^+ increased with plasma treatment. Scans were taken over the endosperm on the dorsal surface of each grain. Scale bars = 10 µm. Abbreviations: P30 (30-minute plasma); P90 (90-minute plasma). 214
Figure 7-1. Diagram of psyllium germination layout for optimal observations of BBCH stages 00-09 (see Table 7-2 for growth stage descriptions) of germination. 222
Figure 7-2. Mean percent germination for all treatments and grain types. (A-E) represent the means of combined experiment data (n = 100+). (F) compares the means of treatments for each grain type and highlights the variation in germination with prolonged plasma exposure. Data is presented as mean ± SEM. Abbreviations: T+V (Tumbler + vacuum); P15 (15-minute plasma); P30 (30-minute plasma); P60 (60-minute plasma); P90 (90-minute plasma); ns (non-significant). P-values are in comparison to the Untreated control; *p<0.05; **p<0.01; ***p<0.001; ****p<0.0001..... 226
Figure 7-3. Maize percent of grain with visible fungal contamination in relation to different treatments. It is suspected that high levels of fungal infection may have inhibited germination on the control Untreated and T+V grains. Data is presented as mean ± SEM. Significance to both control treatments is displayed as **p<0.01; ****p<0.0001. The lack of error bars on both the Untreated and T+V controls indicate that every grain displayed visible fungal contamination. Abbreviations: T+V (Tumbler + vacuum); P15 (15-minute plasma); P30 (30-minute plasma); P60 (60-minute plasma); P90 (90-minute plasma)..... 227
Figure 7-4. SEM micrograph showing damage to the pericarp covering the embryo on a 90-minute plasma-treated grain. More detailed images and comparisons with other treatments can be seen in Chapter 4, Figures 4-3 and 4-5. 228

Figure 7-5. Growth and development scores for seedlings across the germination time frame. Data is presented as mean ± SEM. Note that barley data was not collected due to COVID-19 restrictions to controlled environment cabinet access. Abbreviations: P30 (30-minute plasma); P90 (90-minute plasma). . 231

Figure 7-6. Code used with the BiometryTraining package in RStudio to create a randomised complete block design and Latin square design. 233

Figure 7-7. Seedlings grown in Jiffy-7® pellets for growth and development measurements. (A) Maize at 7 days after emergence (DAE); (B) wheat at 6 DAE (C) field pea at 11 DAE; (D) psyllium at 16 DAE. 237

Figure 7-8. Seedling height following emergence from the soil. Data is presented as mean ± SEM. Abbreviations: T+V (Tumbler + vacuum); P15 (15-minute plasma); P30 (30-minute plasma); P60 (60-minute plasma); P90 (90-minute plasma)..... 239

Figure 7-9. Growth of individual replicates over the course of six days following emergence. Black rectangles display the stagnation of growth in many replicates which contributed to large but insignificant differences in mean growth rate. Abbreviations: T+V (Tumbler + vacuum); P15 (15-minute plasma); P30 (30-minute plasma); P60 (60-minute plasma); P90 (90-minute plasma). 240

Figure 7-10. Wheat seedling growth trial. (A) Seedling height recorded for 10 days from emergence at 4 DAS. (B) Dry weights of above ground plant material harvested at 10 days after emergence, 14 DAS. Data is presented as mean ± SEM. Abbreviations: T+V (Tumbler + vacuum); P90 (90-minute plasma); ns (non-significant); **p<0.01; ***p<0.001. 241

Figure 7-11. Maize seed-to-seed pot growth experiment. Images were captured at 4, 8, 12 and 18 weeks after sowing. Overall, there were no visible differences between the treatments. 243

Figure 7-12. Maize harvest data at 18 weeks after sowing. (A) Mean height of plants from soil level to the base of the tassel. (B) Mean dry weights of all above ground vegetative material. Data is presented as mean ± SEM with significance accepted at p<0.05. Abbreviations: T+V (Tumbler + vacuum); P90 (90-minute plasma); ns (non-significant). 243

Figure 7-13. Ethylene trial results for wheat, Triticum aestivum ‘Scepter’ [sic]. (A) Comparisons of percent germination. (B) Comparisons of the mean BBCH score for each treatment at 4 DAS. The dotted line represents radicle protrusion/germination at stage 05. Data is presented as mean ± SEM. Abbreviations: AVG (2-aminoethoxyvinyl glycine treatment); P45 (45-minute plasma); P90 (90-minute plasma); ns (non-significant); *p<0.05; **p<0.01; ****p<0.0001. All pairwise comparisons were calculated based on two-way ANOVA with Tukey’s multiple comparison tests. 252

Figure 7-14. Images of wheat grains from one plate of each treatment at 4 DAS. This visualisation highlights the influence of prolonged plasma exposure on seedling development as seen in the H_2O treatments (left). It also displays the impact of unintentionally high concentrations of ethylene (centre). It is of note that ethylene treatment improved development of P45 grains when compared to the Untreated ethylene grains. 253

Figure 7-15. Percent germination and mean BBCH scores at 6 DAS in maize grains, Zea mays ‘B73.’ (A) Comparisons of percent germination. (B) Comparisons of the mean BBCH score for each treatment at 6 DAS. The dotted line represents radicle protrusion/germination at stage 05. Data is presented as mean ± SEM. Abbreviations: AVG (2-aminoethoxyvinyl glycine treatment); (P60 (60-minute plasma); P90 (90-minute plasma); ns (non-significant); *p<0.05; **p<0.01. All pairwise comparisons were calculated based on two-way ANOVA with Tukey’s multiple comparison tests. 254

Figure 7-16. Concentrations of 8-OHdG per ng of DNA for each grain type and plasma treatment compared to the Untreated control. There were no significant differences between treatments within each grain type. Data is presented as mean ± SEM with significance accepted at p<0.05. Abbreviations: P30 (30-minute plasma); P90 (90-minute plasma); ns (non-significant)..... 262
Figure 8-1. Pilot trial plates of wheat grain with four plasma treatments compared to the Untreated and T+V controls. Plates were incubated for seven days to determine the potential fungal pathogens and levels of contamination. Multiple species of fungi and bacteria are visible across all treatments. Abbreviations: T+V (tumbler + vacuum); P15 (15-minute plasma); P30 (30-minute plasma); P60 (60-minute plasma); P90 (90-minute plasma). 274
Figure 8-2. Comparison of the contaminated wheat with food quality wheat. There is a log 3 increase in colony-forming units in the contaminated grain, suggesting heavy levels of filamentous fungal pathogens across the contaminated samples. Data is presented as mean ± SEM; ****p<0.0001. 276
Figure 8-3. (A) Comparisons of colony-forming unit counts per grain type and treatment on a log scale. Data is presented as mean ± SEM with significance accepted at p<0.05; n = 15. Letters indicate differences between means Plasma treatment significantly reduces the number of culturable colony-forming units. (B) Individual CFU/mL values plotted for each replicate. This figure highlights the variability within treatments, which is likely due to the heterogeneity of the naturally occurring microbial load. Abbreviations: T+V (Tumbler + vacuum); P30 (30-minute plasma); P60 (60-minute plasma); P90 (90-minute plasma); P120 (120-minute plasma). 278
Figure 8-4. Images of one group of representative technical replicate plates from each treatment. Dilutions are indicated in the bottom right corner of each treatment.

Filamentous fungi are notably absent on 120-minute plasma treatment plates. Colonies present on this treatment are composed of yeast and bacteria. 279

Figure 8-5. Flag preparations of isolated cultures. (A) Lichtheimia corymbifera; (B) mixed culture of yeast and bacteria; (C) Aureobasidium pullulans; (D) Rhizopus arrhizus; (E) Penicillium corylophilum; (F) Aspergillus niger. No scale bars were set. 280

Figure 8-6. Percent of plates with visible colonies of each species identified through ITS sequencing. Please note that conidia of Alternaria and Bipolaris genera were visible under the microscope but did not appear in culture. Fusarium species were identified via qPCR but also did not appear in culture. 282

Figure 8-7. Graph illustrating the changes in species abundance across treatments. Two-way ANOVA data is presented as the mean. All plates were scored on a +/- scale for the presence/absence of each known species. The number of technical replicate plates (out of 6) with positive scores were summed and used as a total score for each biological replicate as indicated on the y-axis. Abbreviations: T+V (Tumbler + vacuum); P30 (30-minute plasma); P60 (60-minute plasma); P90 (90-minute plasma); P120 (120-minute plasma)..... 283

Figure 8-8. SEM micrographs of mycotoxin contaminated wheat grain samples. (A-E) display the embryo region of the grain. Note the debris within creases on the Untreated grain. (F-J) show the embryo region at 5000 x magnification with microbes clearly visible in the Untreated image and increasingly damaged with plasma exposure. (K-O) are micrographs of the dorsal region of the grain with clear weathering of both grain and microbe surfaces. (P-T) visualise the wheat grain brush which becomes severely damaged with extended plasma treatment. 286

Figure 8-9. SEM micrographs with sample charging. Red arrows highlight the streaking which was more pronounced in Untreated samples and gradually reduced with plasma exposure. 288
Figure 8-10. Comparisons of mean concentrations of Aflatoxins and Zearalenone found in each treatment. DON was detected in the original testing but not present in the sampling of each treatment. Two-way ANOVA data is presented as mean ± SEM. Abbreviations: T+V (Tumbler + vacuum); P30 (30-minute plasma); P90 (90-minute plasma); P120 (120-minute plasma). 290

List of Tables

Table 1-1. Global figures for grain consumption and losses in 2018 (FAO, 2021b). ... 2

Table 1-2. Selected plasma-treated seed germination research including plant species tested, apparatus, and treatment times. CDPJ = corona discharge plasma jet; DBD = dielectric barrier discharge; DCSBD = diffuse coplanar surface barrier discharge; GA = gliding arc; M = downstream microwave; RF = radiofrequency. 8

Table 1-3. Comparisons of features and structures of each of the five grain types (Briggs, 1978; Brooker et al., 1992; Duffus and Cochrane, 1993; Fincher and Stone, 1993; Malick and Safui, 1985; Mejia, 2003; Niemann et al., 2013; Phan et al., 2020; Rathjen et al., 2009; Song et al., 1992; Werker et al., 1979; Wrigley, 2017; Zablatzká et al., 2021). 25

Table 1-4. List of mycotoxins produced by fungal species of interest for the purposes of this thesis. 27

Table 2-1. Percentage of maize grain displaying visible fungal contamination post-treatment with the stand plasma generator, chlorine gas fumigation, bleach, and Untreated control. 39

Table 2-2. Percentage of maize grains displaying visible signs of fungal contamination post-treatment in the plasma tumbler for 60- and 90-minute treatments and the Untreated control. 41

Table 2-3. Established operating parameters for the plasma tumbler system used throughout this work. 41

Table 5-1. Summary of the pilot trial showing colony-forming units extracted from maize, Zea mays ‘B73,’ Untreated, T+V (Tumbler + vacuum), and P90 (90-minute plasma) grain and plated on two types of culture media. 85

Table 5-2. Variations within initial haemocytometer counts and final colony-forming units from plates. The means of haemocytometer counts of the initial inoculum load are compared to the means of the haemocytometer counts from Untreated extraction solutions. 106

Table 6-1. Fragments with significant differences between treatments are listed with accompanying p-values to compare trends between grain types. Highlighted cells show statistically different trends for fragments between treatments shared in all grains. Blank cells indicate that no statistically significant values were found for this fragment within a grain type. Significance was accepted at $p<0.05$. Abbreviations: U (Untreated); P30 (30-minute plasma); P90 (90-minute plasma) 164

Table 6-2. Fitting the Peleg and 2-phase model to the sorption data sets. The R^2 values and means of best-fit values ± 95% CI are listed for each grain type and treatment. 183

Table 7-1. List of germination experimental design factors for each grain type. 222

Table 7-2. Description of BBCH scale from dry seed to emergence. Adapted from Lancashire et al., 1991. 223

Table 8-1. List of dilutions prepared for each plasma treatment…… 269

List of Equations

Equation 3-1. Colony-forming units……51

$$\frac{CFU}{mL} = \frac{number\ of\ colonies\ counted\ on\ a\ plate * dilution\ factor}{volume\ of\ culture\ plated}$$

Equation 6-1. Seed moisture content……...171

$$\frac{Initial\ weight\ (g)}{dry\ weight\ (g)}\ x\ 100 = \%\ moisture\ content$$

Equation 6-2. Peleg equation……..……173

$$M_t = M_0 + \frac{t}{k_1 + (k_2 t)}$$

Fitting interpretation of Peleg model in x y coordinates, assuming M0 = 0:

$$y = \frac{x}{k_1 + (k_2 x)}$$

Equation 6-3. 2-phase equation……...173

$$\frac{(M_t - M_\infty)}{(M_0 - M_\infty)} = p(1 - e^{-k_{M_1} t}) + (1 - p)(1 - e^{-k_{M_2} t})$$

$$M_t = M_0 + (M\infty - M0)\ (p(1 - e^{-k_{M_1} t}) + (1 - p)(1 - e^{-k_{M_2} t}))$$

Fitting interpretation of 2-phase model in x y coordinates, assuming M0 = 0:

$$y = y_\infty p(1 - e^{-k_{M_1} x}) + y_\infty (1 - p)(1 - e^{-k_{M_2} x})$$

Equation 6-4. Mucilage water sorption……205

$$\frac{(Initial\ water\ weight\ (g) - weight\ of\ excess\ water\ (g))}{initial\ weight\ of\ grain\ (g)}$$

$$= water\ sorption\ capacity\ of\ mucilage\ (g)$$

😊